Efficiency and Sustainability of the Distributed Renewable Hybrid Power Systems Based on the Energy Internet, Blockchain Technology and Smart Contracts

Edited by
Nicu Bizon

Printed Edition of the Special Issue Published in *Sustainability*

MDPI

Efficiency and Sustainability of the Distributed Renewable Hybrid Power Systems Based on the Energy Internet, Blockchain Technology and Smart Contracts

Efficiency and Sustainability of the Distributed Renewable Hybrid Power Systems Based on the Energy Internet, Blockchain Technology and Smart Contracts

Editor

Nicu Bizon

MDPI

Editor
Nicu Bizon
Faculty of Electronics,
Communication and Computers
University of Pitesti
Pitesti
Romania

This is a reprint of articles from the Special Issue published online in the open access journal *Sustainability* (ISSN 2071-1050) (available at: www.mdpi.com/journal/sustainability/special_issues/ Distributed_Renewable_Hybrid_Power_Systems).

For citation purposes, cite each article independently as indicated on the article page online and as indicated below:

LastName, A.A.; LastName, B.B.; LastName, C.C. Article Title. *Journal Name* **Year**, *Volume Number*, Page Range.

Contents

About the Editor

Nicu Bizon

Nicu Bizon (senior member, IEEE) was born in Albesti de Muscel, Arges county, Romania, in 1961. He received his 5-year B.S. degree in electronic engineering from the University "Polytechnic"of Bucharest, Romania, in 1986 and his Ph.D. degree in automatic systems and control from the same university in 1996. From 1996 to 1989, he was involved in hardware design with Dacia Renault SA, Romania. Since 2000, he has served as a professor with the University of Pitesti, Romania, and has received two awards from the Romanian Academy, in 2013 and 2016. He is the editor and author of 5 books published in Springer and the author of 206 scientific papers (including 7 and 84 papers in IEEE transactions and conferences, respectively) published in Scopus, which have been cited 1678 times, corresponding to an h-index = 29. His current research interests include power electronic converters, fuel cell and electric vehicles, renewable energy, energy storage system, microgrids, and control and optimization of these systems.

Preface to "Efficiency and Sustainability of the Distributed Renewable Hybrid Power Systems Based on the Energy Internet, Blockchain Technology and Smart Contracts"

The very fast increase in the world's energy demand over the last decade, and the request for sustainable development, can be approached through micro- and nano-grids using hybrid power systems based on the energy internet, blockchain technology, and smart contracts.

This book includes innovative solutions and experimental research, as well as state-of-the-art studies, in the following challenging fields:

- Microgrids; nanogrids; smart grids; smart cities; and smart associations between farms, buildings, parking, and homes;
- Smart grid cyber security using energy internet, blockchain, and smart contract-based applications;
- Operations of smart associations integrated with distributed generation;
- Smart grid architecture and energy management models;
- Fuel cell (FC) systems: modeling, control, optimization, and innovative technologies to improve the fuel economy, lifetime, reliability, and safety in operation;
- Hybrid power systems (HPSs) based on renewable energy sources (RESs) (RES HPS): optimized RES HPS architectures, global maximum power point tracking (GMPPT) control algorithms to improve the energy harvesting from RESs, and advanced energy management strategies (EMSs) to optimally ensure the power flow balance on DC (and/or AC bus) for standalone RES HPSs or grid-connected RES HPSs (microgrids, nanogrids, etc.);
- RES HPSs with a FC system as a backup energy source (FC RES HPS): innovative solutions to mitigate the RES power variability and load dynamics of energy storage systems (ESSs) by controling the generated FC power, DC voltage regulation, and/or load pulse mitigation via active control of the power converters from hybrid ESS;
- FC vehicles (FCVs): FCV powertrain, ESS topologies, and hybridization technologies and EMSs to improve the fuel economy;
- Optimal sizing of FC RES HPSs and FCVs; and
- Business opportunities, open issues, and future trends.

The climate changes that are visible today are a challenge for the global research community. The stationary applications sector is one of the most important energy consumers. Harnessing the potential of renewable energy worldwide is currently being considered to find alternatives to obtaining energy by using technologies that offer maximum efficiency and minimum pollution. In this context, renewable energy sources, fuel cell systems, and other energy generating sources must be optimally combined and connected to the grid system using advanced energy transaction methods.

The first chapter presents networked control systems (NCSs), which attract the attention of control system engineers. This chapter presents an extensive review of NCSs from the perspective of control system design. The evolution of NCSs is broadly divided in three phases, namely NCSs prior to 2000, NCSs during 2001–2010, and NCSs from 2011 onwards, which correspond to the initial status, intermediate status, and the recent status of the developments in the design of NCSs. The advancement of different control techniques during these phases has been discussed comprehensively. This chapter also describes the transition of control systems ffom a continuous

domain to a networked domain, which makes it better than the traditional control systems.

The next three chapters, Chapters 2 to 4, present applications related to microgrids.

Chapter 2 introduces a new concept that allows for small energy producers to deliver excess energy to microgrids using smart transactions based on blockchain technology.

Chapter 3 investigates the power-sharing issues in networked-isolated microgrids containing multiple distributed generators (DGs) and loads connected to different common coupling points (CCPs) if the line parameters or mesh microgrid configuration are unknown. A decentralized droop control algorithm is proposed to achieve active and reactive sharing of different DGs in isolated microgrids with reconfigurable mesh.

Chapter 4 investigates the problems of improving the power factor through correction methods that reduce the load on the transformers and power conductors, leading to a reduction in losses in power supply and reduced costs by eliminating penalties (because they apply only at the common coupling point).

Chapters 5 and 6 present applications related to proton-exchange membrane fuel cell (PEMFC)-based hybrid power systems.

Chapter 5 proposes an effective control strategy to manage the distribution of energy from fuel cells and batteries to power a hybrid electric boat. The main objectives of this real-time control are to reduce hydrogen consumption and to improve the quality of energy transfer for a hybrid electric boat in various demand conditions.

Chapter 6 examines four fuel-saving strategies using power tracking control of the fuel cell boost converter and optimization of the PEMFC system by controlling power regulators. The performance and safe operation of the PEMFC system in the event of load disturbances and variations in renewable energy were estimated and compared with a reference strategy. The percentages of fuel economy are between 2.83% and 4.36% and between 7.69% and 12.94%, in the case of dynamic charging cycles with averages of 5 kW and 2.5 kW, respectively.

The last five chapters, Chapters 7 to 11, present applications related to microgrids based on energy internet, blockchain technology, and smart contracts.

Chapter 7 presents a new market model with social and commercial tiers for improved prosumer trading in microgrids. The proposal is based on a two-tier local market model oriented for prosumers and consumers connected in microgrids, based on the blockchain technologies and other technologies and concepts such as smart grids, crowdsourcing, and energy poverty.

Chapter 8 proposes the scheduled charging of electric vehicles in a secured manner by emphasizing cost minimization Using blockchain technology and an Inter-Planetary File System (IPFS). The charging of vehicles is performed in a Peer-to-Peer (P2P) manner, using Charging Stations (CSs) or Mobile Vehicles (MVs) that are not connected to a central entity.

Chapter 9 discusses carbon credits, which should reduce the environmental pollution and carbon emission of the Earth in the future, and shows that the market for carbon credits will become a critical issue from 2021 onwards. It proposes a market for carbon credits based on blockchain technology to measure carbon emission rights, making transactions more reliable by verifying carbon emissions rights among the UN-SDGs '(United Nations Sustainable Development Goals') 17 tasks.

Chapter 10 analyzes the blockchain-based Internet of Things (IoT) for a smart electric vehicle battery management system. The first implementation uses ethereum as the blockchain framework for developing smart contracts, while the second uses a directed acyclic graph (DAG), on top of the IOTA tangle. The two approaches are implemented and compared, demonstrating that both

platforms can provide a viable solution for an efficient, semi-decentralized, data-driven BMS.

Chapter 11 proposes the implementation of blockchain technology in irrigation systems that integrate photovoltaic power generation systems. The efficiency of the proposed system is monitored not only through digital hardware connected to photovoltaic panels and water pumps but also by using the blockchain technology and smart contracts. A SolarCoin version similar to the Bitcoin cryptocurrency is proposed for energy and water trading.

As this book presents the latest solutions in the implementation of fuel cell and renewable energy in mobile and stationary applications such as hybrid and microgrid power systems based on energy internet, blockchain technology, and smart contracts, we hope that they are of interest to readers working in the related fields mentioned above.

Nicu Bizon
Editor

A Comprehensive Review of the Evolution of Networked Control System Technology and Its Future Potentials

Mayank Kumar Gautam [1] , Avadh Pati [1] , Sunil Kumar Mishra [2] , Bhargav Appasani [2] , Ersan Kabalci [3] , Nicu Bizon [4,5,6,7,*] and Phatiphat Thounthong [8,9]

1   Department of Electrical Engineering, National Institute of Technology, Silchar 788010, India; mayank_rs@ee.nits.ac.in (M.K.G.); avadh@ee.nits.ac.in (A.P.)
2   School of Electronics Engineering, Kalinga Institute of Industrial Technology, Bhubaneswar 751024, India; sunil.mishrafet@kiit.ac.in (S.K.M.); bhargav.appasanifet@kiit.ac.in (B.A.)
3   Department of Electrical and Electronics Engineering, Nevsehir Haci Bektas Veli University, 503000 Nevsehir, Turkey; kabalci@nevsehir.edu.tr
4   Faculty of Electronics, Communication and Computers, University of Pitesti, 110040 Pitesti, Romania
5   ICSI Energy, National Research, 240050 Ramnicu Valcea, Romania
6   Development Institute for Cryogenic and Isotopic Technologies, 240050 Ramnicu Valcea, Romania
7   Doctoral School, Polytechnic University of Bucharest, 313 Splaiul Independentei, 060042 Bucharest, Romania
8   Renewable Energy Research Centre (RERC), Department of Teacher Training in Electrical Engineering, Faculty of Technical Education, King Mongkut's University of Technology North Bangkok,1518 Pracharat 1 Road, Bangkok 10800, Thailand; phatiphat.t@fte.kmutnb.ac.th
9   Group of Research in Electrical Engineering of Nancy (GREEN), University of Lorraine, 2 Avenue de la Forêt de Haye, Vandeuvre lès Nancy CEDEX, F-54000 Nancy, France
*   Correspondence: nicu.bizon@upit.ro

Abstract: Networked control systems (NCSs) are attracting the attention of control system engineers. The NCS has created a paradigm shift in control system technology. An NCS consists of control loops joined through communication networks in which both the control signal and the feedback signal are exchanged between the system and the controller. However, its materialization faces several challenges as it requires the integration of advanced control and communication techniques. This paper presents an extensive review of NCSs from the perspective of control system design. The evolution of NCSs is broadly divided in three phases, namely NCSs prior to 2000, NCSs during 2001–2010, and NCSs from 2011 onwards. This division corresponds to the initial status, intermediate status, and the recent status of the developments in the design of NCSs. The advancement of different control techniques during these phases has been discussed comprehensively. This paper also describes the transition of control systems form continuous domain to networked domain, which makes it better than the traditional control systems. Some important practical applications, which have been implemented using NCSs, have also been discussed. The thrust areas for future research on NCS have also been identified.

Keywords: controller design analysis; networked control systems (NCSs); network security; delays; sampling

1. Introduction

A networked control system (NCS) consists of control loops connected through communication networks, in which both the control signal and the feedback signal are exchanged between the system/plant and the controller. There are two types of approaches for design of NCSs, namely control of network approach and control over network approach. Only the control over network approach-based NCSs are considered in this review. A simple block diagram of this type of networked system is shown in Figure 1.

In an NCS, the plant output is measured using the sensors. These signals are converted into digital signals using the analog-digital (A/D) convertors, which are transmitted to the

controller via a communication network. The controller determines the control signal based on the sensor output, which is transmitted back to the plant using same communication channel. The control signal before being fed to the actuator section of the plant, is converted from digital to analog signal using the digital-analog (D/A) convertor. In this manner, the plant dynamics can be controlled from a remote location.
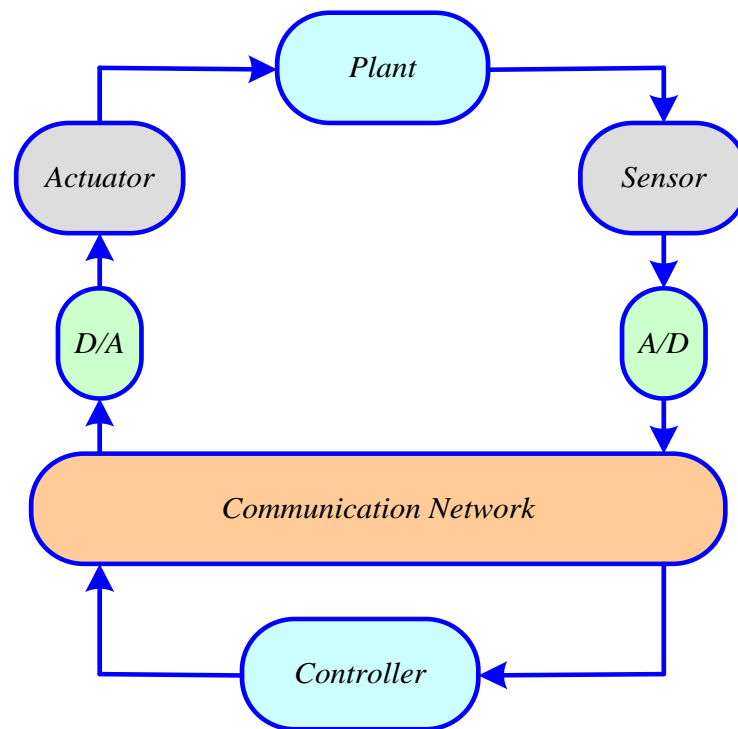
Figure 1. A simple block representation of a networked control system (NCS).

1.1. Advantages and Disadvantages of NCS

There are several underlying advantages of an NCS, which is termed as the next generation control system. Key merits of networked control systems (NCSs) are as follows:

(i)   *Effective reduction of system complexity*: It is possible to minimize the complexity of control systems by interfacing them with the communication network. With the communication network, the data related to multiple plants can be easily stored at a single server which reduces the complexity of control systems.

(ii) *Efficient sharing of network data*: Several parameters pertaining to the plant can be exchanged easily using the communication networks, which helps in the design of control algorithms.

(iii) *Simple to take intellectual decisions based on the information*: The information can be used to make intelligent decisions easily.

(iv) *Eliminates unnecessary wiring*: Today, it is possible to transmit data wirelessly at a very high speed. The wiring for interfacing controllers and plants can also be avoided. The wireless sensor networks are advanced enough to make the wireless control is a reality.

(v)   *Simple to scale the networks by adding additional sensors, actuators, and controller*: The wireless sensors and actuators can be replaced easily, which reduces the maintenance cost of the NCS. The controllers can also be replaced economically as compared to the traditional wired controllers. The expansion of sensors, actuators and controllers can also be achieved easily.

(vi) *Cyber-physical interface for tele-execution of control*: The NCS provides a platform for cyber-physical interface and tele-execution of controls. The NCS permits the remote control of the plant.

(vii) *Wide range of applications*: Applications in the area of distributed power systems, robots, unmanned aerial vehicles (UAVs), automobiles, space discovery, terrestrial discovery, industrial unit automation, remote problem-solving and troubleshooting, perilous environments, aircraft, production plant monitoring, and many more. More and more applications of NCS are coming into existence every day.

The NCS is also plagued by several problems. The disadvantages of NCS are:

(i.) *Loss of ability to determine the time of incoming data*: The time at which the data arrives cannot be determined exactly, so uniform sampling cannot be used.

(ii.) *Loss of data integrity*: Data may be lost during the transmission process, so it cannot give the complete information.

(iii.) *Communication Latency*: In remotely located NCSs, due to the communication latency, the control action may not be implemented with immediate effect.

(iv.) *Complexity and Congestion*: As the number of nodes increases, so does the complexity of the communication system, causing congestion and time delays. Therefore, the deployment in an industry with tens of thousands of sensors and actuators can be a challenging task.

1.2. Designing of Control System from Continuous Domain to Networked Control Domain

In the beginning, control signals were generated using analog computers. Frequency analysis and Laplace transform were the primary tools for analysis. The main drawbacks of this system are its limited accuracy, limited bandwidth, drift, noise, and limited capabilities to manage nonlinearities. Known delays could be handled at the time of control synthesis using the well-known Smith predictor.

Digital controllers replaced the analog technology with the advancement of processors. However, controlling an analog plant with a discrete electronic system inevitably introduces timing distortions. In particular, it will become necessary to sample and convert the sensor measurements to digital data and also convert them back to analog values. Sampling theory and z transform became the standard tools for the design and analysis of digital control systems analysis. For z transform, it is assumed that the sampling is uniform. Thus, for the design of digital controllers, periodic sampling became the standard. Note that, at the infancy of digital controls, as the computing power was poor and memory was expensive, it was vital to minimize the complexity of the controllers and the operating power. It is not obvious that the periodic sampling assumption is always the best choice. For example, adaptive sampling has been used in Reference [1], where the sampling frequency is changed based on the derivative of the error signal, and is far better than equidistant sampling in terms of computed samples (but possibly not in terms of disturbance rejection [2]). A summary of these efforts is provided in References [3,4]. However, with the decreasing computational costs, interest in adaptive sampling reduced, and the linearity preservation property of equidistant sampling has helped it to stay the undisputed standard.

From the computing side, real-time scheduling modeling and analysis were introduced in Reference [5]. This scheduling was based on restrictive assumptions, one of them being the periodicity of the tasks. Even if more assumptions were progressively introduced to cope with the practical problems, the periodicity presumption remains popular [6]. Moreover, the topology of the network can vary with time, allowing the mobility of the control devices. Hence, the whole control system can be highly adaptive in a dynamic environment. In particular, wireless communications allow for the rapid deployment of networks for connecting remotely located devices. However, networking also has problems, such as variable delays, message de-sequencing, and periodic data loss. These timing uncertainties and disturbances are in addition to the problems introduced by the digital controllers. Figure 2 shows the trade-off between control performance and the sampling rate.
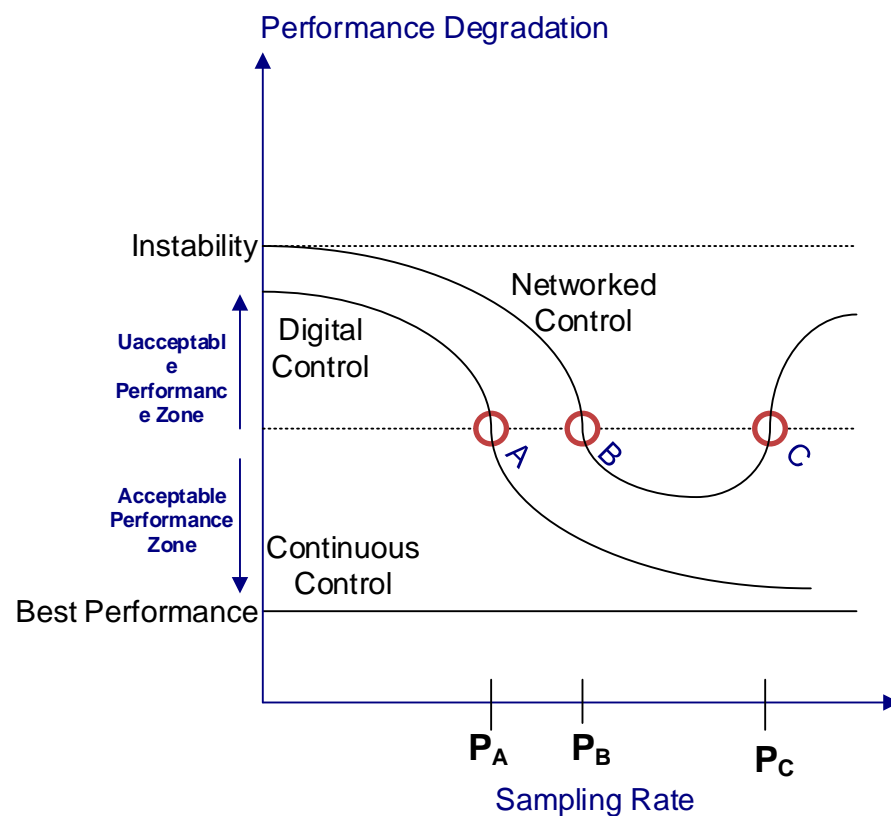
Figure 2. Trade-off between control performance and the sampling rate.

Figure 2 shows that the control performance is only applicable for a range of sampling rate from P_B to P_C. Increasing the sampling rate above P_C increases the network-induced delays. This will result in the degradation of control performance.

Based on the above discussion, the difference between the conventional control systems and the NCS is been summarized in Table 1 as:

Table 1. Differences between networked and conventional control systems.

Parameters	Networked System	Conventional System
Vital Function	Control of physical equipment	Data processing and transfer
Applications	Manufacturing, processing and utility distribution	Corporate and home environments
Hierarchical Process	Deep, functionally separated hierarchies	Shallow, integrated hierarchies
Failure Mode and its effect	High	Low
Reliability Requirement	High	Moderate
Deterministic	High	Low
Data Composition	Small packets of periodic and aperiodic traffic	Large, aperiodic packets
Reliability	Required	Not required
Operating Environment	Hostile conditions, often featuring high levels of dust, heat, and vibration	Clean environments, often specifically intended for sensitive equipment

1.3. Co-Design Approach for the NCSs

The design of an NCS integrates the domains of control system, communication, and real-time computing. The increasing complexity of the computer systems, and their networks, requires advanced methods specifically suited for the NCS. The main issue to be addressed is the achievement of the control objective (i.e., a combination of security, performance, and reliability requirements), despite the disturbances. For instance, sharing of common computing resources and communication bandwidths by competing control loops, alongside the other functions, introduces random delays and data losses. Moreover, the use of heterogeneous computers and communication systems increases the complexity of the NCS.

Control plays a significant role in interconnected complex systems for their reliable performance [7]. The interconnection of elements and sub-systems, coming from different technologies, and which are subject to various constraints, calls for a design that can solve the conflicting constraints. Besides achieving the desired performance in normal situations, the reliability and safety-related problems are of concern for the system developers. A fundamental concept that is dependability, which is the device property that features various attributes, such as access, reliability, safety, confidentiality, integrity, and maintainability [8]. Being confronted with faults, errors, and failures, a system's dependability could be achieved in numerous ways, i.e., fault prevention, fault threshold, and fault forecasting [9].

Except in the event of failures due to hardware or software components, most procedures run with nominal behavior, but, neither the process nor the execution resource parameters are completely known or modeled. One method is to allocate the system resources conservatively, which results in the wastage of resources. From the control viewpoint, specific inadequacies to be considered include poor timing, delays, and data loss. Control usually deals with modeling uncertainty, powerful adaptation, and disturbance attenuation. More correctly, as shown with recent results obtained on NCS [10], control loops tend to be robust and can tolerate networking and computing disturbances, up to a certain level. Therefore, the timing deviations, such as jitter or data loss, as long as they remain within the bounds, may be viewed as the nominal features of the system, but not as exceptions. Robustness allows for provisioning the execution resources according to needs that are average than for worst cases, and to take into account system reconfiguration only once the failures surpass the abilities of the controller tolerance that is running.

An NCS is composed of a collection of heterogeneous devices and information subsystems. For designing the NCS, many conflicting constraints must be simultaneously fixed before reaching a satisfactory solution that is implementable. Issues related to networking control tracking performance, robustness, redundancy, reconfigurability, energy consumption, expense effectiveness, etc., are to be addressed. Traditional control usually deals with a procedure that requires a solitary computer, and the limitations of the communication links and computing resources usually do not notably affect its performance. Existing tools dealing with the modeling and identification, robust control, fault diagnosis and isolation, fault tolerant control, and flexible real-time scheduling need to be enhanced, adapted, and extended to handle the networked characteristics of the control system. Finally, the thought of a co-design system approach has emerged that allows the integration of control, as well as communication within the NCS design [10].

1.4. Main Contributions

The NCS is an emerging area of the control system. It is worth reviewing the state-of-the-art developments in NCS. Although many review papers have been published in this area, to the best of the authors' knowledge, these focused only on a certain dimension of the NCS, and a comprehensive approach was lacking. In this paper, a comprehensive review on the evolution of NCSs in last the 30 years is discussed. The evolution of NCS is broadly divided in three phases as: (i) prior to 2000, (ii) 2001–2010, and (iii) 2011 onwards. The reason for this division is to understand the initial, the intermediate, and the latest developments related to NCS. The main focus of this discussion would be on the advancement

of different control techniques during these phases. Based on the extensive review, the different types of NCSs and their related challenges are described. At the end, this review paper highlights the following innovations in the field of NCS: new novel methods for selecting the best sampling time in the NCS, new jitter compensation techniques, developing the theory and practice for control systems operating in a distributed and asynchronous packet-based environment, stability analysis of networked control systems in the presence of network-induced delays and packet dropouts (due to propagation delay and also due to the network congestion), and developing of advanced networked control methods that provide the desired performance in the presence of uncertainties and adversaries. This review paper also highlights some important practical applications that are implemented using the NCSs. Lastly, the important future research areas for NCSs are discussed.

The remaining sections are as follows: Section 2 reviews the development of NCS prior to 2000 AD; The development of NCS from 2001 AD to 2010 AD is discussed in Section 3; The advancement of NCS in recent phase after 2011 AD is discussed in Section 4; Section 5 describes about different topologies of NCSs; Section 6 presents different types of NCSs and their related challenges; Section 7 discusses some of the vital practical applications of the NCSs; Section 8 is the conclusion, along with the observations and potential future developments.

2. Initial Phase of NCS Prior to 2000

The NCS concept is not a recent phenomenon. It emerged in the early 1970s, with the progress of computation, as well as communication, technologies. However, the computation and communication technologies were still in the nascent stages and so the NCSs were designed as decentralized control systems, which remained prominent for the next three decades. One of the earliest works on decentralized NCS was proposed by Reference [11], where algebraic and geometric methods were discussed to obtain stable results. A dual-mode decentralized scheme for the networked control of a commodity's flow has been presented in Reference [12]. First, local controllers located at network nodes, exchange simple messages with their neighbors to determine the confined optimum flows. Second, the local controllers adjust their flows to reach the optimal equilibrium state in finite time.

The stabilization of the decentralized linear time-invariant multivariable (LTI-MultiVar) system was proposed in Reference [13] by employing numerous local feedback control rules. A necessary and sufficient condition was obtained from the above rule for the stabilization of the given system. Later, in Reference [14], the properties of the closed loop were studied for both controllable and observable *k-channel* linear systems, by applying the consequences of decentralized feedback. In addition, the theory of a complete system was established. Complete systems can be made both controllable and observable for all channels by applying non-dynamic decentralized feedback.

Some development in the field of decentralized control was achieved in 1980s. In Reference [15], a new dynamic interaction measure was defined by using the perception of structured singular value (SSV) for multivariable systems under feedback. To predict the stability of the decentralized systems and to measure the loss of performance, dynamic interaction measure was used. Later, in Reference [16], F. Lin et al. presented several important studies on decentralized control systems. The decentralized regulation and synchronization for partially surveyed discrete-time-event systems was studied. In Reference [17], which was illustrated using a simple production system. This study was later extended in Reference [18], and it was concluded that decentralized supervision would be easier to design and use.

In the 1990s, several NCS-related ideas evolved based on the concepts developed in the recent years, such as smart networks for control, decentralized control of complex systems, supervisory control, control in multimedia wireless networks, quasi-decentralized control, scheduling, event-triggered control, stability analysis, and so on [19–31].

The decentralized control of systems, which is complex in nature, were described in Reference [19], wherein topics, such as stabilization, optimization, estimation and control, output control, decompositions, and reliable control, were discussed in detail. In Reference [20], the author discussed the role of distributed, as well as centralized, networks for control. The authors also differentiated the above two categories in different ways. It also discussed the benefits and drawbacks of data networks, as well as the control networks. In a discrete-time system [21], the events must be within the imposed time constraints. To achieve a given control objective, a controller can hinder, permit, or pressurize several events in the system. In Reference [22], the network-level management and control issues were discussed. The quasi-decentralized control for complex systems was analyzed in Reference [23] using the concept of power system stabilization to design a sample system.

Three types of data: periodic data, sporadic data, and messages, have been proposed in Reference [24] for the planning of the NCS. As a basic parameter, delay bound was used, which guarantees the stability of the given system using Lyapunov's theorem. The above method can adjust the sampling period to be as minimum as possible, allocating all the network bandwidth. The basic properties of real time distributed systems were compared in Reference [25]. In addition, the characteristics of time triggered and event-triggered distributed systems in robotics were discussed in References [26,27] using the artificial intelligence, particularly focusing on the predictability, resource utilization, extensibility, etc. In Reference [28], the authors achieved the asymptotic stability and improved controller performance by scheduling the use of the network.

At the end of 20th century, a basic controller called an event-based proportional–integral–derivative (PID) controller was described in Reference [29], decreasing the resource consumption, only with the deprivation in the performance of trivial control. The proposed work was validated with simulations on a double-tank process. Next, two types of algorithms were suggested in Reference [30] for approximating the plant operation: one was an open-loop arrangement analyst, and the other was a closed-loop arrangement analyst/predictor. Again, the NCS's stability was analyzed in Reference [31], showing the effects of sampling rate manipulation and network delay on the system stability.

The above historical developments are summarized in tabular form in Table 2 on the basis of area/network/parameter.

Table 2. Summarized discussion of development of NCS prior to 2000.

S.No.	Papers	Parameter/Area/Network
1	[11–19,23]	Decentralized, Robust Control Network
2	[20–22,24–29]	Smart, Wireless and Discreet Control Networks
3	[30,31]	Stable and Robust Networks

Table 2 shows the distribution of available papers in the different areas prior to year 2000: on decentralized-based networks, there are around 10 papers; on smart network-based systems, there are around 9 papers (during this period, the smart networks are in development stage); stable and robust networks can be found in all types of networks. The table here describes about the evolution of networked systems from decentralization of the available conventional networks. As there are many shortcomings in decentralized systems, the evolution of smart/wireless networks/discreet event-based networks came into existence. The distribution of the papers prior to 2000 is shown in Figure 3. The majority of the works are related to decentralized networks, followed by smart networks, and only a small percentage of works dealt with stable/robust networks.
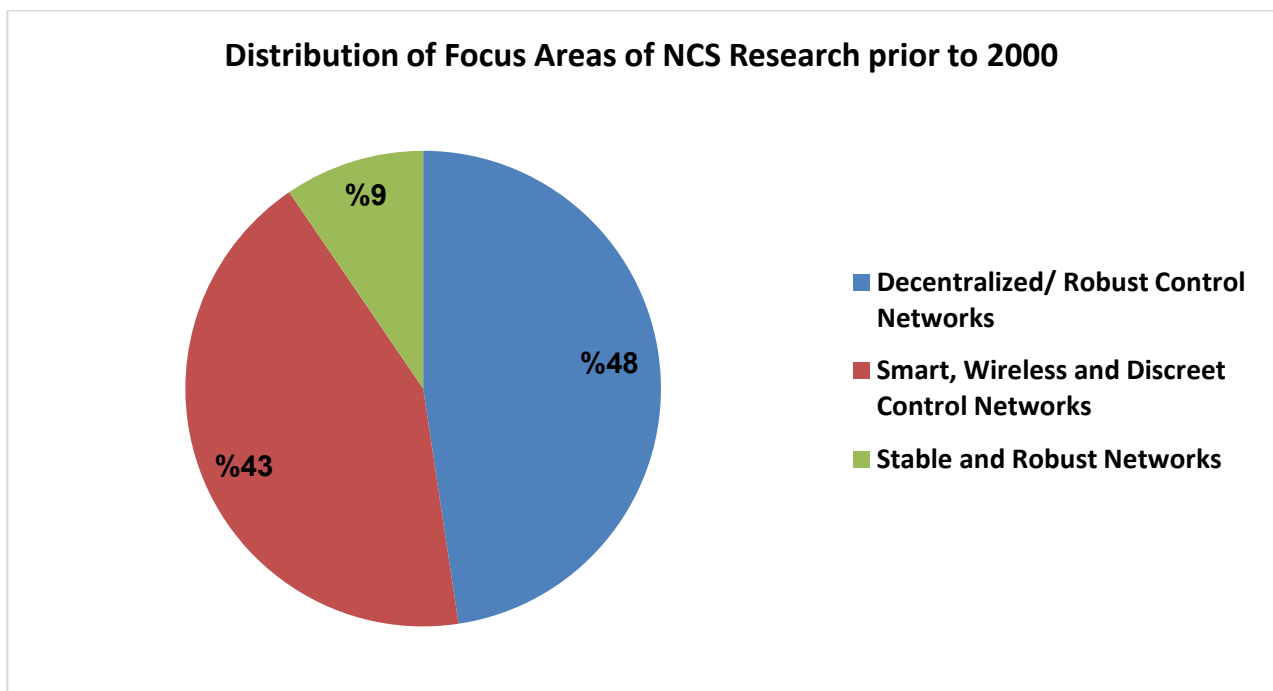
Figure 3. Distribution of focus areas of NCS research prior to 2000.

3. Development of NCS between 2001 to 2010

During this period, the key concepts of NCS, which were proposed earlier, received more attention, and the volume of research increased tremendously. One of the main themes of this period was the controller design for NCS with stability analysis and time delay. An important work on scheduling method for NCS was proposed by Reference [32]. This method guaranteed the stability using Lyapunov method. Next, a work on the impact of modern networked architecture on control act of NCS was published by Reference [33]. In Reference [34], the procedures for selecting the message recognizers for vigorously scheduled networked systems were proposed and validated. In Reference [35], recital benefits were established by dispensing with queues and by vigorous traffic scheduling on the network.

An uncomplicated and easy model of a network system was proposed in Reference [36], in which local controllers connected by a network was addressed. In Reference [37], it was discussed that any complex self-motivated communications network typically has several layers and executive units and would be at risk of several disturbances. Therefore, the requirement for efficient and intelligent control of the systems must be used [38]. In Reference [39], an original networked control protocol, called try once-discard, has been proposed for multiple-input and multiple-output (MIMO) NCSs.

A style technique of memoryless-quantizers in sampled-data models was planned by Reference [40]. The objective was quadratic stability within the continuous time (CT) domain. In Reference [41] a general framework for the NCSs was given, where all elements were assumed to be connected through a communication network. They used the uncertainty threshold principle to point out that, with the bound conditions, even in an undisturbed NCS there would be data rates that degrade the performance of networked control due to the network induced delays and can lead the system to the instability [42].

In Reference [43], web-based multi-rate control systems were presented. It was suggested that the effect of web time delay on the control performance can be reduced by using the time delay compensation. A novel networked control strategy developed by Reference [44], analyzes the soundness of the networked systems with unsystematic delay in the communication. It consisted of a network control predictor and a traditional controller. The soundness criteria of a networked system were analytically derived for random

communication delays. In Reference [45] a state observer for the networked systems with a delay in the time period was designed. Authors claimed that the state observer supported the satisfactory performance of the NCS, even with delay in the time period. Another review paper [46], which appeared within the same year, was centered on network-induced delays, sampling amount, jitter, information packet dropout, network programming, and stability of Ss.

In Reference [47], authors studied the result of a network within the feedback circuit of an NCS. A random packet-loss model for the network was considered. A classical work on the design of robust H-infinity (H∞) controllers for NCSs with uncertainties was given by Reference [48] that additionally considered the network-induced delay and information dropout. Next, the delays due to the sensor-to-controller and to-actuator were sculptured as two Markov/stochastic chains in Reference [49]. Input/output delay approach was considered by Reference [50] to style the strong sampled-data strong control. Enough LMI conditions were obtained by Lyapunov–Krasovskii functionals. In Reference [51], the straight line stability and straight line persistent disturbance attenuation problems were investigated for NCSs under the effects of random access delays and packet dropout. A robust controller was designed in Reference [52] for the NCSs with random time-delays, using the linear matrix inequality (LMI). The performance analysis of the event-triggered control for the detector sampling in a NCS was carried out by Reference [53]. The analytical formula for analyzing the mean and, therefore, the rate of event-driven traffic versus the sampling resolution was obtained. The simulation results in support of the obtained formula were additionally discussed.

A fault detection technique for NCSs supporting the parity relation and Principal Component Analysis (PCA) was projected in Reference [54]. The projected methodology noticed an honest decoupling from the unknown and random network-induced delay. In Reference [55] a fault bearing control methodology for the nonlinear NCSs with communication constraints was given. In Reference [56], the Tagaki-Sugeno (T-S) model was utilized to design a networked system with completely different delays induced by the network. When analyzed with the existing system modeling methods, this approach does not need the data of the actual delays induced by the network. The work in Reference [57] focused on the networked system with random time delays and, additionally, bestowed a brand new modeling methodology for the linear and nonlinear NCS with time delays that are random in nature and named those models as similar T-S fuzzy models.

A system supported bionic principles was introduced by Reference [58] to demonstrate the information obtained from an oversized range of numerous sensors. By means of that structure symbolization, the quantity of data to be processed was considerably reduced. In Reference [59] the event-triggered control was revisited, from an input-to-output perspective. Review of many modern results on evaluation, investigation, and controller synthesis for networked systems were administered in Reference [60]. Another paper, by Reference [10], surveyed appropriate work from the areas of systems and process control, detection, and estimation. Input delay approach, during which the sample-and-hold circuit can be implanted into an analog system with an input delay which is time-varying, was revised in Reference [61]. The loss of data-packets in the NCSs was mentioned in Reference [62]. In Reference [63], a mathematical model of a small rotorcraft was presented. The identification methodology and state estimation using Extended Kalman Filter were discussed. Control algorithms, based on PI, LQG and SDRE approaches, focused on rotorcraft were also proposed.

In Reference [64], the impact of a network within the electrical circuit of a system was discussed. They used an unsystematic loss of data-packet model for the network, and showed the results for discrete-time period systems with stochastic process jumping constraints. In Reference [65] the exponential stability of Nonlinear Time Varying (NLTV) impulsive systems was established with the help of Lyapunov functions separated at the impulse times. In Reference [66], it was observed that for NCSs with delays and output feedback stabilization, there was a deviation in the mean-square stability due to the random

communication situations. In Reference [67], a state feedback controller was proposed for the stabilization of an uncertain linear networked control systems with random communication time delays, which differs from the Lyapunov–Razumikh methodology. In Reference [68], a sufficient condition was obtained for the exponential stability of the networked systems, and they also the mentioned relationship between the dropout rate of the data-packets. An occurrence-based discrete-time model (an exponential unsure system with delay) was proposed by Reference [69] that showed that the stability of the projected system can be achieved by finding an effect for a switched stochastic system with an additive norm delimited uncertainty.

In Reference [70], the state feedback controllers were considered for a closed-loop NCS that is represented as a delay in switched systems. A technical note involved with the stabilization drawback of NCS was revealed by Reference [71]. In Reference [72], compensation ways were studied, within the structure of NCS, while considering the protocol characteristics. A general framework was projected initially, wherever the zero-order hold had the logical capability of selecting the most recent control input packet. A category of period of time control systems during which every control task triggers its next unleash supported the worth of the last sampled state were examined by Reference [73]. In Reference [74], a memory less quantizer for steadying a single-input discrete-time Linear Time Invariant (LTI) system with random loss in data-packets, was proposed within the sense of unsystematic quadratic stability. Nesic et al. [75] generalized and unified a variety of recent developments in the literature pertaining to quantized control systems (QCS) and NCS. They provided a unified framework for the controller style with division and time planning via an emulation-like approach. Improved stability conditions were derived in Reference [76] for sampled-data feedback control systems with falteringly Linear Time Variant (LTV) sampling intervals. The cause of robust $H\infty$ control was researched by Reference [77] for sampled-data systems with probabilistic sampling. By Linear Matrix Inequality (LMI) approach, enough situations were produced, that bonded the robust mean-square exponential stability of the system.

An event-driven state-feedback type of control technique in which a control input generator mimicked a continuous feedback between two successive event times was published by Reference [78]. In Reference [79], focus was given on different factors, such as networking technology, delay network induced delay, resource allocation of networks, scheduling, fault bearing capacity, etc. In Reference [80], an original totally time period dependent Lyapunov function was proposed in the construction of the input delay that improves the existing results. In Reference [81], the cause of the NCSs having exponential stability with the increase in delay time-periods, was studied. The cause of robust fault calculation for a class of tentative networked systems with arbitrary communication delays induced by the network was inspected by Reference [82], which also described the delays by Markov processes. In Reference [83], wireless sensor networks for networked manufacturing systems were proposed.

The above historical development is summarized in tabular form in Table 3 on the basis of area/network/parameter as follows.

The above, Table 3, gives a structured information about the distribution of papers in different areas published during the phase from 2001 to 2010. On scheduled networks, there are around 6 papers; on stability analysis-based systems, there are around 15 papers; on complex and interactive networks, there are around 5 papers; on communication and event-based networks there are around 4 papers, etc. Event-based approach was still in the developmental phase as it was a new technique. Delay-based systems were popular during this stage that were used to overcome the drawbacks of the research prior to year 2000. So, scheduled, autonomous, event-based, and communication-based approaches came into existence during this phase. The major drawbacks prior to year 2000 were: security issues, effect of delay on networked systems, effect of packet dropouts in communication networks, etc. So, to overcome these issues, scheduled approach-based network came into existence. The distribution of the papers during this phase are shown in Figure 4. The

major focus was on delay-based approaches in networked system to improve the flow of information in networked system and make the system stable.

Table 3. Summarized discussion of development of NCS from 2001 to 2010.

S.No.	Papers	Parameter/Area/Network
1	[32,35,38,46,47,79]	Scheduled Networks
2	[34,36,39–41,46,47,49–51,57,62,71,76,81]	Stability Analysis/Approach
3	[37,42,46,47,75]	Complex/Interactive Networks
4	[10,43,46,63]	Internet/Communication Based Multi-rate Control Networks
5	[46,53,75,78]	Event Based Networks
6	[33,44–46,48–50,52,54–56,61,65–68,70,72,74,77,80,82]	Delay/Fault Detection/Packet Loss
7	[46,58,83]	Autonomous Networks
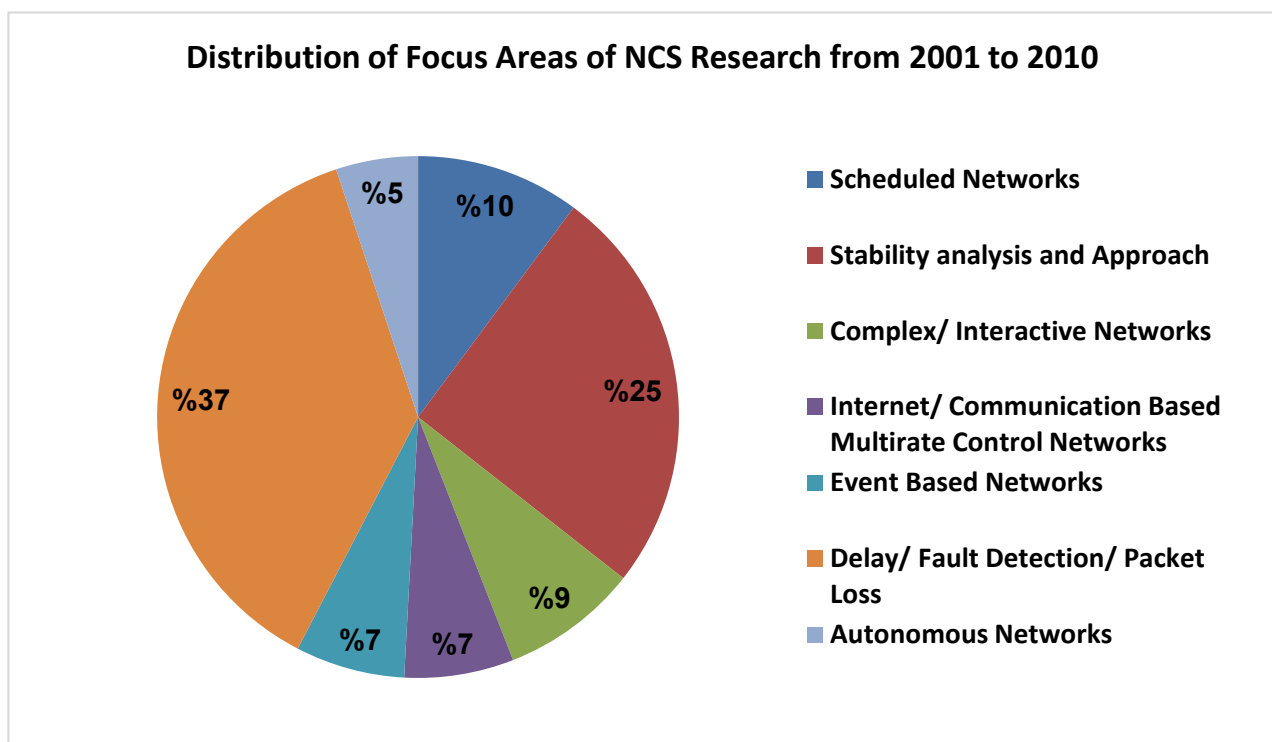
Figure 4. Distribution of focus areas of NCS research from 2001 to 2010.

4. Development of NCS from 2011 Onwards

In the last decade, highly developed control methods were employed for improving the performance of NCS in terms of system stability, delays, event-triggering algorithms, network security, etc. In addition, the discrete time NCSs have received a considerable amount of attention.

Model-based predictive NCSs (MBPNCSs) were proposed by Reference [84] that compensated for the random delays and for the data losses in data transmission. The performance of the system was improved with the help of a predictive control scheme. In Reference [85], an approach for stabilization via discontinuous Lyapunov function was proposed, where sampling intervals that varied in terms of their nature, the dropouts, and

network delays were taken into account. In Reference [86], a *H2/H∞* control of random time delayed networked systems was proposed. In Reference [87], the stability investigation of a NCS was achieved, where the communication between the controller and the plant input is through a digital channel, with dropouts in data-packets and finite-level quantization. Again, in Reference [88], authors describe the stability of NCSs with respect to time-varying transmission intervals.

For discrete-time models, in Reference [89], the difficulty of the networking-based *H∞* filtering method was described. A Markov jumping model based method was described to design *H∞* filters, in which the filter gains depend on both the network delays and dropouts in data-packets. In Reference [90], a novel method was presented to calculate the stability of continuous linear systems with input containing the sampled data. In a technical note, Reference [91] presented a new method with control packet loss. In Reference [92], a networked control loop was considered in which the "slave" portion was a plant, and the "master" portion was the remote controller and observer. In networks, the fault detection of linear systems with restricted loss of data packets was proposed by Reference [93]. In Reference [94], a modern control system mapped on Networks-on-Chip was presented. The proposed architecture was supposed to play a pivotal role in real time applications like missile control system, robot trajectory, and satellite vehicle orbital trajectory control system. In Reference [95], a NCS framework for the coordinated control of distributed generation sources in smart power grids was proposed. The system measurements were transmitted to the controller through a real-time communication network and the effects of delays and packet dropouts due to the communication network were modeled.

An event-triggered transmission scheme was proposed by Reference [96] for a sampled-data control system. In Reference [97], an event-triggering method was designed to decrease the network communication load, which could also be used to decide the time moment of the sampled signals. In Reference [98], a methodology for the technological investigation of iterative learning control for sampled-data systems was proposed. In Reference [99], a new Lyapunov functional was constructed to drive some stability criteria. Then, a channel utilization-based switched controller was designed to asymptotically stabilize the networked system in the sense of mean-square. It was shown that the proposed approach enhances the robustness of the networked control system to data drift and external disturbances. In Reference [100], the cascade control was employed for stabilization of the singular NCSs. In Reference [101], a network-based output controlled T-S fuzzy system was investigated that is steadied using a delayed fuzzy static controller, and not by any non-delayed static controller. In Reference [102], a novel robust variable sampling period controller (RVSPC) was developed that takes into account random time delays and losses in data-packets. In Reference [103], a decentralized event-triggered dissipative control was studied for systems having diverse physical characteristics. In Reference [104], a distributed NCS scheme was proposed by considering the communication delays. The results were applied to reduce the inter-area swing oscillations in a power grid. A brief overview of NCSs was presented by Reference [105] regarding the system configurations, challenging issues, and the methodologies.

In Reference [106], a time-triggered zooming algorithm for the dynamic quantization at the sensor side was proposed that led to an exponentially stable closed-loop system. The algorithm included proper initialization of the zoom parameter. An exhaustive explanation of the various types of networked control techniques is given by Reference [107]. The *H∞* output feedback control of NCSs with time delay and dropout in data-packets were considered in Reference [108], whereas Reference [109] discovered the nonlinear networked systems with tracking control problem. In Reference [110], the data that uses self-healing technology was reviewed as input and was justified as big data. In Reference [111] the method for time-delays in large-scale networked systems connecting sensors, controllers, and actuators was developed. A new sampling and control strategy was proposed by Reference [112] to search a sub-optimal sampling sequence and control input sequence to minimize the disordering of data-packets. Further, in Reference [113], an original state

space model was set up, in which both the tracking error and the state variables were combined and optimized. The optimal estimation problem in lossy NCSs with randomly dropped control data-packets was elaborated in Reference [114]. In Reference [115], the problem of Sliding Mode Controller (SMC) for NCSs was considered with semi-stochastic switching, popularly known as Markov or stochastic switching and having unsystematic dimensions. In Reference [116], a phenomenon of self-triggered sampling was proposed for a networked system with considerations of data losses and delay in communication. In Reference [117], both the *D*-stability, as well as the properties of finite *L2*-gain, were studied for a class of uncertain discrete-time systems with time varying network-induced delays [118,119].

A summary of the distributed NCSs was presented by Reference [105]. In Reference [120], stochastic nonlinear time-delay systems were considered that take the help of observer-based fuzzy output-feedback control (OFOFC). In Reference [121], the stochastic linear systems with random data dropout designed by a Bernoulli random variable were described. In Reference [122], the state and fault estimation problem for Linear Time (LT) switched systems with immediate disturbances and faults, was considered. Also, the two types of observer-based approaches were considered.

A procedure to evaluate the wellbeing of Centralized Power Systems (CPSs) in the event of cyber-attacks was described by Reference [123]. The problem of switched type networked systems with external disturbance and faults was investigated in Reference [124]. In Reference [125], the main cause of $H\infty$ control for uncertain discrete-time domain T-S fuzzy systems was considered.

The problem of state estimation for linear stochastic methods with event-triggered communication and packet loss was determined in Reference [126]. In Reference [127] event-triggered coordination for multi-agent structures/systems was elaborated. A survey on the distributed type of control and distributed type of filtering had been provided by Reference [128] for industrial CPSs, explained by different mathematical equations. In Reference [129], the problem of event-based network-induced time-varying delays with output tracking control for nonlinear NCSs approximated by type-2 fuzzy systems was investigated. In Reference [130], the authors addressed the concern for multi-layer, data-driven cyber-attacks, developed to boost ICS cyber security. In Reference [131], the control of automotive active suspension system using Proportional Integral Derivative (PID) and Linear Quadratic Regulator (LQR) methods was discussed. In Reference [132], a closed-loop controller model considering cyber-attacks and the mixed-triggering scheme, was proposed. In Reference [133], a robust fault detection scheme for networked control systems (NCSs) was developed with limited quality of services (QoS), such as network-induced time delay, data dropout, and error sequence. In Reference [134], a survey on time-delay approach to networked control systems (NCSs) was provided, which discusses the fundamental network-induced issues in NCSs and the main approaches to the modeling of NCSs. Again, an investigation on distributed type of control and distributed type of filtering for CPSs described by dynamic mathematical modeling equations was presented by Reference [135]. In Reference [136], a scheme called robust approximation-based model predictive control (RAMPC) was developed for the constrained networked control systems (NCSs) subject to external disturbances. This paper also provides a roadmap to evaluate the permissible sampling period and also evaluates the necessary conditions for the feasibility of the RAMPC.

In Reference [137], a sampled-data control problem was investigated for connected vehicles subject to switching topologies, communication delays, and external disturbances. It used an advanced tracking error-based sampled-data platoon control method. In Reference [138], authors were concerned with the modeling and controlling using the mixed event-triggered mechanism (ETM) for NCSs with varying time-delays and uncertainties. In Reference [139], authors investigated about the switching-like event-triggered control for networked control systems (NCSs) under the malicious denial of service (DoS) attacks. In Reference [140] authors proposed an iterative learning control (ILC) scheme to synchro-

nize an array of non-identical neural network systems based on time-varying delay in a repetitive environment. In Reference [141], authors considered a resilient event-triggered control problem for a class of networked systems subject to randomly occurring deception attacks. In Reference [142], a novel method is proposed for line selection and fault location in a distribution network based on a cloud-edge-terminal hierarchical fault monitoring and control system. Reference [143] focuses on the event-triggered control problem for networked switched systems with actuator saturation. Here, an event-triggering strategy is developed based on discrete event-triggered samplings.

In Reference [144], authors investigated the stability problem for networked control systems. They have taken into consideration the input delays and multiple communication imperfections containing time-varying transmission intervals and transmission protocols. Reference [145] focused on addressing the sliding mode control problem of continuous-time nonlinear networked control systems. In Reference [146], the problem of fault-tolerant sampled-data $H\infty$ control for a networked control system with random time delays and actuator faults is investigated. In Reference [147], the problem of event-triggered finite-time control for networked switched control systems with extended dissipative performance was investigated. In Reference [148], the authors proposed a scheduling approach which can minimize the impact of delays and conflicts on the network, to improve the system stability, which results in an economical allocation of network resources, minimizes the traffic congestion, and improves the overall performance of the NCS.

In Reference [149], the authors discussed about the effect of limited bandwidth on the system's performance, particularly when the sampling period was small. In Reference [150], the authors discussed the amalgamation of control and communication in NCSs that offers remarkable achievement in the design and analysis of such controlled systems. In Reference [151], the authors discussed the LMI approach to effectively compensate for the random network-induced delays and provide the desired control performance. In Reference [152], a new ETM was proposed, under which data packets could be actively dropped within consecutive steps, thereby, saving more communication resources than the existing ETM. In Reference [153], the authors proposed the descriptive analysis about classification of cyber-attacks and threats related to security in industrial control systems. In Reference [154], the authors proposed a new quantization structure, and a mathematical treatment of this structure was given to illustrate the advantage for the quantization effects.

The above developments can be summarized in tabular form in Table 4 on the basis of area/network/parameter as follows.

Table 4. Summarized discussion of development of NCS from 2011 onwards.

S.No.	Papers	Parameter/Area/Network
1	[86,89–91,99–103,107,112,113, 119,122,128,131,136]	Model/Sampling Based Networks
2	[85,88,90–92,97,98,100,101,107, 114,117,132,144]	Stability Analysis/Approach
3	[86,87,91,93,98,100,101,106– 108,112,113,115– 125,129,130,132–134,137– 142,144–146,149,151]	Delay/Fault Detection/Packet Loss
4	[92,93,99,107,109,110,114,121, 125,126,137,140,145]	Internet/Communication Based Multi-rate Control Networks
5	[95,104,105,107,111,118,128, 135,142]	Distributed Networked Control Approach
6	[96,97,103,107,126,127,129,135, 138,139,143,147,152,154]	Event Based Networks
7	[98,107]	Interactive Networks

Table 4 gives the structured information on the distribution of papers in different areas published from the year 2011 onwards. The major focus of research during this phase was on the delay-based networks. The difference between the works published in the earlier phases is that the security approach, model-based approach, and the sampled-based approach involve the incorporation of delays. Secondly, the advanced model-based networked approaches, such as Model-Predictive Control (MPC), OFOFC networks, etc., were proposed, which make the networked system more stable and improve its performance. Figure 5 shows the distribution of papers during this phase. It can be clearly noticed that major focus is on the delay-based approach, which covers approximately 37% of the research contribution. The stability approach is also very important as the stability depends on delay. If the delay is maximum, the system has to be designed to make it stable. To achieve this purpose, many event-based techniques were developed.
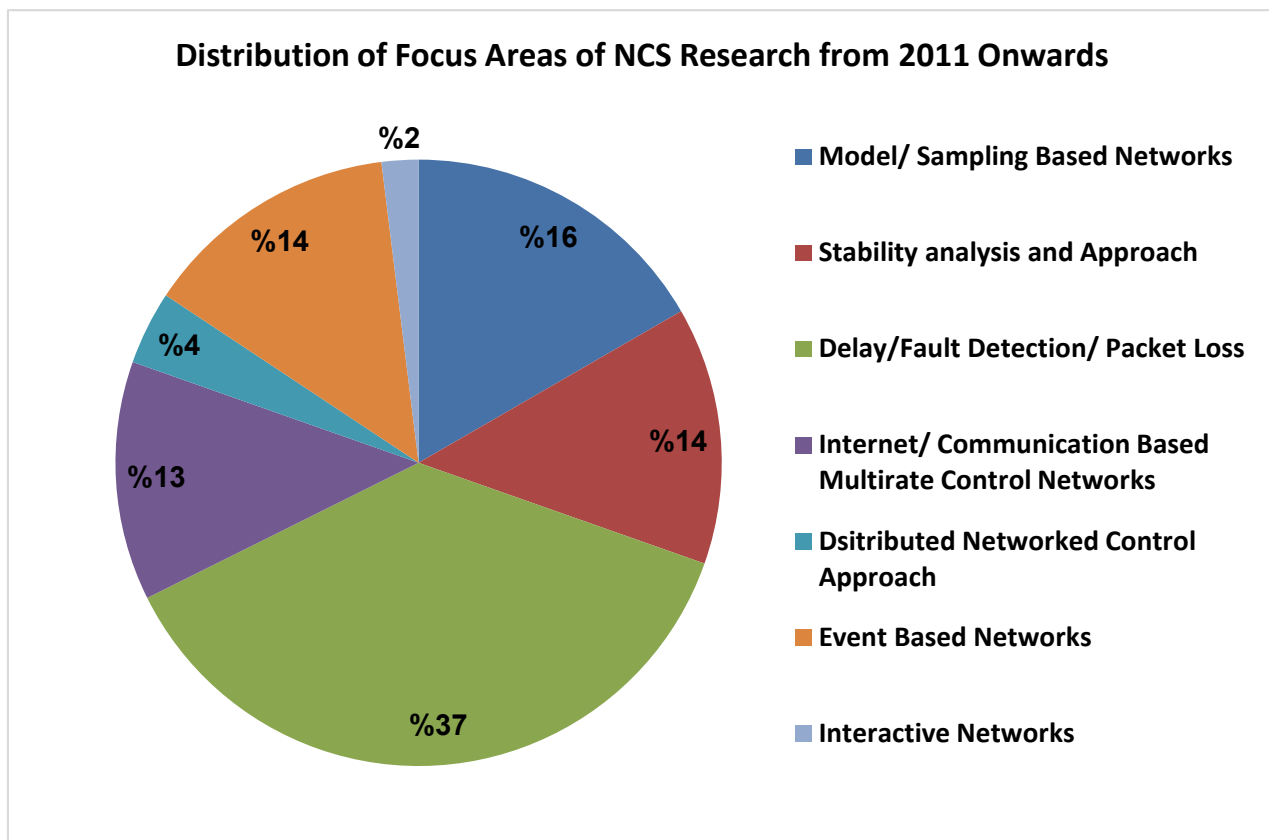
Figure 5. Distribution of focus areas of NCS research from 2011 onwards.

5. Topologies in NCSs

Basically, there are three types of network topologies available in NCSs, namely centralized topology, decentralized topology, and distributed topology. A brief discussion on these topologies is given below.

5.1. Centralized Topology

The centralized topology is shown in Figure 6. Here, the sensed data is sent to a centralized controller for data fusion. Suitable data fusion methods are necessary to obtain the fused data which are utilized for computing processes and executions.
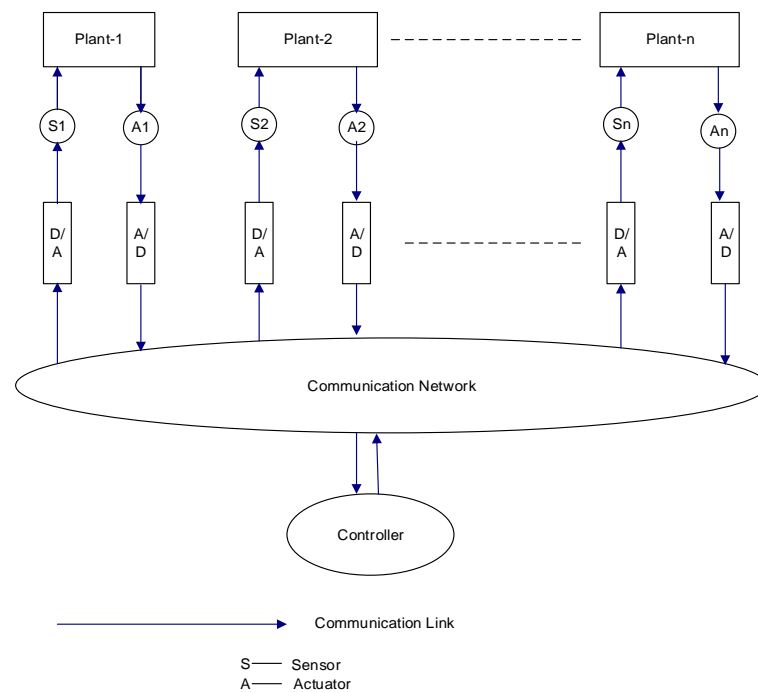
Figure 6. Centralized topology.

5.2. Decentralized Topology

This topology is shown in Figure 7. Each controller node depends only on the local information that the controller possesses for making its local decision. In this topology, the controller nodes do not share their information with the corresponding neighboring nodes. These types of topologies are helpful in reducing the time taken to analyze and synthesize the NCSs. Here, the controllers are decentralized controllers.
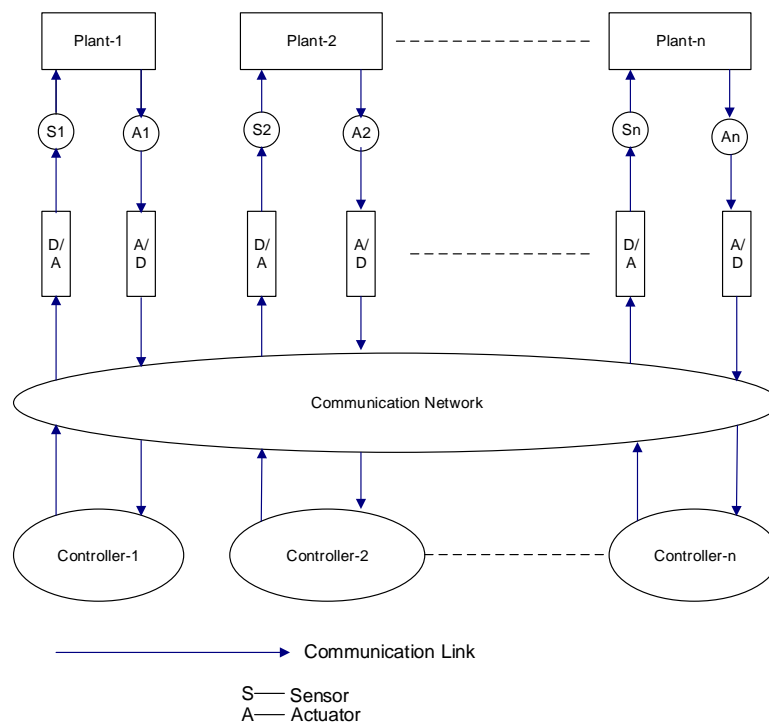
Figure 7. Decentralized topology.

5.3. Distributed Topology

The pictorial representation of the distributed topology is shown in Figure 8. One example of distributed topology can be found in Reference [155], where the load frequency control of a networked multi-area power system was discussed. There are two important characteristics of this topology: the subsystem's information is exchanged with the help of shared communication network, and the plant consists of a huge number of simple interacting units that are interconnected to achieve a desired objective. In this topology, each controller is allowed to share its local information with the corresponding neighboring controllers. Thus, the distributed controllers are capable to coordinate their behavior by transmitting/receiving information to/from other controllers within their corresponding neighboring area. Here, the controllers are distributed controllers. Advantages of this type of topology are: modularity, scalability, and robustness.
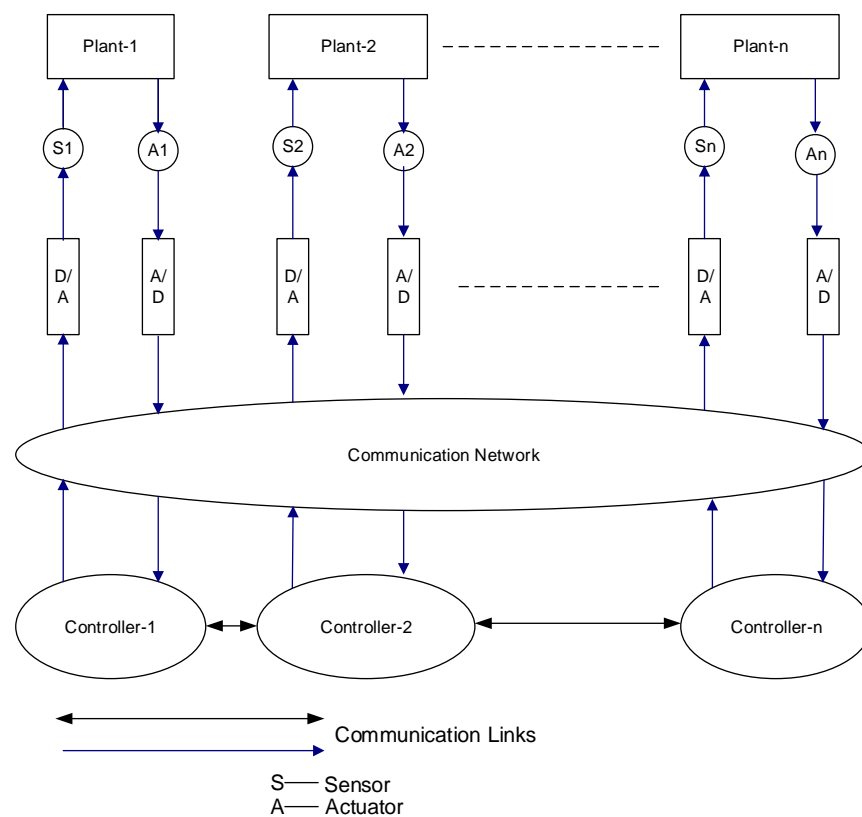
Figure 8. Distributed topology.

5.4. Distribution of Literature Based on the Topologies of NCSs

Table 5 gives a summary of the literature based on the topology. It can clearly be seen that the majority of research works use decentralized topology as the controller works independently for the given number of plants, and it has many advantages over the centralized topology, such as network time reduction in sending the data, less network congestion, maximum number of paths available for transmission, etc. The distributed topology is in the developmental stage and has tremendous applications in the NCSs. Focus is now shifting towards the distributed topologies of NCSs. Figure 9 clearly shows that the major focus has been on decentralized (i.e., 59%) topology, followed by the distributed topology, that has share of 32%. Centralized topology has been the least preferred topology, with a share of 9%.

Table 5. Summarized discussion of different types of NCS topologies.

S.No.	NCS Topology	Reference No.
1	Centralized Topology	[20,48,83,96,97,128]
2	Decentralized Topology	[10–31,43,46,53,63,75,78,96,97,103,104,107,126, 127,129,135,138,139,143,147,152,154]
3	Distributed Topology	[20,25–27,46,58,83,95,104,105,107,111,118,126– 129,134,135,142,155]
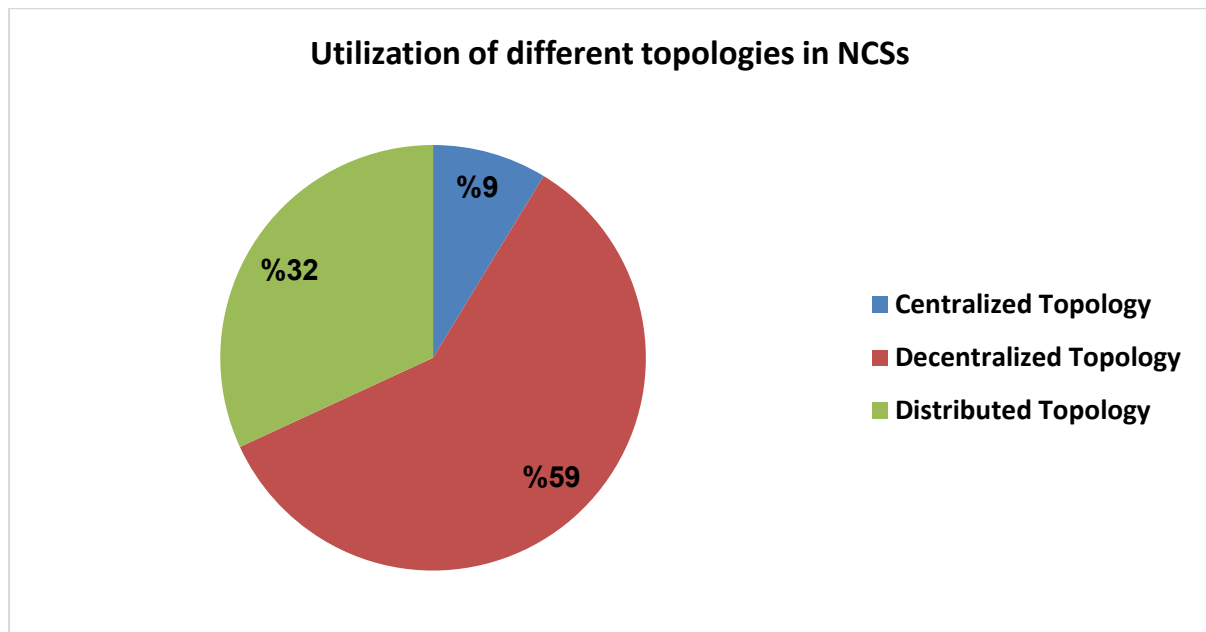
Figure 9. Utilization of different topologies.

6. Types and Challenges of NCS

Based on the above review, we have identified types of NCSs and the related challenges, which are discussed in this section.

6.1. Types of NCS

The types of NCS developed in the literature are shown in Figure 10.
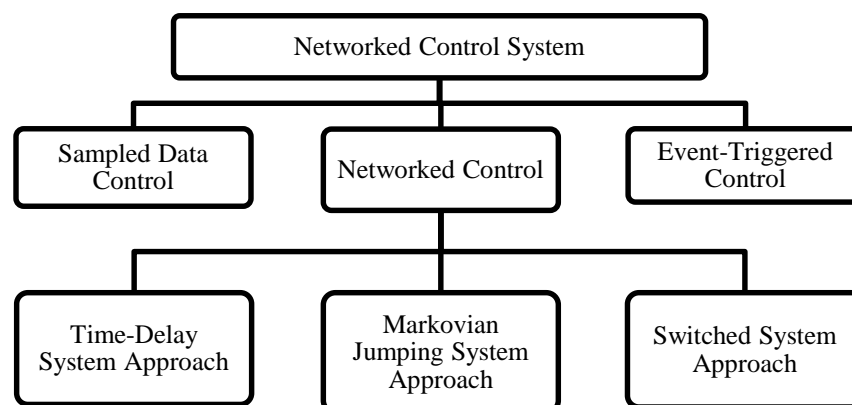
Figure 10. Types of NCS.

6.1.1. Sampled-Data Control

If all the control parts are placed in the similar venue, the resulting NCS is often considered to be a digital unit. Since the late 1950s, sampled data control theory has been very well developed for digital control systems. The strategy of delay in the input to this type of control, firstly planned in 1988 [79], has gained resurgent popularity, thanks to the advent of the LMI methodology and also to the advancement of network control technologies. The upper limit of two successive samples and the associated controller is often easily determined using the input delay technique.

6.1.2. Networked Control

Delays caused by the network and the packet losses are still difficult issues for NCSs. Reckoning on managing the network delays and the packet dropouts, different ways to measure stability, and managing styles for NCSs have been developed over the past decade. A brief review of a few of them is discussed below.

6.1.3. A Time-Delay System Approach

The delay in the input method for a sampled system motivates a time-delay system method [77]. Using this approach, the closed loop system is represented as a process with a time-varying lag. The delay in communicating the data from the sensors to the controller and from the controller to the actuators and the respective data-packet dropouts are indirectly incorporated within the input-delay. This approach obtains the maximum delay that the system can tolerate and still maintain its performance. On the other hand, it indicates the worst delay induced by the network and the corresponding packet dropouts that the networked system can tolerate. In the worst case scenario, the results obtained from this approach are definitely conservative [70].

6.1.4. A Markovian-Jumping System Approach

This approach is developed for the investigation and control of the networked systems. Network delays were considered, where the closed-loop NCSs were represented as stochastic-process systems and associated with Linear Quadratic Gaussian (LQG) optimum controllers [66]. The stabilization issue in networked systems is mentioned employing this system approach [39]. Its price remarking that the conception of packets-dropout of data dependent Lyapunov functions is established [71], resulting in some less traditional stability criteria. The Markovian approach is planned for NCSs with delays induced by the network [86]. The key plan is to model the sensor to the controller and the controller to the actuator delays as Markov chains, thus reproducing the closed-loop NCSs as a Markovian process with two modes portrayed by two Markov chains.

6.1.5. A Switched System Approach

This method with arbitrary switching is employed within the investigation and control of these systems. There are a variety of methods on how to build the networked system as a switched-system by means of arbitrary switching. Most of them support the discrete-time method, whereas few of them on the continuous-time method. Based on the idea that the control signal varies with time, a discrete-time switched model is developed [92], where the sampling amount is split into a variety of subintervals on which the controller operates better than the sampling frequency. With this model, the stability and the chronic disturbance attenuation were investigated for the NCSs. It is to be noted that the constraint on delays due to the network is not simple for some NCSs. So, to get rid of this constraint, efforts are created; see, e.g., References [49,68,88].

6.1.6. Event-Triggered Control

In this, the completion of control assignment is decided by the occurrence of an incident, instead of slip away of a fixed fundamental quantity as in the control of time-triggered systems. One of the main advantages of this type of control is the resource

consumption with less control performance degradation. This control technique has received plenty of interest and has become a booming topic within the field of NCSs; see, e.g., References [29,72,89]. A key purpose of this control technique is to style an acceptable triggering circumstance that decides whether or not a control task is accomplished. Because of the above benefits, this control approach involves the fore. A variety of problems for these type of systems is tackled, such as Euclidean Norm, L_2, investigation and control style, tracking control, dynamic output feedback control, $H\infty$ filtering, and accord of multi-agent systems.

6.2. Challenges of NCS

Apart from several advantages, there are many key challenges that have received a considerable attention of the research community. Many solutions have been proposed in the past, and many more are being proposed every day. Next, we will discuss some of the key challenges of NCS. Figure 11 presents a flow diagram of the challenges involved in the implementation of the NCS.
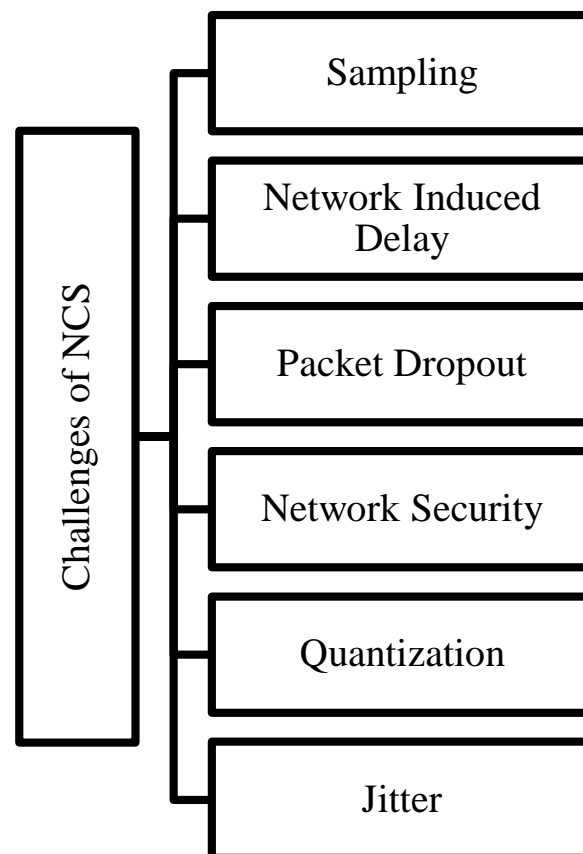
Figure 11. Challenges of NCS.

6.2.1. Sampling

Before being transmitted over a communication network, the continuous signals should be sampled for simplicity. For sampling the above continuous-time signals, there are basically two ways: one is time-triggered, and another is event-triggered. In time-triggered sampling also known as Riemann sampling, the sampling moment happens at fixed time intervals. Periodic sampling was usually employed in the early digital management systems, as the analysis and style of these sampled systems is simple. At the instance the value of the sampled signal approaches zero, the output obtained is equivalent to the continuous-time system. Another sampling is event-triggered, which is generally denoted as Lebesgue sampling. In this the sampling occurs when an event is triggered. This sampling significantly reduces the network traffic volumes. Over the last decade, there

has been an increasing interest in the control of NCSs through event-triggering because of its advantage over time-triggering; see, e.g., References [59,73,78].

In NCSs, the limited bandwidth restricts the system performance [149]. This occurs when the sampling period is small, thereby generating a lot of data that overloads the network and causes congestion. It may result in increased packet losses and longer delays, which degrades the performance. The relationship between the sampling period, the network load, and the system performance in an NCS is illustrated in Figure 12 [150]. For instance, decreasing the sampling period through the values corresponding to points "a" and "b", the device performance improves. In addition, the device performance deteriorates as a result of network congestion when the sampling period is reduced, as indicated by the values corresponding to points "b" to "c". An optimal sampling period exists at which the system performance is the best (point "b" in Figure 12).
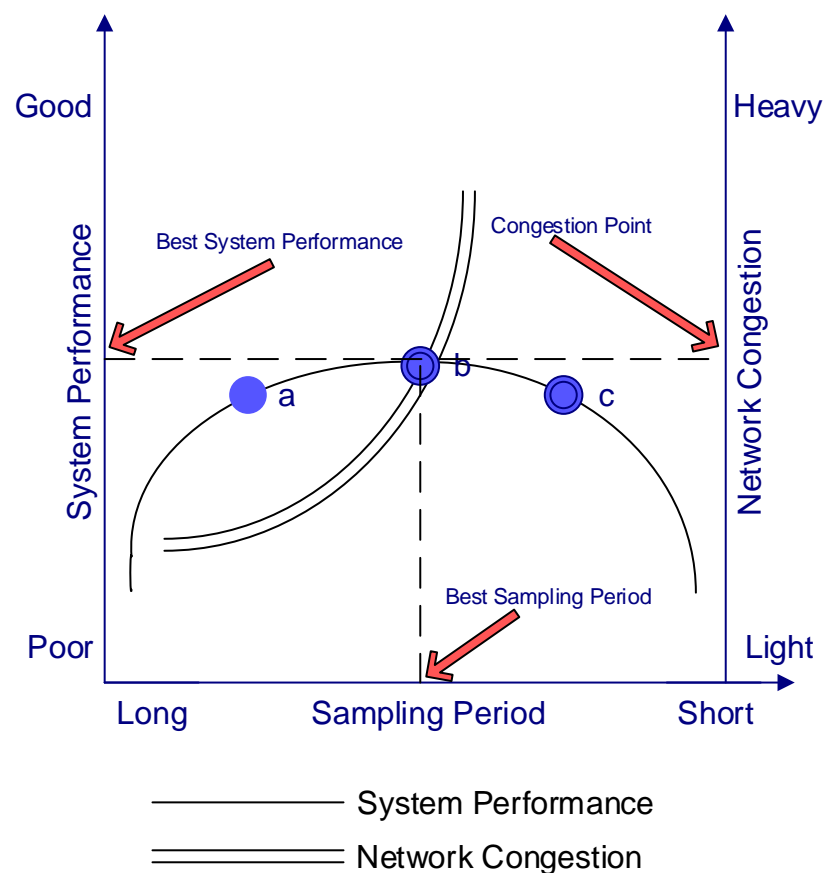
Figure 12. Relationship between system performance, network congestion and sampling period.

Table 6 shows the quantitative data for the sampling rate considered in the different research works. There are mainly periodic and aperiodic sampling approaches. In periodic case, the lowest sampling rate considered was 22.1 ms [40], whereas the highest sampling rate considered was 1730 ms [149]. For the case of aperiodic sampling, the lowest range is between 4 ms to 4.7 ms in Reference [119], whereas the highest range was between 30 ms to 1380 ms in Reference [96].

Table 6. Sampling rate considered in different studies.

Reference	Type of Sampling	Sampling Interval/Sampling Interval Range (*in ms*)
[1]	Aperiodic	16 to18
[4]	Periodic	40, 80
[40]	Periodic	22.1
[50]	Periodic	785
[65]	Periodic	132.77
[77]	Aperiodic	10 to 11
[80]	Aperiodic	104 to 169
[93]	Periodic	40
[96]	Aperiodic	30 to 1380
[103]	Aperiodic	0 to 299
[119]	Aperiodic	4 to 4.7
[137]	Periodic	100
[146]	Aperiodic	20 to 100
[149]	Periodic	1730

6.2.2. Network-Induced Delay and Packet Dropout

In the literature, many delay induced network models have been proposed [48,49,60, 70,84,86,98–100,118]. In Reference [84], four main delay models were discussed, namely: (a) constant delay model, (b) stochastic delay model, (c) Markov chain model, and (d) hidden Markov model. Reasons for these types of delays are: limited bandwidth, network traffic, and transmission protocols [99]. Two types of delays mainly occur: (i) sensor to-the controller delays and (ii) controller to-the actuator delays. Since network-induced delays depend on the networking circumstances [60], they are sometimes time-varying, unpredictable, and the upper bound is unknown. As a consequence, network-induced delays are ordinarily sculptured as interval time-varying delay [48,100] and a Markov chain with known transition chances [49,86], with partially transition chances [89] and with arbitrary shift [70]. As mentioned, in Reference [98], network-induced delays have been seen as a cause of degradation of performance of the system or possibly the cause for system instability. In Reference [118] authors proposed an algorithm based on the gradient push-sum method to solve the Electronic Data Processing (EDP) in a distributed manner over the communication networks with time-varying topologies and communication delays. This proposed algorithm is guaranteed to solve the EDP if the time-varying directed communication network is uniformly jointly strongly connected. There are some systems where the presence of communication delay may have a positive effect on the system performance as in Reference [119]. In Reference [151] authors proposed LMI approach to determine the two-mode-dependent static output feedback controller gains to compensate for the random network-induced delays efficiently and provide the desired control performance.

Table 7 shows the quantitative data for the delay range considered in the different studies carried out in the literature. The highest delay considered was 6 s [66].

Data-packet dropout is a vital issue, which is due to the defective transmission pathway. Limited bandwidth and bulk data transfer over one line are responsible for this defective transmission. Many studies have considered packet losses in the NCSs [41,63,69,75,88,92,94,109,113,114]. These issues often occur because of exchanging the data amongst the various devices, which degrades the performance and can destabilize the system. Due to traffic congestion, the data-packet loss is also a major concern. Mostly, the dropout effect is also known as a Bernoulli or Markov process. In most communication networks, different data packets suffer different delays, which produces a situation where a

data packet sent earlier may arrive at the destination later, or vice versa; see Figure 13 [46]. This phenomenon is referred to as data packet disorder. Table 8 shows the quantitative data of the packet loss rate considered in the different studies existing in the literature. The highest packet loss rate considered was 80% in Reference [63].

Table 7. Delay data considered in different studies.

Reference	Type of Delay	Delay/Delay Range (*in ms*)
[41]	Random Delay	160 to 132
[45]	Network-Induced Time Delay	15 to 35
[49]	Random Delay	0 to 2000
[50]	Time-Varying Delay	0 to 1000
[52]	Random Delay	0 to 1000
[56]	Random Delay	0 to 3000
[66]	Random Delay	2000 to 6000
[67]	Random Delay	0 to 123
[68]	Network Induced Delay	0 to 100
[70]	Network Induced Delay	500 to 1550
[80]	Variable Delay	104 to 169
[103]	Variable Delay	0 to 300
[137]	Constant Delay	250
[146]	Constant Delay	500
[149]	Constant Delay	1730
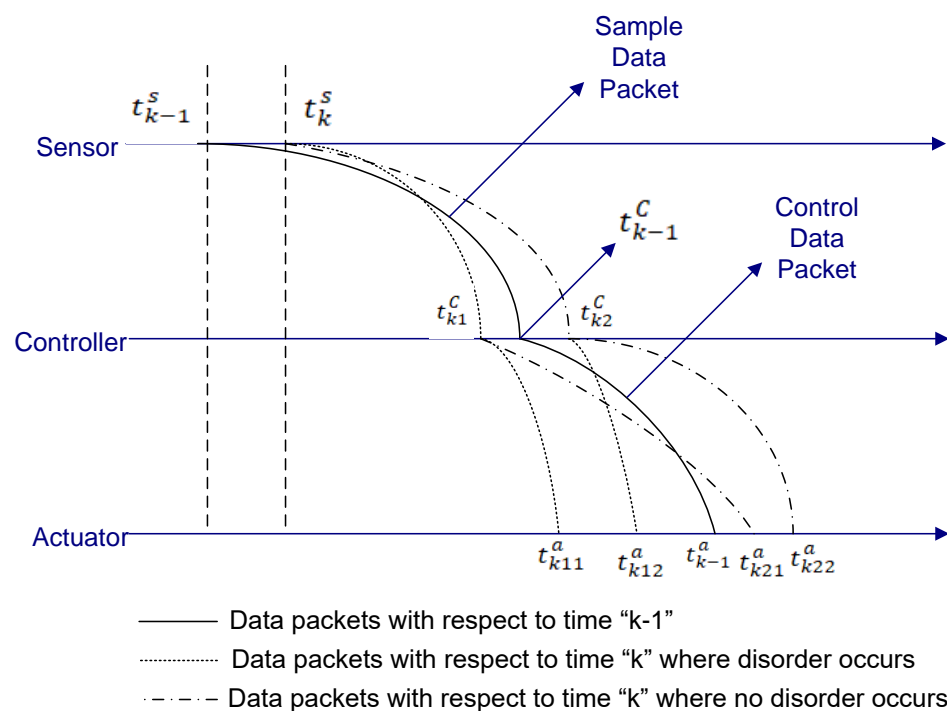
Figure 13. Data packet dropouts/disorder in NCSs.

Table 8. Packet loss rate considered in different studies.

Reference	Loss Rate/Loss Rate Range (in %)
[41]	10
[62]	0 to 80
[67]	26.39
[74]	25 to 31
[91]	25
[93]	10
[108]	30 to 70
[113]	20 to 40

6.2.3. Network Security

Security of NCSs is one in the various foremost challenges that is receiving much attention these days [123,130,132]. Any network is prone to interception, particularly the wireless networks. Hence, network security is usually involved. Attacks to the NCS (as shown in Figure 14) will be described in brief as: A1 and A3 symbolize deception attacks, where a person sends forged data from either the sensors or the controllers. The forged data consists of: faulty activity, like the incorrect time of activity or the incorrect sender id. The person will instigate these types of attacks by getting the key or by cooperating with some attacks on sensors (A1) or controllers (A3). Attacks A2 and A4 signifies Denial of Service (DoS) attacks, where the person is barred by the controller from attaining device measurements. To launch DoS attacks, the person jams the associated communication channels, negotiates the devices to stop, and attacks the routing protocols. Attack A5 symbolizes an on-the-spot attack against the actuators. So, attempts should be made to prevent the negotiation of the actuators and the other direct attacks against the physical system, for example, by securing the attacked-physical system, observation cameras, etc. In Reference [152], a new ETM is proposed, under which data packets could be actively dropped within consecutive steps, saving more communication resource than the existing ETM. Here, mainly the effect of DoS attacks obeying Bernoulli distribution is considered and analyzed. Figure 15 shows that the numbers of security events have increased, which is reported by the industrial control systems (ICSs) cyber emergency response team.
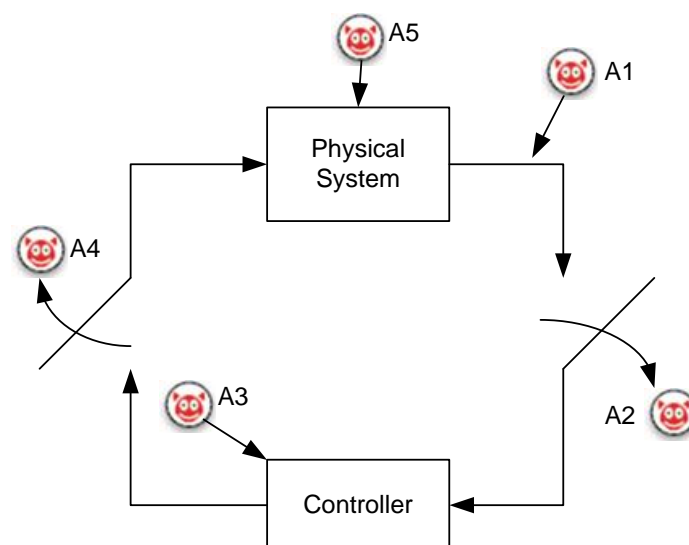
Figure 14. Cyber-attacks on NCSs.

Security Incidents/Data Breaches
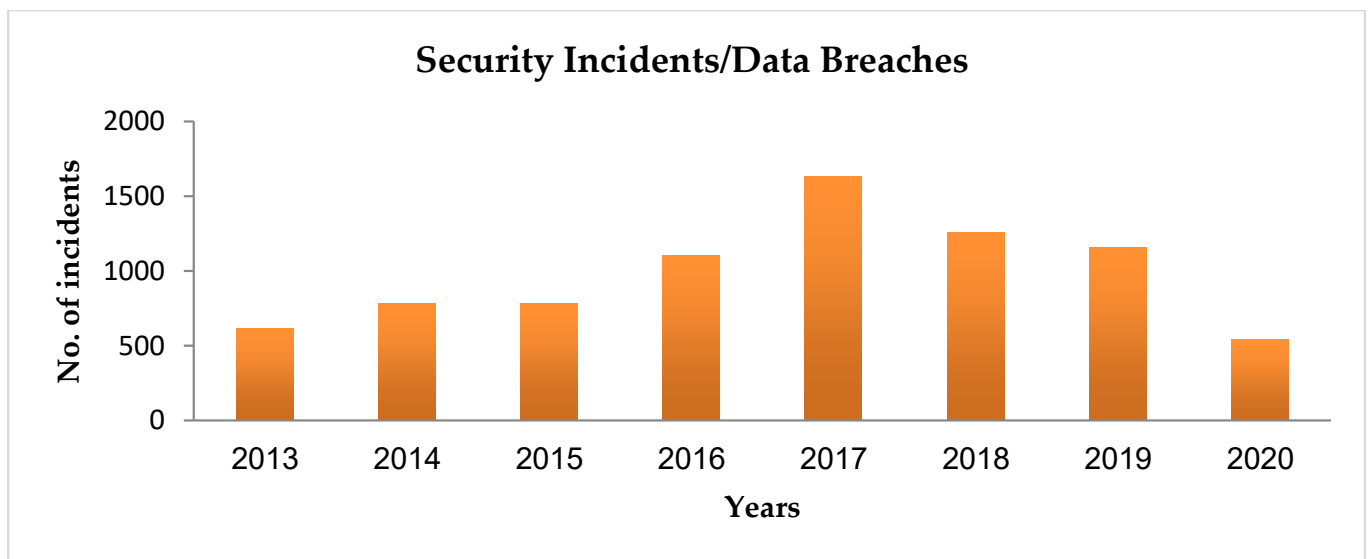
Figure 15. Industrial control systems security incidents year by year.

In Figure 15, it can be seen that in the beginning, the security incidents were on the rise, but there is a drastic decrease in the security incidents from 2017 to 2020 because of the protective measures taken and the development of advanced networked security approaches in NCSs. Advanced NCSs security techniques are being developed so that the NCSs are safer to operate [153].

6.2.4. Quantization

In these systems, signals are typically quantified by a quantifier prior to sending over a communication network. A quantifier is the same as a nonlinear mapper that maps segments of real sets to completely diverse levels. The quantity of these levels is intimately joined for the flow of information between the physical plant and the filter. In step with the finite period of the word-quantization error, unit of measurement is ineluctable, that has negative effects on the NCS performance. For an NCS subject to quantization, associated random data-packet dropouts [74] were considered, where some relationship is disclosed between the magnitude of the quantization and data-packet dropout. For the NCS subject to finite-level quantization and dropouts in data packets, the results of the step-size quantifier and, additionally, the external variety of consecutive data-packet dropouts on the NCS attenuation level of disturbance are inspected [87]. An integrated generalized framework for the investigation and elegance of networked controlled systems is projected through an associated emulation-like approach that gives a distinct approach through the study of quantization effects on NCSs [75]. The uniform quantizer maps real-valued function to a finite number of quantization regions with arbitrary shape, as in Reference [106]. In Reference [154], the authors proposed a new quantization structure, and a mathematical treatment of this structure is given to illustrate the advantage for the quantization effects.

6.2.5. Jitter

Jitter is generally defined as the distortion of a signal or image caused by poor synchronization. It is defined by the Institute of Electrical and Electronics Engineers (IEEE) [46] as "time-related, abrupt, spurious variations in the duration of any specified related interval", and it arises due to clock drift, branching in the code, scheduling, communication, and use of certain computer hardware structures, e.g., cache memory. Jitter can be classified into two types: delay jitter [156] and rate (sampling) jitter [157]. The goal of delay jitter is to minimize the difference between delay times of different packets. The goal of rate jitter is to minimize the difference between inter-arrive times [156].

7. Practical Applications of NCS

Apart from review of theoretical developments, many practical applications of NCS have been implemented to date. Some of the important areas of application of NCSs will be discussed briefly.

7.1. Autonomous Mobile Robots/Controlled Networks

For robots, the authority to perform and act dynamically is of vital importance. By itself, they comprise of mobile systems where the changes in environment activate changes in what purposes the system should convene the quality approach to structure the system, typically stated within the artificial intelligence literature because the behavior-based artificial intelligence framework [16,26,27]. Most plans are to spot completely different types of controllers and responses to sensory inputs, with desired mechanism performance. This practice of structuring the system into split behaviors, dedicated to playing bound responsibilities, has gained vital momentum in AI society. In Reference [158], implementation of a cloud service for remote control of a robotic manipulator is addressed, and an optimal control model restriction and control event-triggered communication are studied to be applied to a Robotic Manipulator as a Service. One more such example of the controlled network is the autonomous vehicular system designed by Toyota company called Prius, shown in Figure 16 [159]. This autonomous vehicular system consists of functions, such as automatic controlling the steering, acceleration, and brakes. This function is called Move-Box which is developed by Netherlands Organization for Applied Scientific Research. It functional system works as a line between the Peripheral Component Interface (PCI) extensions for Instrumentation (PXI) which is placed on the roof of vehicle. An eHorizon system designed by Continental company is proficient in controlling the vehicle by using Global Positioning System (GPS).
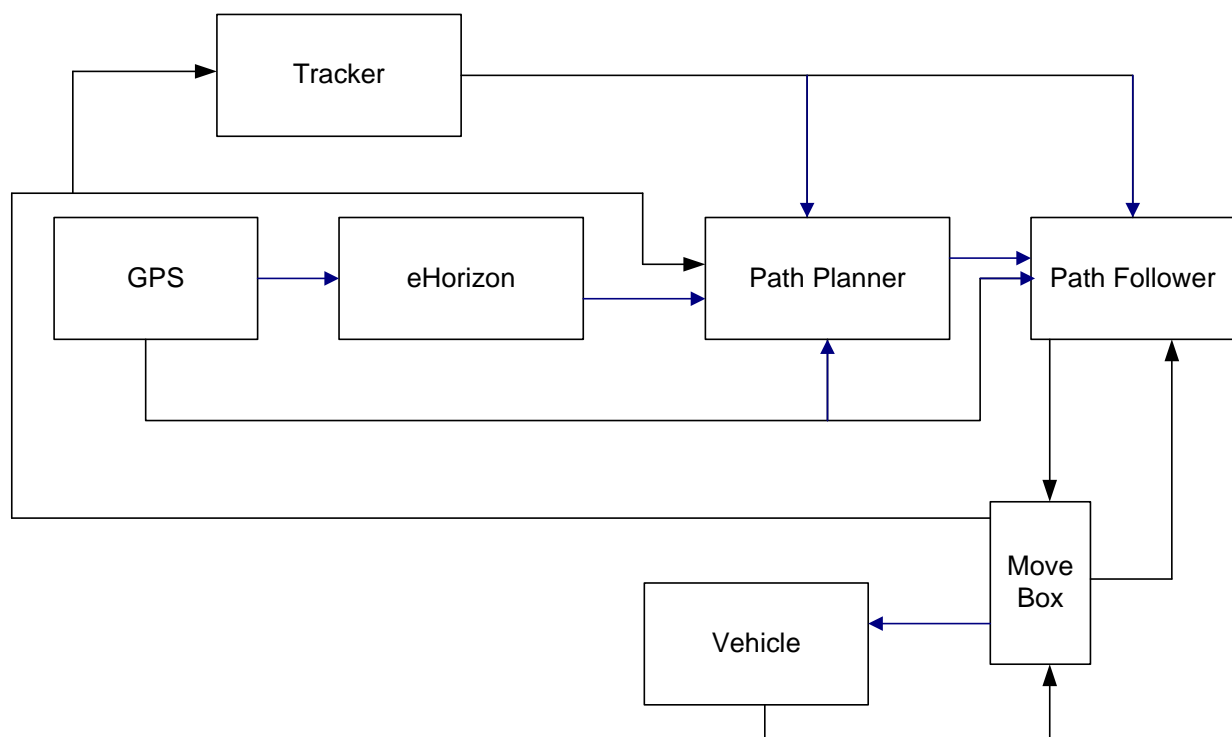
Figure 16. Components of autonomous vehicular system.

7.2. Power Systems and Smart Grids

Gradually proceeding to reliable information transmission to far-flung areas over communication networks, it is very difficult to reproduce the consequences of the commu-

nication system in the situation of stability in power grids. These types of communication system networks set up random variable time-delays and packet-dropouts in the data being transmitted. There are so many approaches to check such type of communication systems, commonly known as NCS [60]. Intensive analysis persists in control system theory to model the consequences of data-packet delays and dropouts because of the transmission of sensor, as well as actuator, signals via a constrained communication network on desired system stability [39]. Power grids are amongst the biggest styles of systems that are made-up by the human. For performance and transient stability analysis functions, the facility network has to be studied as a full because of the extremely interactive nature of its parts. Another issue is that the growth of an influence network beside time that moves it aloof from its properly designed initial structure and causes degradation of performance, stability and dependableness. Supported by these facts, it is expected that a networked management theme is ready to realize a superior performance compared to the historically decentralized controllers that use solely the regionally measured info [104].

In Reference [95], a modern coordinated NCS framework is designed for grids to control distributed generation sources. Measurements of the system are being transmitted to the networked-controller through the above mentioned period of time communication system network. The consequences of data transmission delays and data-dropouts are because of the communication system network is sculptured. Because this modern communication system network has become vital for grids, future power systems should be designed ready for instability.

In Reference [155], a distributed supervisory strategy for load/frequency control problems in networked multi-area power systems is discussed. Coordination between the control center and the areas is accomplished via data networks subject to communication latency, which is modeled by time-varying time-delay.

Figure 17 shows the block diagram of networked control of smart grid [160]. The block "Power System" shows the open-loop power system which is to be controlled. To this effect, real-power deviations in some of the lines are measured in real-time using current transformers (CTs) and potential transformers (PTs), and represented by y(t) in the block diagram. They are sampled and sent over the communication network as discrete data-packets, y(k). User datagram protocol is used for packet transmission, and packet-loss occurs during transmission. The final data which is received at the control unit after packet loss is given by y'(k). The control unit consists of a LQG controller, which is a combination of a Kalman filter and a linear quadratic regulator (LQR). Kalman filter uses the reduced-power system model and the output data-packets arriving at the controller, y'(k), to estimate the states, x'(k). The state estimates are then multiplied by the LQR gain to produce the control signals, u(k), which are then sent with the help of communication network to the actuators.

7.3. Manufacturing Systems

With the growth in economic processes that specialize in high price with low volume, the producing system design is growing from ancient centralized model to the distributed model and then proceeds to the modern networked system/model. In present situations, the producing systems are designed as in a networked model framework with the help of networking communication systems which consist of the diverse collections of manufacturing devices. Such a type of modern networked producing system monitors and controls by provision of maximizing the standard of service provided by the prevailing manufacturing resources [83].

A typical Industrial Manufacturing Control System is shown in Figure 18 [161]. It consists of large number of control loops, Human-Machine Interface (HMIs), remote diagnostics section, sensors, and actuators, built on layered network architectures, with the help of networked layer. A control loop consists of sensors, actuators, and controllers to deploy certain controlled processes. A sensor is a device that produces a measurement of some physical property and then sends this information as controlled variables to the

controller. The controller interprets the signals and generates corresponding manipulated variables, based on a control algorithm and target set points, which it transmits to the actuators. Actuators are used to deploy the controlled processes based on the commands being received through the controller.

Although Radio-Frequency Identification (RFID) is widely used for the application of asset tracking, it requires a power supply for the operation. But, for some cases, where is no power supply available, such as monitoring the activities of the aircraft cabin's maintenance workers, wireless sensor networks (WSN) is the best choice for workers as it requires no power supply [83].

7.4. Missiles

The system algorithms implementation in networks-on-chip is very helpful to address the varied problems with missile control systems, like power consumption, congestion management, and loss of data packets. Consideration of on-chip implementation of NCSs began to grow due to its potential in numerous applications; it conjointly provided several challenges for researchers to attain reliable and economical control. Moreover, the NCS has been analyzed for many years and has given rise to several necessary research topics in missile control systems [94]. With the progress in digital control systems, the data bus transmit scheme has secured more attention. However, communication networks inevitably introduce time delay. To compensate the time delay effects, an application of fuzzy controller to such a system was shown in Reference [162].
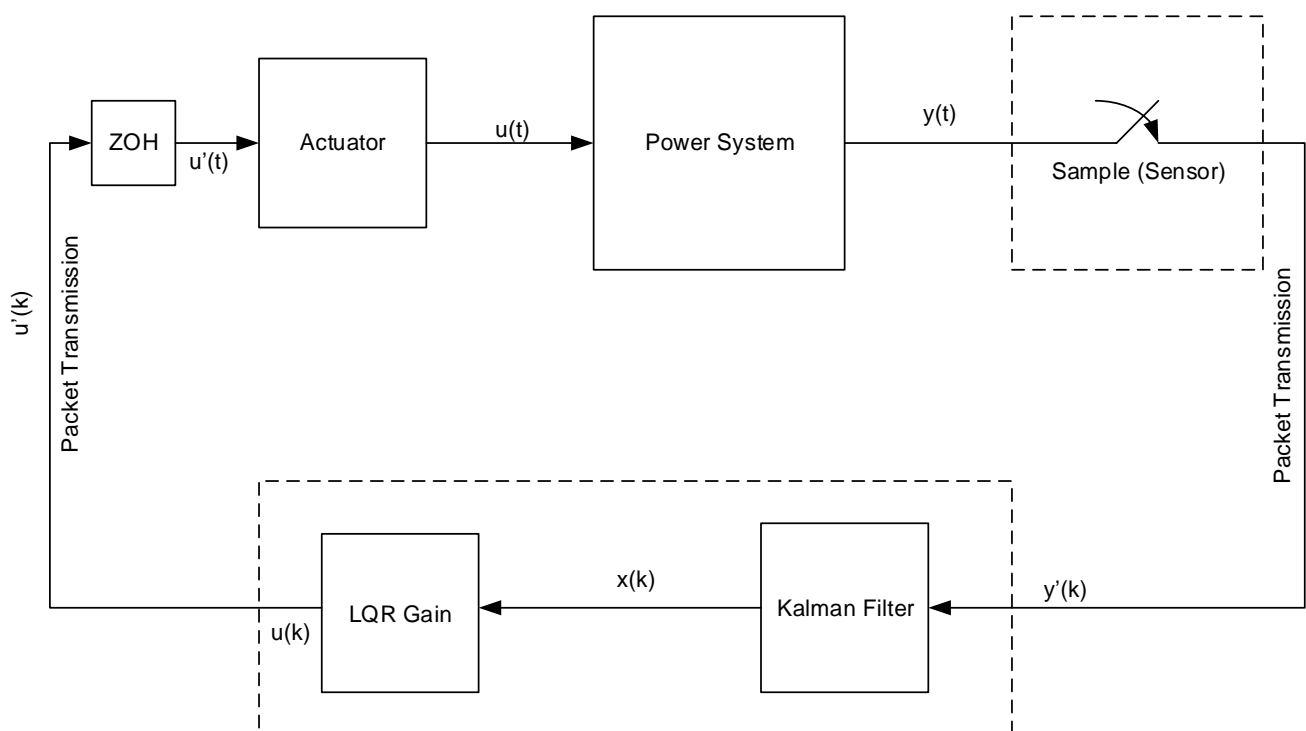
Figure 17. Layout of the networked control of the smart grid.
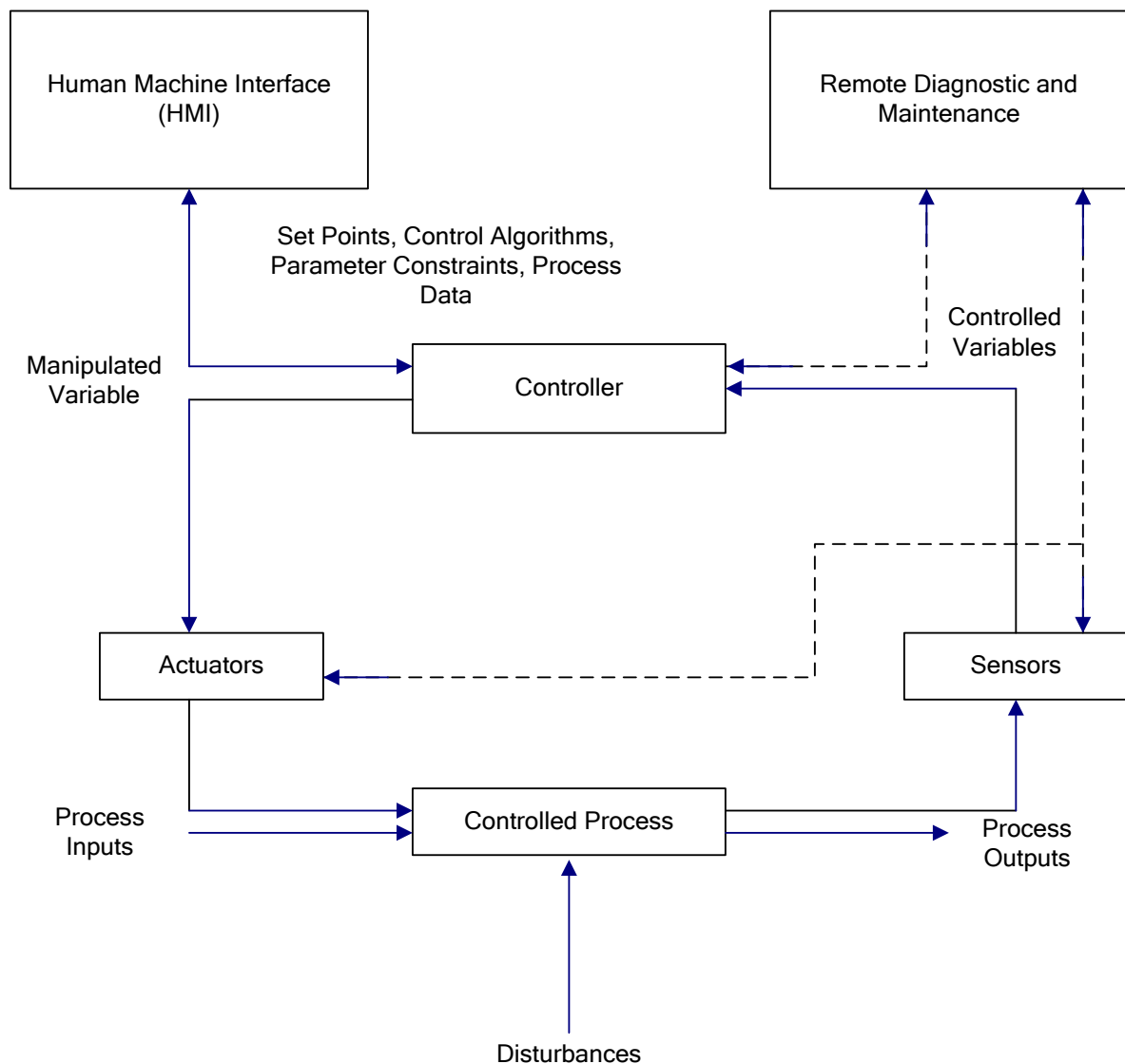
Figure 18. Industrial Manufacturing Control System.

7.5. UAVs

Today, unmanned aerial vehicles (UAVs) have become more and more well-liked in a wide field of applications. Though principally for military functions within the earlier period, it is noticed that there are various areas which may prove helpful [163]. For example, in the agriculture domain, they are applied in field observations or for chemical distributions. They patrol as a fireguard for forests or are used for traffic observation within the cities. They may also be used for automatic landscape photographing. They are terribly attention-grabbing, like in educational analysis, e.g., as flying laboratories, a workplace for control algorithms, or as an education gear for college scholars [63].

Figure 19 shows the diagram of an autonomous UAV. The block diagram consists of various control modules, sensors, actuators (valves, motors), communication modules, etc., which acts as a bridge between the remote access system and the UAV system. The remote control system can access the information, as well as send the useful commands to the UAV. The power available in the vehicle is calculated by the computing power module.
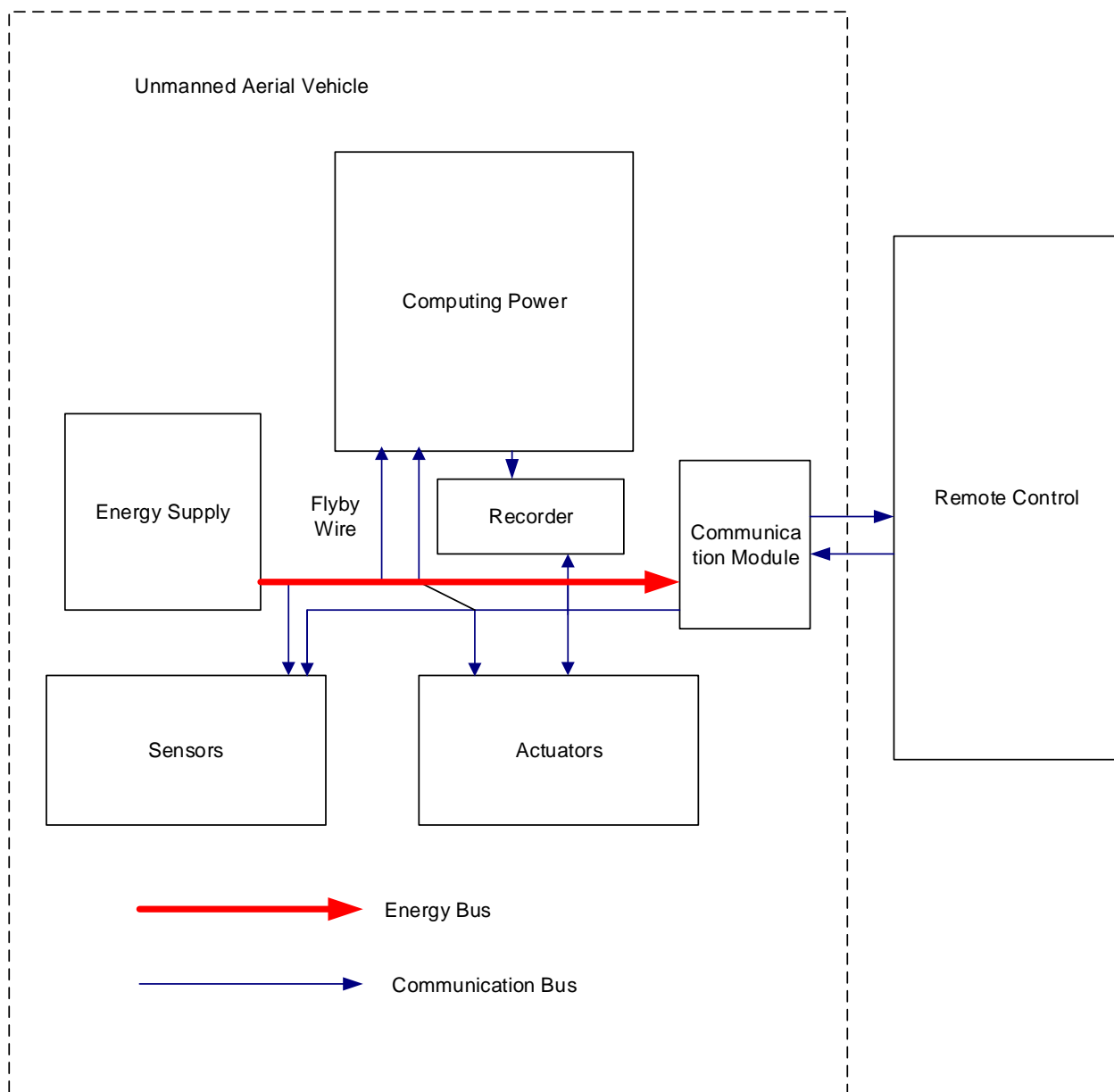
Figure 19. Flow diagram of autonomous unmanned aerial vehicles (UAV).

7.6. Quasi-Decentralized Control System

In order to achieve robust stability for a wide range of power system operating conditions, there is a need to break the limit imposed by the decentralized controller structure by implementing a quasi-decentralized control structure. Figure 20 is a block diagram to represent such a scheme. Since time-synchronized phases of Alternating Current (AC) voltages and currents are essential for the coordinated control, synchronous sampling control units based on the Global Positioning System (GPS) are used for this purpose.
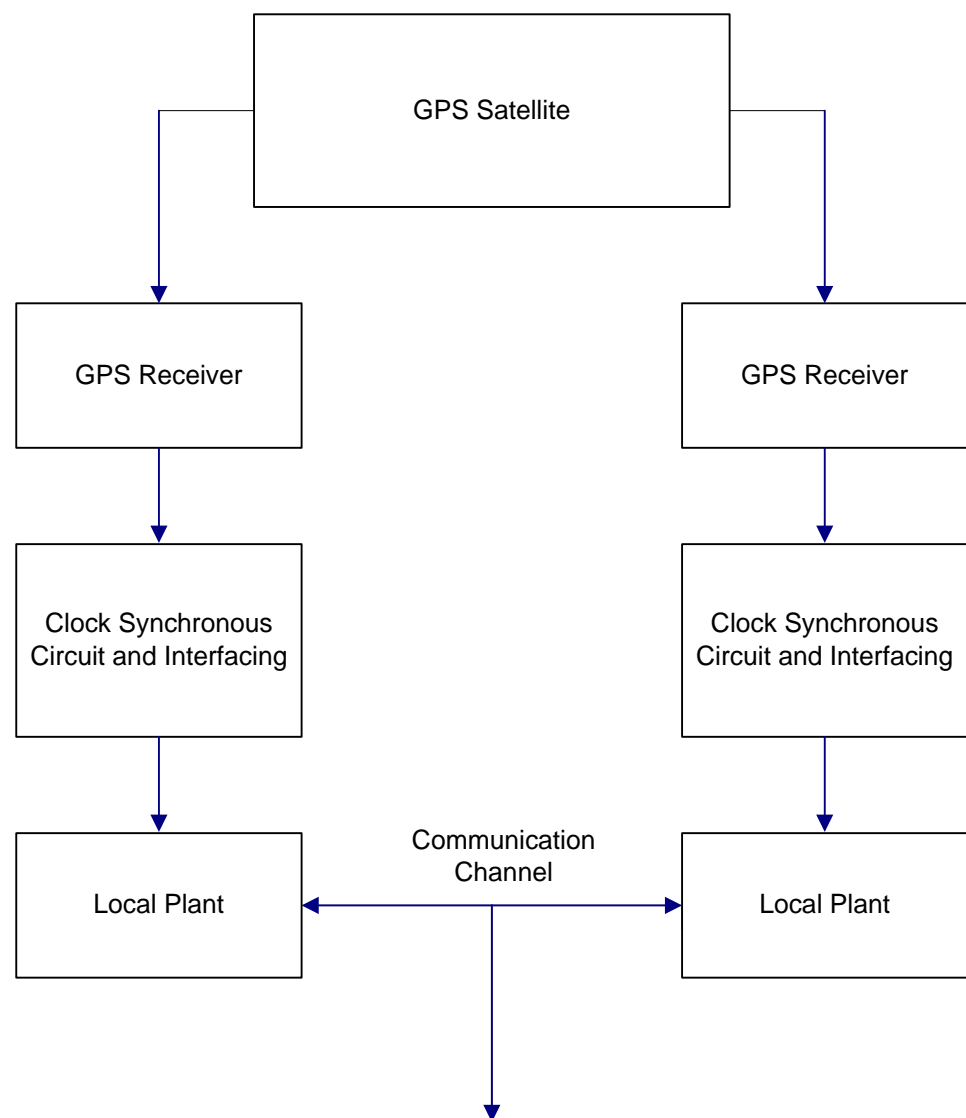
Figure 20. Quasi decentralized system for two synchronized plants.

7.7. Cloud Computing

The cloud and networked control systems amalgamate the benefits of cloud computing technology, advanced theory of networked control system, and other recent developed wireless and communication-based approaches. Figure 21 represents the cloud computing-based NCS. This system consists of plants to be controlled, a gateway computer, the cloud, and the network. The cloud is equipped with a large quantity of computational and storage resources; however, the plants have restricted resources. The plants send the sensor data to the cloud through the available network, so that the desired control signals can be evaluated by the cloud. These control signals are then sent back to the plants as the input of the actuator.

In a large-scale networked control system, the bagged information consists of information captured by universal information-sensing mobile devices, sensory technologies related to aerials, such as remote sensing, cameras, microphones, RFIDs, and WSNs [164].
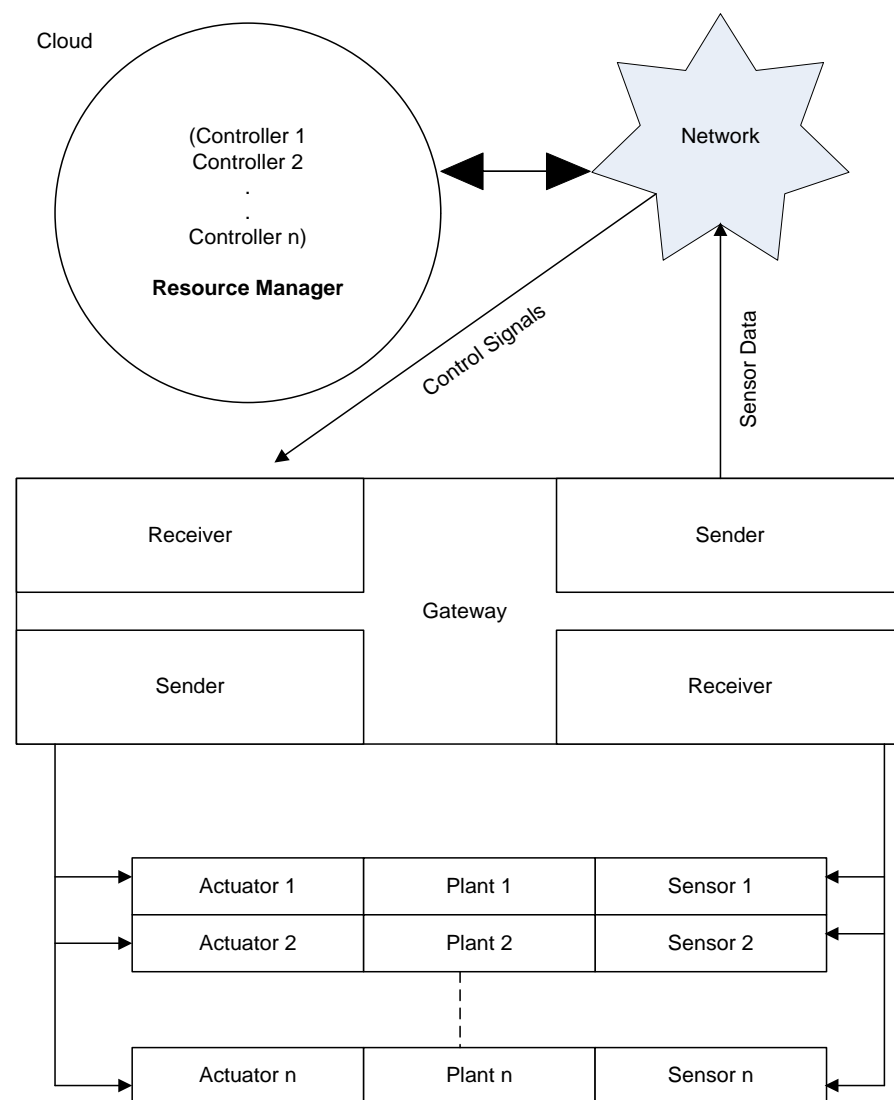
Figure 21. Cloud computing-based NCS.

8. Concluding Remarks and Future Potentials

The progress of NCSs can be termed as the steady progress which was based on evolution of computation and communication technology. The research of NCSs started with decentralized control systems, which later converged to several theories related to the stability analysis of NCSs. Then, many research papers discussed issues, such as sampling, quantization, and time delays. In a recent phase of NCSs development, some new topics, such as controller design for NCSs with event-triggered sampling and cyber-attacks, have received a lot of attention. NCSs have also been implemented for many practical systems, like UAVs, power systems and smart grids, robots, missiles, and manufacturing systems. At present, the components are distributed over long distances, such as in a smart grid, teleoperation control system, etc. Conventional control cannot satisfy the latest challenges, so novel control structures are needed to resolve the newly-presented complex control systems. Even though a lot of advancement has been made in NCSs, their practical applications are very limited. Most of the research works dealt with simple-nodes and simple-system. Multi-sensors (or multi-nodes) and multi-system, in addition to coupling of numerous nodes or subsystems, should be considered in the future research. In accordance with the undeniable fact that the complex NCSs have characteristics of wide area, wide selection, and big data, we ought to combine the network control technology with the computer technology, the cloud storage technology, the data mining technology, and the

wide-area measurement techniques in such a way that more effective control algorithms are developed. The research in NCSs has come a long way since its inception, but, in terms of real-time implementation, there is still a lot of scope. This is definitely going to be taken into account in further research problems.

Abbreviations

S.No.	Abbreviation	Full Form
1	AC	Alternating Current
2	CPSs	Centralized Power Systems
3	CT	Continuous Time
4	DoS	Denial of Service
5	EDP	Electronic Data Processing
6	ETM	Event Triggered Mechanism
7	GPS	Global Positioning System
8	H∞	H- infinity
9	ICSs	Industrial Control Systems
10	ILC	Interactive Learning Control
11	L2	Euclidean Norm
12	LMI	Linear Matrix Inequality
13	LT	Linear Time
14	LQG	Linear Quadratic Gaussian
15	LQR	Linear Quadratic Regulator
16	LTI	Linear Time Invariant
17	LTV	Linear Time Variant
18	MBPNCSs	Model Based Predictive Networked Control Systems
19	MIMO	Multiple Input Multiple Output
20	NCS	Networked Control System
21	NLTV	Nonlinear Time Varying
22	OFOFC	Observer-based Fuzzy Output Feedback Controller
23	PCA	Principal Component Analysis
24	PID	Proportional Integral Derivative
25	QCS	Quantized Control System
26	QoS	Quality of Services
27	RAMPC	Robust Approximation Based Model Predictive Control
28	RFID	Radio-Frequency Identification
29	RVSPC	Robust Variable Sampling Period Controller
30	SMC	Sliding Mode Controller
31	SSV	Structured Singular Value
32	T-S	Takagi Sugeno
33	UAVs	Unmanned Aerial Vehicles
34	WSN	Wireless Sensor Networks
35	ZOH	Zero Order Hold

References

1. Dorf, R.; Farren, M.; Phillips, C. Adaptive sampling frequency for sampled-data control systems. *IEEE Trans. Autom. Control* **1962**, *7*, 38–47. [CrossRef]
2. Smith, M. An evaluation of adaptive sampling. *IEEE Trans. Autom. Control* **1971**, *16*, 282–284. [CrossRef]
3. Hsia, T. Comparisons of adaptive sampling control laws. *IEEE Trans. Autom. Control* **1972**, *17*, 830–831. [CrossRef]
4. Hsia, T. Analytic design of adaptive sampling control law in sampled data systems. *IEEE Trans. Autom. Control* **1974**, *19*, 39–42. [CrossRef]
5. Liu, C.; Layland, J. Scheduling algorithms for multiprogramming in hard real-time environment. *J. ACM* **1973**, *20*, 40–61. [CrossRef]
6. Audsley, N.; Burns, A.; Davis, R.; Tindell, K.; Wellings, A. Fixed priority preemptive scheduling: An historical perspective. *Real-Time Syst.* **1995**, *8*, 173–198. [CrossRef]
7. Murray, R.M.; Aström, K.J.; Boyd, S.P.; Brockett, R.W.; Stein, G. Future directions in control in an information-rich world. *IEEE Control Syst. Mag.* **2003**, *23*, 20–33.
8. Laprie, J.-C. (Ed.) *Dependability: Basic Concepts and Terminology*; Springer: New York, NY, USA, 1992.
9. Avižienis, A.; Laprie, J.C.; Randell, B. *Fundamental Concepts of Dependability*; Report 01145; LAAS: Toulouse, France, 2000.
10. Baillieul, J.; Antsaklis, P.J. Control and communication challenges in networked real-time systems. *Proc. IEEE* **2007**, *95*, 9–28. [CrossRef]
11. Aoki, M. On feedback stabilizability of decentralized dynamic sytems. *Automatica* **1972**, *8*, 163–173. [CrossRef]
12. Lau, R.; Persiano, R.M.; Varaiya, P. Decentralized information and control: A network flow example. *IEEE Trans. Autom. Control* **1972**, *17*, 466–473. [CrossRef]
13. Wang, S.; Davison, E.J. On the stabilization of decentralized control systems. *IEEE Trans. Autom. Control* **1973**, *18*, 473–478. [CrossRef]
14. Corfmat, J.P.; Morse, A.S. Decentralized control of linear multivariable systems. *Automatica* **1976**, *12*, 479–495. [CrossRef]
15. Grosdidier, P.; Morari, M. Interaction measures for systems under decentralized control. *Automatica* **1986**, *22*, 309–319. [CrossRef]
16. Brooks, R. A robust layered control system for mobile robots. *IEEE J. Robot. Autom.* **1986**, *2*, 14–23. [CrossRef]
17. Lin, F.; Wonham, W.M. Decentralized control and coordination of discrete-event systems. In Proceedings of the 27th IEEE Conference on Decision and Control, Austin, TX, USA, 7–9 December 1988; Volume 2, pp. 1125–1130.
18. Lin, F.; Wonham, W.M. Decentralized control and coordination of discrete-event systems with partial observation. *IEEE Trans. Autom. Control* **1990**, *35*, 1330–1337. [CrossRef]
19. Siljak, D. *Decentralized Control of Complex Systems*; Academic: New York, NY, USA, 1991.
20. Raji, R.S. Smart networks for control. *IEEE Spectr.* **1994**, *31*, 49–55. [CrossRef]
21. Lin, F.; Wonham, W.M. Supervisory control of timed discrete-event systems under partial observation. *IEEE Trans. Autom. Control* **1995**, *40*, 558–562. [CrossRef]
22. Schwartz, M. Network Management and Control issues in Multimedia Wireless Networks. *IEEE Pers. Commun.* **1995**, *2*, 8–16. [CrossRef]
23. Yang, T.C. *Research into Quasi-Decentralised Control*; National Grid Company Research Contract; (CHQ/169732/GSI); University of Sussex: Sussex, UK, 1998.
24. Kim, Y.H.; Park, H.S.; Kwon, W.H. A Scheduling Method for Network-based Control Systems. In Proceedings of the American Control Conference, Philadelphia, PA, USA, 24–26 June 1998; pp. 718–722.
25. Kopetz, H. Event Triggered versus Time Triggered Real Time Systems, Trends in Real-Time Operating Systems. In *Operating Systems of the 90s and Beyond*; Session-4; Springer: Berlin/Heidelberg, Germany, 1998.
26. Kortenkamp, D.; Bonasso, R.P.; Murphy, R. (Eds.) *Artificial Intelligence and Mobile Robots*; The MIT Press: Cambridge, MA, USA, 1998.
27. Arkin, R.C. *Behavior Based Robotics*; The MIT Press: Cambridge, MA, USA, 1998.
28. Walsh, G.C.; Ye, H.; Bushnell, L. Stability analysis of networked control systems. In Proceedings of the 1999 American Control Conference, San Diego, CA, USA, 2–4 June 1999.
29. Årzén, K.-E. *A Simple Event-Based PID Controller*; IFAC World Congress: Prague, Czech Republic, 1999.
30. Beldiman, O.; Walsh, G.C. Predictors for networked control systems. In Proceedings of the American Control Conference, Chicago, IL, USA, 28–30 June 2000; pp. 2347–2351.
31. Branicky, M.; Phillips, S.; Zhang, W. Stability of Networked Control Systems: Explicit Analysis of Delay. In Proceedings of the American Control Conference, Chicago, IL, USA, 28–30 June 2000; pp. 2352–2357.
32. Walsh, G.C.; Ye, H. Scheduling of Networked Control Systems. *IEEE Control Syst. Mag.* **2001**, *21*, 57–65.
33. Lian, F.L.; Moyne, J.; Tilbury, D. Time Delay Modeling and Sampling Time Selection for Networked Control Systems. In Proceedings of the Internal Mechanical Engineering Congress and Exposition, New York, NY, USA, 11–16 November 2001.
34. Zhang, W.; Branicky, M.S.; Philips, S.M. Stability of Networked Control Systems. *IEEE Control Syst. Mag.* **2001**, *21*, 84–99.
35. Bushnell, L.G. Special Section on Networks and Control. *IEEE Control Syst. Mag.* **2001**, *21*, 22–29.
36. Ishii, H.; Francis, B.A. Stabilization with control networks. *Automatica* **2002**, *38*, 1745–1751. [CrossRef]
37. Amin, M. Modelling and Control of Complex Interactive Networks. *IEEE Control Syst. Mag.* **2002**, *22*, 22–27.

38. Branicky, M.S.; Phillips, S.M.; Zhang, W. Scheduling and Feedback Co-Design for Networked Control Systems. In Proceedings of the IEEE Conference on Decision and Control, Las Vegas, NV, USA, 10–13 December 2002.

39. Walsh, G.C.; Hong, Y.; Bushnell, L.G. Stability Analysis of Networked Control Systems. *IEEE Trans. Control Syst. Technol.* **2002**, *10*, 438–446. [CrossRef]

40. Ishii, H.; Francis, B.A. Quadratic stabilization of sampled-data systems with quantization. *Automatica* **2003**, *39*, 1793–1800. [CrossRef]

41. Babak, A.S. Stability of Networked Control Systems in the Presence of Packet Losses. In Proceedings of the 2003 IEEE Conference on Decision and Control, Maui Maui, HI, USA, 9–12 December 2003.

42. Yodyium, T.; Chow, M.-Y. Control methodologies in networked control systems. *Control Eng. Pract.* **2003**, *11*, 1099–1111.

43. Yang, S.H.; Dai, C. Multi-rate Control in Internet Based Control Systems. In Proceedings of the Control 2004, Bath, UK, 6–9 September 2004.

44. Liu, G.P.; Mu, J.X.; Rees, D. Networked Predictive Control of Systems with Random Communication Delay. In Proceedings of the Control 2004, Bath, UK, 6–9 September 2004.

45. Chen, Z.; Liu, L.; Zhang, J. Observer Based Networked Control Systems with Network-induced Time Delay. In Proceedings of the IEEE Conference on Systems, Man and Cybernetics, Hague, The Netherlands, 10–13 October 2004.

46. Yu, J.; Yu, S.; Wang, H. Survey on the Performance Analysis of Networked Control Systems. In Proceedings of the IEEE Conference on Systems, Man and Cybernetics, Hague, The Netherlands, 10–13 October 2004.

47. Seiler, P.; Sengupta, R. An $H\infty$ approach to networked control. *IEEE Trans. Autom. Control* **2005**, *50*, 356–364. [CrossRef]

48. Yue, D.; Han, Q.-L.; Lam, J. Network-based robust $H\infty$ control of systems with uncertainty. *Automatica* **2005**, *41*, 999–1007. [CrossRef]

49. Zhang, L.; Shi, Y.; Chen, T.; Huang, B. A new method for stabilization of networked control systems with random delays. *IEEE Trans. Autom. Control* **2005**, *50*, 1177–1181. [CrossRef]

50. Fridman, E.; Shaked, U.; Suplin, V. Input/output delay approach to robust sampled-data $H\infty$ control. *Syst. Control Lett.* **2005**, *54*, 271–282. [CrossRef]

51. Lin, H.; Antsaklis, P. Stability and persistent disturbance attenuation properties for a class of networked control systems: Switched system approach. *Int. J. Control* **2005**, *78*, 1447–1458. [CrossRef]

52. Huo, Z.H.; Fang, H.J. Robust $H\infty$ filter design for networked control system with random time delays. In Proceedings of the 10th IEEE International Conference on Engineering of Complex Computer Systems, Shanghai, China, 16–20 June 2005; pp. 333–340.

53. Miskowicz, M. The event-triggered integral criterion for sensor sampling. In Proceedings of the IEEE International Symposium on Industrial Electronics, (IEEE ISIE'05), Dubrovnik, Croatia, 20–23 June 2005; pp. 1061–1066.

54. Ye, H.; He, R.; Liu, H.; Wang, G.Z. A new approach for fault detection of networked control systems. In Proceedings of the 14th IFAC Symposium on System Identification, IFAC, New Castle, Australia, 29–31 March 2006; pp. 654–659.

55. Huo, Z.H.; Fang, H.J. Fault-tolerant control research for networked control system under communication constraints. *Acta Autom. Sin.* **2006**, *32*, 659–666.

56. Zheng, Y.; Fang, H.J.; Wang, H.O. Takagi-Sugeno Fuzzy model- based fault detection for networked control systems with Markov delays. *IEEE Trans. Syst. Man Cybern. Part B Cybern.* **2006**, *36*, 924–929. [CrossRef] [PubMed]

57. Fang, H.J.; Zhang, H.; Fang, Y.W.; Yang, F. Quasi T-S fuzzy models and stable controllers for networked control systems. In Proceedings of the 6th World Congress on Intelligent Control and Automation, Dalian, China, 21–23 June 2006; pp. 220–223.

58. Pratl, G.; Dietrich, D.; Hancke, G.; Penzhorn, W. A new model for autonomous, networked control systems. *IEEE Trans. Ind. Inf.* **2007**, *3*, 21–32. [CrossRef]

59. Tabuada, P. Event-triggered real-time scheduling of stabilizing control tasks. *IEEE Trans. Autom. Control* **2007**, *52*, 1680–1685. [CrossRef]

60. Hespanha, J.; Naghshtabrizi, P.; Xu, Y. A survey of recent results in networked control systems. *Proc. IEEE* **2007**, *95*, 138–162. [CrossRef]

61. Mirkin, L. Some remarks on the use of time-varying delay to model sample-and-hold circuits. *IEEE Trans. Autom. Control* **2007**, *52*, 1109–1112. [CrossRef]

62. Xiong, J.; Lam, J. Stabilization of linear systems over networks with bounded packet loss. *Automatica* **2007**, *43*, 80–87. [CrossRef]

63. Spinka, O.; Kroupa, S.; Hanzalek, Z. Control System for Unmanned Aerial Vehicles. In Proceedings of the 5th IEEE International Conference on Industrial Informatics, Vienna, Austria, 23–27 July 2007; Volume 1.

64. Jiang, X.; Han, Q.-L.; Liu, S.; Xue, A. A new *H1* stabilization criterion for networked control systems. *IEEE Trans. Autom. Control* **2008**, *53*, 1025–1032. [CrossRef]

65. Naghshtabrizi, P.; Hespanha, J.; Teel, A. Exponential stability of impulsive systems with application to uncertain sampled-data systems. *Syst. Control Lett.* **2008**, *57*, 378–385. [CrossRef]

66. Gao, H.; Meng, X.; Chen, T. Stabilization of networked control systems with a new delay characterization. *IEEE Trans. Autom. Control* **2008**, *53*, 2142–2148. [CrossRef]

67. Huang, D.; Nguang, S. State feedback control of uncertain networked control systems with random time-delays. *IEEE Trans. Autom. Control* **2008**, *53*, 829–834. [CrossRef]

68. Zhang, W.-A.; Yu, L. Modelling and control of networked control systems with both network-induced delay and packet-dropout. *Automatica* **2008**, *44*, 3206–3210. [CrossRef]

69. Hetel, L.; Daafouz, J.; Lung, C. Analysis and control of LTI and switched systems in digital loops via an event-based modelling. *Int. J. Control* **2008**, *81*, 1125–1138. [CrossRef]

70. Zhang, W.-A.; Yu, L. A robust control approach to stabilization of networked control systems with time-varying delays. *Automatica* **2009**, *45*, 2440–2445. [CrossRef]

71. Xiong, J.; Lam, J. Stabilization of networked control systems with a logic ZOH. *IEEE Trans. Autom. Control* **2009**, *54*, 358–363. [CrossRef]

72. Vatanski, N.; Georges, J.; Aubrunb, C.; Rondeaub, E.; Jämsä-Jounela, S. Networked control with delay measurement and estimation. *Control Eng. Pract.* **2009**, *17*, 231–244. [CrossRef]

73. Wang, X.; Lemmon, M. Self-triggered feedback control systems with finite-gain stability. *IEEE Trans. Autom. Control* **2009**, *45*, 452–467. [CrossRef]

74. Tsumura, K.; Ishii, H.; Hoshina, H. Tradeoffs between quantization and packet loss in networked control of linear systems. *Automatica* **2009**, *45*, 2963–2970. [CrossRef]

75. Nesic, D.; Liberzon, D. A unified framework for design and analysis of networked and quantized control systems. *IEEE Trans. Autom. Control* **2009**, *54*, 732–747. [CrossRef]

76. Fujioka, H. Stability analysis of systems with aperiodic sample-and hold devices. *Automatica* **2009**, *45*, 771–775. [CrossRef]

77. Gao, H.; Wu, J.; Shi, P. Robust sampled-data H1 control with stochastic sampling. *Automatica* **2009**, *45*, 1729–1736. [CrossRef]

78. Lunze, J.; Lehmann, D. A state-feedback approach to event-based control. *Automatica* **2010**, *46*, 211–215. [CrossRef]

79. Gupta, R.; Chow, M. Networked control system: Overview and research trends. *IEEE Trans. Ind. Electron.* **2010**, *57*, 2527–2535. [CrossRef]

80. Fridman, E. A refined input delay approach to sampled-data control. *Automatica* **2010**, *46*, 421–427. [CrossRef]

81. Sun, X.M.; Liu, G.-P.; Wang, W.; David, R. Stability analysis for networked control systems based on average dwell time method. *Int. J. Robust Nonlinear Control* **2010**, *20*, 1774–1784. [CrossRef]

82. Huang, D.; Nguang, S.K. Robust fault estimator design for uncertain networked control systems with random time delays: An ILMI approach. *Inf. Sci.* **2010**, *180*, 465–480. [CrossRef]

83. Zhuang, L.Q.; Zhang, D.H.; Wong, M.M. *Wireless Sensor Networks for Networked Manufacturing Systems, Factory Automation*; Intech Open: Rijeka, Croatia, 2010.

84. Onat, A.; Naskali, T.; Parlakay, E.; Mutluer, O. Control over imperfect networks: Model-based predictive networked control systems. *IEEE Trans. Ind. Electron.* **2011**, *58*, 905–913. [CrossRef]

85. Liu, K.; Fridman, E. Networked-based stabilization via discontinuous Lyapunov functionals. *Int. J. Robust Nonlinear Control* **2011**, *22*, 420–436. [CrossRef]

86. Shi, Y.; Yu, B. Robust mixed H2/H∞ control of networked control systems with random time delays in both forward and backward communication links. *Automatica* **2011**, *47*, 754–760. [CrossRef]

87. Ishido, Y.; Takaba, K.; Quevedo, D. Stability analysis of networked control systems subject to packet-dropouts and finite-level quantization. *Syst. Control Lett.* **2011**, *60*, 325–332. [CrossRef]

88. Donkers, M.; Heemels, W.; van de Wouw, N.; Hetel, L. Stability analysis of networked control systems using a switched linear systems approach. *IEEE Trans. Autom. Control* **2011**, *56*, 2101–2115. [CrossRef]

89. Zhang, X.-M.; Han, Q.-L. Network-based H∞ filtering for discrete time systems. *IEEE Trans. Signal Process.* **2012**, *60*, 956–961. [CrossRef]

90. Seuret, A. A novel stability analysis of linear systems under asynchronous samplings. *Automatica* **2012**, *48*, 177–182. [CrossRef]

91. Chen, W.H.; Zheng, W.X. An improved stabilization method for sampled-data control systems with control packet loss. *IEEE Trans. Autom. Control* **2012**, *57*, 2378–2384. [CrossRef]

92. Kruszewski, A.; Jiang, W.; Fridman, E.; Richard, J.P.; Toguyeni, A. A switched system approach to exponential stabilization through communication network. *IEEE Trans. Control Syst. Technol.* **2012**, *20*, 887–900. [CrossRef]

93. Liu, B.; Xia, Y.Q.; Yang, Y.; Fu, M.Y. Robust fault detection of linear systems over networks with bounded packet loss. *J. Frankl. Inst.* **2012**, *349*, 2480–2499. [CrossRef]

94. Sehgal, V.K.; Khanna, R.; Garg, G.; Singhal, N.; Sahu, N.; Gupta, S. Modern Control System Mapping on Networks-on-Chip. In Proceedings of the Third International Conference on Intelligent Systems Modelling and Simulation, Kota Kinabalu, Malaysia, 8–10 February 2012; pp. 31–36.

95. Sivaranjani, S.; Thukaram, D. Networked control of smart grids with distributed generation. In Proceedings of the 2013 Annual IEEE India Conference (INDICON), Mumbai, India, 13–15 December 2013; pp. 1–6.

96. Peng, C.; Han, Q.-L. A novel event-triggered transmission scheme and L2 control co-design for sampled-data control systems. *IEEE Trans. Autom. Control* **2013**, *58*, 2620–2626. [CrossRef]

97. Yue, D.; Tian, E.; Han, Q.-L. A delay system method for designing event-triggered controllers of networked control systems. *IEEE Trans. Autom. Control* **2013**, *58*, 475–481. [CrossRef]

98. Abidi, K.; Xu, J. Iterative learning control for sampled-data systems: From theory to practice. *IEEE Trans. Ind. Electron.* **2014**, *58*, 3002–3015. [CrossRef]

99. Wang, Y.-L.; Han, Q.-L. Modelling and controller design for discrete time networked control systems with limited channels and data drift. *Inf. Sci.* **2014**, *269*, 332–348. [CrossRef]

100. Du, Z.; Yue, D.; Hu, S. H∞ stabilization for singular networked cascade control systems with state delay and disturbance. *IEEE Trans. Ind. Inf.* **2014**, *10*, 882–894. [CrossRef]

101. Zhang, D.; Han, Q.-L.; Jia, X. Network-based output tracking control for a class of T-S fuzzy systems that cannot be stabilized by nondelayed output feedback controllers. *IEEE Trans. Cybern.* **2015**, *45*, 1511–1524. [CrossRef]

102. Truong, D.Q.; Ahn, K.K. Robust Variable Sampling Period Control for Networked Control Systems. *IEEE Trans. Ind. Electron.* **2015**, *62*, 5630–5643. [CrossRef]

103. Zhang, X.; Han, Q. A Decentralized Event-Triggered Dissipative Control Scheme for Systems with Multiple Sensors to Sample the System Outputs. *IEEE Trans. Cybern.* **2016**, *46*, 2745–2757. [CrossRef]

104. Tavassoli, B.; Amraee, T.; Amanzadeh, M. Design and evaluation of distributed networked control for a dual-machine power system. In Proceedings of the 2017 Iranian Conference on Electrical Engineering (ICEE), Tehran, Iran, 2–4 May 2017; pp. 871–876.

105. Ge, X.; Yang, F.; Han, Q.-L. Distributed networked control systems: A brief overview. *Inf. Sci.* **2017**, *380*, 117–131. [CrossRef]

106. Liu, K.; Fridman, E.; Johansson, K.H. Dynamic quantization of uncertain linear networked control systems. *Automatica* **2015**, *59*, 248–255. [CrossRef]

107. Zhang, X.-M.; Han, Q.-L.; Yu, X. Survey on recent advances in networked control systems. *IEEE Trans. Ind. Inform.* **2016**, *12*, 1740–1752. [CrossRef]

108. Chen, H.F.; Gao, J.F.; Shi, T.; Lu, R.Q. H infinity control for networked control systems with time delay, data packet dropout and disorder. *Neurocomputing* **2016**, *179*, 211–218. [CrossRef]

109. Chen, Z.; Zhang, B.; Li, H.; Yu, J. Tracking control for polynomial fuzzy networked systems with repeated scalar nonlinearities. *Neurocomputing* **2016**, *171*, 185–193. [CrossRef]

110. Khatib, E.J.; Barco, R.; Munoz, P.; De La Bandera, I.; Serrano, I. Self-healing in mobile networks with big data. *IEEE Commun. Mag.* **2016**, *54*, 114–120. [CrossRef]

111. Freirich, D.; Fridman, E. Decentralized networked control of systems with local networks: A time-delay approach. *Automatica* **2016**, *69*, 201–209. [CrossRef]

112. Li, J.; Er, M.J.; Yu, H. Sampling and control strategy: Networked control systems subject to packet disordering. *IET Control Theory Appl.* **2016**, *10*, 674–683. [CrossRef]

113. Lu, R.; Xu, Y.; Zhang, R. A new design of model predictive tracking control for networked control system under random packet loss and uncertainties. *IEEE Trans. Ind. Electron.* **2016**, *63*, 6999–7007. [CrossRef]

114. Lin, H.; Su, H.; Shu, Z.; Wu, Z.G.; Xu, Y. Optimal estimation in UDP-like networked control systems with intermittent inputs: Stability analysis and suboptimal filter design. *IEEE Trans. Autom. Control* **2016**, *61*, 1794–1809. [CrossRef]

115. Liu, X.; Yu, X.; Ma, G.; Xi, H. On sliding mode control for networked control systems with semi-Markovian switching and random sensor delays. *Inf. Sci.* **2016**, *337*, 44–58. [CrossRef]

116. Peng, C.; Han, Q.L. On designing a novel self-triggered sampling scheme for networked control systems with data losses and communication delays. *IEEE Trans. Ind. Electron.* **2016**, *63*, 1239–1248. [CrossRef]

117. Chen, Q.; Liu, A. D-stability and disturbance attenuation properties for networked control systems: Switched system approach. *J. Syst. Eng. Electron.* **2016**, *27*, 1108–1114. [CrossRef]

118. Yang, T.; Lu, J.; Wu, D.; Wu, J.; Shi, G.; Meng, Z.; Johansson, K.H. A Distributed Algorithm for Economic Dispatch over Time-Varying Directed Networks with Delays. *IEEE Trans. Ind. Electron.* **2017**, *64*, 5095–5106. [CrossRef]

119. Selivanov, A.; Fridman, E. Sampled-Data Implementation of Derivative-Dependent Control Using Artificial Delays. *IEEE Trans. Autom. Control* **2018**, *63*, 3594–3600. [CrossRef]

120. Wang, G.Q.; Liu, X.Q.; Shi, P. Observer-based fuzzy adaptive output-feedback control of stochastic nonlinear multiple time delay systems. *IEEE Trans. Cybern.* **2017**, *47*, 2568–2578. [CrossRef]

121. Shen, D.; Zhang, C.; Xu, Y. Two updating schemes of iterative learning control for networked control systems with random data dropouts. *Inf. Sci.* **2017**, *381*, 352–370. [CrossRef]

122. Yin, S.; Gao, H.; Qiu, J.; Kaynak, O. Descriptor reduced-order sliding mode observers design for switched systems with sensor and actuator faults. *Automatica* **2017**, *76*, 282–292. [CrossRef]

123. Kwon, C.; Hwang, I. Reachability analysis for safety assurance of cyber-physical systems against cyber-attacks. *IEEE Trans. Autom. Control* **2018**, *63*, 2272–2279. [CrossRef]

124. Li, M.; Chen, Y. Robust adaptive sliding mode control for switched networked control systems with disturbance and faults. *IEEE Trans. Ind. Inform.* **2018**, *15*, 193–204. [CrossRef]

125. Wei, Y.L.; Qiu, J.B.; Shi, P.; Wu, L.G. A piecewise-Markovian Lyapunov approach to reliable output feedback control for fuzzy affine systems with time-varying delays and actuator faults. *IEEE Trans. Cybern.* **2018**, *48*, 2723–2735. [CrossRef]

126. Sun, Y.-C.; Yang, G.-H. Event-triggered state estimation for networked control systems with lossy network communication. *Inf. Sci.* **2019**, *492*, 1–12. [CrossRef]

127. Nowzari, C.; Garcia, E.; Cortés, J. Event-triggered communication and control of networked systems for multi-agent consensus. *Automatica* **2019**, *105*, 1–27. [CrossRef]

128. Ding, D.; Han, Q.L.; Wang, Z.; Ge, X. A Survey on Model-based Distributed Control and Filtering for Industrial Cyber-Physical Systems. *IEEE Trans. Ind. Inform.* **2019**, *15*, 1551–3203. [CrossRef]

129. Pan, Y.; Yang, G.H. Event-based output tracking control for fuzzy networked control systems with network-induced delays. *Appl. Math. Comput.* **2019**, *346*, 513–530. [CrossRef]

130. Zhang, F.; Kodituwakku, H.A.D.E.; Hines, J.W.; Coble, J. Multi-Layer Data-Driven Cyber-Attack Detection System for Industrial Control Systems Based on Network, System, and Process Data. *IEEE Trans. Ind. Inform.* **2019**, *15*, 4362–4369. [CrossRef]

131. Youness, S.F.; Lobusov, E.C. Networked Control for Active Suspension System. In Proceedings of the 13th International Symposium Intelligent Systems (INTELS'18), Washington, DC, USA, 24–28 July 2019; pp. 123–130.

132. Liu, J.; Wu, Z.-G.; Yue, D.; Park, J.H. Stabilization of Networked Control Systems with Hybrid-Driven Mechanism and Probabilistic Cyber Attacks. *IEEE Trans. Syst. Man Cybern.* **2019**. [CrossRef]

133. Ye, H.; Wen, L. Robust Fault Detection Filter Design of Networked Control Systems. *IEEE Access.* **2019**, *7*, 141144–141152. [CrossRef]

134. Liu, K.; Anton, S.; Emilia, F. Survey on time-delay approach to networked control. *Annu. Rev. Control* **2019**, *48*, 57–79. [CrossRef]

135. Yi, X.; Yang, T.; Wu, J.; Johansson, K.H. Distributed event-triggered control for global consensus of multi-agent systems with input saturation. *Automatica* **2019**, *100*, 1–9. [CrossRef]

136. Wang, T.; Kang, Y.; Li, P.; Zhao, Y.B.; Yu, P. Robust model predictive control for constrained networked nonlinear systems: An approximation-based approach. *Neurocomputing* **2020**, *418*, 56–65. [CrossRef]

137. Wen, S.; Guo, G. Sampled-Data Control for Connected Vehicles with Markovian Switching Topologies and Communication Delay. *IEEE Trans. Intell. Transp. Syst.* **2020**, *21*, 2930–2942. [CrossRef]

138. Liu, B.; Liu, Y. Mixed Event Triggered Mechanism Modeling and Controlling for Networked Control Systems with Time Varying Delays and Uncertainties. *Asian J. Control* **2020**, *22*, 1–15. [CrossRef]

139. Peng, C.; Sun, H. Switching-Like Event-Triggered Control for Networked Control Systems under Malicious Denial of Service Attacks. *IEEE Trans. Autom. Control* **2020**, *65*, 3943–3949. [CrossRef]

140. Qiang, H.; Lin, Z.; Zou, X.; Sun, C.; Lu, W. Synchronizing non-identical time-varying delayed neural network systems via iterative learning control. *Neurocomputing* **2020**, *411*, 406–415. [CrossRef]

141. Wang, K.; Tian, E.; Liu, J.; Wei, L.; Yue, D. Resilient control of networked control systems under deception attacks: A memory-event-triggered communication scheme. *Int. J. Robust Nonlinear Control* **2020**, *30*, 1534–1548. [CrossRef]

142. Deng, F.; Zu, Y.; Mao, Y.; Zeng, X.; Li, Z.; Tang, X.; Wang, Y. A method for distribution network line selection and fault location based on a hierarchical fault monitoring and control system. *Int. J. Electr. Power Energy Syst.* **2020**, *123*, 106061. [CrossRef]

143. Qi, Y.; Xu, X.; Lu, S.; Yu, Y. A waiting time based discrete event-triggered control for networked switched systems with actuator saturation. *Nonlinear Anal. Hybrid Syst.* **2020**, *37*, 100904. [CrossRef]

144. Liu, K.-Z.; Sun, X.-M.; Teel, A.R.; Liu, J. Stability analysis for networked control systems with sampling, transmission protocols and input delays. *Nonlinear Anal. Hybrid Syst.* **2021**, *39*, 1–25. [CrossRef]

145. Liu, Y.-A.; Tang, S.; Liu, Y.; Kong, Q.; Wang, J. Extended dissipative sliding mode control for nonlinear networked control systems via event-triggered mechanism with random uncertain measurement. *Appl. Math. Comput.* **2021**, *396*, 125901.

146. Fang, F.; Ding, H.; Liu, Y.; Park, J.H. Fault tolerant sampled-data H∞ control for networked control systems with probabilistic time-varying delay. *Inf. Sci.* **2021**, *544*, 395–414. [CrossRef]

147. Gao, H.; Shi, K.; Zhang, H. A novel event-triggered strategy for networked switched control systems. *J. Frankl. Inst.* **2021**, *358*, 251–267. [CrossRef]

148. Tian, Z. Deadband feedback-based scheduling approach for networked control system with variable sampling period. *Trans. Inst. Meas. Control* **2021**. [CrossRef]

149. Zhang, H.; Hui, G.; Wang, Y. Stabilization of networked control systems with piecewise constant generalized sampled data hold function, International Journal of Innovative Computing. *Inf. Control* **2013**, *9*, 1159–1170.

150. Zhao, Y.-B.; Sun, X.-M.; Zhang, J.; Shi, P. Networked Control Systems: The Communication Basics and Control Methodologies. *Math. Probl. Eng.* **2015**, *2015*, 639793. [CrossRef]

151. Haghighi, P.; Tavassoli, B. Robust H_∞ output feedback design for networked control systems with partially known delay probabilities. *Optim. Control Appl. Methods* **2020**, *41*, 1052–1067. [CrossRef]

152. Guo, L.; Yu, H.; Hao, F. Event-triggered control for stochastic networked control systems against Denial-of-Service attacks. *Inf. Sci.* **2020**, *527*, 51–69. [CrossRef]

153. Ahmadian, M.M.; Shajari, M.; Shafiee, M.A. Industrial control system security taxonomic framework with application to a comprehensive incidents survey. *Int. J. Crit. Infrastruct. Prot.* **2020**, *29*, 100356. [CrossRef]

154. Song, J.-S.; Chang, X.-H. H∞ controller design of networked control systems with a new quantization structure. *Appl. Math. Comput.* **2020**, *376*, 125070. [CrossRef]

155. Casavola, A.; Franze, G. Coordination strategies for networked control systems: A power system application. In Proceedings of the 2008 10th International Conference on Control, Automation, Robotics and Vision, Hanoi, Vietnam, 17–20 December 2008; pp. 503–508.

156. Cervin, A.; Henriksson, D.; Lincoln, B.; Årzén, K.E. Jitterbug and True Time: Analysis Tools for Real- Time Control Systems. In Proceedings of the 2nd Workshop on Real-Time Tools, Copenhagen, Denmark, 1 August 2002.

157. Nilson, J. Real-Time Control Systems with Delays. Ph.D. Thesis, Lund Institute of Technology, Lund, Sweden, 1998.

158. Pillajo, C.; Hincapié, R.; Pilatasig, E. Implementation of a network control system for a Robotic Manipulator as cloud service. In Proceedings of the 2015 CHILEAN Conference on Electrical, Electronics Engineering, Information and Communication Technologies (CHILECON), Santiago, Chile, 28–30 October 2015; pp. 791–795.

159. De Winter, A.; Baldi, S. Real-Life Implementation of a GPS-Based Path-Following System for an Autonomous Vehicle. *Sensors* **2018**, *18*, 3940. [CrossRef] [PubMed]

160. Singh, A.K.; Singh, R.; Pal, B.C. Stability Analysis of Networked Control in Smart Grids. *IEEE Trans. Smart Grid* **2015**, *6*, 381–390. [CrossRef]

161. Falco, J.; Stouffer, K.; Wavering, A.; Proctor, F. *IT Security for Industrial Control Systems*; NIST Internal Report (NISTIR); National Institute of Standards and Technology (NIST), U.S. Department of Commerce: Gaithersburg, MD, USA, 2002.

162. Xu, Z.; Xu, H. Application of Fuzzy Controller to Missile Networked Control Systems. In Proceedings of the 2008 4th International Conference on Wireless Communications, Networking and Mobile Computing, Dalian, China, 12–17 October 2008; pp. 1–4.

163. Prouty, R. *Helicopter Performance Stability and Control*; Krieger Publishing Company Inc.: Malabar, FL, USA, 2003; p. 560.

164. Segaran, T. ; *Hammerbacher. J. Beautiful Data: The Stories behind Elegant Data Solutions*; O_Reilly Media: Sebastopol, CA, USA, 2009.

Article

Unification of Edge Energy Grids for Empowering Small Energy Producers

Evangelos K. Markakis [1], Yannis Nikoloudakis [1], Kalliopi Lapidaki [2], Konstantinos Fiorentzis [1]
and Emmanuel Karapidakis [1,*

[1] Department of Electrical and Computer Engineering, Hellenic Mediterranean University, GR-71004 Heraklion, Greece; emarkakis@hmu.gr (E.K.M.); gnikoloudakis@hmu.gr (Y.N.); kfiorentzis@hmu.gr (K.F.)

[2] Adrestia Research and Development PPC, GR-71202 Heraklion, Greece; lapidaki@adrestia.eu

* Correspondence: karapidakis@hmu.gr

Abstract: The current energy landscape is largely comprised of big stakeholders, who are often the monopolistic drivers of their local market. This fact does not leave any room for smaller players to participate in this procedure by contributing their part in the energy pool. Moreover, the dynamic demand for power along with the current power production rate are not corelated, rendering the power distribution grid, a best effort network, prone to power failures, due to the inevitable irregularities in demand. This paper introduces a novel concept that allows small energy producers, such as solar panel grids, to offer their production excess through an intelligent energy brokerage blockchain-based framework. The proposed framework ingests the vast amounts of bigdata stemming from the distributed smart energy grids smart metering and allows for automatic commercial transactions of power between the participants of a dedicated marketplace. Values dynamically fluctuate depending on the real-time offer and demand and the grid's state. Thus, all partaking stakeholders are able to take the most out of their product by leveraging the intelligence provided by the energy marketplace, and contribute to the overall stabilization of the energy grid.

Keywords: energy grids; energy producers; cold spinning reserve; DLT; brokerage; SMEs; energy optimisation

1. Introduction

The way we interact with our world around us in almost every aspect of our lives, from how we monitor our environment to how we power our homes and communities is revolutionized, through the collection of vast amounts of information, from a variety of heterogeneous Internet of Things (IoT) devices [1] and Energy net metering [2], which can help to evolve and transform the electric Grid optimization [3]. This information can have an immediate impact towards the improvement of our wellbeing, by providing unprecedented insights on the intelligent and proactive control [4] and monitoring of how power is delivered from a powerplant and used throughout our communities. In this respect, existing energy grids are tightly coupled with a vast network of smart devices and sensors, capable of generating enormous volumes of heterogenous data [5] (bigdata), daily. These data flows, which are difficult to manage and control, can be either dropped, or dismissed, or in some cases underutilized, thus minimizing their impact on benefiting energy grids' optimization. The processing of the collected data, due to its wide diversity, requires intelligent decision-support systems that must utilize current market trends, while also empowering energy distributors to optimize their grids. It is reported by the world economic forum that the deployment and installation of smart meters could generate between 30€ to 60€ [6] in annual savings per customer, raising this number to billions of Euros in total savings.

Current power systems consist of several Gensets (Electricity generators) for cold spinning reserve (ancillary services) [7,8], which are activated trough industrial networks [8] (Scada, PLCs, etc), in case of unexpected events (i.e., power disturbances or total failures) in the distribution grid. These units, along with Power Factor Correctors are capable of correcting reactive power (Q) in addition to active power production, both for on-premises issues, and even more for Neighbor or Total Line issues. Currently these gensets are off-line during any disturbance of the grid, thus not contributing to the system's stability optimal performance. This modus operandi leaves a huge room for improvement, through which both the owner/consumers of the units as well as the whole nearby distribution network can benefit, resulting to the overall enhancement of the power network, and reaching the required power quality.

Currently, the peak-load demand distribution [9] is never a straight line. This fact, apart from the disastrous results it can bring within the distribution lines, can also significantly raise the running costs of electric grids, and also impose. Being aware of this uneven distribution can help identify "cheaper" time-periods [10] of electricity production lifecycle the current energy market is not exploiting. Furthermore, the energy market is primarily comprised of large Power providers, who are leaving no room for Small and Medium-sized Enterprises (SMEs) [11], who are usually based on renewable energy sources, to take part in the power-production market. These small players are mostly "forced" to sell their produced energy to the large power distributors; thus, are abolishing any leverage they could have to influence the energy market. An optimized distributed ledger powered energy market where energy producers and distributors can buy and sell energy automatically, according to a set of criteria, defined by the stakeholders and influenced by the demand, or unexpected events (i.e., power failures in large geographical areas, or big sports events that increase the demand), could mitigate this imbalance. Utilizing public blockchain networks optimized for smart contracts (e.g., Ethereum blockchain [12]), will empower small power suppliers (i.e., solar panels) to securely record the excess power output on the block chain and sell it to large power distributors, or allow themselves to become large power distributors, while at the same time increase their revenue by omitting intermediaries.

In addition, the revolutionization of the smart cities and smart communities, integral part of which are the smart power grids, stems from the immerging ICT era, empowered by the 5G and the distributed Edge Computing paradigms. These immersive technologies introduce the concept of network technology "recycling" and unification [13] for creating a common access playground that can provide a variety of services to the end-users/clients or edge Supervisors (Neighbor based). The advancements of 5G and Edge Computing provide a "fertile" environment for enabling intelligent decision-making, where and when they are needed the most, at the source where the data flows of heterogeneous source are generated. At the same time, the combination of Edge Computing with energy in Hybrid approaches can enable total management in numerous fields. In this paper we present a novel unification of the edge that can be used for the optimization and the empowerment of small energy producers and the utilization of the data stemming from all energy producers and energy sensors of the network.

2. System Description

The system is based on the well-known three-layered architectural [14–16] approach, able to work cooperatively in every part of the grid Network. Starting from the "extreme edge" layer we have the data and energy generating layer that consists of all near-the-edge devices. These devices can be probes, sensors, smart meters, and monitoring devices that are creating an interconnected heterogeneous network of things, in a unified community. This enhancement is supported by an edge layer, which is able to interconnect communities in larger groups, creating clusters called "suburbs" that are able to monitor the power consumption of a specific area in real-time, and enable the smooth out-of-the-peak load-demand distribution by enabling, in an automated manner, the cold spinning reserve (ancillary services) by the use of industrial networks (Scada, PLCs, etc). Finally, an energy

layer is introduced, which can unify and support "suburbs" to provide common energy resource-utilization and at the same time help in the necessary resource supplement management. The key idea is to partition the three-layer infrastructure, consisting of the extreme edge, the edge, and the energy layers into logical virtual networks whose membership can partially overlap with that of other Fog grids and to dynamically reshape this segmentation to ensure fine-grained management of the available resources.

To achieve the above, we are borrowing the successful model of Distributed networks in a hybrid form, where a peer can be "primus inter pares". In this context we enable two types of interconnected elements (Figure 1). The first type work as regular objects, named Edge Nodes (EN) and the latter are Enablers Edge Nodes (EEN). The achieved unification creates a community playground, SMEs can provide their produced power and translate into a digital energy unit, though a novel element named EnergyStore, which takes under consideration the power consumption and the market requests in power in real-time. Though the proposed system we bypass the "obligation" of small energy producers [17] to sell their produced energy to the large power distributors; thus, they partake in the common energy market as equals, directly competing with large power producers. Secondly, we introduce the dynamic cold spinning reserve in the total "suburb" peak load equation, which can efficiently support power-offloading and improve the peak load graph. Finally, we present a distributer ledger powered energy market, where energy producers and distributors can buy and sell energy automatically, according to a set of criteria defined by the stakeholders and influenced by the current market demand, and unexpected events throughout the grid (i.e., power failures in large geographical areas, or big sports events that increase the demand). An EN can be any end-device having at least some processing and communication capabilities that will allow us to deploy our solution on it and thus transform the device into a fully operational edge node. An EN interacts with its corresponding EEN, firstly to inform it about the device's available resources, and secondly to receive and carry out the assigned computational or/and networking tasks.
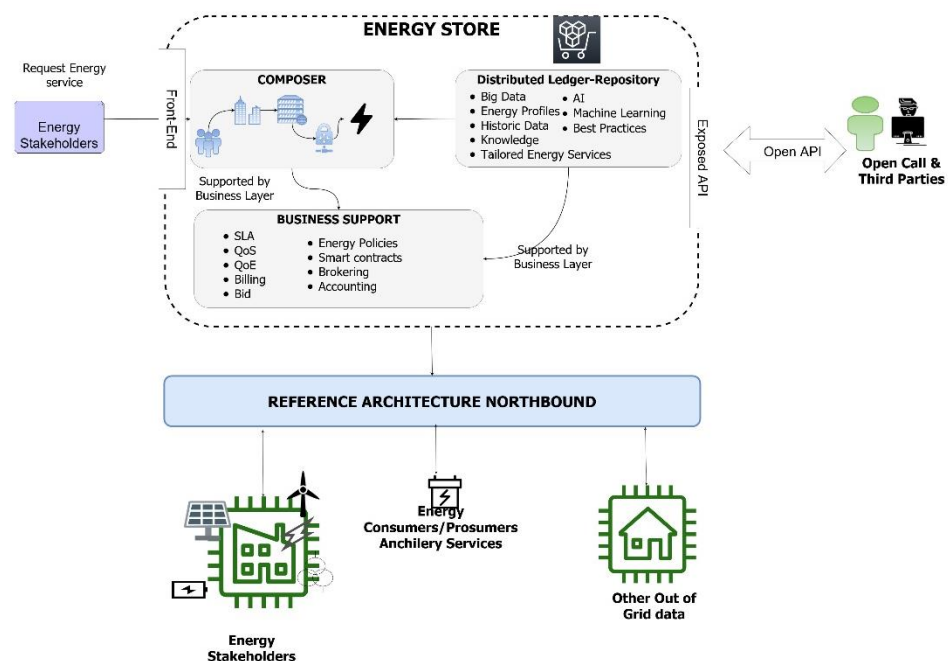
Figure 1. High level architecture of the Energy Store.

An EEN plays two roles within the proposed ecosystem, namely the role of the edge intra-supervisor and the role of the edge's envoy to the edge orchestrator. As an intra-supervisor, an EEN: (a) Oversees the formation of the extreme edge network by performing operations such as the (de)registering of extreme nodes; (b) queries the registered edge nodes about their state and their available resources; and (c) creates a logical topology of

the extreme and edge network along with a virtual pool of the ENs available resources. As an envoy, an EEN interacts with the edge orchestrator towards (a) (de)registering an extreme edge network to the edge overlay; (b) providing a "copy" of the EEN's virtual pool of resources and energy, therefore enabling edge orchestrator to have a clear image for the available energy resources across the whole ecosystem; and (c) mediating between orchestrator and ENs for reserving resources, assigning energy tasks or even deploying cold-spinning elements. Following hybrid Peer to Peer (P2P) paradigm, an EEN is selected from the currently running ENs taking into account several attributes like energy production, energy consumption element, computation processing and power level/type, etc. Recognizing that the unrestrained membership of Edge nodes in the selection process could pose security threats, we are providing a Security as a Service (SaaS) tool that can provide the means for "screening" the candidates list based on the stakeholder's policies. The EEN is elected from the existing ENs; it manages ENs and it is the point of contact to the orchestrator.

3. Energy Store

Energy Store is itself a distributed system following the decentralization and digitalization trends [18]. This toolset will deal with energy monitoring of the edge deployment including sensors, actuators, devices, gateways, and the software deployed at the edge. Additionally, it will provide the needed services to provide updates triggered by the system administrator or by the users using the Service Store. The Store subsystem of the proposed platform allows for optional or third-party software installation to the edge system, in a plug-n-play manner.

The edge layer will facilitate the software components and PaaS capabilities that will allow third-party systems to safely integrate into the platform. The toolset provides a set of services that enable the energy monitoring of legacy subsystems as well as the integration of services that connect the legacy systems to the rest of the platform. This toolset will leverage existing services to facilitate the deployment of new services and updates.

4. Brokering Ability

In this section we introduce the brokerage module that lives inside the Energy Store that acquires all energy sources and brokers them focusing on achieving revenue for all energy producers. The ability to interconnect and unify the production of multiple energy producers provides multiple new revenue streams with the ability to create tailored products (e.g.," green contracts" from only "green" energy producers). The brokerage system performs various functionalities, namely discovery, integration, aggregation, customization, quality assurance and optimization.

Discovery deals with the identification and selection of existing energy services to allow the creation of user-tailored contracts. This functionality allows the Energy Store to list all energy offerings from different providers, where end-users can directly compare similar energy services, their ratings, and other relevant features.

Integration is related to the provision of energy-based environment in order to integrate separate energy systems. The integration aims at either facilitating power exchange between separate systems or realizing collaborative business processes within the existing energy systems.

Aggregation concerns the provision of energy services that comprise multiple third-party energy producers. An aggregated energy service may allow users to interact with the interfaces of the third-party services directly (for instance, through a smart-meter interface), or indirectly, through a common interface that encapsulates the individual services and possibly add common functionality such as cold-spinning reserve, coupling capacitors and capacitor dividers.

Customization enables the implementation of new functionalities to enrich the offered energy services, by means of extension rather than modification of that services' implementation e.g., include only "green" energy sources.

Quality assurance ensures that one or more energy services achieve specific quality expectations. This can be performed by service testing, policy enforcement, SLA monitoring, and possibly by self-management mechanisms triggered, to restore service quality.

Optimization enables the opportunistic improvement of the consumption or provisioning of an energy service with respect to various criteria, such as cost, functionality, or performance.

The overall architecture of the brokerage module is depicted in Figure 2.
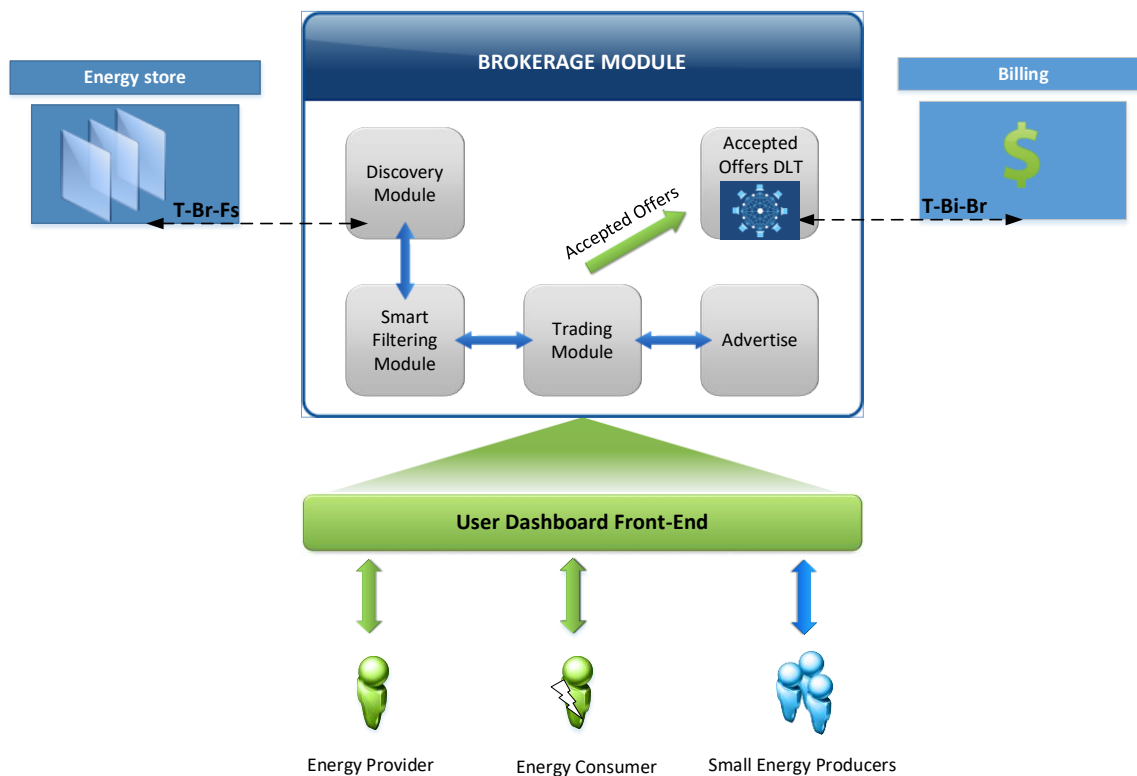
Figure 2. Brokerage module internal architecture.

It consists of five main modules that are used in various interactions, as shown in the Figure above:

- Energy Discovery Module

This module retrieves all the available and tradable energy units from the small energy grids.

- Smart Filtering Module

This module applies a smart filtering to the list of the available energy services, based on the users' preferences and the SLA parameters.

- Trading Module

This module provides all the interaction between the service provider and the function providers. The Trading module is used for requesting a new trade/offer from the Energy Providers (EP).

- Energy Contract Advertise Module

This module is responsible for the advertisement/return of all tradable Energy Services to the EPs.

- Accepted Offers DLT

This module is responsible for updating the distributed Ledger for the accepted offers in order to be available for the accounting module for billing purposes and provide transparent transactions to all involved parties.

According to the proposed mechanism, the EP browse the offerings from the energy contracts' catalogue that match its requirements. If the requested function supports Brokering/Trading, the internal modules will try to fulfil the criteria set by the EP. Furthermore, the brokerage module initiates the appropriate bid/trading policies according to the EP's request in collaboration with the Energy Discovery module.

The high-level architecture of the brokerage module along with the interaction inside the Marketplace is described below and depicted above in the high-level architecture of the brokerage module along with the interaction inside the Marketplace.

1. The EP provides the Energy Contract request and the initial price to the brokerage module.
2. The brokerage module informs the Energy Producers (EPRs) regarding the request and the initial price.
3. EPR send their bids for the functions (Power produced Price, Infrastructure cost, Setup price and the SLA specification)
4. The brokerage module initiates an auction to maximize its revenue based on the produced power price, setup price, infrastructure cost and SLA specification.
5. The brokerage module informs the bidding results.
6. Depending on the type of auction, an iteration continues until a bidding winner is found.
7. The brokerage module announces the final results.
8. The winner acknowledges the results.
9. The brokerage module indicates the Energy Contract price, which is provided by the EPRs that won the bidding, to the EP.
10. The EP accepts the price.
11. The EP receives the energy contract.
12. Finally, all setup prices will be sent to the accounting module through the SLA management module.

According to the trading process (i.e., auction-based algorithm in XX), the Energy brokerage module determines the optimal allocation solution, considering the maximization of Energy Provider's income. Consequently, the brokerage module undertakes the trading procedure that collects bids from Energy Producers (EPRs), in order to lease the produced power to the energy customers, through the EP. The brokerage module computes the assigning solution through this mechanism together with price and SLA per service.

4.1. Infrastructure Cost of Brokering

Infrastructure costs are calculated with the use of the algorithm described below Algorithm 1. The overhead lines cost OL_cost, underground and subsea cables (US_Cost), onshore AC substation Cost (OAS_Cost) and the HVDC converter stations and Transformer's cost (HVDCCT_COST) are calculated based on the prices stemming from various Energy Infrastructure providers on the internet [18]. Furthermore, when the auction-based algorithm is followed, the sellers (i.e., EPRs) that are denoted as $S = \{1, 2, \ldots, s\}$, lease the Energy Services, denoted as $V = \{1, 2, \ldots, v\}$, to $b = 1$ buyers (EPs). The EP is able to buy/lease Energy Services, denoted as x_v for a specific time period t_i, by reporting a price $P(b) = \{x_v, t_i\}$ (i.e., bid price of Energy Services considering specific requirements), while the EPRs lease Energy Services y_v, providing a function cost f_v, for a specific time t_i and with a specific SLA L_v, by reporting a price $P(S) = \{f_v, y_v, t_i, L_v\}$ (i.e., asking price of Energy Services considering specific requirements). Finally, the pair (b,v) in the pseudo-code bellow represents possible combinations of solutions, regarding "v" Energy Service to EP.

In case EP benefit must be maximized, an optimization problem is formulated as follows, based on linear programming, i.e., the following equation:

$$max : \sum_{s=1}^{s} (|P(b) - P(S)|) \tag{1}$$

Algorithm 1 List of steps for Infrastructure Cost Calculation.

---

1. Inputs: Energy Services, Demand
2. Access service catalog store
3. Estimate the initial price per Energy Services
4. Create and advertise price-portfolio
5. Receive EPRs offers P(S) and EP bids P(b), where P(S) = {fv, yv, ti, Lv} and P(b) = {xv, ti}
6.   **for all** offers and bids **do**:
7.   Sort P(S) and P(b) in descending order based on price, function cost and SLA and create the auction-portfolio
8.   **end for**
9. Calculate the highest valuation S[b,v] for all Energy Services (i,v) {1, 2, . . . , v}
10. set Soptimal = S[b,v] //Random solution for algorithm initiation
11.   for each bid P(b)do //Iteration process in order to find the best solution
12.   **if** (S[b,v]) $\leq$ (S[b + 1, v + 1]) // Check if the current solution is better or not to the neighbour solution
13.   then save the new solution (S[b + 1, v + 1]) to the best found
14.   **end if**
15.   **end for**
16. **return** Best Solution

In this respect and to facilitate competition among Function Providers (EPRs) a novel brokerage platform is designed that will allow (i) the customers to search for available offerings, (ii) auctioning between the third-party function developers (EPRs) and the EP, in order to find the best price for the Energy Services that will be part of each Energy Contract.

Furthermore, while the provision of Energy Services encompasses several system functionalities, Energy Service trading can be regarded as one part of the process that deals with the economic aspects. The trading process determines all the issues related with Energy Services selling and buying (e.g., direct trading between service provider and function provider or via a brokerage module), while pricing is a major issue that determines the value (or worth) of the Energy Services to the service provider and the function provider.

Another issue is the competition/cooperation among function and service providers, as well as customers involved in Energy Services trading. Depending on the Energy Services trading model, the Energy Service access may require permission through the cooperation of service provider and function provider, through a payment process. To determine the optimal network function provision during the trading process, optimization and decision theory techniques can be used.

4.2. Brokering with an Energy Blockchain

The blockchain is a distributed ledger recording the events of all Power producers that generate data, processing and sharing. It is composed of a growing number of blocks. In our Broker, each block contains one or more events identified by event hash. An event hash is computed by hashing the event content, as the event fingerprint. A block also has a block header, which contains (shown in figure down):

- Root of all the event hashes in the block.
- Timestamp: The time of when the block is created.
- Block hash: The hash code computed based on the hash of the last block, the root, and the timestamp.

The cascaded hash computing at the event level (event hash), the block level (root), and the chain level (block hash) ensures the content immutability of a blockchain. If someone wants to modify the block information, he/she has to modify the entire chain. Yet, any tampering with the content can be easily detected by re-generating the hash codes and comparing them with the original ones.

In our Brokerage model, the blockchain service manages the immutable information of energy data. Two types of events are recorded on a blockchain: Energy generation event and session creation event.

Energy Generation Event. An energy generation event is created when an energy record file or a cold spinning reserve is requested to be started. It contains overhead lines cost OL_cost, underground and subsea cables (US_Cost), onshore AC substation Cost (OAS_Cost) and the HVDC converter stations and Transformers cost (HVDCCT_COST), signature, event type, last chunk location in chain, etc.

Session Creation Event. A session creation event is created when a Energy consumer takes an action in the system. It contains the start time, end time, public key of the provider and the requester for identifying the session participants, as well as the signature.

The operation of the proposed engine will be based on pioneering mathematical models (e.g., game theory) for analyzing, compiling, combining, and correlating all related information and data from different levels patterns and contexts in a privacy-aware manner. These techniques will provide the basis required for supporting the processing and storage of Energy contracts gathered from various sources in a unified structure in order to discover the relationships between Energy producers and Energy consumers along with the timeline of the contract, including a map of affected power producers and a set of meaningful chain of contract.

5. Conclusions

This paper introduces a novel concept that allows small energy producers, such as solar panel grids, to offer their production excess through an intelligent energy brokerage blockchain-based framework. These units, along with Power Factor Correctors (ancillary services) are capable of correcting reactive power (Q) in addition to active power production, both for on-premises issues, and even more for Neighbor or Total Line issues. Currently these gensets are off-line during any disturbance of the grid, thus not contributing to the system's stability optimal performance. This modus operandi leaves a huge room for improvement, through which both the owner/consumers of the units as well as the whole nearby distribution network can benefit, resulting to the overall enhancement of the power network, and reaching the required power quality. Additionally, the utilization of the small energy producers in the optimization equation along with the ability to commonly contribute to the energy grid provides a new approach of operation. In this paper we describe a novel framework that ingests the vast amounts of bigdata stemming from the distributed smart energy grids though the net metering and allows for automatic commercial transactions of power between the participants of a dedicated marketplace. Values dynamically fluctuate depending on the real-time offer and demand and the grid's state. Thus, all partaking stakeholders are able to take the most out of their product, by leveraging the intelligence provided by the energy marketplace, and contribute to the overall stabilization of the energy grid.

Data Availability Statement: Not applicable.

Conflicts of Interest: The authors declare no conflict of interest.

References

1. Jamal, H.; Arshad, M.N.; Butt, Y.; Shafiq, H.; Manan, A.; Arif, A.; Janjua, M.K. Design of an economical and reliable net-metering device for residential consumption measurement using IoT. In Proceedings of the 2020 59th Annual Conference of the Society of Instrument and Control Engineers of Japan (SICE), Chiang Mai, Thailand, 23–26 September 2020; pp. 1747–1752.
2. Poullikkas, A.; Kourtis, G.; Hadjipaschalis, I. A review of net metering mechanism for electricity renewable energy sources. *Int. J. Energy Environ. (Print)* **2013**, *4*, 975–1002.
3. Nguyen, T.A.; Byrne, R.H. Maximizing the cost-savings for time-of-use and net-metering customers using behind-the-meter energy storage systems. In Proceedings of the 2017 North American Power Symposium (NAPS), Morgantown, WV, USA, 17–19 September 2017; pp. 1–6.
4. Zobaa, A.F.; Vaccaro, A. (Eds.) *Computational Intelligence Applications in Smart Grids: Enabling Methodologies for Proactive and Self-Organizing Power Systems*; World Scientific: Singapore, February 2015. [CrossRef]
5. Ahsan, U.; Bais, A. Distributed big data management in smart grid. In Proceedings of the Wirel Opt Commun Conference (WOCC) 2017, Newark, NJ, USA, 7–8 April 2017; pp. 1–6.
6. Fiorentzis, K.; Karapidakis, E.; Tsikalakis, A. Cost Analysis of Demand-Side Generating Assets Contribution to Ancillary Services of Island Power Systems. *Inventions* **2020**, *5*, 34. [CrossRef]
7. Danish, S.M.S.; Ahmadi, M.; Danish, M.S.S.; Mandal, P.; Yona, A.; Senjyu, T. A coherent strategy for peak load shaving using energy storage systems. *J. Energy Storage* **2020**, *32*, 101823. [CrossRef]
8. Rashidinejad, M.; Song, Y.H.; Javidi, M.H. Ancillary Services (I): Pricing and Procurement of Reserves. In *Operation of Market-oriented Power Systems*; Springer: London, UK, 2003; pp. 223–252.
9. Iskakova, A.; Nunna, H.K.; Siano, P. Ethereum Blockchain-Based Peer-To-Peer Energy Trading Platform. In Proceedings of the 2020 IEEE International Conference on Power and Energy (PECon), Penang, Malaysia, 7–8 December 2020; pp. 327–331.
10. Majidi, M.; Nojavan, S.; Zare, K. Optimal stochastic short-term thermal and electrical operation of fuel cell/photovoltaic/battery/grid hybrid energy system in the presence of demand response program. *Energy Convers. Manag.* **2017**, *144*, 132–142. [CrossRef]
11. O'Keeffe, J.M.; Gilmour, D.; Simpson, E. A network approach to overcoming barriers to market engagement for SMEs in energy efficiency initiatives such as the Green Deal. *Energy Policy* **2016**, *97*, 582–590. [CrossRef]
12. Aloqaily, M.; Boukerche, A.; Bouachir, O.; Khalid, F.; Jangsher, S. An energy trade framework using smart contracts: Overview and challenges. *IEEE Netw.* **2020**, *34*, 119–125. [CrossRef]
13. Markakis, E.; Mastorakis, G.; Mavromoustakis, C.X.; Pallis, E. (Eds.) *Cloud and Fog Computing in 5G Mobile Networks: Emerging Advances and Applications*; Institute of Engineering and Technology: England, UK, 2017; Volume 70, p. 440, ISBN-13: 978-1-78561-083-7.
14. Patlitzianas, K.D.; Ntotas, K.; Doukas, H.; Psarras, J. Assessing the renewable energy producers' environment in EU accession member states. *Energy Convers. Manag.* **2007**, *48*, 890–897. [CrossRef]
15. Markakis, E.K.; Karras, K.; Sideris, A.; Alexiou, G.; Pallis, E. Computing, caching, and communication at the edge: The cornerstone for building a versatile 5G ecosystem. *IEEE Commun. Mag.* **2017**, *55*, 152–157. [CrossRef]
16. Markakis, E.; Negru, D.; Bruneau-Queyreix, J.; Pallis, E.; Mastorakis, G.; Mavromoustakis, C.X. A p2p home-box overlay for efficient content distribution. In *Emerging Innovations in Wireless Networks and Broadband Technologies*; IGI Global: Hershey, PA, USA, 2016; pp. 199–220.
17. Di Silvestre, M.L.; Favuzza, S.; Sanseverino, E.R.; Zizzo, G. How Decarbonization, Digitalization and Decentralization are changing key power infrastructures. *Renew. Sustain. Energy Rev.* **2018**, *93*, 483–498. [CrossRef]
18. Agency for the Cooperation of Energy Regulators (ACER). *Report on Unit Investment Cost Indicators and Corresponding Reference Values for Electricity and Gas Infrastructure Electricity Infrastructure Version 1.1 August 2015 Infrastructure Reference Costs*; ACER Agency: Ljubljana, Slovenia, 2015.

Article

New Decentralized Control of Mesh AC Microgrids: Study, Stability, and Robustness Analysis

Youssef Hennane [1,2,*], Abdelmajid Berdai [2], Jean-Philippe Martin [1], Serge Pierfederici [1] and Farid Meibody-Tabar [1]

1 Laboratoire Énergies & Mécanique Théorique et Appliquée LEMTA, Centre National de la Recherche Scientifique CNRS, Université de Lorraine, 54000 Nancy, France; jean-philippe.martin@univ-lorraine.fr (J.-P.M.); serge.pierfederici@univ-lorraine.fr (S.P.); farid.meibody-tabar@univ-lorraine.fr (F.M.-T.)

2 Electrical Engineering Department, National Superior School of Electricity and Mechanics (ENSEM), Hassan II University, Route d'El Jadida, km 7, Oasis, Casablanca BP 8118, Morocco; a.berdai@gmail.com

* Correspondence: youssef.hennane@univ-lorraine.fr; Tel.: +33-7-53067573

Abstract: In this paper, we investigated the power sharing issues in mesh islanded microgrids that contain several distributed generators (DGs) and loads connected to different points of common coupling (PCC). Firstly, an improved decentralized droop control algorithm is proposed to achieve the active and reactive power sharing of different DGs in reconfigurable mesh islanded microgrids. Accurate power sharing was obtained even though line parameters or the mesh microgrid configuration were unknown. Secondly a state-space model of the whole mesh microgrid was developed, considering several generators with their decentralized controllers, line feeders, and dynamic loads. This model was used to design parameters of droop controllers, to study the asymptotic stability and the robustness properties of the system. All strategies and analyses were validated by simulation based on the generic microgrid detailed in the standard IEEE 9bus test feeder.

Keywords: droop control; mesh microgrids; power sharing; synchronization; system stability; robustness analysis; constant power load; reconfiguration

1. Introduction

Microgrids are able to integrate different distributed generator (DG) systems converting different types of renewable energy and to supply different types of loads. This gives a certain level of independence, allowing them to be connected or disconnected from the main grid. One of the challenges is to synchronize and connect all the distributed generators to an islanded microgrid, while providing the "plug and play" functionality and respecting the active and reactive power sharing between the different distributed generation units (DGs) [1,2]. Currently, the most used methods for power sharing and synchronization in literature are based on the droop control strategy [3–8]. However, most of the microgrids considered in these research works have only a single point of common coupling (PCC), which are connected to all DGs through converters and the loads like in Figure 1. In order to level up the independence of microgrids from the main grid by increasing the penetration rate of distributed generators in microgrids, the choice of mesh multi-PCC microgrids seems to be a good solution. However, the intermittency of renewable energy may cause more instability problems in mesh microgrids due to their higher level of complexity compared to microgrids with single points of common coupling.
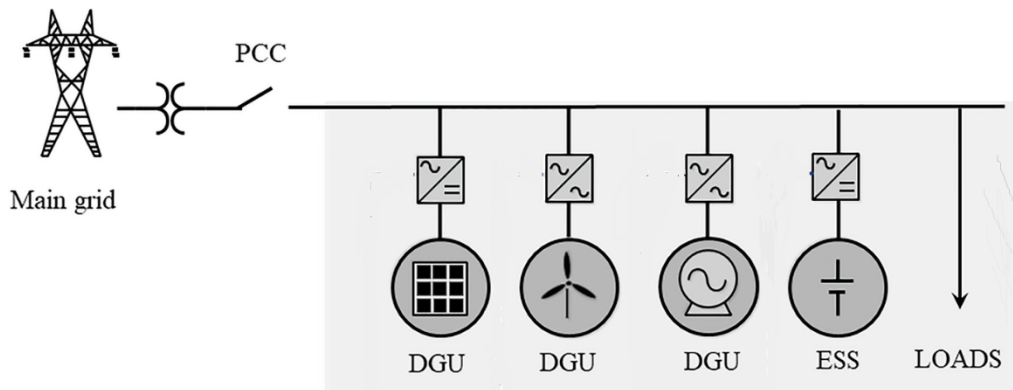
Figure 1. Microgrid with one point of common coupling (PCC).

In mesh multi-PCC reconfigurable microgrids, with many distributed generation sources (DGs) and loads randomly connected to different PCCs, classical synchronization methods and power sharing strategies based on droop control and used in mono-PCC microgrids are less efficient. Indeed, most droop methods assume that the transmission lines are purely inductive or resistive in nature which leads to a linear droop characteristic where active power sharing depends on either frequency or voltage magnitude. However, in microgrids with reconfigurable structure, the sources as well as the networks may become redundant. The changes in the network impedance whenever a branch or source is disconnected in a microgrid means that the active and reactive power cannot be totally decoupled. These changes affect the power sharing among the sources and reduce the stability of the microgrid for any disturbance [9,10].

Much research has focused on solutions that concern the active and reactive power sharing in droop-controlled mesh microgrids [11,12] either by using virtual impedance correction loop and a convergence acceleration strategy to compensate the offset created by the power line impedances and improve the reactive power sharing such as in ref [11], or by adopting a voltage compensation strategy to keep the bus voltage stable at the rated value and improve the reactive power sharing such as in ref [12]. However, only a few studies have focused on active and reactive power sharing in reconfigurable mesh microgrids such as in ref [10], where the authors propose the use of L1 adaptive methods for stable operation of a microgrid with wide range of R/X ratios.

Another problem is the possible unstable behavior of the microgrid caused by the interaction between the DGs and loads as well as the changes in the network configuration. The system stability depends on the type of loads being connected to the microgrid, especially the ones supplied through tightly regulated power converters. These loads behave as constant power loads (CPL) and may cause system instability [13–15]. In the literature, the main studies are based on linearization techniques [16]. The non-linear models of the considered power systems are linearized around an operating point and then studied using linear analysis tools. Moreover, linearization tools only predict the stability of the system for small perturbations [17,18] and cannot guarantee the system stability for large perturbations.

In this paper, a mesh microgrid constituting several PCCs connected to two DGs (DG1 with a nominal power of three megawatts and DG2 with a nominal power of two megawatts) through two transformers (6 kV/20 kV) as well as three loads (LOAD1 with a nominal power of one megawatt, LOAD2 with a nominal power of 1.2 megawatts, and LOAD3 with a nominal power of 1.5 megawatts) are considered. The different PCCs are interconnected with power supply lines, modeled by resistance, inductance and capacitance (RLC) circuits inspired by an IEEE 9-bus test feeder (Figure 2). All the microgrid data are presented in Tables 1 and 2.
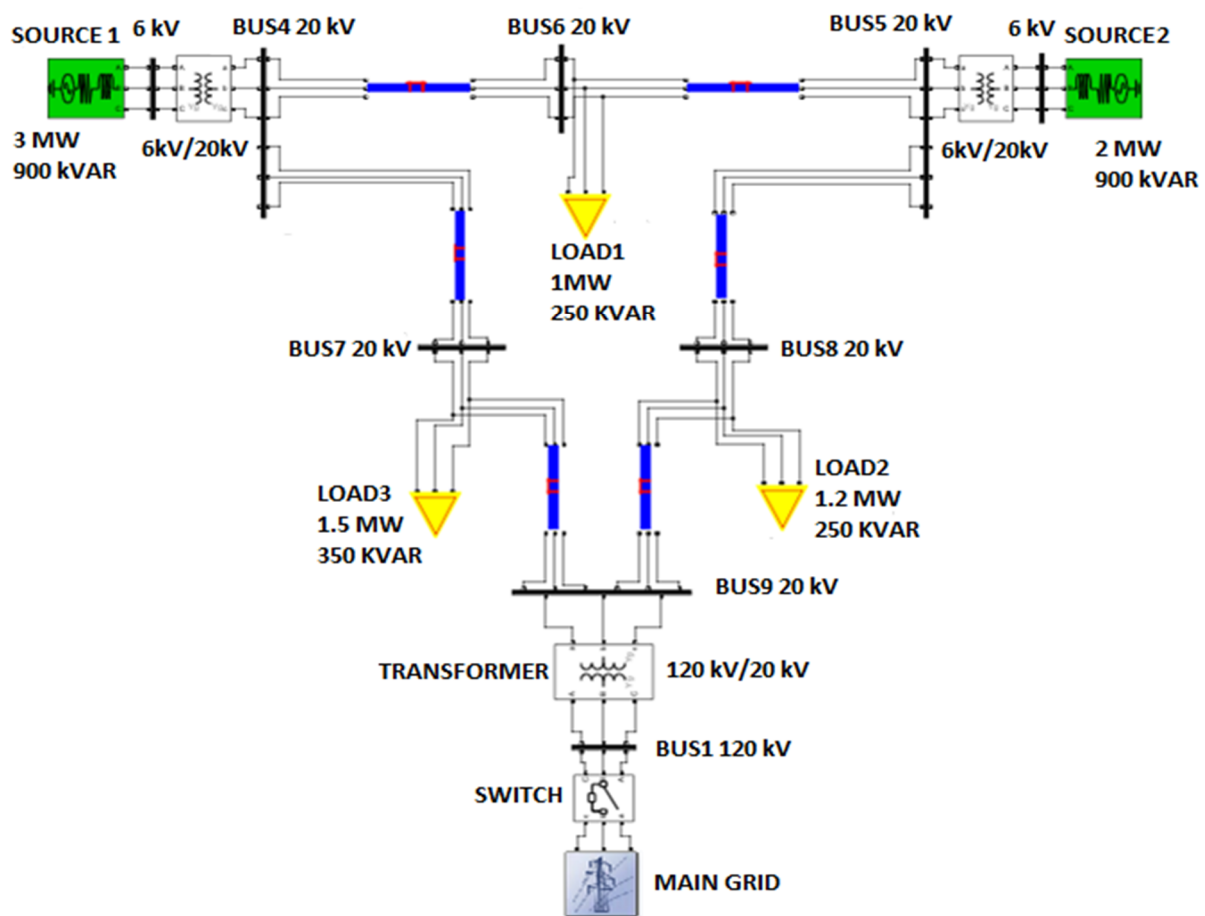
Figure 2. IEEE 9 bus test feeder.

Table 1. Parameters of the considered microgrid power lines.

Lines	Resistance (Ω)	Inductance (mH)	Capacitance (μF)	Points of Connections
Line 1	0.63	7.14	205	Bus 8–Bus 7
Line 2	2.55	11.4	230	Bus 5–Bus 7
Line 3	0.63	7.14	205	Bus 8–Bus 9
Line 4	2	7	180	Bus 9–Bus 6
Line 5	1.7	7.6	153.4	Bus 4–Bus 5
Line 6	1.7	7.6	153.4	Bus 4–Bus 6

Table 2. Sources and load powers.

Sources and Loads	Active Power (Mw)	Reactive Power (Mvar)	Phase to Phase Voltage (kV)	Point of Connection
Source 1	3	0.9	6	Bus 7
Source 2	2	0.9	6	Bus 9
Load 1	1.5	0.35	20	Bus 5
Load 2	1.2	0.25	20	Bus 6
Load 3	1	0.25	20	Bus 8

In order to ensure an accurate power sharing and to provide the "plug and play" function adapted to the considered multi-PCC mesh microgrid, a new droop control and synchronization strategies is applied, such as the one demonstrated in ref [19]. This new droop control in islanded mode consists of removing the decoupling between the

active and reactive power caused by the line impedances and the change in the microgrid configuration. The first DG connected to the microgrid imposes its voltage and frequency. For other DGs, an adapted synchronization strategy is proposed and applied before their interconnection to the microgrid. The simulation results using a model developed in the Simscape feature of MATLAB/Simulink environment enabled the validation of the efficiency of this new droop control.

To study the stability of the microgrid, a state model of the entire meshed microgrid was developed considering its power lines and loads including a CPL as well as its generators, with their decentralized controllers integrating modified droop algorithms. The comparison of the results obtained from the stablished state model and the developed model in Simscape environment confirm the validity of the proposed microgrid state model. This validated state model was then used to study the microgrid stability by calculating its Jacobean matrix and its eigenvalues at each operating point. Based on these results, the root locus, and eigenvalues sensitivity analysis, depending on the parameters of the established model, were performed. The latter made it possible to find the origin of different frequency components by observing the dynamic behavior of different state variables. The analysis of the system stability was then performed by observing the evolution of the system eigenvalues with respect to droop parameters and different load power variations. It will be shown that the system stability may be affected due to unadapted droop control parameters and/or CPL levels.

The established state-model was also used to verify the robustness of the considered mesh microgrid, including the new droop-control that ensured active and reactive power sharing to the modifications caused by the connection of DGs and large load variations (changes in network configuration).

To summarize, the main points of this paper are, firstly, the development of a new droop control strategy for power sharing especially reactive power in mesh islanded microgrids. Unlike in the solutions mostly used by authors for power sharing in reconfigurable mesh microgrids, this modified droop control strategy is decentralized, which means that it does not require any sort of communication between the DGs connected to the microgrids. Thanks to the non-linear term added to the classical droop control, the power coupling phenomenon created by the line impedances and the change in the microgrid configuration is removed. The modified droop control strategy was proven efficient for active and reactive power sharing in different microgrid structures. Additionally, a fast and efficient synchronization strategy did not affect the power sharing. The second major point is the development and validation of a state-space model describing the mesh microgrid and its control. This state-space model was used to study the microgrid stability especially in the presence of active loads such as CPLs. The state model was also used to test the robustness of the modified droop control under different microgrid configurations and different states of charge. The validated state-space model made the manipulation of the system so much easier and allowed many more studies to be carried out on the meshed microgrid. For example, one of many scenarios where the state-space model can be useful is when the CPL-injected power in the microgrid increases, and the state model can easily predict the right value of the capacitor that should be added to the PCC where the CPL is also connected. This means that many future studies can be conducted based on this developed and validated state-space model.

2. Power Sharing and Synchronization Strategies in Mesh Microgrids

2.1. Power Sharing Using Droop Control Strategies

The traditional droop strategy imposing the electrical pulsation and the RMS voltage of a distributed generator via Equations (1) and (2) is efficient in microgrids with a single PCC shown in Figure 1, only if the effect of power line impedance is ignored [4].

$$\omega_i = \omega_n - m_i(P_i - P_{in}), \tag{1}$$

$$E_i = E_n - n_i(Q_i - Q_{in}) \tag{2}$$

$$\text{With}: \; m_i = \frac{\Delta_\omega}{P_{in}}, \; n_i = \frac{\Delta_E}{Q_{in}},$$

where P_i and Q_i are the measured values of the active and reactive power of the *i*th DG, P_{in} and Q_{in} are their nominal values, ω_n and E_n are the nominal values of the pulsation and voltage of the *i*th DG, Δ_ω and Δ_E are the permissible variations of pulsation and voltage, and m_i and n_i are the droop control coefficients. The active and reactive power sharing method is based on a droop control algorithm that sets the frequency and voltage amplitude at the associated PCC for each DG according to Equations (1) and (2).

This droop control does not ensure efficient reactive power sharing even in single PCC micro-grids due to the line impedances. A droop control strategy that has been proven effective for active and reactive power sharing in mono-PCC microgrids (3) and (4) was applied to the complex mesh microgrid in Figure 2, and considering one of the PCC voltages as reference potential of the studied microgrid. The simulation results are presented in Figures 3 and 4.

$$\delta_i = \int \left(K_a(\delta_{in} - \delta_L) - m_i(P_i - P_{in}) \right).dt, \tag{3}$$

$$E_i = \int \left(K_e(E_{in} - E_L) - n_i(Q_i - Q_{in}) \right).dt, \tag{4}$$

(a)

(b)

Figure 3. Evolution of the distributed generator (DG) active (**a**) and reactive (**b**) powers (first DG supplies the microgrid up to 5 s, the second DG is connected to the microgrid at 5 s).
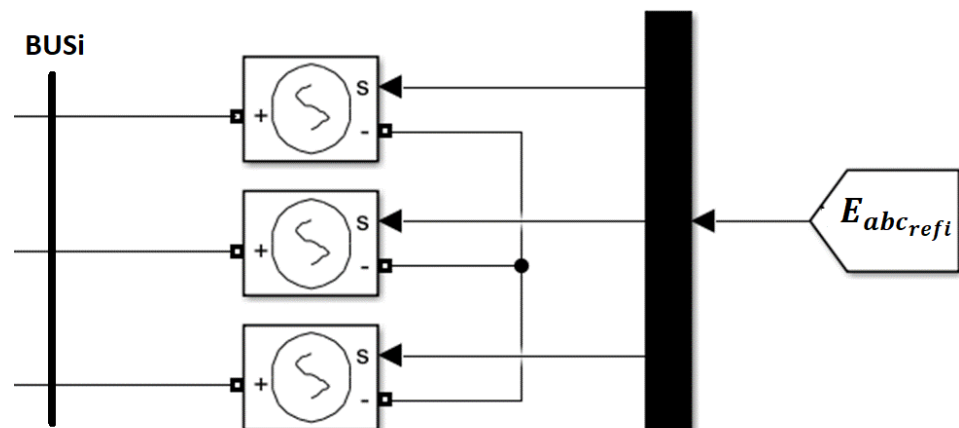
Figure 4. Scheme of the controllable voltage sources DG1 and DG2.

The proposed angular droop aims to indirectly control the voltage at the PCC and its phase to be equal to the nominal values (i.e., E_{in} and δ_{in}). The added integrators can minimize the static error between the feedback signal and the corresponding nominal values. By choosing identical K_a and K_e for each generator, an accurate active and reactive power sharing is achieved which no longer depends on the system impedance and is unaffected by the digital errors and disturbances [9].

In practice, real microgrids can have several PCCs, interconnected by several supply lines with non-negligible impedances. In order to study such a microgrid, a slightly modified IEEE 9bus test feeder is considered, composed of two DGs and three loads, interconnected by RLC lines (Figure 2). It can be noticed that the application of the droop method, based on Equations (3) and (4), on the multi-PCC microgrid of Figure 2 leads to a perfect active power sharing when the second DG is connected at 5 s (Figure 3a). However, the reactive power sharing when the second DG is connected is not achieved (Figure 3b). It can also be remarked that unacceptable disturbing active and reactive power peaks occur due to the lack of synchronization (Figure 3a,b at 5 s).

In mesh microgrids, each line, connecting the *i*th PCC to the *j*th, has a non-negligible inductance ($\lambda_{i,j}$) and resistance ($\rho_{i,j}$), leading to a line voltage drop between these two PCCs that creates a coupling between the active power ($P_{i,j}$) and reactive power ($Q_{i,j}$) exchanged between *i*th and *j*th PCCs, according to Equation (5):

$$\Delta E = \rho_{i,j}I_{i,j}cos\varphi + j\lambda_{i,j}\omega I_{i,j}\sin\varphi = \frac{\rho_{i,j}P_{i,j} + j\lambda_{i,j}Q_{i,j}}{E_i}, \tag{5}$$

where φ is the phase shift between the phase voltage $\overline{E_j}$ and the phase current $\overline{I_{i,j}}$.

To achieve an efficient reactive power sharing in this type of mesh microgrids, the voltage equation in (2) is modified by adding a decoupling term (see Equation (7)) removing the coupling phenomenon between active and reactive power [12]. This coefficient, called J_i, is estimated using a PI controller, forcing the suppression of the error ε_i defined in Equation (8). In steady state, when the error ε_i tends to zero, the reactive power sharing is well ensured between the DGs. This approach allows the primary control of the voltage of the *i*th DG, regardless of the operating point of the loads. It should be noted that E_{ref} in Equation (8) is the measured value of one of the PCC voltages of the studied mesh microgrid acting as the pilot node and considered as its reference potential. The rated voltage of this pilot node is called E_n.

$$\omega_i = \omega_n - m_i\left(P_{fi} - P_{in}\right), \tag{6}$$

$$E_i = E_n - n_i\left(Q_{fi} - Q_{in}\right) - J_i\left(P_{fi} - P_{in}\right), \tag{7}$$

$$\text{With}: m_i = \frac{\Delta_\omega}{P_{in}}, n_i = \frac{\Delta_E}{Q_{in}} \text{ and } \begin{cases} J_i = K_I \int \varepsilon_i dt \\ \varepsilon_i = \left[-\left(\frac{E_{ref}}{E_n} - 1\right) - \left(\frac{Q_i}{Q_{in}} - 1\right)\right] \end{cases}, \tag{8}$$

In the absence of information on E_{ref} the coefficient J is set to 0 and we return to the classical droop.

2.2. Synchronization Strategy in Mesh Islanded Microgrid

Due to the complexity of the mesh microgrids and the intermittency of renewable energies, DGs frequently connect to and disconnect from the microgrid, so a fast and efficient synchronization method is required. To achieve the synchronization of the *i*th DG to the *i*th PCC before their interconnection, the voltage amplitude E_{pcci}, the pulsation ω_{pcci} and the phase θ_{pcci} of the *i*th PCC must be approximately equal to those of the *i*th DG ($E_{DGi}, \omega_{DGi}, \theta_{DGi}$) [2]. To achieve this objective, the errors between the amplitudes, pulsations, and phases of both sides (the *i*th DG and the *i*th PCC) are forced to zero by adding pure integral controllers to the *i*th DG droop control, as shown in Equations (9) and (10) [19]. It should be noted that the binary coefficient B_i in these equations is equal

to one only during the synchronization interval, and equal to zero otherwise. For the pulsation and phase synchronization, the pure integrators are added to the pulsation droop control, Equation (9), and for the voltage synchronization, the pure integrator is added to the voltage droop control, Equation (10).

$$\omega_i = \omega_n - m_i\left(P_{fi} - P_{in}\right) - \left[K_{ai}\int\left(\omega_{DGi} - \omega_{pcci}\right) + K_{bi}\int\left(\theta_{DGi} - \theta_{pcci}\right)\right]B_i, \quad (9)$$

$$E_i = E_n - n_i\left(Q_{fi} - Q_{in}\right) - J_i\left(P_{fi} - P_{in}\right) - \left[K_{ei}\int\left(E_{DGi} - E_{pcci}\right)\right]B_i, \quad (10)$$

To prove the efficiency of the proposed synchronization and power sharing strategies, the mesh microgrid in Figure 2 is modeled using the Simscape toolbox of Matlab/Simulink. Source 1 and Source 2 of Figure 2 are modeled by two controllable voltage sources shown in Figure 4, connected to two different PCCs and controlled by $E_{abc_{refi}}$, which was generated using the modified droop strategy described by Equations (9) and (10), a power calculation bloc, a power filter, park transform and inverse park transform, as explained in the equivalent synoptic diagram describing a droop-controlled DGi in Figure 5. The main microgrid parameters are listed in Table 1. The powers of sources and loads are listed in Table 2.
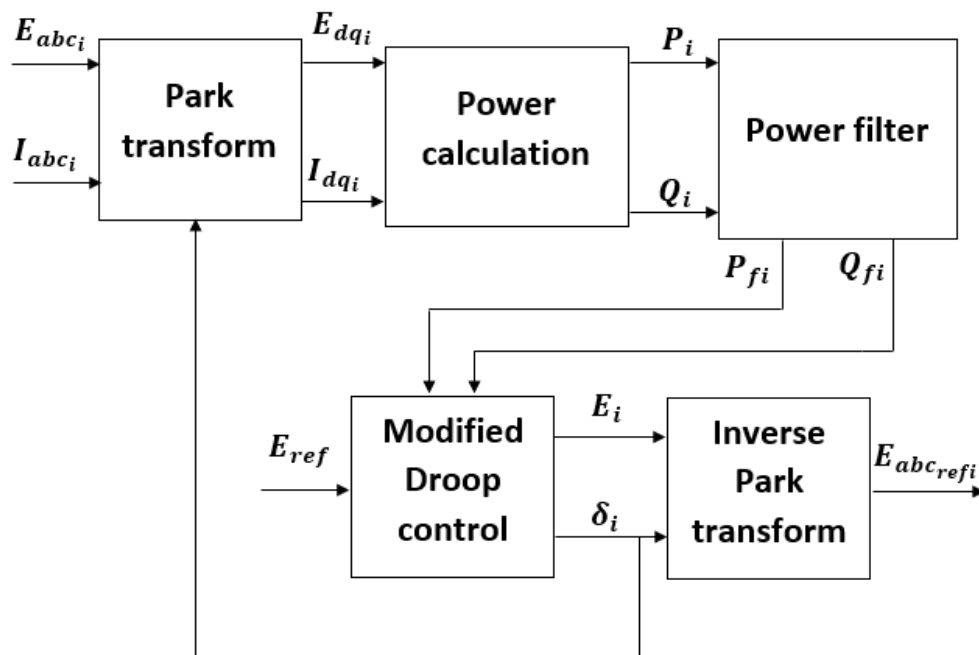
Figure 5. Equivalent synoptic diagram describing a droop-controlled DGi.

Based on this Simscape model, the efficiency of the proposed synchronization and power sharing strategies assumed in Equations (9) and (10) is evaluated. Figure 6a and 6b show the evolution of the active and reactive powers delivered by DG1 and DG2. In the beginning, the first DG (DG1) imposes the frequency of the microgrid as well as the voltages of each PCC; up to t = 5 s, DG1 supplies the loads connected to the microgrid. The second generator (DG2) is synchronized during the interval 1–5, and then it is connected to the microgrid at t = 5 s. The power-sharing of the active and reactive powers are ensured in steady state without being affected by the synchronization procedure. In addition, compared to the previous results shown in Figure 3a,b, the power peaks appearing after the connection of DG2 to the microgrid are considerably attenuated. It should be noted that these performances are maintained with a higher number of DGs connected to the microgrid, even though the results are not presented in this paper.
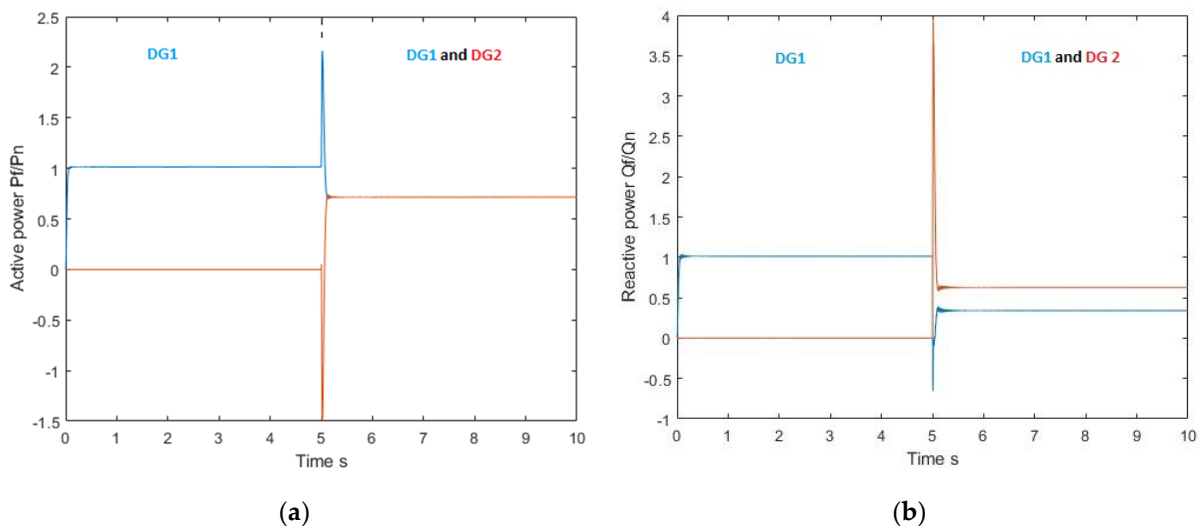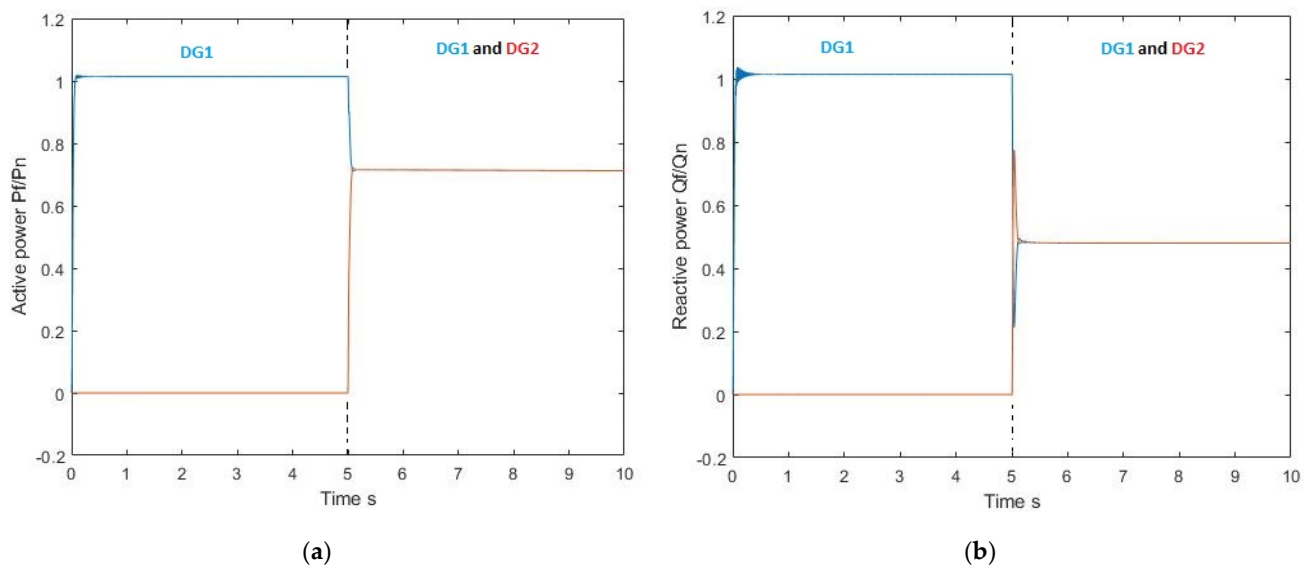
Figure 6. Evolution of the DG active (**a**) and reactive (**b**) powers (first DG supplies the microgrid up to 5 s, the second DG is connected to the microgrid at 5 s).

In order to highlight the effect of the loss of the information on E_{ref}, a simulation test was made using the developed model in Simscape environment, and the results are shown in Figure 5. It consists of connecting both DGs to the microgrid at 0 s using the control strategy defined in Equations (6) and (7). The information on E_{ref} is lost at 4 s and becomes available again at 8 s, and in this scenario Figure 7a,b show the evolution of the active and reactive powers, respectively. The active power sharing is not affected by the loss of information on E_{ref} because it only depends on the frequency, being the same in all the microgrid PCCs. However, the reactive power sharing is totally lost when the information on E_{ref} is absent, but it is easily regained when the information on E_{ref} becomes available again.
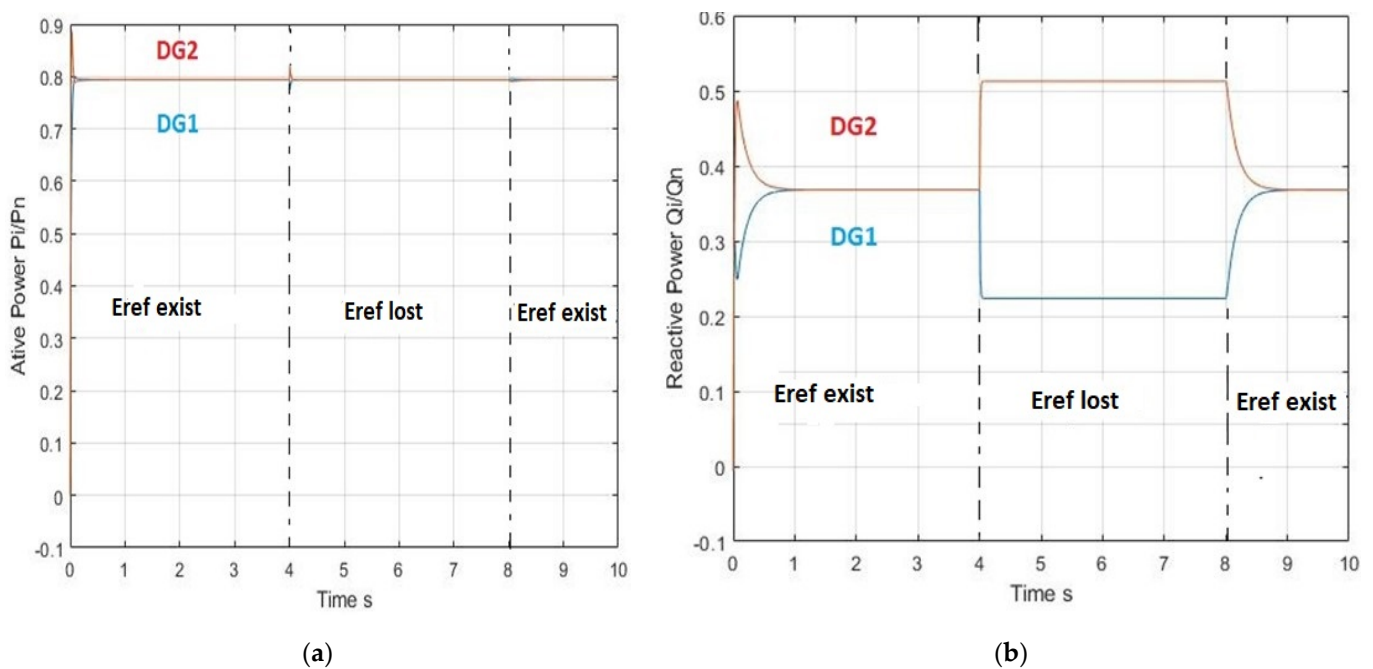
Figure 7. Evolution of the DG active (**a**) and reactive (**b**) powers (both DGs are connected at 0 s).

Even though the considered microgrid including its loads and DGs are well controlled, the synthesis of the droop control parameters is not based on a methodical approach; they are tuned by trial-and-error method using Simscape.

This method cannot guarantee the system stability when the parameters of the load change or additional dynamical constant power loads (CPL) are connected to the microgrid. For example, when a CPL is added to the microgrid it is not evident to foresee the system stability with the variation of its absorbed active power. Figure 8 shows that, as previously, the first DG1 imposes the frequency of the microgrid as well as each PCC voltage of up to t = 5 s and supplies the R–L loads connected to the microgrid. The second generator (DG2) is synchronized and connected to the microgrid at t = 5 s. A dynamic CPL is connected parallel to load 1 (see Figure 2) at t = 7 s, absorbing an active power of 120 kW and zero reactive power. The active power absorbed by this CPL is increased to 500 kW at t = 8 s. It can be remarked that the connection of the CPL absorbing 120 kW does not impact the stability, but when its absorbed power increases to 500 kW the system becomes unstable. Hence, for each modification, the trial-and-error method should be applied again in order to find the eventual new values of the microgrid control parameters which may ensure its stability. In order to overcome this constraint, one solution consists of establishing the state-model that represents the microgrid including its control and studying the microgrid stability by calculating its Jacobean matrix and its eigenvalues at each operating point, as is detailed in the next section.
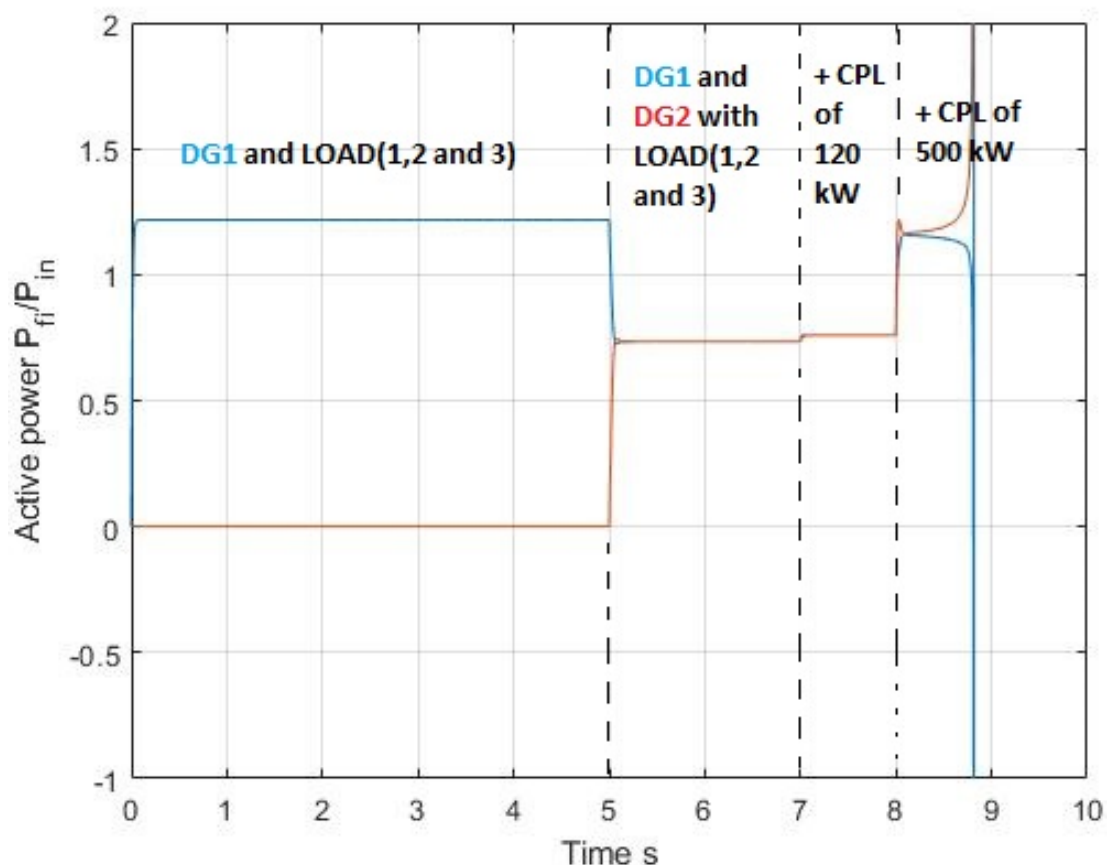
Figure 8. Evolution of the DG active power under different state of charge (first DG supplies the microgrid up to 5 s, the second DG is connected to the microgrid at 5 s).

3. System Modeling for Its Stability Analysis

Due to the interaction between the DGs and the loads, the stability of the microgrids is strongly influenced. Therefore, to study the stability and robustness of the droop-controlled

microgrid, a complete mathematical dynamic model of the whole system is established in this section.

3.1. State-Space Model of a Distributed Generator (DG)

The equations describing the behavior of the *i*th DG are presented on the equivalent synoptic diagram of Figure 9. It is composed of four cascaded blocs for which the relationship between their outputs and inputs are presented in the following.
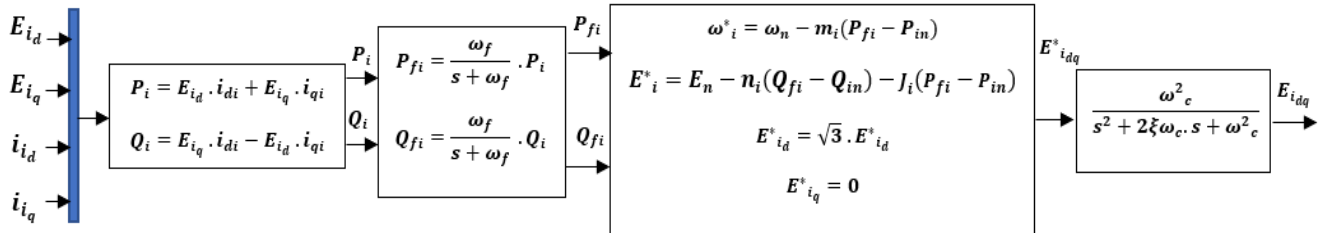
Figure 9. Equivalent synoptic diagram describing a droop-controlled DGi.

In the first bloc (Figure 9), the *i*th DG measured voltages (E_{i_d}, E_{i_q}) and currents (i_{di}, i_{qi}) are used to calculate the instantaneous active and reactive powers using classical Equations (11) and (12).

$$P_i = E_{i_d} \cdot i_{i_d} + E_{i_q} \cdot i_{i_q} \tag{11}$$

$$Q_i = E_{i_q} \cdot i_{i_d} - E_{i_d} \cdot i_{i_q} \tag{12}$$

In the second bloc, the instantaneous active and reactive powers (P_i and Q_i) are filtered using a first-order low-pass filter to obtain the average (filtered) values P_{fi} and Q_{fi} using Equations (13) and (14). It should be emphasized that the cut-off frequency ω_f of the filter is related to the dynamics of the droop control-loop.

$$\frac{d}{dt} P_{fi} = \omega_f \left(P_i - P_{fi} \right) = \omega_f \left(P_i - P_{fi} \right) \tag{13}$$

$$\frac{d}{dt} Q_{fi} = \omega_f \left(Q_i - Q_{fi} \right) = \omega_f \left(Q_i - Q_{fi} \right) \tag{14}$$

The third bloc applies the modified droop control in Equations (6)–(8), using P_{fi} and Q_{fi} to achieve the active and reactive power sharing.

The fourth bloc models the delay imposed by the voltage source inverter (VSI), controlling the *i*th DG output voltages by means of a second-order filter. This filter has a faster dynamic compared to the external droop control loop $\omega_c \gg \omega_f$. The relationship between the output voltage of the *i*th DG and its voltage reference is expressed by the transfer function defined in Equation (15):

$$\frac{E_{i_{dq}}}{E^*_{i_{dq}}} = \frac{\omega_c^2}{s^2 + 2\xi\omega_c.s + \omega_c^2}, \tag{15}$$

3.2. Microgrid Structure and Modeling

Figure 10 shows a microgrid inspired from the IEEE 9bus test feeder that differs slightly from the microgrid of Figure 2 and contains an additional CPL. In fact, this type of load is increasingly present in microgrids and imposes more severe constraints to the system stability. The considered microgrid is composed of two DGs powering three classical inductive loads, modeled by serial R–L circuits, and a CPL load. They are interconnected by RLC power lines to represent a mesh multi-PCC microgrid. The line connecting the PCC_i and PCC_j have a resistance r_{ij}, an inductance l_{ij}, and a capacitance of c_{ij}. Their values are determined knowing the distance between the considered PCCs. The capacitance c_{ij} is connected to the PCC_j.
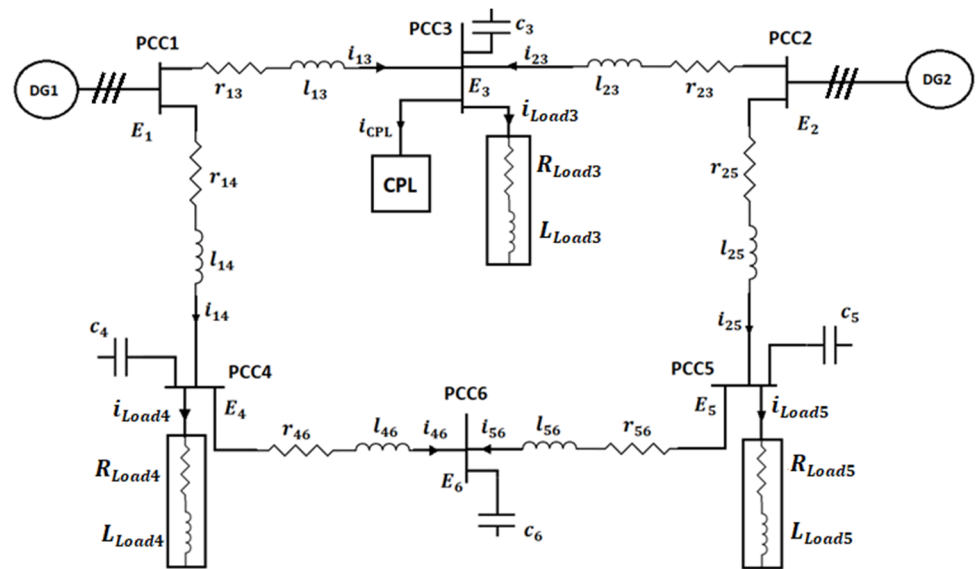
Figure 10. IEEE 9bus test feeder.

In order to study the considered microgrid having two DGs, the state equations are given using a common reference frame for expressing the different variables. The used d–q reference frame is defined in a way that its d-axis is oriented toward the first DG voltage vector ($\overline{E}_1$ Figure 11). Then, the d-axis is shifted by δ_1 with respect to the α-axis, where δ_1 is the argument of the DG1 voltage vector ($\overline{E}_1 = E_1 e^{j\delta_1} = E_{1_\alpha} + jE_{1_\beta}$). The rotating d–q reference frame turns with an electrical speed of $\omega_1 = \frac{d\delta_1}{dt}$ with respect to the fixed reference frame $\alpha - \beta$. When the different DGs are synchronized and connected to the microgrid, their pulsations vary simultaneously. Then, the pulsations of the DG1 and DG2 voltages ($\omega_1 = \frac{d\delta_1}{dt}$ and $\omega_2 = \frac{d\delta_2}{dt}$) are the same (i.e., $\omega_1 = \omega_2 = \omega_{com}$)). Knowing that the phase voltages of DG1 and DG2 (connected to PCC1 and PCC2) have the RMS values of E_1 and E_2, the $\alpha - \beta$ components of $\overline{E}_1$ and $\overline{E}_2$ are obtained using the Concordia transformation T^t_{32} in (16) and (17):

$$\begin{pmatrix} E_{1_\alpha} \\ E_{1_\beta} \end{pmatrix} = T^t_{32} \begin{bmatrix} E_{1_a} \\ E_{1_b} \\ E_{1_c} \end{bmatrix} = \begin{pmatrix} \sqrt{3}.E_1.\cos\delta_1 \\ \sqrt{3}.E_1.\sin\delta_1 \end{pmatrix} \text{ and } \begin{pmatrix} E_{2_\alpha} \\ E_{2_\beta} \end{pmatrix} = T^t_{32} \begin{bmatrix} E_{2_a} \\ E_{2_b} \\ E_{2_c} \end{bmatrix} = \begin{pmatrix} \sqrt{3}.E_2.\cos\delta_2 \\ \sqrt{3}.E_2.\sin\delta_2 \end{pmatrix} \quad (16)$$

$$\text{where}: \ T^t_{32} = \sqrt{\frac{2}{3}}.\begin{bmatrix} 1 & -\frac{1}{2} & -\frac{1}{2} \\ 0 & \frac{\sqrt{3}}{2} & -\frac{\sqrt{3}}{2} \end{bmatrix}, \quad (17)$$
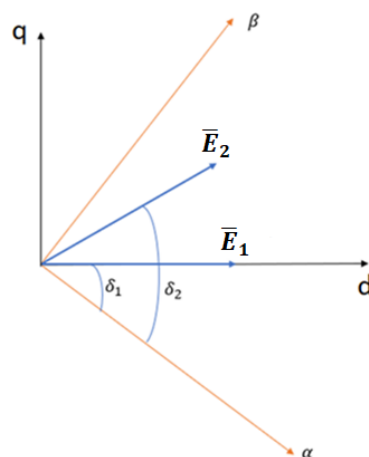
Figure 11. Reference frames $\alpha - \beta$ and d $-$ q.

Then, Equations (18) and (19) give the relationship between the d–q components of the voltage vectors at PCC_1 and PCC_2 and their $\alpha - \beta$ components.

$$DG1: \begin{cases} \begin{pmatrix} E_{1_d} \\ E_{1_q} \end{pmatrix} = P(-\delta_1) \cdot \begin{pmatrix} E_{1_\alpha} \\ E_{1_\beta} \end{pmatrix} = \begin{pmatrix} \cos\delta_1 & \sin\delta_1 \\ -\sin\delta_1 & \cos\delta_1 \end{pmatrix} \cdot \begin{pmatrix} \sqrt{3}.E_1.\cos\delta_1 \\ \sqrt{3}.E_1.\sin\delta_1 \end{pmatrix} \\ \begin{pmatrix} E_{1_d} \\ E_{1_q} \end{pmatrix} = \begin{pmatrix} \sqrt{3}.E_1 \\ 0 \end{pmatrix} \end{cases}, \quad (18)$$

$$DG2: \begin{cases} \begin{pmatrix} E_{2_d} \\ E_{2_q} \end{pmatrix} = P(-\delta_1) \cdot \begin{pmatrix} E_{2_\alpha} \\ E_{2_\beta} \end{pmatrix} = \begin{pmatrix} \cos\delta_1 & \sin\delta_1 \\ -\sin\delta_1 & \cos\delta_1 \end{pmatrix} \cdot \begin{pmatrix} \sqrt{3}.E_2.\cos\delta_2 \\ \sqrt{3}.E_2.\sin\delta_2 \end{pmatrix} \\ \begin{pmatrix} E_{2_d} \\ E_{2_q} \end{pmatrix} = \begin{pmatrix} \sqrt{3}.E_2.\cos(\delta) \\ \sqrt{3}.E_2.\sin(\delta) \end{pmatrix} \text{with}: \ \delta = \delta_2 - \delta_1 \end{cases}, \quad (19)$$

Equation (20) presents a network model of N power lines of a mesh microgrid, interconnecting its PCC_i and PCC_j, where i and $j \in [1, 2, \ldots, N]$ and $i \neq j$ (Figure 10).

$$\begin{cases} \frac{d}{dt}i_{ij_d} = \frac{1}{l_{ij}}\Delta E_{ij_d} - \frac{r_{ij}}{l_{ij}}i_{ij_d} + \omega_{com}i_{ijq} \\ \frac{d}{dt}i_{ij_q} = \frac{1}{l_{ij}}\Delta E_{ij_q} - \frac{r_{ij}}{l_{ij}}i_{ij_q} + \omega_{com}i_{ijd} \\ \text{where}: \quad \Delta Eij_d = \left(E_{i_d} - E_{j_d}\right) \quad \Delta Eij_q = \left(E_{i_q} - E_{j_q}\right) \end{cases}, \quad (20)$$

E_{i_d} and E_{i_q} are the d–q components of PCC_i voltage. The loads considered in this work were serial passive R–L loads and an active CPL (Figure 10). With the sum of the current connected to PCC_i being zero (Kirchhoff current law), Equation (21) relates to all PCCs except the ones connected to the DGs for which the voltages are imposed by their droop controllers.

$$\begin{cases} \frac{d}{dt}E_{i_d} = \frac{1}{C_i}\left(-i_{Loadi_d} - i_{CPLi_d} + \sum_j i_{ji_d}\right) + \omega_{com}.E_{i_q} \\ \frac{d}{dt}E_{i_q} = \frac{1}{C_i}\left(-i_{Loadi_q} - i_{CPLi_q} + \sum_j i_{ji_q}\right) - \omega_{com}.E_{i_d} \end{cases}, \quad (21)$$

It should be noted that $\sum_j i_{ji}$ in Equation (17) is the sum of the currents of the power lines connected to PCC_i. i_{CPLid} and i_{CPLiq} are the d–q components of the current absorbed by the active CPL_i. The non-linear Equation (22) allows the determination of these components knowing the active and reactive powers P_{CPLi} and Q_{CPLi} absorbed by CPL_i.

$$\begin{cases} \begin{pmatrix} P_{CPLi} \\ Q_{CPLi} \end{pmatrix} = \begin{pmatrix} E_{i_d} & E_{i_q} \\ E_{i_q} & -E_{i_d} \end{pmatrix} \cdot \begin{pmatrix} i_{CPLid} \\ i_{CPLiq} \end{pmatrix} \\ \begin{pmatrix} i_{CPLid} \\ i_{CPLiq} \end{pmatrix} = \frac{1}{E_{i_d}{}^2 + E_{i_q}{}^2} \cdot \begin{pmatrix} E_{i_d} & E_{i_q} \\ E_{i_q} & -E_{i_d} \end{pmatrix} \cdot \begin{pmatrix} P_{CPLi} \\ Q_{CPLi} \end{pmatrix} \end{cases}, \quad (22)$$

The d–q components of the R–L load current connected to PCC_i (i_{Loadi_d} and i_{Loadi_q}) can be determined using Equation (23):

$$\begin{cases} \frac{d}{dt}i_{Loadi_d} = \frac{1}{L_{Loadi}}\left(E_{i_d} - R_{Loadi} \cdot i_{Loadi_d}\right) + \omega_{com} \cdot i_{Loadi_q} \\ \frac{d}{dt}i_{Loadi_q} = \frac{1}{L_{Loadi}}\left(E_{i_q} - R_{Loadi} \cdot i_{Loadi_q}\right) - \omega_{com} \cdot i_{Loadi_d} \end{cases}, \quad (23)$$

where R_{Loadi} and L_{Loadi} represent the resistance and inductance of the RL load.

The overall model of the microgrid presented in Figure 10 including its control, defined by the previous equations, has 40 state variables which constitute the elements of the state vector x, described in the following (24):

$$\begin{aligned} [x]^T = & [i_{13_d} \ i_{13_q} \ i_{23_d} \ i_{23_q} \ i_{25_d} \ i_{25_q} \ i_{14_d} \ i_{14_q} \ i_{56_d} \ i_{56_q} \ i_{46_d} \ i_{46_q} \ E_{1_d} \ E_{1_q} \ E_{2_d} \ E_{2_q} \ E_{3_d} \ E_{3_q} \ E_{4_d} \ E_{4_q} \ E_{5_d} E_{5_q} \\ & E_{6_d} \ E_{6_q} \ i_{Load3_d} \ i_{Load3_q} \ i_{Load4_d} \ i_{Load4_q} \ i_{Load5_d} \ i_{Load5_q} \ P_{f1} \ Q_{f1} \ P_{f2} \ Q_{f2} \ \delta \ \dot{E}_{1_d} \ \dot{E}_{1_q} \ \dot{E}_{2_d} \ \dot{E}_{2_q} \ J_i], \end{aligned} \quad (24)$$

Considering the non-linear Equations (7), (11), (12), (19) and (21), the overall microgrid model is non-linear and can be finally put into the following form:

$$\dot{x} = f(x) \text{ with } f : R^n \rightarrow R^n,\ n = 40, \tag{25}$$

3.3. Validation of the State Model

The results concerning the evolution of the microgrid active and reactive powers, obtained under the same conditions using the Simscape model and the established state model, were used to validate the established state model. The same simulation scenario was considered for obtaining the simulation results using both models. Both DGs were connected to the microgrid at 0 s. The simulation results of both considered models are presented in Figure 12a,b, illustrating the evolution of the active and reactive powers of DG1 and DG2. Both models led to similar results; therefore, the established state model is considered validated. Thus, it can be used for studying the microgrid stability, integrating its control. To further confirm the validity of the developed model, Figure 12c shows a zoomed-in view of the transitory state after the connection of both DGs at 0 s.
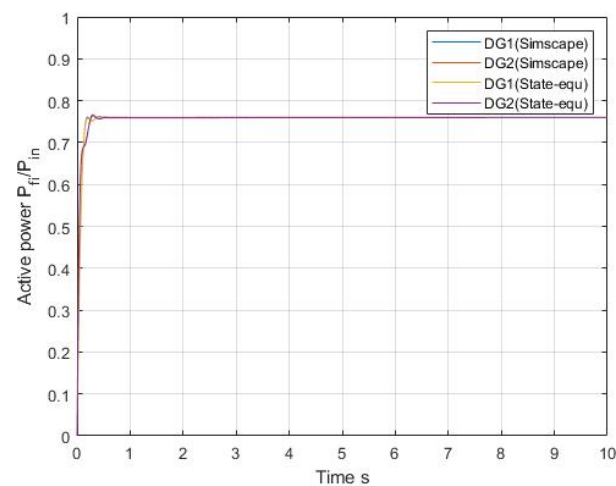
(**a**)
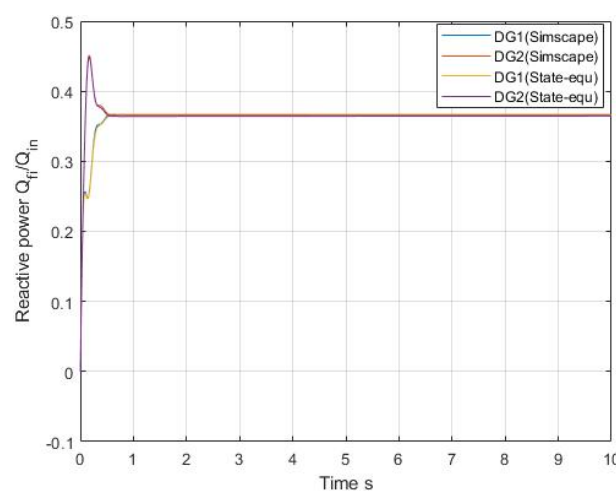
(**b**)

Figure 12. *Cont.*
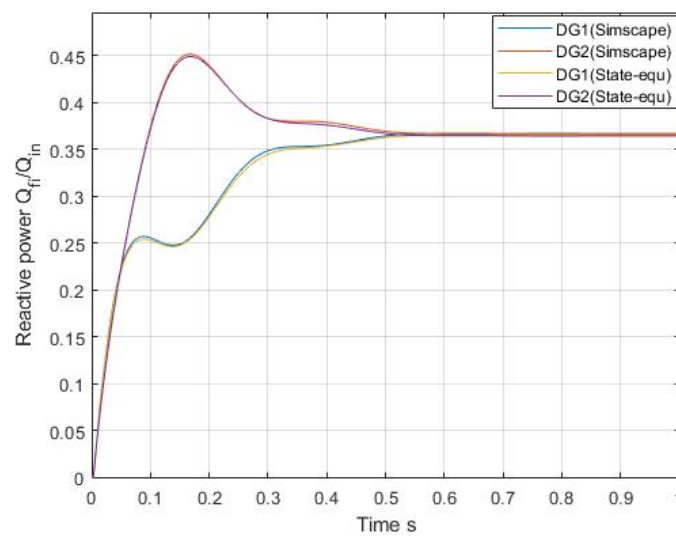
(**c**)

Figure 12. Simulation results obtained using Simscape and the mathematical state-model. Both DGs were connected to the microgrid at 0 s. (**a**) Evolution of the DGs per unit active powers. (**b**) Evolution of the DGs per unit reactive powers. (**c**) Zoomed-in view of the per unit reactive powers around 0 s.

4. Mesh Microgrid Stability and Robustness of its Control

4.1. Jacobian Matrix Eigenvalues

In order to study the stability of the microgrid, defined by the continuous nonlinear differential system (24), and to analyze its dynamic behavior, which is affected by several control parameters, an eigenvalue sensibility analysis was performed by means of the calculation of the eigenvalues of the Jacobian matrix $\left(\frac{\partial f}{\partial x}\right)_{x_0}$ at the operating point $f(x_0) = 0$. The system, i.e., the microgrid, will be asymptotically stable around the operating point x_0 if the real parts of all eigenvalues are strictly negative.

The system parameters are given in Tables 3–5. The classical loads were modelled by serial R–L loads. The values of R and L were chosen depending on the operating point of these loads. The CPL was defined by constant values of its absorbed active and reactive powers, which may vary depending on its chosen operating point. The parameters of the DGs corresponded to their rated powers (available powers) and the parameters imposing the dynamic behavior of their control (ω_f, ω_c, ξ, permissible variations of pulsation Δ_ω and voltage Δ_E).

Table 3. Parameters of the considered microgrid power lines.

Lines	Resistance (Ω)	Inductance (mH)	Capacitance (μF)	Points of Connection
Line 13	0.63	7.14	205	PCC1–PCC3
line 23	0.63	7.14	205	PCC2–PCC3
line 14	2.55	11.4	230	PCC1–PCC4
line 25	2	7	180	PCC5–PCC2
line 56	1.7	7.6	153.4	PCC5–PCC6
line 46	1.7	7.6	153.4	PCC4–PCC6

Table 4. Parameters of the considered microgrid power loads.

Serial RL Loads	Resistance (Ω)	Inductance (H)
Load 1	376.47	0.2496
Load 2	319.467	0.1765
Load 3	252.8977	0.1564
Load CPL	Pc = 100 KW	Qc = 0 VAR

Table 5. Parameters of the considered DGs.

DGs	Rated Active Power (MW)	Rated Reactive Power (Mvar)	Rated Phase to Phase Voltage (kV)	Cut-Off Frequency Power Calculation Filter (rad/s)	Cut-Off Frequency Second Order Filter (rad/s)	Damping Factor	Permissible Variations of Pulsation (for Droop Control)	Permissible Variations of Voltage (for Droop Control)
DG1	$P_{1n} = 3$	$Q_{1n} = 0.9$	20	$\omega_{f1} = 20$	$\omega_{c1} = 1000$	$\xi = 0.7$	$\Delta_\omega = 0.5$	$\Delta_E = 6$
DG2	$P_{2n} = 2$	$Q_{2n} = 0.9$	20	$\omega_{f2} = 20$	$\omega_{c2} = 1000$	$\xi = 0.7$	$\Delta_\omega = 0.5$	$\Delta_E = 6$

The eigenvalues of the system at the considered operating point, corresponding to the parameters of the loads and DGs given in Tables 4 and 5, are shown in Table 6. It can be observed that four of the Jacobian matrix eigenvalues are the negative real numbers, and that the other 36 eigenvalues are two by two the complex conjugate numbers, having negative real parts.

Table 6. Eigenvalues under nominal operating condition.

λ	Value
$\lambda_{1,2}$	$-287 \pm 37,510i$
$\lambda_{3,4}$	$-287 \pm 36,756i$
$\lambda_{5,6}$	$-53 \pm 26,120i$
$\lambda_{7,8}$	$-54 \pm 26,562i$
$\lambda_{9,10}$	$-484 \pm 26,915i$
$\lambda_{11,12}$	$-484 \pm 27,669i$
$\lambda_{13,14}$	$-360 \pm 15,598i$
$\lambda_{15,16}$	$-360 \pm 14,843i$
$\lambda_{17,18}$	$-1766 \pm 377i$
$\lambda_{19,20}$	$-1488 \pm 377i$
$\lambda_{21,22}$	$-1564 \pm 377i$
$\lambda_{23,24}$	$-86 \pm 377i$
$\lambda_{25,26}$	$-254 \pm 377i$
$\lambda_{27,28}$	$-701 \pm 714i$
$\lambda_{29,30}$	$-700 \pm 714i$
$\lambda_{31,32}$	$-700 \pm 714i$
$\lambda_{33,34}$	$-9 \pm 26i$
λ_{35}	-4.4089
λ_{36}	-17.0790
λ_{37}	-19.9387
λ_{38}	-20.0041
$\lambda_{39,40}$	$-700 \pm 714i$

All of the Jacobian matrix eigenvalues have negative real parts, therefore the microgrid including its DG's control and loads can be considered as a stable system around the considered operating point. The study of the considered mesh microgrid stability around other operating points can also be conducted based on the established state model.

In order to perform the sensitivity analysis and find the origin of different frequency components, depending on the parameters of the established model, the parameters of the different constituents of the microgrid, including its control parameters were modified separately. In the following sections, the evolution of eigenvalue trajectories with variation

of the parameters of each microgrid constituent is discussed to verify their impact on the system stability.

4.2. Eigenvalue Trajectory and Sensibility Analysis for Different Values of Power Line Parameters

To vary the parameters of the 6 power lines of the microgrid, the values of the lengths of all of these power lines are modified by 10 steps of 10% (for each line, from its initial length to two times this length), the Jacobean matrix eigenvalues are determined, and their evolution shown on Figure 13. The variation of the parameters of the power lines only impacts the eigenvalues λ_1 to λ_{12}, which are two by two complex conjugate numbers; the other eigenvalues λ_{13} to λ_{40} do not vary significantly with the evolution of the power line parameters. The real parts of the impacted eigenvalues (λ_1 to λ_{12}) become closer to zero but remain sufficiently negative to not impact system stability when the line parameters are increased within the considered interval. However, if the lengths of the power lines become excessively long, the real parts of the impacted eigenvalues may become positives and cause system instability.
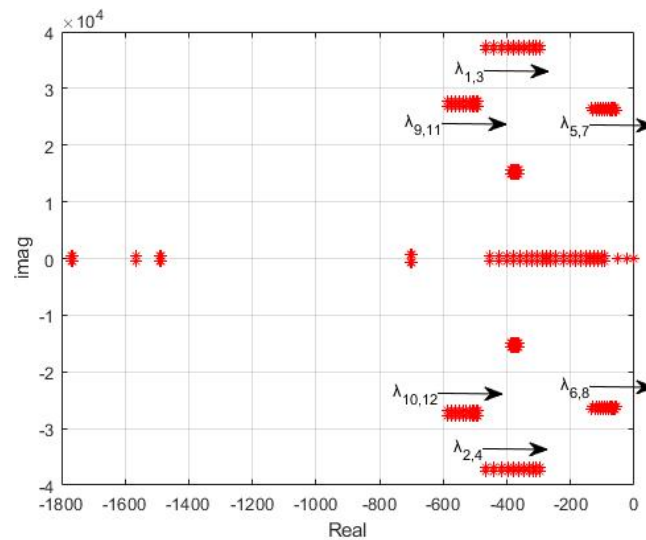
Figure 13. Evolution of eigenvalues corresponding to the change in line parameters.

4.3. Eigenvalue Trajectory and Sensibility Analysis for Different Values of DG Parameters

The same approach as in Section 4.2. is used to study the impact of other parameters that may contribute to the instability of the system. For the considered DGs, the parameters which may impact the system stability are the cut-off frequency ω_f for power calculation (Equations (13) and (14)), the value of the filter's cut-off frequency ω_c of the second order filter (Equation (15)), as well as the frequency drop Δ_ω and the voltage drop Δ_E in Equations (6)–(8).

First, the cut-off frequency ω_f is modified in 10 steps (from its initial value to 10 times this value), the Jacobean matrix eigenvalues are determined, and their evolutions are illustrated in Figure 14. The variation of ω_f impacts the real negative eigenvalues λ_{35}, λ_{36}, λ_{37} and λ_{38} as well as the eigenvalues λ_{33}, λ_{34} which are two complex conjugate numbers. The other eigenvalues do not vary significantly with the evolution of ω_f. It can be seen that when ω_f increases, the eigenvalues λ_{33}, λ_{34}, λ_{36}, λ_{37} and λ_{38} are shifted to the left while λ_{35} moves very slightly toward zero, but its value does not change considerably and stays largely negative (from -4 to -3.6). The system always remains stable when ω_f increases, but the system dynamics become increasingly faster.
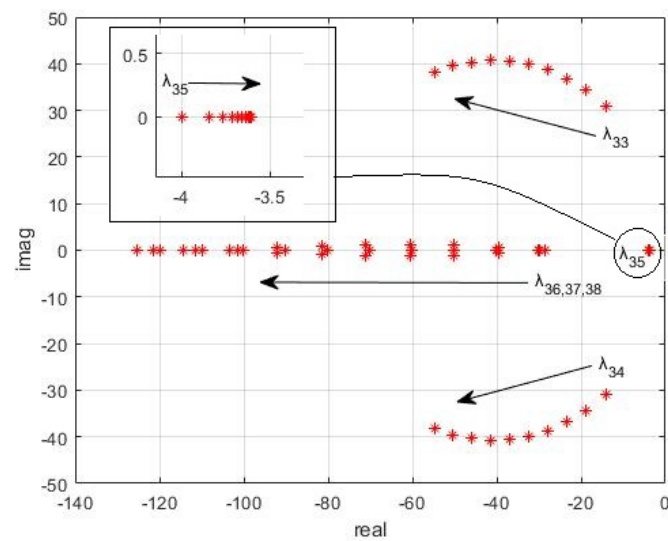
Figure 14. Evolution of eigenvalues corresponding to the change in ω_f ($20 < \omega_f < 200 (\text{rad}/s)$ with ω_f increasing).

To examine the impact of ω_c in Equation (13), representing the delay imposed by the voltage source inverter (VSI) controlling the DG, on the system stability, its value is largely decreased (from its initial value 1000 rad/s to 50 rad/s). The eigenvalues most sensitive to the variation of ω_c are λ_{27} to λ_{32} as well as λ_{39} and λ_{40}, which are two by two of the complex conjugate numbers. As shown in Figure 15, the real parts of the impacted eigenvalues move to the right when ω_c decreases and tend to be positive when ω_c becomes inferior to 50 rad/s, which causes the system instability.
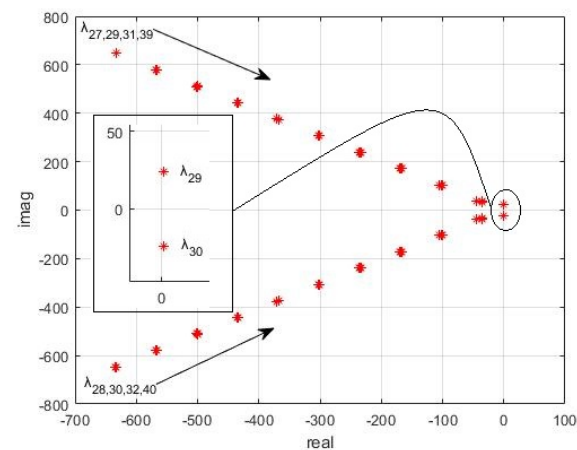
Figure 15. Evolution of eigenvalues corresponding to the change in ω_c ($50 < \omega_c < 1000$ (rad/s) with ω_c decreasing).

To validate these results, the Simscape simulations were made to verify that any value of ω_c inferior to 50 rad/s can cause system instability. The results of the first simulation, made using the Simscape model with $\omega_c = 50$ rad/s, are illustrated on Figure 16a, and those of the second simulation with $\omega_c = 45$ rad/s are shown on Figure 16b. These results confirm the system stability for $\omega_c > 50$ rad/s, as predicted by the stability analysis based on the established state model.
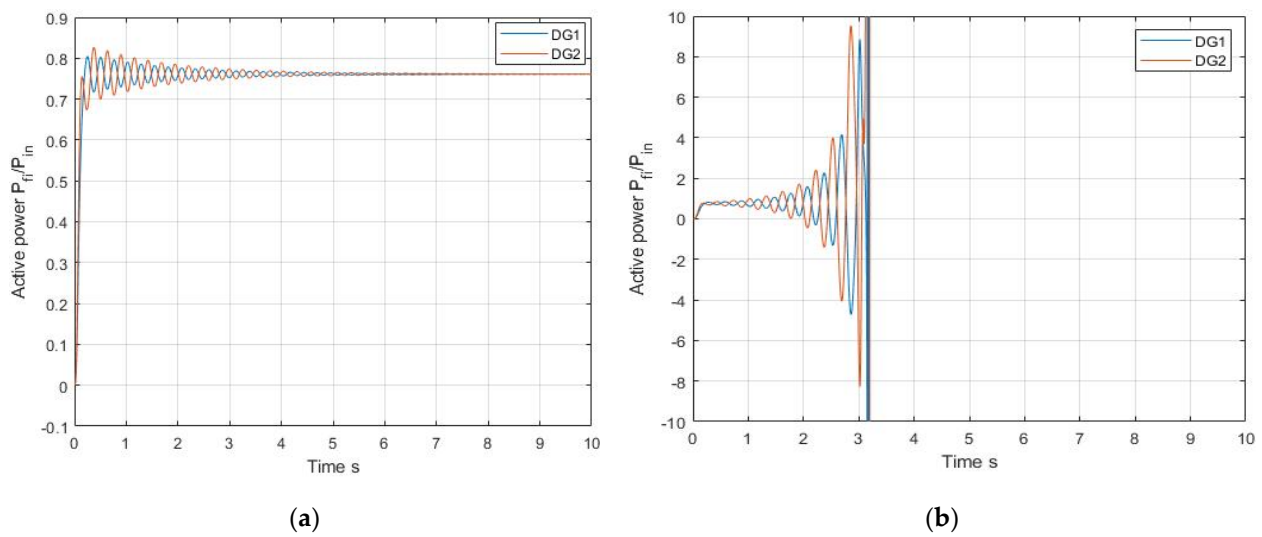
Figure 16. Evolution of the DG active power (Simscape model (both DGs are connected at 0 s)): (**a**) with $\omega_c = 50$ rad/s. (**b**) with $\omega_c = 45$ rad/s.

To evaluate the impact of droop control parameters on the system stability, the frequency drop Δ_ω is increased in 10 steps (from its initial value to 10 times this value). The eigenvalues mostly impacted by this variation are λ_{23} to λ_{26} as well as λ_{33} and λ_{34} which are two by two complex conjugate numbers. As shown in Figure 17 when Δ_ω increases the eigenvalues λ_{23} to λ_{26} move toward the left, while λ_{33} and λ_{34} move toward the right side of the real axis and become positive for $\Delta_\omega \geq 5$ rad/s. By following the same approach as Simscape, simulations were made to verify that any value of Δ_ω superior or equal to 5 rad/s can cause the system instability. The results of the first simulation, made using the Simscape model with $\Delta_\omega = 4.5$ rad/s, are illustrated In Figure 18a, and those of the second simulation with $\Delta_\omega = 5$ rad/s are shown In Figure 18b. These results confirm the system instability for $\Delta_\omega \geq 5$ rad/s, as predicted by the stability analysis based on the established state model.
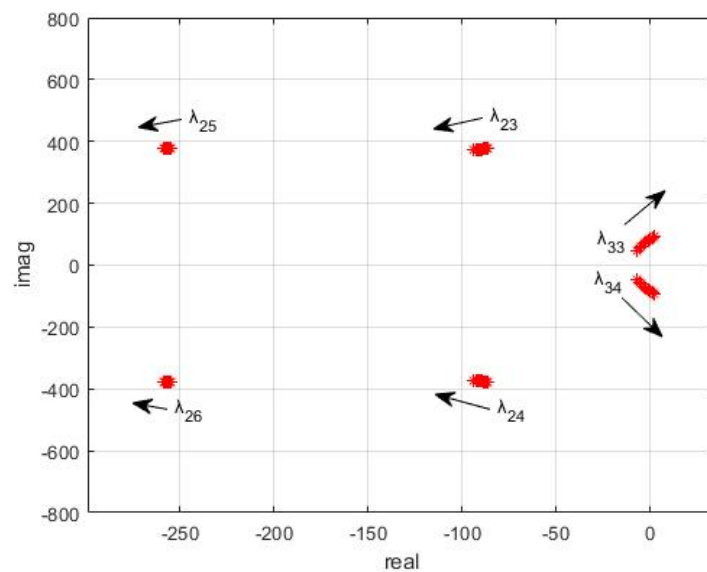
Figure 17. Evolution of eigenvalues corresponding to the change in Δ_ω ($0.5 < \Delta_\omega < 5.5$ (rad/s)) with Δ_ω increasing.
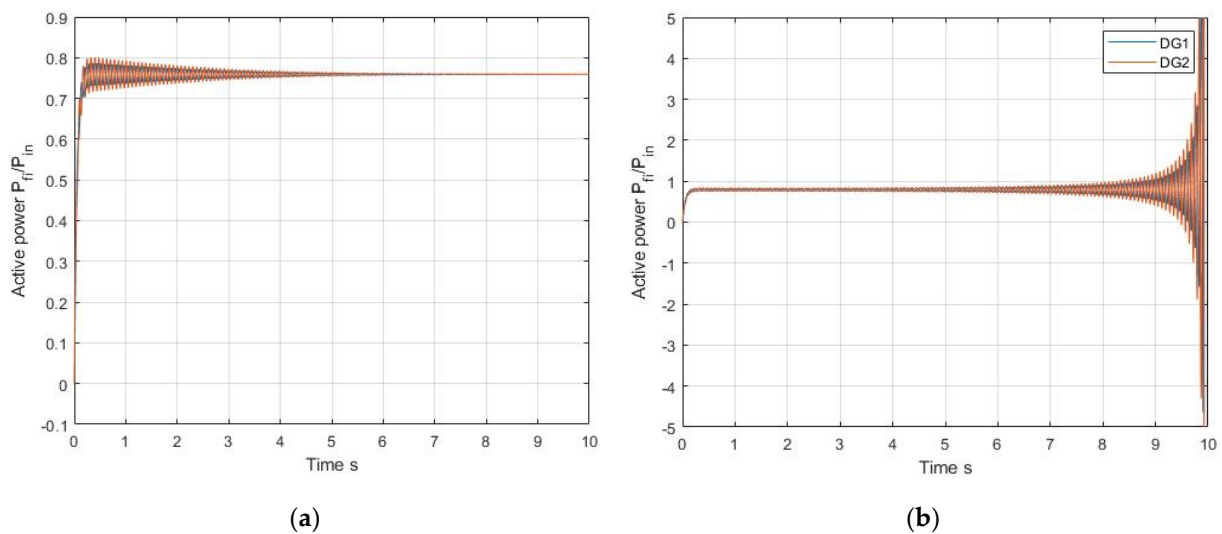
Figure 18. Evolution of the DGs active power (Simscape model, both DGs connected at 0 s): (**a**) Δ_ω = 4.5 rad/s and (**b**) Δ_ω = 4.5.

The voltage drop Δ_E is the last parameter of the DGs for which its impact on the system stability is studied. This has been done by varying Δ_E from its initial value to 10 times this value. The eigenvalues mostly impacted by this variation are λ_{23} and λ_{24}, which are the complex conjugate numbers with a negative real part as well as λ_{36} which is a real negative number. When the voltage drop increases, Figure 19 shows that λ_{36} moves to the left while λ_{23} and λ_{24} move slightly to the right but remain negative. Thus, contrary to Δ_ω, the voltage drop Δ_E has a negligible impact on the system stability.
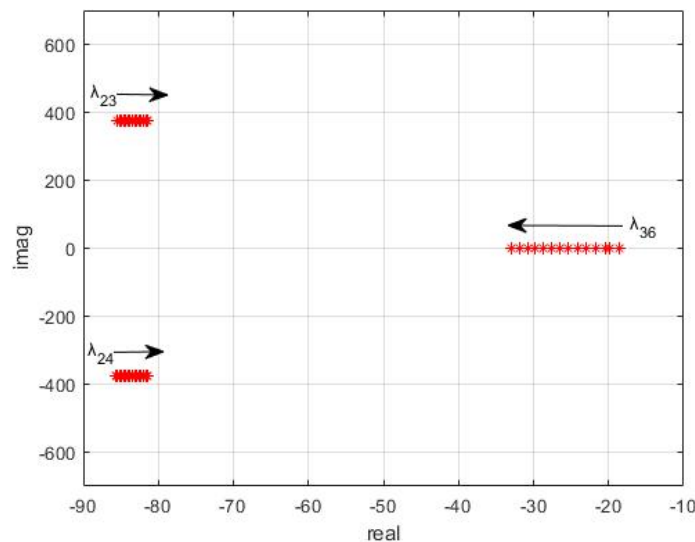
Figure 19. Evolution of Eigenvalues with the change in voltage drop $6 < \Delta_E < 70(V)$ with Δ_V increasing.

4.4. Eigenvalue Trajectory and Sensibility Analysis for Different Values of Load Parameters

In order to explain the effect of load variation on system stability, a study of the variation of dominant eigenvalue trajectories under different load conditions is established. Starting with the CPL type, Figure 20a,b show the trajectory of the eigenvalues under the effect of the change in active P_c and reactive Q_c powers absorbed by the CPL. As the active power or the reactive power absorbed by the CPL increases up to 120 kW (with fixed $Q_c = 0$) and 72 kVAr (with fixed $P_c = 100$ kW), respectively, the eigenvalues λ_5 to λ_8 are the most sensitive to the change of P_c or Q_c of the CPL. The other eigenvalues do not vary

with the evolution of P_c or Q_c. When the active power (P_c) absorbed by the CPL increases from 100 kW up to 120 kW (with fixed $Q_c = 0$), the eigenvalues λ_7 and λ_8 move to the left far away from zero while λ_5 and λ_6 move toward the right but remain sufficiently negative. In the same manner, when the reactive power (Q_c) absorbed by the CPL increases from zero up to 72 kVAr (with fixed $P_c = 100$ kW), the eigenvalues λ_7 and λ_8 move to the left while λ_5 and λ_6 move toward the right. For the considered intervals of the active power and reactive power, the real part of λ_5 and λ_6 remains sufficiently negative and the system stability is not affected. However, when the active power P_c or the reactive power Q_c become greater than certain limits, the real parts of the eigenvalues λ_5 and λ_6 become positive which causes system instability. For example, when Q_c is fixed to zero, the limit value of active power P_c absorbed by the CPL is 124.5 kW, beyond this value, the real part of the eigenvalues λ_5 and λ_6 becomes positive (Figure 21a for $P_c = 124$kW and $P_c = 126$kW) and the system cannot be considered asymptotically stable around the considered operating point. In the same manner, when P_c is fixed to 100 kW, the limit value of reactive power Q_c absorbed by the CPL is 74.3 kVAr; beyond this value, the real part of the eigenvalues λ_5 and λ_6 becomes positive (Figure 21b for $Q_c = 73$ kVAr and $Q_c = 74$ kVAr).
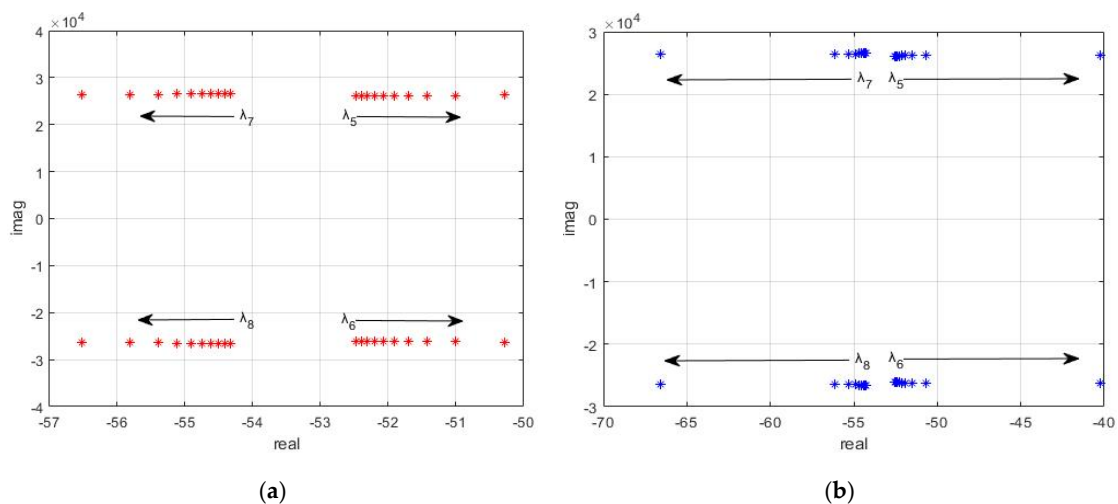
Figure 20. Evolution of eigenvalues with the change of the CPL active and reactive power: (**a**) P_c increasing $100(\text{kW}) < P_c < 120(\text{kW})$ and $Q_c = 0$; (**b**) Q_c increasing $0 < Q_c < 72(\text{kVAr})$ and $P_c = 100$ kW.
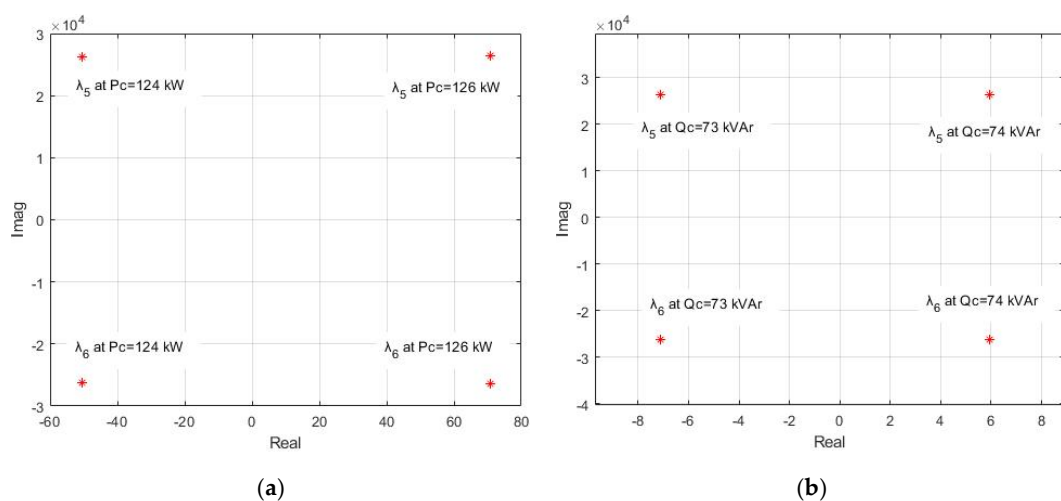
Figure 21. Evolution of the eigenvalues with the change of the CPL active or reactive power around their limited values: (**a**) active power variation from $P_c = 124$ kW to $P_c = 126$ kW when $Q_c = 0$; (**b**) reactive power variation from $Q_c = 73$ kVAr to $Q_c = 74$ kVAr when $P_c = 100$ kW.

To confirm the results concerning the stability limits imposed by the CPL, the Simscape simulations were made for two values of the CPL active power, one less than the active power limit (P_c = 124 kW) and another one higher than this limit (P_c = 125kW) and the results are shown in Figure 22a,b. These results are in perfect accordance with the conclusions drawn from the established state model relating to the impact of the CPL on the stability of the considered system.
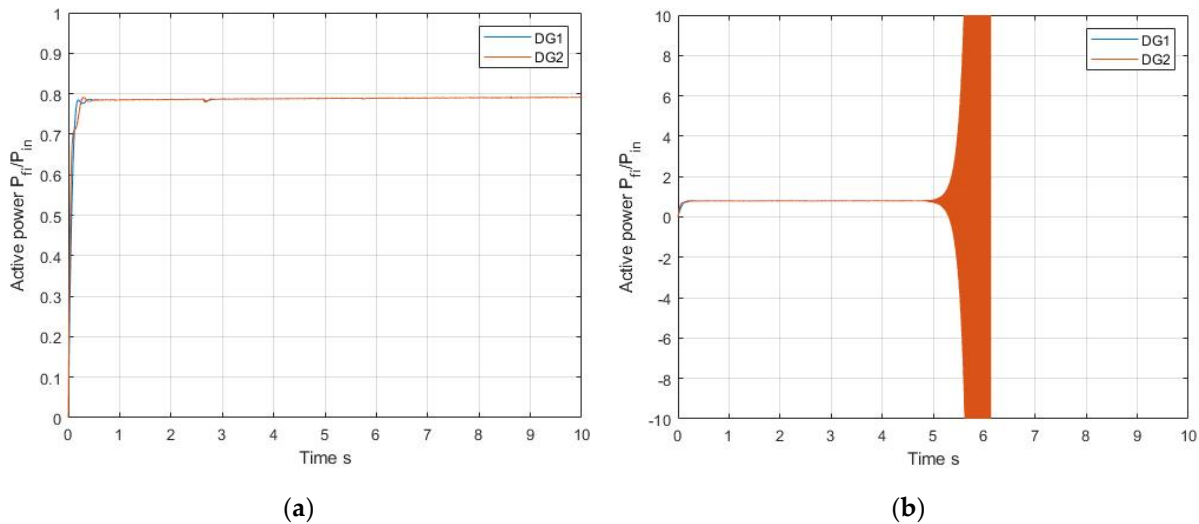
Figure 22. Evolution of the DGs active power (Simscape model with both DGs connected at 0 s): (**a**) P_c = 124 kW. (**b**) P_c = 125 kW.

In order to maintain the microgrid stability for higher values of active power absorbed by the CPL, one solution consists of adding a capacitor to the PCC to which the CPL is connected. Then, the established state model can be used to dimension the necessary capacitor value for the required CPL active power. For the considered microgrid, the CPL is connected to PCC3, and based on the above analysis, the system stability is affected when the CPL active power becomes higher than 124 kW. The latter active power limit can be augmented; for example, to P_c = 620 kW by imposing an adapted value to the capacitor connected to PCC3. This value can be determined using the established state model.

When $Q_c = 0$, the limit value of active power P_c absorbed by the CPL becomes 620 kW when the capacitor c_3 is modified from 0.4 μF to 2 μF. Figure 23 shows that the real part of the eigenvalues λ_5 and λ_6 is negative for P_c = 620 kW and positive for P_c = 625 kW. Then the microgrid stability is ensured up to P_c = 620 kW. This result is in perfect accordance with the Simscape simulation results shown in Figure 24a,b. Hence, the stability analysis based on the established state model can be used as a powerful tool to adjust mesh microgrids to guarantee their stability when their loads or even their architectures change.

Concerning the serial R–L loads in the microgrid, the impact of their variations on the system stability is studied by analyzing the evolution of the eigenvalues mostly impacted by the change under constant power factor of each RL-load connected to a given PCC. In fact, the power factor of classical loads is usually higher than 0.92 and its variation can be neglected. For the three serial RL-loads of the considered microgrid shown in Figures 10 and 25–27 show the evolution of the eigenvalues mostly impacted by varying (from initial value to 50% of this value) the impedances of RL-load3, RL-load4 and RL-load5 under constant power factor, respectively. The most impacted eigenvalues in this case are λ_1 to λ_{12}, which correspond to line current equations and λ_{13} to λ_{20} as well as λ_{25} and λ_{26}, which correspond to the PCC voltage equations. It can be noticed that when the value of each RL-load decreases under constant power factor, the eigenvalues mostly impacted move to the right but remain sufficiently negative and do not impact the system stability as long as the load variation is within the indicated power range.
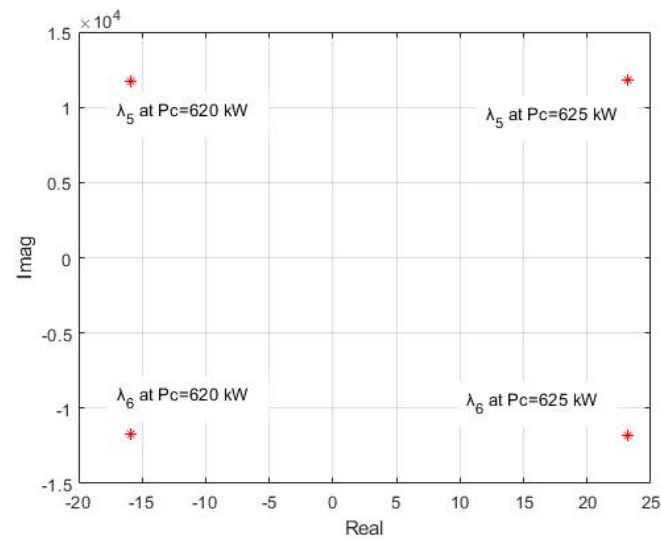
Figure 23. Evolution of the eigenvalues with the change of the CPL active power around its limited value from $P_c = 620$ kW to $P_c = 625$ kW when $Q_c = 0$.

(**a**)

(**b**)
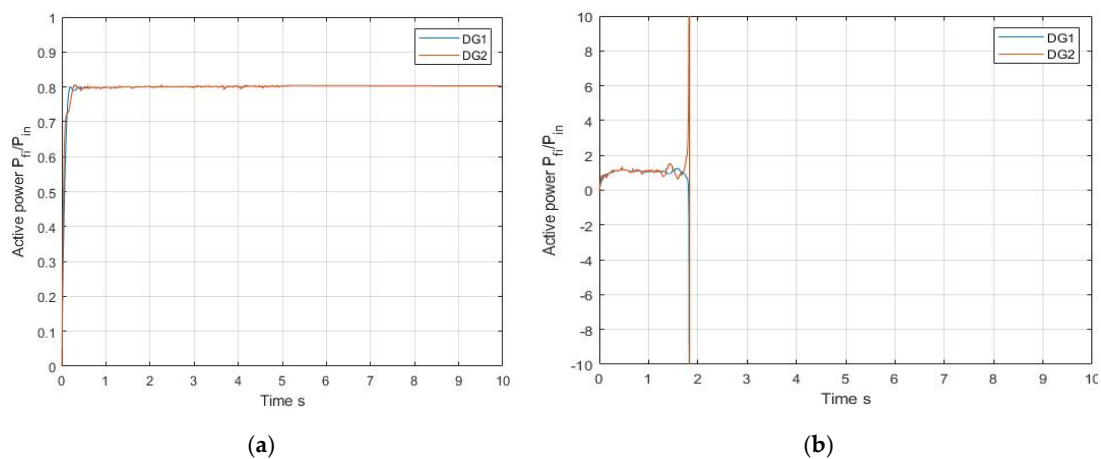
Figure 24. Evolution of the DGs active power (Simscape model with both DGs connected at 0 s): (**a**) $P_c = 620$ kW. (**b**) $P_c = 625$ kW.
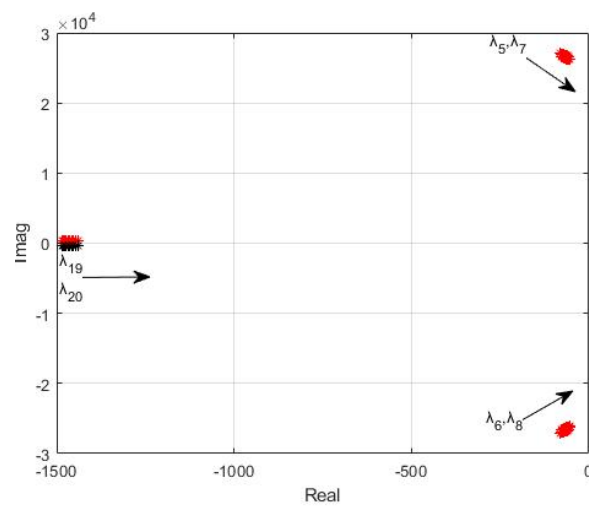
Figure 25. Evolution of eigenvalues corresponding to the decrease in RL-load3 under constant power factor: $175 < R_{Load3} < 376(\Omega)$ and $0.13 < L_{Load3} < 0.25(H)$.
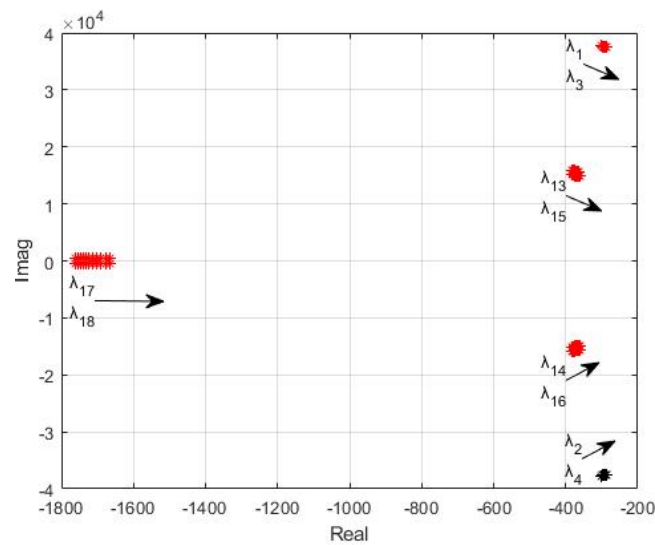
Figure 26. Evolution of eigenvalues corresponding to the decrease in RL-load4 under constant power factor: $155 < R_{Load4} < 319(\Omega)$ and $0.085 < L_{Load4} < 0.17(H)$.
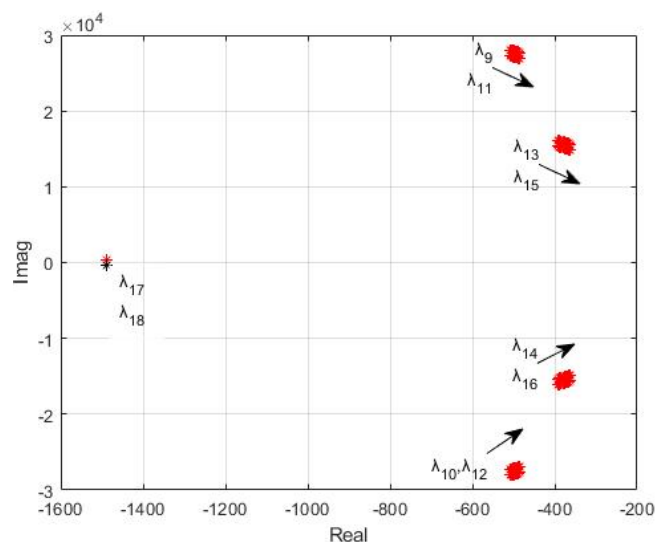
Figure 27. Evolution of eigenvalues corresponding to the decrease in RL-load5 under constant power factor: $126 < R_{Load5} < 252(\Omega)$ and $0.077 < L_{Load5} < 0.1564(H)$.

4.5. Mesh Microgrid Control Robustness

Based on the established and validated state-model, including the modified droop-control that ensures active and reactive power sharing, the considered mesh microgrid control robustness with respect to the modifications caused by the connection of DGs and large load variations is studied. In this simulation, at 0 s, the first DG sets the frequency of the microgrid and the voltages of the PCCs while only the first RL load is connected. Then, the second DG is interconnected to the microgrid at 5 s after being synchronized from 1 s to 5 s. At 8 s, the second RL load is also connected, applying a high positive load step to the microgrid. Finally, at 11 s, the CPL load absorbing an active power of 100 kW is also connected to the microgrid to verify its effect on the active and reactive power sharing.

Due to the modified droop control strategy given by Equations (9) and (10), the active and reactive power sharing is ensured (Figure 28a,b). The convergence of the reactive power of the two DGs under different load conditions is convincingly verified in Figure 28b. In addition, and as foreseen by the stability analysis based on the state-model, the microgrid stability is ensured in different microgrid structure configuration when the CPL active power load does not exceed 124 kW.
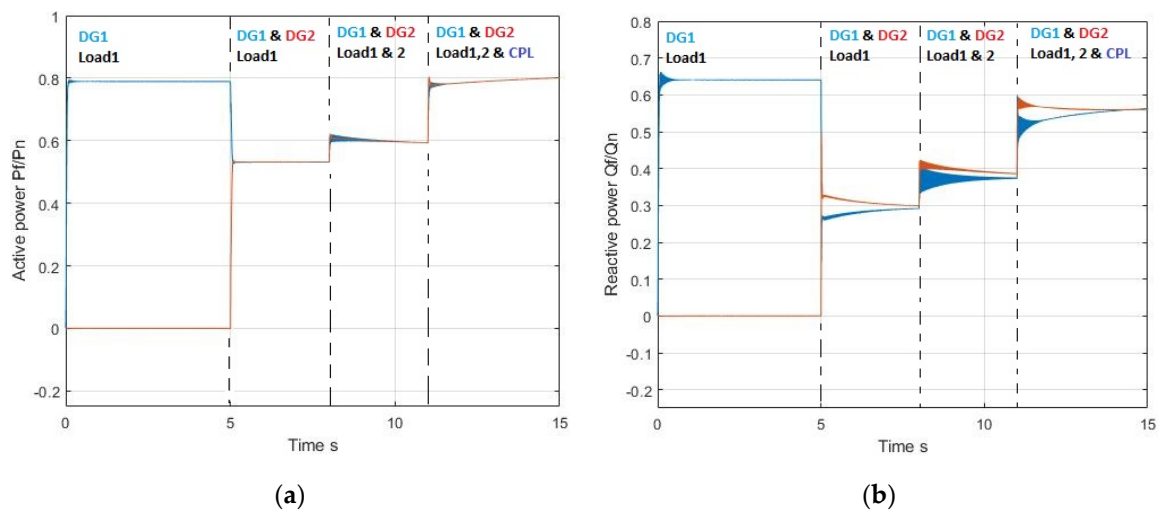
Figure 28. Evolution of the DG active (**a**) and reactive (**b**) powers under different states of charge.

5. Discussion

An improved droop control strategy for synchronization and power sharing was applied on a mesh multi-PCC islanded microgrid. With only the information on the measured RMS voltage value at a pilot node, this strategy has proven its efficiency for fast synchronization as well as active and reactive power sharing between all microgrid DGs. This makes the mesh multi-PCC microgrid eligible to the "plug and play" feature.

In order to study the microgrid stability and its droop control robustness, a state model of the complete system has been proposed and validated based on simulation results achieved using both the Simscape model and proposed state-model. Then, the stability analysis of the considered non-linear system at each operating point was performed using the Jacobean matrix of the state model. In practice, the dynamic behavior of different state variables and the origin of different frequency components were found by studying the evolution of the system eigenvalues with respect to the parameters of the power lines, DGs and different loads. It was found that the most influent system parameters on its stability were the DGs control parameters and the CPL active power level.

In addition, it has been shown through an example that the established state model, which allows the study of system stability, can be used as a powerful tool to adjust certain mesh microgrid parameters to guarantee its stability when the absorbed active power level of its CPLs becomes too high. Finally, the validated microgrid state-model, including the modified droop-control that ensures active and reactive power sharing, also achieved mesh microgrid control robustness with respect to the modifications caused by the connection of DGs and large load variations, which means that the new droop control is always effective under different network configurations.

The developed modified droop control strategy can be adapted and used for power sharing in grid-connected mesh microgrids, and the synchronization strategy can also be adapted for a seamless transfer from an islanded microgrid to a grid-connected microgrid. As mentioned in the Introduction, the developed and validated state-space model can be the base for many future studies in mesh microgrids.

Author Contributions: Conceptualization, Y.H., A.B., S.P. and F.M.-T.; methodology, S.P. and F.M.-T.; software, Y.H.; validation, A.B., J.-P.M., S.P. and F.M.-T.; formal analysis, Y.H.; investigation, Y.H.; resources, S.P., F.M.-T. and A.B.; data curation, Y.H.; writing—original draft preparation, Y.H.; writing—review and editing, F.M.-T. and S.P.; visualization, Y.H.; supervision, A.B., J.-P.M., S.P. and F.M.-T.; project administration, A.B., J.-P.M., S.P. and F.M.-T.; funding acquisition, A.B., J.-P.M., S.P. and F.M.-T. All authors have read and agreed to the published version of the manuscript.

Institutional Review Board Statement: Not applicable.

Informed Consent Statement: Not applicable.

Data Availability Statement: No suggested Data Availability Statements.

Conflicts of Interest: The authors declare no conflict of interest.

References

1. El-Khattam, W.; Salama, M.M. Distributed generation technologies, definitions and benefits. *Electr. Power Syst. Res.* **2004**, *71*, 119–128. [CrossRef]
2. Zhang, L.; Harnefors, L.; Nee, H.-P. Power-Synchronization Control of Grid-Connected Voltage-Source Converters. *IEEE Trans. Power Syst.* **2010**, *25*, 809–820. [CrossRef]
3. Haizhen, X.; Xing, Z.; Fang, L.; Debin, Z.; Rongliang, S.; Hua, N.; Wei, C. Synchronization strategy of microgrid from islanded to grid-connected mode seamless transfer. In Proceedings of the IEEE International Conference of IEEE Region 10 (TENCON 2013), Xi'an, China, 22–25 October 2013.
4. Tayaba, U.B.; Roslan, M.A.B.; Hwai, L.J.; Kashif, M. A review of droop control techniques for microgrid. *Renew. Sustain. Energy Rev.* **2017**, *76*, 717–727. [CrossRef]
5. Xiaofei, X.; Hong, L.; Zhipeng, L. Research on new algorithm of droop control. In Proceedings of the Chinese Control and Decision Conference (CCDC), Guiyang, China, 25–27 May 2013.
6. Huang, X.; Wang, K.; Qiu, J.; Hang, L.; Li, G.; Wang, X. Decentralized Control of Multi-Parallel Grid-Forming DGs in Islanded Microgrids for Enhanced Transient Performance. *IEEE Access* **2019**, *7*, 17958–17968. [CrossRef]
7. Han, H.; Hou, X.; Yang, J.; Wu, J.; Su, M.; Guerrero, J.M. Review of Power Sharing Control Strategies for Islanding Operation of AC Microgrids. *IEEE Trans. Smart Grid* **2016**, *7*, 200–215. [CrossRef]
8. Moussa, H.; Shahin, A.; Martin, J.-P.; Pierfederici, S.; Moubayed, N. Optimal angle droop for power sharing enhancement with stability improvement in islanded microgrids. *IEEE Trans. Smart Grid* **2017**, *9*, 5014–5026. [CrossRef]
9. Dheer, D.K.; Kulkarni, O.V.; Doolla, S.; Rathore, A.K. Effect of Reconfiguration and Meshed Networks on the Small-Signal Stability Margin of Droop-Based Islanded Microgrids. *IEEE Trans. Ind. Appl.* **2018**, *54*, 2821–2833. [CrossRef]
10. Trivedi, A.; Singh, M. Adaptive Droop Control for AC Microgrid with Small Mesh Network. *IEEE Trans. Ind. Electron.* **2018**, *65*, 4781–4789. [CrossRef]
11. Zhu, Y.; Zhuo, F.; Shi, H. Accurate power sharing strategy for complex microgrid based on droop control method. In Proceedings of the IEEE 10th International Symposium on Power Electronics for Distributed Generation Systems (PEDG), Xi'an, China, 3–6 June 2019.
12. Jiao, J.; Guo, S.; Tan, C.; Xue, Y.; Hua, X. Research on Improved Droop Control Method of DC Microgrid Based on Voltage Compensation. In Proceedings of the 2020 5th International Conference on Power and Renewable Energy (ICPRE), Shanghai, China, 12–14 September 2020; pp. 391–395. [CrossRef]
13. Jusoh, A.B. The instability effect of constant power loads. In Proceedings of the National Power and Energy Conference PECon 2004, Kuala Lumpur, Malaysia, 29–30 November 2004; pp. 175–179.
14. Cespedes, M.; Xing, L.; Sun, J. Constant-power load system stabilization by passive damping. *IEEE Trans. Power Electron.* **2011**, *26*, 1832–1836. [CrossRef]
15. Marx, D.; Magne, P.; Nahid-Mobarakeh, B.; Pierfederici, S.; Davat, B. Large signal stability analysis tools in DC power systems with constant power loads and variable power loads—A review. *IEEE Trans. Power Electron.* **2012**, *27*, 1773–1787. [CrossRef]
16. Kabalan, M.; Singh, P.; Niebur, D. Large signal Lyapunov-based stability studies in microgrids: A review. *IEEE Trans. Smart Grid* **2016**, *8*, 2287–2295. [CrossRef]
17. Bottrell, N.; Prodanovic, M.; Green, C.T. Dynamic stability of a microgrid with an active load. *IEEE Trans. Power Electron.* **2013**, *28*, 5107–5119. [CrossRef]
18. Rasheduzzaman, M.; Mueller, J.A.; Kimball, W.J. An accurate small-signal model of inverter- dominated islanded microgrids using dq reference frame. *IEEE J. Emerg. Sel. Top. Power Electron.* **2014**, *2*, 1070–1080. [CrossRef]
19. Hennane, Y.; Martin, J.; Berdai, A.; Pierfederici, S.; Meibody-Tabar, F. Power Sharing and Synchronization Strategies for Multiple PCC Islanded Microgrids. *Int. J. Electr. Electron. Eng. Telecommun.* **2020**, *9*, 156–162. [CrossRef]

Improving the Efficiency and Sustainability of Power Systems Using Distributed Power Factor Correction Methods

Ciprian Mihai Coman [1,2,*], Adriana Florescu [3] and Constantin Daniel Oancea [4]

[1] ITC Department, Tesagon International SRL, Ploiesti 100029, Romania
[2] Faculty of Electronics, Telecommunications and Information Technology, Politehnica University of Bucharest, Bucharest 060042, Romania
[3] Department of Applied Electronics and Information Engineering, Faculty of Electronics, Telecommunications and Information Technology, Politehnica University of Bucharest, Bucharest 060042, Romania; adriana.florescu@upb.ro
[4] Department of Measurements, Electrical Devices and Static Converters, Faculty of Electrical Engineering, Politehnica University of Bucharest, Bucharest 060042, Romania; daniel.oancea@upb.ro
* Correspondence: ciprian@tesagon.com

check for updates

Abstract: For the equipment connected to the three-phase or single-phase grid, the power factor represents an efficiency measure for the usage of electrical energy. The power factor improvement through correction methods reduces the load on the transformers and power conductors, leading to a reduction of losses in the mains power supply and a sustainable grid system. The implications at the financial level are also important. An example of load that generates a small power factor is represented by a motor without mechanical load or having a small mechanical load. Given the power factor correction (PFC), the costs are reduced through the elimination of penalties, applying only in the common coupling point (CCP). The advantages of using equipment for the power factor correction are related also to their long operation duration and the easiness of their installation. The device presented in this article takes advantage of the advances in information and communication technology (ICT) to create a new approach for telemetry and remote configuration of a PFC. This approach has flexibility and versatility, such that it can be adapted to many loads, easily changing the capacitance steps and settings of the power factor correction device.

Keywords: power factor; reactive power; capacitance; harmonics; telemetry; Industry 4.0

1. Introduction

The power factor is a measure of the efficiency of the use of electricity. Improved power factor correction reduces the load of the transformers and conductors of electrical installations. The implications are also financial in nature, a low power factor increasing the cost of consumed electrical energy [1–4].

Reactive power is an important parameter of the electrical power that leads to a decreased power factor. It is generated by two main factors: reactive elements and unbalances in the three-phase systems [5]. For example, AC rotary machines will induce extra losses when unbalanced load current and reactive power are absorbed by a single-phase load. Sensitive electronic equipment is particularly disturbed by the low power factor generated by unbalanced current. There are many authors that explored ways to reduce the extra costs generated by reactive power [6–11].

The use of capacitors for the correction of the power factor is related to the long service life and the ease of installation. It should be kept in mind that the capacitor batteries introduce disturbances in

the network when they are connected and disconnected. The maximum value of the voltage does not exceed (in the absence of harmonics) twice the maximum value of the rated voltage, when switching the discharged capacitors [12].

In the case of a capacitor already charged at the time of switching off, the overvoltage can reach a maximum value approaching three times the peak nominal value. When considering the automatic step change of capacitor batteries, care must be taken that the section of capacitors to be supplied is completely discharged [1,12].

An overexcited synchronous condenser is another option to correct the power factor. Basically, it is a synchronous electric drive/generator in the no load electric drive state, but with overexcited current. This is a much more expensive option because of the special design needed (e.g., oversized windings and special rotor shaft), which is the main disadvantage. An advantage is the missing disturbances in the power network.

Good management of an electrical energy consumer network includes the evaluation of the power factor and actions to improve it. For the reliable measurement of power, reactive power, the appearance of the resonance phenomenon needs to be taken into consideration and has been studied by various authors, with several approaches being published in various articles [13–15]. We use mathematical models to describe the performance of the power factor corrector, similar to the ones described in [16]. There are also principles for optimization of the power factor in a closed network, such as the proportional-integral-derivative (PID) algorithm [17].

In the context of increasing the penetration of the intermittent renewable energy sources, the concept of microgrids (MG) becomes more frequent as a solution to these issues. There are efforts being made to improve the solutions available to microgrid developers in order to compensate the power factor and the load asymmetries inside the microgrid by utilizing advanced functionalities enabled by grid tied inverters of photovoltaics and energy storage systems [18,19].

Advanced operational capabilities of power electronic based distributed energy resources (DERs) can be employed to compensate power quality phenomena such as harmonics, interharmonics, and current/voltage unbalances [15,19–22]. Hence, smart and multi-functional inverters are capable of providing multiple ancillary services to the MG, along with dedicated resources such as automatic power factor correction equipment.

The problems of degrading power factor and reactive power are mainly present in the industrial environment, where the frequency of inductive loads is significant, most commonly from electric motors. Due to rapid advances in ICT, the digital transformation is expanding across all domains. In the industrial environment, most often, it takes the form of Industry 4.0 ecosystems that integrate several technologies and concepts such as the Internet of Things (IOT), big data, cloud computing, and smart metering, in order to allow real-time monitoring and controlling of a complex industrial system using remote computers and mobile devices [23–27].

Similar applications are employed in ship main propulsion power monitoring systems. In the particular application explored in [28], wireless telemetry technology was used alongside the MODBUS communication protocol.

The topic of power factor correction has been previously explored and presented in the literature, using different approaches. In [29], a new digital power factor correction (PFC) control strategy was presented, based on digital signal processor speed to solve the problem of limited switching frequency. In [30], a programmable logic controller (PLC) was used to control switch capacitors for PFC near a three-phase electric induction motor. More complex PFC decision algorithms were analyzed in [31], and a new teaching learning based optimization (TLBO) approach was studied along with a cloud based data warehouse for electrical parameters. The power factor has different limits depending on the country. A value of about 0.8 is suitable for industrial loads. Under semi-industrial/mixed conditions, a value of 0.85 is a common value, while 0.9 is generally used/considered for residential areas.

In order to improve electrical energy efficiency through the current quality, this paper analyzes the performances of a proposed distributed power factor correction methodology. For this purpose, a new

design and implementation of a PFC are performed. It uses an industrial decision device manufactured by Ducati Energia [32,33], five capacitor batteries that can be engaged incrementally, ICT in general, and IOT in particular. This approach has flexibility and versatility, such that it can be adapted to many loads, easily changing the capacitance steps and the settings of the power factor correction device. The switching overvoltage problem is solved using the decision software to prevent a switch from taking place before the capacitors are discharged. Tests are performed on a motor with no load, at initial PF of 0.64. Using the correction device, the PF is improved to 0.8. Our goal is to create a versatile solution that is easy to adapt and configure in industrial settings, not to push the PF to the ideal value of one.

The rest of the paper is organized as follows. Section 2 presents the general architecture of the PFC system, along with the materials and methods used. Details on the implementation of the experimental model are presented in Section 3, while Section 4 presents the measured results at the switching moment. The paper concludes in Section 5.

2. Background, Materials, and Methods

2.1. Background

In the sinusoidal regime, for single-phase or three-phase circuits symmetrically charged, for which the RMS values of the voltages and currents on the three phases (but also the phase differences between the corresponding phasors) are equal, the power factor is defined as the positive and subunit ratio between the active power P and the apparent power S [34]. Regarding the power factor notations, the PF notation is used in the U.S. regulations, while the λ notation is used in the European regulations.

$$1 \geq \lambda \equiv PF = \frac{P}{S} \geq 0 \tag{1}$$

For a linear and passive dipole, we have for the power factor the expression:

$$\lambda \equiv PF = \frac{P}{S} = \frac{U \cdot I \cdot \cos \varphi}{U \cdot I} = \cos \varphi, \ 0 \leq \cos \varphi \leq 1 \tag{2}$$

The PF is easily determined from the power triangle. Thus, the power factor is the ratio of active power to apparent power. If mathematically, this ratio is also described by the cosine of the angle between the two powers, in reality, the coincidence between the two sizes will exist only if the waveform of the current is sinusoidal (that is, if they are not harmonic):

$$PF = \frac{P}{S} \ \cos(\varphi) = \frac{P_1}{S_1} \tag{3}$$

where P and S are the active, respectively the apparent, total power, and P_1 and S_1 are the active power, respectively the apparent, power given by the fundamental (1st order harmonic).

In the non-sinusoidal regime, the components that define the power factor (the active power P, respectively the apparent power S) are the same with the mention that the apparent power S is written according to the three orthogonal components: the active power P, the reactive power Q, and the deforming power D, so that Equation (2) changes into (4):

$$\lambda \equiv PF = \frac{P}{S} = \frac{P}{\sqrt{P^2 + Q^2 + D^2}} \tag{4}$$

Even if there is no reactive power, the power factor remains lower than 1, due to the deforming power specific to the non-sinusoidal regime. Generally, the cancellation of the reactive power does not improve the power factor as it does in the sinusoidal regime. It is possible that by reducing the

reactive power, the deforming power increases even more. This means that in the non-sinusoidal mode, by adding capacitors, it is sometimes possible to even worsen the power factor.

The reactive factor and the deforming factor are defined. The reactive factor is defined as the ratio between the reactive power and the active power in the circuit, at one point [34]:

$$\rho = \frac{Q}{P} \tag{5}$$

while the deforming factor represents the ratio between the deforming power and the non-deforming power:

$$\tau = \frac{D}{\sqrt{P^2 + Q^2}} \tag{6}$$

Relation (4) turns into Relation (7), where cos ξ is a notation given by (8):

$$\lambda \equiv PF = \frac{P}{S} = \frac{P}{\sqrt{P^2 + Q^2}} \cdot \frac{\sqrt{P^2 + Q^2}}{\sqrt{P^2 + Q^2 + D^2}} = \cos \varphi \cdot \cos \xi, \tag{7}$$

$$\cos \xi = \frac{\sqrt{P^2 + Q^2}}{\sqrt{P^2 + Q^2 + D^2}} < 1 \tag{8}$$

The expression of the power factor can be rewritten as (9):

$$\lambda = PF = \frac{1}{\sqrt{1 + \rho^2}} \cdot \frac{1}{\sqrt{1 + \tau^2}} \tag{9}$$

In the non-sinusoidal regime, the definition of the power factor does not express the degree of use of the power available in the network, because the sources of harmonics are not the generators of the network, but actually the nonlinear receivers.

In the non-sinusoidal mode, two values for the power factor are defined and measured: the power factor for the fundamental component (fundamental 50/60 Hz power factor or displacement power factor (DPF)) and the total power factor (PF) (true/total power factor):

$$\lambda_1 \equiv DPF = \cos \varphi_1 = \frac{P_1}{S_1} \tag{10}$$

$$\lambda \equiv PF = \frac{P}{S} = \frac{P}{U \cdot I} \tag{11}$$

In the U.S., the penalties applied to industrial consumers are based on the value of the fundamental power factor given by Relation (10) above [34]. The total power factor includes the influence of the harmonics on the active power, and the apparent power provides information on the efficiency of the use of the active power at the consumer.

An expression can be established for the total power factor in the non-sinusoidal regime, depending on the current and voltage distortion factors. To do this, the expressions of active power and apparent power are written. The active power in the non-sinusoidal regime is given by the sum of the active powers corresponding to each harmonic in part, generating two components, the fundamental active power and the harmonic active power (the deforming residue of the active power):

$$P = \sum_{h=1} U_h \cdot I_h \cdot \cos(\alpha_h - \beta_h) = \sum_{h=1} U_h \cdot I_h \cdot \cos \varphi_h = P_1 + P_H \tag{12}$$

$$P_1 = U_1 \cdot I_1 \cdot \cos \varphi_1 \tag{13}$$

$$P_H = \sum_{h=1} U_h \cdot I_h \cdot \cos \varphi_h \tag{14}$$

The apparent power of an electric dipole is defined by the product of the RMS values of the voltage and current, denoted by S in Relation (15). Similarly, the apparent power in the non-sinusoidal regime can be decomposed into the fundamental apparent power S1 given by Relation (16) and the harmonic apparent power (the residual apparent power) SN given by Relation (17). The fundamental apparent power, S1, and its components P1 and Q1 are of great interest because they intervene in the circulation of powers in the circuit. In the non-sinusoidal mode, the apparent power can be expressed according to the RMS value of the voltage and the RMS value of the current, according to (18):

$$S = U \cdot I \tag{15}$$

$$S_1 = U_1 \cdot I_1 \tag{16}$$

$$S_1^2 = P_1^2 + Q_1^2 \tag{17}$$

$$S^2 = (U \cdot I)^2 = \left(U_1^2 + U_H^2\right) \cdot \left(I_1^2 + I_H^2\right) = S_1^2 + S_H^2 \tag{18}$$

The power factor can be rewritten in a form that takes into account the Total Harmonic Distortion factor for the voltage (THD_U) and the Total Harmonic Distortion factor for the current (THD_I) both defined below [34]:

$$k_{dI} \equiv THD_I = \frac{I_H}{I_1} = \sqrt{\frac{\sum_{h\neq1} I_h^2}{I_1^2}}; k_{dU} \equiv THD_U = \frac{U_H}{U_1} = \sqrt{\frac{\sum_{h\neq1} U_h^2}{U_1^2}} \tag{19}$$

$$\lambda \equiv PF = \frac{P}{S} = \frac{P_1 + P_H}{\sqrt{S_1^2 + S_N^2}} = \frac{\frac{P_1}{S_1} \cdot \left(1 + \frac{P_H}{P_1}\right) \cdot DPF}{\sqrt{1 + \frac{S_N}{S_1}^2}} = \frac{\left(1 + \frac{P_H}{P_1}\right) \cdot DPF}{\sqrt{1 + THD_I^2 + THD_U^2 + (THD_I + THD_U)^2}} \tag{20}$$

For $THD_U < 5\%$ and for $THD_I > 40\%$, the relation between the total power factor and the fundamental power factor can be written with the approximate formula (21):

$$\lambda \equiv PF = \frac{1}{\sqrt{1 + THD_I^2}} \cdot DPF = \frac{I_1}{I} \cdot \cos \varphi_1 \tag{21}$$

The meanings of the quantities in (21) are: I_1 is the RMS value of the fundamental component of the current; I is the RMS value of the non-sine current; and φ_1 is the offset angle between the curves of the fundamental components of the voltage and the current.

Many modern equipment such as switching power supplies or speed adjustment equipment have the fundamental power factor close to 1, but the total power factor can be 0.5–0.6. In order to avoid non-compliant situations, it is necessary to measure both the fundamental power factor and the total power factor. The modern measuring devices (for example, the electric meters) can measure both DSP (PF1) and PF. For industrial consumers, PF is lower than DPF.

A special mention is that in the case of three-phase systems, in the sinusoidal and non-sinusoidal regime, the arithmetic power factor and the vector power factor are defined. In the case of the sinusoidal regime, these values are described below.

The arithmetic apparent power (A, B, C represent the three phases) in (22):

$$S_a = \sum_{x \in A,B,C} S_x = S_A + S_B + S_C = \sum_{x \in A,B,C} \sqrt{P_x^2 + Q_x^2} \tag{22}$$

where $S_{A,B,C}$, $P_{A,B,C}$, and $Q_{A,B,C}$, represent the apparent power, the active power, and the reactive power on the phase.

Geometrical apparent power can be written as:

$$S_g = \sqrt{P^2 + Q^2} \tag{23}$$

$$P = \sum_{x \in A,B,C} P_x = P_A + P_B + P_C \tag{24}$$

$$Q = \sum_{x \in A,B,C} Q_x = Q_A + Q_B + Q_C \tag{25}$$

but can also be written in the form (26):

$$S_g = \left| P_A + P_B + P_C + j \cdot (Q_A + Q_B + Q_C) \right| = \left| P + j \cdot Q \right| \tag{26}$$

Following the conference of the American Institute of Electrical Engineers in 1920, two definitions for the arithmetic power factor, respectively geometrical, were proposed:

$$\lambda_a \equiv PF_a = \frac{P}{S_a} = \frac{P_A + P_B + P_C}{S_A + S_B + S_C} \tag{27}$$

$$\lambda_g \equiv PF_g = \frac{P}{S_g} = \frac{P_A + P_B + P_C}{\left| \underline{S_A} + \underline{S_B} + \underline{S_C} \right|} \tag{28}$$

in which the apparent complex powers on the phases are given by:

$$\underline{S_A} = P_A + j \cdot Q_A; \; \underline{S_B} = P_B + j \cdot Q_B; \; \underline{S_C} = P_C + j \cdot Q_C \tag{29}$$

If we have the case of the non-sinusoidal regime, the powers are described below. The apparent arithmetic power (A, B, C represent the three phases) is given in (30). In addition to the sinusoidal regime, it is the appearance of deforming power.

$$S_A = \sqrt{P_A^2 + Q_A^2 + D_A^2}; S_B = \sqrt{P_B^2 + Q_B^2 + D_B^2}; S_C = \sqrt{P_C^2 + Q_C^2 + D_C^2} \tag{30}$$

The apparent arithmetic power is:

$$S_a = S_A + S_B + S_C \tag{31}$$

while the geometrical apparent power is given in (30), and its components are given in (31):

$$S_g = \sqrt{P^2 + Q^2 + D^2} \tag{32}$$

$$P = P_A + P_B + P_C; Q = Q_A + Q_B + Q_C; D = D_A + D_B + D_C \tag{33}$$

In order to characterize the apparent power in the case of unbalanced loads, the term equivalent apparent power is introduced. This can be correlated with losses in power lines and in transformers, in the same way that we have an apparent power for balanced loads. Compared to (34), an equivalent current I_e and an equivalent phase voltage U_e can be defined in (35):

$$S = \sqrt{3} \cdot U \cdot I \tag{34}$$

$$S_e = 3 \cdot U_e \cdot I_e \tag{35}$$

For a three-phase circuit with a neutral conductor, the equivalent voltage is given by (36):

$$U_e = \sqrt{\frac{U_a^2 + U_b^2 + U_c^2}{3}} \tag{36}$$

For a three-phase circuit without a neutral conductor, the equivalent voltage can be calculated with (37):

$$U_e = \sqrt{\frac{U_{AB}^2 + U_{BC}^2 + U_{CA}^2}{9}} \tag{37}$$

The RMS value of the equivalent current is evaluated according to the RMS values of the currents, I_A, I_B, and I_C in (38):

$$I_e = \sqrt{\frac{I_A^2 + I_B^2 + I_C^2}{3}} \tag{38}$$

For the particular case of a balanced and linear load, we have $U_e = U$, $I_A = I_B = I_C = I_e = I$, and the apparent power is written according to Relation (39):

$$S_e = S = \sqrt{3} \cdot U \cdot I \tag{39}$$

Finally, the equivalent power factor results in (40):

$$\lambda_e \equiv PF_e = \frac{P}{S_e} \tag{40}$$

2.2. Materials and Methods

For the equipment connected to the three-phase or single-phase network, the power factor is a measure of the efficiency of the use of electricity. Improved power factor correction reduces the load of transformers and conductors of electrical installations. In ideal conditions, the power factor would be 1. An example of a load that produces a low power factor is an engine without a mechanical load or a low mechanical load.

Correcting the power factor leads to increasing the capacity of the network infrastructure and reducing losses in transformers and cables. One method of reducing the power factor, considering that most loads are inductive, is the use of electric capacitor batteries.

The advantages of using electric capacitors for power factor correction are related to the long service life and ease of installation. It should be kept in mind that the capacitor batteries introduce disturbances in the network when they are connected and disconnected. The use of capacitor batteries in automated power factor correction equipment uses several steps, thus ensuring load flexibility.

Creating a database with information on the evolution of the power factor, but also of other current parameters, can only improve the decision of choosing the optimal method for the correction of the power factor, based on the statistical analysis.

There are a number of standards that a device used for power factor correction must meet. Voltages and currents are measured in TrueRMS value. The entire design of the R5 device from Ducati Energia meets the standards: IEC/EN 61010-1, IEC/EN 61000-6-2, IEC/EN 61000-6-4, IEC/EN 61326-1, EN 62311, EN 301-489-1, EN 301-489-3, EN 300-220-2, and EN 300-330.

The switches for connecting/disconnecting the capacitor batteries were specially designed for this operation, being provided with resistors for limiting the current. It was not necessary to use a possible fourth contact for neutral, as the capacitor batteries were connected in a delta configuration according to the manufacturer's recommendations for the power factor correction device. Their supply was through a general switch. The fuses for supplying the Ducati device and the control circuits were dimensioned at 2 A, and the power part was protected by a tripolar safety of 25 A.

The equipment was designed to be used for the 3×120 V three-phase network, but could also be used for the 3×230 V three-phase network, with minimal modifications.

The electrical diagram, according to the manufacturer's recommendations, is shown in Figure 1. The T1 transformer was only required if the capacitor battery contactor coils were operating at a voltage different from that of the mains supply.
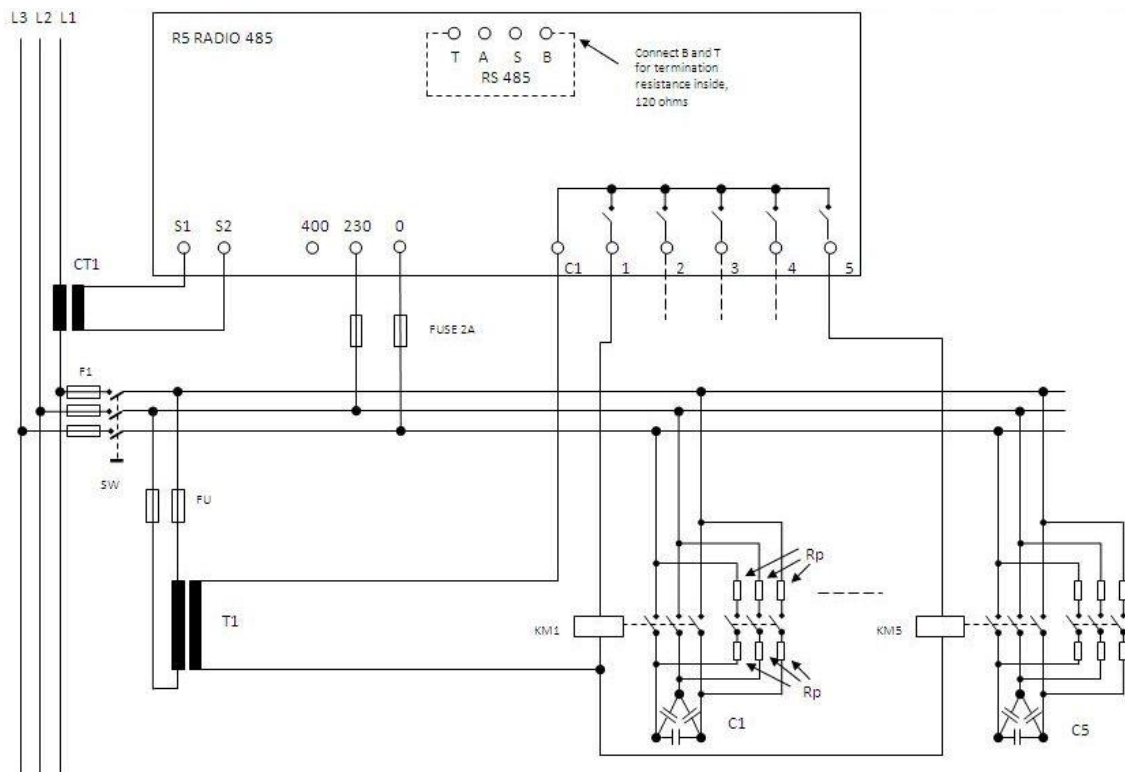
Figure 1. Power factor correction (PFC) device power diagram for three-phase current.

The current transformer was Class 0.5 with the ratio of currents 10/1. It was considered that the equipment would be used for laboratory experiments, for loads up to 10kW. For each particular industrial implementation, the capacitors battery must be adapted to the load, and the decision system parameters must be configured for the algorithm to know the parameters of the system it controls. The components and devices used and the necessary conductors were installed in a box with dimensions of $500 \times 400 \times 250$. The safety measures imposed by the use of dangerous voltages were respected. Thus, safety measures were taken against electrocution by using terminals according to the European standards (they did not have accessible metal elements), and for unauthorized access, an alarm was provided that triggered when the door of the panel was opened, when the panel was powered. The operation of the panel was started with a key, thus avoiding the unauthorized use of the equipment. For each step of the capacitor stack, a light was installed to signal the change. Light indicators were also used to signal the presence of voltage on each phase.

The power factor correction equipment was optimally positioned near the load (electric motor). The minimum costs were when the power factor correction equipment was installed in a central position, within the installation. Usually, the power factor correction equipment is installed near the consumption measurement point (meter).

The relationships underlying the calculations for determining the power factor compensation capacity are contained in (41) and (42). If it is desired to obtain a certain power factor, not fully compensating it, we can use the relation obtained from the triangle of powers, which directly calculates the reactive power needed to be compensated by the capacitor (43). The initial angle between the voltage and current phases is φ_1, and the target phase shift is φ_2. The load was a serial network

consisting of a resistor (R) and an inductance (L), which simulated a real inductive load. This was to be offset by a C_C capacity. The reactive power to be compensated is denoted with Qc.

$$I = \frac{U}{Z} \; Z = \sqrt{R^2 + X_L{}^2} \; P = R \cdot I^2 \; S = U \cdot I \; Q = X_L \cdot I^2 \tag{41}$$

$$X_C = \frac{U^2}{Q_c} \; C_C = \frac{1}{2 \cdot \pi \cdot f \cdot X_C} \tag{42}$$

$$Q_C = P \cdot (\tan(\varphi_1) - \tan(\varphi_2)) \tag{43}$$

To make the calculations easier, one can imagine a simple application that can determine, for a particular consumer, the capacity needed to achieve full or partial compensation of the power factor. Here, MS Excel was used for the calculation; see Figure 2. Yellow is the initial (primary) size and red the intermediate size. Green is the measurements in direct relation with the determination of the compensating capacity, partial or total, of the power factor. The application calculated the same value for the compensation capacity using two different calculation methods.
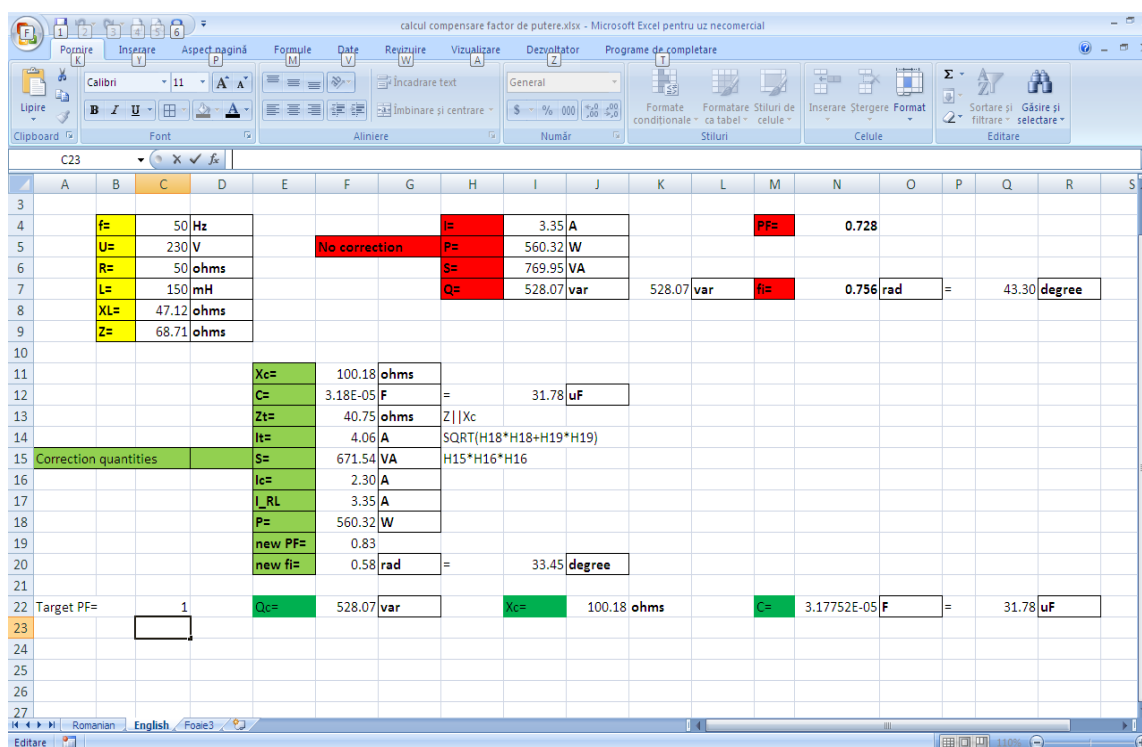
Figure 2. Application for determining the capacity for power factor compensation.

To verify the calculations, a simulation was performed in LTSpice; see Figures 3 and 4. The circuit elements were chosen for a phase shift of approximately 45 degrees. The circuit resistance was chosen to be 50 ohms, and the inductance resulted from 150 mH, from the triangle of impedances. For the total compensation of the phase shift determined by the resistor-inductor (RL) circuit R_1L_1, a capacitor C_1 with a capacity of approximately 32 µF was obtained, connected in parallel with the RL circuit considered. The presented circuit was single-phase (chosen for simplicity and clarity), and for the three-phase circuits, the situation was similar.
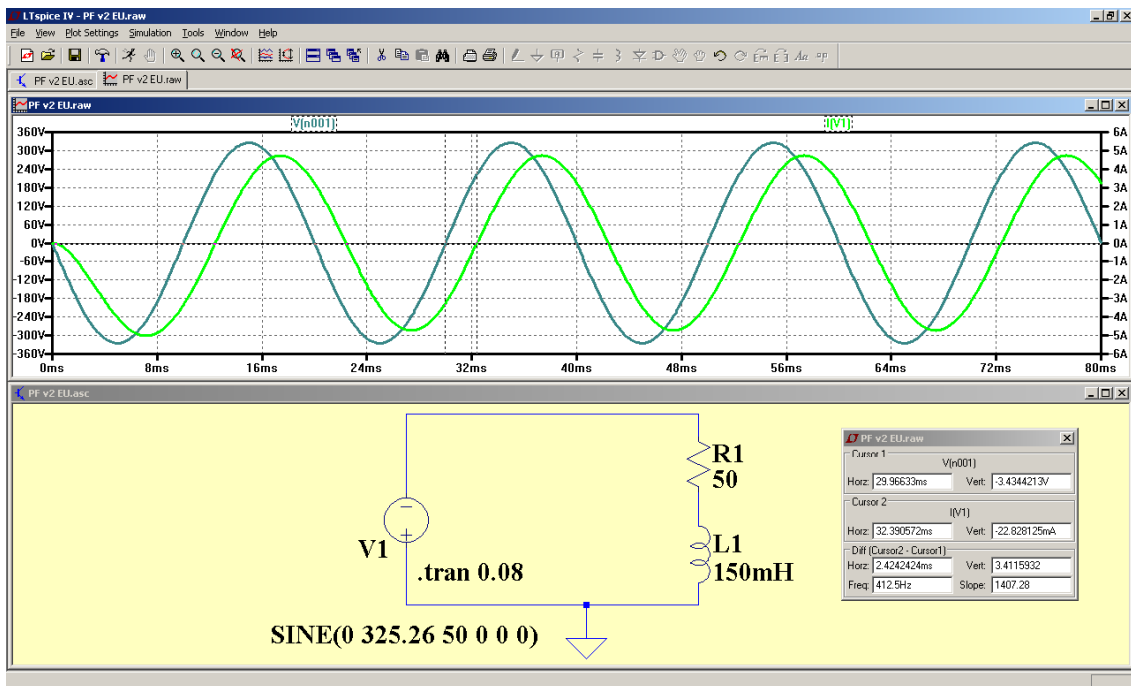
Figure 3. Scheme for simulating the operation of an RL circuit.
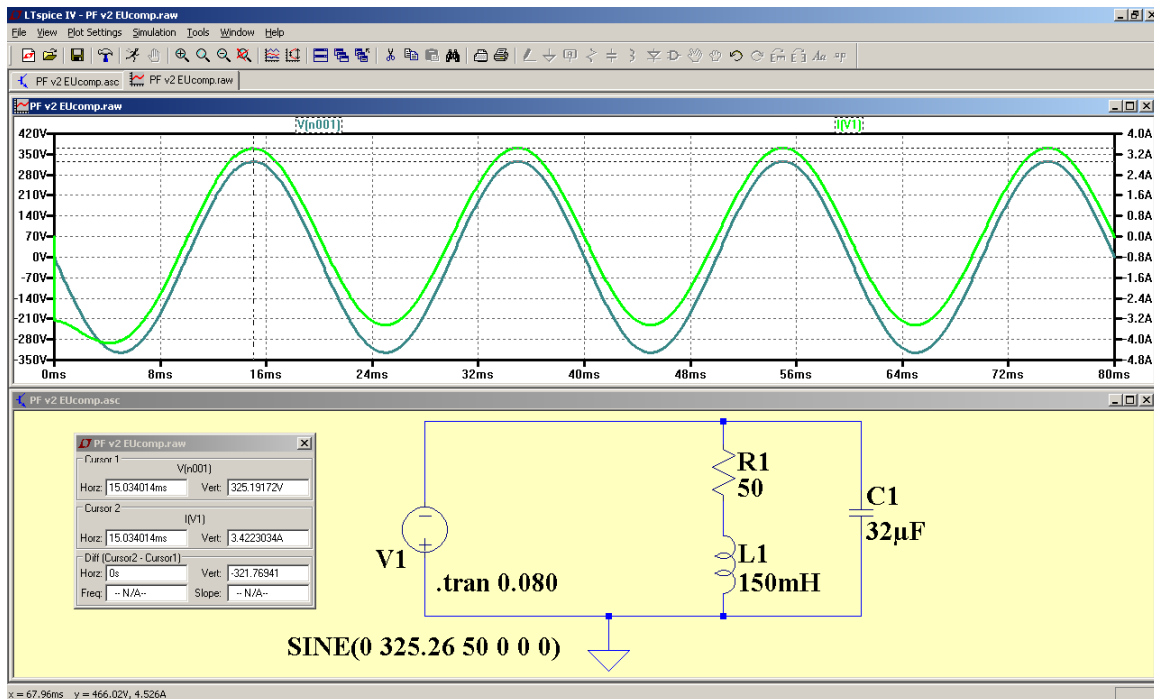
Figure 4. Scheme for simulating the phase compensation function using a capacitor.

3. Results

3.1. Power Factor Compensation Equipment

For a power factor compensation circuit, equipment consisting of a Ducati Energia R5 485 device that controlled a five-step capacitor battery and a Raspberry Pi 3 IoT device with the corresponding program for greater functionality were developed, with more command and control possibilities

and a high degree of automation; see Figure 5. The R5 device could be configured to work on both single-phase and three-phase networks.
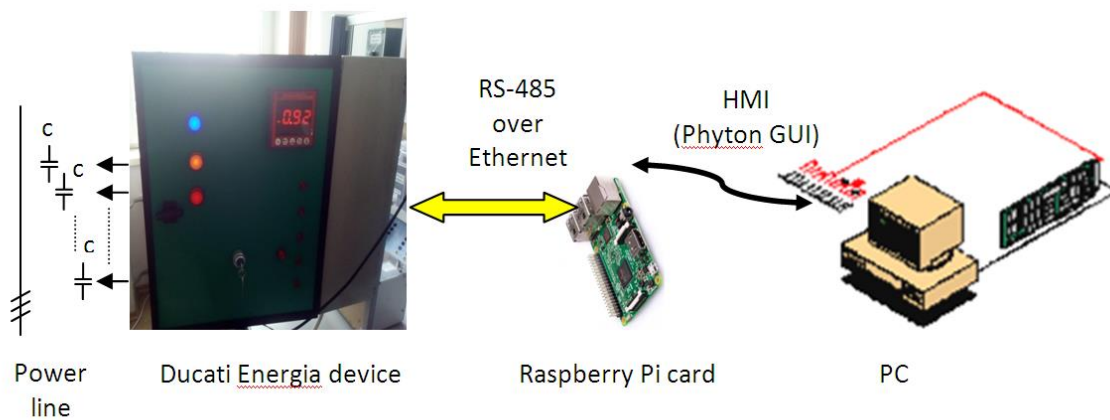
Figure 5. Schematic representation of the proposed assembly for power factor correction.

The Ducati Energia R5 device ensured quality analysis in the monitored electrical network, by calculating the cosine of the phase difference between the current and the voltage. Its configuration was achieved both from the buttons on the front panel, but especially by the much greater number of possibilities, using the communication through the MODBUS/RS485 protocol. In addition, the MODBUS protocol could also read data on the network (voltages, currents, powers, phases, total harmonic distortion (THD), etc.). Starting from formula (19), the THD is here calculated based on another equivalent consecrated formula (44), where the current was measured and I_{RMS} easily computed, and the fundamental harmonic was calculated using Fast Fourier Transform (FFT).

$$\text{THD} = \sqrt{\left(\frac{I_{RMS}}{I_1}\right)^2 - 1} \tag{44}$$

The capacitor battery schematic is presented in Figure 1 and the implementation in Figure 6. There were five steps, the first two using three monophasic capacitors each and the next three using triphasic capacitors, as follows:

Step I: 3×9.6 µF, 0.83 kvar, 1.6 A, 525 V
Step II: 3×11.6 µF, 0.83 kvar, 1.73 A, 480 V
Step III: 6.6 µF, 1 kvar, 1.4 A, 400 V
Step IV: 6.6 µF, 1 kvar, 1.4 A, 400 V
Step V: 9.95 µF, 1.5 kvar, 2.2 A, 400 V

The implemented MODBUS protocol was based on six callable functions, two of which were of particular interest: Function 03: "READ HOLDING REGISTERS" and Function 06: "PRESET SINGLE REGISTER", the first one for reading data and the second one for configuring the device for correction of the fault power [9,10].

Function 03: "READ HOLDING REGISTERS" reads one or more memory adjacent locations, each one being one or two words in size. It is possible to read up to 12 or 24 consecutive measures. Table 1 describes the read request format (from master to slave) and Table 2 describes the reply format (from slave to master). The standard abbreviations are used in the tables below: address (Addr), function (Func), cyclic redundancy check (CRC), register (Reg), high (H), low (L), most significant word (MSW), least significant word (LSW), integer (Int), voltage transformer (VT), current transformer (CT).

Figure 6. Capacitor battery implementation.

Table 1. Read request format (from master to slave).

Addr	Func	Data Start Register H	Data Start Register L	Data # of Regs H	Data # Regs L	CRC	CRC
1Fh	03h	00h	11h	00h	08h	17h	B7h

Table 2. Read reply format (from slave to master).

Addr	Func	Byte count	Data Out Reg 0012 H	Data Out Reg 0012 L	… …	Data Out Reg 0018H	Data Out Reg 0018L	CRC	CRC
1Fh	03h	10h	10h	EFh	… … ..	3Bh	40h	xxh	yyh

The interpretation of the reply is as follows:

- Addressed slave (Addr = 1 Fh)
- Function code request (Func = 03)
- Number of data byte following (Byte count = 10 h)
- Data byte fields requested by the master (Data Out)
- Cyclic redundancy check (CRC)

The physical address is always obtained from the measured address reduced by one unit. Examples of addresses and what is read from them are given in Table 3. There are hundreds of addresses with possible readable values [9,10]. The device implementation monitors Line 1, but the commands are available for implementations with several devices. Here, in Table 3, we have some examples of functions. The schematic in Figure 1, which is recommended by the Ducati manufacturer [33], monitors only one line, but is able to work in three-phase systems as well. According to the references, R5 Ducati is a power factor automatic controller for single-phase and three-phase networks with or

without neutral connection. The only precaution is when using the R5 Ducati device in a one-phase power system to select working phases. Using numerical methods, because of the integrated controller, the R5 Ducati device computes additional necessary quantities.

Table 3. Examples of readable addresses and the results returned.

Add.	Word	Measurement Description	Unit	Format
0002	2	Frequency	Tenths of Hz	Unsigned Long
0004	2	Three-phase Equivalent Voltage	V	Unsigned Long
0006	2	Linked Voltage (Line 1–Line 2)	V	Unsigned Long
0008	2	Linked Voltage (Line 2–Line 3)	V	Unsigned Long
0010	2	Linked Voltage (Line 3–Line 1)	V	Unsigned Long
0012	2	Voltage between Phase and Neutral Line 1	V	Unsigned Long
0014	2	Voltage between Phase and Neutral Line 2	V	Unsigned Long
0016	2	Voltage between Phase and Neutral Line 3	V	Unsigned Long
0018	2	Three-phase Equivalent Current	Hundredths of A	Unsigned Long
0020	2	Current Line 1	Hundredths of A	Unsigned Long
0022	2	Current Line 2	Hundredths of A	Unsigned Long
0024	2	Current Line 3	Hundredths of A	Unsigned Long
0026	2	Three-phase equivalent power factor*	Hundredths	bit-Signed /Unsigned Long
0028	2	Power factor Line 1*	Hundredths	bit-Signed Long
0030	2	Power factor Line 2*	Hundredths	bit-Signed Long
0032	2	Power factor Line 3*	Hundredths	bit-Signed Long
0034	2	Three-phase equivalent active power	W	bit-Signed Long
0036	2	Average three-phase equivalent active power	W	bit-Signed Long
0038	2	Maximum three-phase equivalent active power	W	bit-Signed Long
0040	2	Active power Line 1	W	bit-Signed Long
0042	2	Active power Line 2	W	bit-Signed Long
0044	2	Active power Line 3	W	bit-Signed Long
0046	2	Average active power Line 1	W	bit-Signed Long
0048	2	Average active power Line 2	W	bit-Signed Long

Function 06: "PRESET SINGLE REGISTER" lets the user set the setup parameters of the Ducati Energia device. Table 4 presents examples of the addresses of this function.

Table 4. Configuration function.

Addr.	Words	Parameter Description	Min.	Max.	Format
0002	1	VT Ratio (not available for R5 and R8)	1	500	Unsigned Int
0004	1	CT Ratio (not available for R5 and R8)	1	1250	
0006	1	Average period	1	60	Unsigned Int
0200	1	CT primary (Ampere)	1	10,000	Unsigned Int
0202	1	CT secondary (Ampere)	1	5	Unsigned Int
0204	1	CT phase insertion 0 = L1 (R); 1 = L2 (S); 2 = L3 (T);	0	2	Unsigned Int
0206	1	Enable CT inversion 0 = Disabled; 1 = Enabled;	0	1	Unsigned Int
0208	1	Enable cogeneration 0 = Disabled; 1 = Enabled;	0	1	Unsigned Int
0210	1	Frequency mode 0 = 50 Hz; 1 = 60Hz; 2 = Auto;	0	2	Unsigned Int

Table 4. *Cont.*

Addr.	Words	Parameter Description	Min.	Max.	Format
0212	1	VT primary (MSW) (Volts)	50	200,000	Unsigned Int
0214	1	VT primary (LSW) (Volts)	(210 for R5)	(160,000 for R5)	Unsigned Int
0216	1	VT secondary (Volts)	50	525	Unsigned Int
0218	1	Voltage phase 0 = L1n; 1 = L2n; 2 = L3n; 3 = L12; 4 = L23; 5 = L31;	0	5	Unsigned Int
0220	1	Step nominal voltage (Volts)	50	5000	Unsigned Int

3.2. Application Development

The application was developed in Phyton, an interpreter programming environment, which is relatively easy to follow and also ensures the possibility of an adequate interface. In this case, the user interface is in the form of an HTML page, for maximum compatibility of the application.

Flask is a micro web framework written in Python. It is classified as a microframework because it does not require particular tools or libraries. It was chosen for this application due to its small footprint and easy to use features.

The accessible routes to the application were split into two categories: public and private. The public routes were index and login, which were accessible for everyone, while the private routes required identification with a username and password and included read, admin, and logout.

In order to establish a connection to the remote power factor correction device, the MODBUS protocol was used. The function is presented below:

def get_instrument():

 # default minimalmodbus instrument parameters are MODBUS *standard (19200 8N1):*
#instrument.serial.port   # this is the serial port name
#instrument.serial.baudrate = 19200   # Baud
#instrument.serial.bytesize = 8
#instrument.serial.parity   = serial.PARITY_NONE
#instrument.serial.stopbits = 1
#instrument.serial.timeout   = 0.05   # seconds
#instrument.mode = minimalmodbus.MODE_RTU   # rtu or ascii mode
instrument = minimalmodbus.Instrument('/dev/ttyUSB0', 3) # port name, slave address (in decimal)
instrument.serial.baudrate = 9600
instrument.debug = 0
return instrument

The device registers held values of different lengths and precisions, using singed or unsigned number representations. In order to ensure an extensible and robust application, we defined a list with registers that could be read and a list of registers that could be written. We present an example to showcase the properties of each register:

readOnlyRegisters = (

{
* 'registerAddress': 1,*
* 'numberOfRegisters': 2,*
* 'name': 'Frequency',*

```
    'unit': 'Hz',
    'multiplier': 0.1,
    'isSigned': False,
}
 . . . .
}
writeOnlyRegisters = (

{
    'registerAddress': 5,
    'numberOfRegisters': 1,
    'name': 'Average period',
    'options': None,
    'min': 1,
    'max': 60,
}
 . . . .
}
```

For each property, it was necessary to use a fractional multiplier, due to unsigned integer representation. For example, 0.1 was used for frequency, thus from the tenths number representation, and the frequency was brought to the unitary level.

Figure 7 shows the general appearance of the application, accessed with a web browser (the captures were made from two different operating systems, Windows 10 and Raspbian, just to show the compatibility of the realized application). The data were read on the first page, and for the configuration, a more secure connection procedure was needed to avoid unauthorized configurations, which could cause damage.
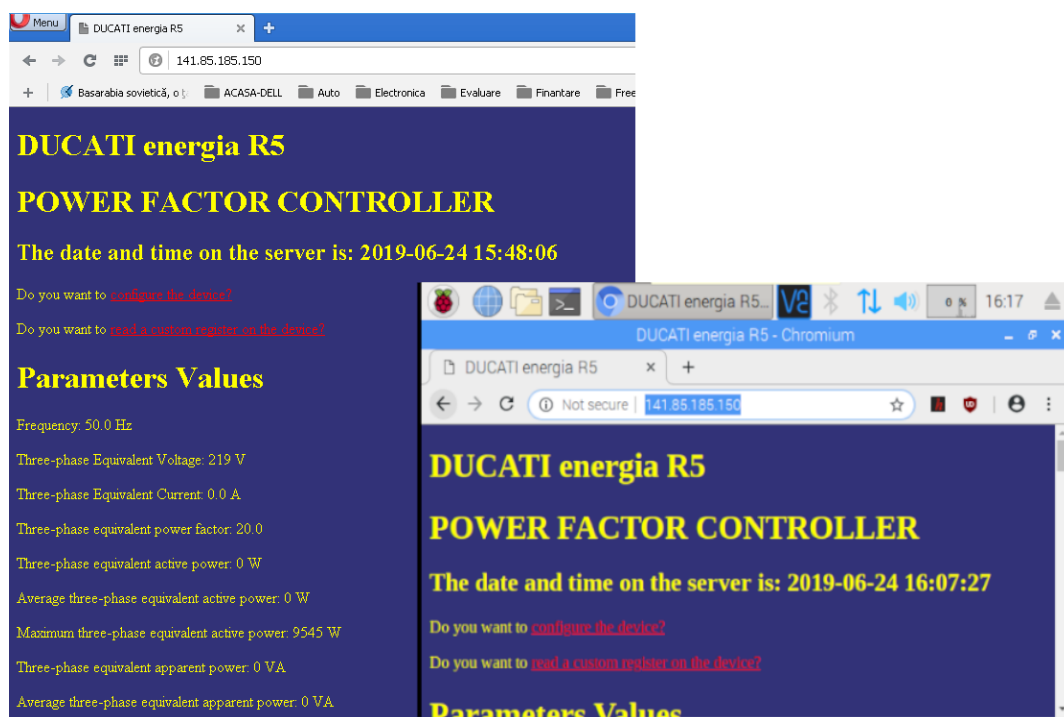
Figure 7. Appearance of the main user interface (left under Windows OS, right under Raspbian OS).

4. Discussion

In order to observe the influence on the network at the connection of the capacitor battery, the voltage waveform was captured (Figure 8), where the X axis is the time representation (10 ms/div) and the Y axis the amplitude representation (1 V/div). The complexity of this measuring system was to achieve the best solution for accurate measurement. For example, choosing the best ratio of the current transformer and the best value of the secondary circuit of the current transformer resistor was necessary to achieve the best linearity and sensitivity of measurement system. Both the reduction of the current and the modification of its phase were observed after the important variation of the current from the moment of commutation, aspects that were expected to happen. The representation scale was 1 V vertically and 10 ms horizontally, per division. For the measurement, a current transformer was used, with the higher frequency band, in order not to attenuate the transient regime. For current transformers, it is mandatory to use a secondary circuit with a resistor, to prevent a faulty state in the case of open circuit. Additionally, the resistor helped convert current into voltage in order to be easily readable by the oscilloscope. The oscilloscope probes used were equipped with a 1:10 divider, in order to attenuate the measured signal. The current transformers used were manufactured by Talema India and were of the type AC1010-AC1020. For the secondary, it was provided with five turns and a load resistance of two steps, 1.8 kohms and 270 ohms (the selection was made using a jumper); see Figure 9. In this way, a higher sensitivity could be obtained from the current transformer (1.8 kohms) or better linearity (270 ohms). The observed power factor improved from 0.64 to 0.8, using a capacity of 9.6 μF and an electric motor running without load. Regarding the resistors in Figure 9, for the current transformer, it was mandatory to have a resistor in secondary circuit, because when we had an open circuit, it could be a faulty state. Additionally, this resistor converted the current into voltage to be easily readable by the oscilloscope.
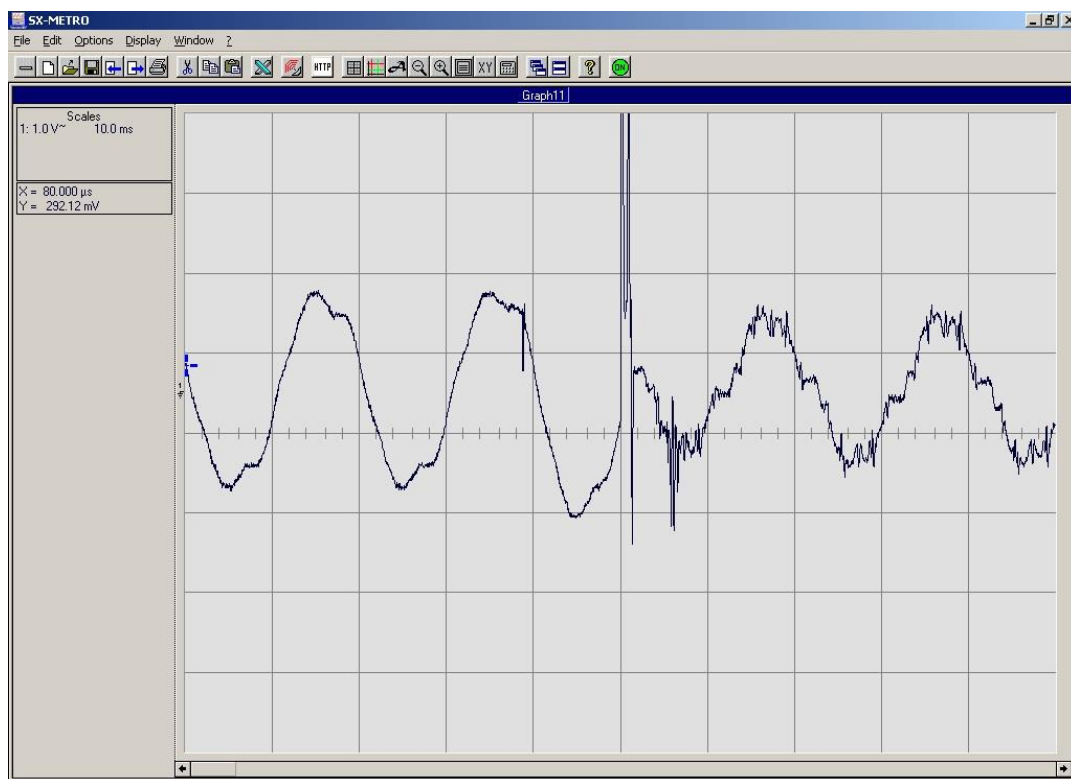
Figure 8. The appearance of the current before and after the switching moment.
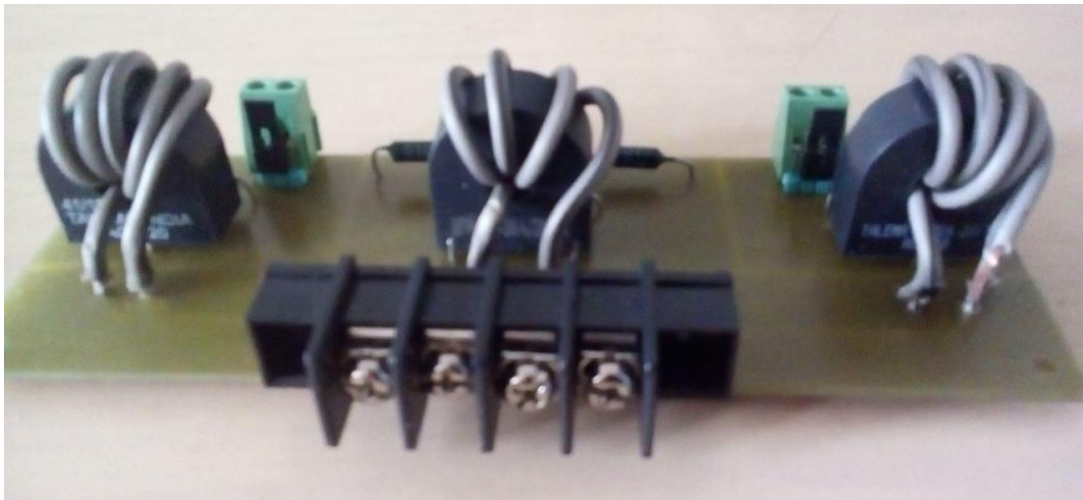
Figure 9. Current transformers used to visualize the waveform of the current at the time of switching.

During the testing of the equipment, the aim was to highlight the moment when a step connection of the capacitor batteries took place. The most convenient to use, which also provided galvanic isolation, was a broadband frequency current claw device, from DC to over one hundred kHz. The wider the frequency band, the better the transient regime was obtained. As a load, a 2.2 kW three-phase asynchronous motor was used.

The capacitors were specially designed for the correction of the power factor and contained resistors for their discharging so that at the next switching, they were not loaded with a significant voltage. This was why the equipment did not perform frequent switching, allowing no less than one minute between two switches, so that there was enough time for the capacitors to be discharged.

The interpretation of the switching moment was qualitative, highlighting the moment when it took place, and its effect on the amplitude and phase of the current. Using the PF correction device and a custom built telemetry module, we were able to adjust the configuration of the PF device remotely, as well as read and record on a server the electric current parameters. While the PF improvement was not better than other existing methods, this implementation outlined the ability to use telemetry to identify potential issues and improve the PF correction efficiency.

This power factor correction device can be a component in the emerging field of smart grids because of the remote control and measurement capabilities. It can be easily integrated in the smart grid environment using secure communication capabilities.

PF correction is very important from an economic point of view as well. In Romania, the pricing of reactive electricity to consumers, with differentiation in the case of domestic consumers, is made according to the average power factor, reported at a neutral PF, currently equal to 0.92. For a PF between 0.65 and 0.92, the pricing is done according to the energy price. If the PF is less than 0.65, the payment is calculated at three times the price of the reactive energy [35].

The estimated cost of the entire device, considering only component costs without the manufacturing process, was around 700 Euro. On the market, the price is around 165 Euro/kVA. Additionally, the cost increases when installing the power factor correction equipment (cables, settings, etc.). The comparison is valid only for the same principle of design; the cost increases considerably when another principle is used (e.g., synchronous electric drive).

For a test load of 10 kw, a benefit of 20–30% of energy efficiency was estimated. The estimation was made over five days, but to be more accurate, a longer period of time is required, e.g., several months. Due to seasons, an accurate estimation of the energy efficiency must be made over one year.

5. Conclusions

The importance of controlling and maintaining the power factor is undeniable, due to the effects that a small power factor can have on the network. There is not only an unjustified consumption, but also the possibility of the occurrence of damage, when the content of harmonics is important.

The paper presents not only a general view on the power factor and its influence on the functioning of the network, but also the dimensioning and practical realization of a proposed equipment that improves the power factor of a consumer, by connecting capacitors to the power line.

A new PFC circuit based on telemetry and remote configuration was designed and tested. The main advantage of the achieved equipment was that it could be configured and programmed remotely through an Internet connection, allowing for easy fine tuning of the algorithm's configuration parameters to achieve potentially better operation based on the time feedback loop and artificial intelligence. This is an interesting idea that will be further explored in future work. Other advantages were related to the fact that the application was designed to ensure portability and flexibility in the operation of the equipment at various load levels depending on the targeted implementation.

The configuration possibilities of the Ducati Energia R5 device are multiple, starting with both single-phase and three-phase operation and continuing with setting parameters for the capacitors used and reaching limits for triggering alarms.

The obtained results confirmed the presented theory perfectly and showed the correctness of the equipment design. The energy losses measured on the test equipment were reduced by 20% over a short test period of five days. Accurate statistical data would require longer period tests (e.g., one year). Loss of equipment efficiency is a consequence of an improper power factor. When a plant operates with a low power factor, the amount of useful energy available inside the plant at distribution transformers is considerably reduced due to the amount of reactive energy that the transformers must carry. Less current means less losses in the distribution system of the plant, because the losses are proportional to the square of the current (I^2R).

The recorded data regarding the transient regime clearly showed that the current variations could be important. In this situation, the capacities used were of a small value (μF), so the results were proportional. The influence on the obtained data was also due to the current probe. The higher the frequency band, the more spectacular the transition (by amplitude and duration).

Another interesting idea for future work can be the scheme of the measuring system for data acquisition. Simplifying the design, it consisted of conditional circuits (current transformer) and an oscilloscope. The complexity of the measuring system was focused to achieve the most accurate measurement; for example, to choose the best ratio of current transformer and the best value of secondary circuit of the current transformer resistor, which is necessary to reach the best linearity and sensitivity of the measurement system.

References

1. Apetrei, D.; Chicco, G.; Neurohr, R.; Albu, M.M.; Postolache, P. Power quality monitoring. Data relevance and usefulness. In Proceedings of the 15th IEEE Mediterranean Electrotechnical Conference MELECON, Valletta, Malta, 28 Febrauary 2010; pp. 1630–1635.
2. Golkar, A.; Golkar, A.M. Reactive power pricing in deregulated electricity market. In Proceedings of the 20th International Conference and Exhibition on Electricity Distribution—Part 1, Prague, Czech Republic, 8–11 June 2009.
3. Li, J.; Geng, X.; Li, J. A Comparison of Electricity Generation System Sustainability among G20 Countries. *Sustainability* **2016**, *8*, 1276. [CrossRef]
4. Bhatia, A. *Power Factor in Electrical Energy Management*; PDHonline Course: Fairfax, VA, USA, 2012.
5. Graña-López, M.; García-Diez, A.; Filgueira-Vizoso, A.; Chouza-Gestoso, J.; Masdías-Bonome, A. Study of the Sustainability of Electrical Power Systems: Analysis of the Causes that Generate Reactive Power. *Sustainability* **2019**, *11*, 7202. [CrossRef]
6. Emanuel, A.E. Apparent and reactive powers in three-phase systems: In search of a physical meaning and a better resolution. *Eur. Trans. Electr. Power* **2007**, *3*, 7–14. [CrossRef]
7. Robbins, B.A.; Dominguez-Garcia, A.D. Optimal Reactive Power Dispatch for Voltage Regulation in Unbalanced Distribution Systems. *IEEE Trans. Power Syst.* **2015**, *31*, 2903–2913. [CrossRef]
8. Pereira, B.R.; Da Costa, G.R.M.M.; Contreras, J.; Mantovani, J.R.S.; Da Costa, G.R.M. Optimal Distributed Generation and Reactive Power Allocation in Electrical Distribution Systems. *IEEE Trans. Sustain. Energy* **2016**, *7*, 975–984. [CrossRef]
9. Kirkham, H.; Emanuel, A.; Albu, M.; Laverty, D. Resolving the reactive power question. In Proceedings of the 2019 IEEE International Instrumentation and Measurement Technology Conference (I2MTC), Auckland, New Zealand, 20–23 May 2019; pp. 1–6.
10. Chang, W.-N.; Liao, C.-H. Development of an SDBC-MMCC-Based DSTATCOM for Real-Time Single-Phase Load Compensation in Three-Phase Power Distribution Systems. *Energies* **2019**, *12*, 4705. [CrossRef]
11. Shin, H.-K.; Cho, J.-M.; Lee, E.-B. Electrical Power Characteristics and Economic Analysis of Distributed Generation System Using Renewable Energy: Applied to Iron and Steel Plants. *Sustainability* **2019**, *11*, 6199. [CrossRef]
12. Asprou, M.; Kyriakides, E.; Albu, M. The effect of PMU measurement chain quality on line parameter calculation. In Proceedings of the 2017 IEEE International Instrumentation and Measurement Technology Conference (I2MTC), Torino, Italy, 22–25 May 2017; pp. 1–6.
13. Oancea, C.-D. Power factor evaluation in data acquisition systems. In Proceedings of the 2017 9th IEEE International Conference on Intelligent Data Acquisition and Advanced Computing Systems: Technology and Applications (IDAACS), Bucharest, Romania, 21–23 September 2017; Volume 1, pp. 481–484.
14. Oancea, C.D. Analysis of the performance of the mark-space method for determining the power in single-phase circuits. In Proceedings of the 2017 International Conference on Electromechanical and Power Systems (SIELMEN), Iaşi, Romania, 12–13 October 2017; pp. 448–451.
15. Stoica, S.-D. The Circulation of Reactive Power and the Appearance of Resonance Phenomenon at the Final User's Premises. In *UPB Scientific Bulletin, Series C: Electrical Engineering*; Politechnica University of Bucharest: Bucharest, Romania, 2011; Volume 73.
16. Olaru, D.; Floricău, D. Model Analysis for Sinusoidal Power Factor Corrector. In *UPB Scientific Bulletin, Series C: Electrical Engineering*; Politechnica University of Bucharest: Bucharest, Romania, 2012; Volume 74, pp. 273–282.
17. Fulga, N.; Popescu, M.O.; Popescu, C. On the Transients Optimization and the Power Factor Correction of the Static Converters. In *UPB Scientific Bulletin, Series C: Electrical Engineering*; Politechnica University of Bucharest: Bucharest, Romania, 2008; Volume 70, pp. 51–60.
18. Sa'Ed, J.; Amer, M.; Bodair, A.; Baransi, A.; Favuzza, S.; Zizzo, G. A Simplified Analytical Approach for Optimal Planning of Distributed Generation in Electrical Distribution Networks. *Appl. Sci.* **2019**, *9*, 5446. [CrossRef]
19. Charalambous, A.; Hadjidemetriou, L.; Zacharia, L.; Bintoudi, A.; Tsolakis, A.; Tzovaras, D.; Kyriakides, E. Phase Balancing and Reactive Power Support Services for Microgrids. *Appl. Sci.* **2019**, *9*, 5067. [CrossRef]

20. Hadjidemetriou, L.; Kyriakides, E. Accurate and efficient modelling of grid tied inverters for investigating their interaction with the power grid. In Proceedings of the 2017 IEEE Manchester PowerTech, Manchester, UK, 18–22 June 2017; pp. 1–6.

21. Ali, Z.; Christofides, N.; Hadjidemetriou, L.; Kyriakides, E. An advanced current controller with reduced complexity and improved performance under abnormal grid conditions. In Proceedings of the 2017 IEEE Manchester PowerTech, Manchester, UK, 18–22 June 2017; pp. 1–6.

22. Sangwongwanich, A.; Yang, Y.; Sera, D.; Soltani, H.; Blaabjerg, F. Analysis and Modeling of Interharmonics From Grid-Connected Photovoltaic Systems. *IEEE Trans. Power Electron.* **2018**, *33*, 8353–8364. [CrossRef]

23. Coman, C.M.; Florescu, A. Electric grid monitoring and control architecture for industry 4.0 systems. In Proceedings of the 2018 International Symposium on Fundamentals of Electrical Engineering (ISFEE), Bucharest, Romania, 1–3 November 2018; pp. 1–6.

24. Lin, C.; Chen, M. Design and implementation of a smart home energy saving system with active loading feature identification and power management. In Proceedings of the 2017 IEEE 3rd International Future Energy Electronics Conference and ECCE Asia (IFEEC 2017—ECCE Asia), Kaohsiung, Taiwan, 3–7 June 2017; pp. 739–742.

25. Tuballa, M.L.; Abundo, M.L. A review of the development of Smart Grid technologies. *Renew. Sustain. Energy Rev.* **2016**, *59*, 710–725. [CrossRef]

26. Mnati, M.J.; Bossche, A.V.D.; Chisab, R.F. A Smart Voltage and Current Monitoring System for Three Phase Inverters Using an Android Smartphone Application. *Sensors* **2017**, *17*, 872. [CrossRef] [PubMed]

27. Tureczek, A.M.; Nielsen, P.S. Structured Literature Review of Electricity Consumption Classification Using Smart Meter Data. *Energies* **2017**, *10*, 584. [CrossRef]

28. Bonisławski, M.; Hołub, M.; Borkowski, T.; Kowalak, P. A Novel Telemetry System for Real Time, Ship Main Propulsion Power Measurement. *Sensors* **2019**, *19*, 4771. [CrossRef]

29. Zhang, W.; Feng, G.; Liu, Y.-F.; Wu, B. New digital control method for power factor correction. *IEEE Trans. Ind. Electron.* **2006**, *53*, 987–990. [CrossRef]

30. Jain, R.; Sharma, S.; Sreejeth, M.; Singh, M. PLC based power factor correction of 3-phase Induction Motor. In Proceedings of the 2016 IEEE 1st International Conference on Power Electronics, Intelligent Control and Energy Systems (ICPEICES), Delhi, India, 4–6 July 2017; pp. 1–5.

31. Cano-Ortega, A.; Sánchez-Sutil, F.; Hernandez, J.C. Power Factor Compensation Using Teaching Learning Based Optimization and Monitoring System by Cloud Data Logger. *Sensors* **2019**, *19*, 2172. [CrossRef] [PubMed]

32. Quick Setup Power Factor Controller (PFC) R5. Available online: https://www.ducatienergia.com/media/products/180221-1623-guida-rapida-r5-v0l-ita-eng.pdf (accessed on 1 February 2020).

33. Assembly and Use Instructions R5 Power Factor Controllers. Available online: https://www.ducatienergia.com/media/products/180221-1625-mu-mid-r5-d-eng.pdf (accessed on 1 February 2020).

34. *Carmen Ionescu Golovanov, Measurement of Electrical Quantities in the Electric Power System*; AGIR Publishing House: Bucharest, Romania, 2009.

35. *Electricity Pricing for Captive Consumers, SCE-POC-09-19/01.11.2002*; Instructions for Charging Electricity to Captive Consumers: Bucharest, Romania, 2006.

Article

Real-Time Control Strategy of Fuel Cell and Battery System for Electric Hybrid Boat Application

Ahmed Al Amerl [1,2,]*[ID]**, Ismail Oukkacha** [1]**, Mamadou Baïlo Camara** [1,]*[ID] **and Brayima Dakyo** [1]

1   GREAH, EA 3220, University of Le Havre, 76600 Le Havre, France; ismail.oukkacha.ge@gmail.com (I.O.); brayima.dakyo@univ-lehavre.fr (B.D.)
2   Electrical Department, University of Kufa, AL Najaf 54001, Iraq
*   Correspondence: ahamedsaad@yahoo.com (A.A.A.); mamadou-bailo.camara@univ-lehavre.fr (M.B.C.)

Abstract: In this paper, an effective control strategy is proposed to manage energy distribution from fuel cells and batteries for hybrid electric boat applications. The main objectives of this real-time control are to obtain fast current tracking for the batteries' system, the DC bus voltage stability by using a fuel cell, and energy load distribution for a hybrid electric boat under varying demand conditions. The proposed control strategy is based on a combination of frequency approach and current/voltage control of interleaved boost converters to reduce the hydrogen consumption by the fuel cell and improve the quality of energy transfer. The frequency approach was dedicated to managing the DC power-sharing between the load, the fuel cell, and the batteries' storage system by extracting the power references. The closed loop control system utilized to control the energy is based on the DC/DC converters. The performance evaluation of the proposed control strategy has been tested through a real-time experimental test bench based on a dSPACE board (DS1104).

Keywords: interleaved boost converter; DC/DC converter; hybrid electric boat; energy storage system (ESS); RST control

1. Introduction

Calculating the total number of boats in the world is an inexact science, but it is stated by some reports in 2017 that there are estimated to be more than 30 million recreational boats on the planet, not including cruise ships [1]. The Electric Boat and Ship Market was valued at USD 5 billion in 2020 and expected to reach USD 10 billion by 2026 registering a compound annual growth rate (CAGR) of above 11% during the forecast period (2021–2026). It is recorded that the CO_2 emissions from boats form about 3–5% of the world's CO_2 emissions, which equates to about one billion tons [2].

The necessity of reducing pollutant emissions together with environmental issues requires special actions from boat manufacturers and researchers to propose alternative clean energy such as fuel cells (FCs) [3]. Thanks to the success of hydrogen fuel cells in heavy-duty vehicles, FCs (nowadays) are being integrated into different marine vessels. Fuel cells are playing the main role in reducing the greenhouse gas (GHG) emissions of marine industries on the ports and water. For marine vessels, fuel cells are the only viable, true zero-emission option. Just like batteries, fuel cells produce electricity with high efficiency through an electro-chemical process. The difference is, with a fuel cell, energy is stored separately in the form of hydrogen fuel. As long as fuel is available, the fuel cell power systems will produce electricity as a generator. The only emissions from a fuel cell are water vapor and heat.

Nearly more than 10 years ago, there was plenty of effort on hydrogen FCs to be the carbon-free future for transportation applications, such as recreational boating. Both hydrogen FCs and batteries can produce clean energy without any CO_2 emissions. Although batteries are less costly than *FC*, hydrogen cells do not need to recharge or run down as long as there is a stable source of hydrogen [4]. However, due to the slowness

of *FC* at starting and operation, the utilization of batteries as auxiliary sources with *FC* is, in fact, crucial to guarantee a smooth driving speed of the electric boats. In addition, the hybrid plane can integrate storage devices, such as a pack of batteries, to allow a significant reduction in hydrogen consumed by *FC* [5]. Batteries are a zero-emission power solution for smaller vessels that operate with short duty cycles. However, the lower power density and greater weight limit the use of batteries in many applications.

The hybrid energy system of *FC* and ESS is widely used in transportation applications such as Hybrid Electrical Vehicles (HEV) [6]. Most of the studies in [7–10] has been simulated under a different type of platform such as Simulink, SimPowerSystem, HOMER, etc. In the HEV application, *FC*, lithium-ion battery and ultracapacitors system was used to power the electric vehicle based on a fuzzy logic system [7]. The control of voltage and current through the DC/DC converters is based on the frequency energy management and sliding mode control.

Another nonlinear control system has been simulated to manage the power through the boost and boost-buck converters [8]. This control system has been designed to adapt the nonlinear characteristics of power electronic elements and the time-variant system. The closed loop control system has been designed to meet the requirements of system stability based on the sources (*FC* and SC). Various ESS has been combined with *FC* to ensure energy supply in the HEV, based on different topologies that respect the design of advanced charge systems [9]. A Simulink simulation has been used to carry out a mathematical model for hybrid systems consisting of *FC*/battery source for boat applications. The batteries are directly connected to the DC microgrid without any control, while the *FC* is controlled through DC/DC converters based on operation state scenarios [10]. However, most of these studies [5–10] have been modeled based on many assumptions and approximations to represent the physical operation of the system and still need to actualize.

Some other researchers have been invested in the hardware in the loop and experiments to test the control strategies applied to HEV. The supercapacitor (SC) bank has been used at a transient state of operation, in addition to the *FC* [11]. The Lyapunov nonlinear control method has been applied to the simulation system based on HEV to estimate the converter control parameters. The New European Driving Cycle (NEDC) has been used to evaluate the proposed energy management method through simulation tests compared to the experimental one [12]. The DC network has linked between multi-source *FC*, lithium batteries and ultracapacitors through DC/DC converters and an asynchronous machine through a DC/AC inverter. In [13], the authors proposed a closed loop control system to manage the distributed power between the multi-source system and load that represent the Hybrid Electric Boat (HEB). The main goal of the control system is to share the load profile between sets of two variable speed diesel generators and an auxiliary source (ESS) that is connected through the bidirectional DC/DC converter.

In 2019, the CO_2 emissions are increasing to reach 1.5 billion tons because of the significant growth in demand on all fossil fuels. To avoid these emissions, many countries, such as China, Europe and the United States, are using renewable energies in the power sector. In this context, the multi-source system consisting of wind and PV with battery has been experimentally tested to minimize the generation of a diesel system [14]. The MPPT has been used to control the PV and wind while the main goal of the battery was the compensation of intermittent power fluctuations in the system. In [15], the authors proposed a hybrid system to respect the environmental concerns and respond to the energy demand. A DC/DC converter is used to integrate PV to the DC grid in case of failure in the production of wind energy delivered through a three-phase bidirectional AC/DC converter. A survey of challenges that faced the integration of renewable energy sources has been presented in [16].

Compared to other types of stored energy, both *FC* and ESS technologies have low environmental effects. The system based on *FC* has better ability to work for more operating time than batteries. On the other hand, batteries require fewer spare components and have a low price. The results of real-time monitoring on transport applications such as

boats can gain a wide view of the challenges and advantages of using *FC* and ESS energy technologies. For this reason, *FC* energy and lithium-ion battery storage systems will be searched in this paper.

A hybrid electric system consisting of *FC* and a pack of batteries has been proposed in this paper. An efficient control strategy to manage the flow of energy between the two sources and boat power demand (load) has been presented. The system has been constructed based on the continuity of hydrogen into the fuel cell, which is considered to be the main source to provide the majority of the load whereas the Electrical Storage System (ESS) supplies the complement of the request power during the peak load and *FC* start up. The proposed control strategy has adopted the combination between the frequency approach and RST control system. The frequency approach has been modified to control the time constant in real-time implementation based on the health state of ESS. The main goals of this real-time control strategy are to maintain the reliability of the hybrid system and to secure the two sources from unsecured operation conditions, in addition to minimizing the hydrogen consumption.

The organization of this paper includes the configuration of the proposed hybrid system in Section 2. In Section 3, the control strategies of *FC* and pack of a battery system based on DC/DC converters have been detailed. Section 4 is devoted to the energy management system based on frequency approach to share the load power by controlling the DC bus voltage and the bidirectional current of the battery system. Section 5 gives a presentation of the experimental results on a reduced scale system, and finally, the conclusion remarks are described in the Section 6.

2. Structure of Hybrid Electric Boat System

The studied HEB system presented in Figure 1 consists of two types of resources (*FC* combined with the lithium batteries) and the load represented by electric boat power demand. The DC grid is connected to the *FC* through an interleaved boost converter and a pack of batteries (power source) through a buck-boost DC/DC converter. The variable load has been linked to the DC/AC inverter as shown in the HEB system configuration.
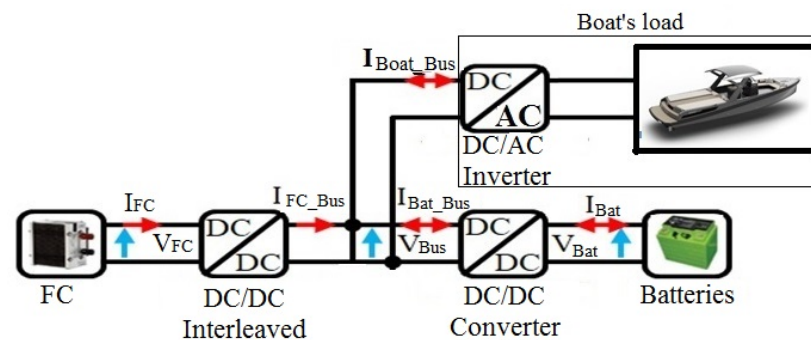
Figure 1. Hybrid Electric Boats system configuration.

In this paper, a pack of battery storage energy is utilized to overcome the disadvantages of the slow operation of the *FC* (especially at startup). The main contribution of the *FC* source is to control and maintain the continuity of DC bus voltage with or without output current of ESS. In addition, the DC energy supplied from the *FC* of the proposed system is based on interleave boost converters because of their advantages such as higher efficiency, reduced ripple currents, and substantially reducing losses.

The batteries can contribute to providing appropriate and smooth DC power generation for boat and reduce the amount of energy required from the *FC* source. The DC/DC and DC/AC converters are used for current control to improve the quality of energy transfer, to reduce the hydrogen consumption by the *FC*, using ESS in real-time conditions. Batteries ESS capacity was determined to be able to store the energy from *FC* source at charging time and return it at discharge time to meet the fast shortages in demand.

The load profile of HEB is proposed to represent boat freight transport with rated 60 kW from Le Havre to Paris in France.

3. Simulation of Power Control Strategy

3.1. Control Strategy for Bus Link Voltage

The DC energy produced by *FC* has been controlled through the interleaved boost converter that is connected to the DC bus link. The main objective of this control strategy is to stabilize and maintain the DC bus voltage during the load variation and to keep the *FC* as the primary source in this system. The boost interleaved converter protects the *FC* source from any revert energy during regeneration status by ESS. The topology of the three-phase interleaved boost converter shown in Figure 2 consists of three parallel switches controlled by Pulse Width Modulation (PWM) signals with three freewheeling diodes for each phase with three same inductances and three diodes in series.
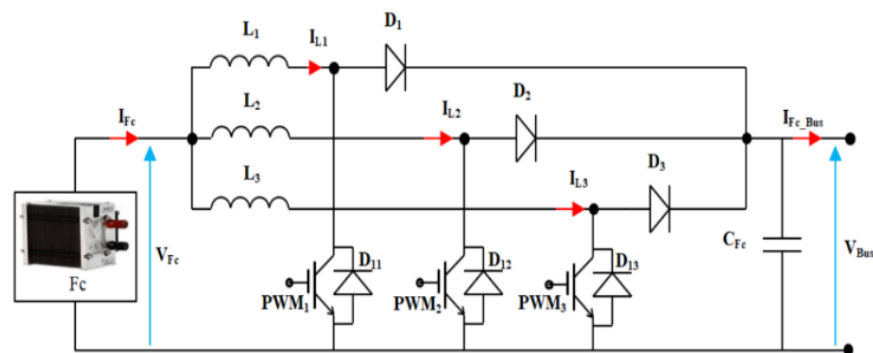
Figure 2. Interleaved boost converter.

The three switches are used to improve the output waveform and increase the delivery power of the converter. During the design of interleaved converter, the size of the converter filter is considered to reduce the ripple of the output current of the three paths. In order to take advantage of the three IGBT switches on the control design, the three PWM signals are phase shifted by 120° as shown in Figure 3. The ratio of the input current ripple to the current ripple is often used as a comparison criterion between different interleaved boost converter topologies [17].
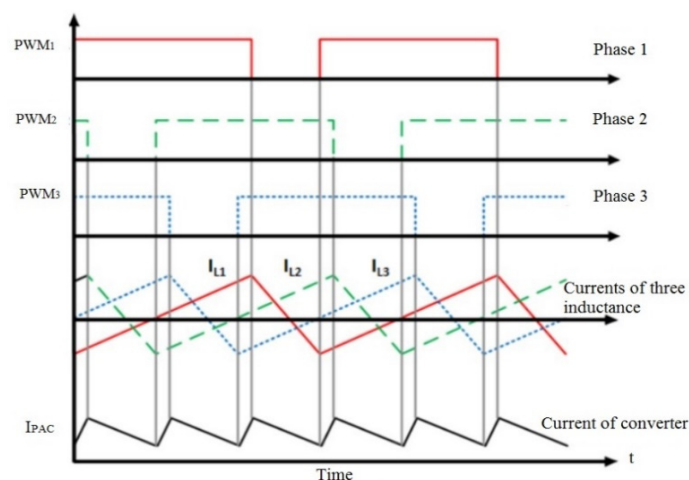
Figure 3. Three PWM signals and current for interleaved converter.

The model of a three-phase interleaved boost converter can be represented by the following three equations:

$$
\begin{cases}
L_1 \cdot \frac{dI_{L1}}{dt} = V_{FC} - (1 - \alpha_1) \cdot V_{Bus} \\
L_2 \cdot \frac{dI_{L2}}{dt} = V_{FC} - (1 - \alpha_2) \cdot V_{Bus} \\
L_3 \cdot \frac{dI_{L3}}{dt} = V_{FC} - (1 - \alpha_3) \cdot V_{Bus}
\end{cases}
\tag{1}
$$

where V_{FC} is the fuel cell voltage (measured in V); α is the duty ratio of PWM signal; L is the inductance (measured in mH); V_{Bus} is the DC Bus link voltage in (measured in V); i_{L1} is the current of conductance (measured in A); dt is the change of time in second.

The proposed control of voltage control is based on the RST polynomial method that requires tracking the reference voltage. The synthesis of this method can define the overshoot and the rise time of the measurement but has to take into account the delays as well as the nature of the disturbances and the set points [18,19]. The RST polynomial controller offers better respond and robustness toward the parametric variations in comparison with a PI controller [20].

In order to achieve minimal static error with disturbance rejection, the RST polynomials used for DC bus voltage control are presented by the following equations:

$$
\begin{cases}
S_{FC}(z^{-1}) = 1 - z^{-1} \\
T_{FC}(z^{-1}) = R_{FC}(z^{-1}) = t_{0FC} + t_{1FC} \cdot z^{-1} \\
t_{0FC} = 2 \cdot \left(1 - e^{-\omega_{FC} \cdot T_e} \right) \cdot \frac{C_T}{T_e} \\
t_{1FC} = \left(e^{-\omega_{FC} \cdot T_e} - 1 \right) \cdot \frac{C_T}{T_e} \\
C_T = C_{Fc} + C_{Bat}
\end{cases}
\tag{2}
$$

where T_e is the sampling period, ω_{FC} represent the bandwidth for controlling the voltage, C_T is the total capacitance in the bus.

In HEB, the voltage bus should be kept constant, which is considered in this control to be the voltage reference. In addition, the *FC* is the main principle that controls the DC bus voltage through the linked interleaved boost converter. Indeed, the current of the *FC* source is not controlled and will be imposed by the evolution of the system. That means, the *FC* current is deduced from Kirchhoff's current law and equal to the load current after subtracting the contributions from the pack of batteries, it can be calculated by:

$$
I_{Fc} = \frac{V_{Bus}}{V_{FC}} \cdot I_{FC\_Bus}
\tag{3}
$$

The main construction of RST voltage control with Anti-windup that used in the different controller to minimize performance degradation has shown in Figure 4.

3.2. Control Strategy of the Current System

In this section, the main principle of the control strategy is based on sharing of the load's current between *FC* and a pack of batteries. Therefore, the HEB load profile and the *FC* limited generation have been studied to select the size and number of batteries required [21]. The main factors have been considered to determine the rated power output of batteries were the maximum difference of the output power of *FC* and HEB load, the maximum value of stored power, and the searched over the duration of *SoC*.
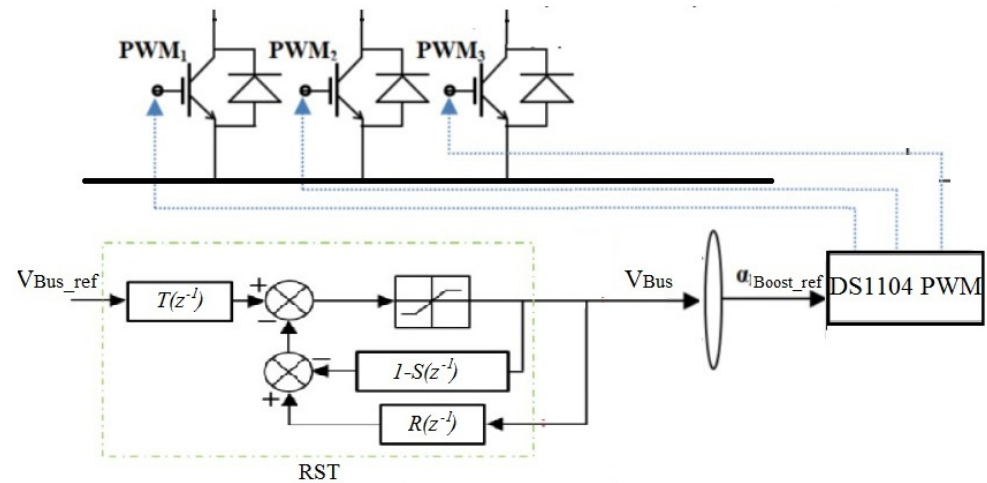
Figure 4. RST polynomial controller with Anti-windup.

The ESS power control sub-system includes the pack of batteries interfaced with a buck/boost converter to control the current between the DC bus and batteries. Lithium-ion batteries have been considered in this study because of their high energy density and efficiency in comparison to the other battery types such as NiMH, NiCd, or lead-acid. The battery output voltage is considered to be nonlinear functional because of the battery's state of charge (*SoC*) and the nonlinear current. The battery's voltage V_{Bat} is calculated by using the following equation [22].

$$V_{Bat} = V_{op} - R_{Bat} * i_{Bat} - K_b \frac{Q}{Q - i_t}.i_t + A_b e^{-B.i_t} - K_b \frac{Q}{Q - i_t}.i^* \tag{4}$$

where V_{op} is the voltage of open circuit, i_{Bat} is the current of open circuit, R_{Bat} is the total internal resistance of batteries, Q is the total capacity of batteries, K_b is polarization constant, i^* is filtered current of batteries, B is exponential capacity, i_t is actual charge batteries current, A_b is exponential voltage.

The term ($K_b \frac{Q}{Q - it}.i_t$) is called the polarization voltage that affect the *SoC*, which reflects the performance of the battery. The *SoC* of batteries plays the main role in stabilizing the bus voltage of DC link and buffering the power fluctuations. The battery voltage during the charging state increases after the pack of batteries is fully charged and referred to the polarization resistance (Pol_{res}) that can be found by:

$$Pol_{res} = K \frac{Q}{it - 0.1Q} \tag{5}$$

According to the above parameters, the model of the Li-ion battery can be represented as in Figure 5.

In this HEB system, the load profile of the boat is only at the positive part, which means there will be only one direction of current pass from the DC link to the boat's load through the DC/AC converter and has no reverted current. In *FC* source with a high voltage gain needs controller connected to an interleaved DC/DC boost converter to ensure their optimal operation and maintain the voltage of the DC link constant.
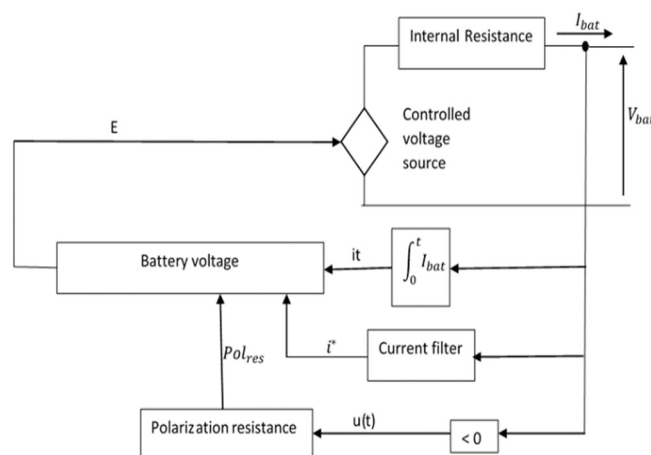
Figure 5. Model of Li-ion battery [23].

ESS units are connected to the DC bus via bidirectional DC/DC converters as shown in Figure 6. The reference current for the pack of batteries is obtained from the implemented frequency management approach and from the power balance linked to the converter as expressed in the following equation, where the losses in the converter are neglected:

$$I_{Bat} = \frac{V_{Bus}}{V_{Bat}} I_{Busbat} \tag{6}$$

In buck-boost converter, the battery current is controlled by changing the value of the duty cycle rate ($\propto$) in both cases buck and boost. Normally, the duty cycle changed from 0 to 1 but increases the response time and protects the IGBT devices; it is recommended to limit these values according to the maximum and minimum voltage of the batteries.

$$\propto_{Buck\_Bat} = \frac{V_{Bat} + V_{control\_loop\_output}}{V_{Bus}} \tag{7}$$

$$\propto_{Boost\_Bat} = 1 - \frac{V_{Bat} - V_{control\_loop\_output}}{V_{Bus}} \tag{8}$$
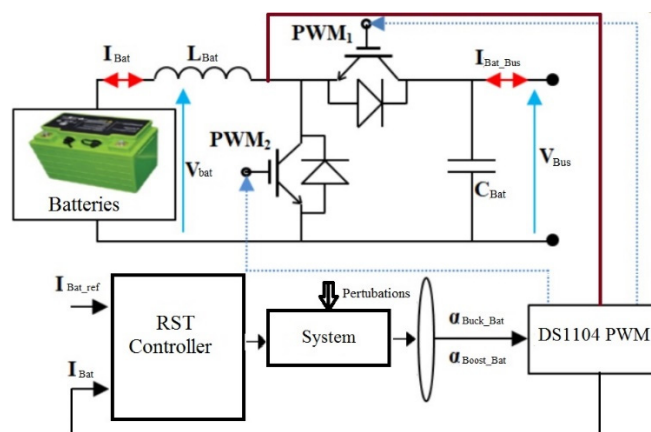
Figure 6. Battery current control system-based boost-buck converter.

At the load side, the same control technique has been used to control the current in the DC link side, according to the changes on the load profile through the frequency approach to manage the energy from sources as shown in Figure 7.
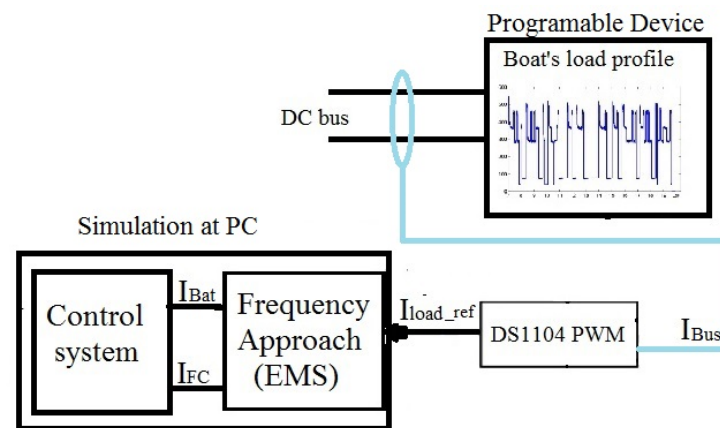
Figure 7. Control system and boat's load profile.

4. Frequency Approach for Control Strategy

The control of power is unidirectional for the fuel cell and load, while for the pack of the batteries is bidirectional. The distribution of power into the DC grid is controlled by using the frequency approach, which considers the power balance, state of charge (*SoC*) for batteries, and the limited power of *FC* and batteries. All these constraints can be described by the following equations:

Power balance:

$$P_{FC}(t) \pm P_{Bat}(t) = P_{Load}(t) \tag{9}$$

SoC:

$$SoC_{min}(t) \leq SoC(t) \leq SoC_{max}(t) \tag{10}$$

FC power limits:

$$P_{FC\ min}(t) \leq P_{FC}(t) \leq P_{FC\ max}(t) \tag{11}$$

Pack of batteries power limits:

$$P_{Bat\ min}(t) \leq P_{Bat}(t) \leq P_{Bat\ max}(t) \tag{12}$$

This control strategy is based on three main control systems to determine the switch state of the converters and on-times as shown in Figure 8. It has been proposed to control these dynamic interactions by taking into account the frequency content of the fluctuations. If the DC bus voltage is controlled to a constant value, the disturbances will be transferred to the currents.

The current reference of batteries is extracted from the load demand using the low-pass filter (LPF) based on DC bus voltage controller as shown in Figure 9. Due to profile variances for boats' demand in terms of start and operation status, the batteries current reference (I_{Bat_ref}) will use to control the state (buck/boost) of DC/DC converter at the side of the pack of batteries. The current control system is based on the changes of converter operation mode. The converter mode is operated as the follow principle: If sign $I_{Bat\_ref} > 0$, the converter operates in boost mode and pack of battery supply energy to DC-bus. Otherwise, the converter operates in buck mode and batteries store energy.
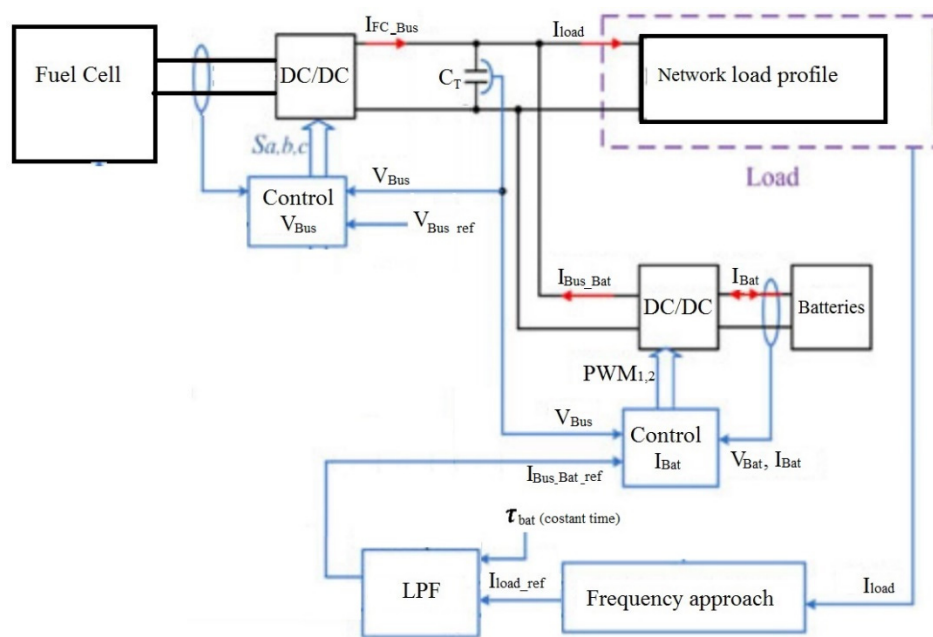
Figure 8. The proposed control strategy.
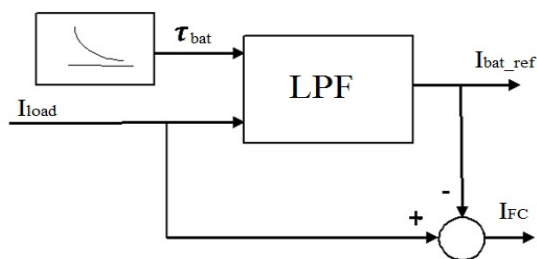
Figure 9. Batteries current reference extraction method.

The approach of low-pass filter (LPF) has been determined by identifying the functions as described in Figure 10. This method has been developed to control the time constants of the filter during the real-time operations, according to the healthy state of batteries such as *SoC*, capacitance and resistance. The currents of load are broken down into low frequency components to estimate the reference of battery power and high frequency ones, where the component of the high frequency is utilized to estimate the *FC* current.
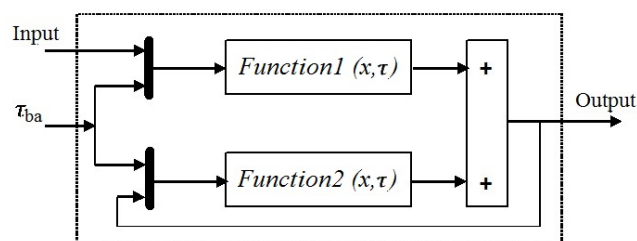
Figure 10. Control of LPF time constants in real-time.

The parameters of the functions that define the control of LPF time constant can be expressed as follows:

$$\begin{cases} Function1(x, \tau_{Bat}) = \frac{x.T_s\ (1+z)}{(T_s\ +2\tau_{Bat})z} \\ Function2(x, \tau_{Bat}) = \frac{\tau_{Bat}(2x-T_s\ )}{(T_s\ +2x)z} \\ \tau_{Bat} \approx \frac{\rho_{eBat}}{2*\pi*\rho_{pBat}} = \frac{Energy_{Bat}}{2*\pi*Power_{Bat}} \end{cases} \qquad (13)$$

5. Simulation Results for Frequency Approach

To demonstrate the feasibility of the HEB, the simulations of the energy management strategy are done using Matlab/Simulink software. The rated power for the simulated system is considered as 60 kW, and all other parameters for the rest of the system are detailed in Table 1. These parameters are obtained from the data sheet of the battery [24], from previous work [25] and the setting for the control system.

Table 1. HEB system parameter.

Description	Symbol	Parameters
Voltage of battery cell	$V_{Batmin} \sim V_{Batmax}$	2.8 V~3.8 V
Parallel resistances	R_1, R_2	0.033, 0.375 Ω
Parallel capacitances	C_1, C_2	92, 499 F
Battery power density	ρ_{PBat}	310 W/Kg
Battery energy density	ρ_{EBat}	102 Wh/Kg
Initial value of battery *SoC*	$SoC(t_0)$	97%
Number of batteries in series	N_{s_Bat}	59
Number of batteries in parallel	N_{P_Bat}	1
Electric wiring resistance for battery	R_{bwi}	4.5 m Ω
Capacitance of DC-link	$C_{Fc} = C_{Bat} = C_{Bus}$	3.3 mF
I_{Bat} smoothing inductances	L_{Bat}	12 mH
Parameters for battery's current control	$t_{0Bat}; t_{1Bat}$	85.84; 55.13
Parameters for DC-link voltage control	$t_{0Fc}; t_{1Fc}$	3.27; 3.23
Parametric coefficients	$\lambda_1; \lambda_2$ $\lambda_3; \lambda_4$	-0.984; 0.00312 7.22×10^{-5}; -1.061×10^{-4}
PWM frequency	f_d	2 kHz
Low pass filter time constant	τ_{Bat}	189 s
O2 and H2 Pressures	$P_{O2}; P_{H2}$	0.209 atm; 1.476 atm
Thickness of polymer membrane	L	25×10^{-4} cm
FC active area	Ar	67 cm^2
Maximum density of current	J_{max}	0.672 A/cm^2

The adopted energy management splits the load energy demand into several components according to the number and nature of the onboard energy sources. In this HEB case, the system contains two energy sources: fuel cells and a pack of batteries. The fuel cells stack has lower dynamic performance compared to the battery pack. Therefore, the *Fc* contribution will cover the low frequency component extracted from the load current demand, furthermore the *Fc* stack is considered to be the system's main source, and the DC-bus voltage is controlled through it.

On the other hand, the high frequency component is ensured by the battery pack because it benefits from higher dynamic characteristics than the *Fc*, and it is considered to be an auxiliary energy source. The load current separation is performed using a low pass filter.

In this simulation, the DC-bus voltage is set to a constant point as shown in Figure 11, so that the current flows through the bus link to share the load demand with the multi-source system (fuel cells stack and battery pack) according to the proposed modified frequency separation approach. The implemented voltage control strategy maintains the DC-bus voltage around the constant reference value. For this simulation, the V_{Bus} reference value is fixed to 374 V. According to the simulation result, the voltage control is satisfied since the measure is very close to the set point with minor fluctuations due to the load current variations.
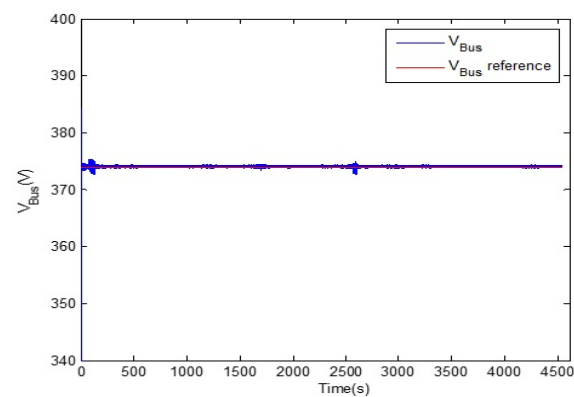
Figure 11. DC-bus voltage control result.

Figure 12 shows the profile of HEB for the total duration (4572.5 s) with a high peak of 95 A and minimum current of 2 A.
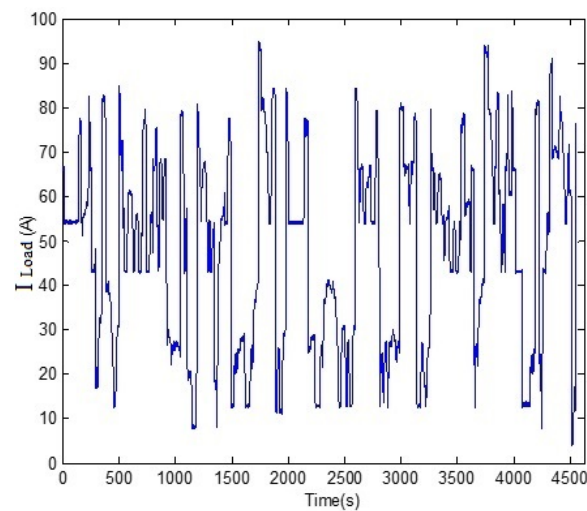
Figure 12. HEB load current profile.

Figure 13 shows the *Fc* stack current contribution, which represents the low frequency component of the load power requirement. Compared to the batteries and the load ones, I_{Fc} frequency variation is moderate. The *Fc* stack terminal voltage is illustrated in Figure 14. Regarding the voltage response, and beside the first voltage drop due to *Fc* voltage activation, V_{FC} does not fluctuate significantly compared to V_{bat}; this means that the *FC* stack is not requested during transient load states.

The battery pack current and voltage are presented, respectively, in Figures 15 and 16. The battery pack ensures the high frequency of the load power requirement. It can be noted from the above figures that when there is a considerable load demand, it will cause a fast-discharging current from the battery. On the other hand, during large load power drops, the battery voltage increases due to the recovered current. Finally, when the load demand is stable with no high frequency solicitations, the battery voltage is stable.
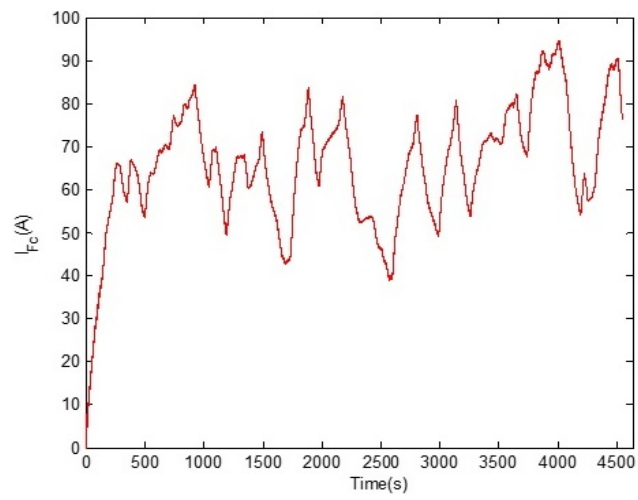
Figure 13. Fuel cells stack current contribution.
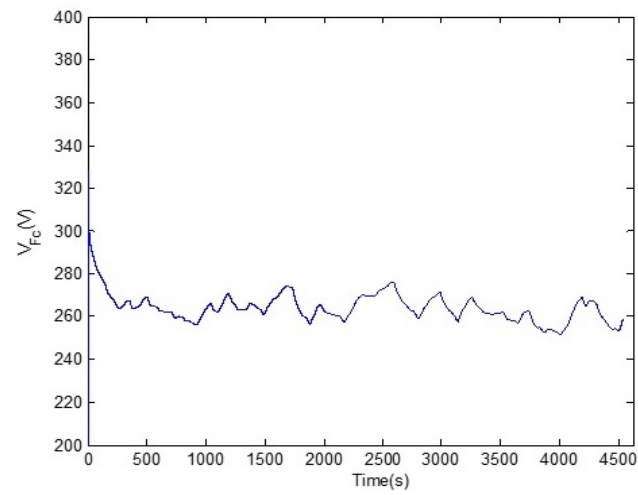
Figure 14. Fuel cells stack voltage.
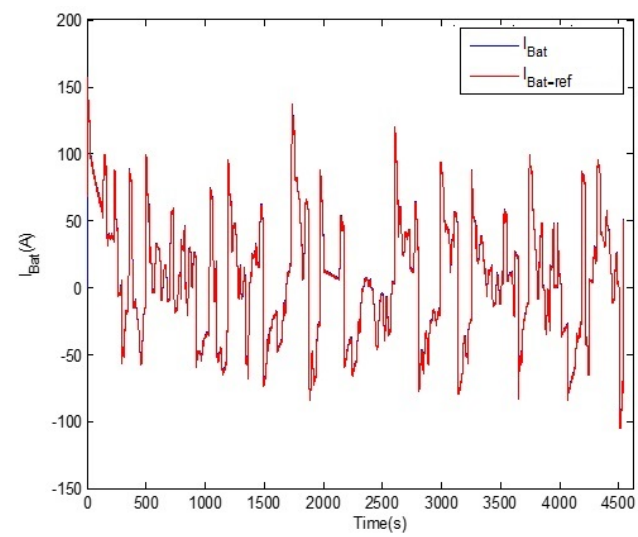
Figure 15. Current contribution of the batteries pack.
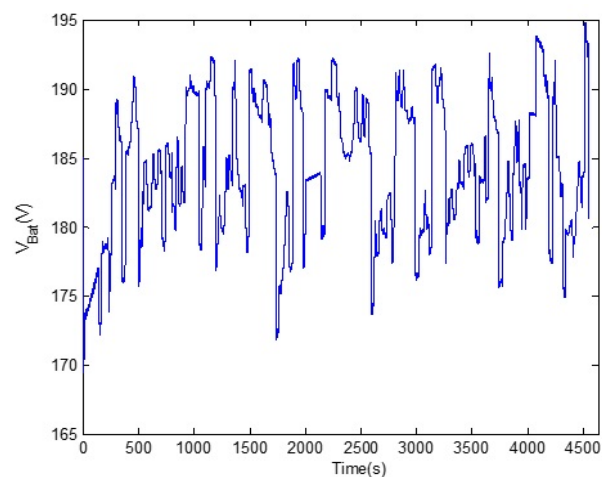
Figure 16. Voltage of pack of the batteries.

6. Experimental Verification of the Control Strategies

According to the available equipment in the laboratory, the tests are done on a reduced scale of 71. The experimental test bench as shown in Figure 17. The system consists of two PC systems (1 and 2) that are used to control and measure the test bench. The fuel cell (8) is connected through the interleaved boost converter (3) to the DC bus supplied by a pack of batteries with a total of 500 Ah (6) through DC/DC buck-boost converter (5). The pack of batteries consists of five batteries type LiFePO4 in the series each has 12 V/100 Ah. The load profile (7) has been implemented in programmable DC load (4) which is linked in the DC bus link through the unidirectional buck converter (4).
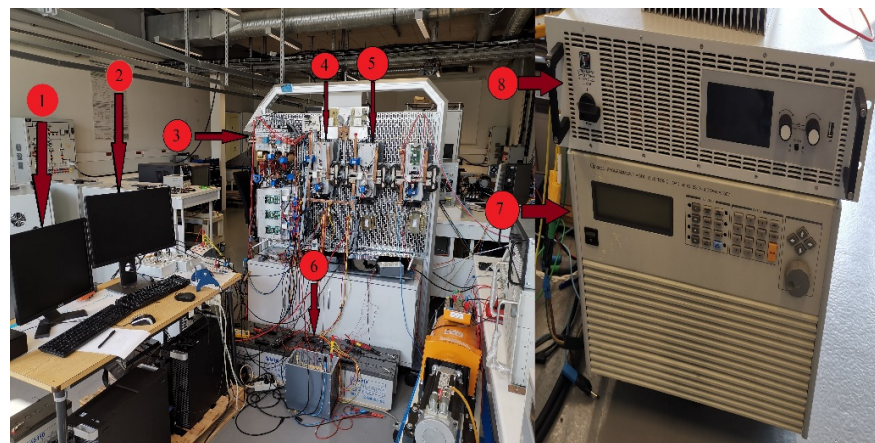
Figure 17. Test bench for HEB system.

The voltage reference of the DC bus was fixed to 105 V due to limited voltage of the batteries, while the *FC* voltage source was 70 V. The output current of the *FC* system is covered by the high frequency components for the frequency approach based on load reference current. The parameters of HEB system used in the test bench are presented in Table 2.

Table 2. Parameters of HEB System.

Parameters	Values
FC nominal voltage	70 V
Max current *FC* output	40 A
Max. voltage *FC* output	400 V
Max. current for IGBT DC/DC	300 A
Max. current for IGBT interleaved	600 A
Nominal voltage of Li-ion battery	12 V
Capacity of Li-ion battery	100 Ah
Initial state of battery charge	75%
Nominal discharge current	17.39 A
Internal resistance of battery	0.00465 ohms
Number of cells in series	5
DC-bus capacitors	400 uF
Current smoothing inductances	1 mH
Sampling period	1 ms
Switching frequency	10 kHz

The power management between the *FC* and pack of batteries sources of the HEB has been developed based on the performance of individual energy sources and the suitable controllers for each of them have been adopted. The main principle of the energy management system has been done in Figure 18. The pack of batteries and *FC* source must share the power with variable load in order to maintain the power balance in the HEB system. The control strategies are based on extracting voltage and current references for *FC* and batteries, respectively.
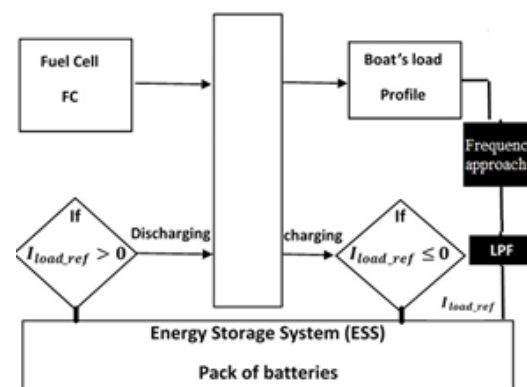
Figure 18. Management scheme for load sharing.

During the startup and rapid demand, the power output of the *FC* source cannot follow the power load required. The deficit of power in these conditions will fluctuate the frequency on the HEB that leads to the current reference for a pack of batteries to discharge batteries depending on the magnitude of deficit current. The batteries cells absorb the additional power as storage energy. If the production power exceeds the maximum capacity of storage batteries, the control system of interleaved boost converter needs to decrease the *FC* output power to maintain the stability of the DC bus link voltage.

In Figure 19, the experimental test shows that the proposed control of DC bus voltage has been maintained around the set point as a reference, with some acceptable error in measurements. The PC1 is used to implement and control the real-time simulation through the Dspace (DS1104 controller) by changing the ratio of duty of IGBT by controlling for PWM for the interleaved boost converter. The measurement of voltage bus has been used to track the reference value required.
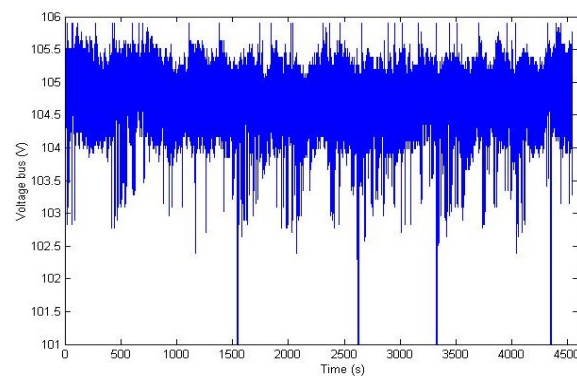
Figure 19. Result of DC bus voltage control.

The *FC* voltage results are presented in Figure 20, which is close to the limit voltage requested (70 V). The interleaved boost converter has been controlled to determine the direction and amplitude of current between the DC bus and the fuel cell source as shown in Figure 21.
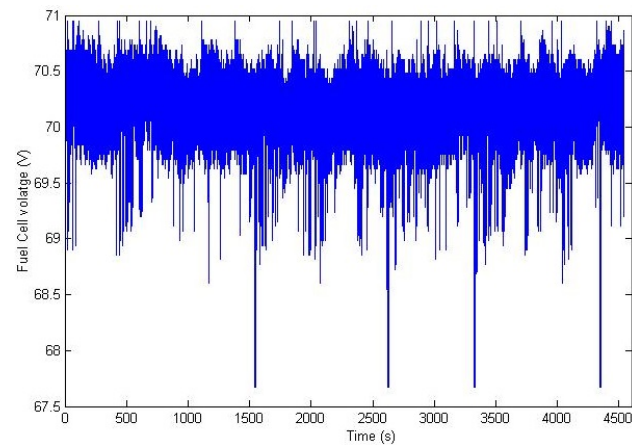
Figure 20. Measured voltage of the *FC*.
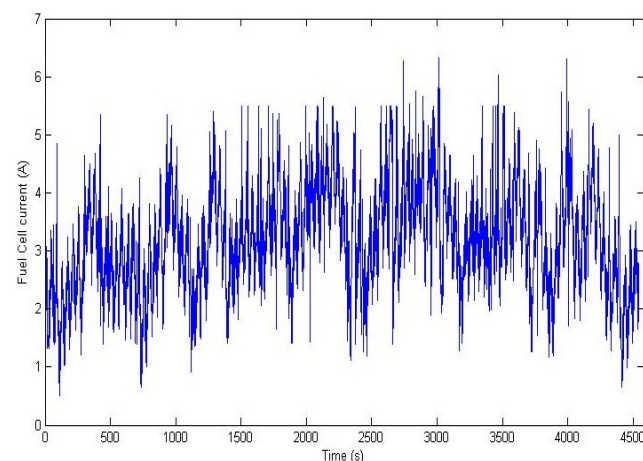
Figure 21. Measured current of *FC*.

The profile has been rescaled according to the laboratory equipment after adding some noise to have dynamic performance. The variation of demand has been controlled in real-time implementation to track the profile of boat's load, as presented in Figure 22. The maximum and minimum current of load demand is 8 and 0.7 A, respectively. It shows that the fluctuations of current from the load have been controlled by the PC2 through another

Dspace (DS1104 controller) to obtain the best correction between the simulated load profile and the production required for the real-time implementation.
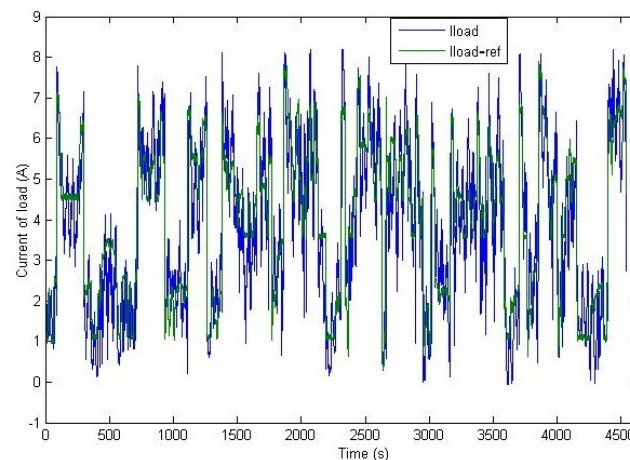
Figure 22. Load current control result.

The control strategy of the batteries' current is based on the RST method to track the current reference extracting from the proposed modified frequency approach. The constant time of frequency approach has been calculated by the simulation part at 189 s taking into account the healthy state of the pack of batteries. The result of battery voltage control with the state of charge management during HEB operation is illustrated in Figure 23. The battery controller keeps the voltage limitation less than maximum value and more than minimum value to avoid the batteries' deterioration. The unpredictable battery voltage depends on the components of high frequency for load current.
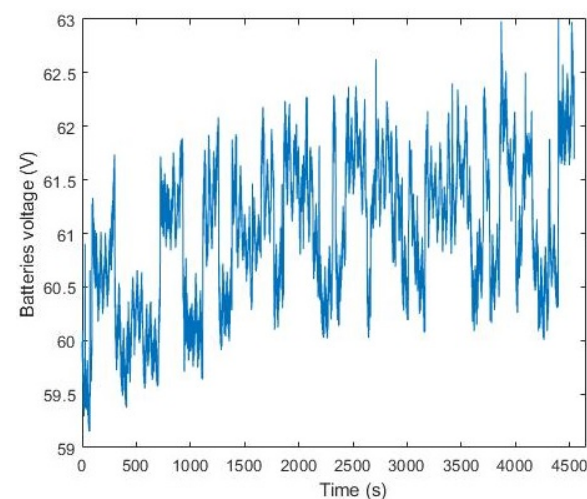
Figure 23. Batteries voltage.

When I_{bat_ref} is in the charging status (negative areas), the exceeding production of energy is stored in the batteries. Otherwise, in the discharge status (positive areas), the storage energy is used to ensure the compensation of this energy. The real-time simulation in PC2 sends the PWM for IGBTs into the converter to control the buck-boost converter. The state of the converter as buck or boost is determined according to the sign of current reference extracting from the modified frequency approach. The ratio of a duty cycle is controlled by the RST method to track the reference current required and its direction is shown in Figure 24. The amplitude of batteries current is fluctuating between positive and negative parts to determine the buck and boost state, respectively.
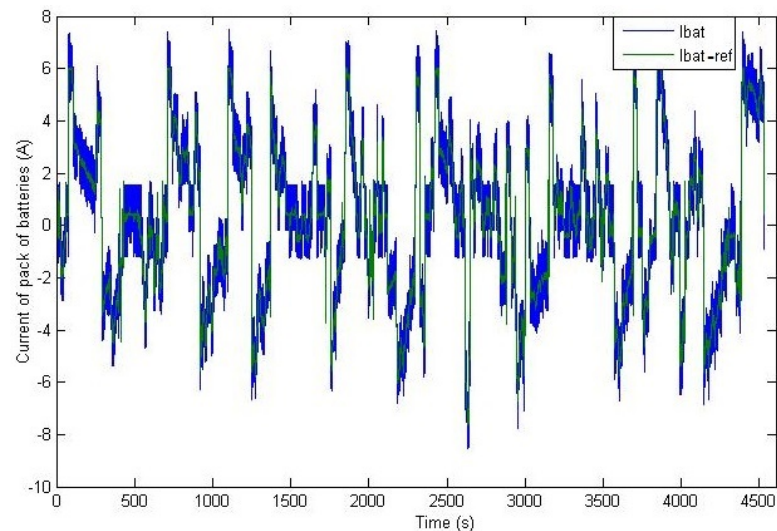
Figure 24. Measured current on the batteries compared to its references.

7. Conclusions

This paper presents the study of an HEB based on *FC* source and storage batteries. To achieve an efficient energy production of the proposed system, the energy management was based on maximizing the share of the pack of batteries and minimizing the contribution of the *FC* source. Since the energy produced by *FC* is slow at the startup and has rapid load changes, the producing energy is supplied by the ESS. A set of the batteries was connected to the DC-bus link through DC/DC buck-boost converter in order to compensate for the fluctuations of high frequency current from *FC* sources. The time constant of the frequency approach has been selected for an efficient management system based on the health state of the batteries and load profile. The simulations evaluated the performances of the proposed modified frequency approach to demonstrate its ability to respect the *SoC* conditions of batteries. The performances of the proposed DC grid concept are validated through the experimental tests, using dSPACE real-time platform (CP1104) to demonstrate the feasibility of the HEB. The results from the experimental tests in reduced scale are satisfactory and show the efficiency of the proposed control strategy.

Nomenclature

Pn	PMSG rated power
Rt	Radius of the wind turbine
ρ	Air density
Rs	PMSG resistance
Ls	Inductance of the PMSG
J	Total moment of inertia for a wind
Usef	Line to line RMS voltage in the stator
Vdcref	DC-bus voltage reference
Rres; Lres	Grid parameters
R; L	Parameters of the filter
C	DC-bus capacitor
φ	Magnetic induced flux
τ	Pitch actuator time constant

References

1. European Commission. *The EU Blue Economy Report 2019*; European Commission: Brussels, Belgium, 2019.
2. International Renewable Energy Agency. *Navigating the Way to a Renewable Future: Solutions to Decarbonise Shipping*; International Renewable Energy Agency: Abu Dhabi, UAE, 2019.
3. Cruz-Pérez, N.; Santamarta, J.C.; Rodríguez-Martín, J.; Ioras, F.; Bruccoleri, M. Incamp: Master'S Degree in the Carbon Neutral Management of Sport Marinas. In Proceedings of the EDULEARN20 Proceedings, Online Conference, 6–7 July 2020; Volume 1, pp. 151–156.
4. IEA. *The Future of Hydrogen for G20*; IEA G20: Paris, France, 2019.
5. Balestra, L.; Schjølberg, I. Modelling and simulation of a zero-emission hybrid power plant for a domestic ferry. *Int. J. Hydrog. Energy* **2021**, *46*, 10924–10938. [CrossRef]
6. Khaligh, A.; Li, Z. Battery, ultracapacitor, fuel cell, and hybrid energy storage systems for electric, hybrid electric, fuel cell, and plug-in hybrid electric vehicles: State of the art. *IEEE Trans. Veh. Technol.* **2010**, *59*, 2806–2814. [CrossRef]
7. Snoussi, J.; Ben Elghali, S.; Benbouzid, M.; Mimouni, M.F. Auto-adaptive filtering-based energy management strategy for fuel cell hybrid electric vehicles. *Energies* **2018**, *11*, 2118. [CrossRef]
8. El Fadil, H.; Giri, F.; Guerrero, J.M.; Tahri, A. Modeling and nonlinear control of a fuel cell/supercapacitor hybrid energy storage system for electric vehicles. *IEEE Trans. Veh. Technol.* **2014**, *63*, 3011–3018. [CrossRef]
9. Sharma, S.; Panwar, A.K.; Tripathi, M.M. Storage technologies for electric vehicles. *J. Traffic Transp. Eng.* **2020**, *7*, 340–361.
10. Han, J.; Charpentier, J.F.; Tang, T. An energy management system of a fuel cell/battery hybrid boat. *Energies* **2014**, *7*, 2799–2820. [CrossRef]
11. Nazir, M.S.; Ahmad, I.; Khan, M.J.; Ayaz, Y.; Armghan, H. Adaptive control of fuel cell and supercapacitor based hybrid electric vehicles. *Energies* **2020**, *13*, 5587. [CrossRef]
12. Tani, A.; Camara, M.B.; Dakyo, B. Energy management based on frequency approach for hybrid electric vehicle applications: Fuel-cell/lithium-battery and ultracapacitors. *IEEE Trans. Veh. Technol.* **2012**, *61*, 3375–3386. [CrossRef]
13. Zhou, Z.; Camara, M.B.; Dakyo, B. Coordinated power control of variable-speed diesel generators and lithium-battery on a hybrid electric boat. *IEEE Trans. Veh. Technol.* **2017**, *66*, 5775–5784. [CrossRef]
14. Lawan, M.M.G.; Raharijaona, J.; Camara, M.B.; Dakyo, B. Power control for decentralized energy production system based on the renewable energies—Using battery to compensate the wind/load/PV power fluctuations. In Proceedings of the 2017 6th International Conference on Renewable Energy Research and Applications, ICRERA 2017, San Diego, CA, USA, 5–8 November 2017.
15. Kumar, M.; Singh, S.N.; Srivastava, S.C. Design and control of smart DC microgrid for integration of renewable energy sources. In Proceedings of the IEEE Power and Energy Society General Meeting, San Diego, CA, USA, 22–26 July 2012.
16. Badal, F.R.; Das, P.; Sarker, S.K.; Das, S.K. A survey on control issues in renewable energy integration and microgrid. *Prot. Control Mod. Power Syst.* **2019**, *4*, 1–27. [CrossRef]
17. Uno, M.; Inoue, M.; Sato, Y.; Nagata, H. Bidirectional Interleaved PWM Converter with High Voltage-Conversion Ratio and Automatic Current Balancing Capability for Single-Cell Battery Power System in Small Scientific Satellites. *Energies* **2018**, *11*, 2702. [CrossRef]
18. Sant'Ana, W.C.; Salomon, C.P.; Lambert-Torres, G.; Da Silva, L.E.B.; Bonaldi, E.L.; De Oliveira, L.E.L.; Filho, J.S.; Mollica, D. Modeling and control of AC current and DC voltage of PWM converters using polynomial RST and PI controllers. In Proceedings of the 14th Brazilian Power Electronics Conference, COBEP 2017, Juiz de Fora, Brazil, 19–22 November 2017.
19. Arazi, M.; Payman, A.; Camara, M.B.; Dakyo, B. Analysis of a bidirectional resonant converter for wide battery voltage range in electric vehicles application. In Proceedings of the 2017 IEEE Vehicle Power and Propulsion Conference, Belfort, France, 11–14 December 2017.

20. Oukkacha, I.; Camara, M.B.; Dakyo, B. Energy Management in Electric Vehicle based on Frequency sharing approach, using Fuel cells, Lithium batteries and Supercapacitors. In Proceedings of the 7th International IEEE Conference on Renewable Energy Research and Applications, ICRERA 2018, Paris, France, 14–17 October 2018; pp. 986–992.

21. Benrabeh, A.; Khoucha, F.; Herizi, O.; Benbouzid, M.E.H.; Kheloui, A. FC/battery power management for electric vehicle based interleaved DC-DC boost converter topology. In Proceedings of the 2013 15th European Conference on Power Electronics and Applications, EPE 2013, Lile, France, 2–6 September 2013.

22. Wang, C.; Mi, Y.; Fu, Y.; Wang, P. Frequency control of an isolated micro-grid using double sliding mode controllers and disturbance observer. *IEEE Trans. Smart Grid* **2018**, *9*, 923–930. [CrossRef]

23. Motapon, S.N.; Dessaint, L.-A.; Al-Haddad, K. A comparative study of energy management schemes for a fuel-cell hybrid emergency power system of more-electric aircraft. *IEEE Trans. Ind. Electron.* **2014**, *61*, 1320–1334. [CrossRef]

24. Bellache, K.; Camara, M.B.; Dakyo, B.; Sridhar, R. Aging characterization of lithium iron phosphate batteries considering temperature and direct current undulations as degrading factors. *IEEE Trans. Ind. Electron.* **2020**, *68*, 9696–9706. [CrossRef]

25. Camara, M.B.; Gualous, H.; Gustin, F.; Berthon, A.; Dakyo, B. DC/DC converter design for supercapacitor and battery power management in hybrid vehicle applicationspolynomial control strategy. *IEEE Trans. Ind. Electron.* **2010**, *57*, 587–597. [CrossRef]

Efficient Operation of the Hybrid Power System Using an Optimal Fueling Strategy and Control of the Fuel Cell Power Based on the Required Power Tracking Algorithm

Nicu Bizon [1,2,3,*], **Phatiphat Thounthong** [4,5] **and Damien Guilbert** [5]

[1] Faculty of Electronics, Communication and Computers, University of Pitesti, 110040 Pitesti, Romania
[2] ICSI Energy, National Research and Development Institute for Cryogenic and Isotopic Technologies, 240050 Ramnicu Valcea, Romania
[3] Doctoral School, Polytehnic University of Bucharest, 313 Splaiul Independentei, 060042 Bucharest, Romania
[4] Renewable Energy Research Centre (RERC), Department of Teacher Training in Electrical Engineering, Faculty of Technical Education, King Mongkut's University of Technology North Bangkok, 1518, Pracharat 1 Road, Bangsue, Bangkok 10800, Thailand; phatiphat.t@fte.kmutnb.ac.th
[5] Groupe de Recherche en Energie Electrique de Nancy (GREEN), Université de Lorraine, GREEN, F-54000 Nancy, France; damien.guilbert@univ-lorraine.fr
*   Correspondence: nicu.bizon@upit.ro

Abstract: In this paper, four fuel economy strategies using power tracking control of the fuel cell boost converter and fuel cell optimization through the control of the fueling regulators were analyzed. The performance and safe operation in conditions of load disturbances and variations of renewable energy were considered. A benchmark strategy was used as a well-known strategy, which was based on the static feed-forward control of the fueling regulators. One of the four strategies is new and was based on switching the optimization reference to air and fuel regulators based on a threshold of the required power from the fuel cell system. The advantages of using the power tracking control and the optimization based on two variables instead of one are highlighted in sizing the battery capacity and its lifetime, and obtaining fuel economy respectively. The percentages of fuel economy for the analyzed strategies compared to the reference strategy are between 2.83% and 4.36%, and between 7.69% and 12.94%, in the case of a dynamic load cycle with an average of 5 kW and 2.5 kW, respectively.

Keywords: hybrid power system; nano-grid; fuel cell; fuel economy; power tracking; optimization

1. Introduction

A hybrid power system (HPS) includes renewable energy sources, power generators, DC and AC loads, and energy and power storage devices that ensure the balance of power flows in conditions of stability and safe operation of the entire system [1]. One or more HPSs are usually integrated into a nano-grid or a mini-grid [2]. Depending on the size (kW), capability, and complexity of a grid, they are classified into mini-grids, micro-grids, nano-grids, and pico-grids [3]. For example, a nano-grid can produce or consume energy in interaction with other mini-, micro- or nano-grids [4]. Thus, the HPS based on fuel cell (FC) systems as backup energy source proposed in this study can emulate the operation of a nano-grid by including the power demand on the AC bus (from AC load and power exchanged with the grid in grid-connected mode) in the power profile of the DC load.

Due to the growing global energy demand in recent years [5], the reduction of fossil fuel resources [6] and the increase in greenhouse gas emissions have been contributing to climate change

and global warming [7]. Hence, sustainable energy development policies have been imposed [8]. The increasing use of renewable energy sources (RES) in the last decade has clearly shown that they are a sustainable option for providing the energy needed for decades to come [9].

However, it is worth mentioning that each RES has a variable profile (even intermittent), so regardless of how the combination of RESs available in a certain location (where in addition to solar energy, there can be energy generated by wind, rivers, tides, biomass and so on) the balance of power flows must be compensated to ensure the stability of HPS [10]. Given that FC technology has matured and costs have been declining year by year, the FC system is frequently used as an auxiliary power source (instead of a diesel generator) to reduce the battery capacity. However, since fuel cells feature slow dynamics, they cannot be employed to respond to dynamic solicitations from the loads connected to the DC bus. Therefore, the use of a hybrid energy storage system (ESS) such as the combination batteries/ultracapacitors is required to compensate the dynamic operations [11].

If FC HPS is not connected to the grid (being included in a nano-grid), it is recommended that the excess renewable energy be stored in hydrogen tanks using an electrolyzer [12]. If FC HPS is connected to the grid, this surplus energy can be sold on the energy market when the price is the best.

This results in a hybridization of the grids by including complementary technologies for energy generation and storage [13], with the aim of attenuating the variability of RES power by integrating complementary technologies and efficient control of power converters [14]. Thus, the objectives of this paper are as follows:

1. To analyze four fuel economy strategies using power tracking control (PTC) of the FC boost converter and optimization through global extremum seeking (GES)-based control of the fueling regulators, as (1) performance compared with a benchmark strategy, and (2) safe operation in conditions of load disturbances and variations of renewable energy;
2. To design and test a new fuel economy strategy using PTC and optimization through GES-based control that is switched to the fuel and air by using a tuned power threshold to maximize the fuel economy;
3. To highlight the operation of the HPS in conditions of load disturbances and variations of renewable energy under PTC and related advantages in sizing the battery capacity and its lifetime.

   Secondary objectives are focused on:

1. Identifying performance indicators to recognize the strategies of a subclass among other subclasses belonging to the same class of optimization strategies;
2. Proposing indicators that will allow estimation of fuel consumption over a predicted load cycle up to the first refueling station if the consumption during a standard load cycle is known.

The novelty of this study compared to other similar studies (including those published by the authors) is given by the following elements presented and validated in this study:

1. A new fuel economy strategy based on switching the optimization reference to air and fuel regulator considering a threshold of the required power from the fuel cell system is proposed and analyzed as performance compared to the original reference strategies and a commercial benchmark strategy.
2. Considering a variable power profile for the load demand and the renewable power, the advantages in design and operation of the battery stack due to the charge-sustained mode for battery using the new power tracking control proposed for the FC system are highlighted as follows: a reduced capacity and size is needed for the battery; an increased battery lifespan could be obtained avoiding the frequent charge-discharge cycles that appear in other strategies proposed in the literature; maintenance costs can be reduced (due to the fact that it is not necessary to monitor the state of charge (SOC) of the battery, because the final SOC will be almost equal to the initial SOC).

3. The advantages of using a new optimization fuel strategy based on two variables instead of one are highlighted by fuel economy obtained under variable power profile for the load demand and the renewable power.

4. New performance indicators to recognize the strategies of a subclass among other subclasses are proposed and validated using the four strategies analyzed here.

So, besides the introduction, the paper is structured into a further four sections as follows. Section 2 presents the HPS model, detailing in subsections the PTC, GES control, and fueling strategies analyzed in this paper. Section 3 presents the results obtained in stationary and dynamic regimes of HPS. Finally, Section 4 comparatively analyzes the results and Section 5 concludes the paper.

2. Modeling of the Hybrid Power System

The structure of the hybrid power system (HPS) is shown at the top of Figure 1, which presents the HPS diagram and details the following subsystem: the energy management unit that contains the PTC, the optimal fueling strategy, the real-time optimization algorithm, and the semi-active ESS topology. The renewable power level on the DC bus is controlled by the k_{RES} parameter (see the HPS diagram at the top of Figure 1). The FC power will be generated based on the PTC to compensate the power flow balance on the DC bus and operate the battery in charge-sustained mode.

The inverter system and AC load have been equated at the DC bus level with a DC load. DC load is modeled by a controlled current source, resulting in a dynamic power (P_{load}) required from the power sources connected to the DC bus (see for example, Figure 2). Non-polluting energy sources such as photovoltaic panel arrays [15] and wind turbine farms [16] may provide renewable energy, but the available renewable power profile is variable (depending on weather, season, etc.) [17], and the DC bus power balance must be dynamically compensated by the ESS [18]. Consequently, it will result in a variable profile for ESS power due to the changed power with DC bus, with frequent charge-discharge cycles, which reduce the battery life [19]. Furthermore, battery pack capacity must be oversized to provide the DC power needed under a variable power profile from RES, such as that shown in Figure 3a or Figure 4a (P_{RES1} and P_{RES2} for $k_{RES} = 1$ and $k_{RES} = 2$). RES is also modeled by a controlled current source to easily change the RES power profile.

The battery/ultracapacitors hybrid ESS (see bottom of the Figure 1) uses a semi-active topology (with the battery connected directly to the DC bus and the ultracapacitors stack connected to the DC bus via a bidirectional DC-DC power converter), which is the most widely used in the literature because it ensures a trade-off between cost, performance, and flexibility in control.

The ESS power is shown in Figures 3b and 4b for $k_{RES} = 1$ and $k_{RES} = 2$, respectively. In the first case, the battery is discharged and the state-of-charge (SOC) will decrease. In the second case, the battery operates in charge-discharge cycles, but in average value (AV) it seems to operate in charge-sustained mode (so, the final SOC will be approximately equal with the initial SOC of 80%). However, it is observed that there are charge and discharge cycles that must be taken into account in the design of the battery capacity. Note that $P_{load(AV)} = 5$ kW, $P_{RES1(AV)} \cong 2.5$ kW, and $P_{RES2(AV)} \cong 5$ kW, so $P_{ESS1(AV)} \cong 2.5$ kW, and $P_{ESS2(AV)} \cong 0$.

Battery pack operation in charge-sustained mode with SOC variations within the admissible limits due to a reduced level of the ESS power exchanged with DC bus has the following advantages: no battery capacity oversizing and SOC monitoring is required.

Therefore, it is necessary to use a backup energy source to operate the battery pack in charge-sustained mode ($P_{ESS(AV)} \cong 0$) with a reduced level of the ESS power exchanged with DC bus [20]. If a clean solution is desired, then the fuel cell (FC) system can be used [21].
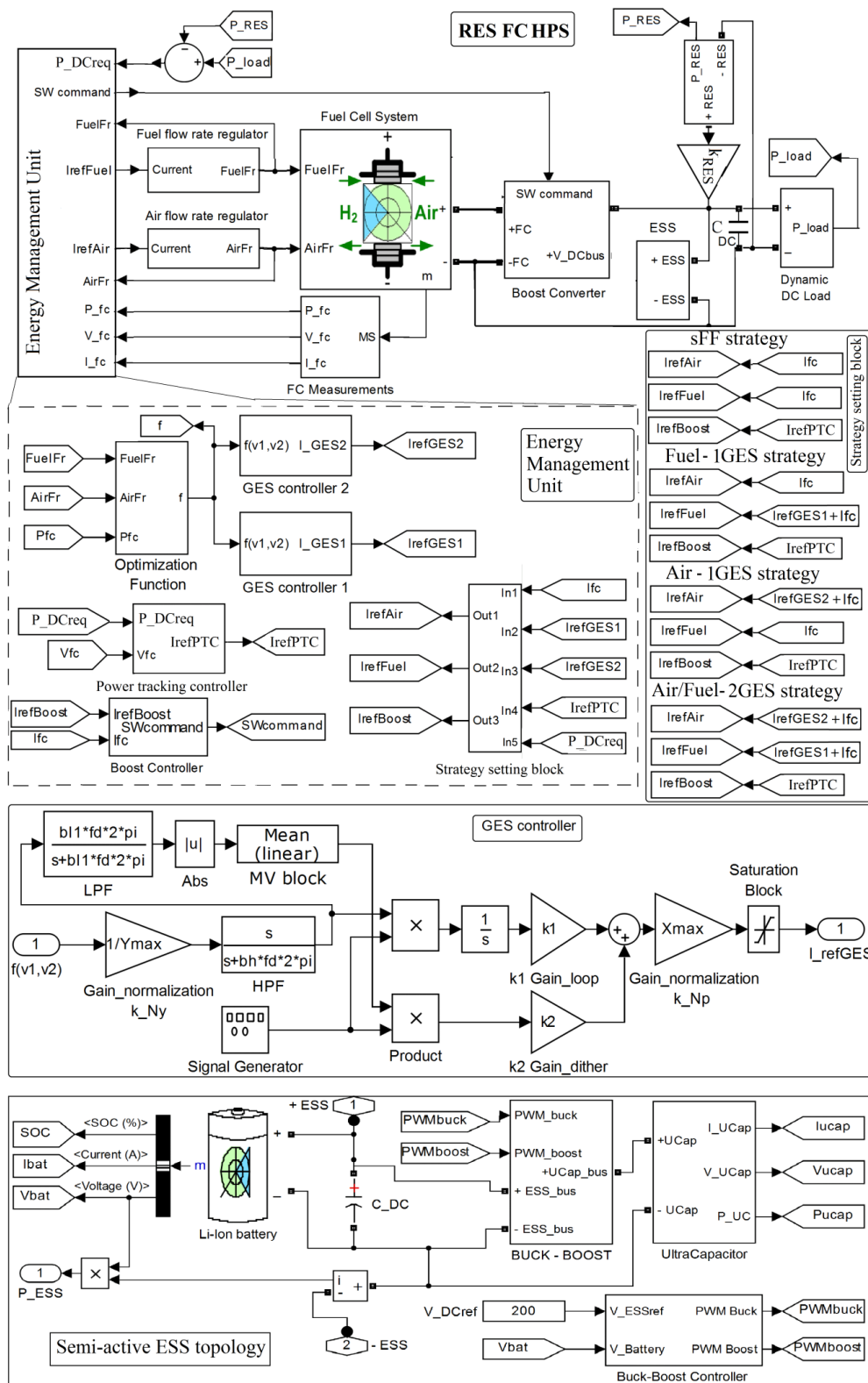
Figure 1. Hybrid power system (HPS).
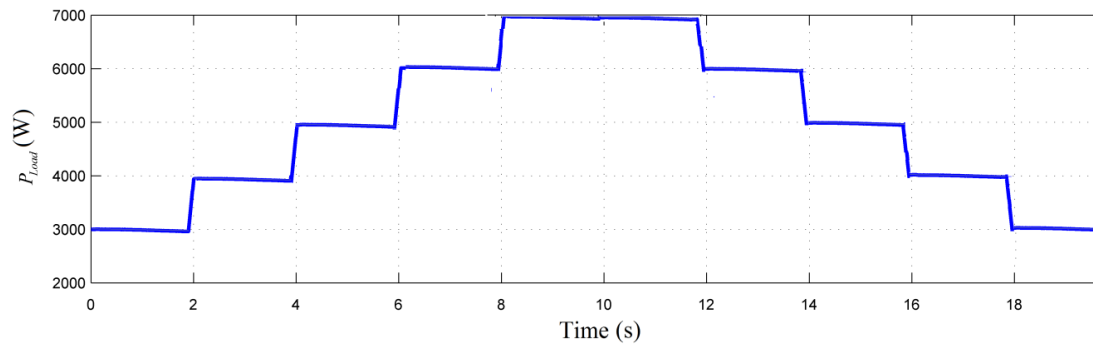
Figure 2. Load power profile.
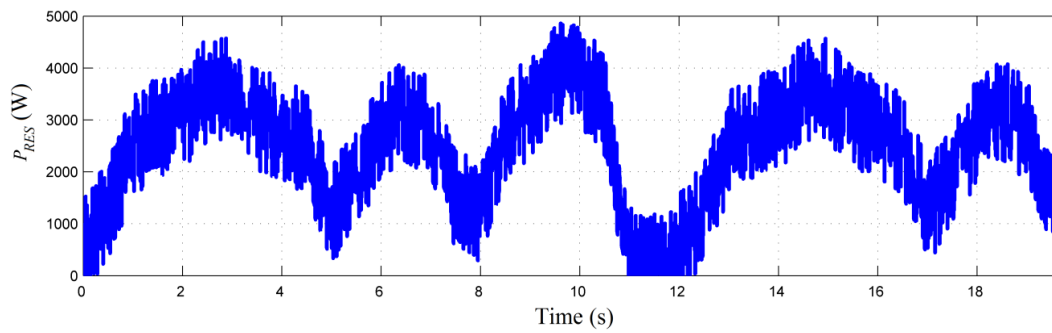
(**a**)
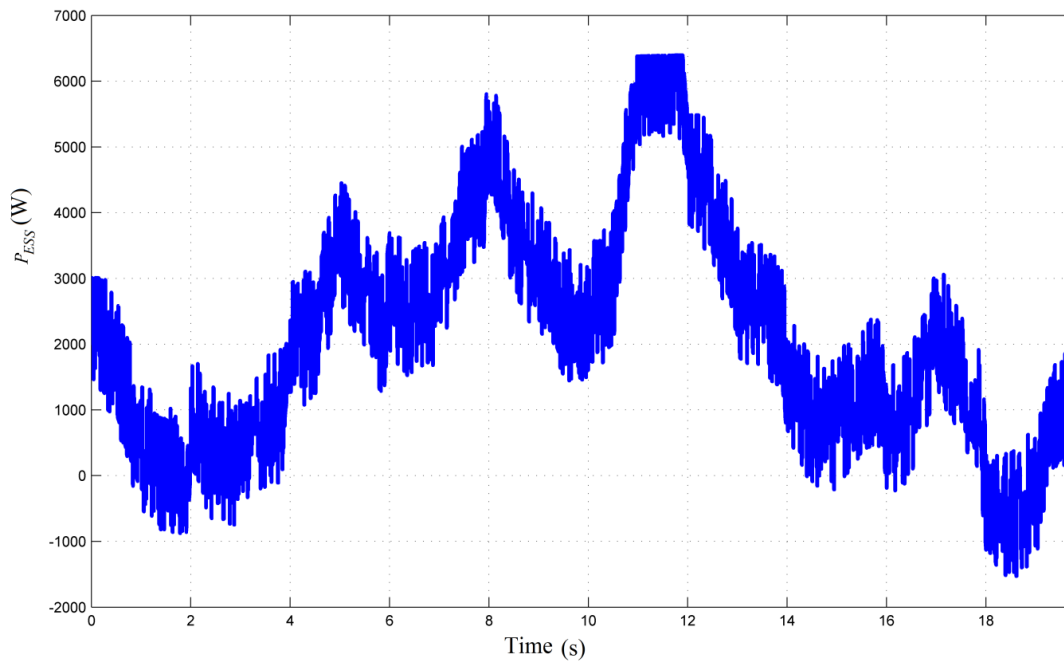
Figure 3. The first power profile for the renewable energy source (RES), P_{RES1} for $k_{RES} = 1$ (**a**) and energy storage system (ESS), P_{ESS1} for $k_{RES} = 1$ (**b**).
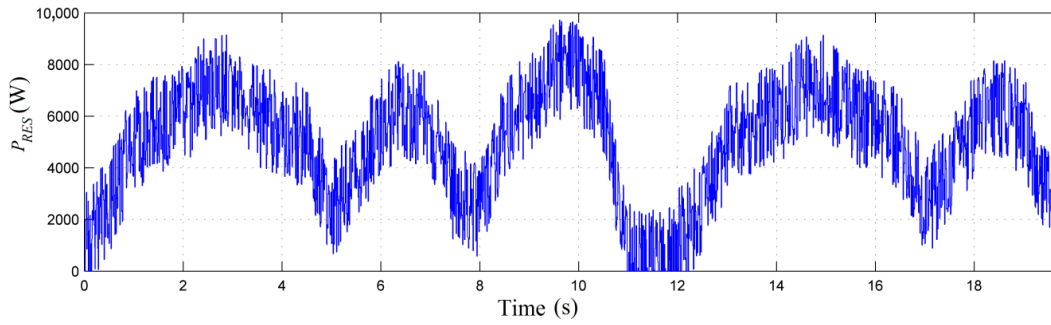
(**a**)
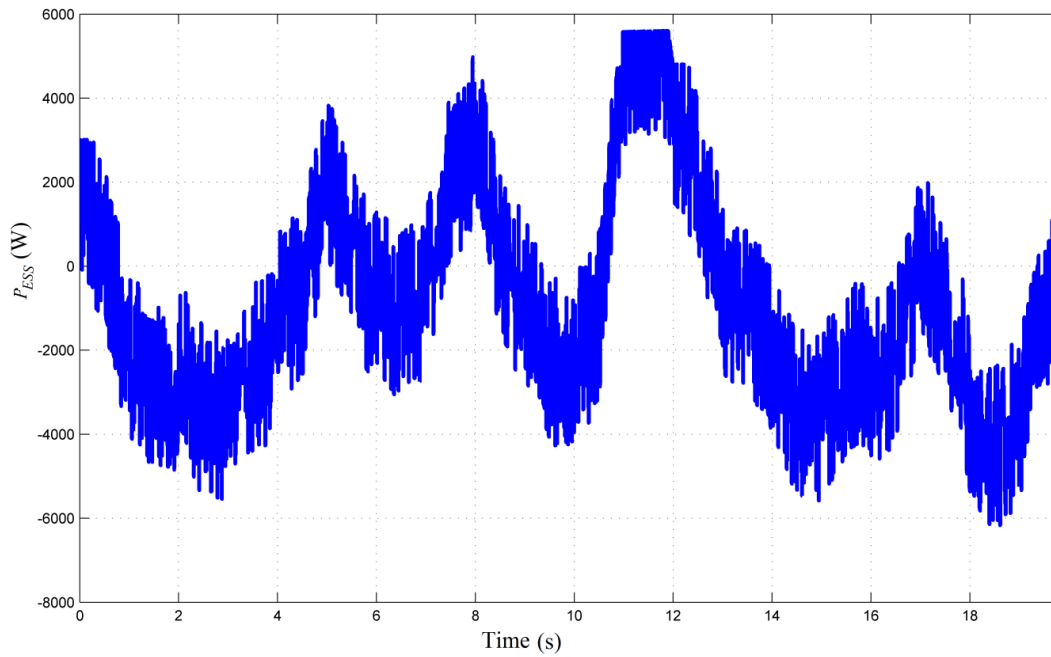
(**b**)

Figure 4. The second power profile for the RES, P_{RES2} for k_{RES} = 2 (**a**) and ESS, P_{ESS2} for k_{RES} = 2 (**b**).

In this study, a proton-exchange membrane fuel cell (PEMFC) and an electrolyzer was used. The electrolyzer must be supplied with excess power $(P_{RES} - P_{load}) > 0$, when the FC system does not have to generate power (being switched off or operating in standby mode) [22]. If $P_{RES} < P_{load}$ and $P_{ESS(AV)} \cong 0$, then the FC system must generate the power requested to compensate for the DC power flow balance $(P_{DCreq} = P_{load} - P_{RES} > 0)$. Power P_{DCreq} is generated via a DC-DC boost converter (with efficiency η_{Boost}). Thus, FC net power must be $P_{FCnet} = P_{DCreq}/\eta_{Boost}$ under the PTC that generates the switching (SW) command.

The oxygen and hydrogen flow rates (*AirFr* and *FuelFr*) of the PEMFC system is controlled with air and fuel regulators having as references $I_{ref(Air)}$ and $I_{ref(Fuel)}$ [23]:

$$AirFr = \frac{60000 \cdot R \cdot (273 + \theta) \cdot N_C \cdot I_{ref(Air)}}{4F \cdot (101325 \cdot P_{f(O2)}) \cdot (U_{f(O2)}/100) \cdot (y_{O2}/100)} \tag{1}$$

$$FuelFr = \frac{60000 \cdot R \cdot (273 + \theta) \cdot N_C \cdot I_{ref(Fuel)}}{2F \cdot (101325 \cdot P_{f(H2)}) \cdot (U_{f(H2)}/100) \cdot (x_{H2}/100)} \tag{2}$$

where $N_C, \theta, U_{f(H2)}, U_{f(O2)}, P_{f(H2)}, P_{f(O2)}, x_{H2}, y_{O2}$ are default parameters explained in [24].

For a given FC net power under PTC reference ($I_{ref(PTC)}$), the fuel consumption can be minimized by using an optimal fueling strategy to set in real-time the references $I_{ref(Air)}$ and $I_{ref(Fuel)}$ [25].

The aforementioned references ($I_{ref(PTC)}$, $I_{ref(Air)}$ and $I_{ref(Fuel)}$) are outputs of the energy management unit that contains the PTC, the optimal fueling strategy, and the real-time optimization algorithm. The design of the energy management unit will be detailed in the next sections.

2.1. Control of the Fuel Cell Power Based on the Required Power Tracking Algorithm

The PTC has been designed based on the DC power flow balance as follows:

$$C_{DC}u_{DC}du_{DC}/dt = p_{DC} + p_{RES} + p_{ESS} - p_{Load} \tag{3}$$

where $p_{DC} = \eta_{boost}p_{FCnet}$ is the power generated by the FC system via DC-DC boost converter, p_{FCnet} is FC net power, p_{RES} is RES power, p_{ESS} is ESS power and p_{Load} is load power.

DC voltage u_{DC} is regulated to V_{DCref} = 200 V by controlling the power exchanged by a 50 F ultracapacitors (UC) stack with DC bus via a bidirectional DC-DC converter and filtered by a 0.01 F capacitor (C_{DC}). Therefore, a semi-active ESS topology was designed [20,21] and implemented here using a 100 Ah lithium-ion battery pack and a 50 F UC stack (see bottom of Figure 1).

If

$$p_{DC} = \eta_{Boost}p_{FCnet} = p_{DCreq} = p_{Load} - p_{RES} \tag{4}$$

then

$$C_{DC}u_{DC}du_{DC}/dt = p_{ESS} \tag{5}$$

So, on average value (AV):

$$P_{ESS(AV)} = 0 \tag{6}$$

However, due to implementation of the optimal fueling strategy, the FC net power may differ a bit to the value resulting from (4), being approximate to that value:

$$p_{FCnet} \cong \frac{p_{Load} - p_{RES}}{\eta_{Boost}} \Rightarrow I_{FC} \cong \frac{p_{Load} - p_{RES}}{V_{FC}\eta_{Boost}} \tag{7}$$

So, the FC current reference ($I_{ref(PTC)}$) obtained from the PTC will be given by (8):

$$I_{ref(PTC)} = \frac{p_{Load} - p_{RES}}{V_{FCnet}\eta_{Boost}} = \frac{p_{DCreq}}{V_{FCnet}\eta_{Boost}} \tag{8}$$

The optimal fueling strategy is selected using the strategy-setting block (see the energy management unit presented in the middle of Figure 1). Note that for all strategies, the boost controller has FC current (I_{FC}) as one input and the second input ($I_{ref(Boost)}$) is set to PTC reference ($I_{ref(PTC)}$). Thus, using, for example, a boost controller with 0.1 A hysteresis, the FC current will track the PTC reference.

The battery pack and ultracapacitors stack will compensate for the energy and power imbalances in DC power flow balance (3) due to the implementation of the optimization strategy and slow power response of the FC system (using 100 ms time constant and 100 A/s slope limiters in the fueling regulators).

The references $I_{ref(Air)}$ and $I_{ref(Fuel)}$ were specifically established for each fueling strategy analyzed in this study (see the strategy-setting block presented in the middle of Figure 1), as will be presented in the next section.

2.2. Fueling Strategies

In order to compare the performance of the fueling strategies analyzed in this study, a well-known control strategy, applied in many commercial applications and known in the literature as the static feed-forward (sFF) control [26], will be used as a reference.

In sFF strategy, the fueling regulators are both controlled by FC current, so the references $I_{ref(Air)}$ and $I_{ref(Fuel)}$ are set as follows:

$$I_{ref(Fuel)} = I_{FC} , \; I_{ref(Air)} = I_{FC} \tag{9}$$

Optimizing the operation of the FC system referred in this study to the minimization of total fuel consumption ($Fuel_T = \int FuelFr(t)dt$) using an optimization function given by (10):

$$f(x, AirFr, FuelFr, P_{load}, P_{RES}) = 0.5 \cdot P_{FCnet} + k_{fuel} \cdot Fuel_{eff} \tag{10}$$

where x is the vector of FC state variables [26], $Fuel_{eff} \cong P_{FCnet}/FuelFr$ is the fuel consumption efficiency and $k_{fuel} = 25$ (Lpm/W) to minimize the fuel consumption. This value of the k_{fuel} parameter has been obtained by sensitivity analysis performed in the range 0–50 (Lpm/W) for the optimization function given by (10) [23,25].

The global extremum seeking (GES) [27] was selected as the search algorithm of the maximum for function f in conditions of load disturbances and variations of renewable energy. The search variables were $v_1 = AirFr$ and $v_2 = FuelFr$ and the GES model (which is shown in the bottom of Figure 1) will be detailed in the next section.

For the fueling strategies analyzed in this study, the references $I_{ref(GES1)}$ and $I_{ref(GES2)}$ generated by GES controllers were specifically established to the references $I_{ref(Air)}$ and $I_{ref(Fuel)}$ as follows.

For the strategy using optimization through GES-based control of the fuel regulator (labelled below as Fuel-1GES strategy), the settings were:

$$I_{ref(Fuel)} = I_{FC} + I_{ref(GES1)}, \; I_{ref(Air)} = I_{FC} \tag{11}$$

For the strategy using optimization through GES-based control of the air regulator (labelled below as Air-1GES strategy), the settings were:

$$I_{ref(Air)} = I_{FC} + I_{ref(GES2)}, \; I_{ref(Fuel)} = I_{FC} \tag{12}$$

For the strategy using optimization through GES-based control of both air and fuel regulators (labelled below as Air/Fuel-2GES strategy), the settings were:

$$I_{ref(Fuel)} = I_{FC} + I_{ref(GES1)}, \; I_{ref(Air)} = I_{FC} + I_{ref(GES2)} \tag{13}$$

A new strategy was proposed using optimization through GES-based control switched to the fuel and air (labelled below as Air/Fuel-2GES SW strategy). A power threshold to maximize the fuel economy was used, so the settings are given by (14):

$$I_{ref(Fuel)} = \begin{cases} I_{FC}, \; if \; P_{DCreq} \le P_{ref} \\ I_{FC} + I_{ref(GES1)}, \; if \; P_{DCreq} > P_{ref} \end{cases} , \; I_{ref(Air)} = \begin{cases} I_{FC} + I_{ref(GES2)}, \; if \; P_{DCreq} \le P_{ref} \\ I_{FC}, \; if \; P_{DCreq} > P_{ref} \end{cases} \tag{14}$$

Air/Fuel-2GES SW strategy uses the best fuel saving strategy between Fuel-1GES and Air-1GES strategies on power ranges defined by the threshold P_{ref} (see Figure 5). Therefore, an increase in fuel economy is expected (see the results section), but two GES controllers are used instead of one as used in Fuel-1GES strategy or Air-1GES SW strategy.
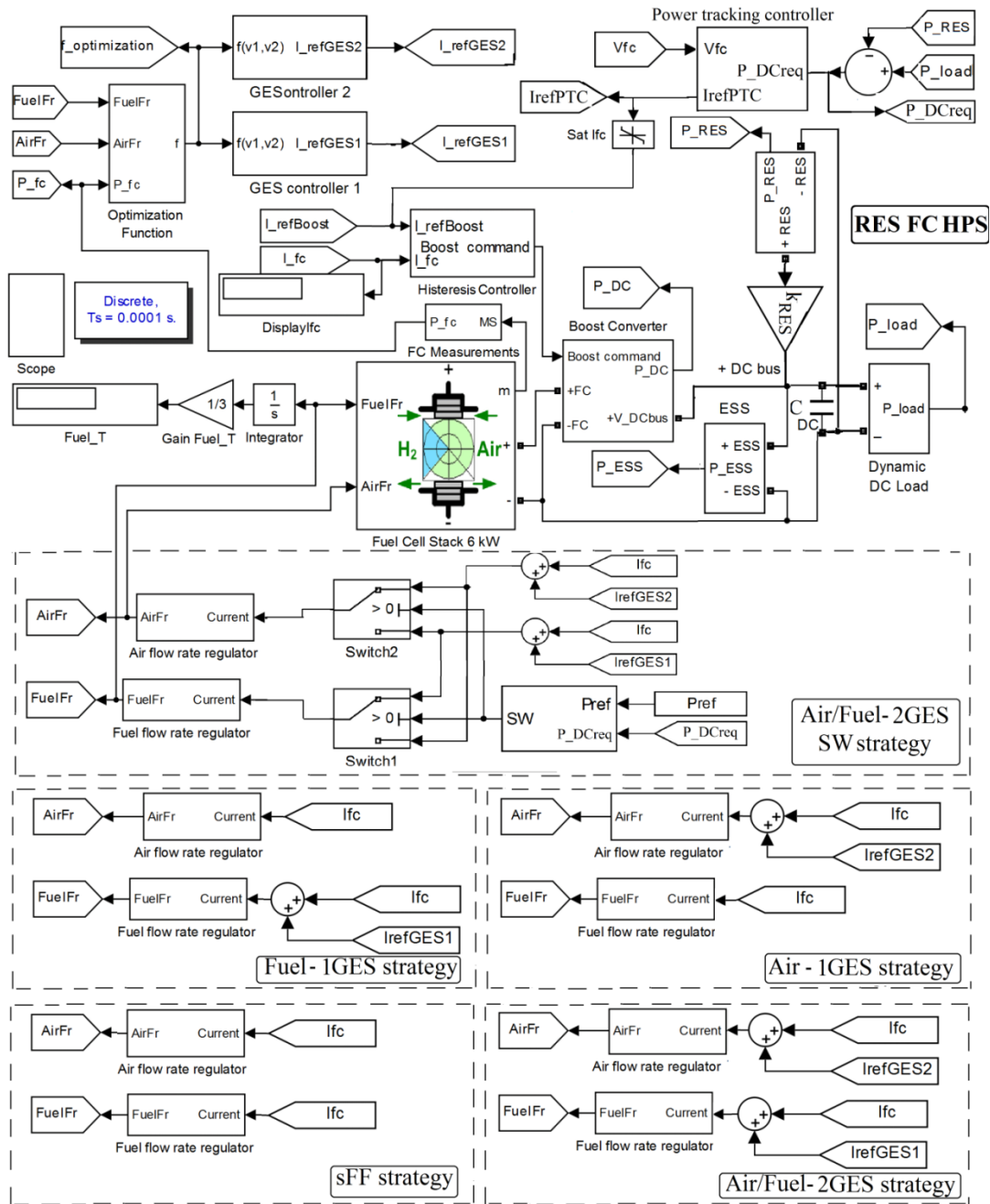
Figure 5. Diagram of the proposed strategies.

The additional use of an optimization controller will increase the complexity of the strategy somewhat, even if the optimization controller based on the GES scheme is not difficult to implement [28,29] (see next section).

2.3. GES-Based Optimization Controller

The GES-based optimization controller is presented at the bottom of Figure 1. Signals are processed based on the operational relationships (15) [30]:

$$y = f(v_1, v_2), y_N = k_{Ny} \cdot y \tag{15a}$$

$$\dot{y}_f = -\omega_h \cdot y_f + \omega_h \cdot y_N, \ y_{HPF} = y_N - y_f, \ \dot{y}_{BPF} = -\omega_l \cdot y_{BPF} + \omega_l \cdot y_{HPF} \tag{15b}$$

$$\omega_h = b_h\omega, \ \omega_l = b_l\omega, \ s_d = \sin(\omega t), \ \omega = 2\pi f_d \tag{15c}$$

$$y_{DM} = y_{BPF} \cdot s_d, \dot{y}_{Gradient} = y_{DM}, p_1 = k_1 \cdot y_{Gradient} \tag{15d}$$

$$y_M = \left| \frac{1}{T_d} \cdot \int y_{BPF} dt \right|, \ p_2 = k_2 \cdot y_M \cdot s_d \tag{15e}$$

$$I_{ref(GES)} = k_{Np} \cdot (p_1 + p_2) \tag{15f}$$

The step in signals processing and used parameter are follows [30]:

- Normalization of FC power (y = p_{FCnet}) is performed using k_{Ny} = 1/1000;
- Approximation the first harmonic (y_{BPF}) is performed with a band-pass filter having the cut-off frequencies $\omega_l = b_l\omega$ and $\omega_h = b_h\omega$, where $\beta_l = 1.5$ and $\beta_h = 0.1$.
- Two sinusoidal dithers, $s_{d1} = \sin(\omega_1 t)$ and $s_{d2} = \sin(\omega_2 t)$ are used (with $f_{d1} = 50$ Hz and f_{d2} = 100 Hz, where $f_d = \omega/2\pi$) to perform demodulation (y_{DM});
- Signal y_{DM} is integrated to obtain the search gradient ($y_{Gradient}$);
- The tracking signal (p_1) and the location signal (p_2) are tuned using k_1 = 1 and k_2 = 2;
- Normalization of the search signal ($p = p_1 + p_2$) is performed using k_{Np} = 20.

The values of the normalization gains k_{Ny} and k_{Np} were chosen in correlation with the range of the FC power, respectively the search range for the references $I_{ref(GES1)}$ and $I_{ref(GES2)}$ generated by GES controllers [30], which established the references $I_{ref(Air)}$ and $I_{ref(Fuel)}$ as mentioned above. It is worth mentioning the 99.9% tracking accuracy and very low power ripple obtained in stationary regimes [31]. The efficient and safe operation of the FC system using the strategies mentioned above were evaluated in stationary and dynamic regimes, considering the fuel economy and the oxygen excess ratio as an indicator of performance and health respectively [32].

The initial simulation conditions are as follows: the initial battery SOC of 80%, the initial voltage on the ultracapacitors stack and DC capacitor of 100 V (V_{UC} (0) = 100 V) and 200 V (V_{C_DC} (0) = 200 V), and initial FC current of 0 A (I_{FC} (0) = 0 A) in order to highlight the initial transitory regime. Different values were considered for the initial values mentioned above. A value of the FC current close to the FC current reference ($I_{ref(PTC)}$) given by (8) reduced the initial transitory regime.

2.4. Oxygen Excess Ratio

The oxygen excess ratio (*OER*) was evaluated using (16) [33]:

$$OER = \frac{c_3 \cdot I_{FC}^3 + c_2 \cdot I_{FC}^2 + c_1 \cdot I_{FC} + c_0}{d_1 \cdot I_{FC} + d_0} \tag{16}$$

where: $c_0 = 402.6$, $c_1 = 8.476 \cdot 10^{-5}$ [1/A], $c_2 = -0.81252$ [1/A²], $d_3 = 0.02673$ [1/A³], $d_0 = 0.997$, and $d_1 = 61.38$.

The obtained results in stationary and dynamic regimes will be presented in the next sections.

3. Results

3.1. Performance of Strategies Fuel-1GES, Air-1GES and Air/Fuel-2GES SW

The performance of strategies Fuel-1GES, Air-1GES, and Air/Fuel-2GES SW were analyzed for different levels of load by total fuel consumption during 20 s (see Table 1). The P_{ref} threshold for best fuel economy should be chosen around 3 kW (see Figure 6). The values in the last column are summarized for P_{ref} = 3.2 kW.

Table 1. Fuel consumption of strategies Fuel-1GES, Air-1GES, and Air/Fuel-2GES.

P_{load}	$\Delta Fuel_{T(Air\text{-}1GES)}$	$\Delta Fuel_{T(Fuel\text{-}1GES)}$	$\Delta Fuel_{T(Air/Fuel\text{-}2GES)}$
(kW)	(L)	(L)	(L)
2	1.22	−0.09	−0.09
3	−0.25	−0.24	−0.24
4	−0.71	−0.25	−0.71
5	−1.03	−0.46	−1.03
6	−2.08	−1.58	−2.08
7	−10.56	−4.24	−10.56
8	−22.92	−18.48	−22.92
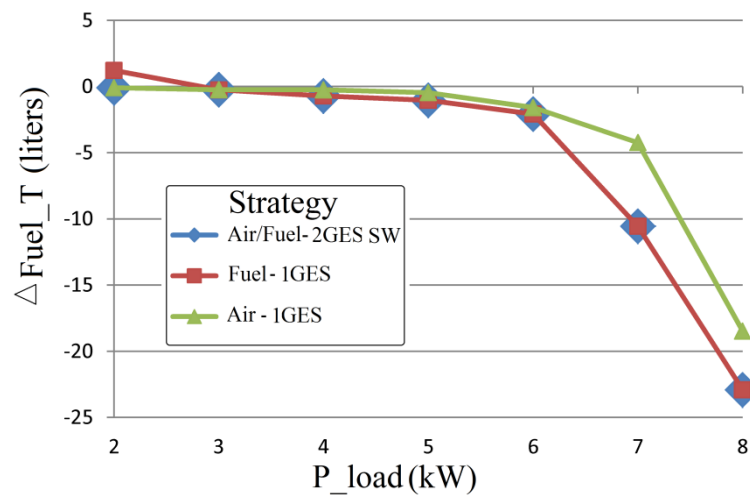
Figure 6. Fuel consumption of strategies Fuel-1GES (global extremum seeking), Air-1GES and Air/Fuel-2GES.

Thus, an increase in fuel economy is expected during dynamic load cycles with levels in the range of zero power to maximum power.

The performance of the strategies mentioned above were evaluated using the load cycle shown in Figure 2. The expected increase in fuel economy will be highlighted in the next section.

3.2. Fuel Consumption for FC HPS (with k_{RES} = 0)

Fuel consumption during the load cycle of 20 s shown in Figure 2 is reported in the first row of Table 2 for strategies sFF, Fuel-1GES, Air-1GES, Air/Fuel-2GES SW, and Air/Fuel-2GES. The fuel economy compared to sFF strategy is presented in the second row of Table 2 using (17).

$$\Delta Fuel_{T(strategy)} = Fuel_{T(sFF)} - Fuel_{T(strategy)} \tag{17}$$

Table 2. Fuel consumption, fuel economy, and percentages of fuel economy compared to $Fuel_{T(sFF)}$ (k_{RES} = 0) during the load cycle shown in Figure 2.

Strategy / Parameter (Unit)	sFF	Fuel-1GES	Air-1GES	Air/Fuel-2GES SW	Air/Fuel-2GES
$Fuel_{T(strategy)}$ (liters)	286.5	278.4	279.4	275.2	274
$\Delta Fuel_{T(strategy)}$ (liters)	0	8.1	7.1	11.3	12.5
$\%Fuel_{T(strategy)}$ (%)	0	2.83	2.48	3.94	4.36

The last row of Table 2 presents the percentages of fuel economy compared to $Fuel_{T(sFF)}$, evaluated by using (18):

$$\%Fuel_{T(strategy)} = 100 \cdot \left(\frac{Fuel_{T(sFF)} - Fuel_{T(strategy)}}{Fuel_{T(sFF)}} \right) \tag{18}$$

As was expected, the fuel economy increased for all strategies compared to sFF strategy and for Air/Fuel-2GES SW strategy compared to the strategies Fuel-1GES and Air-1GES.

To highlight other aspects of the analyzed strategies (such as battery operation in charge-sustained mode or values of other performance indicators) and then discuss them comparatively in the discussion section, the behavior of the FC RES HPS using $k_{RES} = 0$ and strategies sFF, Fuel-1GES, Air-1GES, and Air/Fuel-2GES is presented in Figures 7–10 respectively. The graphs show the load power profile (P_{load}), oxygen excess ratio (OER), ESS power (P_{ESS}), airflow rate ($AirFr$), fuel flow rate ($FuelFr$), total fuel consumption ($Fuel_T$), fuel efficiency ($Fuel_{eff}$), and electrical energy efficiency of FC system ($\eta_{sys} \cong P_{FCnet}/P_{FC}$).

The behavior of Air/Fuel-2GES SW strategy is not presented because its operation is based on the switching of strategies Fuel-1GES and Air-1GES depending on the chosen threshold P_{ref}, so the waveforms would evolve in the same logic.

OER varied within the admissible limits for all the analyzed strategies, highlighting a safe operation for the FC system. OER variation will be detailed in Section 3.4 for FC RES HPS with $k_{RES} = 0$ and $k_{RES} = 1$.

ESS power was almost zero during constant load levels (stationary regimes), except for transient regimes when the power balance was dynamically compensated by ESS, highlighting a battery operation in the charge-sustained mode for all the analyzed strategies.
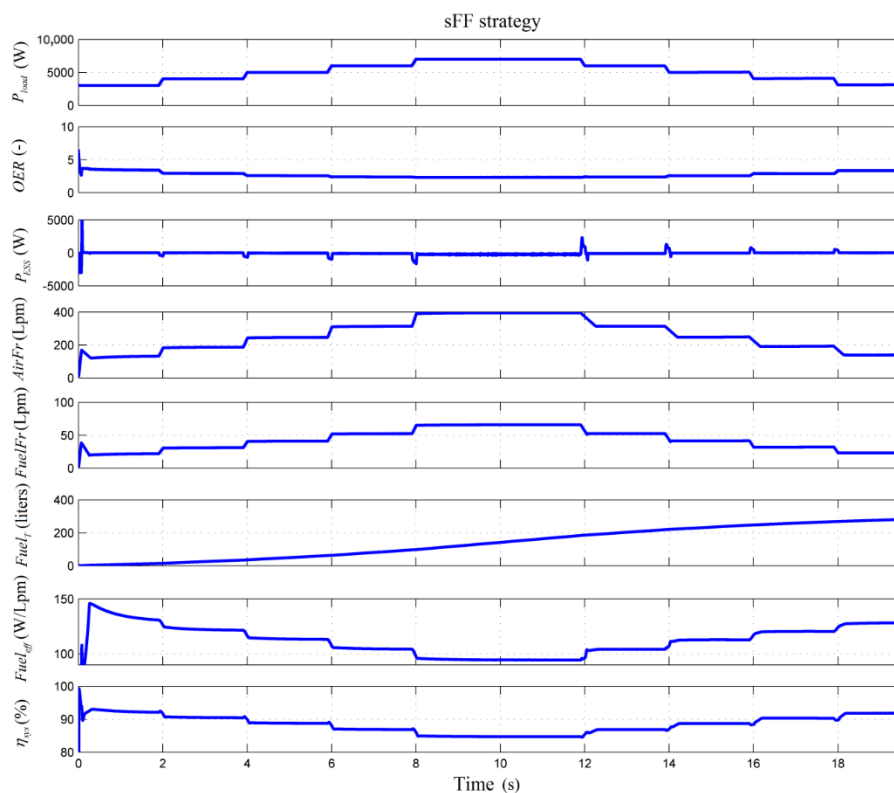
Figure 7. Main waveforms for fuel cell (FC) RES HPS using $k_{RES} = 0$ and static feed-forward (sFF) strategy.
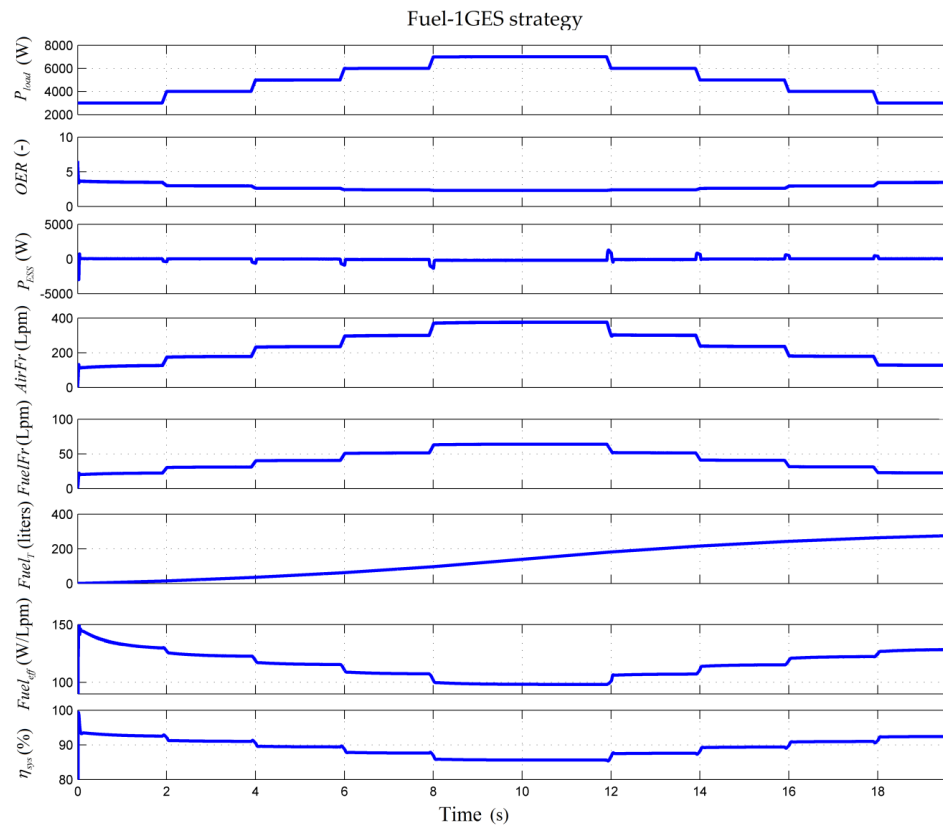
Figure 8. Main waveforms for FC RES HPS using $k_{RES} = 0$ and Fuel-1GES strategy.
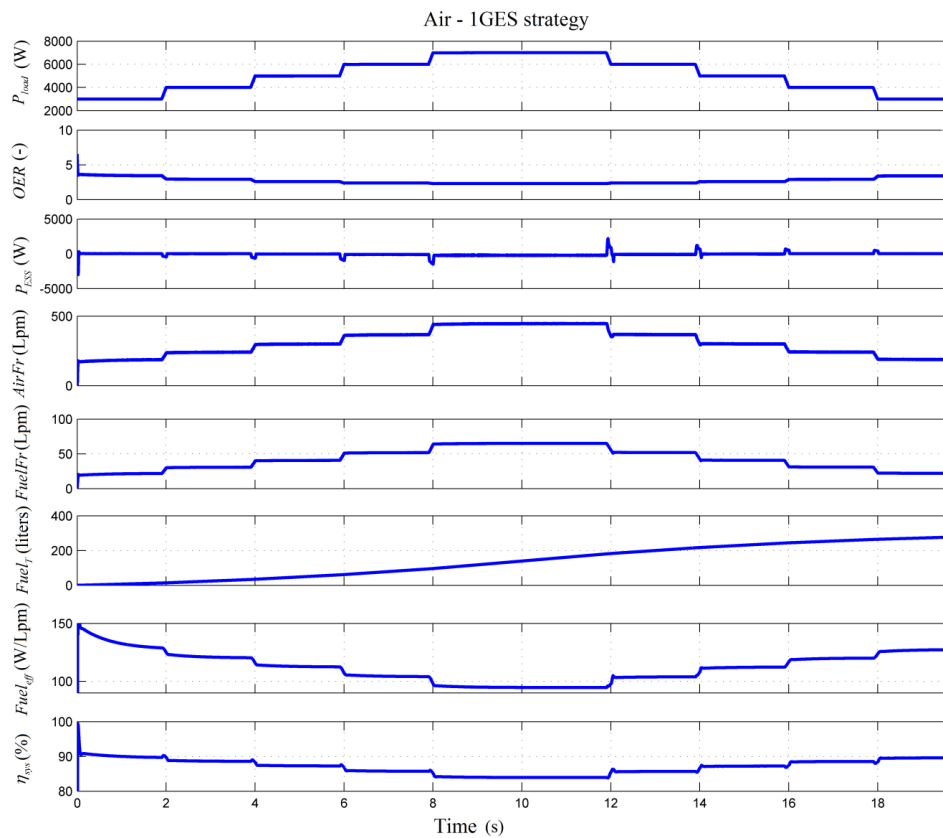
Figure 9. Main waveforms for FC RES HPS using $k_{RES} = 0$ and Air-1GES strategy.
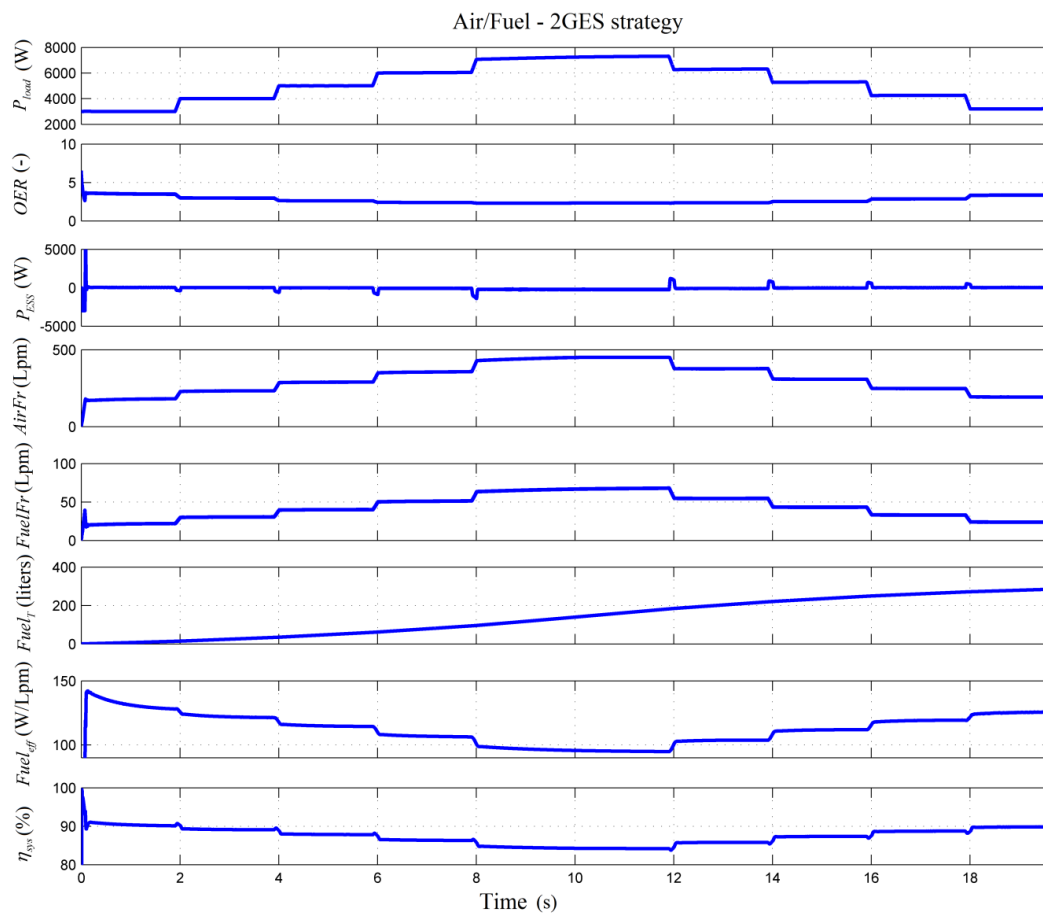
Figure 10. Main waveforms for FC RES HPS using $k_{RES} = 0$ and Air/Fuel-2GES strategy.

Fueling flow rates (*AirFr* and *FuelFr*) were set by FC current in sFF strategy, so both followed the PTC reference ($I_{ref(PTC)}$). *AirFr* and *FuelFr* were set by FC current in the strategies Fuel-1GES and Air-1GES respectively. So, compared to sFF strategy, minor changes were seen in *FuelFr* and *AirFr* which were used in optimization by the strategies Fuel-1GES and Air-1GES respectively. Air/Fuel-2GES strategy used both fueling flow rates in optimization, so minor changes were seen in both fueling flow rates compared to sFF strategy.

The values of total fuel consumption have been provided in the first row of Tables 2 and 3 for each analyzed strategy and the load cycle of 20 s shown in Figure 2.

Table 3. Fuel consumption, fuel economy, and percentages of fuel economy compared to $Fuel_{T(sFF)}^{RES}$ ($k_{RES} = 1$) during the load cycle and RES power profile shown in Figures 2 and 3a.

Strategy / Parameter (Unit)	sFF	Fuel-1GES	Air-1GES	Air/Fuel-2GES SW	Air/Fuel-2GES
$Fuel_{T(strategy)}^{RES}$ (liters)	123.6	113.9	114.1	107.6	108.2
$\Delta Fuel_{T(strategy)}^{RES}$ (liters)	0	9.7	9.5	16	15.4
$\%Fuel_{T(strategy)}^{RES}$ (%)	0	7.85	7.69	12.94	12.46

Two important indicators for evaluating the performance of a strategy are fuel efficiency (*Fuel_eff*) and electrical energy efficiency of the FC system ($\eta_{sys} \cong P_{FCnet}/P_{FC}$). An exhaustive analysis (for $k_{fuel} = 0$, 25, and 50 (Lpm/W) of these performance indicators for seven strategies proposed in the literature

(including strategies Fuel-1GES, Air-1GES, and Air/Fuel-2GES) is presented in [34] compared to the sFF strategy. Here η_{sys} variation is presented to highlight the similar values obtained for FC net power.

FC power variation will be detailed in Section 3.4 for FC RES HPS with $k_{RES} = 0$ and $k_{RES} = 1$. The next section will present the results for FC RES HPS with power support in maintaining to DC power balance from RES, i.e., for $k_{RES} = 1$.

3.3. Fuel Consumption for FC RES HPS with $k_{RES} = 1$

Fuel consumption, the fuel economy, and the percentages of fuel economy compared to the sFF strategy during the 20 s load cycle and RES power profile shown in Figures 2 and 3a are given in Table 3 for strategies sFF, Fuel-1GES, Air-1GES, Air/Fuel-2GES SW, and Air/Fuel-2GES. The fuel economy and the percentages of fuel economy were evaluated using (19) and (20).

$$\Delta Fuel_{T(strategy)}^{RES} = Fuel_{T(sFF)}^{RES} - Fuel_{T(strategy)}^{RES} \tag{19}$$

$$\% Fuel_{T(strategy)}^{RES} = 100 \cdot \left(\frac{Fuel_{T(sFF)}^{RES} - Fuel_{T(strategy)}^{RES}}{Fuel_{T(sFF)}^{RES}} \right) \tag{20}$$

As was expected, fuel consumption decreased due to the contribution of the RES power on DC bus (see the first row of Tables 2 and 3). Note also that the fuel economy increased for the Air/Fuel-2GES SW strategy compared to the strategies Fuel-1GES and Air-1GES (see the second row of Tables 2 and 3). It is also worth mentioning that here the fuel economy was better for the Air-1GES strategy compared to the Fuel-1GES strategy (because the FC power requested was lower due to the contribution of the RES power on DC bus). This also explains better fuel economy for the Air/Fuel-2GES SW strategy compared to the Air/Fuel-2GES strategy (see the second row of Tables 2 and 3).

To compare HPS operation with and without RES power support to DC power balance, the same strategies were used. So, the behavior of the FC RES HPS using $k_{RES} = 1$ and strategies sFF, Fuel-1GES, Air-1GES, and Air/Fuel-2GES is presented in Figures 11–14 respectively. The structure of the graphs is identical to the one mentioned above for Figures 7–10, except for the inclusion of RES power as in the second graph in Figures 11–14.

The values of total fuel consumption presented in the seventh graph have been registered in see the first row of Table 3 for each analyzed strategy.

The following observations can be made for the FC RES HPS using $k_{RES} = 1$:

- ESS power was also almost zero for all strategies, except that it was noisy due to the noise added on RES power, highlighting the battery operation in the charge-sustained mode for FC RES HPS with $k_{RES} = 1$ as well.
- Fueling flow rates (*AirFr* and *FuelFr*) would have evolution as was explained for FC RES HPS with $k_{RES} = 0$, except that for FC RES HPS with $k_{RES} = 1$ the PTC reference and FC currentfollowed the shape of power requested on DC bus, $p_{DCreq} = p_{Load} - p_{RES}$
- It is worth mentioning the low values of the performance indicators (*Fuel*$_{eff}$ and $\eta_{sys} \cong P_{FCnet}/P_{FC}$) during the operation of the FC system at low power. This mode of operation should be avoided by shutting down the FC system, but shutting down and starting of the FC system are complex processes [35]. An appropriate strategy must therefore be implemented in case the FC system operates for a long time at low power. However, these aspects are not in the objectives of this paper.
- OER varied within the admissible limits for all the analyzed strategies, highlighting a safe operation for FC RES HPS using $k_{RES} = 1$.

So, as it was mentioned, OER variation will be presented and commented on in the next section for FC RES HPS with $k_{RES} = 0$ and $k_{RES} = 1$.
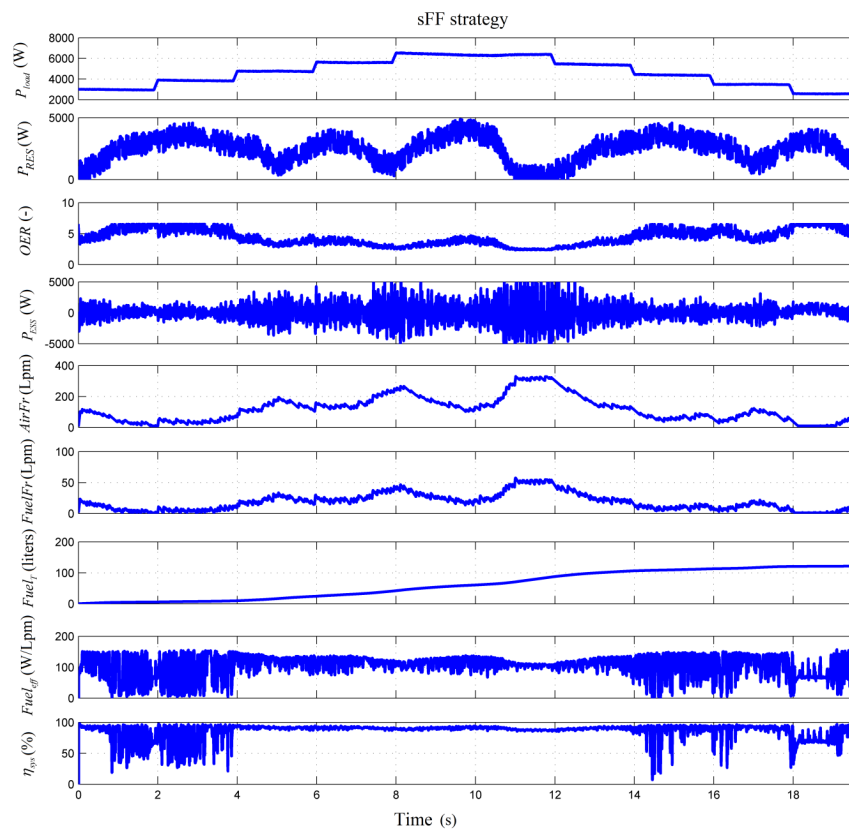
Figure 11. Main waveforms for FC RES HPS using $k_{RES} = 1$ and sFF strategy.
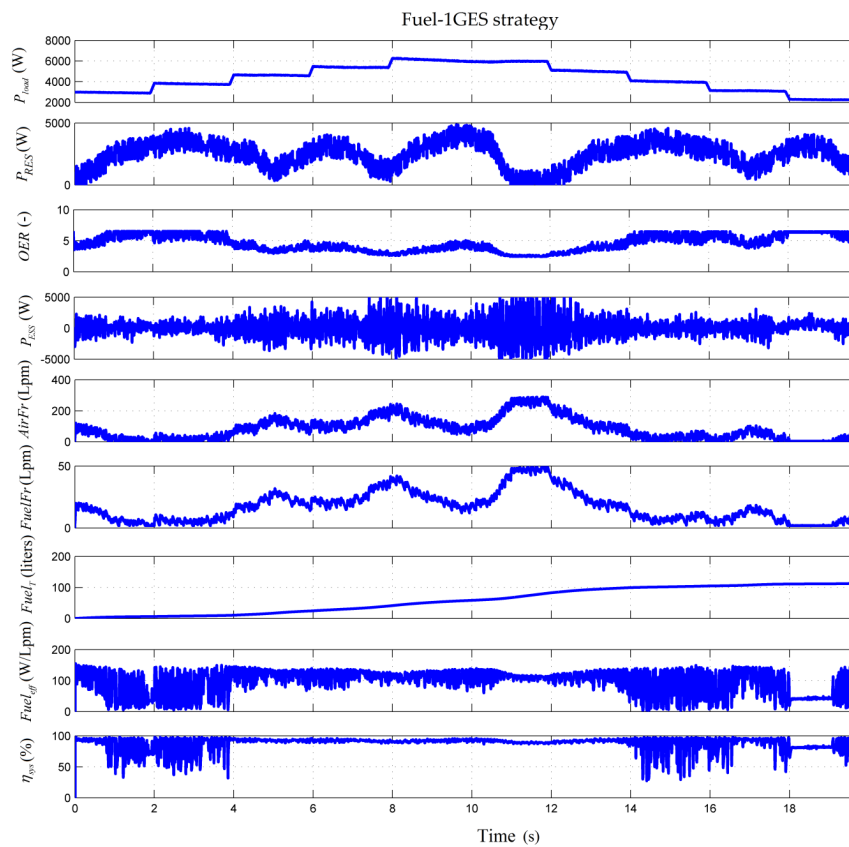
Figure 12. Main waveforms for FC RES HPS using $k_{RES} = 1$ and Fuel-1GES strategy.
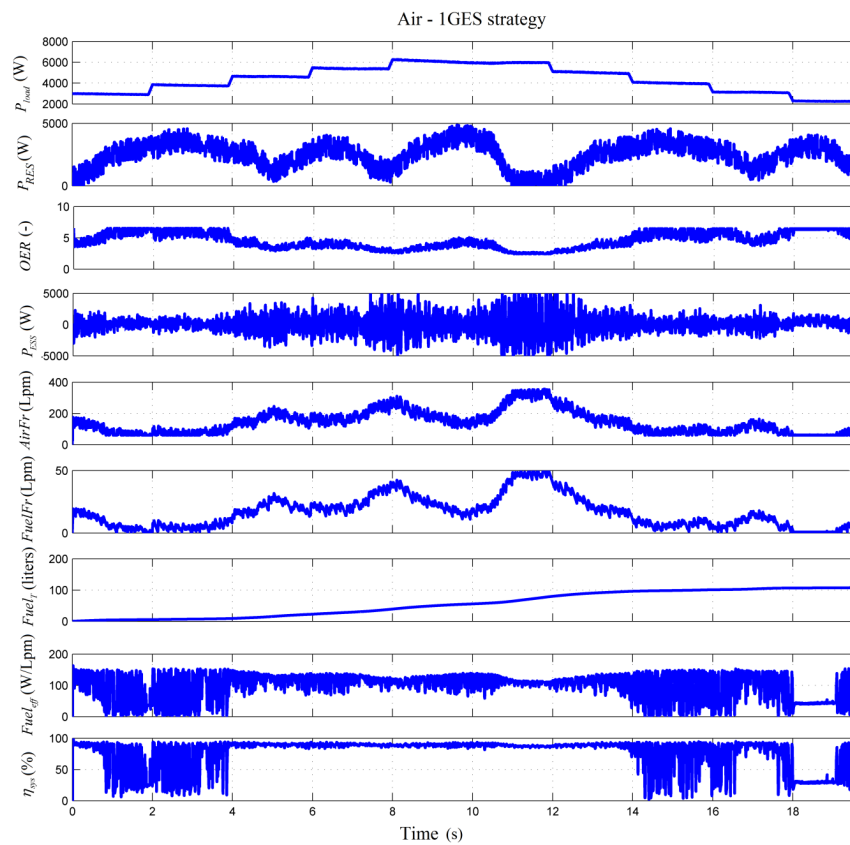
Figure 13. Main waveforms for FC RES HPS using $k_{RES} = 1$ and Air-1GES strategy.
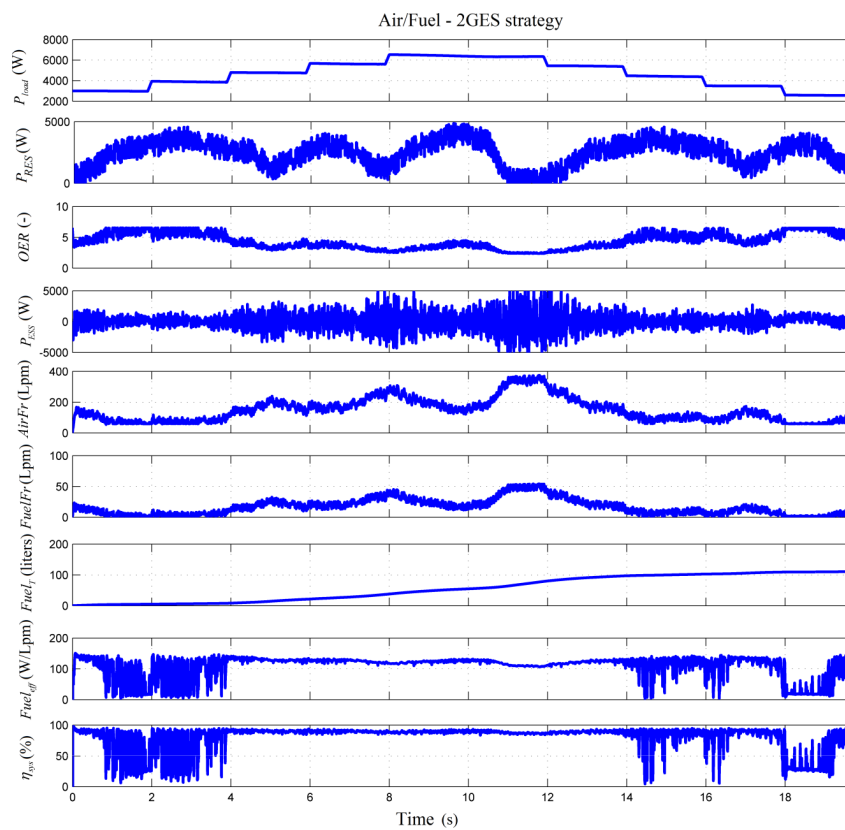
Figure 14. Main waveforms for FC RES HPS using $k_{RES} = 1$ and Air/Fuel-2GES strategy.

3.4. Oxygen Excess Ratio for FC RES HPS with $k_{RES} = 0$ and $k_{RES} = 1$

The oxygen excess ratio of FC RES HPS with $k_{RES} = 0$ is presented in Figure 15 for all strategies. OER varied within the limits of 2.2 and 3.6, which demonstrates the safe operation of HPS without RESs ($k_{RES} = 0$).
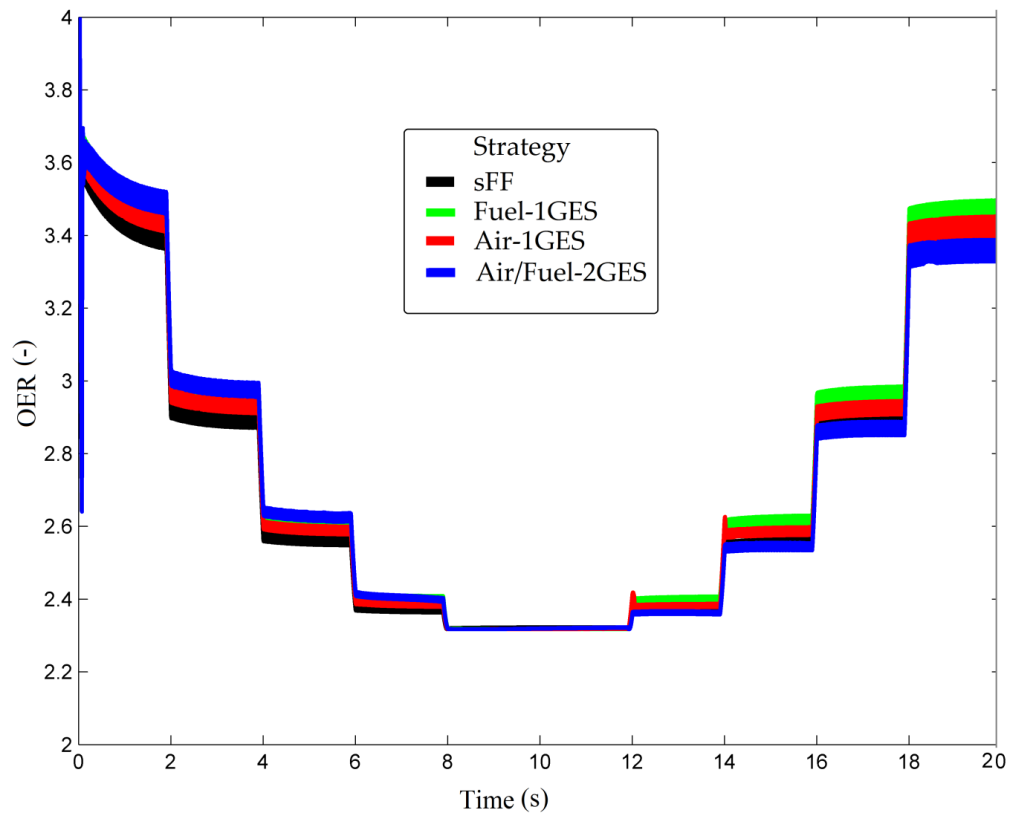
Figure 15. Oxygen excess ratio for FC RES HPS with $k_{RES} = 0$.

Oxygen excess ratio of FC RES HPS with RESs ($k_{RES} = 1$) is presented in Figures 16–19 using the strategies sFF, Fuel-1GES, Air-1GES, and Air/Fuel-2GES respectively. OER variations were represented in different Figures to highlight small variations from one strategy to another (as is the case with ESS power for example). OER varied approximately in the range from 2.3 to 7, so within the allowed limits of safe operation of the FC system.

The same situation (with some minor differences between the representations obtained using the strategies analyzed in this study) applied in the case of FC net power (see next section).
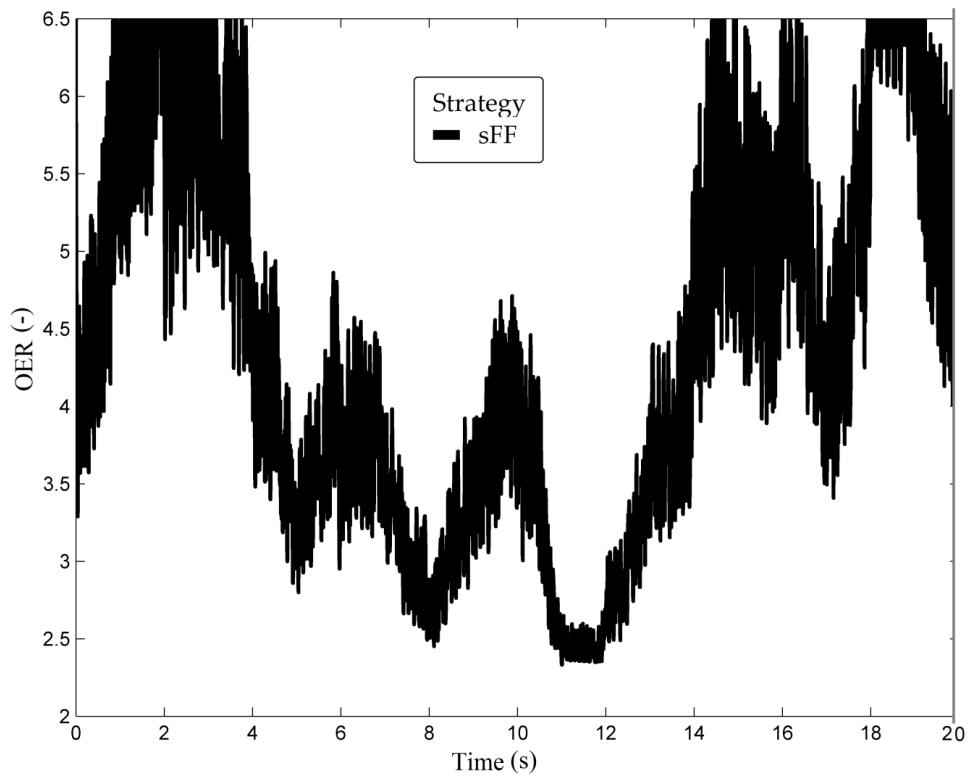
Figure 16. Oxygen excess ratio for FC RES HPS with $k_{RES} = 1$ and sFF strategy.
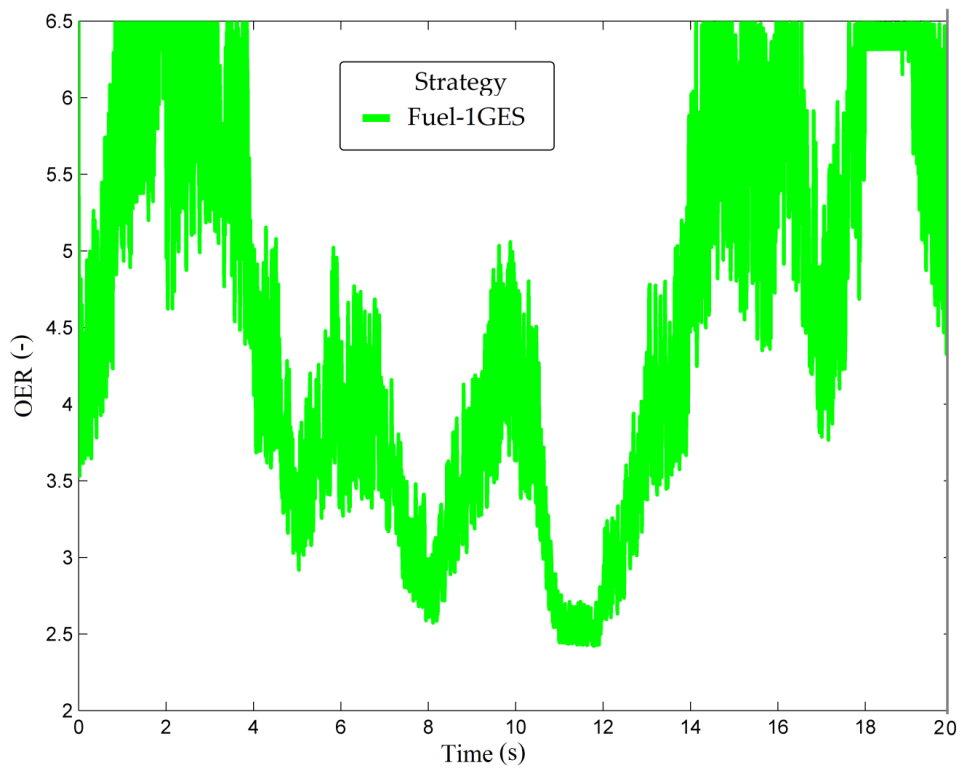
Figure 17. Oxygen excess ratio for FC RES HPS with $k_{RES} = 1$ and Fuel-1GES strategy.
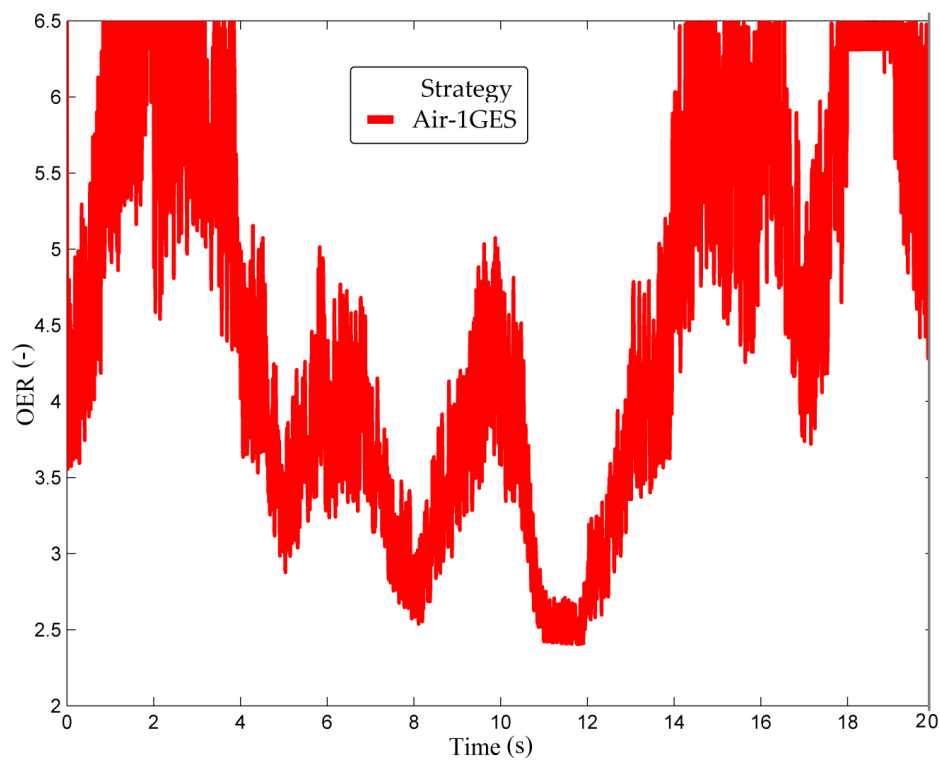
Figure 18. Oxygen excess ratio for FC RES HPS with k_{RES} = 1 and Air-1GES strategy.
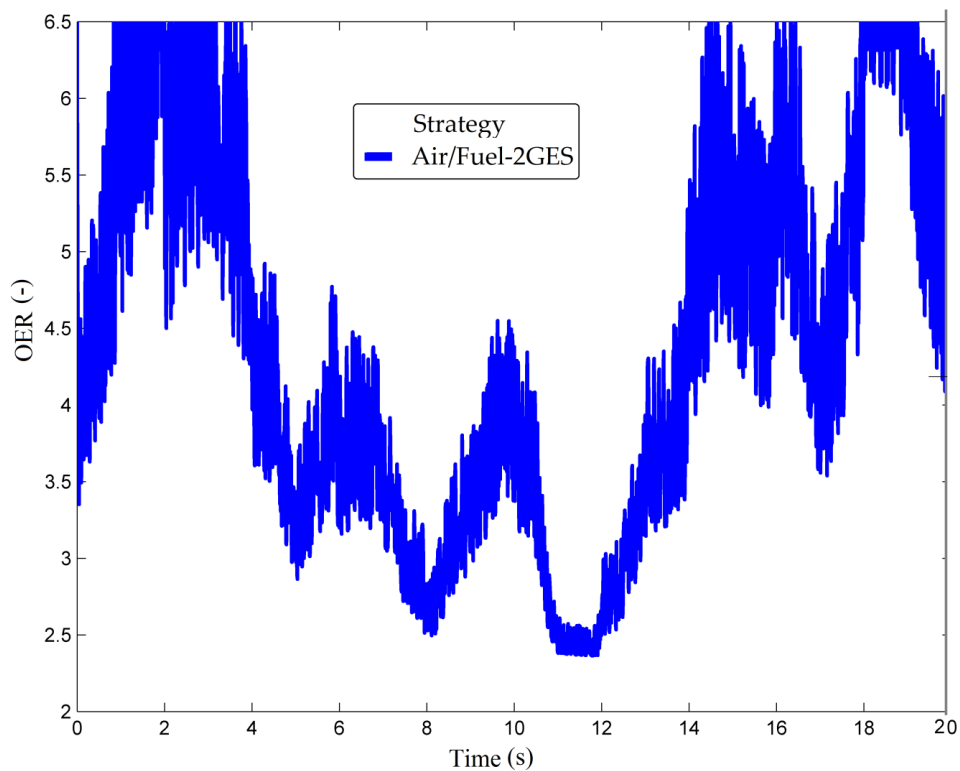
Figure 19. Oxygen excess ratio for FC RES HPS with k_{RES} = 1 and Air/Fuel-2GES strategy.

3.5. FC Net Power Requested from FC RES HPS with k_{RES} = 0 and k_{RES} = 1

FC net power requested to sustain the DC power flow balance of FC RES HPS with k_{RES} = 0 and k_{RES} = 1 are presented in Figures 20 and 21 for all strategies analyzed in this study.
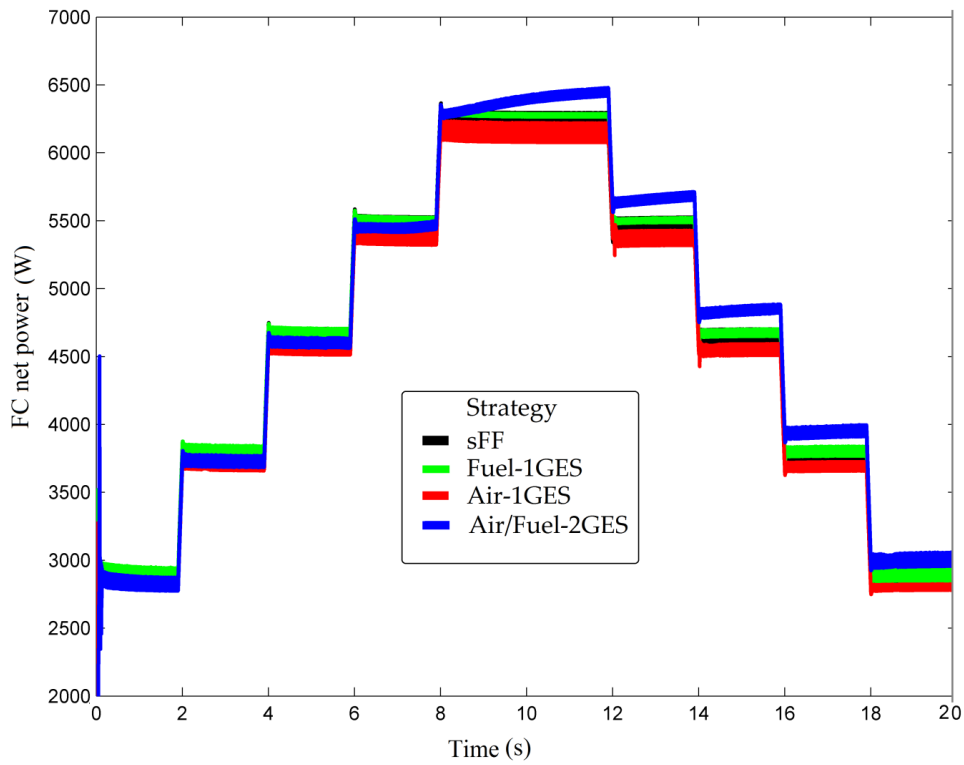
Figure 20. FC net power requested from FC RES HPS with $k_{RES} = 0$.
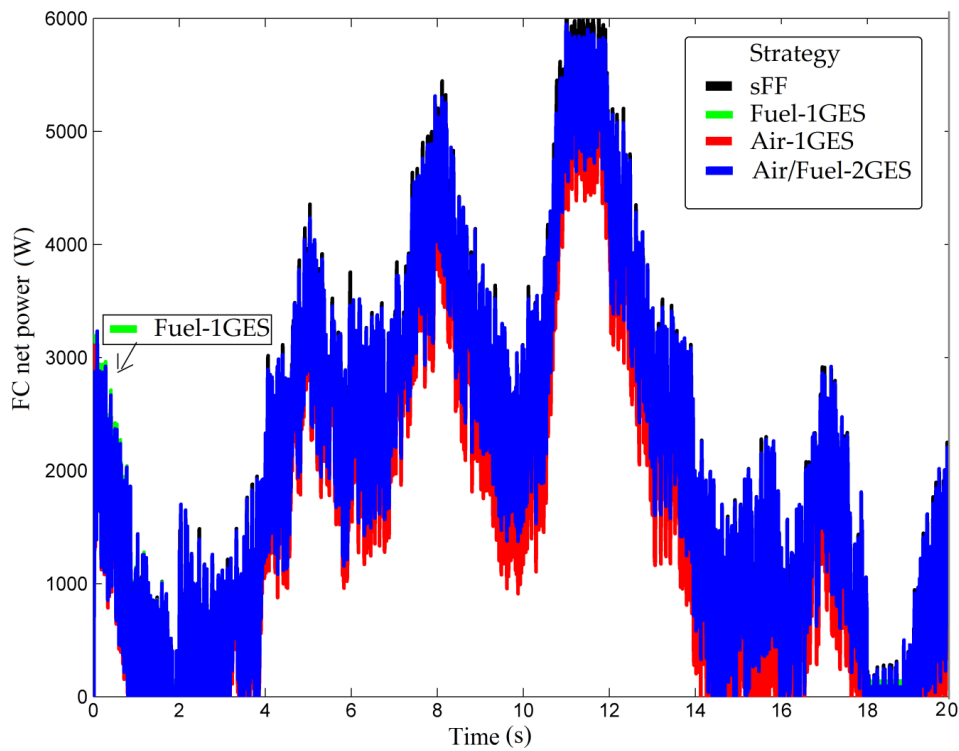
Figure 21. FC net power requested from FC RES HPS with $k_{RES} = 1$.

One issue that may be of interest in using these strategies, which are part of the class of strategies that use the same setting, is whether it can be identified based on the measurements made.

In addition to other discussions of the results obtained, the next section will show how to identify whether the strategy uses one or two GES controllers by simply processing the fuel consumption measurements for HPS with $k_{RES} = 0$ and $k_{RES} = 1$.

4. Discussion

The results obtained for HPS with $k_{RES} = 0$ and $k_{RES} = 1$ in Sections 3.1 and 3.2 are summarized in Tables 4 and 5, where other indicators have been calculated and discussed below.

Table 4. Fuel consumption for FC RES HPS with $k_{RES} = 0$ and $k_{RES} = 1$.

Parameter (Unit) \ Strategy	sFF	Fuel-1GES	Air-1GES	Air/Fuel-2GES SW	Air/Fuel-2GES
$Fuel_{T(strategy)}$ (liters)	286.5	278.4	279.4	275.2	274
$Fuel_{T(strategy)}^{RES}$ (liters)	123.6	113.9	114.1	107.6	108.2
$Fuel_{T(strategy)} - Fuel_{T(strategy)}^{RES}$ (liters)	162.9	164.5	165.3	167.6	165.8
$\dfrac{Fuel_{T(strategy)}^{RES}}{Fuel_{T(strategy)}}$ (%)	43.14	40.91	40.84	39.10	39.49

Table 5. Fuel economy for FC RES HPS with $k_{RES} = 0$ and $k_{RES} = 1$.

Parameter (Unit) \ Strategy	Fuel-1GES	Air-1GES	Air/Fuel-2GES SW	Air/Fuel-2GES
$\%Fuel_{T(strategy)}$ (%)	2.83	2.48	3.94	4.36
$\%Fuel_{T(strategy)}^{RES}$ (%)	7.85	7.69	12.94	12.46
$\%Fuel_{T(strategy)}^{RES} - \%Fuel_{T(strategy)}$ (%)	5.02	5.21	9.00	8.10
$\dfrac{\%Fuel_{T(strategy)}^{RES}}{\%Fuel_{T(strategy)}}$ (-)	2.78	3.10	3.28	2.86

Ratio $\dfrac{Fuel_{T(strategy)}^{RES}}{Fuel_{T(strategy)}}$ was in range of 39.1 to 40.91 for the strategies analyzed in this study (Fuel-1GES, Air-1GES, Air/Fuel-2GES SW and Air/Fuel-2GES), highlighting the contribution of RESs to DC power flow balance compared to load demand (measured by the ratio between the average values of these powers).

If the dependency relationship is chosen linearly, then $\dfrac{Fuel_{T(strategy)}^{RES}}{Fuel_{T(strategy)}} \cong 1.2 \cdot \dfrac{P_{load(AV)} - P_{RES1(AV)}}{P_{load(AV)}} - 0.2$. This is verified in two points, as follows:

$$P_{load(AV)} = 5 \ kW, P_{RES1(AV)} = 0 \Rightarrow 1 = \frac{Fuel_{T(strategy)}^{RES}}{Fuel_{T(strategy)}} \cong 1.2 \cdot \frac{P_{load(AV)} - P_{RES1(AV)}}{P_{load(AV)}} - 0.2 = 1.2 \cdot \frac{5}{5} - 0.2 = 1 \quad (21)$$

$$P_{load(AV)} = 5 \ kW, P_{RES1(AV)} = 2.5 \ kW \Rightarrow 0.4 \cong \frac{Fuel_{T(strategy)}^{RES}}{Fuel_{T(strategy)}} \cong 1.2 \cdot \frac{P_{load(AV)} - P_{RES1(AV)}}{P_{load(AV)}} - 0.2 = 1.2 \cdot \frac{5 - 2.5}{5} - 0.2 = 0.4 \quad (22)$$

Minor differences between the ratio's values obtained with each strategy do not help to define some subclasses. However, the values obtained (close to 40), which was much higher than the value of 43.14 obtained in the case of sFF strategy, shows that all strategies use a similar technique to reduce fuel consumption.

Fuel economy for FC RES HPS with $k_{RES} = 0$ and $k_{RES} = 1$ is computed in Table 5 as percent from fuel consumption using sFF strategy.

Ratio $\dfrac{\%Fuel_{T(strategy)}^{RES}}{\%Fuel_{T(strategy)}}$ was in range of 2.78 to 3.28 for strategies analyzed in this study, highlighting the same thing as the $\dfrac{Fuel_{T(strategy)}^{RES}}{Fuel_{T(strategy)}}$ ratio (the contribution of RESs to DC power

flow balance compared to load demand). In this case, the linear dependence is given by $\frac{\%Fuel^{RES}_{T(strategy)}}{\%Fuel_{T(strategy)}} \cong 2.2 \cdot \frac{P_{load(Max)}-\left(P_{load(AV)}-P_{RES1(AV)}\right)}{P_{load(Max)}-P_{load(AV)}} - 1.2.$

Considering $P_{load(Max)} = \eta_{boost} \cdot P_{FCnet(Max)} \cong 7.6~kW$, this relation is verified in two points, as follows:

$$P_{load(AV)} = 5~kW, P_{RES1(AV)} = 0 \Rightarrow 1 = \frac{\%Fuel^{RES}_{T(strategy)}}{\%Fuel_{T(strategy)}} \cong 2.2 \cdot \frac{P_{load(Max)}-\left(P_{load(AV)}-P_{RES1(AV)}\right)}{P_{load(Max)}-P_{load(AV)}} - 1.2 = 2.2 \cdot 1 - 1.2 = 1 \quad (23)$$

$$P_{load(AV)} = 5~kW, P_{RES1(AV)} = 2.5~kW \Rightarrow$$
$$\Rightarrow 3 \cong \frac{\%Fuel^{RES}_{T(strategy)}}{\%Fuel_{T(strategy)}} \cong 2.2 \cdot \frac{P_{load(Max)}-\left(P_{load(AV)}-P_{RES1(AV)}\right)}{P_{load(Max)}-P_{load(AV)}} - 1.2 = 2.2 \cdot \frac{7.6-(5-2.5)}{7.6-5} - 1.2 \cong 3.115 \quad (24)$$

However, the difference $\%Fuel^{RES}_{T(stategy)} - \%Fuel_{T(stategy)}$ clearly shows that two subclasses can be defined: (1) the class of the strategies Fuel-1GES, Air-1GES (which use one GES controller) and (2) the class of the strategies Air/Fuel-2GES SW and Air/Fuel-2GES (which use two GES controllers). It is worth mentioning that the fuel economy was biggest when using Air/Fuel-2GES SW or Air/Fuel-2GES strategies because these use two GES controllers instead of one. This means a search with two variables in a larger search space.

Other findings of the study performed for HPS with $k_{RES} = 0$ and $k_{RES} = 1$ in Sections 3.1 and 3.2 were the following:

- If the power to be generated by the FC system is small (mainly between 0 and P_{ref}) and a single GES controller strategy is used, then the Air-1GES strategy is recommended. Otherwise, Fuel-1GES strategy is recommended;
- If the power to be generated by the FC system is higher (mainly between P_{ref} and $P_{FC(max)}$) and two GES controllers are used, then the Air/Fuel-2GES strategy is recommended. Otherwise, Air/Fuel-2GES SW strategy is recommended;
- The battery pack operates in charge-sustaining mode if PTC is used for a strategy applied to HPS under dynamic load cycle, without or without RES power; and
- Even if the differences in fuel economy are not major, the definition of specific indicators mentioned above can classify strategies into subclasses or estimate fuel consumption.

The main findings of the study performed for HPS with $k_{RES} = 0$ and $k_{RES} = 1$ in Sections 3.3 and 3.4 were the following:

- The safe operation of HPS is ensured by each analyzed strategy, even in conditions of high load dynamic and large variations of renewable energy power;
- FC net power requested to sustain the DC power flow balance of FC RES HPS under dynamic load cycle and variation of RES power is almost the same due to the optimal value found by each strategy in the search region, which is limited around the current value of the current FC; so these optimal values are close to each other.

This problem of recognizing subclasses of performance from the same class of optimization strategies can also arise for FC HPS (i.e., FC vehicles) by considering two different load cycles and evaluating the performance indicator $\%Fuel^{load1}_{T(stategy)} - \%Fuel^{load2}_{T(stategy)}$.

Furthermore, taking into account different load cycles, the validity of linear relationships such as those introduced below will be verified for other strategies proposed in the literature:

$$\frac{Fuel^{load1}_{T(strategy)}}{Fuel^{load2}_{T(strategy)}} \cong a_1 \cdot \frac{P_{load1(AV)}}{P_{load2(AV)}} - a_2 \quad (25)$$

$$\frac{\%Fuel^{load1}_{T(strategy)}}{\%Fuel^{load2}_{T(strategy)}} \cong a_3 \cdot \frac{P_{load(Max)} - P_{load1(AV)}}{P_{load(Max)} - P_{load2(AV)}} - a_4 \quad (26)$$

where $Fuel^{load}_{T(strategy)}$ is the fuel consumed during the load cycle, $\%Fuel^{load}_{T(strategy)} = 100 \cdot \left(\frac{Fuel^{load}_{T(reference)} - Fuel^{load}_{T(strategy)}}{Fuel^{load}_{T(reference)}} \right)$ is computed using a reference strategy, and parameters a_i, i = 1–4, are specifically determined for each strategy.

Evaluating these ratios would allow a rough estimate of fuel consumption over a predicted load cycle up to the first refueling station based on the fuel consumption on a standard load cycle or during the previous load cycle. Thus, the warning system would signal when it is necessary to refuel from nearby stations.

5. Conclusions

In this study, four fuel economy strategies that use fuel cell optimization through the control of the fueling regulators in the conditions and one reference strategy were analyzed in the conditions in which all strategies used power tracking control of the fuel cell boost converter.

The performance of a strategy (measured for example by the fuel consumption of the FC system) depended on the level of power required from the FC system during a load cycle. Thus, the energy management unit must have a subsystem for selecting the best strategy based on the current value of the load demand and RES power.

If the optimization strategy uses two GES controllers (extending the search for the optimal in two coordinates), then it is recommended to use the Air/Fuel-2GES SW strategy for $0 < P_{FC} < P_{ref}$, and the Air/Fuel-2GES strategy for $P_{ref} < P_{FC} < P_{FC(max)}$. The percentages of fuel economy for strategies Air/Fuel-2GES SW and Air/Fuel-2GES compared to the reference strategy were of 3.94% and 4.36%, and of 12.94% and 12.46%, in the case of a dynamic load cycle with an average of 5 kW and 2.5 kW.

The next research work will focus on testing if the identified indicator ($\%Fuel^{RES}_{T(stategy)} - \%Fuel_{T(stategy)}$) can recognize subclasses of performance from the same class of optimization strategies. For this, experimental validation to evaluate model accuracy will be performed using the general indicator ($\%Fuel^{load1}_{T(stategy)} - \%Fuel^{load2}_{T(stategy)}$). The results presented in this paper highlight the fact that this approach has great chances of being confirmed.

The use of only ultracapacitors stacks instead of hybrid battery/ultracapacitors ESS will also be analyzed in terms of compensation and size performance for use in FC vehicles.

References

1. Mirsaeidi, S.; Dong, X.; Said, D.M. Towards hybrid AC/DC microgrids: Critical analysis and classification of protection strategies. *Renew. Sustain. Energy Rev.* **2018**, *90*, 97–103. [CrossRef]
2. Burmester, D.; Rayudu, R.; Seah, W.; Akinyele, D. A review of nanogrid topologies and technologies. *Renew. Sustain. Energy Rev.* **2017**, *67*, 760–775. [CrossRef]
3. International Renewable Energy Agency (IRENA). *Off-Grid Renewable Energy Systems: Status and Methodological Issues*; IRENA: Abu Dhabi, UAE, 2015; Available online: https://www.irena.org/-/media/Files/IRENA/Agency/Publication/2015/IRENA_Off-grid_Renewable_Systems_WP_2015.pdf (accessed on 29 June 2020).
4. Kumar, S.; Krishnasamy, V.; Neeli, S.; Kaur, R. Artificial intelligence power controller of fuel cell based DC nanogrid. *Renew. Energy Focus* **2020**, *34*, 1–9. [CrossRef]
5. Global Energy Review 2020—Analysis-IEA. Available online: https://www.iea.org/reports/global-energy-review-2020 (accessed on 29 October 2020).

6. Anastasiadis, A.G.; Konstantinopoulos, S.A.; Kondylis, G.P.; Vokas, G.A.; Papageorgas, P. Effect of fuel cell units in economic and environmental dispatch of a Microgrid with penetration of photovoltaic and micro turbine units. *Int. J. Hydrogen Energy* **2017**, *42*, 3479–3486. [CrossRef]

7. Pashaei-Didani, H.; Nojavan, S.; Nourollahi, R.; Zare, K. Optimal economic-emission performance of fuel cell/CHP/storage based microgrid. *Int. J. Hydrogen Energy* **2019**, *44*, 6896–6908. [CrossRef]

8. Ullah, S.; Haidar, A.M.A.; Hoole, P.; Zen, H.; Ahfock, T. The Current State of Distributed Renewable Generation, Challenges of Interconnection and Opportunities for Energy Conversion based DC Microgrids. *J. Clean. Prod.* **2020**, *12*, 122777. [CrossRef]

9. Pourbehzadi, M.; Niknam, T.; Aghaei, J.; Mokryani, G.; Shafie-khah, M.; Catalão, J.P.S. Optimal operation of hybrid AC/DC microgrids under uncertainty of renewable energy resources: A comprehensive review. *Int. J. Electr. Power Energy Syst.* **2019**, *109*, 139–159. [CrossRef]

10. Yamashita, D.Y.; Vechiu, I.; Gaubert, J.-P. A review of hierarchical control for building microgrids. *Renew. Sustain. Energy Rev.* **2020**, *118*, 109523–109540. [CrossRef]

11. Bai, W.; Abedi, M.R.; Lee, K.Y. Distributed generation system control strategies with PV and fuel cell in microgrid operation. *Control. Eng. Pract.* **2016**, *53*, 184–193. [CrossRef]

12. Brunaccini, G.; Sergi, F.; Aloisio, D.; Randazzo, N.; Ferraro, M.; Antonucci, V. Fuel cells hybrid systems for resilient microgrids. *Int. J. Hydrog. Energy* **2019**, *44*, 21162–21173. [CrossRef]

13. San Martín, J.I.; Zamora, I.; San Martín, J.J.; Aperribay, V.; Eguia, P. Hybrid fuel cells technologies for electrical microgrids. *Electr. Power Syst. Res.* **2010**, *80*, 993–1005. [CrossRef]

14. Md Hossain, A.; Roy Pota, H.; Md Hossain, J.; Blaabjerg, F. Evolution of microgrids with converter-interfaced generations: Challenges and opportunities. *Int. J. Electr. Power Energy Syst.* **2019**, *109*, 160–186. [CrossRef]

15. Han, Y.; Chen, W.; Li, Q.; Yang, H.; Zare, F.; Zheng, Y. Two-level energy management strategy for PV-Fuel cell-battery-based DC microgrid. *Int. J. Hydrog. Energy* **2019**, *44*, 19395–19404. [CrossRef]

16. Yu, D.; Zhu, H.; Han, W.; Holburn, D. Dynamic multi agent-based management and load frequency control of PV/Fuel cell/ wind turbine/ CHP in autonomous microgrid system. *Energy* **2019**, *173*, 554–568. [CrossRef]

17. San, G.; Zhang, W.; Guo, X.; Hua, C.; Xin, H.; Blaabjerg, F. Large-disturbance stability for power-converter-dominated microgrid: A review. *Renew. Sustain. Energy Rev.* **2020**, *127*, 109859–109870. [CrossRef]

18. Fahad Zia, M.F.; Elbouchikhi, E.; Benbouzid, M. Microgrids energy management systems: A critical review on methods, solutions, and prospects. *Appl. Energy* **2018**, *222*, 1033–1055.

19. Zhang, Y.; Wei, W. Model construction and energy management system of lithium battery, PV generator, hydrogen production unit and fuel cell in islanded AC microgrid. *Int. J. Hydrogen Energy* **2020**, *45*, 16381–16397. [CrossRef]

20. Bizon, N. Load-following Mode Control of a Standalone Renewable/Fuel Cell Hybrid Power Source. *Energy Convers. Manag.* **2014**, *77*, 763–772. [CrossRef]

21. Bizon, N.; Lopez-Guede, J.M.; Kurt, E.; Thounthong, P.; Mazare, A.G.; Ionescu, L.M.; Iana, G. Hydrogen Economy of the Fuel Cell Hybrid Power System optimized by air flow control to mitigate the effect of the uncertainty about available renewable power and load dynamics. *Energy Convers. Manag.* **2019**, *179*, 152–165. [CrossRef]

22. Zhang, Y.; Wei, W. Decentralized coordination control of PV generators, storage battery, hydrogen production unit and fuel cell in islanded DC microgrid. *Int. J. Hydrog. Energy* **2020**, *45*, 8243–8256. [CrossRef]

23. Bizon, N. Real-time optimization strategy for fuel cell hybrid power sources with load-following control of the fuel or air flow. *Energy Convers. Manag.* **2018**, *157*, 13–27. [CrossRef]

24. SimPowerSystems TM Reference. *Hydro-Québec and the MathWorks*; MathWorks Inc.: Natick, MA, USA, 2010.

25. Bizon, N.; Mazare, A.G.; Ionescu, L.M.; Enescu, F.M. Optimization of the Proton Exchange Membrane Fuel Cell Hybrid Power System for Residential Buildings. *Energy Convers. Manag.* **2018**, *163*, 22–37. [CrossRef]

26. Pukrushpan, J.T.; Stefanopoulou, A.G.; Peng, H. *Control of Fuel Cell Power Systems*; Springer: New York, NY, USA, 2004.

27. Bizon, N.; Kurt, E. Performance Analysis of Tracking of the Global Extreme on Multimodal Patterns using the Asymptotic Perturbed Extremum Seeking Control Scheme. *Int. J. Hydrog. Energy* **2017**, *42*, 17645–17654. [CrossRef]

28. Etouke, P.O.; Nneme, L.N.; Mbihi, J. An Optimal Control Scheme for a Class of Duty-Cycle Modulation Buck Choppers: Analog Design and Virtual Simulation. *J. Electr. Eng. Electron. Control Comput. Sci. JEEECCS* **2020**, *6*, 13–20. Available online: https://jeeeccs.net/index.php/journal/article/view/142 (accessed on 29 June 2020).

29. Nneme, L.N.; Lonla, B.M.; Sonfack, G.B.; Mbihi, J. Review of a Multipurpose Duty-Cycle Modulation Technology in Electrical and Electronics Engineering. *J. Electr. Eng. Electron. Control Comput. Sci. JEEECCS* **2018**, *4*, 9–18. Available online: https://jeeeccs.net/index.php/journal/article/view/101 (accessed on 29 June 2020).

30. Bizon, N.; Thounthong, P.; Raducu, M.; Constantinescu, L.M. Designing and Modelling of the Asymptotic Perturbed Extremum Seeking Control Scheme for Tracking the Global Extreme. *Int. J. Hydrog. Energy* **2017**, *42*, 17632–17644. [CrossRef]

31. Bizon, N.; Thounthong, P. Fuel Economy using the Global Optimization of the Fuel Cell Hybrid Power Systems. *Energy Convers. Manag.* **2018**, *173*, 665–678. [CrossRef]

32. Ramos-Paja, C.A.; Spagnuolo, G.; Petrone, G.; Emilio Mamarelis, M. A perturbation strategy for fuel consumption minimization in polymer electrolyte membrane fuel cells: Analysis, Design and FPGA implementation. *Appl. Energy* **2014**, *119*, 21–32. [CrossRef]

33. Restrepo, C.; Ramos-Paja, C.A.; Girala, R.; Calvente, J.; Romero, A. Fuel cell emulator for oxygen excess ratio estimation on power electronics applications. *Comput. Electr. Eng.* **2012**, *38*, 926–937. [CrossRef]

34. Bizon, N. *Optimization of the Fuel Cell Renewable Hybrid Power Systems*; Springer: London, UK, 2020.

35. Mane, S.; Mejari, M.; Kazi, F.; Singh, N. Improving lifetime of fuel cell in hybrid energy management system by Lure-Lyapunov based control formulation. *IEEE Trans. Ind. Electron.* **2017**, *64*, 6671–6679. [CrossRef]

Article

New Market Model with Social and Commercial Tiers for Improved Prosumer Trading in Microgrids

Bogdan-Constantin Neagu *[ID], **Ovidiu Ivanov**[ID], **Gheorghe Grigoras**[ID], **Mihai Gavrilas** and **Dumitru-Marcel Istrate**

Department of Power Engineering, Gheorghe Asachi Technical University of Iasi, 700050 Iasi, Romania; ovidiuivanov@tuiasi.ro (O.I.); ggrigor@tuiasi.ro (G.G.); mgavril@tuiasi.ro (M.G.); mistrate@tuiasi.ro (D.-M.I.)
* Correspondence: bogdan.neagu@tuiasi.ro; Tel.: +40-232-70-11-10

check for updates

Abstract: In the deregulated electricity markets, trading prices are determined by the offer-demand mechanism, and retail consumers can negotiate tariffs with their supplier of choice. For classic wholesale suppliers, the tariffs are determined by the prices of transactions performed on the wholesale market. In parallel with becoming eligible for participating in the market, the consumers use increasingly local generation sources based mostly on renewable electricity generation equipment such as Photovoltaic (PV) panels, and become prosumers. They want to be able to sell back to the market the generation surplus, in order to obtain the maximum benefits from their initial investment. This paper proposes a two-tier local market model oriented for prosumers and consumers connected in microgrids, based on the blockchain technologies and other technologies and concepts such as smart grids, crowdsourcing and energy poverty. Its goals are to improve the possibilities of local prosumers to sell electricity to local consumers and to increase their profitability, compared to the trading model often used in developing markets, of selling the surplus back to the grid via aggregators. The research aims to contribute to the sustainable development of the electricity sector using new and renewable sources of energy, state-of the art technologies and smart contracts, leading to prosumer proliferation and electricity cost reduction for consumers.

Keywords: local electricity market; smart grids; energy crowdsourcing; renewable energy sources; prosumers; blockchain technology; energy poverty; smart contracts

1. Introduction

The European Commission's strategic framework envisages an improved and modernized European energy market, aimed at creating secure, sustainable, accessible and decentralized energy networks in response to the global challenge of greenhouse gas emissions [1]. In the context of the next generation of digital energy networks, and in the presence of multiple decentralized microgrids, managing the energy generation from various and complementary sources will result in gaining more flexibility in meeting demand and lowering costs for the community. The adoption of a decentralized electricity distribution network, in which ordinary consumers can also be energy producers, named 'prosumers', and can sell their surplus generation to the network, thus getting involved in market transactions inside a community represents an alternative to current traditional networks. It is expected that an increasing number of end-users will want to become active in the electricity sector, which will lead to a large number of transactions. A possible tool for enabling the creation of such microgrid-level markets is the blockchain technology which could provide secure and reliable means of communication and data management between the end-users [2].

Blockchain technology was created as a solution to the problem of mistrust and data security. The first steps in the development of the technology were taken in 1991, when Stuart Haber and

W. Scott Stornetta first spoke about a cryptographically secure blockchain [3]. In 1993, together with Dave Bayer, they integrated optimal Merkel type trees in the concept [4]. Following the financial crisis of 2008, the concept of blockchain as a distributed database was developed, proposing a solution to change the way monetary transactions are carried out through various financial institutions. With the help of a peer-to-peer (P2P) communications network and a distributed data server, a blockchain database can be autonomous [5].

In the recent years, billions of dollars have been invested in research on blockchain technology in an attempt to make the most of its potential and understand how appropriate it is in the different economic domains [6]. But not all domains are fully ready to assimilate the blockchain technology. In each particular case, the current technological opportunities must be analyzed, as well as the challenges that the end-users face and how a new decentralized architecture could create value for them. The electricity industry is an extremely suitable candidate for blockchain technology-based innovation, with its complex supply chain that requires transparency and improved data processing and its highly transactional trading market that would gain advantage from faster settlement. The transparency and immutability of the blockchain can empower end-users of this industry and consumers.

A blockchain system is primarily based on a decentralized ledger of transactions that take place in a network. This network consists of nodes owned by independent entities that use a cryptographic protocol to validate the transactions that are entered in the ledger and to ensure that the entered data cannot be altered or changed. It is immutable, secure and completely transparent. Fully decentralized and replicated to node level, blockchain networks are harder to penetrate and manipulate by dangerous entities.

The blockchain system, coupled with other innovative technologies such as smart grids, big data mining and remote sensing, has the potential to provide solutions to various challenges in the energy sector and to contribute to the achievement of energy efficiency objectives, including to compensate for the funding gap for various projects in the field [7]. The technologies regarding blockchain-based platforms will lead to fundamental changes that will require the involvement of the distribution and supply companies, manufacturers of equipment, regulators and, last but not least, end-users [8,9].

A review of renewable and sustainable energy published in [6] provides a thorough analysis of more than 140 blockchain research projects and startups in the energy sector, from countries belonging all around the world. The electricity sector has a high potential to implement the blockchain technology as part of addressing several challenges [7,10,11]:

- Climate change. The need to integrate in existing electricity distribution systems renewable energy sources (RES) has led to the development of technologies such as PV panels and wind turbines, whose costs are constantly decreasing. The consumers who choose to install such generation sources become prosumers, which presents a challenge for the current structure of electricity networks. They can create technical difficulties for the Distribution Network Operators (DNOs) in ensuring the energy balance. However, electricity generation at the household level (classically with PV panels on the roof) is a great opportunity for the development of blockchain technology-based architectures, because it capitalizes on the distributed nature of electricity generation with unprecedented efficiency.
- The development of technologies that allow the transition to active distribution networks. The technological solutions refer to the communications and networking components, inverters, bidirectional smart metering systems, energy storage solutions. This evolution allows greater control at network level. Electricity becomes a controllable, storable and easily quantifiable product, suitable for trading through smart contracts.
- The creation of energy communities managed by local energy production cooperatives formed by community members. The microgrids which integrate the blockchain technology can represent a solution for connecting the poorest consumers to cleaner and cheaper energy, but also for energy savings and more responsible and accessible consumption. In some EU member states, European Federation of Renewable Energy Cooperatives (REScoop) have explicitly set social goals, such as

reducing energy poverty. They meet those objectives by developing solidarity schemes aimed at lowering the energy bills of vulnerable members, providing them with services and training in reducing consumption. They also use the gains from RES energy generation to increase the living standards of vulnerable and low-income households.

- Simplifying the architecture of the current trading models. The implementation of a blockchain-based prosumer network leads to the elimination of a large number of intermediaries in the electricity trading process.

Among the technical advantages of this technology can be underlined the following: better management of power generation, fewer hours of supply interruption, secure energy transactions, increased distributed generation. The main economic advantages refer to protecting the identities of the traders, creating a distributed economy, reducing the tax burdens, data protection and control, and compensation for producers [12,13].

Another concept that can be associated with local electricity trading in microgrids is the mitigation of energy poverty. 'Energy poverty' can be defined as the lack of access to clean, renewable, affordable energy, which leads to costly energy bills [14]. The concept lies at the intersection of energy sustainability and social issues mitigation, being characterized by three realities: high energy prices, low or stagnating incomes, and energy inefficient homes in urgent need of renovations.

The mitigation of energy poverty can be achieved using crowdsourcing, a concept first introduced in 2005 by James Surowiecki [15], which can be defined as utilizing contributions from peers and the collective wisdom of the crowd to alleviate a problem. It can also be an effective approach to enable the crowd to provide a service in a community within a limited geographical area by using smart metering [16].

In Romania, according to Order 228/28.12.2018 published by ANRE (Romanian Energy Regulatory Authority), the prosumers can trade electricity generated from renewable sources such as photovoltaics (PV), biomass, wind, cogeneration. The suppliers are bound to buy the surplus at the weighted average day-ahead market price from the previous year [17], with the advantage of the exemption from the payment of the distribution network tariff. This trading system is the most basic, limiting the options of both parties [18]. More advanced trading models should be considered to increase the benefits of the prosumers and consumers who trade electricity in a local market organized at the microgrid or community level.

Usually, in classic wholesale electricity markets, electricity is traded using bilateral contracts with negotiated prices, for long periods (years, months, weeks). This trading manner helps to reduce the prices for the buyers, and provides stability and predictability for the producers. For shorter trading intervals, such as in the day-ahead (SPOT) markets, the merit order price setting mechanism is preferred, which ensures maximum benefits for producers when the demand is high and can lead to higher prices for suppliers and end-users.

On the other hand, the electricity quantities traded in local grids by prosumers are much smaller, and the trading intervals need to be smaller, because of renewable generation uncertainty. At the same time, the generation from prosumers needs to be incentivized to promote the proliferation of renewable electricity. Thus, a market model for microgrids should take into consideration creating advantages simultaneously for prosumers and consumers.

In this regard, the paper presents a new trading approach for prosumers that uses the blockchain technology for creating a local market at microgrid level, forecasts for consumer buy offers, obtained using technologies such as remote sensing tools, and the energy crowdsourcing concept for energy poverty mitigation. The proposed model takes as reference the trading model for excess prosumer generation used in Romania and applicable to developing markets, which consists in selling back the available electricity at fixed tariffs back to the grid. The authors propose a diversification of the trading methods and settlement procedures by creating a local trading mechanism intended to provide flexible market model that can be adapted to specific microgrid conditions and rules agreed at the community level. The proposed market model has two trading levels. The primary level is

intended for main trading. The secondary, two-tier market is designed by the authors for increasing the prosumer profitability and lowering consumer electricity cost while accommodating particular scenarios that can arise in real conditions. The considered scenarios are: mitigating energy poverty for vulnerable consumers, selling remaining prosumer surplus to consumers who do not participate in the primary market but have bilateral contracts with certain prosumers, allowing occasional access to the market in exchange for a tariff, and reducing the effect of erroneous consumer buy offers caused by inaccurate forecasts or temporary unusual consumption patterns. The primary market model offers two trading alternatives: 'first-come-first-served' (FCFS), and merit-order (MO). The secondary market proposes two tiers with three trading methodologies, which can be optionally used, in number and order, according to the specific needs of particular microgrids: energy poverty mitigation, tariff access and invite access. The proposed alternatives are tested in a case study, on an existing low voltage (LV) electricity distribution network from Romania which has microgrid characteristics, in order to assess the effects of the chosen trading methods on the profits achieved by prosumers and consumers.

The proposed market model provides flexible tools for incentivizing the sustainable development of local communities based on environment protection and economic and social inequality mitigation through the use of modern technology tools, by encouraging local trading of electricity generated from renewable, clean primary sources.

The results of the case study show that by using the local trading mechanisms designed for the primary and secondary markets, the prosumers can sell more electricity, at lower prices for the community and better individual profit. If the benefits are consistent, this can lead to the increase of distributed generation sources in microgrids, thus a more sustainable development of the electricity generation sector.

By lowering consumer prices, the sustainable economic and social development of communities is also encouraged. Not least, these goals are envisioned to be achieved by obtaining in parallel the modernization of the electricity distribution infrastructure, by using smart grid communication and energy management tools and involving digital instruments (specialized trading software and blockchain).

The remainder of the paper is structured as follows. Section 2 presents a literature review regarding the research proposed in the paper. Section 3 describes the proposed market model for microgrids. In Section 4 are presented the results of the case study, with a comparison between the proposed trading strategies, outlining their particularities. The paper ends with the sections dedicated for discussions and references, and annexes.

2. Literature Review

Recent studies have considered combining the operation of small-scale renewable energy sources (SSRES) in distribution networks and deregulated electricity markets. The range of these studies is covering unit commitment [19] and economic dispatch problems [20], in addition to scheduling of SSRES [21], and the uncertainty of renewable generation [22]. The main trends and approaches currently described in the literature are briefly summarized in the following paragraphs.

As it was presented in the introduction section, in Europe there are currently over 3400 green energy cooperatives (REScoop). In accordance with [23–26], the REScoop notion is defined in EU directives as "local energy communities", according to data from the Federation of Green Energy Cooperatives in Europe. More than one million European citizens are participating in REScoops to invest together in the transition from fossil fuels to clean primary energy resources and energy efficiency. In Romania, starting in 2020, the first established REScoop proposes that future members who generate energy (prosumers) will be able to sell the surplus to other members, rather than to an aggregator, following the concept of 'prosumer-friendly' [27].

In another perspective, paper [28] considers a P2P electricity trading method using a private Ethereum blockchain ledger where all bids are encrypted for anonymity and peer matching is done by a functional encryption-based contract.

Regarding the energy crowdsourcing in prosumer-enabled electrical networks, a small number of published papers is available in the literature [16,29]. The existing studies consider a two-stage algorithm for minimizing the cost of generation and the energy losses by prior rescheduling of user loads and SSRES.

In other work, a particular local energy market model was considered in [30], which integrates different P2P energy trading platforms based on unidirectional market clearing price (MCP) for a microgrid. Moreover, the settlement considers an MCP or P2P mechanism.

The future active distribution network (ADN) is a P2P community based on active energy agent (AEA) users [31]. The maximization of social welfare in local prosumer generation trading with an auction-based mechanism is used in [32]. The same first author considers that in a microgrid the energy flows in a transactive way and the transactions are based on bilateral contracts between peers [33]. Another concept of prosumer surplus trading based on the transactive energy concept is proposed in the literature [34–37]. Paper [34] uses a Stackelberg game-based method for solving the transactive energy problem, in which the DNO and the SSRES aggregators are participating simultaneously in the Local Electricity Market (LEM) and Wholesale Electricity Market (WEM). A comprehensive cost–benefit model for prosumer load sharing was proposed in [35], using game theory and considering non-cooperative game models of the microgrids for prosumers energy surplus. In the same context, a particular social welfare-based concept on transactive energy or demand response (DR) is applied in [36,37] using negotiated prices.

Another way to trade surplus are DR programs, whereby the LEM operators play a vital role in managing the exchange of data, to ensure the notification flow between balancing authorities, service companies and end-users. First, the microgrid operator assesses the electricity consumption patterns based on the structure of variable electricity tariffs and prices to establish trading plans. They also sign bilateral P2P contracts with end-users to take direct control of specific energy assets [38]. This information is aggregated to create commitment portfolios—load reduction schedules that are provided to network operators in exchange for compensation commensurate with the size of the capacity involved [39]. In the event of a system emergency or demand, the DSO shall request the aggregator to reduce or increase a portion of the contracted portfolio. For this reason, the aggregator receives additional compensation which can take the form of tariff reductions, incentive payments and invoice credits.

Using online platforms [40–46], the consumers can become prosumers who create and distribute their own information about the energy generation. Some authors proposed a demurrage mechanism (DM) and Home Energy Management (HEM) for prosumers' energy surplus in an LEM based on blockchain [41]. A particular P2P business model for 48 residential prosumers with PV panels installed in a Swedish village is proposed in [42]. This article identifies some new potential opportunities for optimizing the LEM and its variables for the best gain, taking into account that a significant influence is represented by the integration of energy demand, generation supply, and LEM rules. The aforementioned study can be used to provide information for regulatory bodies to create a fair, useful and cost-effective P2P electricity trading framework for prosumers. Another comprehensive platform for prosumers' digitalization was recommended in [43], and market simulations are developed in [44,45] for consumers integration in microgrids. In the same manner, a virtual platform was proposed in [46] for efficient management of multiple energy prosumers (MEP).

The presence of decentralized energy sources demands the analysis of the problem of continuity of energy supply to operators whose activities significantly depend on electricity. There are EU countries where power outages amount to about 20 min per year, but in other cases the average power outages range from 450 to 500 min [47]. Prosumers' microinstallations ensure the business continuity for producers in such countries and negotiated surplus trading increases social welfare [48]. Because the SSRES efficiency depends on atmospheric conditions and regional climate, even minor temporary changes in weather conditions can cause significant variability in power generation at different time and space scales. Methodologies based on the remote sensing of atmospheric conditions are the primary

source of information for the development of numerical forecasting models that support the planning and operation of power systems in the presence of intermittent energy sources [49]. For local trading of such electricity surplus, the LEM operators consider the blockchain concept [11,12,16,28,29,40,41,48] or direct bilateral contracts [50,51]. These market models aim to provide secure and affordable energy supply for the end user, which is essential for the functioning of an economy in which energy poverty is reduced and the needs of vulnerable social groups are taken into account [52–54]. Social welfare is obtained by the authors in [53], where the smart P2P contracts are considered as a distributed optimization problem, solved with a virtual aggregator based on the Alternating Direction Method of Multipliers (ADMM). All the LEM actions can be completed by the peers who do not necessarily trust each other through an agreement algorithm which defines the speed of the transactions. One of the most used algorithms is the Proof-of-Work (PoW) [55]. Nonetheless, previous articles about energy sustainability have paid limited attention to prosumer engagement, management and administration. For example, according to [56,57] each of the providers can have a proper trading platform with specific architecture for sustainable planning of the local microgrid or region.

From other perspectives, the prosumer surplus trading process based on the specific transactive energy microgrids are examined by the researchers in [58–60]. The prosumers' aggregation to one group with the same interest based on virtual microgrids is analyzed by the authors in [61] for bill cost reduction as a particular energy poverty mitigation or social welfare. The aforementioned problem can be solved in smart buildings by using ADMM for energy sharing between the players, as is shown in [62,63].

In [64] remarkable directions for cost-effective use of digital cryptocurrencies in smart grid dynamic management are thoroughly explained to cover the challenging viewpoints of blockchain technology. The LEM is favorable for prosumers because the participation of the before-mentioned players is concrete in the purchase of energy surplus, but the revenues from the surplus traded are proportional between sellers [65]. Common consumers do not produce electricity and are only active in the purchasing process [66]. The load flexibility can change the trading offers. Other perspectives consider peak loads in the prosumer's vicinity with smart P2P subscribed capacity prices in [67], or the crowdsourcing concept for surplus energy planning or sharing, as is used in [68], or considering the indispensable local energy storage systems [69].

The main concepts taken from the literature and discussed above are compared with the market model proposed in the paper, in Table 1. In addition, the last column considers the type of settlement used in the market.

The objective of the local market is to enable an overlay social network of smart devices that facilitates the communication and trading process between players from LEM, prosumers, consumers and microgrid. They should share a common goal, such as optimal energy management, taking into account that the solution with local energy storage systems (as is battery banks) is too expensive [70,71], and without technical possibility for energy poverty mitigation.

Table 1. A comparison between the proposed model and the literature state-of-the-art survey.

Reference No.	Blockchain	P2P Contracts	Energy Crowdsourcing	REScoop	Energy Poverty	Settlement Procedure
[16,29]	Yes	Yes	Yes	No	No	Negotiated
[28]	Yes	Yes	No	Yes	No	Negotiated
[24,25,44,49,57]	No	No	No	Yes	No	Negotiated
[26,27]	Yes	No	No	Yes	No	Negotiated
[30–32,35,38,42,56,60,65]	No	Yes	No	No	No	Negotiated or MCP

Table 1. *Cont.*

Reference No.	Blockchain	P2P Contracts	Energy Crowdsourcing	REScoop	Energy Poverty	Settlement Procedure
[33,34,36,37,43,45]	No	No	No	No	No	Negotiated
[39,46,50,51,69,71]	No	Yes	No	Yes	No	Negotiated or MCP
[40,41,54,58,59]	Yes	Yes	No	No	No	Negotiated
[53]	Yes	Yes	No	No	Yes	Negotiated
[48,55,64]	Yes	No	No	No	No	Negotiated
[61,66]	No	No	No	No	Yes	Negotiated or MCP
[62,63]	No	Yes	No	No	Yes	Negotiated
[68]	No	Yes	Yes	No	No	Negotiated
Proposed model	Yes	Yes	Yes	Yes	Yes	Negotiated and MCP

3. Materials and Methods

In LV electricity distribution networks or local microgrids, there is an increasingly larger number of residential consumers who are opting to install local generation resources to gain independence from the grid. The predominant choice is the use of PV panels systems that are easier to install at household residences and provide energy by converting the solar irradiation into electricity. This trend is incentivized by the subsidies offered by governments worldwide. As the number of individual houses adopting this technology increases, new opportunities arise regarding the trading models used for selling the excess generation. Residences become prosumers, entities capable of consuming, producing and selling electricity. The prosumers will use their own generated electricity mainly to cover their individual consumption and when the generation exceeds this amount, they will sell the surplus to the grid. The simplest method of surplus trading is to sell the entire available quantity back to the supplier, though an aggregator entity, at a regulated price. However, this is the least profitable approach, as the regulated prices are usually low [72], and the benefits can be seen only by the suppliers/network operators, and the prosumers. New trading methods for microgrids are currently envisioned in the literature, aiming to create local electricity markets that would provide benefits for all the players involved (aggregators, prosumers and consumers). A main requirement for implementing such initiatives is the conversion of the classic electricity distribution infrastructures into intelligent or smart grids, capable of real-time communication between the supply and consumer buses, and centralized operation management and data processing at microgrid level.

In line with these trends, previous research efforts by the authors, published in [40], proposed an algorithm for prosumer surplus transactions at the microgrid level, using P2P contracts and blockchain technology. The market mechanism considers trading priorities set at central level and based on consumer or prosumer prices, or custom priorities determined by the prosumer–consumer geographical distances and the 'first-come-first-served' (FCFS) principle.

This paper extends the previous research considering an improved and extended market model, with two trading phases (primary and secondary). The basic flowchart of the proposed market model is depicted in Figure 1.

The primary market includes the blockchain approach from [40] and adds a supplementary trading method based on the merit order used in wholesale markets. These methods can be used as alternatives for trading.

A second market segment, with two tiers, is proposed to help the prosumers and consumers to better manage the sell and buy offers that can be affected by errors. Crowdsourcing and energy poverty mitigation are used for this purpose.
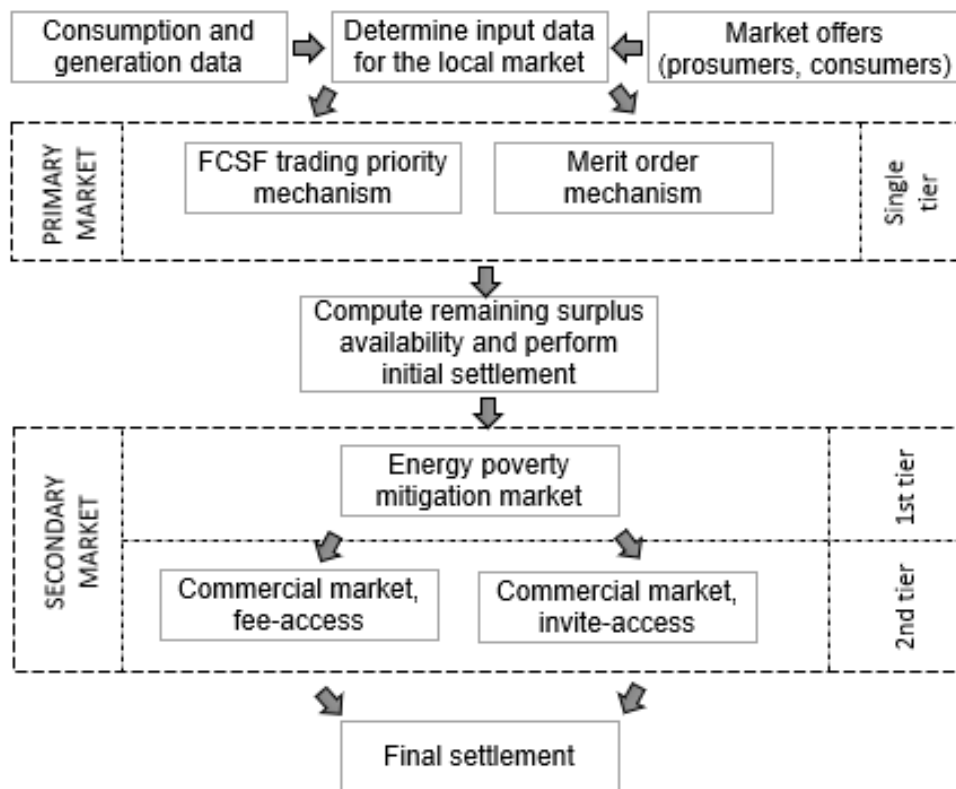
Figure 1. The basic diagram of the proposed market algorithm.

The sell offers are the result of the surplus that the prosumers can generate but cannot use locally. The buy offers placed by the consumers in the local market are usually the result of forecasts made with variable precision. In the case of trading electricity obtained from PV panels, the forecasts must consider weather data obtained with technologies such as remote sensing and big data mining. Thus, the offers placed by the consumers in the market can be affected by errors which will result in mismatches between the needed and traded quantities.

In the Romanian market model, when the electricity acquired from the local market is less than the demand, the consumers would buy the rest at higher prices from the national grid, and the generators would be forced to sell any surplus to the aggregator, at a lower price.

On the other hand, if trading is performed in a local market, when the consumers forecasts are higher than the actual demand, the buyers would be forced to sell the excess quantities to the aggregator if sufficient and cheap storage facilities are not available.

The newly proposed algorithm provides market mechanisms designed to alleviate these problems. The following general assumptions are made:

- The prosumer and consumer selling and buying offers are managed by the local non-profit aggregator using two possible market mechanisms integrated in a blockchain trading system:

  ○ A primary market built on the blockchain technology, ensuring anonymity and security for the placed orders.
  ○ A secondary market with a two-tier trading mechanism for minimizing the imbalance between the offers placed in the blockchain system and the actual traded quantities.

- The primary market can use two alternative price-setting methods based on blockchain technology: the 'first-come-first-served' (FCFS) method or the merit-order method used in traditional day-ahead markets.
- The secondary market provides two optional trading tiers:

○ The energy poverty mitigation tier, aimed at low-income consumers who otherwise could not afford to participate in the market.

○ The commercial tier, with two options, aimed for expanding the market through crowdsourcing, with two types of consumers: those participating occasionally, in exchange for a fee, and consumers who do not participate directly with offers but are represented (invited) in the market by other consumers.

- For the invite option of the commercial tier, any consumer Ci can acquire electricity from the second market layer only if has signed previously a P2P contract with a specific prosumer Pj.
- The selling price of a prosumer or consumer can vary hourly, but in the paper is set constant for all trading intervals. This approach is modelling the practice used for traditional differentiated tariffs where the peak and night prices are outside the hours when PV panels can generate electricity, and the case where no storage capabilities are installed in the network. Electricity is sold on the market for the surplus intervals, and settlement is performed at the end of each trading interval.
- If the local surplus exceeds the demand traded in the market, the surplus will be sold to the aggregator/market administrator, at regulated tariffs.
- The secondary two-tier market components are optional, but the case study considers all the available options, in order to better demonstrate the advantages of the proposed trading algorithm.

3.1. Input Data for the Local Market

The input data required for trading consist of the quantities and prices associated with the consumption and local generation measured in the market. This information is provided in six matrices: $C = C\,(h, i) \in \mathbb{R}^{nhxNCM}$, $CO = CO\,(h, i) \in \mathbb{R}^{nhxNCM}$ and $PCO = PCO\,(h, i) \in \mathbb{R}^{nh \times NCM}$ for consumption quantity, offers and price offers, and $G = G\,(h, j) \in \mathbb{R}^{nh \times NPM}$, $GO = GO\,(h, j) \in \mathbb{R}^{nh \times NPM}$, $PGO = PGO\,(h, j) \in \mathbb{R}^{nh \times NPM}$ for generation quantity, offers and price offers, where *NCM* and *NPM* are the number of consumers and prosumers participating at hour *h* in the market. It is considered that generally *NCM* < *NC* and *NPM* < *NP*, *NC* and *NP* being the number of consumers and prosumers connected in the microgrid.

Trading in the primary market can occur at any hour *h* when there are consumer buying offers placed in the blockchain system (1), and there is generation surplus offered for selling (2).

$$\sum_{i=1}^{NCM} CO(h, i) > 0 \tag{1}$$

$$\sum_{j=1}^{NPM} GO(h, j) > 0 \tag{2}$$

Surplus occurs when the local generation of a prosumer exceeds its individual consumption (3) and the surplus is traded in the market (4).

$$S(h, j) = G(h, j)\text{-}C(h, j), \; j = 1..NPM \tag{3}$$

$$S(h, j) \Rightarrow GO(h, j) \tag{4}$$

The consumer quantity offers for the primary market use two types of representation:

- as actual consumption value measured in [W], when the price is set according to the blockchain priority model, as in [40];
- as a multiple of 100 W for the price setting according to the day-ahead merit order model used in wholesale markets.

The prosumers can choose to sell their surplus directly to the aggregator for a fixed regulated tariff, or in the primary local market. In the paper, it is considered that all the available surplus is traded through sell offers placed in the market blockchain system.

The secondary market is activated at any hour *h* when at least one of the following conditions is fulfilled:

- The sum of the buy offers is lower than the aggregated offers placed by the prosumers, i.e., the prosumers need to sell the remaining surplus:

$$\sum_{i=1}^{NCM} CO(h,i) < \sum_{j=1}^{NPM} GO(h,j) \tag{5}$$

- The buy offer of a consumer *i* is greater than the actual consumption because of the forecast error or representation model used in the market (multiple of 100 kW).

$$CO(h,i) > TCO(h,i), \; i = 1..NCM \tag{6}$$

where *TCO(h,i)* is the quantity of electricity actually traded by the consumer *i* at hour *h*, which can be equal to or less than the offer placed on the market.

3.2. The Primary Market

This market segment is the main trading tool for the prosumers and consumers in the microgrid. As outlined previously, two alternatives are provided for determining the consumer and prosumer trading priority: 'first-come-first-served' and merit order. Both methods use the consumer (buy) and prosumer (sell) offers placed in a centralized secure and anonymous blockchain system established at the microgrid or market level. The blockchain system is preferred because it guarantees trading fairness, all players being unaware of the offers placed by others, thus minimizing the risk of market manipulation.

Another assumption used in the paper is that, by means of an automated system comprising smart metering, two-way communication and continuous monitoring at the microgrid level, the algorithm has immediate access to measured and forecasted data at consumer and prosumer buses. For examining the possible effects on trading, two consumer offer mechanisms are considered:

- Consumers place on the market buy offers for the entire consumption at hour *h*, in order to minimize their electricity bill by attempting to buy the maximum quantity of electricity from the local market, at lower prices, rather than from the main grid, at higher prices.
- Consumers place on the market buy offers determined by forecast techniques using big data analysis or remote sensing techniques.

The first type of offer is used in the FCFS trading method, where a generic consumer *i* places fixed-price-per-kWh and variable quantity offers, the trading order being determined by the time tag of the offer. The quantities for these offers are determined in the settlement phase, based on consumption measurements taken from the microgrid. The flowchart of this trading method is given in Figure 2.
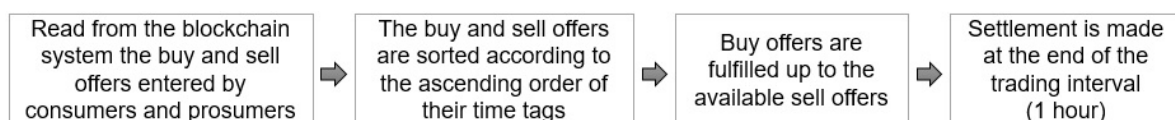
Figure 2. The basic diagram of the primary market 'first-come-first-served' trading mechanism.

The second type of offer is used in the merit-order trading mechanism. The buy offer prices and quantities are placed in the blockchain system by the consumers before the trading interval. Quantities

are given as multiples of 100 W and prices are given for each kWh. The flowchart of this trading method is given in Figure 3. The trading order and price are determined by the standard merit-order method, provided in Figure 4, where the trading price is determined as the market clearing price (MCP).
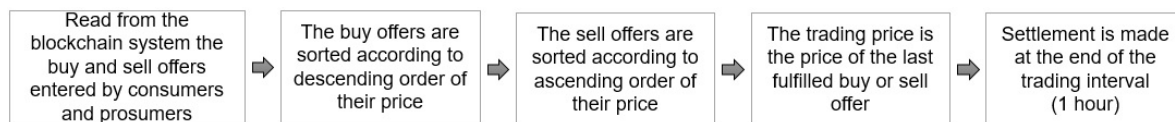
Figure 3. The basic diagram of the primary market merit-order trading mechanism.
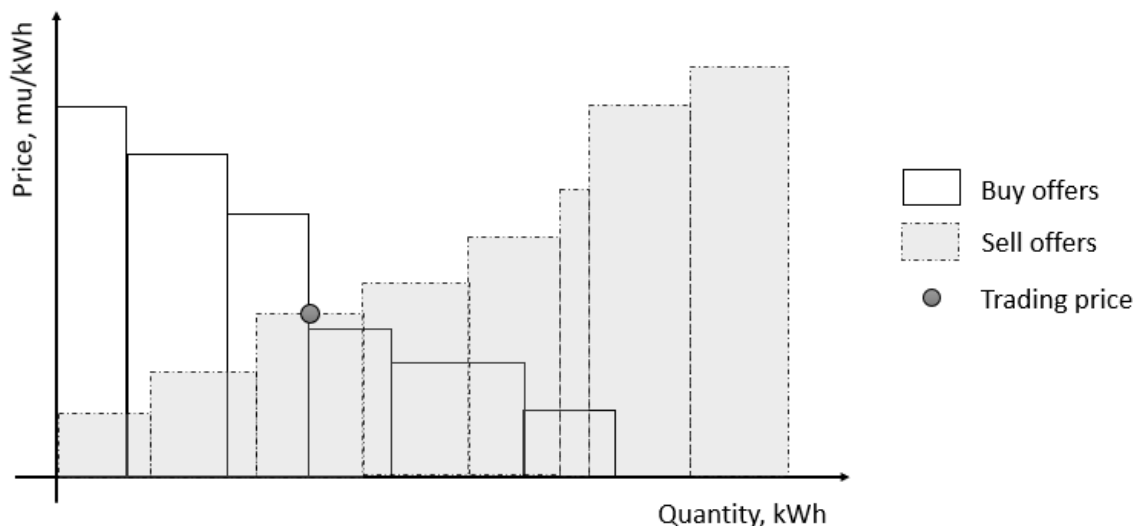
Figure 4. The merit-order trading mechanism.

For both methods, the prosumer sell offers are given as the full available surplus *S(i,h)*, in kWh.

The maximum amount of traded electricity *TC* is determined by the minimum between the aggregated buy and sell offers:

$$TC = \min\left(\sum_{i=1}^{NCM} CO(h, i), \sum_{j=1}^{NPM} GO(h, j)\right) \tag{7}$$

The settlement price of a transaction *t* made by a prosumer *j* or consumer *i* is given by the amount of traded electricity *C(h,t)* and its price *P(h,t)*, determined by each transaction, *TP(h,t)*, which can be different from the sell or buy offer price submitted by the players in the market, *PCO(h,i)*, *PGO(h,j)*.

$$TP(h, t) = C(h, t) \cdot P(h, t) \tag{8}$$

The basic flowchart of the primary market algorithm uses the steps presented in Figure 5.
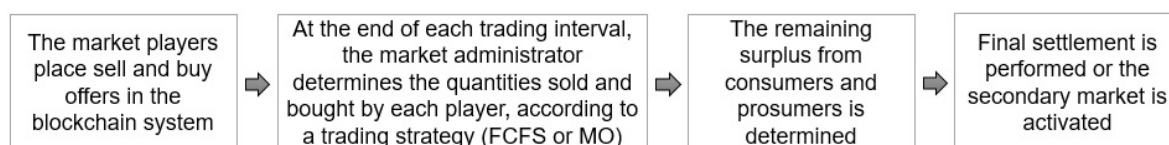
Figure 5. The flowchart of the primary market trading algorithm.

The trading mechanisms used in the primary market can lead to electricity quantities that cannot be traded locally. Three scenarios can lead to this situation:

- At given hours, the total local generation available in the market (sell offers) exceed the total consumption (buy offers).
- If the merit-order method is used, the buy offers are given as multiples of 100 W, while the sell offers are the $S(h,i)$ quantities. This leads to $S(h,i)$ fractions that cannot be fulfilled.
- The consumers place in the market buy offers that exceed their real consumption, following forecast errors or significant accidental deviations from the daily demand pattern.

All these quantities can amount to an important value over longer time periods. If they are not traded in the local market, the prosumers would sell at minimum price to the aggregator, while the consumers would buy electricity at standard, high tariffs.

The algorithm proposed in the paper offers the possibility of extending the primary market with a two-tier secondary market, in order to make prosumer and consumer surplus quantities available for trading in the local network.

3.3. The Secondary Market—The Energy Poverty Tier

The local market is profitable mostly to consumers with high demand, who can better benefit from the energy cost reduction obtained from the difference between the grid tariffs and the price per kWh offered by the local producers. These consumers are also usually those who have the financial resources to install the physical and software infrastructure required to access the market.

On the other hand, amongst the consumers connected in a microgrid can exist a number of low-income consumers, who in traditional networks would be classified as belonging to vulnerable categories and suffer from energy poverty. The paper proposes an optional secondary market tier in which the surplus that cannot be traded in the primary market would be automatically allocated in the initial settlement phase (see Figure 1) to such vulnerable consumers who, in normal conditions, would not be able to access the local market.

The surplus can come from both prosumers and consumers, as summarized in the previous subsection. In all the cases, the electricity quantities will result from the mismatch between the quantities offered for trading (higher)—$CO(h,i)$ or $GO(h,j)$—and actual traded quantity, determined by the existing (lower) generation availability $TC(h,j)$ or realized consumption $TC(h,i)$:

$$\begin{aligned} TC(h,i) &= CO(h,i)\text{-}TC(h,i), \ i=1\ldots NCM, \ \textit{for consumers} \\ TC(h,j) &= GO(h,j)\text{-}TC(h,j), \ j=1\ldots NPM, \ \textit{for prosumers} \end{aligned} \tag{9}$$

Thus, consumers who were buyers in the primary market can act as sellers in the secondary market, together with the prosumers.

The quantities sold to vulnerable consumers in the secondary market are determined using the merit-order method where the buyers' prices are set as 0 mu/kWh (mu is the monetary units) and the quantities are ranked in descending order. The cost for traded kWh can be set using as reference the price obtained by the seller in the primary market, the original price offer placed by the seller in the primary market or an agreed fixed tariff, according to the policy agreed in the local market.

This trading scheme offers two benefits. The vulnerable consumers from the microgrid will see social welfare increase by the reduction of their electricity bill, which will be proportional to their consumption in the trading hours interval and the market price. On the other hand, the prosumers with remaining generation surplus and the consumers who have surplus to sell after the initial settlement of the primary market can sell electricity at higher prices than the tariff used by the aggregator.

The flowchart of the first tier of the secondary market is presented in Figure 6.

Since the demand of the vulnerable consumers selected for the energy poverty tier is expected to be low, the remaining surplus after the settlement of the first tier can be further traded in a second tier reserved for commercial trading.
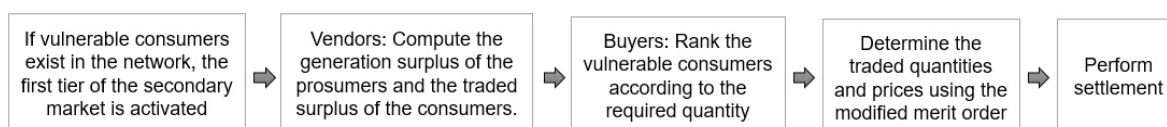
Figure 6. The flowchart of the social inclusion tier of the secondary market.

3.4. The Secondary Market—The Commercial Tier

The commercial tier of the secondary market is designed to incentivize market diversity by allowing other consumers to participate in trading. Several consumer categories are envisioned. Some consumers would not trade continuously and would seek only occasional access to the market, buying the local generation surplus to supply automated receptors such as greenhouse irrigation systems in given hours of preset days. Other types of occasional consumers could benefit from the price difference when trading on the local market, but the initial investment for the infrastructure required to get access to the market would be prohibitive.

Two options are available in the algorithm for this trading segment:

- Option 1: Fee access.
- Option 2: Invite access.

In the fee-access model, the consumers who need only occasional access to the market can submit offers in the secondary market to gain priority access for the surplus remaining after the settlement of the primary market offers. The trading model considers the merit-order priority method described in Figure 5 for the primary market, but where the consumers offer to buy from the market their entire consumption measured in the trading interval, at the lowest price plus a fixed percent fee from the value of the transaction. The merit order is used to determine the succession in which the offers are fulfilled. The financial settlement is made using the MCP, the consumer or the prosumer price offers for all transactions, according to the market policy, and then a fee *f*% is added to the price resulting from the trading mechanism.

$$TP(h,i) = C(h,i) \cdot (PCO(h,i), \ PGO(h,j) \ or \ MCP(h)) \cdot (1 + f\%) \tag{10}$$

The basic flowchart of the fee-access secondary market model is given in Figure 7.
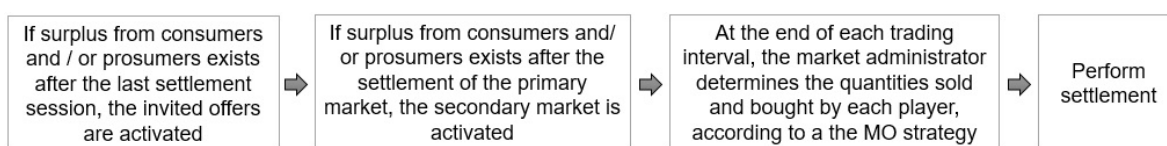
Figure 7. The flowchart of the secondary market fee-access model.

In the invite-access model, existing market players can act as subcontractors for other consumers from the microgrid. Certain prosumers or consumers can still have surplus quantities unsold after the previous settlement sessions have been completed. In order to avoid getting the lowest price per kWh from the market aggregator, they can optionally choose a partner from the microgrid to which the remaining quantities will be sold. The transactions are based on P2P contracts existing between the two entities and notified to the market administrator, who is responsible for the final settlement at market level. The settlement price is agreed between the parties, chosen from the vendor and buyer offers.

The flowchart of the secondary market invite-access model is provided in Figure 8.
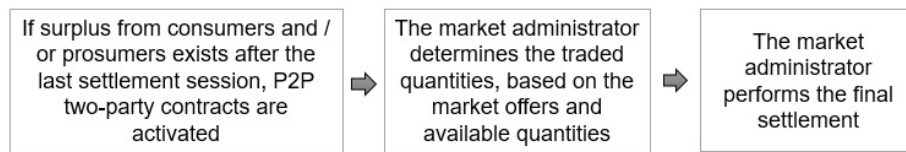
Figure 8. The flowchart of the secondary market invite-access model.

It should be noted that the secondary market models are optional, and their order of activation can be changed according to the priorities of a specific microgrid. Instances can exist where the energy poverty mitigation tier is absent or one or both segments of the secondary commercial tier are used.

4. Results

The new market was tested on an LV distribution network from Romania, with 28 buses and two four-wire three-phase bundled feeders, with an average distance between the connection points of 40 m. The network supplies only single-phase residential consumers, some of whom also have PV generation capabilities. The load and generation profiles used in the study are considered as daily 24-hour measured values, as provided from the smart metering infrastructure existing in the LV microgrid. The 24-hour load profiles for the network buses are presented in Table A1 in Appendix A.

Each bus, except bus 1, which is a branching point, has one residence connected. The prosumers are located at buses 3, 6, 7, 10, 15, 25 and 27, as shown in the one-line diagram from Figure 9. Their 24-hour generation profiles were modeled using representative data for this type of generation and are provided in Appendix A, Table A2. The prosumers will use the generated electricity primarily for supplying their own hourly demand, and wish to sell the remaining surplus to the consumers participating in the local market set up at microgrid level and managed by a non-profit aggregator. From Table 2 and Figure 10, it is seen that generation occurs only in the 06:00–18.00 interval, when solar energy is available. The surplus is maximized in the 10:00–13:00 interval and minimized towards the evening time, when the peak load hours are near.
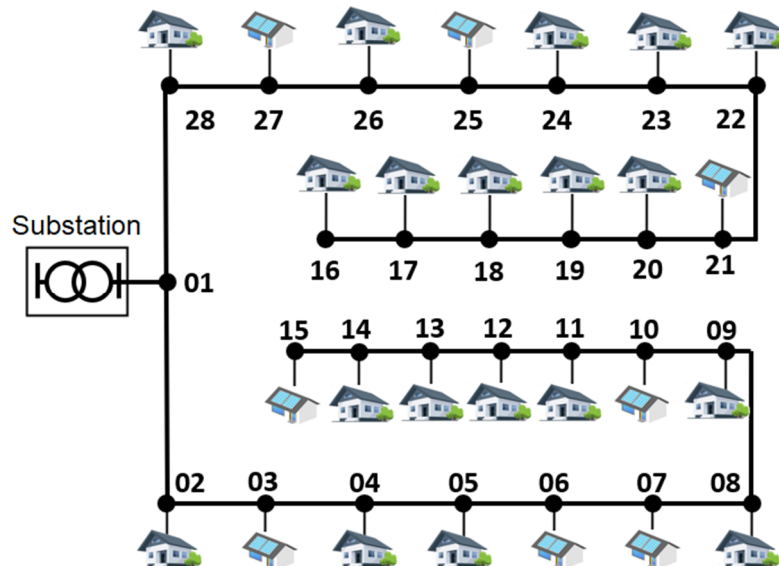
Figure 9. The low voltage (LV) microgrid used in the case study.

Table 2. The prosumers' electricity surplus, in kWh.

Hour	P27	P21	P7	P15	P6	P3	P10	P25	Total
h6	0.000	1.588	0.000	1.948	0.000	1.208	2.496	3.052	10.292
h7	0.000	1.805	0.263	1.585	0.000	1.806	2.616	3.487	11.562
h8	0.668	1.726	0.704	1.586	0.000	2.879	0.714	3.826	12.103
h9	1.437	1.749	1.056	2.228	0.741	2.836	1.279	3.956	15.282
h10	1.607	2.292	1.093	1.302	1.116	3.251	2.794	4.232	17.687
h11	1.655	2.038	1.400	2.775	1.886	3.372	0.000	4.175	17.301
h12	1.595	1.822	1.225	1.880	2.328	3.392	0.980	4.060	17.282
h13	1.508	0.685	1.413	2.826	2.294	3.462	0.826	4.240	17.254
h14	1.372	1.182	1.385	2.945	1.347	3.178	0.000	4.214	15.623
h15	1.106	2.028	1.048	1.546	1.184	2.331	0.000	3.702	12.945
h16	0.563	0.819	0.410	1.325	0.000	2.133	0.000	3.209	8.459
h17	0.000	0.000	0.000	1.062	0.000	1.134	0.046	2.877	5.119
h18	0.000	1.170	0.000	1.161	0.000	1.221	0.914	2.599	7.065
Total	11.511	18.904	9.997	24.169	10.896	32.203	12.665	47.629	167.974
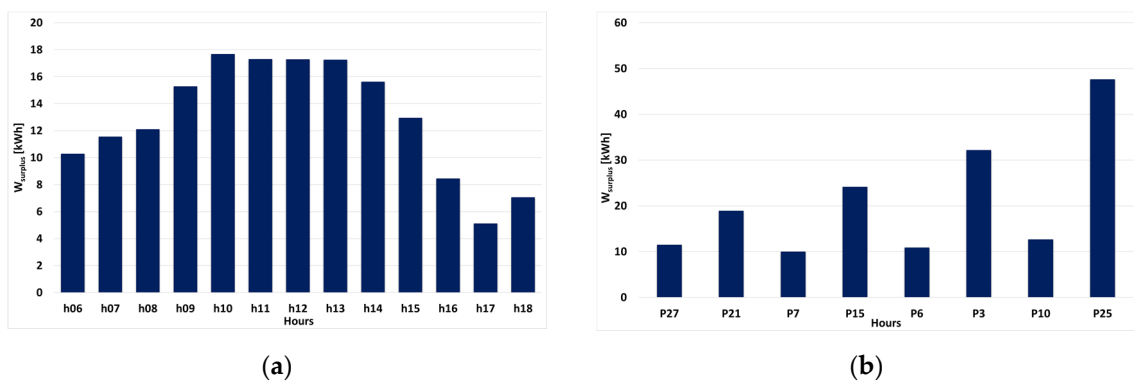
Figure 10. The total electricity surplus: (**a**) hourly; (**b**) for each prosumer.

4.1. The Primary Market

From the 27 consumers existing in the microgrid, the case study considers that only 11 are participating in the primary market as buyers (from buses 5, 8, 9, 11, 12, 14, 16, 19, 20, 24, 26), chosen mainly between the residences with high daily electricity demand. For each hour *h*, they can submit to the market two types of offers according to the traded quantity: the entire hourly demand and forecasted values, in multiples of 100 kW, as discussed in Section 3.2. For the forecasted offers, the values used in the case study are given in Table A3 in Appendix A, and in Figure 11, only for the hour intervals in which prosumer generation exists.
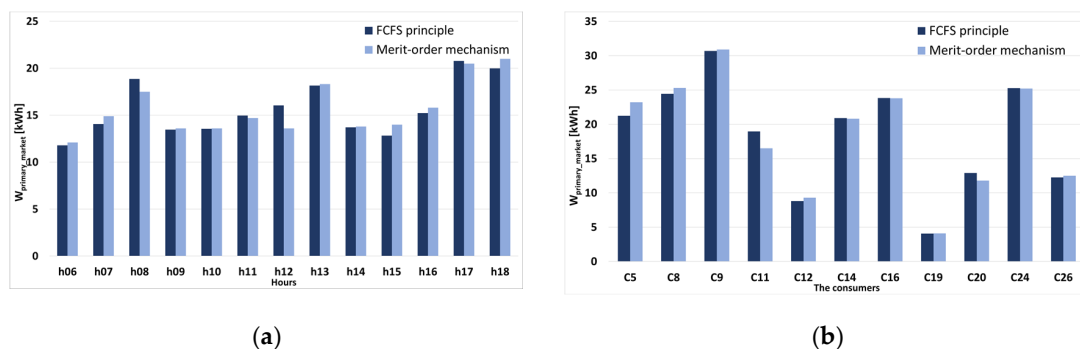
Figure 11. The buyer quantity offers in the primary market: (**a**) hourly; (**b**) for each consumer.

The sellers who place offers in the primary market are the prosumers with generation surplus. It is considered that they wish to sell the entire surplus on the market to maximize their revenue. The quantities offered, derived from Tables A1 and A2, are presented in Table 2 and Figure 10, where it can be seen that surplus exists for trading in all hourly intervals from 06:00 to 18:00, but there are prosumers who cannot trade electricity at some hours (for example, P27 or P6).

For all quantity offers, the consumers and the prosumers must also provide in the blockchain system of the primary market the desired price offers, which are given in Tables A4 and A5 in Appendix A. These values were set between 0.39 and 0.6 mu/kWh for consumers, and in the 0.4–0.55 mu/kWh range for prosumers. The higher maximum prices for consumers were chosen taking into account the merit-order method, in which the offers with the highest prices are prioritized. Furthermore, both the prosumers' and consumers' price offers were set higher than the regulated tariff to incentivize the trading in the local market.

If the market would not be present, the total electricity surplus quantity (167.97 kWh) would be traded by the aggregator back in the grid, at a regulated tariff. Using the reference value of 0.251 mu/kWh applied in Romania [73,74], the total revenue of the prosumers would be of 42.16 mu/day.

For demonstrating the advantages and disadvantages of each trading priority method used in the market, FCFS and MO, the case study results are be provided as comparisons between these alternatives.

As it can be seen from Figure 11, there are hours when the MO offers differ from the total demand used in the FCFS offers. This can happen because of two reasons: the forecast error and the standardized offer type (multiple of 100 W) used by the MO method. On the other hand, the offers placed by the consumers in the market are identical for both trading methods, and equal to the available surplus (Figure 10), because one of the main objectives of the local market is to enable prosumers to sell the entire surplus locally, and offers given as multiples of 100 W would impede the achievement of this goal.

The traded quantities and revenues/costs for each prosumer/consumer and hourly interval are given in Figures 12 and 13 and Tables 3–6.

(**a**)   (**b**)
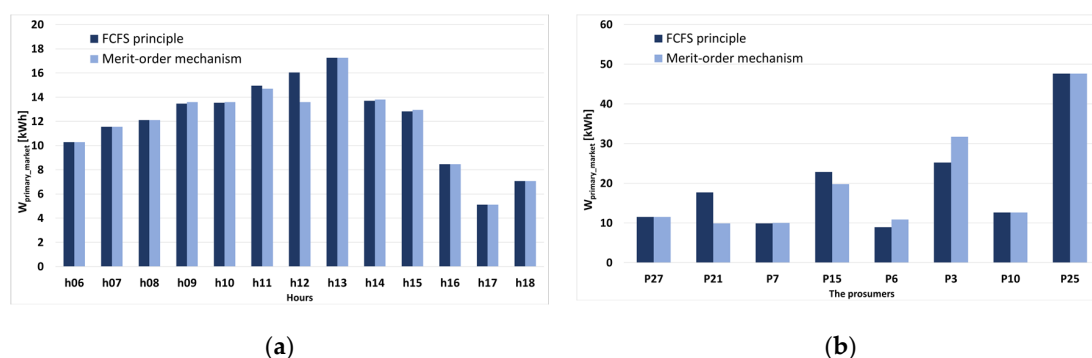
Figure 12. The traded quantities of the sellers in the primary market: (**a**) hourly; (**b**) for each prosumer.

(**a**)   (**b**)
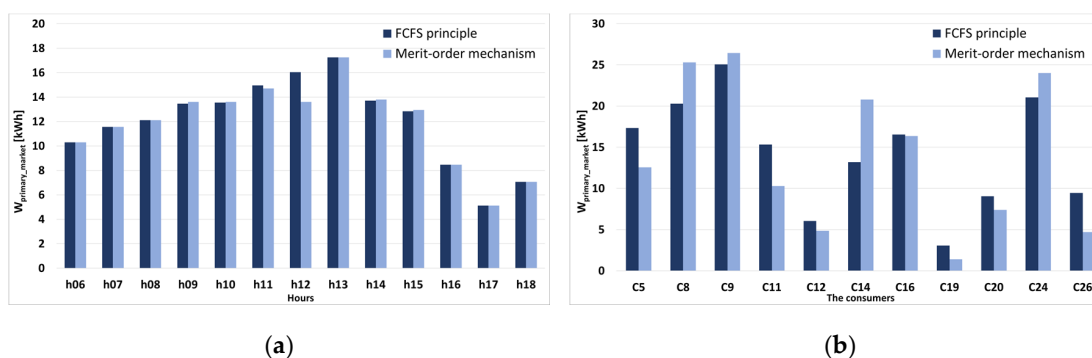
Figure 13. The traded quantities of the buyers in the primary market: (**a**) hourly; (**b**) for each consumer.

The data from Tables 3–6 show some interesting results regarding the hourly and daily offers and traded quantities for the consumers and prosumers.

The local generation surplus (167.97 kW) is insufficient to supply all the consumer needs (203.43 kWh). From Table 3, it is seen that, for the chosen consumption, local generation and primary market offers, when using the FCFS trading priority, the consumers can trade quantities lower than their consumption, and will need to buy the rest from the grid, at higher tariffs. If the MO trading priority is used, Table 4 shows that the hourly buy offers placed by the consumers are usually not fully fulfilled, but the traded quantities exceed the consumption. This leads to a surplus with the consumers, which will be traded to the grid, at regulated tariffs, or sold in the secondary market.

For prosumers, there are trading intervals where the surplus exceeds the traded prosumer offer and traded consumer quantities which are equal (for example, at *h11*, as seen from Tables 4 and 6). This suggests that the prosumer will not be able to sell their entire surplus because of lack of demand. Additionally, applying the FCFS and MO trading priorities in fulfilling the market offers has different effects on the traded quantities, both hourly and for individual prosumers or consumers. If the FCFS trading priority is used, the total quantity traded by the prosumers is larger (Table 5) because the prosumer surplus offers can be matched more closely by the consumer offers. This means that if the MO trading priority is used, it is expected to have more surplus unsold to the local consumers, thus reducing the profitability of the prosumers. In this case, they would have to sell extra surplus to the grid in exchange for the regulated tariff, which is lower than the local consumer offers. As it can be seen from Table 6, the generation surplus remaining after the primary market is concentrated in the 09:00–14:00 interval, while the evening and morning intervals see the highest deficit in local generation (Table 4).

Table 3. The daily offer, traded and remaining quantities for each buyer in the primary market, kWh.

Consumer	C5	C8	C9	C11	C12	C14	C16	C19	C20	C24	C26	Total
Consumption (offers FCFS)	21.25	24.44	30.70	18.96	8.79	20.92	23.84	4.08	12.90	25.27	12.26	203.41
offers MO	23.2	25.30	30.9	16.50	9.30	20.80	23.8	4.10	11.80	25.20	12.50	203.40
traded FCFS	17.32	20.29	25.07	15.33	6.04	13.20	16.54	3.08	9.05	21.04	9.44	156.40
traded MO	12.55	25.30	26.42	10.30	4.85	20.80	16.36	1.40	7.40	24.02	4.70	154.10
rem. FCFS	3.93	4.15	5.62	3.64	2.75	7.72	7.30	1.01	3.85	4.23	2.82	47.01
rem. MO	10.65	0	4.48	6.20	4.45	0	7.44	2.70	4.40	1.18	7.80	49.30

Table 4. The hourly offer, traded and remaining quantities in the primary market for all buyers, kWh.

Hour	h06	h07	h08	h09	h10	h11	h12	h13	h14	h15	h16	h17	h18	Total
Consumption (offer FCFS)	11.8	14.06	18.87	13.47	13.55	14.96	16.04	18.16	13.7	12.83	15.23	20.77	19.99	203.43
offer MO	12.1	14.9	17.5	13.6	13.6	14.7	13.6	18.3	13.8	14	15.8	20.5	21	203.40
traded FCFS	10.29	11.56	12.1	13.47	13.55	14.96	16.04	17.25	13.7	12.83	8.46	5.12	7.07	156.40
traded MO	10.29	11.56	12.1	13.6	13.6	14.7	13.6	17.25	13.8	12.95	8.46	5.12	7.07	154.10
rem. FCFS	1.51	2.5	6.77	0	0	0	0	0.91	0	0	6.77	15.65	12.92	47.03
rem. MO	1.81	3.34	5.40	0	0	0	0	1.05	0	1.05	7.34	15.38	13.93	49.30

Table 5. The daily offer, traded and remaining quantities for each seller in the primary market, kWh.

Prosumer	P27	P21	P7	P15	P6	P3	P10	P25	Total
surplus	11.51	18.90	10.00	24.17	10.90	32.20	12.67	47.63	167.97
traded FCFS	11.51	17.72	9.88	22.87	8.92	25.20	12.67	47.63	156.40
traded MO	11.51	9.89	10.00	19.80	10.90	31.71	12.67	47.63	154.10
rem. FCFS	0	1.18	0.11	1.30	1.98	7.00	0	0	11.58
rem. MO	0	9.02	0	4.37	0	0.49	0	0	13.88

Table 6. The hourly offer, traded and remaining quantities in the primary market, for all sellers, kWh.

Hour	h06	h07	h08	h09	h10	h11	h12	h13	h14	h15	h16	h17	h18	Total
Surplus	10.29	11.56	12.10	15.28	17.69	17.30	17.28	17.25	15.62	12.95	8.46	5.12	7.07	167.97
traded FCFS	10.29	11.56	12.10	13.47	13.55	14.96	16.04	17.25	13.70	12.83	8.46	5.12	7.07	156.40
traded MO	10.29	11.56	12.10	13.60	13.60	14.70	13.60	17.25	13.80	12.95	8.46	5.12	7.07	154.10
rem. FCFS	0	0	0	1.82	4.14	2.35	1.24	0	1.92	0.11	0	0	0	11.58
rem. MO	0	0	0	1.68	4.09	2.60	3.68	0	1.82	0	0	0	0	13.88

The profitability of the FCFS and MO trading priorities can be assessed from Figure 14 and Tables 7 and 8 for the buyers and Figure 15 and Tables 9 and 10 for the sellers. The market model offers the possibility of performing financial settlement in three assumptions for the prices: using the market clearing price (MCP), the consumer offers (COP) and the prosumer offers (POP), because different microgrids can pursue different objectives when establishing the local market. For example, using POP coupled with MO in the primary market can be an advantage for the buying consumers, who will buy electricity at lower prices from the local prosumers instead of paying the standard residential tariff. Using the MCP favors the prosumers with lower prices. In generation surplus scenarios, they can sell electricity at a higher clearing price. Using the COP will be an advantage for the prosumers, who will be able to obtain settlement prices larger than their initial offers.

The sellers/vendors with the highest cost/revenue can be considered as making the most profit because quantities are bought by consumers at a price lower than the standard LV residential tariff, while the sell offers are settled by the vendors at a price higher than the resell tariff to the grid.
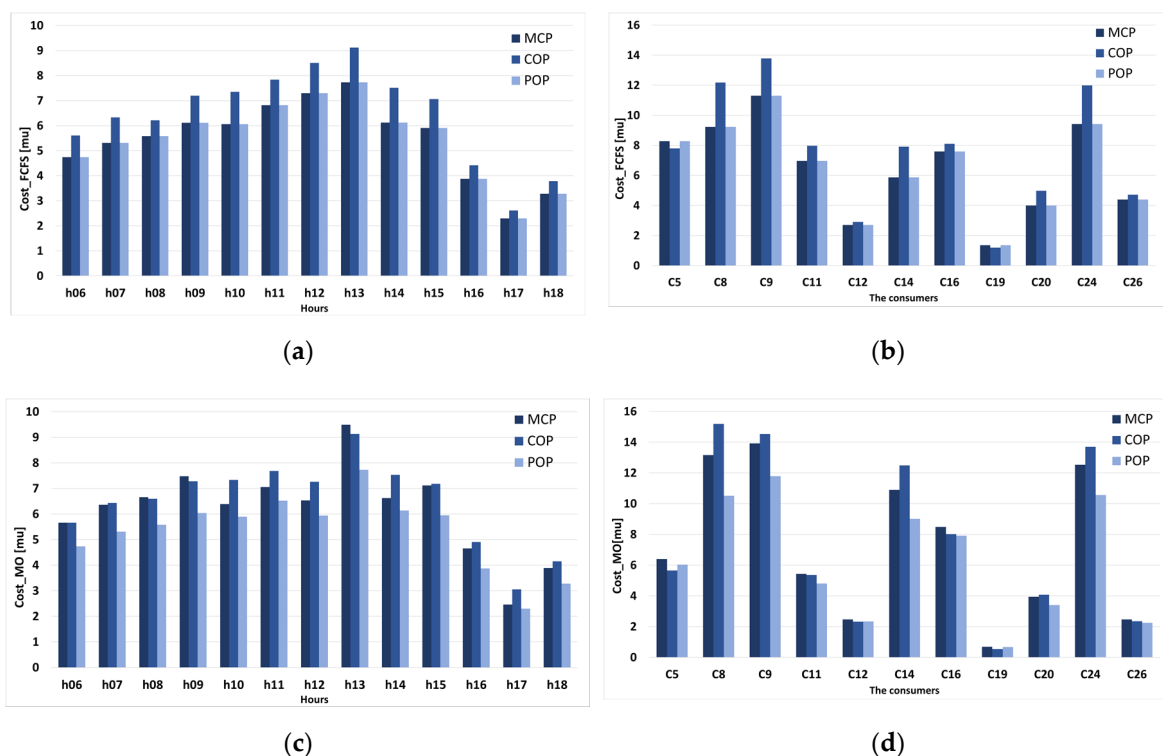
Figure 14. The primary market cost for buyers: (**a**) The hourly values, first-come-first-serve (FCFS); (**b**) The values for each consumer, FCFS; (**c**) The hourly values, MO; (**d**) The values for each consumer, MO.

(**a**)

(**b**)

(**c**)

(**d**)
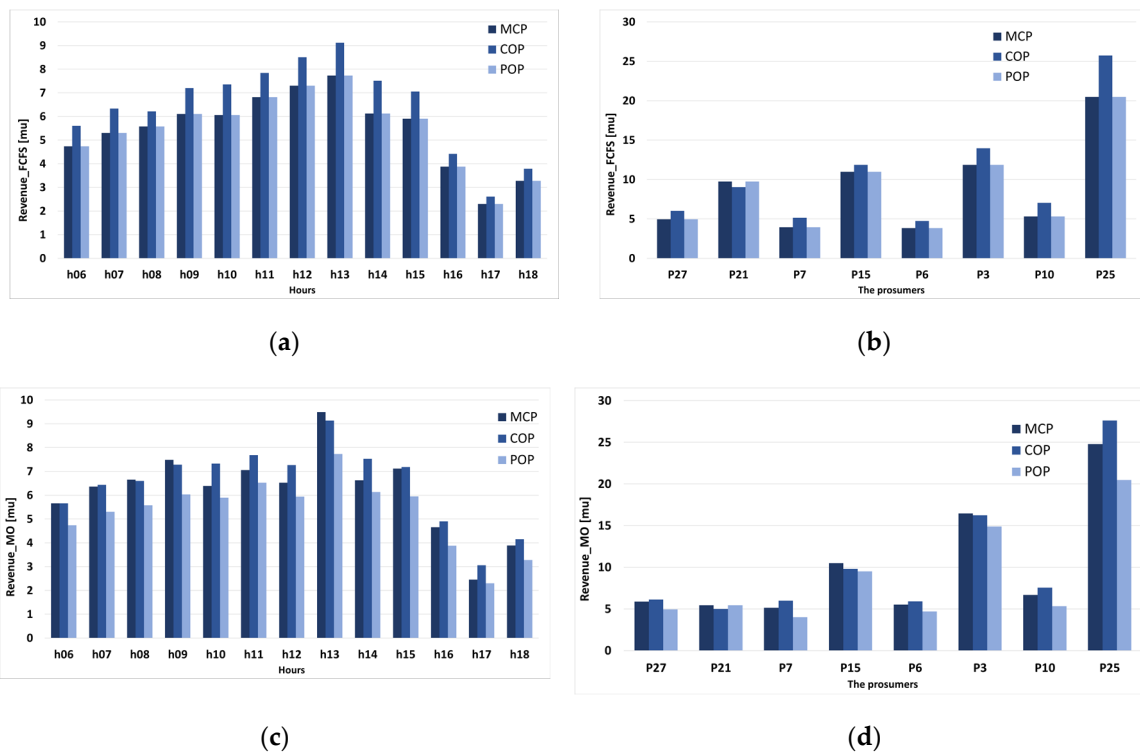
Figure 15. The primary market revenue for sellers: (**a**) The hourly values, FCFS; (**b**) The values for each prosumer, FCFS; (**c**) The hourly values, MO; (**d**) The values for each prosumer, MO.

For the scenario considered in the case study, Figures 14 and 15 show that the highest revenues are obtained by prosumers when the consumer offer prices (COP) are used for settlement. If the FCFS trading priority is used, the MCP and POP settlements give the same results, because the methodology from [40] uses as settlement price the prosumer offers, and the MCP and POP trading priorities would result the same, as the buy offer price is not relevant and thus considered 0 um/kWh for all buyers. For the MO trading priority, the MCP settlement results in higher trading prices than POP, because the trading price for all sellers and buyers is determined by the price unrestricted merit order used in wholesale markets (Figure 4).

As it can be seen from Tables 7–10, the players who get the most advantage from the local market are C8, C9, C24, the consumers without generation capability that have the highest demand, and P15, P3, P25, the prosumers with the largest daily surplus.

Table 7. The daily cost for each buyer in the primary market, mu.

Consumers		C5	C8	C9	C11	C12	C14	C16	C19	C20	C24	C26	Total
FCFS	MCP	8.28	9.23	11.30	6.96	2.70	5.87	7.59	1.36	4.00	9.42	4.39	71.11
	COP	7.80	12.17	13.79	7.97	2.90	7.92	8.10	1.20	4.98	11.99	4.72	83.54
	POP	8.28	9.23	11.30	6.96	2.70	5.87	7.59	1.36	4.00	9.42	4.39	71.11
MO	MCP	6.40	13.15	13.91	5.44	2.47	10.89	8.49	0.68	3.94	12.53	2.46	80.36
	COP	5.65	15.18	14.53	5.36	2.33	12.48	8.01	0.55	4.07	13.69	2.35	84.20
	POP	6.03	10.52	11.79	4.80	2.34	9.00	7.91	0.67	3.41	10.56	2.25	69.28

Table 8. The hourly cost in the primary market for all buyers, mu.

Consumers		h06	h07	h08	h09	h10	h11	h12	h13	h14	h15	h16	h17	h18	Total
FCFS	MCP	4.74	5.31	5.58	6.11	6.06	6.81	7.30	7.73	6.12	5.90	3.87	2.30	3.28	71.11
	COP	5.60	6.33	6.21	7.20	7.35	7.84	8.51	9.12	7.51	7.06	4.42	2.61	3.79	83.54
	POP	4.74	5.31	5.58	6.11	6.06	6.81	7.30	7.73	6.12	5.90	3.87	2.30	3.28	71.11
MO	MCP	5.66	6.36	6.66	7.48	6.39	7.06	6.53	9.49	6.62	7.12	4.65	2.46	3.89	80.36
	COP	5.66	6.43	6.60	7.28	7.33	7.68	7.26	9.13	7.53	7.18	4.90	3.05	4.15	84.20
	POP	4.74	5.31	5.58	6.04	5.90	6.52	5.94	7.73	6.13	5.95	3.87	2.30	3.28	69.28

Table 9. The daily revenue for each seller in the primary market, mu.

Prosumers		P27	P21	P7	P15	P6	P3	P10	P25	Total
FCFS	MCP	4.95	9.75	3.95	10.98	3.83	11.85	5.32	20.48	71.11
	COP	6.02	9.04	5.15	11.86	4.74	13.95	7.04	25.74	83.54
	POP	4.95	9.75	3.95	10.98	3.83	11.85	5.32	20.48	71.11
MO	MCP	5.88	5.44	5.13	10.50	5.51	16.44	6.67	24.78	80.36
	COP	6.11	4.98	6.00	9.80	5.90	16.25	7.54	27.61	84.20
	POP	4.95	5.44	4.00	9.51	4.69	14.90	5.32	20.48	69.28

Table 10. The hourly revenue in the primary market for all sellers, mu.

Prosumers		h06	h07	h08	h09	h10	h11	h12	h13	h14	h15	h16	h17	h18	Total
FCFS	MCP	4.74	5.31	5.58	6.11	6.06	6.81	7.30	7.73	6.12	5.90	3.87	2.30	3.28	71.11
	COP	5.60	6.33	6.21	7.20	7.35	7.84	8.51	9.12	7.51	7.06	4.42	2.61	3.79	83.54
	POP	4.74	5.31	5.58	6.11	6.06	6.81	7.30	7.73	6.12	5.90	3.87	2.30	3.28	71.11
MO	MCP	5.66	6.36	6.66	7.48	6.39	7.06	6.53	9.49	6.62	7.12	4.65	2.46	3.89	80.36
	COP	5.66	6.43	6.60	7.28	7.33	7.68	7.26	9.13	7.53	7.18	4.90	3.05	4.15	84.20
	POP	4.74	5.31	5.58	6.04	5.90	6.52	5.94	7.73	6.13	5.95	3.87	2.30	3.28	69.28

4.2. The Secondary Market—The Energy Poverty Mitigation Tier

The proposed local market model uses in the secondary market an optional energy poverty mitigation tier, designed to include a category of consumers that can usually will not be able to trade on the market because of their low income or other social vulnerabilities. The microgrid community can decide to assist these consumers by supporting the reduction of their electricity bill. The simplest way to achieve this goal is to automatically allocate the prosumer surplus available after the settlement of the primary market to cover the demand of such consumers. In the data used for the case study, a single consumer, C28, fulfills the requirements of a vulnerable consumer. As seen in Table A1, its total daily consumption amounts to 3.31 kWh, with 1.79 kWh in the 06:00–18:00 interval.

Since the two trading priority methods (FCFS and MO) give in the primary market different results regarding the trading participants and quantities at each hour, a similar behavior is propagated in the secondary market. Thus, the trading results will be presented in the same manner as for the primary market, as a comparison between the cases in which the primary market uses the FCFS or the MO in determining the priorities of the traded quantities. It is considered that the secondary market uses the same price offers entered in the blockchain system for the primary market.

According to the data from Tables 3 and 5, after the settlement of the primary market, prosumers P21, P7, P15, P6, P3, P25 have unsold surplus if the FCFS trading priority is used. No consumers can participate in the secondary market, because they cannot have surplus after trading. If the MO priority is used, the prosumers with available surplus are P21, P15, P3, and also there are consumers which have placed in the primary market offers exceeding their real consumption, and can become sellers on the secondary market (C5, C9, C11, C12, C16, C19, C20, C24, and C26). The hours in which the sellers are having surplus after the primary market are presented in Appendix B, Tables A6 and A7. The only entity buying in this market is C28, and its hourly buy offer match its entire consumption (See

Table A1). However, these are total quantities, and each seller can trade different surplus quantities in each hour. This will lead to the necessity of prioritization of the sell offers, and subsequent settlement between C28 and possibly multiple sellers. The quantities traded hourly are presented in Appendix B, Tables A8 and A9. The sell offers and traded quantities are given in Figures 16 and 17. Tables 11–14 summarize the daily and hourly offers and quantities traded by buyers and sellers.

(a)

(b)
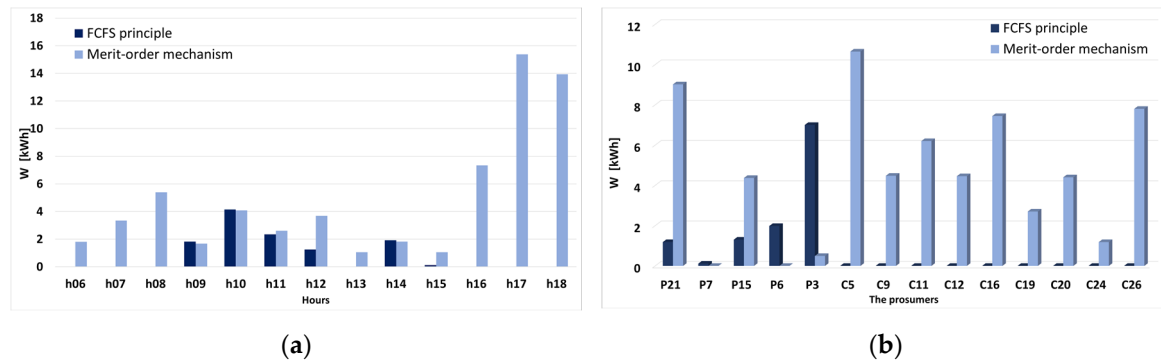
Figure 16. The sell offers of the vendors in the energy poverty mitigation market: (**a**) hourly; (**b**) for each prosumer/consumer.

(a)

(b)
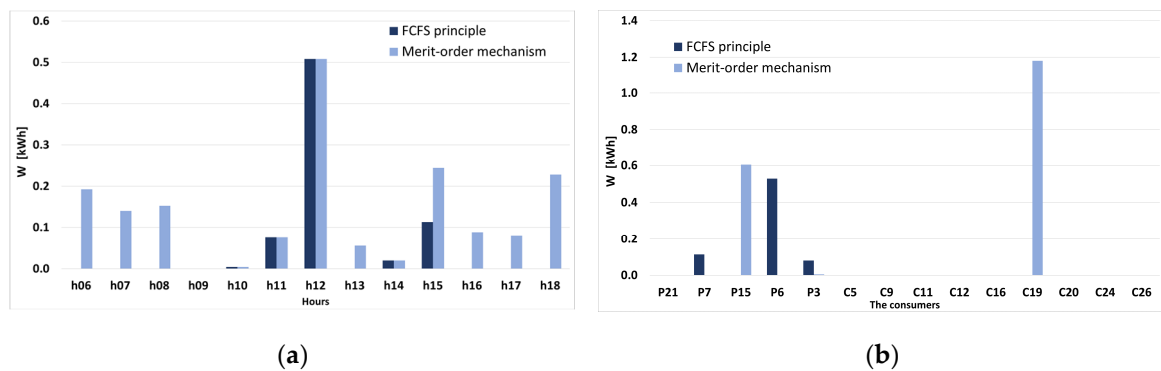
Figure 17. The traded quantities of the vendors in the energy poverty mitigation market: (**a**) hourly; (**b**) for each prosumer.

Table 11. The daily traded quantities for consumer C28 in the energy poverty mitigation market, kWh.

Consumer	C28
Consumption (offers FCFS)	1.79
offers MO	1.79
traded FCFS	0.72
traded MO	1.79
rem. FCFS	1.07
rem. MO	0

Table 12. The hourly traded quantities in the poverty mitigation market for consumer C28, kWh.

Hour	h06	h07	h08	h09	h10	h11	h12	h13	h14	h15	h16	h17	h18	Total
Consumption (offer FCFS)	0.19	0.14	0.15	0	0	0.08	0.51	0.06	0.02	0.24	0.09	0.08	0.23	1.79
offer MO	0.19	0.14	0.15	0	0	0.08	0.51	0.06	0.02	0.24	0.09	0.08	0.23	1.79
traded FCFS	0	0	0	0	0	0.08	0.51	0	0.02	0.11	0	0	0	0.72
traded MO	0.19	0.14	0.15	0	0	0.08	0.51	0.06	0.02	0.24	0.09	0.08	0.23	1.79
rem. FCFS	0.19	0.14	0.15	0	0	0	0	0.06	0	0.13	0.09	0.08	0.23	1.07
rem. MO	0	0	0	0	0	0	0	0	0	0	0	0	0	0

Table 13. The daily traded quantities for each vendor in the energy poverty mitigation market, kWh.

Vendor	P21	P7	P15	P6	P3	C5	C9	C11	C12	C16	C19	C20	C24	C26	Total
surplus FCFS	1.18	0.11	1.30	1.98	7.00	0	0	0	0	0	0	0	0	0	11.58
surplus MO	9.02	0	4.37	0	0.49	10.65	4.48	6.20	4.46	7.44	2.70	4.40	1.18	7.80	63.18
traded FCFS	0	0.11	0	0.53	0.08	0	0	0	0	0	0	0	0	0	0.72
traded MO	0	0	0.60	0	0.00	0	0	0	0	0	1.18	0	0	0	1.79
rem. FCFS	1.18	0.00	1.30	1.45	6.92	0	0	0	0	0	0	0	0	0	10.86
rem. MO	9.02	0.00	3.76	0	0.49	10.65	4.48	6.20	4.46	7.44	1.52	4.40	1.18	7.80	61.39

Table 14. The hourly traded quantities in the energy poverty mitigation market for all vendors, kWh.

Hour	h06	h07	h08	h09	h10	h11	h12	h13	h14	h15	h16	h17	h18	Total
surplus FCFS	0	0	0	1.82	4.14	2.35	1.24	0	1.92	0.11	0	0	0	11.58
surplus MO	1.81	3.34	5.40	1.68	4.09	2.60	3.68	1.05	1.82	1.06	7.34	15.38	13.94	63.18
traded-FCFS	0	0	0	0	0.00	0.08	0.51	0	0.02	0.11	0	0	0	0.72
traded-MO	0.19	0.14	0.15	0.00	0.00	0.08	0.51	0.06	0.02	0.24	0.09	0.08	0.23	1.79
rem. FCFS	0	0	0	1.82	4.14	2.27	0.73	0	1.90	0	0	0	0	10.86
rem. MO	1.62	3.20	5.25	1.68	4.08	2.53	3.17	0.99	1.80	0.81	7.25	15.30	13.71	61.39

Figures 16 and 17 and Tables 11–14 reveal significantly different trading scenarios on the energy poverty mitigation market when the two trading priority methods (FCFS and MO) are used in the primary market. For FCFS, 3 out of 5 prosumers will trade electricity with C28, while if MO were to be used, only P15 and P3 will sell electricity, the rest of the buying offer being fulfilled by just one consumer, C19. Also, if the secondary market is activated, the available surplus rises when MO is used from 13.88 kWh in the primary market to 63.18 kWh, due to the presence of the consumers who need to sell the surplus generated by the forecast error or offer quantity rounding. In the absence of the secondary market, these two quantities would be sold back to the grid at minimal price. Thus, in addition to allowing prosumer to sell more surplus, the secondary market offers a mechanism for minimizing the effect of consumption forecast errors at the consumer side when the MO trading priority method is used. However, the prosumer and consumer surplus to be sold back to the grid remain high, at 13.27 kWh and 48.12 kWh respectively (Table 13).

The costs of the consumer C28 and revenues of the vendors in the energy poverty market tier are given in Tables 15–18 and Figures 18 and 19. The financial settlement is performed in this case using as reference only the vendor price offer, similar to POP from Tables 7–10, because with just one vulnerable consumer trading in the market, the COP is viable only if the consumer would buy at a fixed tariff, and MCP results are the same as POP when COP is not specified.

The results show that the vendor revenues are lower than in the primary market, because of the smaller traded quantities, but they can become significant if they are averaged over longer periods (months, years). The consumer C28 will pay less in the local market than when buying electricity from the grid, and the MO trading priority maximizes its earnings and the number of hourly intervals in which trading can be made. A more profitability analysis will follow in the Discussions section, for all the trading segments considered in the market algorithm.
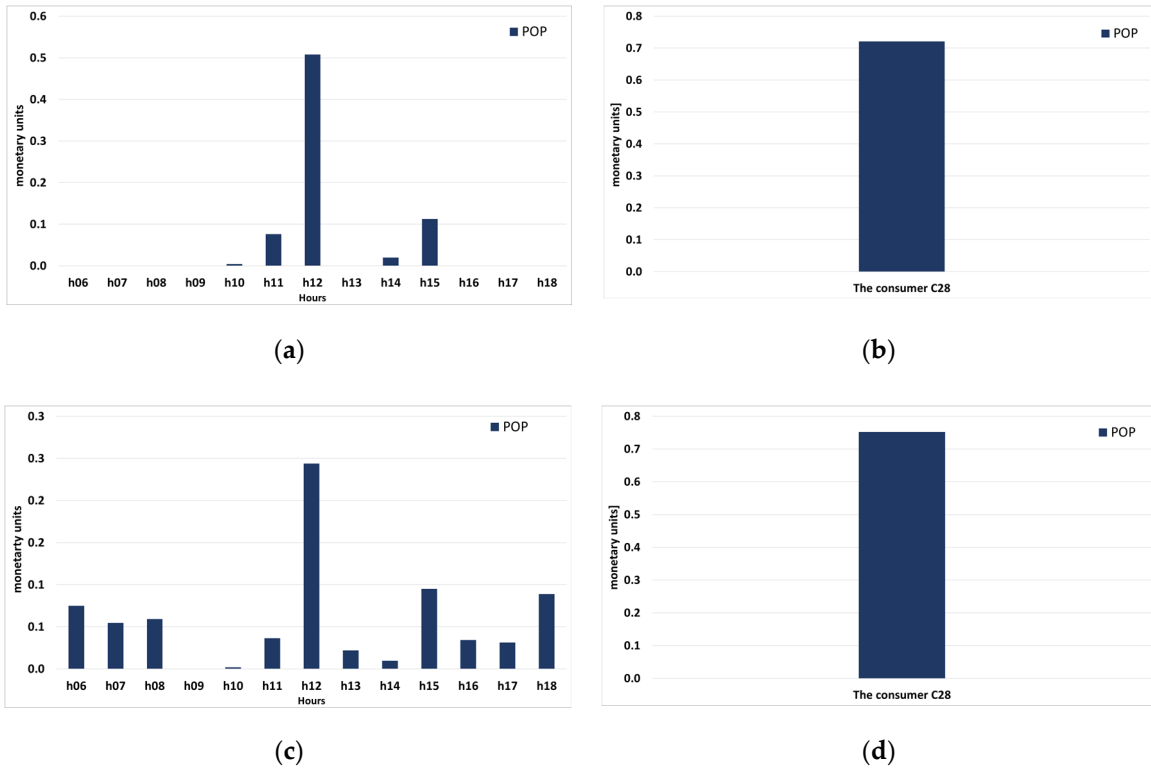
Figure 18. The energy poverty mitigation market cost for buyers: (**a**) hourly values, FCFS; (**b**) daily values for each consumer, FCFS; (**c**) hourly values, MO; (**d**) daily values for each consumer, MO.
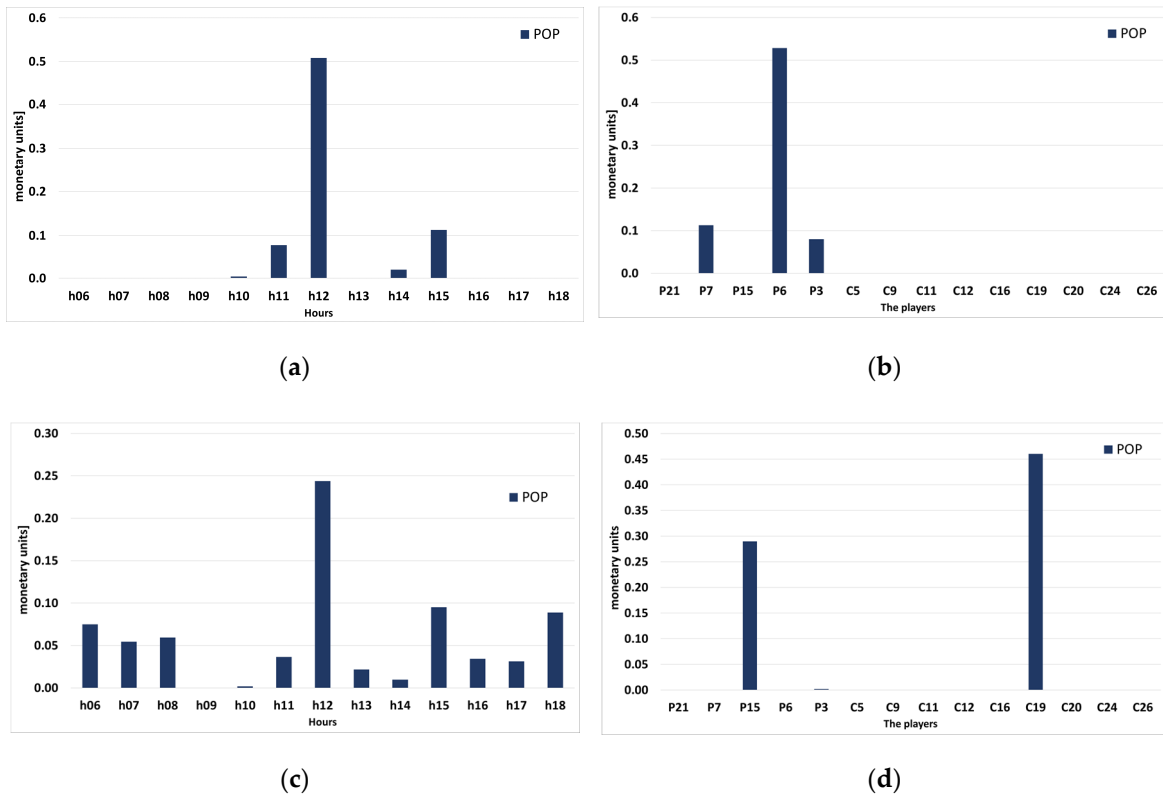
Figure 19. The energy poverty mitigation market revenue for vendors: (**a**) hourly values, FCFS; (**b**) daily values for each consumer, FCFS; (**c**) hourly values, MO; (**d**) daily values for each consumer, MO.

Table 15. The daily cost for each consumer in the energy poverty mitigation market, mu.

Consumers		C28
FCFS	POP	0.72
MO	POP	0.75

Table 16. The hourly cost for all buyers in the energy poverty mitigation market, mu.

Consumers		h06	h07	h08	h09	h10	h11	h12	h13	h14	h15	h16	h17	h18	Total
FCFS	POP	0	0	0	0	0.00	0.08	0.51	0	0.02	0.11	0	0	0	0.72
MO	POP	0.07	0.05	0.06	0	0.00	0.04	0.24	0.02	0.01	0.10	0.03	0.03	0.09	0.75

Table 17. The daily revenue for each vendor in the energy poverty mitigation market, mu.

Vendors		P21	P7	P15	P6	P3	C5	C9	C11	C12	C16	C19	C20	C24	C26	Total
FCFS	POP	0	0.11	0	0.53	0.08	0	0	0	0	0	0	0	0	0	0.72
MO	POP	0	0	0.29	0	0.00	0	0	0	0	0	0.46	0	0	0	0.75

Table 18. The hourly revenue in the energy poverty mitigation market for all vendors, mu.

Prosumers		h06	h07	h08	h09	h10	h11	h12	h13	h14	h15	h16	h17	h18	Total
FCFS	POP	0	0	0	0	0.00	0.08	0.51	0	0.02	0.11	0	0	0	0.72
MO	POP	0.07	0.05	0.06	0	0.00	0.04	0.24	0.02	0.01	0.10	0.03	0.03	0.09	0.75

4.3. The Secondary Market—The Commercial Tariff Access Tier

As seen previously, the vendors can remain after the primary market with surplus available for selling. Both prosumers and consumers can become sellers on the secondary market. The energy poverty mitigation tier can help to reduce the surplus, but, if the vulnerable consumers have low demand and are in low numbers, the quantities still remaining after the settlement can be significant. For the demand-generation balance and the set of offers used in the case study, the total primary market surplus is of 63.18 kWh and reduces only to 61.39 kWh after the energy poverty mitigation market, if the MO trading method is used. For the FCFS method, the remaining surplus decreases from to 11.58 kWh to 10.86 kW. For further reducing the quantity sold to the grid, the local market model uses the second tier of the secondary market, operated according to the MO trading priority method used in the primary market, but with different market participants.

The sellers that can enter this market segment are the same as for the energy poverty mitigation market: prosumers with remaining surplus and consumers whose offers placed in the blockchain system of the primary market exceed their actual demand, thus becoming surplus. The buyers are consumers from the same microgrid who did not participate in the primary market, but are ready to occasionally buy surplus from the secondary market when it is available, at market prices. In exchange for this facility, they pay an extra fee, according to the formula from Equation (10). The quantities are determined automatically in the settlement phase of the energy poverty market or at the end of the primary market, if the EP tier is not used. The sell price offers are the offer prices entered by prosumers in the blockchain system of the primary market. For consumers the buy prices are: C13–0.47 mu/kWh, C17–0.30 mu/kWh, C18–0.42 mu/kWh, lower than the average offers from the primary market, in order to minimize the effect of the added tariffs. The fulfilment priority for the buy and sell offers is determined using the MO strategy from Figure 4, and the actual quantities and financial exchanges between sellers and buyers are settled as in the primary market.

Using as reference the trading data from Table 13, the sellers participating in the market are P21, P15, P6 and P3, if the FCFS method is used in the primary market, and P21, P15, P3, C5, C9, C11, C12, C16, C19, C20, C24, and C26. The buyers are three consumers that did not participate in the primary market, namely C13, C17 and C18. The fee applied for all the consumers is a 10% increase of the final

buy price, and it is charged by the market administrator. For evaluating all the possibilities regarding the financial settlement, all three price alternatives will be considered: MCP, COP and POP, similar to the primary market. The quantities offered and actually traded by each vendor and buyer in the two primary market methodologies (FCFS and MO) are given in Appendix C, Tables A10–A14.

The results show that the use of the MO in the primary market leads to higher quantities traded in the tariff-access market tier, while if the FCFS priority is chosen, prosumer surplus is lower. The hourly results for the market and the daily quantities traded by the prosumers and the consumers are summarized, as for the previous market tiers, in Figures 20–23 and Tables 19–22.

The results from Tables 19–22 show that the tariff-access consumers are able to acquire 7.67 kWh for the FCFS primary market trading priority, exclusively from prosumer surplus. 21.28 kWh are bought for the MO trading priority method, mainly from consumer surplus, as it can be seen in Table 21. When the MO method is used, the consumer buy offers are fulfilled from the most part from the local market (Table 20), only 1.2 kWh remaining to be bought from the grid. After the settlement of the two commercial market tiers, the prosumers lower their unsold surplus to only 3.19 kWh (FCFS) or 4.7 kWh (MO), while the consumer surplus remains high, at 35.94 kWh. The prosumer surplus is available mainly in the 09:00–14:00 interval, while the consumer surplus can be accessed outside this interval, between 06:00–8:00 and 15:00–18:00 (see Table A11).

Because of the larger quantities bought by the three consumers, the fee-access tier is more profitable for the surplus vendors, compared to the energy poverty mitigation market. In addition, considering the lower price offers used for the tariff-access consumers, the COP settlement option is the best choice for the consumers, incurring the lowest costs (see Table 25). For the FCFS trading priority method, MCP and POP give the same results, which suggests that the merit order clearing price is determined by higher vendor price offers (Table 26).
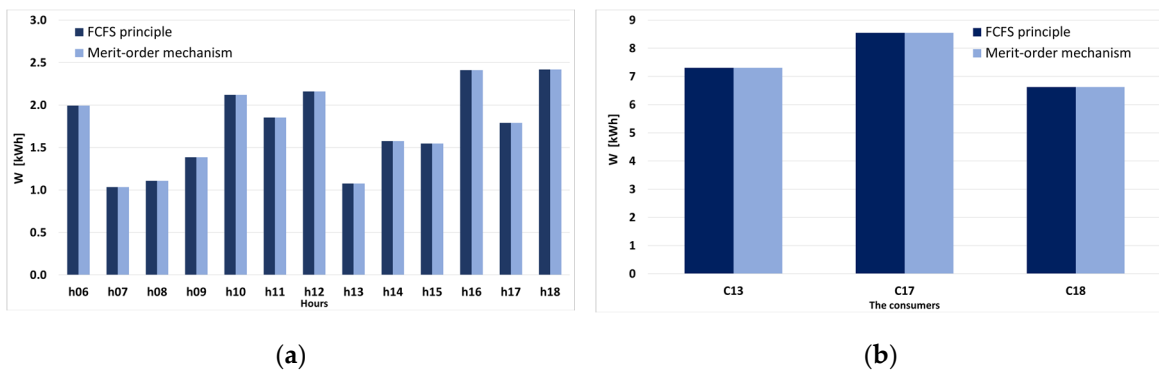
Figure 20. The buyer quantity offers in the secondary tariff-access market: (**a**) hourly; (**b**) per consumer.
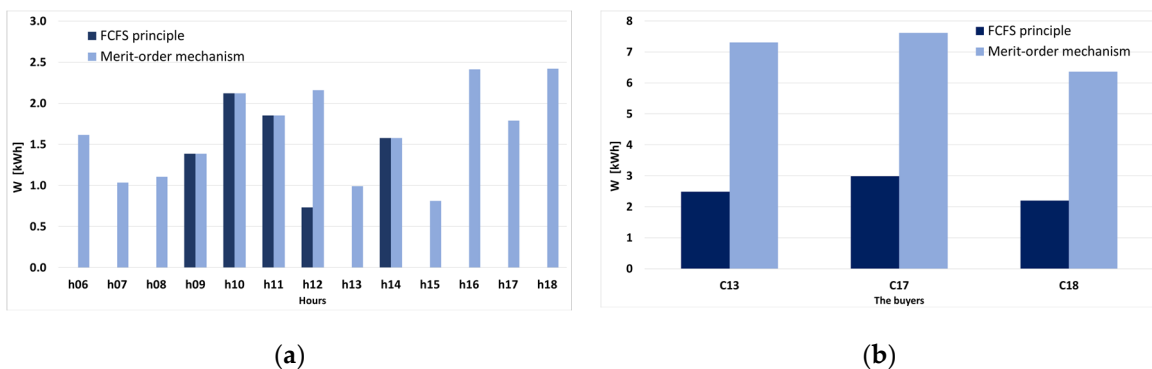
Figure 21. The buyer quantities traded in the secondary tariff-access market: (**a**) hourly; (**b**) for each consumer.
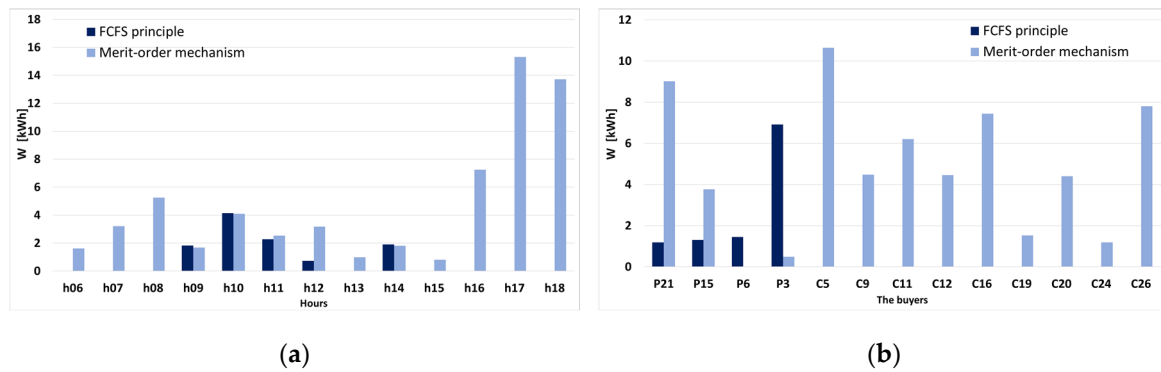
Figure 22. The seller quantity offers in the secondary tariff-access market: (**a**) hourly; (**b**) for each seller.
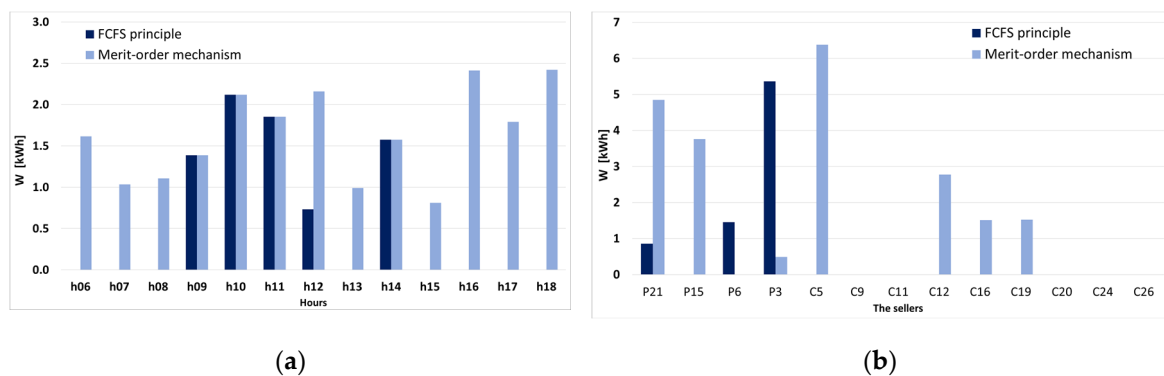
Figure 23. The buyer quantities traded in the secondary tariff-access market: (**a**) hourly; (**b**) for each seller.

Table 19. The daily traded quantities for each buyer in the secondary tariff market, kWh.

Consumer	C13	C17	C18	Total
offer FCFS	7.30	8.55	6.62	22.48
offer MO	7.30	8.55	6.62	22.48
traded FCFS	2.49	2.99	2.20	7.67
traded MO	7.30	7.61	6.36	21.28
rem. FCFS	4.82	5.57	4.43	14.81
rem. MO	0.00	0.94	0.26	1.20

Table 20. The hourly traded quantities in the secondary tariff market for all buyers, kWh.

Hour	h06	h07	h08	h09	h10	h11	h12	h13	h14	h15	h16	h17	h18	Total
offer FCFS	1.99	1.03	1.11	1.39	2.12	1.85	2.16	1.08	1.58	1.55	2.41	1.79	2.42	22.48
offer MO	1.99	1.03	1.11	1.39	2.12	1.85	2.16	1.08	1.58	1.55	2.41	1.79	2.42	22.48
traded FCFS	0	0	0	1.39	2.12	1.85	0.73	0	1.58	0	0	0	0	7.67
traded MO	1.62	1.03	1.11	1.39	2.12	1.85	2.16	0.99	1.58	0.81	2.41	1.79	2.42	21.28
rem. FCFS	1.99	1.03	1.11	0.00	0.00	0.00	1.43	1.08	0.00	1.55	2.41	1.79	2.42	14.81
rem. MO	0.38	0.00	0.00	0.00	0.00	0.00	0.00	0.09	0.00	0.74	0.00	0.00	0.00	1.20

Table 21. The daily traded quantities for each vendor in the secondary tariff market, kWh.

Vendor	P21	P15	P6	P3	C5	C9	C11	C12	C16	C19	C20	C24	C26	Total
surplus FCFS	1.18	1.30	1.45	6.92	0	0	0	0	0	0	0	0	0	10.86
surplus MO	9.02	3.76	0.00	0.49	10.65	4.48	6.20	4.46	7.44	1.52	4.40	1.18	7.80	61.39
traded FCFS	0.86	0	1.45	5.36	0	0	0	0	0	0	0	0	0	7.67
traded MO	4.84	3.76	0	0.49	6.38	0	0.00	2.78	1.51	1.52	0	0	0	21.28
rem. FCFS	0.32	1.30	0	1.56	0	0	0	0	0	0	0	0	0	3.19
rem. MO	4.17	0	0	0	4.27	4.48	6.20	1.68	5.94	0	4.40	1.18	7.80	40.11

Table 22. The hourly traded quantities in the secondary tariff market for all vendors, kWh.

Hour	h06	h07	h08	h09	h10	h11	h12	h13	h14	h15	h16	h17	h18	Total
surplus FCFS	0	0	0	1.82	4.14	2.27	0.73	0	1.90	0	0	0	0	10.86
surplus MO	1.62	3.20	5.25	1.68	4.08	2.53	3.17	0.99	1.80	0.81	7.25	15.30	13.71	61.39
traded FCFS	0	0	0	1.39	2.12	1.85	0.73	0	1.58	0	0	0	0	7.67
traded MO	1.62	1.03	1.11	1.39	2.12	1.85	2.16	0.99	1.58	0.81	2.41	1.79	2.42	21.28
diff FCFS	0	0	0	0.43	2.02	0.42	0.00	0	0.32	0	0	0	0	3.19
diff MO	0	2.16	4.14	0.30	1.96	0.67	1.01	0	0.23	0	4.84	13.51	11.29	40.11

The costs of the buyers and the revenues of the vendors in this market tier are summarized in Figures 24 and 25 and Tables 23–26, for all three available settlement policies (MCP, COP, POP).
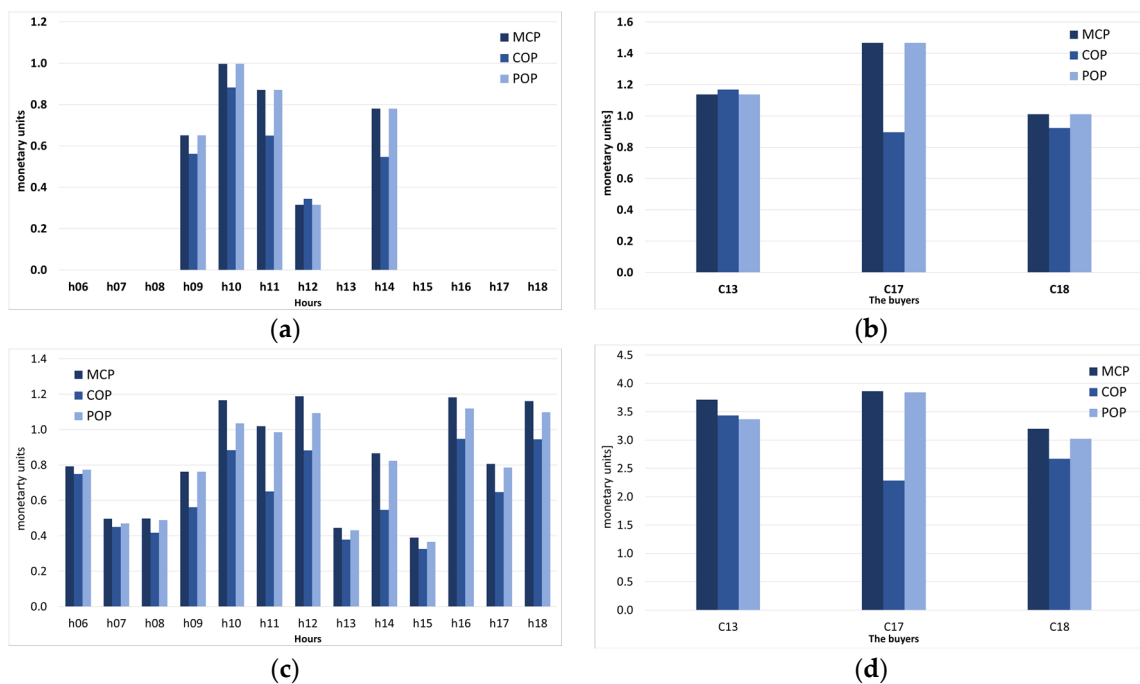
Figure 24. The tariff-access market cost for buyers: (**a**) hourly values, FCFS; (**b**) daily values for each consumer, FCFS; (**c**) hourly values, merit-order (MO); (**d**) daily values for each consumer, MO.

(**a**)

(**b**)

(**c**)

(**d**)
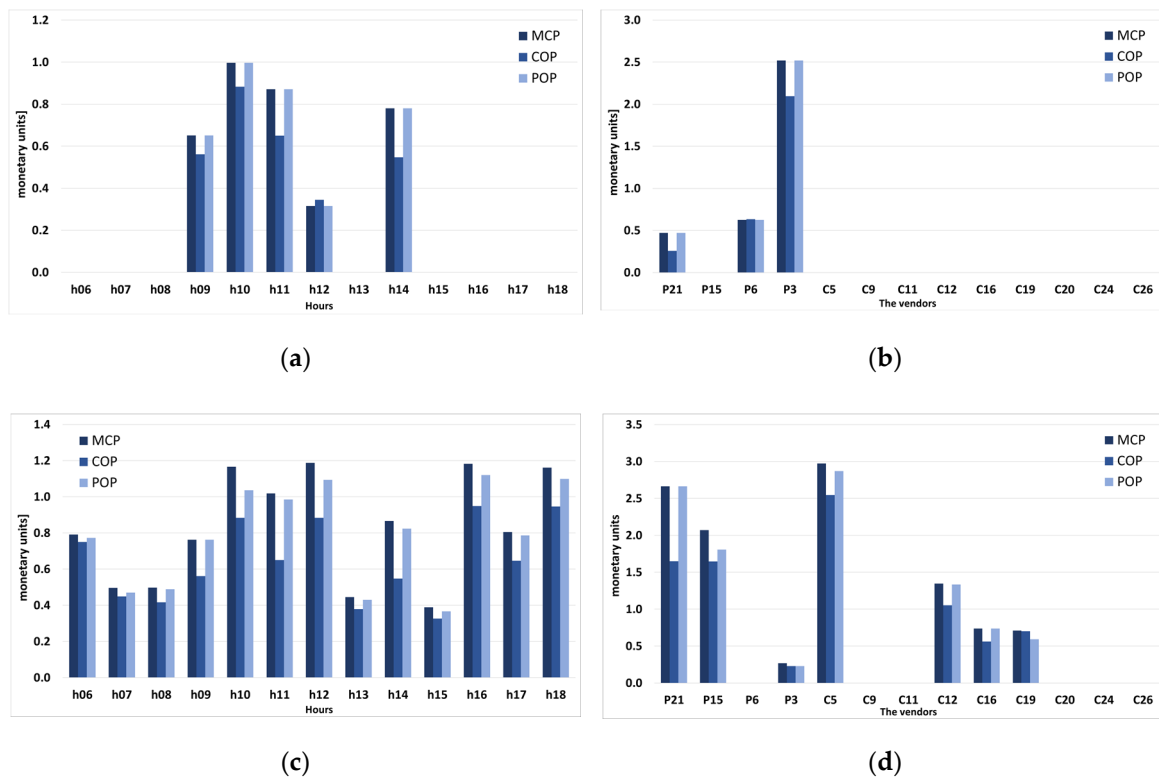
Figure 25. The tariff-access market revenue for vendors: (**a**) hourly values, FCFS; (**b**) daily values for each consumer, FCFS; (**c**) hourly values, MO; (**d**) daily values for each consumer, MO.

Table 23. The daily cost for each consumer in the tariff-access market, mu.

	Consumers	C13	C17	C18	Total	Total + 10% Fee
FCFS	MCP	1.14	1.47	1.01	3.61	3.98
	COP	1.17	0.90	0.92	2.99	3.29
	POP	1.14	1.47	1.01	3.61	3.98
MO	MCP	3.71	3.86	3.20	10.77	11.85
	COP	3.43	2.28	2.67	8.39	9.23
	POP	3.37	3.84	3.02	10.23	11.26

Table 24. The hourly cost for all buyers in the tariff-access market, mu.

Consumers		h06	h07	h08	h09	h10	h11	h12	h13	h14	h15	h16	h17	h18	Total	Total + 10% Fee
FCFS	MCP	0	0	0	0.65	1.00	0.87	0.32	0	0.78	0	0	0	0	3.61	3.98
	COP	0	0	0	0.56	0.88	0.65	0.34	0	0.55	0	0	0	0	2.99	3.29
	POP	0	0	0	0.65	1.00	0.87	0.32	0	0.78	0	0	0	0	3.61	3.98
MO	MCP	0.79	0.50	0.50	0.76	1.17	1.02	1.19	0.45	0.87	0.39	1.18	0.81	1.16	10.77	11.85
	COP	0.75	0.45	0.42	0.56	0.88	0.65	0.88	0.38	0.55	0.33	0.95	0.65	0.95	8.39	9.23
	POP	0.77	0.47	0.49	0.76	1.04	0.99	1.09	0.43	0.82	0.37	1.12	0.79	1.10	10.23	11.26

Table 25. The daily revenue for each vendor in the tariff-access market, mu.

Vendors		P21	P15	P6	P3	C5	C9	C11	C12	C16	C19	C20	C24	C26	Total
FCFS	MCP	0.47	0	0.62	2.52	0	0	0	0	0	0	0	0	0	3.61
	COP	0.26	0	0.63	2.10	0	0	0	0	0	0	0	0	0	2.99
	POP	0.47	0	0.62	2.52	0	0	0	0	0	0	0	0	0	3.61
MO	MCP	2.66	2.07	0	0.27	2.97	0	0	1.35	0.74	0.71	0	0	0	10.77
	COP	1.65	1.65	0	0.23	2.55	0	0	1.05	0.56	0.70	0	0	0	8.39
	POP	2.66	1.81	0	0.23	2.87	0	0	1.33	0.74	0.59	0	0	0	10.23

Table 26. The hourly revenue in the tariff-access market for all vendors, mu.

Prosumers		h06	h07	h08	h09	h10	h11	h12	h13	h14	h15	h16	h17	h18	Total
FCFS	MCP	0	0	0	0.65	1.00	0.87	0.32	0	0.78	0	0	0	0	3.61
	COP	0	0	0	0.56	0.88	0.65	0.34	0	0.55	0	0	0	0	2.99
	POP	0	0	0	0.65	1.00	0.87	0.32	0	0.78	0	0	0	0	3.61
MO	MCP	0.79	0.50	0.50	0.76	1.17	1.02	1.19	0.45	0.87	0.39	1.18	0.81	1.16	10.77
	COP	0.75	0.45	0.42	0.56	0.88	0.65	0.88	0.38	0.55	0.33	0.95	0.65	0.95	8.39
	POP	0.77	0.47	0.49	0.76	1.04	0.99	1.09	0.43	0.82	0.37	1.12	0.79	1.10	10.23

4.4. The Secondary Market—The Commercial Invite Access Tier

An alternative proposed in the local market model for the tariff-access secondary market is an invite-access market tier. This solution, while it has lower impact on the surplus reduction at market level, is viable for individual prosumers and consumers which are in the situation of frequently having unsold surplus after the final settlement. The invite-access strategy proposes that long-term P2P contracts can be established between seller–buyer pairs, stipulating that the buyer can automatically access the unsold surplus of the seller when it is available. In this case, the settlement is not performed at market level, but only for the two parties involved, and it can be considered that the buyer is an 'invited guest' in the local market.

The market diagram from Figure 1 considers the invite-access market as an alternative to the tariff-access market, but this approach is not mandatory, as the energy mitigation market, the tariff-access market and the invite-access market can be used in any desired order or number in the architecture of the local market.

Considering the layout from Figure 1 and the data from Tables 2, A2, A7 and A13, the evolution of the surplus of prosumer P21 in the MO primary market priority case is the one seen in Table 27. The prosumer is able to sell 4.844 kWh on the tariff-access market.

Table 27. The surplus of prosumer P21 in the primary and secondary markets (energy poverty mitigation and tariff-access), kWh.

Hour	Initial Generation	Surplus			
		Initial	After the Primary Market	After the Secondary Market, 1st Tier	After the Secondary Market, 2nd Tier (Tariff-Access)
h01	2.361	1.588	0	0	0
h02	2.785	1.805	0	0	0
h03	3.286	1.726	0	0	0
h04	3.329	1.749	1.682	1.682	0.296
h05	3.639	2.292	2.292	2.292	1.963
h06	3.751	2.038	2.038	2.038	0.672
h07	3.735	1.822	1.822	1.822	1.014
h08	3.812	0.685	0	0	0
h09	3.742	1.182	1.182	1.182	0.227
h10	3.461	2.028	0	0	0
h11	2.832	0.819	0	0	0
h12	2.403	0	0	0	0
h13	2.237	1.17	0	0	0
Total	41.373	18.904	9.016	9.016	4.172

On the other hand, if the prosumer has a P2P contract with consumer C22 who did not participate in the primary market, and the tariff access option is not activated, then it would be possible to sell in the invite-access market almost the same quantity, as can be seen in Table 28. Furthermore, a scenario can be imagined in which the invite market is activated first, followed by the tariff-access market, in which case prosumer P21 would be able to sell their entire surplus in the local blockchain market. Thus, if the market model is optimally configured, it can lead to the maximization of the local trading, thus minimizing the surplus sold to the grid at regulated tariffs.

Table 28. Comparison between the quantities sold by prosumer P21 in the tariff- and invite-access markets, kWh.

Hour	Surplus, P21	Consumption, C22	Electricity Sold in the Tariff-Access Market	Electricity Sold to C22 in the Invite-Access Market
h06	0	1.340	0	0
h07	0	0.960	0	0
h08	0	0.270	0	0
h09	1.682	0.420	1.386	0.420
h10	2.292	1.000	0.329	1.000
h11	2.038	0.930	1.366	0.930
h12	1.822	1.050	0.808	1.050
h13	0	1.020	0	0
h14	1.182	0.970	0.955	0.970
h15	0	1.010	0	0
h16	0	1.110	0	0
h17	0	1.540	0	0
h18	0	1.630	0	0
Total	9.016	13.250	4.844	4.370

5. Discussion

The results presented in the case study show that the secondary market has a positive effect regarding the surplus quantities sold by the prosumers in the local market. A key aspect that still needs to be discussed is the profitability of the local market, with its two components. Using Tables 3, 5, 11, 13, 19 and 21 for quantities, the influence of the primary and secondary markets on the quantities sold by the prosumers and consumers back to the grid is determined in Tables 29 and 30.

Table 29. The evolution of the electricity quantities bought from the grid in the time interval 06:00–18:00, before and after trading on each market segment, kWh.

Trading Priority in PM	Initial Consumption (No Market)	Traded in PM	Consumer Surplus for SM	Consumption Bought from the Grid after PM	Traded in SM1	Traded in SM2	Consumption Bought from the Grid after SM
FCFS	203.41	156.4	0	47.01	0.72	7.67	38.62
MO	203.41	154.1	49.31	98.62	1.79	21.28	75.55

Table 30. The evolution of the surplus quantities sold to the grid in the hourly interval 06:00–18:00, after trading on each market segment, kWh.

Market Player Type	PM Trading Priority	Initial Surplus	Traded in PM	Surplus after PM	Traded in SM1	Traded in SM2	Surplus after SM
prosumers	FCFS	167.97	156.4	11.58	0.72	7.67	3.18
	MO	167.97	154.1	13.88	0.6	9.1	4.17
consumers	FCFS	0	0	0	0	0	0
	MO	0	0	49.31	1.18	12.68	35.45

Table 29 shows that the offer quantities used in the MO trading priority determine a 49.3 kWh surplus at the consumers, which represents electricity traded but not consumed. This represents a high value, at 25% of the total consumption, and is mainly determined by hourly demand forecast errors. In the absence of the secondary market, the entire quantity would be sold to the grid, and the price mismatch between the buy price on the market (high) and sell price to the grid (low) would represent a cost increase for the consumers. Thus, accurate demand forecasts could reduce the costs for the consumers participating in the market. Additionally, it can be seen that the FCFS trading priority results in lower quantities sold back to the grid, as consumer surplus is absent.

Table 30 shows that the secondary market makes a significant contribution to reducing the prosumer surplus from 11.58/13.88 kWh to 3.18/4.17 kWh. Here, it can be seen that while the bulk of the surplus is sold on the primary market, the secondary market allows an important increase

of local generation sold locally. The primary market helps prosumers to sell the majority of their surplus in the local market, and the supplementary market tiers allow consumers to mitigate forecast errors by acting as sellers, and also reduce the share of surplus prosumer generation sold back to the grid. These trading options can have, depending on local conditions, positive effects in increasing the number of prosumers in the microgrid and reducing the electricity acquired by the consumers from the grid, at higher prices and taxes. In other words, social and environmental sustainability can be improved.

The reduction of local generation quantities sold back to the grid has positive financial effects for both prosumers and consumers. In the absence of the local market, the prosumers would sell any surplus to the grid at the regulated price. The market allows them to obtain better prices, which are still attractive for consumers as long as they do not exceed the tariff paid for the electricity imported from the grid. On the other hand, by participating in the local market, the consumers have the chance of paying less for electricity. From Tables 7, 9, 15, 17, 23 and 25, the costs and revenues for the sellers and vendors on each market segment can be summarized in Tables 31 and 32, for the 06:00–18:00 interval of the analyzed day.

Table 31. Comparison between the costs of the consumers in each market segment and for each settlement price, mu.

Trading Priority in PM	Settlement Price	PM	SM1	SM2	SM	Total PM + SM
FCFS	MCP	71.11	0	3.98	3.98	75.09
	COP	83.54	0	3.29	3.29	86.83
	POP	71.11	0.72	3.98	4.7	75.81
MO	MCP	80.36	0	11.85	11.85	92.21
	COP	84.2	0	9.23	9.23	93.43
	POP	69.28	0.75	11.26	12.01	81.29

Table 32. Comparison between the vendor revenues on all market segments, mu.

Sellers	Revenue without Local Market	PM Trading Priority	Settlement Price	PM	SM1	SM2	SM	Total PM + SM	Total PM + SM + Grid
prosumers	42.16	FCFS	MCP	71.11	0	3.61	3.61	74.72	75.52
			COP	83.54	0	2.99	2.99	86.53	87.33
			POP	71.11	0.72	3.61	4.33	75.44	76.24
		MO	MCP	80.36	0	5	5	85.36	86.41
			COP	84.2	0	3.53	3.53	87.73	88.78
			POP	69.28	0.29	4.7	4.99	74.27	75.32
consumers	12.38	FCFS	MCP	0	0	0	0	0	
			COP	0	0	0	0	0	12.38
			POP	0	0	0	0	0	
		MO	MCP	0	0	5.77	5.77	5.77	14.67
			COP	0	0	4.86	4.86	4.86	13.76
			POP	0	0.46	5.53	5.99	5.99	14.89

Table 31 shows that the highest costs for the consumers occur when the COP settlement is used, while the POP settlement offers the best buy prices from the market. In Table 32, it can be seen that the prosumer revenues can double when the primary and secondary markets are used, with the highest profits being achieved on the primary market. The secondary market is, however, useful for the consumers who need to sell surplus remaining from the primary market, increasing their daily revenue by up to 200% (14.89 mu, compared to 12.38 mu).

Using the traded quantities and factoring the costs and revenues presented above, a comparison can be made between the daily electricity costs for the aggregated network demand in the 06:00–18:00 interval. Table 33 shows that the combined effect of the primary and secondary markets can decrease the cost by up to 26% when the FCFS trading prioritization is used. For MO prioritization, because

of the significant consumer surplus in the primary market, the cost increases when MCP or COP settlement is used, but the effect of the secondary market is to compensate a fraction of the increase.

Table 33. Comparison between the influence of the primary secondary market on the electricity costs for the microgrid, time interval 06:00–18:00, mu.

PM Trading Priority	Settlement Price	Cost with Regulated Tariff	Cost with PM	Cost with PM and SM	% Reduction PM	% Reduction PM + SM
	MCP	136.89	102.75	101.08	24.94	26.16
FCFS	COP	136.89	115.18	112.82	15.86	17.59
	POP	136.89	102.75	101.80	24.94	25.64
	MCP	136.89	146.73	137.29	−7.19	−0.29
MO	COP	136.89	150.57	139.42	−9.99	−1.84
	POP	136.89	135.65	126.15	0.91	7.85

It is important to note that the results presented in the paper are highly dependent on the input data used for the case study. The profits of the prosumers and the cost reductions for the consumers are affected by the quantities and prices offered in the market by both parties and can vary significantly from the results presented in the paper. Also, depending on local constraints, the trading tiers of the secondary market can be used only partially and in a different order. The case study presents a scenario of a complete market trading sequence to show the capabilities of the proposed model.

The results presented in Tables 29–33 use for the commercial tier of the secondary market only the tariff-access option.

6. Conclusions

The paper proposes a new local market for active microgrids, designed to maximize the surplus sold by the prosumers to the local consumers. The local market requires smart grid features in the microgrid and a blockchain ledger for submitting buy and sell offers. Trading is performed in two phases, first on a primary marked, followed by a two-tier secondary market. The case study shows that the secondary market can help the prosumers to sell more surplus to the local consumers, increasing their profitability. The advantages of the local market can be discussed from several perspectives:

- The reduction of electricity quantities traded back to the grid (at lower prices) for prosumers;
- The reduction of electricity costs for consumers, brought by acquiring cheaper electricity from the local prosumers;
- The increase of profits for prosumers, by selling larger quantities to local consumers, at higher prices than the regulated tariff used to sell back to the grid. This can also be seen as an incentive for increasing sustainable electricity generation from renewable resources;
- The energy poverty mitigation for some consumers, an aspect regarding economic and social sustainability.

However, as main disadvantages, accurate demand forecasts are necessary for the consumers if the MO trading method is used, for optimal market benefits. Furthermore, the implementation of the proposed market model is dependent on several prerequisites: the implementation of smart grid capabilities in the microgrid, the creation of adequate regulations by regional or national authorities, and the development of residential renewable electricity generation, all these being in incipient development stages across the world.

The proposed algorithm is a comprehensive tool of the trading process for consumers and prosumers in microgrids, considering the current regulation framework regarding prosumer activity in the Romanian electricity market, and future research directions considered by the authors aim to extend its capabilities for social inclusion, analyzing the influence of storage capabilities on local market trading dynamics and profitability, and considering new trading options, by comparison with similar real local market models, as they become available in the literature.

7. Patents

National Patent Application "Innovative method of decision-making assistance aimed at streamlining the management of prosumer activity", Romania, 2020, in press.

Abbreviations

ADMM	Alternating Direction Method of Multipliers
ADN	Active Distribution Network
AEA	Active Energy Agent
ANRE	Romanian Energy Regulatory Authority
C	Consumers/Consumption Quantity
CO	Consumption Offers
COP	Consumer Offers Price
DM	Demurrage Mechanism
DNOs	Distribution Network Operators
DR	Demand Response
EU	European Union
f%	fee added to the price resulting from trading mechanism
FCFS	First-Come-First-Served
G	Generation Quantity
GO	Generation Offers
HEM	Home Energy Management
kWh	kilowatt-hours
LEM	Local Electricity Market
LV	Low Voltage
MCP	Market Clearing Price
MEP	Multiple Energy Prosumers
MO	Merit-order
mu	Monetary units
NC	Total Number of Consumers
NCM	Number of Consumers participating in the Market
NP	Total Number of Prosumers
NPM	Number of Prosumers participating in the Market
P	Prosumer/Price
P2P	Peer-to-Peer
PCO	Price of Consumption Offers
PGO	Price of Generation Offers
PM	Primary Market
POP	Prosumer Offers Price

PoW	Proof-of-Work
PV	Photovoltaic
REScoop	European Federation of Renewable Energy Cooperatives
S	Surplus
SM	Secondary Market
SSRES	Small-Scale Renewable Energy Sources
TC	The Maximum Amount of Traded Electricity by Consumers
TP	Transaction of Prosumers
TCO	The Quantity of Electricity Actually Traded
WEM	Wholesale Electricity Market

Appendix A. Input Data for the Primary Market

Table A1. The hourly demand profiles for the entire microgrid, in kW (27 consumers).

Hour	C2	C3	C4	C5	C6	C7	C8	C9	C10
h1	0.616	2.010	0.273	0.000	1.370	2.418	1.152	1.936	0.310
h2	0.608	1.908	0.078	0.020	1.520	2.210	1.664	1.368	0.678
h3	0.557	2.004	0.048	0.260	1.910	2.149	2.056	1.376	0.300
h4	0.522	2.010	0.306	0.040	1.770	2.151	2.048	2.048	0.640
h5	0.522	1.902	0.063	0.050	1.990	2.192	1.816	1.528	0.360
h6	0.571	2.004	0.165	0.250	2.070	2.299	1.168	2.992	0.468
h7	0.529	1.836	0.213	0.125	2.280	2.364	0.720	3.352	0.748
h8	0.592	1.236	0.060	4.710	2.530	2.543	1.704	2.240	3.208
h9	0.562	1.302	0.312	1.290	1.850	2.382	1.976	2.112	2.815
h10	0.616	1.200	0.258	0.525	1.850	2.549	1.944	2.192	1.483
h11	0.860	1.188	0.243	2.985	1.460	2.426	1.904	2.232	4.538
h12	0.535	1.146	0.423	1.895	1.180	2.414	1.872	2.144	3.295
h13	0.641	1.140	0.198	4.595	1.650	2.450	2.456	2.048	3.650
h14	0.322	1.374	0.378	0.930	1.950	2.418	2.632	2.176	5.230
h15	0.181	1.944	0.321	0.260	1.810	2.444	1.896	2.256	4.293
h16	0.214	1.542	0.207	0.535	2.640	2.467	2.072	2.328	3.895
h17	0.781	2.148	0.495	2.125	2.810	2.553	2.080	2.288	3.028
h18	0.764	1.902	0.282	1.025	2.720	2.757	2.016	2.336	1.980
h19	0.426	1.968	0.336	0.140	3.580	3.042	2.720	2.464	1.768
h20	0.426	1.968	0.336	0.140	3.580	3.042	2.720	2.464	1.768
h21	0.496	1.956	0.207	0.210	5.310	3.515	2.672	3.136	3.033
h22	0.561	1.986	0.405	0.480	5.390	3.248	2.488	1.312	5.695
h23	0.554	1.872	0.246	0.195	4.750	3.075	2.432	1.336	4.033
h24	0.578	1.986	0.045	0.100	3.170	2.713	2.088	1.184	1.180
h06–18	7.168	19.962	3.555	21.250	26.800	32.066	24.440	30.696	38.631

Hour	C11	C12	C13	C14	C15	C16	C17	C18	C19
h1	0.230	0.585	0.142	0.910	2.783	2.220	0.210	0.360	0.345
h2	0.220	0.765	0.078	0.920	2.411	1.320	0.000	0.525	0.286
h3	0.200	0.585	0.352	0.925	2.548	0.942	0.000	0.534	0.243
h4	0.200	0.675	0.440	1.225	2.313	0.972	0.045	0.636	0.213
h5	0.200	0.660	0.062	1.345	2.288	0.954	0.000	0.444	0.237
h6	1.240	0.570	1.416	1.290	2.426	1.044	0.115	0.462	0.242
h7	1.400	0.900	0.482	1.325	3.239	1.374	0.075	0.477	0.281
h8	1.440	0.630	0.182	1.520	3.798	3.984	0.475	0.450	0.287
h9	1.170	0.765	0.502	1.430	3.097	2.184	0.380	0.504	0.278
h10	1.130	0.645	1.046	1.120	4.371	1.986	0.495	0.579	0.268

Table A1. *Cont.*

Hour	C11	C12	C13	C14	C15	C16	C17	C18	C19
h11	1.390	0.555	0.150	1.170	2.994	1.986	1.130	0.573	0.285
h12	1.740	0.630	1.032	1.265	3.763	2.844	0.630	0.498	0.315
h13	1.760	0.615	0.056	1.760	2.999	1.566	0.420	0.600	0.301
h14	1.200	0.570	0.056	2.000	2.759	0.930	0.980	0.540	0.329
h15	0.280	0.750	0.236	1.840	3.807	0.798	0.955	0.357	0.312
h16	0.460	0.555	1.024	1.815	3.317	1.152	0.965	0.423	0.350
h17	3.180	0.825	0.232	2.015	3.214	1.944	0.970	0.588	0.366
h18	2.570	0.780	0.890	2.365	2.940	2.046	0.960	0.570	0.468
h19	2.890	0.780	0.458	2.480	3.445	2.460	1.450	0.678	0.443
h20	2.890	0.780	0.458	2.480	3.445	2.460	1.450	0.678	0.443
h21	3.210	0.630	0.864	2.580	3.278	1.884	1.385	0.753	0.454
h22	3.260	0.570	1.326	2.365	2.475	1.374	1.660	0.621	0.482
h23	2.815	0.720	0.376	2.060	2.073	1.380	1.235	0.750	0.509
h24	1.780	0.570	0.200	1.495	2.769	1.158	0.880	0.390	0.328
h06–18	18.960	8.790	7.304	20.915	42.724	23.838	8.550	6.621	4.082

Hour	C20	C21	C22	C23	C24	C25	C26	C27	C28
h1	0.973	0.636	0.790	0.049	1.266	0.384	0.248	0.024	0.973
h2	1.013	0.484	0.780	0.056	1.194	0.384	0.296	0.000	1.013
h3	0.733	0.448	0.730	0.749	1.056	0.388	0.260	0.000	0.733
h4	0.453	0.460	0.920	1.148	1.032	0.392	0.292	0.000	0.453
h5	0.680	0.520	0.800	1.148	1.014	0.400	0.208	0.000	0.680
h6	0.773	0.512	1.340	1.148	1.020	0.396	0.356	0.192	0.773
h7	0.980	0.428	0.960	1.946	1.122	0.376	0.700	0.140	0.980
h8	1.560	0.368	0.270	1.393	1.116	0.352	0.336	0.152	1.560
h9	1.580	0.408	0.420	1.596	1.110	0.356	0.144	0.000	1.580
h10	1.347	0.408	1.000	2.975	1.110	0.360	0.128	0.004	1.347
h11	1.713	0.668	0.930	1.519	1.242	0.620	0.204	0.076	1.713
h12	1.913	0.412	1.050	2.492	1.260	0.344	0.320	0.508	1.913
h13	3.127	0.344	1.020	1.974	1.266	0.324	0.476	0.056	3.127
h14	2.560	0.428	0.970	1.974	1.260	0.332	0.384	0.020	2.560
h15	1.433	1.068	1.010	2.240	1.206	0.940	0.456	0.244	1.433
h16	2.013	0.424	1.110	2.296	1.134	2.500	0.352	0.088	2.013
h17	4.000	0.448	1.540	1.778	1.140	2.544	2.000	0.080	4.000
h18	1.067	0.468	1.630	1.939	1.260	2.820	0.876	0.228	1.067
h19	1.907	0.436	1.570	1.750	1.296	2.104	1.824	0.000	1.907
h20	1.907	0.436	1.570	1.750	1.296	2.104	1.824	0.000	1.907
h21	2.473	1.092	1.280	1.106	1.212	2.144	0.728	0.408	2.473
h22	2.253	1.484	1.110	1.092	1.194	2.084	0.688	0.412	2.253
h23	1.933	1.364	0.710	1.092	1.194	2.248	0.256	0.532	1.933
h24	1.260	0.880	0.840	0.763	1.176	2.008	0.324	0.144	1.260
h06–18	12.900	24.066	6.384	13.250	25.270	15.246	12.264	6.732	1.788

Table A2. The hourly generation profiles for the prosumers in the microgrid, in kW (8 prosumers).

Hour	P27	P21	P7	P15	P6	P3	P10	P25
h1	0	0	0	0	0	0	0	0
h2	0	0	0	0	0	0	0	0
h3	0	0	0	0	0	0	0	0
h4	0	0	0	0	0	0	0	0
h5	0	0	0	0	0	0	0	0
h6	0.249	2.361	2.183	4.374	2.011	2.212	1.965	4.072

Table A2. *Cont.*

Hour	P27	P21	P7	P15	P6	P3	P10	P25
h7	0.518	2.785	2.627	4.824	2.132	2.642	2.364	4.609
h8	1.004	3.286	3.247	5.384	2.357	3.115	2.922	4.942
h9	1.581	3.329	3.438	5.325	2.592	3.139	3.094	5.066
h10	1.735	3.639	3.642	5.673	2.966	3.451	3.278	5.342
h11	1.859	3.751	3.826	5.769	3.346	3.561	3.443	5.417
h12	1.915	3.735	3.639	5.643	3.509	3.539	3.275	5.320
h13	1.984	3.812	3.863	5.825	3.945	3.603	3.477	5.506
h14	1.756	3.742	3.803	5.704	3.297	3.553	3.423	5.474
h15	1.562	3.461	3.492	5.353	2.994	3.276	3.143	4.908
h16	0.915	2.832	2.877	4.642	2.541	2.675	2.589	4.343
h17	0.495	2.403	2.305	4.276	2.352	2.283	2.075	4.017
h18	0.308	2.237	2.105	4.101	1.791	2.123	1.895	3.859
h19	0	0	0	0	0	0	0	0
h20	0	0	0	0	0	0	0	0
h21	0	0	0	0	0	0	0	0
h22	0	0	0	0	0	0	0	0
h23	0	0	0	0	0	0	0	0
h24	0	0	0	0	0	0	0	0

Table A3. The forecasted quantity offers of the buyers (consumers) for the primary market, MO trading priority, in kWh (11 consumers).

Trading Interval	C5	C8	C9	C11	C12	C14	C16	C19	C20	C24	C26
h6	0.30	1.10	3.20	1.30	0.60	1.20	2.00	0.20	0.50	1.20	0.50
h7	0.40	0.80	3.40	1.40	0.80	1.30	2.00	0.30	2.10	2.00	0.40
h8	4.10	1.70	2.10	1.30	0.60	1.40	3.50	0.30	0.60	1.50	0.40
h9	1.50	2.00	2.20	1.00	0.80	1.50	2.00	0.20	0.40	1.60	0.40
h10	0.80	1.90	2.10	1.00	0.80	1.10	2.00	0.30	0.40	2.80	0.40
h11	3.20	1.90	2.20	0.90	0.60	1.20	2.00	0.30	0.30	1.50	0.60
h12	2.00	2.00	2.10	0.00	0.60	1.30	2.00	0.30	0.50	2.40	0.40
h13	4.70	2.50	2.00	1.50	0.70	1.80	1.80	0.30	0.70	2.00	0.30
h14	1.10	2.40	2.20	1.20	0.70	2.00	1.00	0.30	0.60	2.00	0.30
h15	0.60	2.10	2.20	0.70	0.80	1.80	1.00	0.30	1.30	2.20	1.00
h16	0.60	2.20	2.30	0.70	0.70	1.90	1.00	0.40	1.20	2.30	2.50
h17	2.60	2.40	2.40	2.50	0.70	2.10	1.50	0.40	1.60	1.80	2.50
h18	1.30	2.30	2.50	3.00	0.90	2.20	2.00	0.50	1.60	1.90	2.80

Table A4. The offer prices submitted by the buyers (consumers) in the primary market, in mu/kWh.

Trading Interval	C5	C8	C9	C11	C12	C14	C16	C19	C20	C24	C26
h6–h18	0.45	0.6	0.55	0.52	0.48	0.6	0.49	0.39	0.55	0.57	0.5

Table A5. The offer prices submitted by the sellers (prosumers) in the primary market, in mu/kWh.

Trading Interval	P27	P21	P7	P15	P6	P3	P10	P25
h6–h18	0.43	0.55	0.4	0.48	0.43	0.47	0.42	0.43

Appendix B. Data for the Energy Poverty Mitigation Market

Table A6. The sell offer quantities for the energy poverty mitigation tier (kWh), FCFS trading priority.

Hour	P21	P7	P15	P6	P3	Total
h06	0	0	0	0	0	0
h07	0	0	0	0	0	0
h08	0	0	0	0	0	0
h09	0	0	0	0	1.815	1.815
h10	0	0	1.302	0	2.840	4.142
h11	0	0	0	0	2.345	2.345
h12	0	0	0	1.241	0	1.241
h13	0	0	0	0	0	0
h14	1.182	0	0	0.739	0	1.921
h15	0	0.113	0	0	0	0.113
h16	0	0	0	0	0	0
h17	0	0	0	0	0	0
h18	0	0	0	0	0	0
Total	1.182	0.113	1.302	1.980	7.000	11.576

Table A7. The sell offer quantities for the energy poverty mitigation tier, MO trading priority, in kWh.

Hour	P21	P15	P3	C5	C9	C11	C12	C16	C19	C20	C24	C26	Total
h06	0	0	0	0.300	0	0	0.600	0.708	0.200	0	0	0	1.808
h07	0	0	0	0.400	0	0	0.800	1.838	0.300	0	0	0	3.338
h08	0	0	0	4.100	0	0	0.600	0.397	0.300	0	0	0	5.397
h09	1.682	0	0	0	0	0	0	0	0	0	0	0	1.682
h10	2.292	1.302	0.493	0	0	0	0	0	0	0	0	0	4.087
h11	2.038	0.563	0	0	0	0	0	0	0	0	0	0	2.601
h12	1.822	1.860	0	0	0	0	0	0	0	0	0	0	3.682
h13	0	0	0	0.746	0	0	0	0	0.3	0	0	0	1.046
h14	1.182	0.641	0	0	0	0	0	0	0	0	0	0	1.823
h15	0	0	0	0.600	0	0	0.155	0	0.300	0	0	0	1.055
h16	0	0	0	0.600	0.241	0.700	0.700	1	0.400	1.200	0	2.500	7.341
h17	0	0	0	2.600	2.400	2.500	0.700	1.5	0.400	1.600	1.181	2.500	15.381
h18	0	0	0	1.300	1.835	3.000	0.900	2	0.500	1.600	0	2.800	13.935
Total	9.016	4.366	0.493	10.646	4.476	6.200	4.455	7.443	2.700	4.400	1.181	7.800	63.176

Table A8. The sell quantities traded in the energy poverty mitigation tier, FCFS priority, in kWh.

Hour	P21	P7	P15	P6	P3	Total
h06	0	0	0	0	0	0
h07	0	0	0	0	0	0
h08	0	0	0	0	0	0
h09	0	0	0	0	0	0
h10	0	0	0	0	0.004	0.004
h11	0	0	0	0	0.076	0.076
h12	0	0	0	0.508	0	0.508
h13	0	0	0	0	0	0
h14	0	0	0	0.020	0	0.020
h15	0	0.113	0	0	0	0.113
h16	0	0	0	0	0	0
h17	0	0	0	0	0	0
h18	0	0	0	0	0	0
Total	0	0.113	0	0.528	0.08	0.721

Table A9. The sell quantities traded in the energy poverty mitigation tier, MO priority, in kWh.

Hour	P21	P15	P3	C5	C9	C11	C12	C16	C19	C20	C24	C26	Total
h06	0	0	0	0	0	0	0	0	0.192	0	0	0	0.192
h07	0	0	0	0	0	0	0	0	0.140	0	0	0	0.140
h08	0	0	0	0	0	0	0	0	0.152	0	0	0	0.152
h09	0	0	0	0	0	0	0	0	0	0	0	0	0
h10	0	0	0.004	0	0	0	0	0	0	0	0	0	0.004
h11	0	0.076	0	0	0	0	0	0	0	0	0	0	0.076
h12	0	0.508	0	0	0	0	0	0	0	0	0	0	0.508
h13	0	0	0	0	0	0	0	0	0.056	0	0	0	0.056
h14	0	0.020	0	0	0	0	0	0	0	0	0	0	0.020
h15	0	0	0	0	0	0	0	0	0.244	0	0	0	0.244
h16	0	0	0	0	0	0	0	0	0.088	0	0	0	0.088
h17	0	0	0	0	0	0	0	0	0.080	0	0	0	0.080
h18	0	0	0	0	0	0	0	0	0.228	0	0	0	0.228
Total	0	0.604	0.004	0	0	0	0	0	1.180	0	0	0	1.788

Appendix C. Data for the Commercial Secondary Market, Fee-Access Method

Table A10. The sell offer quantities for the commercial fee-access tier, FCFS trading priority, in kWh.

Hour	P21	P15	P6	P3	Total
h06	0	0	0	0	0
h07	0	0	0	0	0
h08	0	0	0	0	0
h09	0	0	0	1.815	1.815
h10	0	1.302	0	2.836	4.138
h11	0	0	0	2.269	2.269
h12	0	0	0.733	0	0.733
h13	0	0	0	0	0
h14	1.182	0	0.719	0	1.901
h15	0	0	0	0	0
h16	0	0	0	0	0
h17	0	0	0	0	0
h18	0	0	0	0	0
Total	1.182	1.302	1.452	6.920	10.855

Table A11. The sell offer quantities for the commercial fee-access tier, MO trading priority, in kWh.

Vendor	P21	P15	P3	C5	C9	C11	C12	C16	C19	C20	C24	C26	Total
h06	0	0	0	0.300	0	0	0.600	0.708	0.008	0	0	0	1.616
h07	0	0	0	0.400	0	0	0.800	1.838	0.160	0	0	0	3.198
h08	0	0	0	4.100	0	0	0.600	0.397	0.148	0	0	0	5.245
h09	1.682	0	0	0	0	0	0	0	0	0	0	0	1.682
h10	2.292	1.302	0.489	0	0	0	0	0	0	0	0	0	4.083
h11	2.038	0.487	0	0	0	0	0	0	0	0	0	0	2.525
h12	1.822	1.352	0	0	0	0	0	0	0	0	0	0	3.174
h13	0	0	0	0.746	0	0	0	0	0.244	0	0	0	0.990
h14	1.182	0.621	0	0	0	0	0	0	0	0	0	0	1.803
h15	0	0	0	0.600	0	0	0.155	0	0.056	0	0	0	0.811
h16	0	0	0	0.600	0.241	0.700	0.700	1.000	0.312	1.200	0	2.500	7.253
h17	0	0	0	2.600	2.400	2.500	0.700	1.500	0.320	1.600	1.181	2.500	15.301
h18	0	0	0	1.300	1.835	3.000	0.900	2.000	0.272	1.600	0	2.800	13.707
Total	9.016	3.762	0.489	10.646	4.476	6.200	4.455	7.443	1.520	4.400	1.181	7.800	61.388

Table A12. The sell quantities traded in the commercial fee-access tier, FCFS trading priority.

Hour	21	15	6	3	Total
h06	0	0	0	0	0
h07	0	0	0	0	0
h08	0	0	0	0	0
h09	0	0	0	1.386	1.386
h10	0	0	0	2.120	2.120
h11	0	0	0	1.853	1.853
h12	0	0	0.733	0	0.733
h13	0	0	0	0	0
h14	0.858	0	0.719	0	1.576
h15	0	0	0	0	0
h16	0	0	0	0	0
h17	0	0	0	0	0
h18	0	0	0	0	0
Total	0.858	0	1.452	5.359	7.668

Table A13. The sell quantities traded in the commercial fee-access tier, MO trading priority, in kWh.

Hour	P21	P15	P3	C5	C9	C11	C12	C16	C19	C20	C24	C26	Total
h06	0	0	0	0.300	0	0	0.600	0.708	0.008	0	0	0	1.616
h07	0	0	0	0.400	0	0	0.474	0	0.160	0	0	0	1.034
h08	0	0	0	0.959	0	0	0	0	0.148	0	0	0	1.107
h09	1.386	0	0	0	0	0	0	0	0	0	0	0	1.386
h10	0.329	1.302	0.489	0	0	0	0	0	0	0	0	0	2.120
h11	1.366	0.487	0	0	0	0	0	0	0	0	0	0	1.853
h12	0.808	1.352	0	0	0	0	0	0	0	0	0	0	2.160
h13	0	0	0	0.746	0	0	0	0	0.244	0	0	0	0.990
h14	0.955	0.621	0	0	0	0	0	0	0	0	0	0	1.576
h15	0	0	0	0.600	0	0	0.155	0	0.056	0	0	0	0.811
h16	0	0	0	0.600	0	0	0.700	0.8	0.312	0	0	0	2.412
h17	0	0	0	1.470	0	0	0	0	0.320	0	0	0	1.790
h18	0	0	0	1.300	0	0	0.848	0	0.272	0	0	0	2.420
Total	4.844	3.762	0.489	6.375	0	0	2.777	1.508	1.520	0	0	0	21.275

Table A14. The buy quantities traded in the commercial fee-access tier, MO trading priority, in kWh.

Hour	C13	C17	C18	Total
h06	0	0	0	0
h07	0	0	0	0
h08	0	0	0	0
h09	0.502	0.380	0.504	1.386
h10	1.046	0.495	0.579	2.120
h11	0.150	1.130	0.573	1.853
h12	0.733	0	0	0.733
h13	0	0	0	0
h14	0.056	0.980	0.540	1.576
h15	0	0	0	0
h16	0	0	0	0
h17	0	0	0	0
h18	0	0	0	0
Total	2.487	2.985	2.196	7.668

Table A15. The buy quantities traded in the commercial fee-access tier, MO trading priority, in kWh.

Hour	C13	C17	C18	Total
h06	1.416	0	0.200	1.616
h07	0.482	0.075	0.477	1.034
h08	0.182	0.475	0.450	1.107
h09	0.502	0.380	0.504	1.386
h10	1.046	0.495	0.579	2.120
h11	0.150	1.130	0.573	1.853
h12	1.032	0.630	0.498	2.160
h13	0.056	0.334	0.600	0.990
h14	0.056	0.980	0.540	1.576
h15	0.236	0.218	0.357	0.811
h16	1.024	0.965	0.423	2.412
h17	0.232	0.970	0.588	1.790
h18	0.890	0.960	0.570	2.420
Total	7.304	7.612	6.359	21.275

References

1. Agora-Energiewende, European Energy Transition 2030: The Big Picture. Available online: https://www.agora-energiewende.de/fileadmin2/Projekte/2019/EU_Big_Picture/153_EU-Big-Pic_WEB.pdf (accessed on 1 August 2020).
2. Saevelect, What Is eDREAM? Available online: https://www.todaysoftmag.ro/article/2469/tehnologia-blockchain (accessed on 1 August 2020).
3. Haber, S.; Scott Stornetta, W. How to time-stamp a digital document. *J. Cryptol.* **1991**, *3*, 99–111. [CrossRef]
4. Bayer, D.; Haber, S.; Scott Stornetta, W. *Improving the Efficiency and Reliability of Digital Time-Stamping*; Capocelli, R., de Santis, A., Vaccaro, U., Eds.; Sequences II; Springer: New York, NY, USA, 1993.
5. Toth, L.A. Blockchain Technology, Today Software Magazine. Available online: https://www.todaysoftmag.ro/article/2469/tehnologia-blockchain (accessed on 1 August 2020).
6. Tradesilvania. Why Use Blockchain Technology? Available online: https://tradesilvania.com/ro/ (accessed on 1 August 2020).
7. Stratulat, A.M. Blockchain: A New Paradigm for the Energy System. Available online: https://medium.com/@adrianmihaistratulat/blockchain-o-noua-paradigma-pentru-sistemul-energetic-ac95761b12a2 (accessed on 1 August 2020).
8. Unlimited Energy for Energy Communities from Renewable Sources. Available online: http://fiiprosumator.ro/static/brosura-greenpeace-energie-fara-limite.pdf (accessed on 1 August 2020).
9. Unguru, M. Blockchain technology: Opportunities for the energy sector. *Euro Infor* **2018**, *2*, 53–58.
10. NewsEnergy, Blockchain Technology and Renewables, the Next "Power Couple". Available online: https://newsenergy.ro/tehnologia-blockchain-si-regenerabilele-urmatorul-power-couple/ (accessed on 1 August 2020).
11. Andoni, M.; Robu, V.; Flynn, D.; Abram, S.; Geach, D.; Jenkins, D.; McCallum, P.; Peacock, A. Blockchain technology in the energy sector: A systematic review of challenges and opportunities. *Renew. Sustain. Energy Rev.* **2019**, *100*, 143–174. [CrossRef]
12. Mika, B.; Goudz, A. Blockchain-technology in the energy industry: Blockchain as a driver of the energy revolution? With focus on the situation in Germany. *Energy Syst.* **2020**. [CrossRef]
13. PwC Global Power & Utilities, Blockchain an Opportunity for Energy Producers and Consumers? Available online: https://www.pwc.com/gx/en/industries/assets/pwc-blockchain-opportunity-for-energy-producers-and-consumers.pdf (accessed on 1 August 2020).
14. Maxim, A.; Mihai, C.; Apostoaie, C.-M.; Popescu, C.; Istrate, C.; Bostan, I. Implications and Measurement of Energy Poverty across the European Union. *Sustainability* **2016**, *8*, 483. [CrossRef]
15. Surowiecki, J. *The Wisdom of Crowds*; Anchor: San Diego, CA, USA, 2005.
16. Wang, S.; Taha, A.F.; Wang, J.; Kvaternik, K.; Hahn, A. Energy crowdsourcing and peer-to-peer energy trading in blockchain-enabled smart grids. *IEEE Trans. Syst. Man Cybern. B Cybern.* **2019**, *49*, 1612–1623. [CrossRef]

17. National Regulatory Authority for Energy. *The 228 Order for the Approval of the Technical Norm Technical Conditions for Connection to the Public Electrical Networks of the Prosumers*; National Regulatory Authority for Energy: Bucharest, Romania, 2018.

18. Neagu, B.C.; Grigoras, G.; Ivanov, O. An Efficient Peer-to-Peer Based Blokchain Approach for Prosumers Energy Trading in Microgrids. In Proceedings of the International Conference on Modern Power Systems (MPS), Cluj Napoca, Romania, 21–23 May 2019; pp. 1–4.

19. Mohan, V.; Bu, S.; Jisma, M.; Rijinlal, V.C.; Thirumala, K.; Thomas, M.S.; Xu, Z. Realistic energy commitments in peer-to-peer transactive market with risk adjusted prosumer welfare maximization. *Int. J. Electr. Power Energy Syst.* **2020**, *124*, 106377. [CrossRef]

20. De La Nieta, A.A.S.; Gibescu, M.; Wang, X.; Song, M.; Jensen, E.; Saleem, A.; Bremdal, B.; Ilieva, I. Local economic dispatch with local renewable generation and flexible load management. In Proceedings of the International Conference on Smart Energy Systems and Technologies (SEST), Sevilla, Spain, 10–12 September 2018; pp. 1–6.

21. Ottesen, S.Ø.; Tomasgard, A.; Fleten, S.-E. Prosumer bidding and scheduling in electricity markets. *Energy* **2016**, *94*, 828–843. [CrossRef]

22. Ferruzzi, G.; Cervone, G.; Delle Monache, L.; Graditi, G.; Jacobone, F. Optimal bidding in a Day-Ahead energy market for Micro Grid under uncertainty in renewable energy production. *Energy* **2016**, *106*, 194–202. [CrossRef]

23. Gregg, J.S.; Nyborg, S.; Hansen, M.; Schwanitz, V.J.; Wierling, A.; Zeiss, J.P.; Delvaux, S.; Saenz, V.; Polo-Alvarez, L.; Candelise, C.; et al. Collective action and social innovation in the energy sector: A mobilization model perspective. *Energies* **2020**, *13*, 651. [CrossRef]

24. Candelise, C.; Ruggieri, G. Status and evolution of the community energy sector in Italy. *Energies* **2020**, *13*, 1888. [CrossRef]

25. Marinakis, V.; Doukas, H.; Koasidis, K.; Albuflasa, H. From intelligent energy management to value economy through a digital energy currency: Bahrain city case study. *Sensors* **2020**, *20*, 1456. [CrossRef] [PubMed]

26. Horstink, L.; Wittmayer, J.M.; Ng, K.; Luz, G.P.; Marín-González, E.; Gährs, S.; Campos, I.; Holstenkamp, L.; Oxenaar, S.; Brown, D. Collective renewable energy prosumers and the promises of the energy union: Taking stock. *Energies* **2020**, *13*, 421. [CrossRef]

27. The First Green Energy Cooperative in Romania Will "Open Its Doors" Soon, Including for Prosumers. Available online: https://newsenergy.ro/prima-cooperativa-de-energie-verde-din-romania-isi-va-deschide-portile-in-curand-inclusiv-pentru-prosumatori/ (accessed on 1 August 2020).

28. Son, Y.-B.; Im, J.-H.; Kwon, H.-Y.; Jeon, S.-Y.; Lee, M.-K. Privacy-preserving peer-to-peer energy trading in blockchain-enabled smart grids using functional encryption. *Energies* **2020**, *13*, 1321. [CrossRef]

29. Wang, S.; Taha, A.F.; Wang, J. Blockchain-assisted crowdsourced energy systems. In Proceedings of the IEEE Power & Energy Society General Meeting (PESGM), Porto, Portugal, 9–11 September 2018; pp. 1–5.

30. Morstyn, T.; Teytelboym, A.; Hepburn, C.; McCulloch, M.D. Integrating P2P Energy Trading with Probabilistic Distribution Locational Marginal Pricing. *IEEE Trans. Smart Grid* **2019**, *11*, 3095–3106. [CrossRef]

31. Fu, M.; Xu, Z.; Wang, N.; Lyu, X.; Xu, W. "Peer-to-Peer Plus" electricity transaction within community of active energy agents regarding distribution network constraints. *Energies* **2020**, *13*, 2408. [CrossRef]

32. Khorasany, M.; Mishra, Y.; Ledwich, G. Design of auction-based approach for market clearing in peer-to-peer market platform. *J. Eng.* **2019**, 4813–4818. [CrossRef]

33. Khorasany, M.; Azuatalam, D.; Glasgow, R.; Liebman, A.; Razzaghi, R. Transactive energy market for energy management in microgrids: The monash microgrid case study. *Energies* **2020**, *13*, 2010. [CrossRef]

34. Haghifam, S.; Zare, K.; Abapour, M.; Muñoz-Delgado, G.; Contreras, J. A stackelberg game-based approach for transactive energy management in smart distribution networks. *Energies* **2020**, *13*, 3621. [CrossRef]

35. Liu, Z.; Gao, J.; Yu, H.; Wang, X. Operation mechanism and strategies for transactive electricity market with multi-microgrid in grid-connected mode. *IEEE Access* **2020**, *8*, 79594–79603. [CrossRef]

36. Hwang, Y.M.; Sim, I.; Sun, Y.G.; Lee, H.-J.; Kim, J.Y. Game-theory modeling for social welfare maximization in smart grids. *Energies* **2018**, *11*, 2315. [CrossRef]

37. Singh, P.; Talwariya, A.; Kolhe, M. Demand response management in the presence of renewable energy sources using Stackelberg game theory. *IOP Conf. Ser. Mater. Sci. Eng.* **2019**, *605*, 012004. [CrossRef]

38. Arun, S.L.; Selvan, M.P. Prosumer based demand response for profitable power exchange between end-user and utility. In Proceedings of the 2018 20th National Power Systems Conference (NPSC), Iruchirappalli, India, 14–16 December 2018; pp. 1–6.

39. Liu, T.; Tan, X.; Sun, B.; Wu, Y.; Guan, X.; Tsang, D.H. Energy management of cooperative microgrids with p2p energy sharing in distribution networks. In Proceedings of the 2015 IEEE International Conference on Smart Grid Communications (SmartGridComm), Miami, FL, USA, 2–5 November 2015; pp. 410–415.

40. Neagu, B.-C.; Ivanov, O.; Grigoras, G.; Gavrilas, M. A new vision on the prosumers energy surplus trading considering smart peer-to-peer contracts. *Mathematics* **2020**, *8*, 235. [CrossRef]

41. Yahaya, A.S.; Javaid, N.; Alzahrani, F.A.; Rehman, A.; Ullah, I.; Shahid, A.; Shafiq, M. Blockchain based sustainable local energy trading considering home energy management and demurrage mechanism. *Sustainability* **2020**, *12*, 3385. [CrossRef]

42. Lovati, M.; Zhang, X.; Huang, P.; Olsmats, C.; Maturi, L. Optimal simulation of three peer to peer (p2p) business models for individual pv prosumers in a local electricity market using agent-based modelling. *Buildings* **2020**, *10*, 138. [CrossRef]

43. Martín, D.; Bordel, B.; Alcarria, R.; Sánchez-Picot, Á.; de Rivera, D.S.; Robles, T. Prosumerization Approach to Semantic Ambient Intelligence Platforms. In Proceedings of the International Conference on Ubiquitous Computing and Ambient Intelligence, Philadelphia, PA, USA, 7–10 November 2017; pp. 109–120.

44. Parag, Y. Beyond energy efficiency: A prosumer market as an integrated platform for consumer engagement with the energy system. *Eur. Counc. Energy Effic. Econ. Summer Study* **2015**, *1*, 15–23.

45. Bytschkow, D.; Capone, A.; Mayer, J.; Kramer, M.; Licklederer, T. An OPC UA-based Energy Management Platform for Multi-Energy Prosumers in Districts. In Proceedings of the 2019 IEEE PES Innovative Smart Grid Technologies Europe (ISGT-Europe), Bucharest, Romania, 29 September–2 October 2019; pp. 1–5.

46. Mamounakis, I.; Vergados, D.J.; Makris, P.; Varvarigos, E.; Mavridis, T. A virtual microgrid platform for the efficient orchestration of multiple energy prosumers. In Proceedings of the 19th Panhellenic Conference on Informatics (PCI'15), Athens, Greece, 1–3 October 2015.

47. Küfeoğlu, S.; Lehtonen, M. Comparison of different models for estimating the residential sector customer interruption costs. *Electr. Power Syst. Res.* **2015**, *122*, 50–55. [CrossRef]

48. Samuel, O.; Almogren, A.; Javaid, A.; Zuair, M.; Ullah, I.; Javaid, N. Leveraging blockchain technology for secure energy trading and least-cost evaluation of decentralized contributions to electrification in Sub-Saharan Africa. *Entropy* **2020**, *22*, 226. [CrossRef]

49. Engeland, K.; Borga, M.; Creutin, J.-D.; François, B.; Ramos, M.-H.; Vidal, J.-P. Space-time variability of climate variables and intermittent renewable electricity production—A review. *Renew. Sustain. Energy Rev.* **2017**, *79*, 600–617. [CrossRef]

50. Etukudor, C.; Couraud, B.; Robu, V.; Früh, W.-G.; Flynn, D.; Okereke, C. Automated negotiation for peer-to-peer electricity trading in local energy markets. *Energies* **2020**, *13*, 920. [CrossRef]

51. Narayanan, A.; Haapaniemi, J.; Kaipia, T.; Partanen, J. Economic impacts of power-based tariffs on peer-to-peer electricity exchange in community microgrids. In Proceedings of the International Conference on the European Energy Market, EEM, Lodz, Poland, 27–29 June 2018.

52. Kuzemko, C.; Lawrence, A.; Watson, M. New directions in the international political economy of energy. *Rev. Int. Polit. Econ.* **2019**, *26*, 1–24. [CrossRef]

53. Van Leeuwen, G.; AlSkaif, T.; Gibescu, M.; van Sark, W. An integrated blockchain-based energy management platform with bilateral trading for microgrid communities. *Appl. Energy* **2020**, *263*, 114613. [CrossRef]

54. Huang, H.; Nie, S.; Lin, J.; Wang, Y.; Dong, J. Optimization of peer-to-peer power trading in a microgrid with distributed PV and battery energy storage systems. *Sustainability* **2020**, *12*, 923. [CrossRef]

55. Ghaemi, S.; Khazaei, H.; Musilek, P. ChainFaaS: An open blockchain-based serverless platform. *IEEE Access* **2020**, *8*, 131760–131778. [CrossRef]

56. Anthony, B.; Petersen, S.A.; Ahlers, D.; Krogstie, J.; Livik, K. Big data-oriented energy prosumption service in smart community districts: A multi-case study perspective. *Energy Inform.* **2019**, *2*, 36. [CrossRef]

57. Cornélusse, B.; Savelli, I.; Paoletti, S.; Giannitrapani, A.; Vicino, A. A community microgrid architecture with an internal local market. *Appl. Energy* **2019**, *242*, 547–560. [CrossRef]

58. Eisele, S.; Eghtesad, T.; Campanelli, K.; Agrawal, P.; Laszka, A.; Dubey, A. Safe and private forward-trading platform for transactive microgrids. *arXiv* **2019**, arXiv:1910.12579.

59. Laszka, A.; Eisele, S.; Dubey, A.; Karsai, G.; Kvaternik, K. TRANSAX: A blockchain-based decentralized forward-trading energy exchanged for transactive microgrids. In Proceedings of the 24th International Conference on Parallel and Distributed Systems (ICPADS), Singapore, Singapore, 11–13 December 2018; pp. 918–927.

60. Li, S.; Lian, J.; Conejo, A.; Zhang, W. Transactive energy system: Market-Based coordination of distributed energy resources. *arXiv* **2019**, arXiv:1908.03641.

61. Vergados, D.J.; Mamounakis, I.; Makris, P.; Varvarigos, E. Prosumer clustering into virtual microgrids for cost reduction in renewable energy trading markets. *Sustain. Energy Grids Netw.* **2016**, *7*, 90–103. [CrossRef]

62. Cui, S.; Wang, Y.; Xiao, J. Peer-to-Peer energy sharing among smart energy buildings by distributed transaction. *IEEE Trans. Smart Grid* **2019**, *6*, 6491–6501. [CrossRef]

63. Cui, S.; Wang, Y.; Shi, Y.; Xiao, J. A new and fair Peer-to-Peer energy sharing framework for energy buildings. *IEEE Trans. Smart Grid* **2020**, *11*, 3817–3826. [CrossRef]

64. Ghorbanian, M.; Dolatabadi, S.H.; Siano, P.; Kouveliotis-Lysikatos, I.; Hatziargyriou, N.D. Methods for flexible management of blockchain-based cryptocurrencies in electricity markets and smart grids. *IEEE Trans. Smart Grid* **2020**, *11*, 4227–4235. [CrossRef]

65. Praça, I.; Ramos, S.; Andrade, R.; da Silva, A.S.; Sica, E.T. Analysis and simulation of local energy markets. In Proceedings of the 2019 16th International Conference on the European Energy Market (EEM), Ljubljana, Slovenia, 18–20 September 2019; pp. 1–5.

66. Neves, D.; Scott, I.; Silva, C.A. Peer-to-peer energy trading potential: An assessment for the residential sector under different technology and tariff availabilities. *Energy* **2020**, *205*, 118023. [CrossRef]

67. Almenning, O.M.; Bjarghov, S.; Farahmand, H. Reducing Neighborhood Peak Loads with implicit Peer-to-Peer energy trading under Subscribed Capacity tariffs. In Proceedings of the 2019 International Conference on Smart Energy Systems and Technologies (SEST), Porto, Portugal, 9–11 September 2019; pp. 1–6.

68. Liang, B.; Liu, W.; Sun, L.; He, Z.; Hou, B. An aggregated model for energy management considering crowdsourcing behaviors of distributed energy resources. *IEEE Access* **2020**, *7*, 145757–145766. [CrossRef]

69. Zepter, J.M.; Lüth, A.; Del Granado, P.C.; Egging, R. Prosumer integration in wholesale electricity markets: Synergies of peer-to-peer trade and residential storage. *Energy Build.* **2019**, *184*, 163–176. [CrossRef]

70. Neagu, B.C.; Gavrilaş, M.; Pentiuc, R.D.; Hopulele, E. Optimal Placement of Energy Storage Systems in Microgrids Using a PSO based Approach. In Proceedings of the 2019 IEEE PES Innovative Smart Grid Technologies Europe (ISGT-Europe), Bucharest, Romania, 29 September–2 October 2019; pp. 1–5. [CrossRef]

71. Faraji, J.; Ketabi, A.; Hashemi-Dezaki, H. Optimization of the scheduling and operation of prosumers considering the loss of life costs of battery storage systems. *J. Energy Storage* **2020**, *31*, 101655. [CrossRef]

72. All You Need to Know to Become A Prosumer. Available online: https://energyindustryreview.com/renewables/all-you-need-to-know-to-become-a-prosumer/ (accessed on 4 August 2020).

73. Neagu, B.C.; Grigoras, G. A Fair Load Sharing Approach Based on Microgrid Clusters and Transactive Energy Concept. In Proceedings of the 12th International Conference on Electronics, Computers and Artificial Intelligence (ECAI 2020), Bucharest, Romania, 25–27 June 2020; pp. 1–5.

74. Electricity Market Monitoring Report—April 2020. Available online: https://www.anre.ro/en/electric-energy/legislation/electictricity-market-monitoring/2020 (accessed on 4 August 2020).

Scheduling Charging of Electric Vehicles in a Secured Manner by Emphasizing Cost Minimization Using Blockchain Technology and IPFS

Muhammad Umar Javed [1], Nadeem Javaid [1,*], Abdulaziz Aldegheishem [2], Nabil Alrajeh [3], Muhammad Tahir [4] and Muhammad Ramzan [5,6]

[1] Department of Computer Science, COMSATS University Islamabad, Islamabad 44000, Pakistan; umarkhokhar1091@gmail.com

[2] Traffic Safety Technologies Chair, Urban Planning Department, College of Architecture and Planning, King Saud University, Riyadh 11574, Saudi Arabia; aldeghei@ksu.edu.sa

[3] Biomedical Technology Department, College of Applied Medical Sciences, King Saud University, Riyadh 11633, Saudi Arabia; nabil@ksu.edu.sa

[4] College of Computer Science and Engineering (CCSE), University of Jeddah, Jeddah 21959, Saudi Arabia; mtyousaf@uj.edu.sa

[5] Department of Computer Science and IT, University of Sargodha, Sargodha 40100, Pakistan; muhammad.ramzan@uos.edu.pk

[6] School of Systems and Technology, University of Management and Technology, Lahore 54000, Pakistan

* Correspondence: nadeemjavaidqau@gmail.com

Abstract: In this work, Electric Vehicles (EVs) are charged using a new and improved charging mechanism called the Mobile-Vehicle-to-Vehicle (M2V) charging strategy. It is further compared with conventional Vehicle-to-Vehicle (V2V) and Grid-to-Vehicle (G2V) charging strategies. In the proposed work, the charging of vehicles is done in a Peer-to-Peer (P2P) manner; the vehicles are charged using Charging Stations (CSs) or Mobile Vehicles (MVs) in the absence of a central entity. CSs are fixed entities situated at certain locations and act as charge suppliers, whereas MVs act as prosumers, which have the capability of charging themselves and also other vehicles. In the proposed system, blockchain technology is used to tackle the issues related with existing systems, such as privacy, security, lack of trust, etc., and also to promote transparency, data immutability, and a tamper-proof nature. Moreover, to store the data related to traffic, roads, and weather conditions, a centralized entity, i.e., Transport System Information Unit (TSIU), is used. It helps in reducing the road congestion and avoids roadside accidents. In the TSIU, an Inter-Planetary File System (IPFS) is used to store the data in a secured manner after removing the data's redundancy through data filtration. Furthermore, four different types of costs are calculated mathematically, which ultimately contribute towards calculating the total charging cost. The shortest distance between a vehicle and the charging entities is calculated using the Great-Circle Distance formula. Moving on, both the time taken to traverse this shortest distance and the time to charge the vehicles are calculated using real-time data of four EVs. Location privacy is also proposed in this work to provide privacy to vehicle users. The power flow and the related energy losses for the above-mentioned charging strategies are also discussed in this work. An incentive provisioning mechanism is also proposed on the basis of timely delivery of credible messages, which further promotes users' participation. In the end, simulations are performed and results are obtained that prove the efficiency of the proposed work, as compared to conventional techniques, in minimizing the EVs' charging cost, time, and distance.

Keywords: blockchain; M2V; IPFS; charging scheduling; Great-Circle Distance

1. Introduction

With the huge increase in both population and urbanization, issues such as drastic climate changes, increased gas emissions, and depletion of fossil fuels arise. Rapid progress has been made in the vehicle industry over the past few years, leading to an increase in the number of vehicles. For this reason, road congestion has also increased drastically. This has created huge amounts of environmental pollution, which includes noise pollution, air pollution, land pollution, etc. These factors disturb the global economy and community to a greater extent. This disturbance further leads to the need for new revolutions for mitigating the previously mentioned problems [1]. To reduce the huge amount of energy required by the vehicles, the scientific and research communities have joined hands and started focusing on Electric Vehicles (EVs) as sources of clean energy. EVs have the ability of reducing fuel demands and gas emissions. Autonomous EVs are a cutting-edge technology of the modern era, which includes self-driving cars as well as services like ride-sharing and smart-pay. EVs also act as environment friendly and green energy sources, as they help in de-carbonization owing to the above-mentioned factors. Conventional combustion engines, which used fossil fuels, are replaced by electric motors that run on Renewable Energy Sources (RESs). EVs can be powered either from Charging Stations (CSs) or from the batteries installed within [2]. The EVs that are emerging drastically in the local market aim to make the power grid into a beneficial entity by introducing the concept of the Grid-to-Vehicle (G2V) charging strategy [3].

With immense developments being made in the Information and Communication Technologies (ICT) sector, bi-directional communication and trading are becoming a reality. In Smart Grids (SGs), EVs play major roles in transportation management. EVs can be charged both from RESs and even from other vehicles via a bi-directional trading mechanism.

In recent times, vehicle manufacturers have not only been competing in terms of providing the latest and most modern infrastructures, but also in terms of providing the latest functionalities and services to drivers. It is expected that conventional vehicles will be replaced with autonomous vehicles, and the entire transportation sector will be taken over by EVs in the near future. The reason is because of the immense amount of research being done in this sector, which enables the vehicular industries to manufacture efficient and highly capable vehicles. Moreover, the battery manufacturing industries also aim at manufacturing batteries with long lifetimes and that are capable of storing more charge. Even now, some conventional vehicles are equipped with the latest technologies for making them semi-autonomous. The increasing number of EVs also poses some problems, like the range anxiety problem, the lack of charging spots, and privacy and security issues. The range anxiety problem is the fear of running out of battery power when going on long distances and being unsure of the availability of CSs. Therefore, batteries with large energy storage capabilities are required when going on long travels, which will, in turn, increase the weight of the car, hindering its performance [4].

In conventional energy trading systems, vehicles have to buy energy from the grid, i.e., a central entity, which makes G2V a centralized system. The involvement of a centralized third party means that there exist single-point failure and privacy leakage issues. The entire system is not optimal and inherits great security risks, as the data residing in the central body are quite easily accessible by hackers. To overcome these issues, a Peer-to-Peer (P2P) system is the optimal solution. A P2P system involves energy trading between EVs, i.e., a Vehicle-to-Vehicle (V2V) trading system. This system has the advantage that the centralized body is eliminated, along with the problems associated with it. However, this decentralized system has some problems. EVs with surplus electricity are hesitant to trade energy with other vehicles due to the privacy and security concerns. Users do not trust each other, as the system is not transparent [5].

To overcome the above-mentioned problems, it is the need of the hour that such a decentralized system is introduced that ensures security, privacy, and data immutability. For this, blockchain technology is introduced and incorporated into various fields of life, like Wireless Sensor Networks (WSNs), Internet of Things (IoT) [6,7], energy [8–10], healthcare, agriculture [11], etc. Blockchain is a decentralized technology that eliminates the need for the centralized party and promotes privacy

and trust among entities. In blockchain technology, the transactions are saved in a distributed ledger; copies are available with every node, ensuring transparency. The transaction data are first stored in a block with a unique hash. Then, these blocks are linked together in a chronological manner. For data verification, consensus algorithms, like Proof of Work (PoW), Proof of Stake (PoS), etc., are used in a blockchain network. Agreement of 51% between nodes is required for any action to take place, e.g., the addition of a new vehicle, sharing of a service, etc., in a blockchain network [12].

A number of problems are associated with the charging of EVs, like limited battery capacities, lower numbers of CSs, trust issues, etc. The cost of charging also plays a vital role in charging of EVs. The vehicle users are reluctant to have their vehicles charged at higher costs. The charging behavior of EVs also affects the grids and the CSs. Therefore, the primary focus of the current research is on the scheduling strategies of EVs. The problem of the limited number of CSs can also be resolved using blockchain technology. It will promote trust between users, which will lead to users' willingness to trade energy amongst themselves. The state information of an EV is collected in the first step, and if the battery level is low, i.e., if the charge stored in the battery is less, then a charging request will be broadcasted to the network. Meanwhile, using a Global Positioning System (GPS), the location information of the EV can be traced and sent to the other vehicles of the network. Then, the shortest driving path is calculated from information obtained through the GPS [13]. The remainder of the paper is organized as follows. Section 2 presents an overview of the related work along with a critical analysis. Section 3 put forwards the problem statement of the proposed work. Section 4 covers the discussion of our proposed system models. The proposed charging schedule is given in Section 5. Section 6 is dedicated to the mathematical formulation of the cost functions and the objective function. Section 7 discusses the power flow and the formulation of the associated energy losses in different charging strategies. The incentive provisioning to the users is presented in Section 8. Furthermore, Section 9 discusses the simulation results in a comprehensive manner. Finally, conclusions and directions for future work are given in Section 10.

After reviewing the work done by several authors in [12,14,15], the motivations for the proposed work are summarized as follows:

- There is a need for a charging scenario other than the conventional scenarios, i.e., G2V and V2V, where vehicles are charged using other vehicles, termed Mobile Vehicles (MVs), which act as prosumers;
- A charging schedule should be devised to charge the vehicles efficiently and also to reduce the charging load on the CSs;
- The data storage issue should be tackled by removing redundancy from the data;
- Blockchain technology should be implemented to promote transparency and to ensure security in a P2P trading scenario;
- Such algorithms should be proposed that will reduce the charging cost and time appreciably;
- Users' participation in the proposed model should be increased by giving incentives.

This work is the extended version of [16]. The major contributions made in this paper are as follows:

- All new incoming vehicles are first authorized by a central entity and then added to the network;
- Scheduling algorithms for the charging of EVs are introduced,
- Mobile-Vehicle-to-Vehicle (M2V) communication between vehicles is done and compared with existing V2V and G2V communications;
- The information related to roads and weather conditions is stored after filtration in a centralized entity using the Inter-Planetary File System (IPFS);
- The shortest distance between charging entities is calculated using the Great-Circle Distance formula. Furthermore, both the times taken to traverse this distance and to charge the vehicles are calculated;

- The location of the vehicles is preserved using an encryption technique to promote vehicles' participation;
- Mathematical formulation is done for achieving the reduction in total charging cost;
- The energy losses associated with the power flow in different charging strategies are discussed;
- Both the number of hashes generated and the mining time required are calculated using different difficulty levels;
- Incentives are given to vehicles on the basis of timely responses of credible messages to increase participation rate.

2. Related Work

Nowadays, the Vehicular Network (VN) is getting smarter with every coming day, and research is aiming towards making it an integral part of the smart city infrastructure. EVs play vital roles in distributed RES transportation and management in SGs. EVs are able to get energy both from the CSs as well as from other EVs using V2V trading. In the near future, the traffic sector will be comprised of a huge number of intelligent EVs. To ensure the security and cost reduction, blockchain will surely play a major role. Several research organizations are currently working on integration of blockchain in the vehicular sector. The blockchain technology promises the advantages of decentralization, security, and trust among EVs. The authors of [5] proposed a system using blockchain along with multisignatures to address transaction security issues. However, the proposed model lacks in providing an efficient system, as it is quite expensive to implement. The authors of [14] proposed a blockchain-based system that makes use of consortium blockchain in order to establish a distributed ledger with nominal cost. In the proposed method, Local Aggregators (LAGs) were introduced to audit and verify the transactions.

In [17], the authors used blockchain technology for creating a decentralized, secured, and trusted ecosystem. The proposed ecosystem consisted of a seven-layer blockchain model. The relationship between the Blockchain-based Intelligent Transport System (B^{2}ITS) and Parallel transportation Management Systems (PtMS) was also studied. It was proved that B^{2}ITS along with PtMS can be used for building better future transportation management systems. In [18], the authors proposed that blockchain technology be integrated into Vehicular Ad-hoc Networks. The proposed system was termed VANET. It consisted of two applications: Mandatory applications and optional applications. Mandatory applications consisted of traffic regulation, vehicle taxation, and vehicle insurance, whereas optional applications consisted of weather information and information about roads, traffic jams, etc. The authors of [19] proposed a blockchain model that ensured that users' data remain secure and private. However, it created trust issues. Services associated with wireless softwares and the respective updates were used to illustrate the efficiency of the proposed model. The authors of [20] described the methods for making the EV communication secure by using cryptographic keys and establishing a public key infrastructure. The proposed model used visible light and acoustic side-channel techniques for minimizing the throughput requirement and providing device independence.

In [21], the authors compared different mechanisms employed in the SG for provisioning of incentives to users. Moreover, they also comprehensively considered the cloud-based V2V energy trading process. Comparison between different existing incentive-based trading schemes was done in order to establish an optimized scheme, which will increase the profit. The authors of [22] presented a decentralized security model that ensured that the trading security is enhanced in the P2P network. The scheduling of vehicle charging was also presented and was supported by a realistic infrastructure. A novel RES pricing scheme in smart cities was brought under consideration by the authors of [23] to achieve domestic electricity bill reduction. The charging schedule was performed using an advanced cross-entropy optimization technique. The proposed system was able to cut down the energy cost at both the community level and the individual level. A game-based energy trading model was proposed in [24] to work out the decision-making processes of electricity operators and consumers in VNs. Small Energy Suppliers (SESs) and Energy Consumers (ECs) were incorporated into the proposed system, and such strategies were designed that made the proposed system beneficial for both the SESs

and ECs. By implementing various stochastic dynamic programming methods, the authors of [25] investigated the energy management in a Smart Home (SH) equipped with Plug-in EVs (PEVs) to address the issue of volatility of RES supply while considering the electricity cost.

The uncontrolled EV charging and discharging created problems for the grid and the CSs, e.g., amplifying the voltage peak, reducing the system's stability, and creating voltage dips. Authors discussed the effects of EVs on energy demand and supply, stability, and reliability in [26]. Two different scenarios were discussed: Vehicle-to-Grid (V2G) and G2V. The authors of [27] proposed a double-layered model and tried to properly allocate the EV charging lots. In the first stage, lots were properly allocated, whereas, in the second stage, integration of RESs in the charging lots was studied. The authors of [28,29] studied the user response behavior, multi-resource coordination strategies, and hierarchies of the electricity markets to model incentive programs. Similarly, the authors of [30,31] proposed Micro-Grid (MG) scheduling for EV charging, and also discussed the algorithms that could make EV charging and discharging an easy and efficient task. Ways to reduce the operational costs and environmental pollution were also discussed.

Integrating RESs in EVs can prove to be a beneficial task and can overcome the hazards of environmental pollution. The authors of [32] proposed an MG architecture running on RESs. It is equipped with a charging lot and aggregated EVs. The main objective is to reduce charging cost and also to provide incentives to those EV users who took part in Demand Response (DR) strategies. The authors of [33] proposed a secure service-provisioning mechanism for lightweight clients. Blockchain technology is used to provide security and privacy to the network. In [34], the authors proposed the PageRank mechanism to assign reputation values to the customers. The customer with the highest reputation value is then authorized to add blocks in the blockchain network. Three different types of attacks were addressed using the modified form of Proof of Authority (PoA).

Conventionally, data are stored in a centralized server, which is vulnerable to attacks. The authors of [35] proposed a secure online storage scheme to store the data provided by users in a P2P manner. The users' information is stored in the form of chunks, which protects it from attacks by malicious entities. All of the data and the metadata are stored online, which means that nothing is stored in the user node. The data are not compromised with the passage of time because they are accessed only by the authorized nodes. The proposed work ensures security provision to the users' data. Similarly, to provide security for the medical data of the users, an attribute-based signature scheme with multiple authorities is proposed by the authors of [36]. In the proposed work, the medical data are attested by the respective patients to avoid disclosure of information to untrusted entities. The proposed work is compared with existing works, which further validates its performance. The authors of [37] proposed a blockchain-based data-sharing platform integrated with the IPFS. In the proposed model, the metadata are uploaded to the IPFS and then divided into a number of sectors. The users are assigned roles and are authenticated using digital signatures. The users are asked to give reviews of the data uploaded to IPFS. Upon successful data delivery, users are awarded with incentives. In this way, maximum honest reviews are uploaded against each file. The authors of [38] proposed a blockchain-based framework for document sharing and version control. The proposed work facilitated multi-user collaboration and change tracking in a secured and trusted environment. The documents are stored in the IPFS, which promotes security. In [39], the authors used the IPFS along with blockchain technology to provide a trusted data traceability and authorization protection mechanism. It also provides a transparent auditing track to trace the data delivery from the sender to the receiver. The proposed model is termed BlockIPFS, in which the metadata is stored in the IPFS and the respective hashes in the blockchain network. Table 1 gives a summary of the related work being studied.

2.1. Critical Analysis

In this subsection, different papers used in the related work (see Section 2) are critically analyzed and evaluated on the bases of three different factors, i.e., scalability, privacy, and resource utilization.

Table 1. Summary of related work.

Scenario (s)	Feature (s)	Objective (s)	Limitation (s)
Smart Grid (SG) energy trading [5]	Use of multisignatures	Solve transaction security issues	Expensive implementation due to usage of multisignatures
Consortium blockchain [14]	Local Aggregators (LAGs) are introduced	Audit the transactions	Introduction of LAGs leads to time complexity
Seven-layer blockchain model [17]	Blockchain-based Intelligent Transport System (B²TS) and Parallel transportation Management Systems (PtMS) data	Provide future directions for intelligent vehicles	Combining data from B²TS and PtMS leads to time complexity
Ad-hoc networks [18]	Vehicular Ad-hoc Networks (VANET)	Optimization of applications	Delay and scalability issues
Blockchain-based architecture [19]	Emerging services and software updates	Protect privacy of users	Trust issues between users
Inter-vehicle protocol [20]	Visible light and acoustic side-channel	Minimize throughput and securing communication	Applicable only for small area
Cloud-based Vehicle-to-Vehicle (V2V) [21]	Incentive-based trading schemes	Efficient increase of the generated profit	Single point of failure and data leakage
Decentralized security model [22]	Registration and authentication details	Securing and scheduling vehicle charging	Two-fold security mechanism of vehicle charging leads to computational complexity
Cross-entropy optimization technique [23]	Pricing schemes	Bill reduction for both community and individuals	Time complexity
Contract-based direct trading [24]	Decision-making process and asymmetric information	Provide benefits to both Energy Consumers (ECs) and Small Energy Suppliers (SESs)	Time complexity
Stochastic dynamic programming framework [25]	Energy demands of Smart Homes (SHs) with Plug-in Electric Vehicles (PEVs)	Minimize cost while balancing power demand	Overlooking user satisfaction
Vehicle-to-Grid (V2G) and Grid-to-Vehicle (G2V) systems [26]	Stability and reliability indices	Improvement of stability and reliability	Security issues
Two-stage model [27]	Economic benefits and technical constraints	Allocate Renewable Energy Sources (RESs) and Electric Vehicle (EV) parking lots simultaneously	Space complexity
SG architecture [28,29]	Incentive DR	Provide incentives to consumers	Third-party involvement
Grid-connected Micro-Grids (MGs) [30,31]	MG operational costs, RES costs	Reduce the operational costs	Overlooking user satisfaction
RES-powered MG [32]	RES costs and DR strategy information	Cost reduction and incentives for DR users	Volatile nature of RESs
Cloud- and edge-based network [33]	Services provided by edge servers	Secure service provisioning to Internet of Things (IoT) devices	Spoofing attacks are not considered
Deregulated SGs [34]	Fair data sharing	Provide privacy to customers	Tradeoff between accuracy and privacy
Online data storage scheme [35]	Robustness against attacks	Ensure privacy provisioning to users' data	Time complexity
Medical data sharing [36]	Avoidance of sensitive medical information disclosure	Privacy provisioning to medical data of patients	Time complexity
Data sharing [37]	Secure and authorized data sharing	Honest reviews given to data files	Time complexity
Document sharing [38]	Secure and trusted document sharing and version control	Facilitate multi-user collaboration	Time complexity
Data traceability framework [39]	Transparent and authorized data sharing	Provide transparent audit tracking to track data delivery	Security issues

2.1.1. Scalability

Scalability is defined as the change in a system's response with the change in hardware components or dataset size. The scalability of a system makes it efficient, competitive, and reputable. From all the papers discussed, References [14,19,21,33] considered scalability. However, some limitations still exist in these papers. For example, in [14], scalability is achieved at the expense of temporal complexity. With the increase in the number of iterations, the computational time also increases. In [19], hardware components' scalability is achieved with the increase in number of blocks generated by EVs. This increase in number of blocks requires enhanced privacy provisioning. However, the proposed work lacks in providing the necessary privacy.

2.1.2. Privacy

Privacy is defined as the ability of an individual or a group of individuals to protect themselves from external interferences. It is of vital importance in any network, especially in blockchain technology, which removes the third party and helps in ensuring the privacy of the network users. Security, encryption, authentication, authorization, etc. all come under the umbrella of privacy. Different papers addressed privacy provisioning in blockchain-based models in different ways and for different purposes, like secure P2P energy trading [14], secure energy trading between EVs [22], and fair data sharing in deregulated SGs [34]. Encryption in the proposed networks of different papers also contributes towards privacy provisioning. The aforementioned three papers, along with Reference [19], used different encryption techniques to encrypt the data and promote data security. However, some limitations still exist; e.g., in [19], an asymmetric encryption technique is used, which fails when encrypting bulk transactions.

2.1.3. Resource Utilization

Resource utilization refers to the achievement of maximum output using minimum resources. This is in relation with the consensus mechanisms used in blockchain-based networks. The work done in References [33,34] is efficient in terms of resource utilization because they both use the PoA consensus mechanism. However, other papers mostly used the PoW consensus mechanism, which has the limitations of excessive power consumption and increased resource utilization.

3. Problem Statement

With the rapid advancements made in various fields of life, a huge shift from conventional forms to the latest and most advanced forms is observed. For instance, traditional grids have been transformed into SGs, which solve the issues of load mismanagement and users' participation using two-way communication methods and advanced infrastructures. Previously, the centralized systems were being used to handle various tasks like sharing of data, energy trading, resource sharing, etc. These systems performed well in their respective domains. However, they have the issues of lack of security, trust, and privacy, along with increased costs and a single point of failure. These problems arise due to the vulnerability of the centralized systems to the malicious entities. To tackle these issues, centralized systems are being changed into decentralized systems, which further ensure reduction of vehicles' charging costs, removal of the single point of failure, and minimization of charging time in the vehicular sector. Without a doubt, the decentralized systems have helped a great deal in solving the above-mentioned issues. Still, they face a number of issues, such as lack of increased security or enhanced privacy, absence of trustworthiness, and lack of users' willingness to participate in the VNs, which need to be tackled. The causes of these issues are reliance on intermediate parties, usage of inefficient security protocols, involvement of inexperienced personel, etc. To tackle these issues, blockchain technology is introduced, which has some highly fascinating features like immutability, resistance to tampering, and security.

The concept of the smart city is not new; however, it still requires much work to transform the simpler cities into the smarter ones. A VN is also a major part of a smart city, which is to be made smart, intelligent, and to be powered using RESs. In modern times, vehicles are getting smarter, throttling is getting faster, and infrastructure is becoming more complex. To fully aid the movement of EVs on the roads and to enhance security of the VNs, the first and foremost requirement is the authentication of the vehicles [12]. The vehicles must be authorized before they become part of the network. Once the vehicles are authenticated, they are free to move in the VN without the fear of legal disobedience.

With the drastic increase in the number of vehicles, the issue of data storage also arises. The mobile vehicles communicate with the surrounding vehicles, Roadside Units (RSUs), and CSs, hence generating and sharing a huge amount of data continuously. As a result of this continuous data sharing, issues such as improper data storage and delayed timely response arise, which lead to mismanagement in VNs. The huge and ever-growing increase in the number of vehicles on the roads leads to further issues, such as road congestion and frequent traffic jams. Due to these reasons, road accidents are increasing in number, resulting in the loss of human life in some cases [40]. To further ensure secure and manageable provisioning of information between entities, a decentralized data storage mechanism is required [35]. Furthermore, to decrease the burden of data storage, the data must be filtered and made less redundant. The data filtration will help in solving the issue of data redundancy. Storage of less redundant data improves the efficiency of the overall VN and also solves the issue of delayed response. Due to the rapid migration of people from traditional vehicles to EVs, the need for proficient knowledge of people about the batteries installed within their vehicles is also increasing. Due to the low literacy rates in many countries, the issue of the lack of such awareness is arising. People are less knowledgeable about their vehicles and also about the exact locations of the charging entities, which causes mismanagement in the VNs. Moreover, the lack of knowledge about the methods required to calculate the shortest distance to the nearest charging entities, the time required to cover that distance, and the time required to charge the vehicles leads to burdens on charging entities and irregular flows of energy in the VNs [41]. This further leads to issues like load-shedding and imbalances between energy supply and demand.

To promote users' participation and privacy, incentive provisioning and location privacy are factors that play vital roles. When users are guaranteed that they are being provided with enhanced security and better incentives, they tend to participate actively and without selfishness. However, much work has not been done in providing these two aspects simultaneously; therefore, they demand quick and active attention from the research community [42].

4. Proposed System Model

The proposed blockchain-based VN is comprised of EVs, MVs, CSs, an Authorization Unit (AU), and a TSIU. It covers various aspects, such as authentication of vehicles, charging scheduling of vehicles depending upon distance and charging time calculation, uploading and saving the files related to weather information and road conditions using the IPFS-integrated TSIU along with data redundancy minimization, incentive provisioning based on data credibility and timely responses by vehicles, etc. Moreover, the transaction details of the verified transactions are stored in a blockchain in a distributed manner; copies are kept at every node's end, hence ensuring data integrity, trust, and transparency. Figure 1 shows the proposed system model comprised of all the involved entities. In the figure, different types of charging strategies, i.e., V2V, M2V, and G2V, are given. Moreover, the authorization of new vehicles by the AU is also shown in Figure 1. Along with that, the uploading of data to the RSUs and then to the TSIU and IPFS is also given in the same diagram. Furthermore, the incorporation of blockchain technology in the proposed system model is also shown. The blue arrows used in the diagram show the flow of data between different entities. The stepwise workflow of the proposed system model is given in Section 4.1.
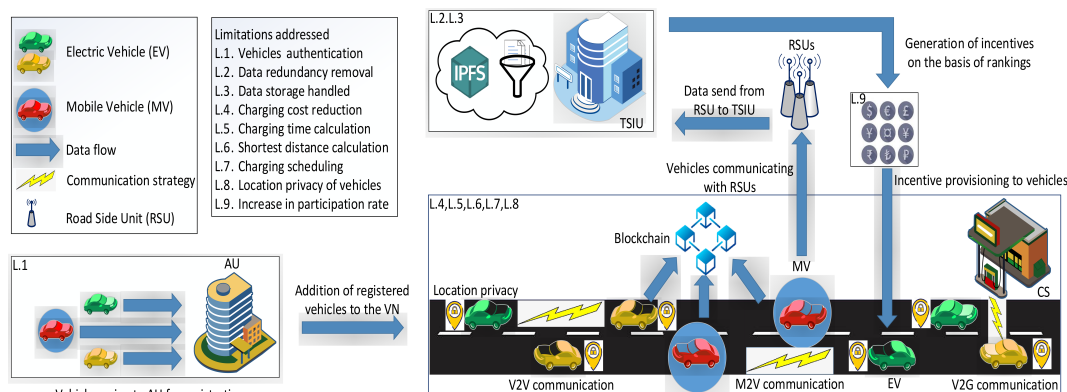
Figure 1. Proposed system model.

The details of the entities involved in charging of vehicles are given below.

- RSUs both store and provide the required information, such as weather conditions, road conditions, congestion and accidents, etc., to the vehicles.
- CSs are the providers of energy/charge to the vehicles. They are situated at certain distances and remain in an active state at all times so that the EVs do not wait for a long time to be charged.
- EVs are the ordinary vehicles; they act as consumers and are powered using electricity. They have batteries installed within, which help to store the charge and keep the vehicles moving. Once the batteries reach a certain level, they need to be charged again. The greater the storage capacity, the greater the distance the vehicles can cover.
- MVs act as prosumers, i.e., they possess the capability of charging themselves using RESs and are capable of providing surplus energy to other neighboring EVs (acting as consumers). When MVs run out of energy and are in need of bulk energy, they send requests to CSs to get energy. Once charged, they are again able to provide energy to EVs moving in that area according to a proper schedule.

Table 2 shows the comparison between the work done in Reference [43] and the proposed work done in this paper. From this comparison, it is inferred that our work is almost 70–80% different from the work done in [43]. Different parameters are considered while carrying out this comparison, such as contributions made, mathematical formulations done, performance parameters chosen, etc.

4.1. Workflow of the Proposed System Model

The workflow of the proposed system model, shown in Figure 1 and discussed in the above section, is given here.

Step 1: Every new incoming vehicle in the network needs to be registered before it can become a part of the network and move freely. This registration is done through the AU, which assigns a pair of public and private keys to the vehicle.

Step 2: After a vehicle becomes a part of the network, it is supposed to send information to the nearest RSUs for storage purposes. This information can be of any type, such weather information, roadside information, or charging selling/buying requests. Meanwhile, the RSUs collect and save the incoming demands and the vehicles' data, keeping a check on the total number of requests being made.

Step 3: As the number of vehicles increases, the amount of information generated and sent to the RSUs also increases. Therefore, the TSIU and IPFS are used to filter the data and reduce data redundancy.

Step 4: When a vehicle needs energy, it broadcasts its request in the network, which includes EVs, MVs, CSs, and RSUs. This request is received by all of the other nearest entities that are part of the network.

Step 5: Upon receiving the request, the RSU decides the best charging entity for the vehicle. For the selection of the charging entity, different factors are considered, such as traveling distance, time taken to cover the distance, etc. The distance between the entities is calculated using the Great-Circle Distance formula.

Step 6: After reaching a suitable charging entity selected by the vehicle, the time required for charging the vehicle is calculated. This time varies with the State of Charge (SoC).

Step 7: After the time required for charging the vehicle is calculated, the total charging cost is calculated, which involves charging cost, distance cost, waiting cost, and reward/penalty cost. All of these costs are summed up to give the final charging cost, which needs to be minimized.

Step 8: The vehicles are also awarded with incentives to increase their participation in the proposed model. The incentives are calculated using reputation values based on two factors: Timely response and credible message delivery. The vehicles with negative reputations are penalized up to a certain threshold value. After that, they are blacklisted and eventually removed from the network.

Table 2. Comparison between work done in [43] and in our paper.

Parameters	Paper [43]	Our Paper
System model	Four major entities are used in the system model, which include agents, EVs, Charging Stations (CSs), and Mobile Charging Vehicles (MCVs). MCVs act as mobile discharging electricity providers in the proposed work	More than four major entities are used in the proposed system model. Agents are replaced by Roadside Units (RSUs) and MCVs are replaced by Mobile Vehicles (MVs) (acting as prosumers)
Blockchain network type	Consortium blockchain is used	Public blockchain is used
Consensus mechanism used	Not explicitly mentioned	Proof of Work (PoW) consensus mechanism is used
Mathematical formulation done	Four different costs are calculated, which are summed to get the total charging cost. Furthermore, user satisfaction is calculated	Distance to the charging entity, time required to travel that distance, time required to charge the vehicles, and time required for data storage are calculated along with four different costs involved in total charging cost
Data used	Real-time data of Beijing are used	Real-time data of four EVs are used
Major contributions	Charging scheduling is done and charging cost is calculated. Furthermore, user satisfaction is also considered. Moreover, a hybrid charging scenario, i.e., Mobile Charging Vehicle-to-Vehicle (MCV2V), is proposed. A double-objective optimization model is used, and an improved algorithm, termed the Non-Dominated Sorting Genetic Algorithm (NSGA), is proposed	Charging scheduling is done and charging cost is calculated. The new charging strategy, i.e., Mobile-Vehicle-to-Vehicle (M2V), is proposed, which is not a hybrid strategy. The data storage issue is solved using the IPFS, in which data is stored after filtration and time for data storage is calculated. Distance to the nearest charging entity and the time taken to cover that distance are also calculated. Furthermore, time taken to charge the vehicles and reputation values are calculated. To promote user participation, an incentive provisioning mechanism is designed and location privacy is also provided.
Performance parameters used	Driving speed, location of charging/discharging entities, time of waiting are used	Gas consumption of smart contracts, mining time taken, and number of hashes generated using blockchain technology are used. Moreover, storage time, traveling time, charging time, reputation values, and charging and traveling costs are also used

Table 3 shows the one-to-one mapping of the identified limitations with the proposed solutions. In the table, the limitations identified and discussed in Section 3 and shown in Figure 1 are referred to

as *L.1–L.9*. The solutions proposed for tackling these limitations are also provided in Table 3 and are referred to as *S.1–S.9*.

Table 3. Mapping of problems with proposed solutions.

Limitation Number	Limitation Identified	Solution Number	Proposed Solution
L.1	Authentication of vehicles	S.1	Authorization Unit (AU) is used to authorize every new incoming vehicle before it becomes part of the network
L.2	Data redundancy removal	S.2	Data filtration is done through the Transport System Information Unit (TSIU), which helps in reducing the data redundancy
L.3	Data storage	S.3	Using the Inter-Planetary File System (IPFS) and TSIU, the data storage issue is solved, as only important and filtered data are saved in the network
L.4	Charging cost reduction	S.4	Mathematical formulation is done to calculate the charging cost and reduce it
L.5	Charging time calculation	S.5	The time taken to charge the vehicles is calculated beforehand to reduce time complexity
L.6	Shortest distance calculation	S.6	The distance between the EV and charging entity is calculated using the Great-Circle Distance formula
L.7	Charging scheduling	S.7	Algorithms are designed to schedule the charging of vehicles
L.8	Location privacy	S.8	Location privacy is achieved using the AES128 encryption scheme
L.9	Lack of user participation	S.9	Users are given incentives to increase their interest and participation in the proposed work

4.2. Authentication of Vehicles

Figure 2 shows the authentication process of the vehicles, which was motivated by [44]. First of all, the new vehicles are directed towards the AU for registration. The arrows pointing towards the AU from the vehicles in Figure 2 show the coming in of new vehicles. The AU assigns unique identity key pairs to the vehicles, consisting of a private key and a public key. The personal data of vehicles are linked and accessed using the private key, whereas the public key is used when the request is to be made in the network. The AU signs every new incoming vehicle digitally using some sort of encryption technique and ensures the security of the vehicles and the network. Only the vehicles with the pair of keys are able to join the network and share information with other vehicles.

4.3. TSIU

The TSIU ensures the reliable transfer of information between the vehicles and the charging entities in a two-way communication manner. The pairs of keys assigned to the vehicles are digitally signed through the AU. The TSIU provides vehicles with various types of information, e.g., the weather conditions, the road congestion information, the locations of the CSs, etc. The vehicle users then decide upon what should be the optimal time and route for traveling using this information. This also helps to combat the range anxiety issue. The vehicle owners know beforehand how much battery charge and time is required for reaching the required destination so that they will not be in constant worry about the availability of the CSs. Figure 3 gives an overview of the TSIU model used. In the figure, different entities exist, such as EVs, MVs, TSIU, etc. The arrows used in the figure show the sharing of data between vehicles and the TSIU. All of the vehicles moving on the road are capable of sharing the road-related information with the TSIU, such as road conditions, number of vehicles, roadside accidents, etc. The TSIU is also capable of sharing this information with all of the vehicles at all times.

As all vehicles are capable of sending the information to the TSIU, this increases the burden on TSIU. To minimize it, the unwanted data are discarded before being sent to the TSIU. For removal of data redundancy, data filtration is performed by comparing the incoming data strings with the

predefined string templates stored in the TSIU. If they both match, then the incoming data string will be stored in the TSIU. Otherwise, it will be discarded. Once the less redundant data are received by the TSIU, they are sent to the IPFS for further reducing the storage issue.
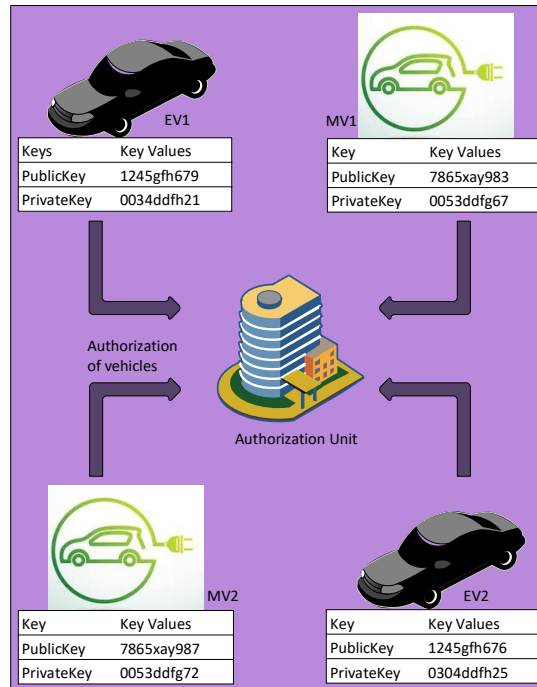

Figure 2. Authentication of vehicles.

4.3.1. IPFS

The vehicles send the information related to weather and road conditions to the TSIU, where this information is stored in the IPFS in a Distributed Hash Table (DHT). The IPFS helps in storing data in a secured distributed manner [45]. The hashes are assigned to each incoming file, and are then forwarded to the blockchain network. Whenever a new vehicle needs some information, it provides the hash to the TSIU, where it is matched with the existing hash. If the hashes are matched, then the information is provided to the vehicle. Otherwise, the request is regarded as fake. Once the information is provided to the network, the blockchain network is updated and a new transaction is stored in a block. The smart contract is written in Solidity and verified in RemixIDE for the IPFS. The main functions involved in the IPFS are: *Add road file, add weather file, get file count, get file ID*, and *assign malicious state*. The first two functions, i.e., *add road file* and *add weather file*, are for storing the files in the IPFS, and have maximum gas consumption. The other functions perform small tasks only; e.g., *get file count* gives the total number of files uploaded to the IPFS, *get file ID* gives the vehicle's ID for a specific file, and *assign malicious state* checks for the malicious status of a vehicle. Therefore, these functions have minimum gas consumption. Figure 4 shows the sequence diagram of the IPFS. However, Algorithm 1 gives the working of the IPFS in the TSIU.

4.4. Location Privacy

In the proposed system model, the location of the vehicles is not shared with other entities in order to increase the vehicles' privacy. This privacy is achieved using the AES128 encryption technique. The actual location of the vehicle in the network is only known to the vehicle authorized by it. Whenever any unauthorized vehicle wants to know the actual location of another vehicle, it first has to get itself authorized by that vehicle. Without authorization, it will only get an encrypted alphanumeric string,

which is almost impossible to decrypt. This location privacy solves the issue of users' hesitance to communicate with other vehicles.

Algorithm 1: Algorithm of IPFS

---

1 Initialization
2 **Inputs:** Weather information file, road condition information file
3 **Output:** Hash for the uploaded file
4 **for** *(Each vehicle, vehicle = 1, ..., n)* **do**
5   Checks for the authorization of the vehicle
6   **if** *Vehicle is authorized* **then**
7   Accepts the information
8   **else**
9   Denies the information and assigns malicious state to the vehicle
10   **end**
11   **end**
12 **end**
13 **for** *Files uploaded by authorized vehicle* **do**
14   Stores the information in the DHT
15   Assign hash to each file stored in the IPFS
16   Sends the hash value to the blockchain
17 **end**
18 **for** *Each new incoming file retrieval request* **do**
19   Checks for the hash of the file provided by the vehicle
20   **if** *Hash is verified* **then**
21   Provides the file
22   **else**
23   Denies the request
24   **end**
25   **end**
26 **end**
27 End
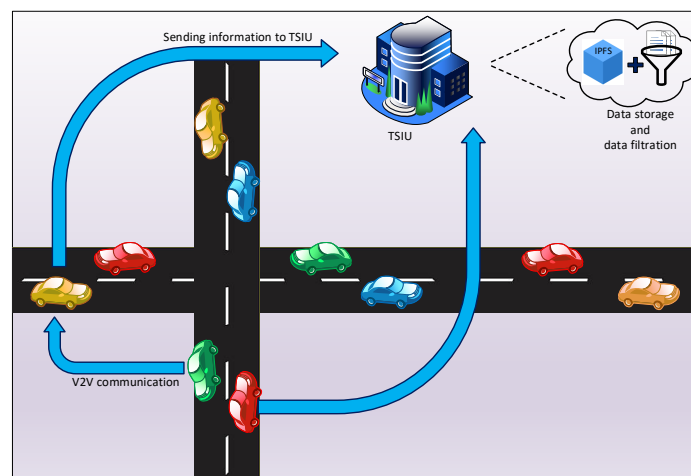
Figure 3. TSIU Model.
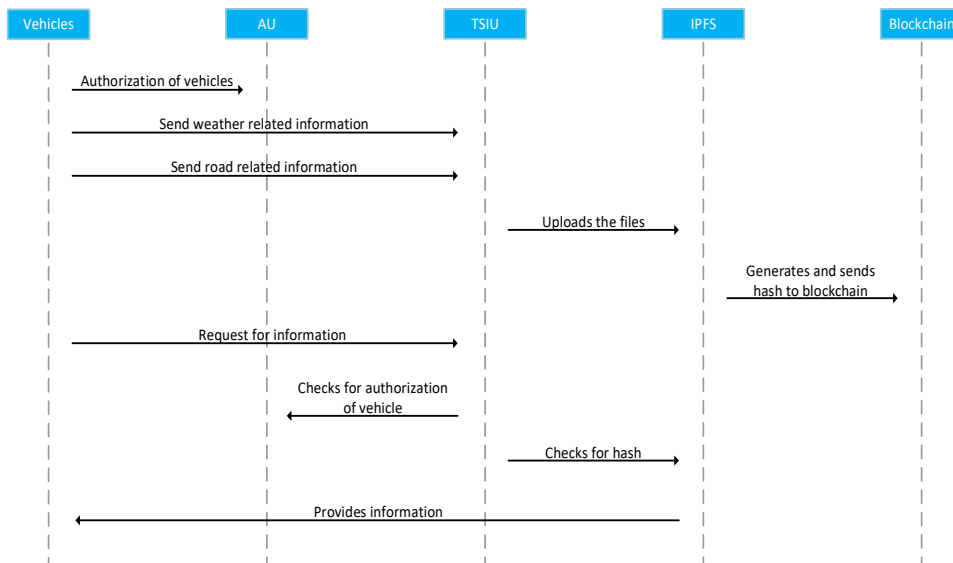
Figure 4. Sequence diagram of the IPFS.

5. Charging Schedule

In this section, the charging schedule of the EVs is discussed. It is important to ensure that the EVs added in the proposed blockchain-based network should have a proper scheduling scenario. For calculation purposes, real-time data are taken from the Electric Vehicle Database [46] and are given in Table 4.

Table 4. Real-time data of EVs.

Manufacturer	Model	Top Speed (kph)	Charging Time (hours)	Battery Capacity (kWh)
BMW	i3	150	4–5	42.2
Kia	e-Soul	156	6–7	42
Nissan	Leaf	144	11–12	40
Volkswagen	e-Golf	150	5–6	35.8

5.1. Scheduling of Vehicle Charging

Figure 5 shows the charging of an EV in three different sources, i.e., using an MV, using another EV, and using a CS. The charging source of the EV is decided by the EV according to the distance and price relationship. If the distance between the EV and the charging source is large, then the price will automatically be high. So, the EV will discard that source and go for the next nearest charging source.
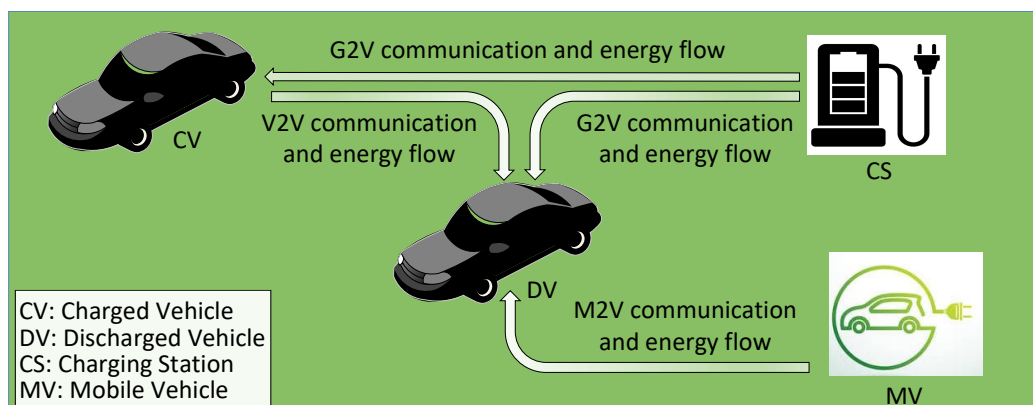
Figure 5. Charging process of an EV using different sources.

5.2. Great-Circle Distance

In this subsection, the distance between vehicles, CSs, and MVs is calculated. This distance calculation is very important for the selection of the entity for charging purpose. This formula gives the shortest distance between two points on a spherical surface. The inputs are the longitude and the latitude values for two different locations. The output is the distance between the provided locations in terms of kilometers or miles [47]. Great-Circle Distance is used in this work because it gives the spherical distance between two entities located on the circumference of the circle. In our work, we set a threshold of 50 km for the selection of the charging entity by an EV. If the charging entity lies outside the 50 km radius, then it will not be selected. Algorithm 2 gives the algorithm for shortest distance selection using Great-Circle Distance. In the algorithm, lines 4–12 record the geographical coordinates of the EVs, MVs, and CSs, respectively. After recording the coordinates, line 13 calculates the distance between an EV and MV, an EV and CS, and an EV and another vehicle using the Great-Circle Distance formula. Furthermore, the conditional statements, e.g., the nested-if loop given in lines 14–26, help in determining the shortest distance.

Algorithm 2: Algorithm for shortest distance selection using the Great-Circle Distance.

---

1 Initialization
2 **Inputs:** EV_{long}, EV_{lat}, MV_{long}, MV_{lat}, CS_{long}, CS_{lat}
3 **Output:** Shortest distance calculation
4 **for** *EV* **do**
5   Take its longitude and latitude values as EV_{long} and EV_{lat}, respectively
6 **end**
7 **for** *MV* **do**
8   Take its longitude and latitude values as MV_{long} and MV_{lat}, respectively
9 **end**
10 **for** *CS* **do**
11   Take its longitude and latitude values as CS_{long} and CS_{lat}, respectively
12 **end**
13 Find distances between vehicle and MV (dis_{M2V}), vehicle and CS (dis_{S2V}), and vehicle and EV (dis_{V2V}) using respective coordinates
14 **if** $dis_{M2V} < dis_{S2V}$, $dis_{M2V} < dis_{V2V}$ *and* $dis_{V2V} < 50km$ **then**
15   Select the distance between vehicle and MV as the shortest distance
16 **end**
17 **else**
18   **if** $dis_{S2V} < dis_{M2V}$, $dis_{S2V} < dis_{V2V}$ *and* $dis_{S2V} < 50km$ **then**
19   Select the distance between vehicle and CS as the shortest distance
20   **end**
21 **end**
22 **else**
23   **if** $dis_{V2V} < 50km$ **then**
24   Select the distance between vehicle and EV as the shortest distance
25   **end**
26 **end**
27 End

5.3. Calculation of Time Taken for Covering the Distance

In this subsection, the total time taken by a vehicle for traversing the distance to the nearest charging entity, obtained using the Great-Circle Distance formula, is calculated. For this calculation, real-time data of four different EVs are used. The time taken by the vehicle for traversing the distance is

given in minutes using Equation (1). The time taken for covering the distance is calculated by dividing the total distance between an EV and the nearest charging entity by the average speed of that EV.

$$Total\ time\ taken = \frac{Total\ distance}{Average\ speed} \tag{1}$$

5.4. Calculation of Time Taken for Charging the Vehicles

In this subsection, the time taken for the charging of the vehicles is calculated. For calculation of the charging time, we make use of the real-time data given in Table 4. The time taken for charging the vehicles is taken in hours and is calculated using Equation (2).

$$Total\ charging\ time = \frac{Battery\ capacity}{Charging\ power} \tag{2}$$

5.5. Charging Scheduling Algorithm

Algorithm 3 gives the charging schedule and cost calculation of the vehicles. Line 1 initializes the algorithm, whereas lines 2 and 3 are for declaring the inputs and the output. Line 4 finds the total number of vehicles present in the network. After finding the total number of vehicles, lines 5–13 calculate the SoC values of the vehicles to check which vehicles need charging and at what percentage. After that, lines 14–26 select the charging entity on the basis of distance.

Algorithm 3: Algorithm of Charging Schedule

---

1 Initialization
2 **Inputs:** Vehicles, EV, MV, CS, dis_{S2V}, dis_{M2V}, dis_{V2V}
3 **Output:** EV charging schedule and cost calculation
4 Find the number of registered vehicles
5 **for** *Each vehicle, vehicle = 1, ..., n* **do**
6   Find State of Charge (SoC) of the vehicles
7   **if** *(Vehicle is discharging)* **then**
8   SoC = 1
9   **else**
10   SoC = 0
11   **end**
12   **end**
13 **end**
14 **for** *Each vehicle, vehicle = 1, ..., n* **do**
15   Find distance between vehicle and MV (dis_{M2V}), vehicle and CS (dis_{S2V}), and vehicle and
       EV (dis_{V2V})
16   **if** *($dis_{M2V} \leq \tau$)* **then**
17   Charge vehicle through MV
18   **else**
19             $dis_{V2V} \leq \tau$
20   Charge vehicle through EV
21   **end**
22   **else**
23   Charge vehicle through CS
24   **end**
25   **end**
26 **end**
27 End

---

6. Mathematical Formulation

This section provides the mathematical formulations of the calculations of the total charging cost and of the objective function in Sections 6.1 and 6.2, respectively.

6.1. Charging Cost Calculation

The total charging cost is calculated by calculating the sum of four individual costs, i.e., charging cost, distance cost, waiting cost, and reward/penalty cost, motivated by [43]. These costs are denoted as C_{1T}, C_{2T}, C_{3T}, and C_{4T}, respectively. These costs are given in Equations (3)–(6).

The first cost is the total charging cost for CSs, EVs, and MVs. P_{CS}, P_{MV}, and P_{EV} are the generation costs per unit for CSs, EVs, and MVs, respectively, whereas C_{CS}, C_{MV}, and C_{EV} are the energy selling costs for CSs, EVs, and MVs, respectively. The product of generation cost with the selling cost provides a complete cost of an entity; when the costs of all three entities are added up, the total charging cost is given, as shown in Equation (3).

$$C_{1T} = (P_{CS} * \sum_{i=1}^{I} C_{CS_i}) + (P_{MV} * \sum_{j=1}^{J} C_{MV_j}) + (P_{EV} * \sum_{k=1}^{K} C_{EV_k}) \tag{3}$$

After calculating the charging cost, the next cost that needs to be calculated is the distance cost. This cost is related to the distance between the charging and discharging entities. The main objective of the vehicles is that they should be charged using their closest entities, either using the CSs, MVs, or other EVs. Equation (4) calculates the total distance cost, where dis_{S2V}, dis_{M2V}, and dis_{V2V} give the distance from vehicle to CS, vehicle to MV, and vehicle to EV, respectively.

$$C_{2T} = (P_{CS} * dis_{S2V}) + (P_{MV} * dis_{M2V}) + (P_{EV} * dis_{V2V}) \tag{4}$$

The third cost, i.e., the waiting cost, also needs consideration. This cost is incurred when the vehicle needs to wait at the time of charging. For instance, a vehicle goes to the CS for charging. At that CS, a number of vehicles are already present for charging purposes. Therefore, this new incoming vehicle is added to the waiting queue. This is also implied even when the vehicle intends to be charged by the MV or the EV. So, for calculating this cost, the distance is calculated, and is then multiplied with the number assigned to the vehicle in the queue. This cost calculation is given in Equation (5).

$$C_{3T} = \left((dis_{S2V} * diff(V, v)) * \left(\sum_{y=1}^{Y} Ve_y + \sum_{z=1}^{Z} Vm_z \right) \right) \tag{5}$$

The fourth cost is the reward/penalty cost. If a certain vehicle saves some units of charge or if it generates some extra units that it can sell to other vehicles, then the particular vehicle is given some reward, and vice versa. Equation (6a), Equation (6b) show the reward and penalty calculations. In the given equations, Q is the price per unit, T_s are the total units saved, and T_w are the units wasted; ev and mv are the numbers of EVs and MVs, respectively.

$$C_{4Tr} = (Q * T_s) * \left(\sum_{l=1}^{L} ev_l + \sum_{m=1}^{M} mv_m \right) \tag{6a}$$

or

$$C_{4Tp} = -(Q * T_w) * \left(\sum_{l=1}^{L} ev_l + \sum_{m=1}^{M} mv_m \right) \tag{6b}$$

Equations (3)–(6) are all summed up to calculate the total cost, as given in Equation (7).

$$C_{Total} = C_{1T} + C_{2T} + C_{3T} + C_{4Tr/4Tp} \tag{7}$$

6.2. Objective Function

The total charging cost is minimized using Equation (11), which is the objective function [43].

$$min\ (C_{Total}) = C_{1T}\ +\ C_{2T}\ +\ C_{3T}\ +\ C_{4T} \tag{8}$$

It is subject to following constraints:

- Minimizing the EV and MV charging costs, as given in Equation (9a), Equation (9b).

$$0 \leq C_{MV} \leq C_{MV}^{max} \tag{9a}$$

$$0 \leq C_{EV} \leq C_{EV}^{max} \tag{9b}$$

- The other is maximizing the units saved or minimizing the units being wasted, as given in Equation (9c).

$$max\ (T_s)\ or\ min\ (T_w) \tag{9c}$$

6.3. Comparison of Equations

In this subsection, the comparison between the existing equations [43] and our proposed equations is given in a tabular form. This comparison helps the reader to understand which changes have been made to the previous equations, which help in further reducing the total charging cost. Table 5 gives the comparison of Equations (3)–(9c). In the first column, the Equations used in [43] are given. The Equations used in our paper are given in the second column. In the third column, the differences between the equations are given.

7. Power Flow and Associated Losses

In the charging of EVs, efficient energy flow plays an important role. This is because EVs may pose serious economical impacts if not charged properly. The major reason behind this economic disturbance is the ultimate loss that is incurred while charging EVs [48]. This loss is further comprised of different losses that occur due to inefficiency of inverters, worn and outdated infrastructure, weather conditions, etc. These losses occur in all types of charging strategies, like V2G, V2V, and M2V. These losses not only pose economic concerns, but also lead to degradation of the lifetime of the batteries installed within the vehicles [49]. The amounts of the economic losses incurred in the V2G are the maximum, while they are minimum in M2V. The reason is because V2G uses conventional fuels for charging vehicles, whereas M2V uses RESs, due to which both the financial and the infrastructural losses are minimized. Figure 6 shows different types of losses incurred in VNs, termed Loss 1, Loss ,2 and Loss 3. Loss 1 is cable loss, which occurs due to the usage of old and worn cables. Loss 2 and Loss 3 are the losses that occur due to inverters' inefficiencies and severe weather conditions, respectively.

7.1. Formulating the Associated Energy Losses

In this subsection, the energy losses associated with the charging of vehicles are formulated along with the parameters they rely on. Equation (10) is used for calculating the Total Power Loss (P_{loss}^{total}) incurred while charging the vehicles.

$$P_{loss}^{total} = (L_{cable} * I_t) + \overline{\eta_{inverter}} + \omega, \tag{10}$$

Table 5. Comparison of equations.

Paper [43]	Our Paper	Difference
$L_1^j = l_s \sum_{m=1}^N s_{jn} + l_m \sum_{r=1}^R m_{jr} + l_d \sum_{k=1}^K d_{jk}$	$C_{1T} = (P_{CS} * \sum_{i=1}^I C_{CS_i}) + (P_{MV} * \sum_{j=1}^J C_{MV_j}) + (P_{EV} * \sum_{k=1}^K C_{EV_k})$	These equations are used for calculating the charging cost in both papers. In [43], the prices charged by charging stations, MCVs, and discharging EVs are multiplied by the amount of energy provided by these entities, respectively. However, in our paper, we multiplied the generation cost with the selling cost and then summed all to get the total cost. Hence, the difference lies in that we do not include the amount of energy provided by the entities during calculation.
$L_2^j = \eta \frac{dis_j}{v_j} + l_d \frac{dis_j}{L}$	$C_{2T} = (P_{CS} * dis_{S2V}) + (P_{MV} * dis_{M2V}) + (P_{EV} * dis_{V2V})$	These equations are used for calculating the cost incurred while traveling, known as the distance cost. In [43], this cost is calculated considering the distance to travel and the time taken to cover that distance. In this paper, this cost is calculated in terms of generation costs and the distance to travel. Hence, the difference is that we are not considering the time in this equation.
$L_3^j = \sum_{z=1}^Z \alpha (Z-z) \frac{V_{jz}}{v_z^c}$	$C_{3T} = \left((dis_{S2V} * \text{diff}(V\nu)) * \left(\sum_{y=1}^Y Ve_y + \sum_{z=1}^Z Vm_z \right) \right)$	This equation is used to calculate the waiting cost while the vehicle waits to be charged. In [43], this cost is calculated as a product of waiting cost and the difference between the number of a specific vehicle and the total number of vehicles. This equation includes the waiting times of all the entities involved and then takes their aggregate. Hence, the difference is that, previously, this equation only involved a single entity, while currently, it involves all types of entities.
$L_4^j = \phi e_j$	$C_{4Tr} = (Q * T_s) * \left(\sum_{l=1}^L ev_l + \sum_{m=1}^M mv_m \right)$ or $C_{4Tp} = -(Q * T_w) * \left(\sum_{l=1}^L ev_l + \sum_{m=1}^M mv_m \right)$	This equation is used to calculate the amount of reward given to the nodes. In [43], only the reward is calculated on the basis of verified transactions. In our case, the reward and penalty are both calculated, which restricts the nodes from malicious activities.
$L_{cj} = L_1^j + L_2^j + L_3^j + L_4^j$	$C_{Total} = C_{1T} + C_{2T} + C_{3T} + C_{4T}$	This equation is the same in both papers, as it only aggregates the equations given above into one equation.
$\min (L_{cj}) = L_1^j + L_2^j + L_3^j + L_4^j$	$\min (C_{Total}) = C_{1T} + C_{2T} + C_{3T} + C_{4T}$	This equation gives the objective functions of both papers. It is similar in both papers because they both aim at reducing the overall charging cost.
$0 \le m_{jr} \le m_r^{max}, 0 \le d_{jk} \le d_k^{max}, c_j^{min} \le e_j \le c_j^{max}$ and $0 \le s_{jn}$	$0 \le C_{MV} \le C_{MV}^{max}, 0 \le C_{EV} \le C_{MV}^{max}$ and $\max (T_s)$ or $\min (T_w)$	These are the constraint equations for the objective function. These are almost same, except that, in our paper, the numbers of units saved or wasted are also considered as constraints for the objective function.
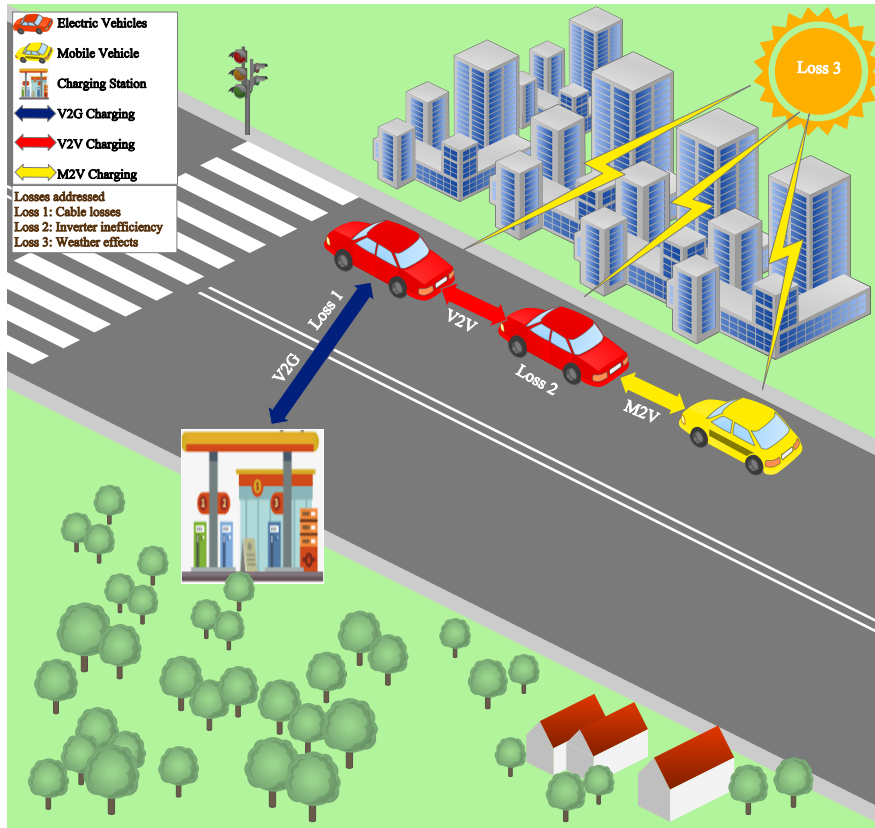
Figure 6. Energy losses in Vehicular Networks (VNs).

where, L_{cable} denotes the cable length, and I_t shows the current passing through the cable at time t. $\overline{\eta_{inverter}}$ represents the inefficiency of an inverter installed within a vehicle and ω denotes the weather effects on the charging process. The ranges of these parameters are given in Table 6. The value of $\overline{\eta_{inverter}}$ depends on the life cycle of the vehicle's battery, while the value of the weather effect coefficient ω depends on the effects caused by weather conditions, i.e., its value is 0 when there is no effect, while the value is 1 in the case of severe weather effects.

Table 6. Parameters and their values.

Parameter	Values
L_{cable}	1–5 m
I_t	16–32 Amperes
$\overline{\eta_{inverter}}$	0–40%
ω	0–1

The objective function is formulated to minimize the P_{loss}^{total}, given in Equation (11). The objective function can be achieved using updated and efficient cables, inverters, batteries, etc., and by increasing the insulation to protect the devices against severe weather effects.

$$Objective\ Function = min(P_{loss}^{total}) \tag{11}$$

This is subject to the constraints provided in Equations (12a)–(12d).

- The length of a cable used for charging the vehicles should lie within a specific range, given in Equation (12a). If a longer cable is used, then the power losses will be greater, and vice versa [50].

$$0 < L_{cable} \leq 5m \tag{12a}$$

- The current supplied at a certain time t should lie within a specific range, taken from [51] and given in Equation (12b).

$$16 Amp \leq I_t \leq 32 Amp \tag{12b}$$

- The inefficiency of an inverter installed within a vehicle should not be greater than a certain limit, given in Equation (12c). There exists a direct relation between the inefficiency of an inverter and the power losses [52].

$$0 \leq \overline{\eta_{efficiency}} \leq 40\% \tag{12c}$$

- The charging infrastructure should not be affected by weather conditions to a great extent. Equation (12d) gives the value of the weather effect coefficient, i.e., ω.

$$0 \leq \omega < 1 \tag{12d}$$

Moving ahead, the losses that occur in the aforementioned strategies are discussed according to case. Cases 1–3 discuss the energy losses in V2G, V2V, and M2V, respectively. The discussions of these cases, along with the mathematical equations, are given below.

- **Case 1: Energy Losses in V2G**

  In this case, the losses incurred in V2G charging of vehicles are discussed. In V2G, maximum economic losses occur, while the power losses are less as compared to the V2V charging strategy. The reason for the maximal economic losses is the usage of conventional fuels in the charging stations. The power losses incurred in V2G are calculated using Equation (10).

- **Case 2: Energy Losses in V2V**

  In V2V charging of vehicles, the maximum amount of power losses occurs. The reason is increased amount of inefficiency of the inverters [52]. Energy trading is done between two vehicles, both equipped with energy inverters; therefore, the inverter inefficiency will be squared, i.e., $\overline{(\eta_{inverter})}^2$. Equation (13) is used to calculate the power loss incurred in V2V charging of vehicles.

$$P_{loss}^{total} = (L_{cable} * I_t) + (\overline{\eta_{inverter}})^2 + \omega \tag{13}$$

- **Case 3: Energy Losses in M2V**

  In M2V, we have the minimum amounts of both economic and power losses. The primary reason is that the Mobile Vehicles (MVs) make use of RESs to generate electricity and have the ability to store and provide the surplus amount of energy to other EVs. The power loss incurred in the M2V charging strategy is calculated using Equation (13).

8. Incentive Provisioning

In the proposed model, the EVs with high message credibility and good timely responses are given reputation and incentives to motivate them further. On the other hand, the EVs that act maliciously or that have low message credibility are penalized. The degree of the penalty is more than the degree of reward given to the vehicles to restrict them from acting maliciously or selfishly. The reputation and incentives are provided on the basis of the following two conditions.

- The vehicles should respond to other vehicles or RSUs in a predefined time. In our case, this value is set to be 15 s.
- The messages delivered by the vehicles should be credible, i.e., having only predefined identities in the message string. The messages with vehicle ID, locations of events, status of events, and times of event occurrence are considered credible.

The vehicles delivering authentic messages are given a reputation value of +1 and are awarded with \$1 as an incentive, whereas the vehicles broadcasting fake messages are given a reputation value

of −1 and penalized $1.5. At the beginning, all vehicles are given equal reputation values. The vehicles that continuously broadcast fake messages are finally blacklisted after their reputation value reaches −1. Figure 7 shows the flowchart of the rewards and penalties incurred by the vehicles.
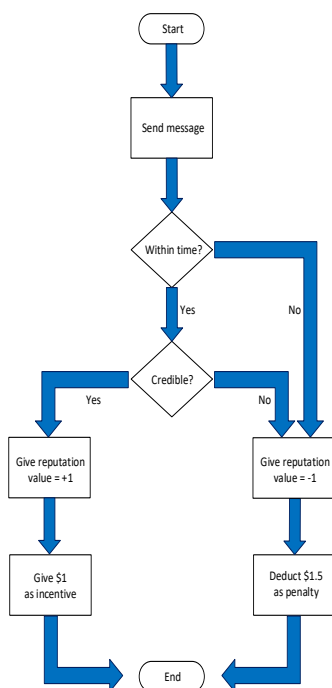
Figure 7. Flowchart of rewards/penalties incurred by vehicles.

9. Results and Discussion

This section covers the simulation results and their discussion.

9.1. Simulation Environment

The simulations are performed in two different environments: Solidity in Visual Studio Code and RemixIDE. Solidity is used for writing smart contracts and is provided by Ethereum. The connectivity of smart contracts with the web interface is done using MetaMask. To log into MetaMask, accounts with digital currency are required. These accounts are provided by Ganache. The smart contracts cover the registration of the vehicles and the nature of the requests being made: Requests accepted and requests denied. In the later stage, the charging schedule was done in Spyder (Python 3.6 package), provided by Anaconda. These simulations were performed on HP 450G ProBook with a 1 TB hard drive and 8 GB RAM.

9.2. Simulation Parameters

Table 7 shows the average values of different simulation parameters that were used in the proposed work. These values are taken from the Electric Vehicle Database [46].

Table 7. Simulation parameters.

Parameters	Values
Battery capacity of an EV	40–45 kWh
Charging time of an EV	6–8 h
Electricity price	10–14 cents/kWh
Maximum number of vehicles in a queue	10
Threshold distance for MV	10 km

Initially, when the smart contract was made and deployed, the transaction and execution costs were calculated. These costs are calculated in terms of 'gas'. Table 8 shows the values of Ether and its multipliers. These values are taken from [53].

Table 8. Values of Ether and its multipliers.

Multiplier	Name
10^0	Wei
10^{12}	Szabo
10^{15}	Finney
10^{18}	Ether

Figure 8 shows the transaction and execution costs in terms of gas for five different functions. These are some of the functions used in the smart contract deployed for vehicles' registration and charging scheduling. It is seen that the function "EV registration" incurs the highest gas consumption, as it is the major function that assigns details to all new EVs added to the system. Similar behavior is observed for "MV registration", the function designed to add new MVs to the network. The transaction costs are always higher than the execution costs because the former costs are linked with the deployment of the contract, whereas the latter costs are incurred while executing a specific function.

Figure 9 shows the comparison between the time taken to store the redundant information and the time taken to store the filtered information in the TSIU. A vivid difference is seen in the aforementioned times. Along with time reduction, the storage burden on the TSIU is also decreased. The data with more than the predefined number of entities, i.e., ID of the vehicle, location of the vehicle, time of reporting, and nature of the event that occurred are discarded, as more data entities will increase the storage burden on the TSIU.

Figure 10 shows the cost comparison between the transaction cost and the execution cost when a vehicle uploads the weather information and road information to the TSIU. The graph shows the gas consumption for five different functions, which are included in the smart contract. It is seen that the gas consumptions of *add weather file* and *add road file* are greater in comparison with other functions. The reason is that these files consist of all of the weather-related information and the road-related information.
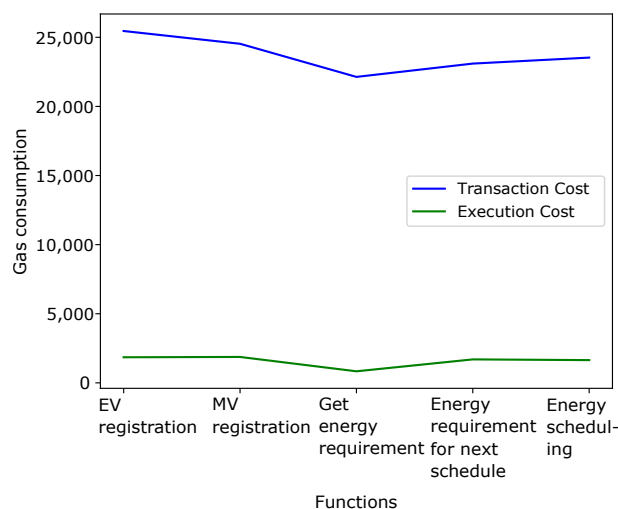
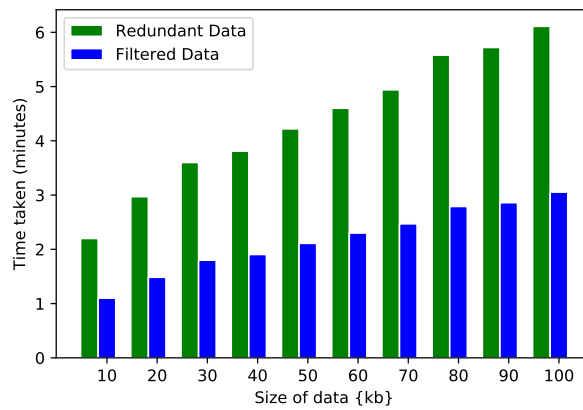**Figure 8.** Gas consumption for EV registration and charging schedule.

Figure 9. Storage time comparison of redundant and filtered data.
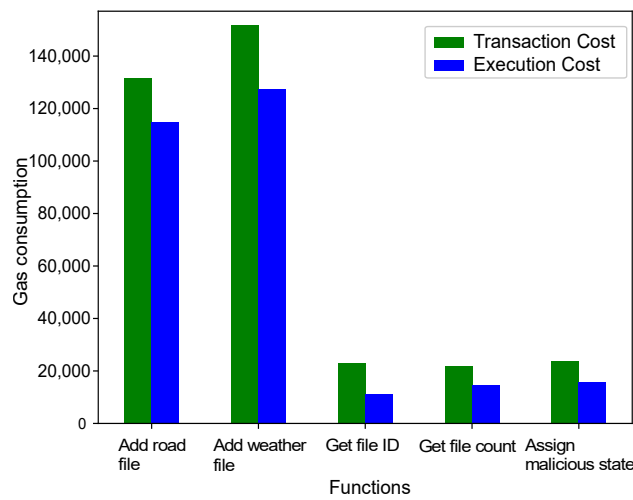
Figure 10. Gas consumption for the IPFS.

Figure 11 shows the average payments and rewards of the charging and discharging EVs. A comparison was done between the existing techniques and the proposed techniques. This graph was motivated by [54]. The graph shows that the costs are reduced as compared to the existing work due to the scheduling algorithm proposed in this paper. The graph also shows that the convergence rate for both the payments of charging EVs and rewards of discharging EVs are fast in comparison with the existing techniques.

Figure 12 shows the charging price and the traveling price of G2V, V2V, and M2V. It is observed that both the charging price and the traveling price are less for the proposed technique, i.e., M2V. This is because, when charging through the CSs, waiting cost and distance cost are also incurred by the vehicles. On the other hand, charging through the EVs incurs the distance cost along with the charging cost of the EVs through CSs. MVs, on the other hand, have lower charging costs because they are equipped with batteries and are self-charged. So, the major cost that exists in M2V is the distance cost. Figure 12 shows the increasing trend with the increasing number of vehicles. The traveling cost consists of fuel costs, maintenance costs, etc.

The time taken by the EVs to be charged is shown in Figure 13. In the figure, real-time data of four different EVs are used, as given in Table 4 in Section 5.3. The charging time is calculated using Equation (2). It is observed from the figure that the time taken to charge the Nissan Leaf is the maximum, as it has the slowest charging speed of all of the vehicles. All EVs are charged using Type-2 chargers, which allow the vehicles to be charged both from single-phase and three-phase main supplies.

Figure 11. Average payments.

Figure 12. Cost comparison of different scenarios.
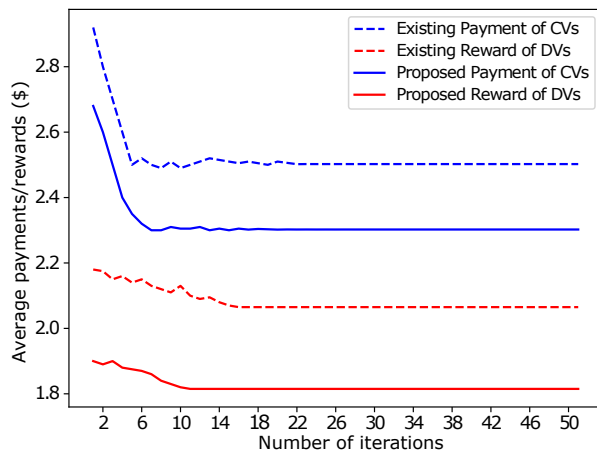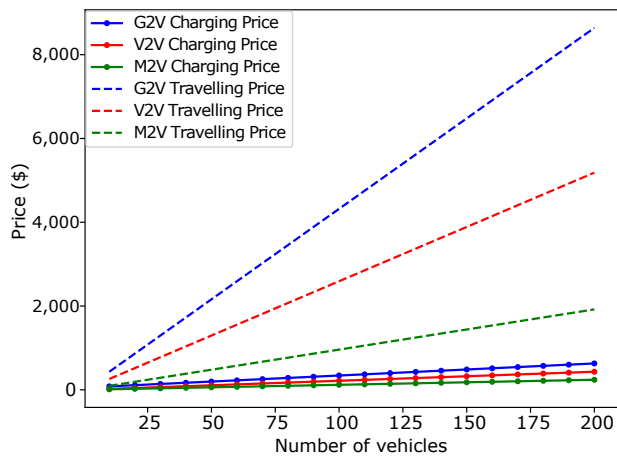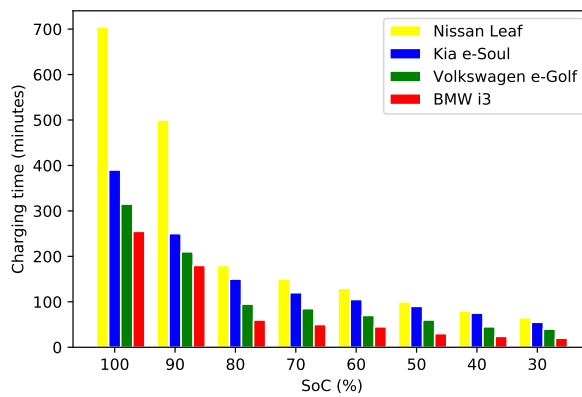

Figure 13. Charging times taken by EVs.

Figure 14 shows the time taken by four different vehicles to cover the distance to the nearest charging entities. For this time calculation, real-time data of four different EVs are used, which are given in Table 4 in Section 5.3. This time is calculated using Equation (1).
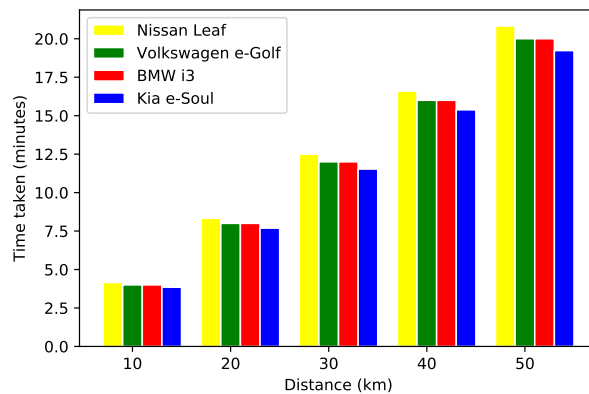
Figure 14. Time taken by EVs to traverse the distance to the nearest charging entity.

The real-time power losses incurred in all three charging strategies, i.e., V2G, V2V, and M2V are shown in Figures 15–18. The comparison of cable losses incurred in the aforementioned charging strategies is shown in Figure 15. It is observed that the cable loss incurred in V2G is the maximum because it also includes the transformer loss along with other losses, like copper loss, hysteresis loss, etc.
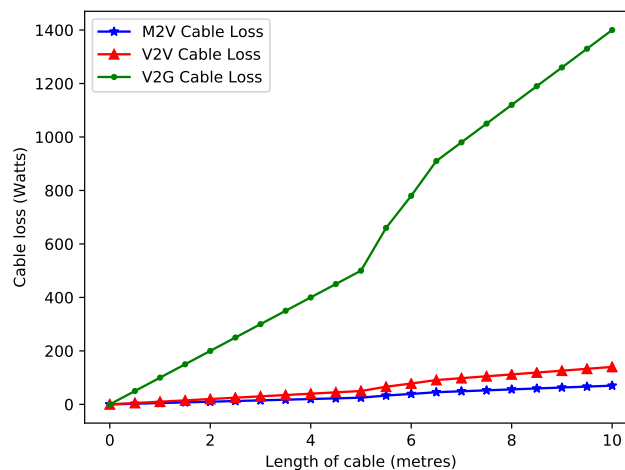
Figure 15. Cable losses incurred.

Figure 16 shows the comparison between the inverter losses of V2G, V2V, and M2V. It is seen that the inverter losses are the greatest for both V2G and M2V because, in these strategies, two inverters are involved simultaneously, which means that the inverters' inefficiencies will be squared.

Moving on, the third type of loss incurred in vehicle charging is due to the effects caused by weather conditions. The comparison between these losses is given in Figure 17. It is observed that the weather losses are the most in V2G because it also involves the weather effects on other devices, such as transformers, circuit breakers, etc.

In Figure 18, the combined losses for the three different strategies are given. The total combined loss involves the cable loss, inverter loss, and loss caused by sever weather effects. It can be seen that V2V has the maximum amount of incurred losses, mainly due to the increase in inefficiency of the inverters.

Figure 19 shows the participation rates of users with the increase in the reputation values, which in turn increases the amount of incentives awarded. These reputation values are given on the basis of timely responses of credible messages. In accordance with these, monetary incentives are given. On the contrary, the incentives are converted into penalties upon false reputation values and are deducted

from users' wallets. The amount of the penalty charged is more than the incentive given to users. This difference in amount restricts the users from acting maliciously.

Figures 20 and 21 show the number of hashes generated and the mining time for the transactions performed against different difficulty levels. It is observed that both the number of hashes generated and the mining time taken increase with the increase in difficulty level. Difficulty is defined as the measure of the complexity for miners to find a hash or a signature for a block in the network. The hash is generated using random numbers. The number of zeros that a signature requires initially determines the difficulty level. The formula for calculating difficulty is given in Equation (14), taken from [55].

$$difficulty = \frac{Hash\ target_{(genesisblock)}}{Hash\ target_{(currentblock)}} \tag{14}$$

where the target is a 256 bit number. The hash target becomes smaller and smaller, thereby making the difficulty greater.

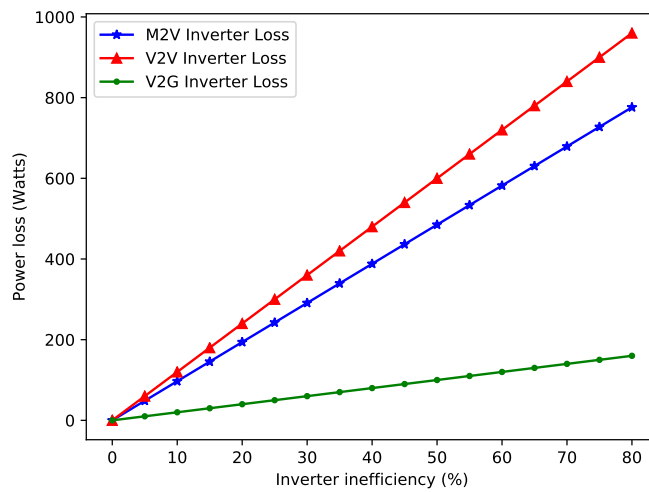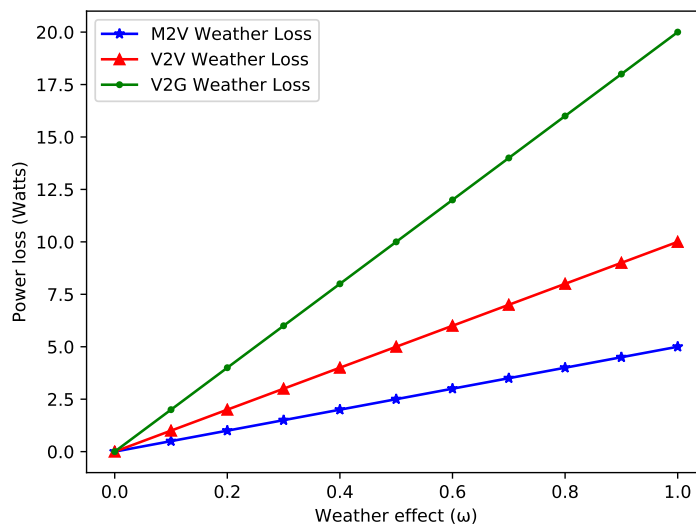**Figure 16.** Inverter losses incurred.
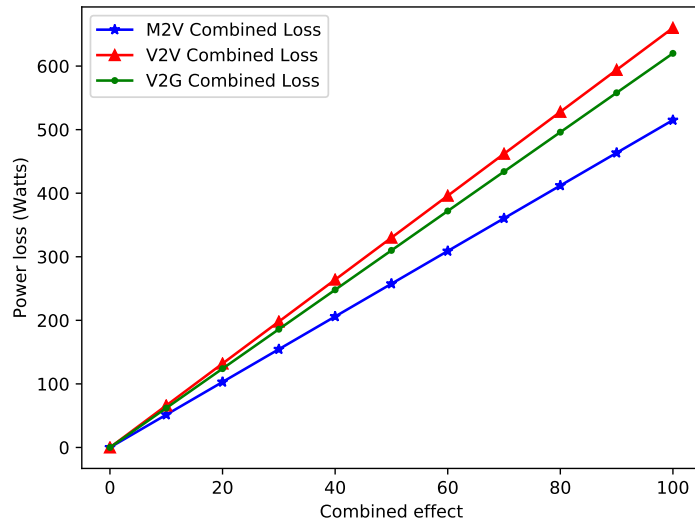

Figure 17. Weather losses incurred.

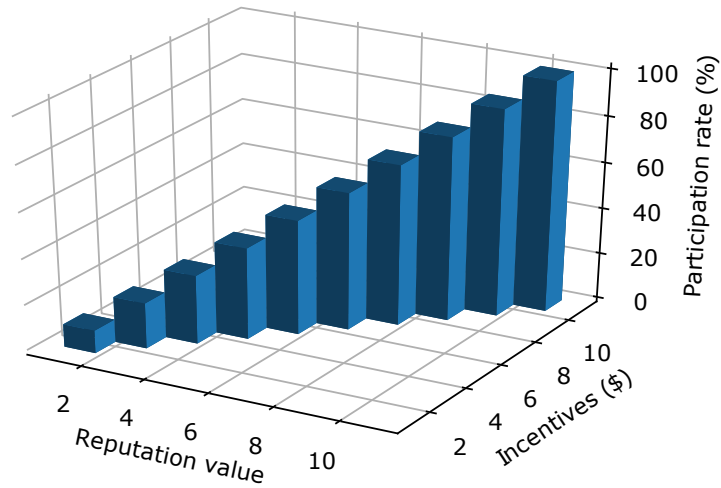**Figure 18.** Combined losses incurred.

Figure 19. Users' participation versus reputation values.
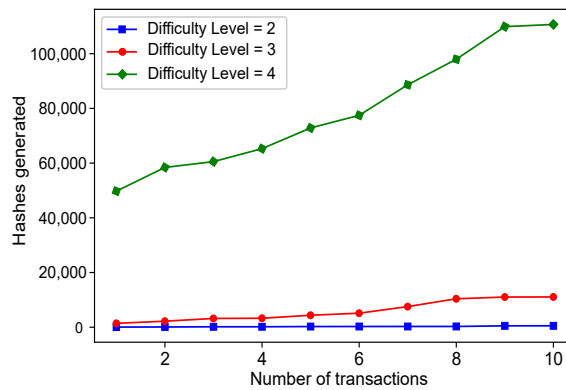
Figure 20. Hashes generated for different transactions.
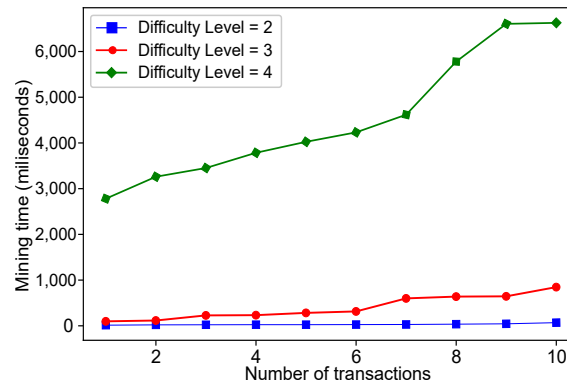
Figure 21. Mining time for different transactions.

Table 9 gives an abstract view of the simulation results given above and maps them with the limitations that they tackle. The limitations identified in Figure 1 and further mentioned in Table 3 are given in Table 9 along with the proposed solutions that are given in Table 3. In the fourth column of Table 9, the validation results are presented and mapped with the identified limitations.

Table 9. Mapping of problems with validation results.

Limitation Number	Limitation Identified	Proposed Solution	Validation Results
L.1	Authentication of vehicles	S.1	No direct validation
L.2	Data redundancy	S.2	To remove data redundancy in the proposed work, data filtration is performed. The comparison between the time taken to store redundant data and filtered data is shown in Figure 9.
L.3	Cost of storing data in the IPFS	S.3	Figure 10 shows the gas consumed while uploading and saving data in the IPFS.
L.4	Charging cost reduction	S.4	Figures 11 and 12 present the cost comparison between different entities. The former shows the difference between reward and payment, whereas the latter shows the difference between three charging scenarios.
L.5	Time taken for vehicles' charging	S.5	The time taken to charge vehicles with different State of Charge (SoC) values is shown in Figure 13.
L.6	Time complexity	S.6	Figure 14 shows the time taken to traverse the distance between a vehicle and the nearest charging entity.
L.7	Charging scheduling	S.7	No direct validation; however, it contributes to the charging cost reduction, which can be seen in Figures 11 and 12.
L.8	Location privacy	S.8	No direct validation; however, the effect can be seen in the increase in participation rate in Figure 19.
L.9	Lack of user participation	S.9	Figure 19 presents a three-dimensional graph relating reputation value, incentives, and the user participation.

Table 10 gives the values of the public key and the private key generated for 10 different vehicles. The public key is open to all the participants of the network, whereas the private key is used only by a specific participant and also for digitally signing the transactions. Table 11 gives all the important details related to the contract creation phase. It is seen that both the execution cost and the transaction cost of contract creation are the greatest because they cover all the functions involved in the smart contract.

Tables 12 and 13 give the details related to the EV and MV registration in the proposed blockchain network. Whenever a new vehicle wants to join the network, it first has to register itself through a central entity. For registration purposes, information consisting of different aspects of a vehicle is required, such as ID, model, make, etc. Moreover, Tables 14 and 15 show the details associated with the scheduling of the energy in the future. Initially, the energy of the current time slot is calculated.

Then, the energy requirement for the next time slot is calculated; finally, energy is scheduled as per the requirements. Table 16 gives the values for the mining time and number of hashes generated

against different difficulty levels in tabular form. In the table, difficulty level is abbreviated as 'Diff. level'. Diff. level 1 is not addressed because it performs transactions in a very short time as compared to other difficulty levels. Difficulty is encountered when mining is performed using PoW. The mining becomes difficult with the increase in the difficulty level. This table makes the comparison between different difficulty levels easy to understand.

Table 10. Keys generated for digital signatures.

Vehicle identity	Public key	Private key
Vehicle 1	04e4c6...47979f	7429f2...886b52
Vehicle 2	04260a...0a95e9	ed9acc...65b48d
Vehicle 3	049b61...bee1ae	35ea24...bf841f
Vehicle 4	047ec6...16a608	24cad1...f49eec
Vehicle 5	04e8a0...9e150f	36aa54...acffac
Vehicle 6	04e4c6...47979f	7429f2...886b52
Vehicle 7	04260a...0a95e9	ed9acc...65b48d
Vehicle 8	049b61...bee1ae	35ea24...bf841f
Vehicle 9	047ec6...16a608	24cad1...f49eec
Vehicle 10	04e8a0...9e150f	36aa54...acffac

Table 11. Contract creation.

Parameter	Value
transaction hash	0x2e104...a93a6
contract address	0x35ef0...450cf
from	0xca35b...a733c
to	EV.(constructor)
transaction cost	998685 gas
execution cost	713861 gas
hash	0x2e104...a93a6
input	0x608...a0029
decoded input	{}
decoded output	–
logs	[]

Table 12. EV registration.

Parameter	Value
transaction hash	0x53cbd...cba6a
from	0xca35b...a733c
to	0x35ef0...450cf
transaction cost	25455 gas
execution cost	1852 gas
hash	0x53cbd...cba6a
input	0x16e...00000
decoded input	{ "address Make": "Honda", "address Model": "X", "uint256 Batterysize": "12" }
decoded output	{}
logs	[]

Table 13. MV registration.

Parameter	Value
transaction hash	0xdabdb...0bbdc
from	0xca35b...a733c
to	0x35ef0...450cf
transaction cost	24531 gas
execution cost	1875 gas
hash	0x53cbd...cba6a
input	0x16e...00000
decoded input	{ "address Make": "Tesla", "address Model": "S", "uint256 Excessenergy": "10" }
decoded output	{}
logs	[]

Table 14. Getting the energy requirements.

Parameter	Value
transaction hash	0x68107...f30b3
from	0xca35b...a733c
to	0x9876e...04485
transaction cost	22135 gas
execution cost	836 gas
hash	0x68107...f30b3
input	0x0bd...e1749
decoded input	{}
decoded output	{ "uint256 Start": "10", "uint256 End": "11", "uint256 Requiredenergy": "5" }
logs	[]

Table 15. Energy requirement for the next schedule.

Parameter	Value
transaction hash	0x16f16...87424
from	0xca35b...a733c
to	0x9876e...04485
transaction cost	23098 gas
execution cost	1698 gas
hash	0x16f16...87424
input	0xba4...00000
decoded input	{}
decoded output	{ "uint256 Start": "11", "uint256 End": "12", "uint256 Requiredenergy": "8" }
logs	[]

Table 16. Mining time and hashes generated against different difficulty levels.

Transactions	Diff. Level = 2			Diff. Level = 3			Diff. Level = 4		
	Mining Time (ms)		Hashes Generated	Mining Time (ms)		Hashes Generated	Mining Time (ms)		Hashes Generated
Transaction 1	14		48	98		1414	2781		49744
Transaction 2	21		84	116		2197	3261		58409
Transaction 3	23		157	228		3203	3452		60456
Transaction 4	25		160	233		3277	3785		65287
Transaction 5	25		243	283		4372	4025		72856
Transaction 6	27		260	315		5125	4232		77465
Transaction 7	29		266	600		7538	4618		88631
Transaction 8	36		273	639		10400	5780		97964
Transaction 9	44		502	645		11035	6605		109892
Transaction 10	69		515	847		11063	6627		110688

Figure 22 shows the output results when a weather information file is added to the IPFS according to the conditions set in the smart contract. Similarly, Figure 23 shows the output when the IPFS assigns a malicious state to a vehicle, denies the file retrieval request, and considers it a malicious request. Figure 24 shows the output results when a user inquires about the total number of files stored already in the IPFS and retrieves the ID of a specific file from the IPFS. Similar outputs are obtained when a road information file is added to the IPFS.
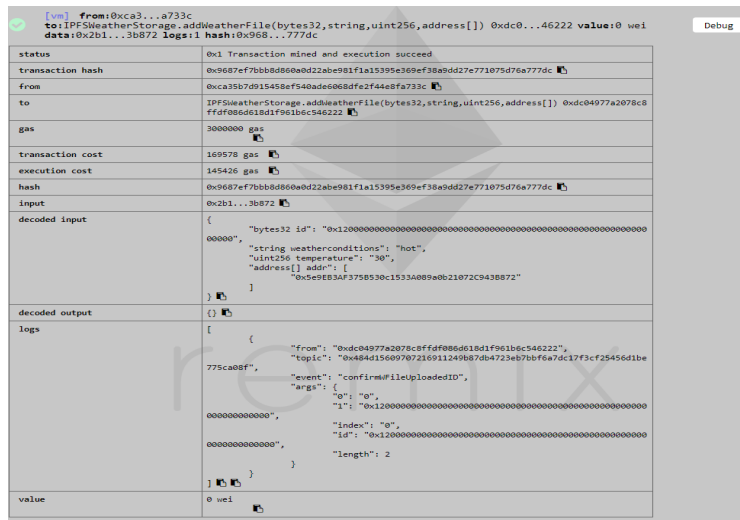
Figure 22. Adding a weather information file to the IPFS.
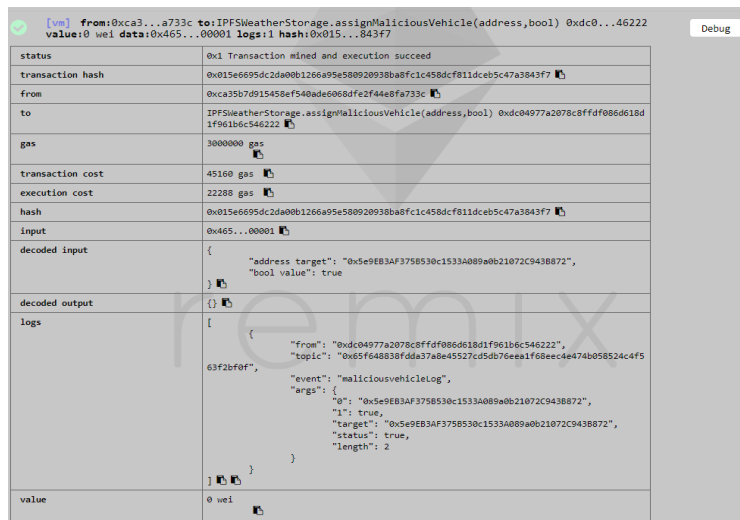
Figure 23. Assigning a malicious state to a vehicle by the IPFS.
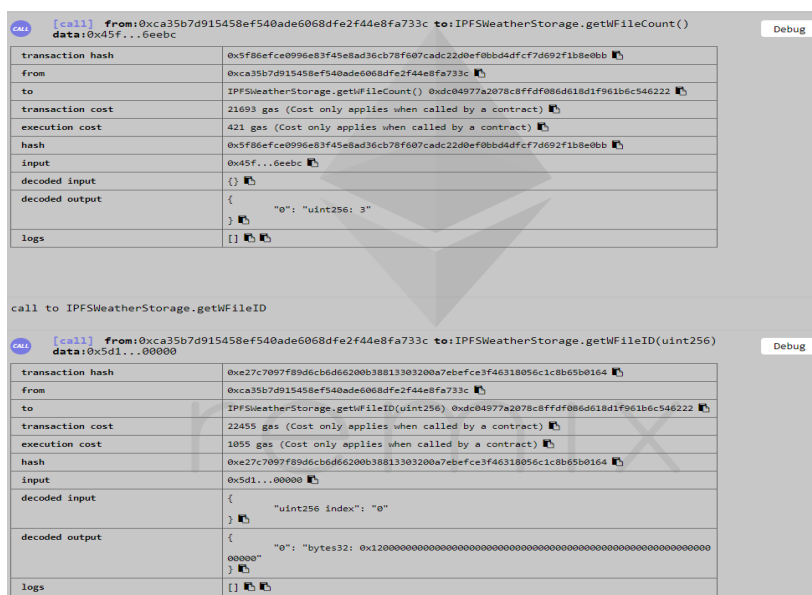
Figure 24. Getting file count and file ID from the IPFS.

10. Conclusion and Future Work

In this paper, the vehicles communicate with each other in a P2P manner for data sharing and energy trading. For an efficient charging schedule of the vehicles, new algorithms are proposed. Using the scheduling algorithm, an efficient cost reduction is observed. The proposed work uses blockchain technology for vehicles' registration and also for ensuring the immutability, security, and tamper proof-nature of the data. In the proposed work, the PoW consensus mechanism is used to achieve consensus between nodes, which makes the entire system trustworthy. The data generated by the vehicles are important entities and are stored in the TSIU after filtration.

Moreover, the shortest distance between an EV and the nearest charging entity is calculated using the Great-Circle Distance formula. The time taken by the EVs to cover this distance and the time taken to charge are also calculated in this work. Moving ahead, user participation is increased by awarding the users with incentives based upon their reputation and also by providing them with location privacy. The locations of vehicles are encrypted using the AES128 encryption technique. The power flow and the associated energy losses are also presented in this work. The mathematical formulation guarantees that all possible costs are calculated and the total charging cost is reduced. The proposed vehicle charging scenario, i.e., M2V, is compared with the existing scenarios, i.e., G2V and V2V, and the results are shown in the simulation section. Furthermore, the simulation results show that the charging cost incurred using M2V is 20%–25% less than in V2V and 35%–40% less than in G2V. It is also observed that the time required to store the data in TSIU is almost 45%–50% less for filtered data in comparison with original data, which reduces the storage complexity. Besides the positive aspects of the proposed system, it still has some limitations. For example, PoW is used in the proposed system, which has the major limitation of being computationally resource-expensive.

In the future, PoW will be replaced with a better consensus mechanism to deal with the issue of excessive resource utilization. Moreover, AES128 will be replaced by a better encryption technique to enhance privacy provisioning.

Conflicts of Interest: The authors declare no conflicts of interest.

Abbreviations

The following abbreviations are used in this paper:

AU	Authorization Unit
B^{2}ITS	Blockchain-based Intelligent Transport System
CS	Charging Station
DHT	Distributed Hash Table
EC	Energy Consumer
ECU	Electronic Control Unit
EV	Electric Vehicle
G2V	Grid-to-Vehicle
ICT	Information and Communication Technologies
IoT	Internet of Things
IPFS	Inter-Planetary File System
IV	Intelligent Vehicle
LAG	Local Aggregator
MDP	Markov Decision Process
MG	Micro-Grid
M2V	Mobile-Vehicle-to-Vehicle
P2P	Peer-to-Peer
PtMS	Parallel transportation Management System
RES	Renewable Energy Sources
PoS	Proof of Stake
PoW	Proof of Work
SES	Small Energy Supplier
SH	Smart Homes
SG	Smart Grid
TSIU	Transport System Information Unit
VN	Vehicular Network
VANET	Vehicular Ad-hoc Network
V2V	Vehicle-to-Vehicle
WSN	Wireless Sensor Network
C_{CS}	CS charging cost
C_{EV}	EV charging cost
C_{MV}	MV charging cost
C_{EV}^{max}	Maximum EV charging cost
C_{MV}^{max}	Maximum MV charging cost
C_{1T}	Charging cost
C_{2T}	Distance cost
C_{3T}	Waiting cost
C_{4Tr}	Reward cost
C_{4Tp}	Penalty cost
CS_{lat}	Latitude of CS
CS_{long}	Longitude of CS
C_{Total}	Total cost
dis_{S2V}	Distance between vehicle and CS
dis_{M2V}	Distance between vehicle and MV
dis_{V2V}	Distance between vehicle and EV
EV_{lat}	Latitude of EV

EV_{long}	Longitude of EV
I_t	Current at time t
L_{cable}	Length of charging cable
MV_{lat}	Latitude of MV
MV_{long}	Longitude of MV
P_{CS}	CS generation price
P_{EV}	EV generation price
P_{MV}	MV generation price
P_{loss}^{total}	Total power loss
Q	Price per unit
T_s	Saved units
T_w	Wasted units
V	Total number of vehicles in queue
v	Number of incoming vehicle
$\overline{\eta_{efficiency}}$	Inverter inefficiency
τ	Threshold distance
δ	Threshold difference between vehicles in charging queue
ω	Weather effect coefficient

References

1. Xie, S.; Zhong, W.; Xie, K.; Yu, R.; Zhang, Y. Fair energy scheduling for vehicle-to-grid networks using adaptive dynamic programming. *IEEE Trans. Neural Netw. Learn. Syst.* **2016**, *27*, 1697–1707.

2. Usman, M.; Knapen, L.; Bellemans, T.; Janssens, D.; Wets, G. Optimal recharging framework and simulation for electric vehicle fleet. *Future Gener. Comput. Syst.* **2020**, *107*, 745–757, doi:10.1016/j.future.2017.04.037.

3. Liu, C.; Chai, K.K.; Zhang, X.; Lau, E.T.; Chen, Y. Adaptive blockchain-based electric vehicle participation scheme in smart grid platform. *IEEE Access* **2018**, *6*, 25657–25665.

4. Noel, L.; de Rubens, G.Z.; Sovacool, B.K.; Kester, J. Fear and loathing of electric vehicles: the reactionary rhetoric of range anxiety. *Energy Res. Soc. Sci.* **2019**, *48*, 96–107.

5. Aitzhan, N.Z.; Svetinovic, D. Security and privacy in decentralized energy trading through multi-signatures, blockchain and anonymous messaging streams. *IEEE Trans. Dependable Secur. Comput.* **2018**, *15*, 840–852.

6. Alghamdi, T.A.; Ali, I.; Javaid, N.; Shafiq, M. Secure Service Provisioning Scheme for Lightweight IoT Devices with a Fair Payment System and an Incentive Mechanism based on Blockchain. *IEEE Access* **2019**, *8*, 1048–1061.

7. Sultana, T.; Almogren, A.; Akbar, M.; Zuair, M.; Ullah, I.; Javaid, N. Data Sharing System Integrating Access Control Mechanism using Blockchain-Based Smart Contracts for IoT Devices. *Appl. Sci.* **2020**, *10*, 488, doi:10.3390/app10020488.

8. Khalid, R.; Javaid, N.; Almogren, A.; Javed, M.U.; Javaid, S.; Zuair, M. A blockchain based load balancing in decentralized hybrid P2P energy trading market in smart grid. *IEEE Access* **2020**, *8*, 47047–47062.

9. Samuel, O.; Almogren, A.; Javaid, A.; Zuair, M.; Ullah, I.; Javaid, N. Leveraging Blockchain Technology for Secure Energy Trading and Least-Cost Evaluation of Decentralized Contributions to Electrification in Sub-Saharan Africa. *Entropy* **2020**, *22*, 226, doi:10.3390/e22020226

10. Yahaya, A.S.; Javaid, N.; Alzahrani, F.A.; Rehman, A.; Ullah, I.; Shahid, A.; Shafiq, M. Blockchain Based Sustainable Local Energy Trading Considering Home Energy Management and Demurrage Mechanism. *Sustainability* **2020**, *12*, 3385, doi:10.3390/su12083385

11. Shahid, A.; Almogren, A.; Javaid, N.; Al-Zahrani, F.A.; Zuair, M.; Alam, M. Blockchain-Based Agri-Food Supply Chain: A Complete Solution. *IEEE Access* **2020**, *8*, 69230–69243.

12. Zhang, T.; Pota, H.; Chu, C.C.; Gadh, R. Real-time renewable energy incentive system for electric vehicles using prioritization and cryptocurrency. *Appl. Energy* **2018**, *226*, 582–594.

13. Luo, Y.; Zhu, T.; Wan, S.; Zhang, S.; Li, K. Optimal charging scheduling for large-scale EV (electric vehicle) deployment based on the interaction of the smart-grid and intelligent-transport systems. *Energy* **2016**, *97*, 359–368.

14. Kang, J.; Yu, R.; Huang, X.; Maharjan, S.; Zhang, Y.; Hossain, E. Enabling localized peer-to-peer electricity trading among plug-in hybrid electric vehicles using consortium blockchains. *IEEE Trans. Ind. Inform.* **2017**, *13*, 3154–3164.

15. Tian, Z.; Jung, T.; Wang, Y.; Zhang, F.; Tu, L.; Xu, C.; Tian, C.; Li, X.Y. Real-time charging station recommendation system for electric-vehicle taxis. *IEEE Trans. Intell. Transp. Syst.* **2016**, *17*, 3098–3109.

16. JJaved, M.U.; Javaid, N. Scheduling charging of electric vehicles in a secured manner using blockchain technology. In Proceedings of the 17th International Conference on Frontiers of Information Technology, Islamabad, Pakistan, 16–18 December 2019.

17. Yong, Y.; Wang, F.-Y. Towards blockchain-based intelligent transportation systems. In Proceedings of the 2016 IEEE 19th International Conference on Intelligent Transportation Systems, Rio de Janeiro, Brazil, 1–4 November 2016.

18. Leiding, B.; Parisa, M.; Dieter, H. Self-managed and blockchain-based vehicular ad-hoc networks. In Proceedings of the 2016 ACM International Joint Conference on Pervasive and Ubiquitous Computing: Adjunct, Heidelberg, Germany, 12–16 September 2016.

19. Dorri, A.; Steger, M.; Kanhere, S.S.; Jurdak, R. Blockchain: A distributed solution to automotive security and privacy. *IEEE Commun. Mag.* **2017**, *55*, 119–125.

20. Rowan, S.; Michael, C.; Meriel, H.; Ciaran Mc, G. Securing vehicle to vehicle data sharing using blockchain through visible light and acoustic side-channels. *arXiv* 2017, arXiv:1704.02553.

21. Zhang, K.; Yuming, M.; Supeng, L.; Sabita, M.; Yan, Z.; Alexey, V.; Magnus, J. Incentive-driven energy trading in the smart grid. *IEEE Access* **2016**, *4*, 1243–1257.

22. Huang, X.; Xu, C.; Wang, P.; Liu, H. LNSC: A security model for electric vehicle and charging pile management based on blockchain ecosystem. *IEEE Access* **2018**, *6*, 13565–13574.

23. Liu, Y.; Hu, S. Renewable energy pricing driven scheduling in distributed smart community systems. *IEEE Trans. Parallel Distrib. Syst.* **2017**, *28*, 1445–1456.

24. Zhang, B.; Jiang, C.; Yu, Ju.; Han, Z. A contract game for direct energy trading in smart grid. *IEEE Trans. Smart Grid* **2018**, *9*, 2873–2884.

25. Wu, X.; Hu, X.; Yin, X.; Moura, S.J. Stochastic optimal energy management of smart home with PEV energy storage. *IEEE Trans. Smart Grid* **2018**, *9*, 2065-2075.

26. Mozafar, M.R.; Amini, M.H.; Moradi, M.H. Innovative appraisement of smart grid operation considering large-scale integration of electric vehicles enabling V2G and G2V systems. *Electr. Power Syst. Res.* **2018**, *154*, 245–256.

27. Amini, M.H.; Moghaddam, M.P.; Karabasoglu, O. Simultaneous allocation of electric vehicles' parking lots and distributed renewable resources in smart power distribution networks. *Sustain. Cities Soc.* **2017**, *28*, 332–342.

28. Vallés, M.; Bello, A.; Reneses, J.; Frías, P. Probabilistic characterization of electricity consumer responsiveness to economic incentives. *Appl. Energy* **2018**, *216*, 296–310.

29. Eissa, M.M. First time real time incentive demand response program in smart grid with "i-Energy" management system with different resources. *Appl. Energy* **2018**, *212*, 607–621.

30. Mortaz, E.; Valenzuela, J. Microgrid energy scheduling using storage from electric vehicles. *Electr. Power Syst. Res.* **2017**, *143*, 554–562.

31. Lu, X.; Zhou, K.; Yang, S. Multi-objective optimal dispatch of microgrid containing electric vehicles. *J. Clean. Prod.* **2017**, *165*, 1572–1581.

32. Aliasghari, P.; Mohammadi-Ivatloo, B.; Alipour, M.; Abapour, M.; Zare, K. Optimal scheduling of plug-in electric vehicles and renewable micro-grid in energy and reserve markets considering demand response program. *J. Clean. Prod.* **2018**, *186*, 293–303.

33. Rehman, M.; Javaid, N.; Awais, M.; Imran, M.; Naseer, N. Cloud based Secure Service Providing for IoTs using Blockchain. In Proceedings of the IEEE Global Communications Conference, Waikoloa, HI, USA, 9–13 December 2019.

34. Samuel, O.; Javaid, N.; Awais, M.; Ahmed, Z.; Imran, M.; Guizani, M. A Blockchain Model for Fair Data Sharing in Deregulated Smart Grids. In Proceedings of the IEEE Global Communications Conference, Waikoloa, HI, USA, 9–13 December 2019.

35. Fukumitsu, M.; Hasegawa, S.; Iwazaki, J.; Sakai, M.; Takahashi, D. A proposal of a secure P2P-type storage scheme by using the secret sharing and the blockchain. In Proceedings of the 2017 IEEE 31st International Conference on Advanced Information Networking and Applications, Taipei, Taiwan, 27–29 March 2017.

36. Guo, R.; Shi, H.; Zhao, Q.; Zheng, D. Secure attribute-based signature scheme with multiple authorities for blockchain in electronic health records systems. *IEEE Access* **2018**, *6*, 11676–11686.

37. Naz, M.; Al-zahrani, F.A.; Khalid, R.; Javaid, N.; Qamar, A.M.; Afzal, M.K.; Shafiq, M. A Secure Data Sharing Platform Using Blockchain and Interplanetary File System. *Sustainability* **2019**, *11*, 7054, doi:10.3390/su11247054.

38. Nizamuddin, N.; Salah, K.; Azad, M.A.; Arshad, J.; Rehman, M.H. Decentralized document version control using ethereum blockchain and IPFS. *Comput. Electr. Eng.* **2019**, *76*, 183–197.

39. Nyaletey, E.; Parizi, R.M.; Zhang, Q.; Choo, K.-K.R. BlockIPFS—blockchain-enabled interplanetary file system for forensic and trusted data traceability. In Proceedings of the 2nd IEEE International Conference on Blockchain, Atlanta, GA, USA, 14–17 July 2019.

40. Su, Z.; Wang, Y.; Xu, Q.; Fei, M.; Tian, Y.; Zhang, N. A secure charging scheme for electric vehicles with smart communities in energy blockchain. *IEEE Internet Things J.* **2018**, *6*, 4601–4613.

41. Wang, Y.; Su, Z.; Zhang, N. BSIS: Blockchain-based secure incentive scheme for energy delivery in vehicular energy network. *IEEE Trans. Ind. Inform.* **2019**, *15*, 3620–3631.

42. Chaudhary, R.; Jindal, A.; Aujla, G.S.; Aggarwal, S.; Kumar, N.; Choo, K.-K.R. BEST: Blockchain-based secure energy trading in SDN-enabled intelligent transportation system. *Comput. Secur.* **2019**, *85*, 288–299.

43. Huang, X.; Zhang, Y.; Li, D.; Han, L. An optimal scheduling algorithm for hybrid EV charging scenario using consortium blockchains. *Future Gener. Comput. Syst.* **2019**, *91*, 555–562.

44. Singh, M.; Kim, S. Branch based blockchain technology in intelligent vehicle. *Comput. Netw.* **2018**, *145*, 219–231.

45. Javed, M.U.; Rehman, M.; Javaid, N.; Aldegheishem, A.; Alrajeh, N.; Tahir, M. Blockchain-Based Secure Data Storage for Distributed Vehicular Networks. *Appl. Sci.* **2020**, *10*, 2011, doi:10.3390/app10062011

46. "EV Database". EV Database. 2020. Available online: https://ev-database.org/ (accessed on 1 May 2020).

47. Porcu, E.; Bevilacqua, M.; Genton, M.G. Spatio-temporal covariance and cross-covariance functions of the great circle distance on a sphere. *J. Am. Stat. Assoc.* **2016**, *111*, 888–898.

48. Abdolmaleki, M.; Masoud, N.; Yin, Y. Vehicle-to-vehicle wireless power transfer: Paving the way toward an electrified transportation system. *Transp. Res. Part C Emerg. Technol.* **2019**, *103*, 261–280.

49. Apostolaki-Iosifidou, E.; Codani, P.; Kempton, W. Measurement of power loss during electric vehicle charging and discharging. *Energy* **2017**, *127*, 730–742.

50. 'Losses In Distribution & Transmission Lines | Electrical India Magazine On Power & Electrical Products, Renewable Energy, Transformers, Switchgear & Cables'. Electrical India Magazine On Power & Electrical Products, Renewable Energy, Transformers, Switchgear & Cables. 2020. Available: https://www.electricalindia.in/losses-in-distribution-transmission-lines/ (accessed on 20 May 2020).

51. Electric Vehicle Charging 101 | Calevip. Calevip.Org. 2020. Available: https://calevip.org/electric-vehicle-charging-101 (accessed on 20 May 2020).

52. Koufakis, A.-M.; Rigas, E.S.; Bassiliades, N.; Ramchurn, S.D. Offline and online electric vehicle charging scheduling with V2V energy transfer. *IEEE Trans. Intell. Transp. Syst.* **2019**, doi:10.1109/TITS.2019.2914087

53. Wood, G. Ethereum: A secure decentralised generalised transaction ledger. *Ethereum Project Yellow Pap.* **2014**, *151*, 1–32.

54. Kim, O.T.T.; Tran, N.H.; Nguyen, V.; Kang, S.M.; Hong, C.S.. Cooperative between V2C and V2V charging: Less range anxiety and more charged EVs. In Proceedings of the 2018 International Conference on Information Networking, Chiang Mai, Thailand, 10–12 January 2018.

55. Nanayakkara, H. Blockchain Mining Difficulty. The Geveo Blog. 2019. Available: http://blog.geveo.com/Blockchain-Mining-Difficulty (accessed on 10 May 2020).

Blockchain of Carbon Trading for UN Sustainable Development Goals

Seong-Kyu Kim [1] and Jun-Ho Huh [2,*]

1   Department of Information Technology, Sungkyunkwan University, Seoul 03063, Korea; guitara7@skku.edu
2   Department of Data Informatics, Korea Maritime and Ocean University, Busan 49112, Korea
*   Correspondence: 72networks@kmou.ac.kr

check for updates

Abstract: Carbon credits should reduce the environmental pollution and carbon emission of the Earth in the future. The market for carbon credits will become a critical issue from 2021, and carbon credits will be applied to systems where individuals can trade. In order for these carbon credits to be traded between individuals, however, a corresponding exchange of carbon credits is needed. Policies, strategies, and technologies are also necessary to measure the trading of carbon credits. This paper aims at making transactions more reliable by applying blockchain technology to measure carbon emission rights. It uses blockchain to verify carbon emissions rights among the UN-SDGs' (United Nations Sustainable Development Goals') 17 tasks. In addition, it introduces the necessary dApp. In fact, we can protect against carbon emissions anomalies by using big data and artificial intelligence in mobile cloud environments. Thus, this paper proposes a blockchain-based carbon emission rights verification system to learn proven data further by using the governance system analysis and blockchain mainnet engine to solve these problems.

Keywords: blockchain; artificial intelligence; information security; UN sustainable development goals; UN SDGs; carbon trading; dApp

1. Introduction

The Kyoto Protocol is a market-based mechanism that formed the framework of the international climate change response system, as described by the United Nations, to ease the burden of cost of greenhouse gas reduction activities by the mandatory reduction bureau. The Kyoto Method consists of carbon emissions trading (ET), a clean development mechanism (CDM), and a joint implementation system (JI); in particular, carbon emission trading (emissions trading) refers to the market wherein greenhouse gas emission rights (emissions trading) are acquired. Where carbon emission rights cover allocations and credits 1), quotas refer to greenhouse gas emission rights paid to major greenhouse gas sources, such as power generation facilities or production facilities, and credits pertain to unit-to-consumption business projects projected for external greenhouse gas reduction projects (BAU-U, BAS-US, etc.). Meanwhile, "market" means that the price of carbon credits is determined by the demand and supply of carbon credits in the market instead of being fixed by policy. This is done in a way that reflects the costs of producing goods or services as the environmental and social costs of climate change [1].

This is in contrast to the carbon tax, wherein the size is determined. According to the World Bank's tally, the carbon emission trading market reached about 10.9 billion USD in 2005 when the Kyoto Protocol took effect and continued to grow at an annual rate of 108%, growing to 143.7 billion USD in 2009. Meanwhile, the growth of the carbon emission trading market slowed down a bit in 2009 when economic activity shrank in the wake of the global financial crisis. Based on the recovery outlook for the global economy, however, the global carbon emission trading market is expected to

reach about 669 billion USD in 2013, according to a report. The carbon emission trading market can be classified in various ways. First, depending on the nature of the carbon emission rights, it can be largely classified as a quota market and a credit market. As shown in Figure 1, Retail allows users to buy and sell goods, energy, etc. using Carbon Impact. In addition, Back-End signed an electronic contract for Carbon Credit, which is a smart contract that is generated by UserProfile, and can use trading rights for carbon transactions in all mobile apps, called Ecosystem. Credit markets are often referred to as project-based markets, which, in turn, can be divided into primary markets and secondary markets. On the other hand, depending on the way the transaction is made, the carbon emission trading market can be classified into OTC (Over-the-Counter) markets and in-house markets. These carbon credits translate into more and more transactions, and they are divided into 17 important subdivisions in the future SDGs (Sustainable Development Goals) at the United Nations. To recognize these carbon credits, carbon credits are accurately measured using non-modifiable blockchain technology and, by extension, proposed by the UN's (United Nations) SDGs as the environmental factors referred to by the UN's SDGs [2].
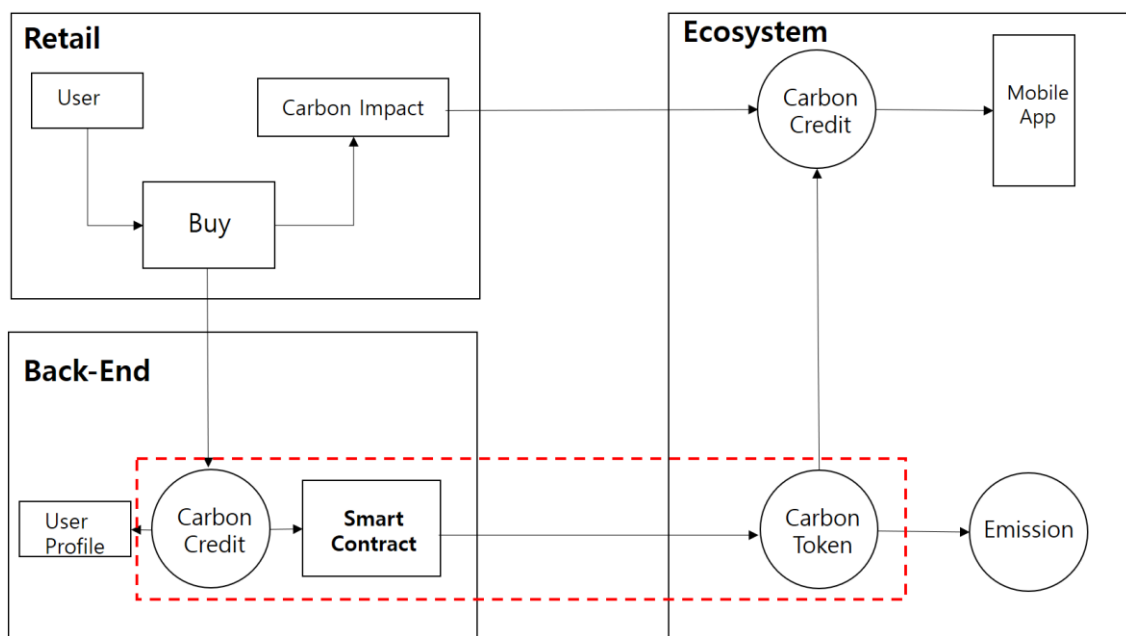
Figure 1. Smart renewable energy and P2P (Peer-to-Peer) blockchain service.

The reason is that the governance system is applied to the carbon credits based on the accuracy of blockchain according to its stability, decentralization, and reliability. To overcome these problems, a hybrid blockchain is proposed. In addition, we use blockchain to verify carbon emission rights in our efforts to manage energy [3]. These efforts are taken a little further in the verification system for blockchain. Therefore, in order to prevent hacking and strengthen security vulnerabilities, the available blockchain network protocol will be applied and changed to the appropriate blockchain network protocol for the greenhouse gas comprehensive information center. In addition, this study provides a scope for the purpose of verifying carbon emission rights using blockchain to conduct transactions between individuals and for the performance of trading of carbon emission rights. The method also aims to instantiate blockchain performance data, Transactions per Second (TPS), and to ensure the transparency and integrity of carbon credits for future P2P (Peer-to-Peer) transactions.

Section 1 discusses the problems of carbon emissions in the UN-SDGs and the artificial intelligence blockchain for verifying the trading rights when future carbon emissions are traded between individuals. When we introduce this blockchain, we talk about the important consensus algorithm. Section 2 presents directions on how to apply blockchain in the UN-SDGs from realized work, and specifically

discusses Information Technology (IT) application and blockchain application for carbon credits and renewable energy. Section 3 describes the UN SDGs' Performance and Blockchain Algorithms for Design and Implementation. Section 4 shows configurations for performance comparison. The actual performance comparison shows 15,000 TPS. Section 5 discusses the direction of future research and current problems. Section 6 concludes with a conclusion on the study of the application of blockchain carbon credits.

2. Background Knowledge

Studies related to blockchains and energy trading have been conducted by several researchers. M. Andoni et al. published their research work titled "Blockchain Technology in the Energy Sector: A Systematic Review of Challenges and Opportunities," whereas S. Wang et al. came up with "Energy Crowdsourcing and Peer-to-Peer Energy Trading in Blockchain-Enabled Smart Grids." F. Luo et al. and K. Gai et al. also released "A Distributed Electricity Trading System in Active Distribution Networks Based on Multi-Agent Coalition and Blockchain" and "Privacy-Preserving Energy Trading Using Consortium Blockchain in Smart Grid," respectively [4–6].

2.1. Carbon Emission

A certified emission reduction (CER; certification reduction or public certification reduction) refers to a confirmation made by the UN that a Clean Development System (CDM) project reduced greenhouse gas emissions. These carbon credits can be traded on the market through the emission trading system. If advanced countries go to developing countries for greenhouse gas reduction projects, the UN will examine and assess them and give them a certain amount of carbon emission rights. This greenhouse gas reduction project is called the Clean Development System (CDM) project. Not only advanced countries, but also developing countries themselves can carry out CDM projects to acquire carbon emission rights, which the Republic of Korea does. This refers to companies in each country that have failed to reduce carbon dioxide (CO2) emissions within a set period of time, paying money to buy rights from businesses that have been able to afford emissions or grow forests. Under the Kyoto Protocol, parties were required to reduce their carbon dioxide emissions by an average of 132% from 2008 to 2012, based on the 1990 emissions [7]. Countries that have succeeded in reducing their emissions have been allowed to buy and sell the corresponding carbon credits. In other words, petrochemical companies and other companies emitting a lot of carbon dioxide must reduce their carbon dioxide emissions themselves or buy rights from forest land owners in countries with low emissions. The Republic of Korea introduced such carbon emission rights from 2015 to 2018 (see Figure 2).
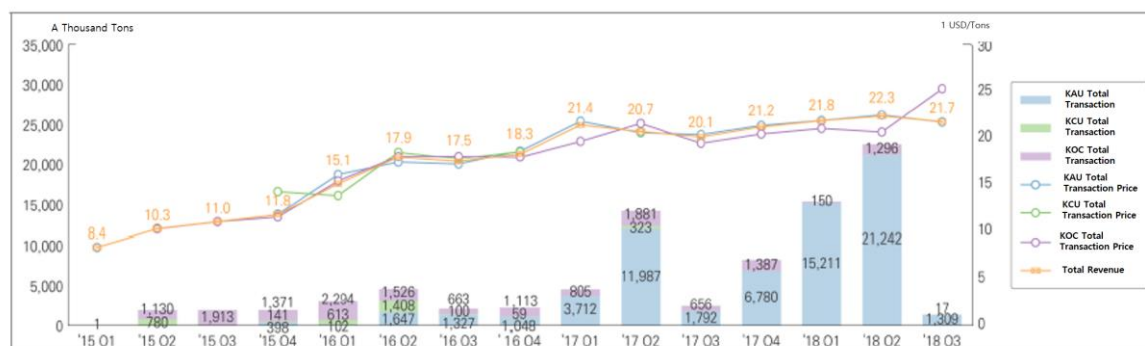

Figure 2. Growth rate of carbon emissions [8].

In addition, the total volume of emissions traded in both in-house and over-the-counter transactions during the branch line result period (2015.1–2018.8) was 86.2 million tons, with 37.5 million tons and 48.7 million tons traded in disability and over-the-counter transactions, accounting for 44% and 56%,

respectively. By emission rights, 66.6 million tons of Korean Allowance Units (KAU), 3.4 million tons of Korean Credit Unit (KCU), and 16.2 million tons of Korean Offset Credit (KOC) were traded, representing 77%, 4%, and 19% of the total. The total volume of transactions per year increased by 208%, 246%, and 134% year-on-year to 5.7 million tons in 2015, 11.9 million tons in 2016, 29.3 million tons in 2017, and 39.2 million tons in 2018, and the last year was similar to 2018, reflecting only the performance of transactions in the first half of the year. In addition, during the same period, the average price increased by 156%, 122%, and 106% year-on-year to 17,1799 KRW in 2016, 20,897 KRW in 2017, and 22,127 KRW in 2018, ending with a double increase compared to the initial average price in 2015. The average transaction price for the entire trading period was 20,279 KRW. In addition, by emission rights, KAU was traded at 15,767 KRW, KOC was 16,703 KRW, and KAU was traded at a relatively higher price than other emission rights, and the market price was slightly higher than the over-the-counter price. Continued increases in transaction prices and expansion of trading volume also affected transaction payments, rising 324%, 333%, and 142% year-on-year to 204.4 billion KRW in 2016, 612.3 billion KRW in 2017, and 868 billion KRW in 2018 from 63.1 trillion KRW in 2015; combined, the total transaction amount was 1.7477 trillion KRW. KAU accounted for 81%, 3%, and 15%, respectively, with 1.4231 trillion KRW; KCU accounted for 54 billion KRW and KOC for 270.6 billion KRW, while the total transaction amount in the market and over-the-counter trading market was 781 billion KRW and 966.7 billion KRW, respectively, representing 45% and 55% of the share, similar to the share of the trading volume [8].

Carbon emission credits refer to the right to emit greenhouse gases, one of the substances giving the Earth's environment a load. When humans emit carbon dioxide (CO_2), nature absorbs it and keeps the CO_2 concentration in the atmosphere at a certain level; when the emission exceeds Earth's own capacity to conserve the environment, however, CO_2 concentration increases gradually, resulting in global warming and climate change. Global CO_2 emissions rose 1.4% (4.6 billion tons) year-on-year to 32.5 billion tons in 2017 from 32.5 billion tons (see Figure 3) [9]. Kyoto Protocol 2, which took effect in 2005 by giving companies the right to emit greenhouse gases only at a manageable level, is set at 41.8 billion tons, or about 5.2% less greenhouse gas emissions from developed countries. The Emission Trading Scheme is a system that uses the advantages of the market mechanism to reduce greenhouse gases to maximize social costs, and the emission trading system is expanding worldwide, including in Korea, allowing companies to trade their remaining or insufficient emission allowances freely [10,11].
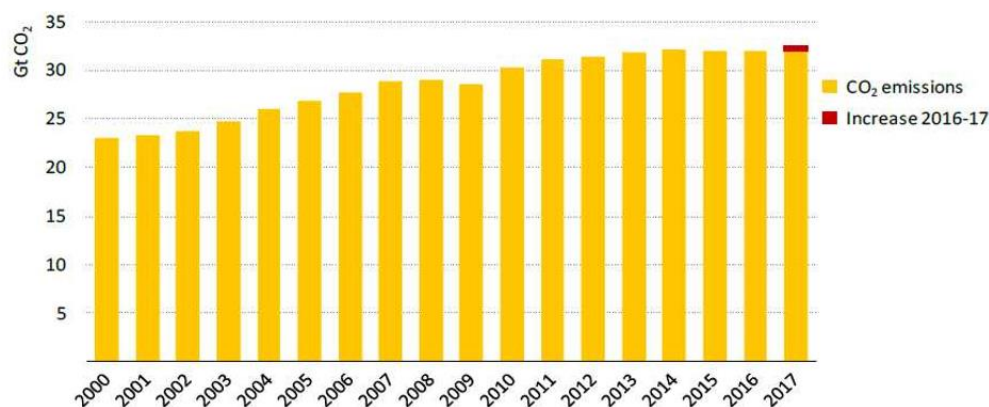
Figure 3. Trend of carbon dioxide (CO_2) emissions related to global energy. Source: Korean Government; "Second National General Management Plan for Greenhouse Gas Statistics (2020–2024)"; KEA Brief Issues of Energy, 2018 [8].

Blockchain technology is considered to be a suitable technology for implementing an emission trading platform that enhances the efficiency, security, and transparency of transactions, since it enables the establishment of multiple trust networks among stakeholders without the need for a Trusted Third Party.

In particular, the effective linkage of emission markets operating in different countries/regions requires the use of blockchain technologies that implement global networks involving multiple members without the need for centralized management. In addition, the climate change response system is changing from the top-down method of allocating greenhouse gas emission rights to developed countries only to the bottom-up formula of self-determination of national reduction targets and methods involving both developed and developing countries. This is a common task of reducing greenhouse gas emissions by establishing a blockchain-based platform wherein the majority of countries around the world participate as members to trade emission rights on their own and jointly verify, record, and store them.

Using this decentralized blockchain technology, the information and transmission details of carbon emission rights can be utilized to incorporate the technologies of blockchain and have safer transactions. In the future, carbon credits are expected to be traded using personal communication in P2P. In the EU (European Union), individuals buy and sell carbon credits. To ensure the safe trade of these carbon credits, we suggest a methodology applied with blockchain technology [12,13].

2.2. UN Sustainable Development Goals

The Sustainable Development Goals (SDGs), as the agenda that the 70th UN General Assembly held in 2015 resolved to achieve by 2030, are 17 shared goals for realizing the ideology of sustainable development. The 2030 Sustainable Development Goals (SDGs), together with the slogan "Leave no one behind," consist of 17 goals and 169 detailed goals for humanity in five areas: Human, earth, prosperity, peace, and partnership [14,15]. In 2015, the expiration of the MDGs' (Millennium Development Goals) implementation target deadline required governments to continue their efforts to achieve their goals and address new issues. Over the past 15 years, the United Nations has been discussing what the global priorities should be. At the Rio+20 meeting in June 2012, we agreed on the post-2015 global development system and came up with 17 new goals or global priorities: Sustainable Development Goals (SDGs) [16].

The MDGs were applied to all countries in principle; in practice, however, the goal was focused on developing countries. SDGs call for all countries, including developed, developing, and underdeveloped, to work toward the prosperity of humankind and to protect the environment. The MDGs were a useful development agenda but had too narrow of a target range, whereas the SDGs are even more comprehensive. The Sustainable Development Goals (SDGs) are flexible in a variety of national situations, allowing countries to select and measure detailed goals and indicators within their most relevant objectives. Even now, countries around the world are making great efforts to implement the Sustainable Development Goals (SDGs). Korea in particular is implementing individual UN-SDGs through government policies and related laws, such as the Framework Act on Sustainable Development, Framework Act on Low-Carbon Green Growth, and Framework Act on International Development and Cooperation [17].

2.2.1. Clean Energy

Energy is the core of the major challenges and opportunities facing the world today. Energy use is essential for jobs, security, climate change, food production, or income growth. Trying to achieve this goal is particularly important because it is linked to other sustainability goals. Focusing on the generalization and efficiency of energy, the increasing use of renewable energy through new economies and job creation will help create sustainable and inclusive communities and address environmental issues such as climate change. Currently, three billion people are at risk of air pollution due to the inability to use clean cooking utensils. Likewise, less than a billion people live without electricity, and 50% of them are found in sub-Saharan Africa. Fortunately, over the past decade, there has been great progress in the use of hydroelectric, solar, and wind power, and energy use per unit of GDP has decreased. Nonetheless, the challenges at hand have not yet been resolved. We need greater access to clean fuel and technology, and more progress needs to be made to integrate renewable energy into the

final energy of buildings, transportation, and industry. Public and private investments in energy need to be increased, with focus on regulatory regimes and innovative business models to change the global energy system [18].

2.2.2. Response to Climate Change

Climate change is now affecting all countries across the continent. It is disrupting the national economy, affecting life, and causing great losses to humanity, communities, and countries today and in the future. Weather patterns are changing, sea levels are rising, climate change is frequent, and greenhouse gas emissions are now at their highest levels. If no action is taken, sea level temperatures are expected to rise above an average of three degrees this century. This has the most effect on the poor and vulnerable. By seeking economic and scalable solutions, the nation can become a cleaner and more resilient economy. The pace of change is accelerating as more people seek ways to use renewable energy and reduce and adapt to greenhouse gas emissions. However, climate change is a transnational global challenge. We need an international level of improvement to help developing countries move toward a low-carbon economy. To strengthen the international response to the threat of climate change, countries adopted the Paris Convention at the Conference of Parties to the United Nations Framework Convention on Climate Change (COP 21), which took effect in November 2016. Under the agreement, all countries agreed to limit the Earth's temperature rise to less than two degrees Celsius. In April 2018, 175 countries ratified the Paris Agreement, and 10 developing countries submitted their first national response plans to combat climate change.

2.2.3. Poverty Eradication

The global poverty rate has been halved since 2000, but one in 10 developing countries still lives below the 1.9 USD-a-day international poverty line, and there are millions of people making less than a day's living expenses. Despite outstanding progress in East Asia and Southeast Asia, 42% of sub-Saharan Africa's population is still suffering from extreme poverty. Poverty means more than just a lack of income and resources to ensure a sustainable livelihood. These include hunger and malnutrition, restrictions on education and living services, social discrimination and exclusion, and restrictions on decision-making participation. Economic development must have a comprehensive goal to provide sustainable jobs and improve the structures of inequality. Social protection needs support to alleviate the suffering of countries at risk of disaster and to overcome economic crises, and these systems will help strengthen the responsiveness of those suffering from unexpected cost losses in the event of disaster and, ultimately, end extreme poverty in areas of absolute poverty.

2.2.4. Famine Species

It is time to rethink how we grow, distribute, and consume food. If done properly, agriculture, forestry, and fishing can provide everyone with nutritious food, generate a significant level of income, and, at the same time, support people-centered rural development and protect the environment. Now, biodiversity is rapidly decreasing due to damage to soil, fresh water, sea, and forests. Climate change is having a devastating effect on the resources we depend on, and it is increasing the risk of disasters, such as drought and flooding. Many farmers are no longer able to make ends meet on their land and have to move to cities to find opportunities, and poor food security causes serious undernourishment, hurting the growth of millions of children or shortening their lifespan. The world's undernourished population is expected to be 815 million, and an additional 2 billion by 2050, which requires fundamental changes in the world's food and agriculture systems. Investment in agriculture is essential to the development of agricultural productivity, and sustainable food production systems are necessary to reduce the risk of malnutrition.

2.2.5. Health and Well-Being

Ensuring a healthy life for all ages and promoting welfare are essential to sustainable development. While significant progress has been made, including increasing human life expectancy and decreasing infant and pregnant women's death rates, a professional improvement in the delivery system is needed to reduce the death rate of fewer than 70 children per 100,000 people by 2030. In order to achieve the goal of reducing early death rates from non-inflammatory diseases by one-third by 2030, efficient techniques are encouraged, such as the use of clean oils in cooking, and training on the dangers of cigarettes is needed. It also takes a lot of effort to eradicate a variety of diseases and to address the ongoing health problems. By focusing on providing effective funding for healthcare systems, improving sanitation, increasing access to medical services, and providing information on preventing environmental pollution, we can make great strides in saving millions of lives.

2.2.6. Quality Education

Quality education is the foundation for sustainable development. In addition to improving the quality of life, providing comprehensive education also helps local people have the creative thinking they need to find innovative solutions to international issues. Currently, more than 265 million children have dropped out of school, and 22% of them are only elementary school students. In addition, even children who go to school lack basic skills, such as reading and calculating. Over the past decade, efforts have been made to increase access to full-course education and to increase women's school enrollment. The eradication of basic illiteracy has increased dramatically, but more effort is needed to achieve universal educational goals and progress. For example, while the equality of primary education between men and women has been achieved, few countries have achieved that goal in the whole course of education. The reason for the lack of quality education is linked to capital issues, such as the lack of trained teachers, poor school facilities, and relatively poor opportunities for rural children. In order to provide quality education to children from poor families, we need to invest in educational scholarships, teacher training workshops, school building and water quality improvement, and school electrical facilities.

2.2.7. Gender Equality

While the Millennium Development Goals (including achieving universal primary education, MDGs) have made progress in gender equality and women's rights and interests, women and girls continue to suffer discrimination and violence throughout the world. Gender equality is not only a basic human right, but a necessary foundation for a sustainable world that pursues peace and prosperity. One in five women between the ages of 15 and 49 stated that they had been victimized by an intimate partner within 12 months of the survey date, and 49 countries currently do not have laws to protect women from domestic violence. Over the past decade, child marriages have been on the decline and progress has been made, with the harmful practice of female genital resection (female circumcision) decreasing by 30%, but more intensive efforts are needed to eradicate this practice. Providing women and girls with education, health care, quality jobs, and increasing their participation in the political and economic decision-making process will bring overall benefits to the sustainable economy, society, and humanity. Therefore, establishing a new legal system for equality of women in the workplace and eradicating harmful practices against women is critical to ending gender discrimination in many countries around the world.

2.3. Blockchain

Blockchain is a distributed computing technology-based data tampering prevention technology. This is a technology that stores managed data in a distributed data storage environment called a "block", where small data are linked in chain form based on the P2P method, so that no one can arbitrarily modify it and anyone can access the results of the change. The block also records all transactions that

were propagated to users prior to the discovery of the block, which is sent equally to all users in a P2P manner, so that the transaction details cannot be modified or omitted arbitrarily. Blocks have links to the date they were found and previous blocks; a collection of these blocks is called a blockchain [18–21].

Simply put, it is a technique that merely sets a bunch of records together. Unlike keeping transaction records on a central server when trading e-money in the past, blockchain shows the transaction records to all users and compares them to prevent forgery. As shown by Bitcoin's initial demonstration of the concept of blockchain and Ethereum's initial implementation of the concept of smart transport, there is a close relationship between blockchain and cryptocurrency. Still, blockchain is not a technology that can be used for cryptocurrency only. Cryptocurrency is said to be subordinate to blockchain.

Thus, technologies or services that have already applied blockchain are being developed. Interestingly, Satoshi Nakamoto solved the problem of developing and applying blockchain instead of developing blockchain first and applying it to Bitcoin, an electronic money system operated only by P2P. This can be seen in "Bitcoin: A Peer-to-Peer Electronic Cash System," the white paper released at the time of the unveiling of Bitcoin to the world. Largely divided into public blockchain, Private blockchain, and concourse blockchain, Bitcoin, which can be seen as the first implementation of the first public blockchain, introduced a proof-of-work approach to verify that the transaction history contained in each "block" was not tampered with by a malicious attacker and to leave only normal blocks. This is done in "proof" fashion, demonstrating that one of the many nodes (partners of the blockchain network) has succeeded in creating a new block that is directly connected to the old blocks (in a chain), which correspond to a work. All nodes (users) participating in the Bitcoin network have the right to create blocks to follow. Still, the next block, considered part of the normal chain on the network, will result in only one. Bitcoin mining refers to the process of changing the non-node value of the block header of new "block candidates" until the result of the execution is less than the "difficulty" value set in the Bitcoin network. The new block candidate will then contain the transaction details made since the last block creation [22–24]. Under this architecture, if more than 50% of nodes are "honest nodes"—a healthy node that does not continue to span blocks containing erroneous transactions—Bitcoin will maintain integrity. If more than 50% of the computing power consumed in mining is an "attacker node" that spans blocks containing erroneous transactions, the integrity of Bitcoin can be destroyed, often referred to as a "51% attack".

The second one is a private blockchain, which refers to a blockchain network where only authorized users (nodes) can participate. If the entire trading history on the network is made transparent, it can be introduced around troubled financial sectors and others [25]. The key feature is that it does not rely on cryptocurrency and, ironically, the reason it exists is that nodes that have validated the validity of a blockchain need a medium for payment. In a private blockchain, an unspecified number of people need not adopt an encryption-waste system because it does not have to serve as a node. There is also a point where the processing speed is fast against the public block chain. This is due to other variance consensus algorithms. Typical solutions include the Linux Foundation, IBM's Hyperledger Fabric, and the Hyperledger Iroha managed by the Linux Foundation and under development by a Japanese company [26–30], Corda of R3. Hyperledger is a blockchain project managed by the Linux Foundation, jointly developed by IBM and Digital Asset, and released as open-source [31]. It enables implementation with the actual code, and IBM provides blockchain solutions based on this project. In the case of a private blockchain by a single entity, it has been regarded as a slow database system with no advantage over a server-based database. Blockchain's security algorithms are aimed at keeping the same data among unreliable players because, if there is one entity, it is only a waste of computation and time. In defense against external attacks, the same effect can be achieved by using a server-based distributed system [32–36], and the scalability, convenience, economy, and performance are also superior to those of the server. Finally, there is the Consortium Blockchain, which combines public and private blockchains [37–45] (see Table 1).

Table 1. Types of blockchains.

	Public Blockchain	Private Blockchain	Consortium Blockchain
Management Subject	All Participants	Managed by the Central Institution	Participants in the Consortium
Network Participating Condition	None	Managed by the Central Institution	None or managed by a selected institution
Transaction Speed	Slow	Fast	Fast
Identification	Anonymous	Identifiable	Identifiable
Transaction Proof	Proof of work algorithm, Transaction verifier cannot be known in advance	Transaction verification is made by the central institution	Transaction verifier is known through certification, Transaction verification and block

Source: Software Policy Institute, 2018 [25].

The rapid increase in world energy demand over the last decade and the requests for sustainable development can be approached through micro- and nanogrids using hybrid power systems based on the energy internet, blockchain technology, and smart contracts. In this way, renewable energy sources, fuel cell systems, and other energy generating sources will be optimally combined and connected to the grid system using advanced energy transaction methods [46]. In particular, this paper's contribution has the point that carbon credits should reduce the environmental pollution and carbon emissions of the Earth in the future. While the size of the carbon emission trading system has grown to a low point, there is a lack of technology to limit it, so research has begun. So, we are talking about the blockchain process for reducing greenhouse gas (GHG) and the measurement, reporting, and verification (MRV) methodology, as well as the verification process in a total of five stages.

For Protocol Design for Hybrid Governance, blockchain talks about how to use and verify IT governance. A procedure for verifying and agreeing on a carbon-tracking AI blockchain platform and a methodology for applying a hybrid governance protocol applicable to the UN SDGs are presented. The procedures of certificate-based hybrid blockchain and authentication of hybrid blockchain based on a cryptographic protocol are applied by applying this methodology: Certification of hybrid blockchain based on MAC (Media Access Control Address) Address, Authentication of Hybrid Blockchain based on ID/password, Hybrid Governance Protocol for Design Pattern, Hybrid Governance Protocol for Visitor Pattern, Hybrid Governance Protocol for Governance Protocol for Protocols, and Hybrid Governance Protocol for Protocols. It will then unveil the source code for the implementation of the hybrid governance protocol.

Thus, this paper proposes a blockchain-based carbon emission rights verification system to further learn proven data using the governance system analysis and blockchain (dApp) mainnet engine to solve these problems.

3. UN SDGs' Performance and Blockchain Algorithms for Design and Implementation

3.1. Issue Raising

Blockchain is also called a public exchange book, and it is not a central manager that manages the transaction book, but is managed instead by all traders together without a central manager. According to the current banking system, all trading books are owned by banks and can be traded only through banks, which can cause major problems in the event of hacking. In contrast, blockchain does not need a central management system, and it is safe from hacking, as all traders have their own transaction books and their books are constantly updated. With the Paris agreement taking effect, carbon emission rights are one of the hottest issues. China recently announced the implementation of the emission

trading system in the power generation sector, and Korea is considering linking the emission market with China and Japan [47,48].

In addition, California and Canada's Quebec have linked emissions trading systems. The European Union has a common emissions trading system. Japan operates a common offset system with 17 developing countries, including Vietnam. In other words, the world is striving to link the carbon markets between countries. This is possible because there is an international agreement called the Paris Agreement, including a common unit of emission calculations called tCO2-eq. In this respect, emissions rights have very similar characteristics to blockchain-based transactions. The maximum permissible amount of greenhouse gas emissions across the globe can be calculated according to the Paris Agreement's goal of curbing global warming (2 °C). In addition, based on each country's greenhouse gas reduction targets, the maximum amount of emissions allowed by the Earth can be defined in the future. The Paris Agreement also applies the same standards to developed and developing countries. In addition, if the maximum greenhouse gas emission capacity of the Earth or the emission rights under the national reduction objective are allocated to the country and businesses, the emission rights can be traded on the same basis with a common worldwide transaction unit: Carbon dioxide equivalent. The Paris Agreement strictly requires prevention of double counting of emissions (reduction) through transparency mechanisms. Blockchain has the advantage of lowering transaction costs and ensuring transparency, as it is managed through common trading accounts around the world. Last year saw the world's first carbon emission trading between a Russian carbon fund and an African carbon emission holding company. In addition, emissions trading using blockchain was a key issue at the International Association of Emissions Trading in Barcelona. The era of the single global emission trading market and emission currency using blockchain could come faster than expected. Blockchain is also a key topic for the fourth revolution in state affairs. Although the UN and others are talking about the possibility of P2P transactions, we are proposing blockchain governance based on blockchain performance and stability through the main algorithms of blockchain.

3.2. Research Methodology

Governance is the generic term for the actions of all decision-making processes that create, update, and discard the formal and informal rules of a system. It consists of factors such as rules, smart tradeoffs, laws (punishment for malicious actors), procedures (what will be done when X occurs), or responsibilities (as to who should do what). The types of governance are largely blockchain governance, project governance, and fund governance. Blockchain governance also proceeds in the form of voting. Of course, voting can be used not only in voting, but also in other ways; also in terms of efficiency, voting is commonly used. The most representative blockchain determines the direction of the network through BIP (Bitcoin Improvement Proposals), EIP (Ethereum Improvement Proposal), developer forums, and various communities; in addition, various blockchains manage the network in slightly different ways. The meaning of project governance is that blockchain networks are a world. Based on this world, we can share on-chain governance and off-chain governance. On-chain governance, the former, refers to a form in which governance can be achieved within a chain without any other elements other than blockchain network components, and blockchain networks can be considered complete as an independent world. Conversely, if governance is done outside the network and it has a direct impact on the blockchain network, this form of governance can be said to be off-chain governance. Fund governance is an act to create a fund to raise the resources needed to create a blockchain ecosystem. Governance is important in blockchain because, over time, the network of blockchain cannot survive without the technology of change that can flexibly cope with the new problems. These quick updates make enterprise and mass market end-user use cases possible. If it takes too long to fix the problem, users will not abandon the service or even participate in it from scratch. Moreover, too-frequent changes divide the community and cause uncertainty to prevail. In a company, a representative's word is law. Thus, changes within a company may be very quick and efficient depending on the capabilities of the representative. In decentralized systems such as blockchain, however, each party has different

incentives. Users, miners, and developers all have different goals. For example, developers were satisfied with Monero's ASIC (Application Specific Integrated Circuit) protection updates, but minor players using ASICs were unhappy, as their profits were shrinking. Eventually, a hard fork broke out, and Monero was divided into several versions. The most important thing in understanding governance is that the incentives that each party constituting governance has may not match. It can be good for users but may be bad for miners (operating companies that implement governance), good for developers but bad for miners. Blockchain governance is designed to achieve network mining agreements through special algorithms. Typical algorithms include Proof-of-Work (PoW), Proof-of-Stake (PoS), and a mix of them. Nonetheless, this governance framework is currently developed and studied extensively, and it has many kinds of governance systems. Funding governance regulates how projects manage the collected funds. Project governance is a kind of meta or meta-meta governance that regulates technology, blockchain governance, funding governance, and meta governance (for example, changing governance procedures altogether). Technology topics include blockchain parameters (block size or gas prices), bug fixes, and new features. On-chain governance is where governance takes place within a blockchain. Ongoing governance involves developers/users/miners alike, and it is largely voted on to modify policies/policy. Off-chain governance is an architecture wherein discussions outside the blockchain are reflected to the blockchain. For example, developers run forums in places like Reddit in a blockchain park, measuring amendments and forming public opinion, and then reflecting them within the blockchain. In cross-chain projects, multiple governance can be implemented simultaneously. For example, in a project called Cosmos, malicious changes cannot be avoided, and rollback procedures must be possible. Blockchain's own token is not a useful incentive or a perfect solution to encourage good behavior. In particular, in situations such as trade shoulder, the token itself can be downgraded as an incentive. In cases like liquid democracy, the centralization of voting rights can be eased but still cannot completely block the populist phenomenon. Because governance is inherently the establishment of mechanisms that address changes in a useful way, several matters are important. In off-chain governance, governance is conducted through online forums outside the blockchain. Developers use the forum to check the revision proposals and their opinions and reflect them as policy changes within the blockchain. Bitcoin mainly runs forums through Reddit. In the case of Etherium, the revised proposals are used to collect public opinion by publishing them on YouTube in lecture form. As such, this paper proposes a Hybrid Governance Protocol, which integrates different types of governance systems. We describe the architecture for introducing blockchain for MRV (Measurement, Reporting, and Verification) application in the GHG (Greenhouse Gas) reduction process. It provides a basic foundation for MRV according to the national CDM (Clean Development Mechanism) methodology. In addition, most nations are developing and equipped with a greenhouse gas reduction zone. There are a lot of data every year, including statistics on greenhouse gas emissions. However, this is because it is the basis for each country to manipulate MRVs. Thus, in order to reduce this GHG, the reduction target must be achieved. There is a lot of discussion about this reduction target. So far, however, the state has arbitrarily granted carbon credits. In addition, each country's guidelines exist, but no clear standardization is made. Thus, the Climate Change and Energy Program emerged as a program to manage climate change and energy. However, these programs are also being challenged by manipulation or by malicious hackers.

Therefore, this research was conducted with Blockchain Agreement Algorithm and Artificial Intelligence Deep Learning Engine for research through verification of GHG reduction and MRV.

In addition, the types of governance structures are largely divided into blockchain governance, project governance, and fund governance.

(1) Blockchain Governance Structure

This refers to an algorithm that verifies accurate data and various data using blockchain. This level of governance is the stage in which all blockchain governance systems are established. It is also in the process of utilizing existing verification algorithms.

(2) Structural Structure Project

The project governance structure is used to establish the ICT (Information Communication Technology) and environmental governance systems required to build and implement carbon emission reduction projects. The project for carbon reduction is a very important step and is related to blockchain agreement algorithms.

(3) Fund Governance Structure

Fund governance refers to the blockchain fund governance structure that is needed when the financial sector funds are made when the carbon emission exchange is formed in future P2P transactions in the financial market of carbon emission rights.

3.3. Blockchain Process for Reducing GHG and MRV

The flexible mechanism for securing liquidity in the greenhouse gas emission trading market allows allocated companies to use emission rights in various and flexible ways in addition to trading emission rights when submitting emission rights in accordance with their target monthly greenhouse gas emission reduction activities. The purpose of flexibility is to secure liquidity in the emission market by diversifying greenhouse gas reduction methods and inducing more greenhouse gas reduction activities by ensuring flexibility in the method of submitting emission rights. Types of flexible mechanisms include banking and borrowing, recognition of early reduction performance, and certification of external reduction projects, such as offset. In addition, to reduce this MRV, a verification platform that is interlinked with these policy segments must be a mix of goods. This is the same for the whole world. This paper used an artificial intelligence blockchain for the verification platform in line with the process of GHG reduction and MRV reduction, and is expected to show a lot of trading volume if the carbon emission trading system comes out as an individual trading system in the future. Therefore, this paper is equipped with a process to perform these verification procedures. The process required for it is shown in Figure 4.
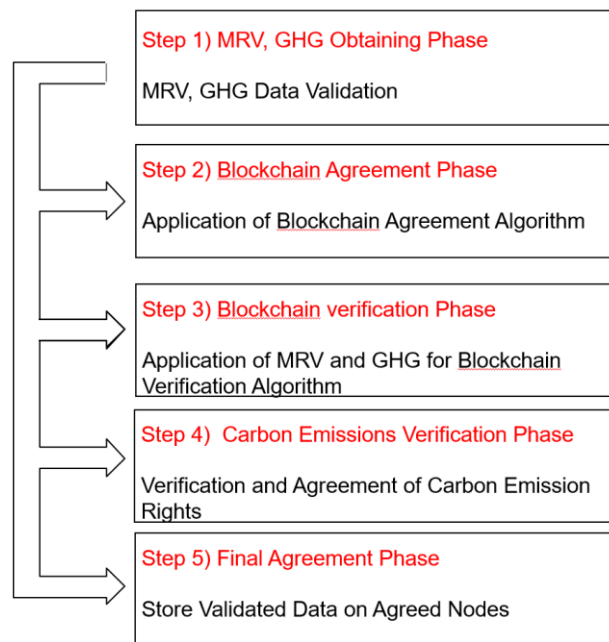
Figure 4. Verification blockchain for measurement, reporting, and verification (MRV) and greenhouse gas (GHG) data.

(1)   Step 1

Large amounts of carbon credits will be created, and individuals will be able to purchase them in the future. Thus, the verification of the data is required to reduce the MRV and GHG required.

(2)   Step 2

Blockchain is a step to propose a blockchain architecture that can achieve a very fast agreement according to Hyper PoR (Proof of Random) consensus algorithm and verify it by these consensus algorithms.

(3)   Step 3

The verification algorithm of the blockchain is used to verify each node and to verify it through work in the mesh network.

(4)   Step 4

Algorithms to agree and verify carbon emission rights are obtained. Carbon emission rights are the steps to verifying carbon credits mined by individuals and exchanges necessary for this reduction.

(5)   Step 5

The final validated data divided into agreed nodes after the data consistency verification process are stored. These storage steps are stored thoroughly prepared for hacking.

3.4. Protocol Design for Hybrid Governance

The Hybrid Governance Protocol is a transaction that occurs on a blockchain network. Transactions that are recorded on the chain are permanent; thus, once they are written in the network, they can never be erased. Still, many problems can arise from relying solely on the chain. The first is slow speed. After a transaction occurs, it takes quite a long time to be confirmed, so it is difficult to process quickly. The second is privacy. In the case of on-chain, there is a problem wherein the transaction history occurring in the blockchain network is disclosed to everyone. The third is cost and scalability. The cost of all the activities occurring in the blockchain network must be paid for by each person, and the slow speed of transactions is a disadvantage.

Blockchain governance protocols are also a concept created to solve the problems in these on- and off-chains. These protocols can be said to be divided into on- and off-chain protocols. On-chain protocols are those other than blockchain network components, a form wherein governance can be achieved in internal strife without a dispute. Under these special circumstances, blockchain is complete in one independent world. In addition, if this is done outside the governance network, and it directly affects the interior of the blockchain network, then this type of protocol should be designed. In other words, it can be defined as the ongoing governance protocol. Still, this governance is very important because the governance protocol of blockchain plays a very important role in designing consensus algorithms. These protocols have a very important role to play. The SDGs announced by the United Nations have 17 categories. This protocol is also characterized by being optimized for carbon emission rights verification.

These protocols can be developed in the same way as governance systems. This paper compares the Internet environment and the distribution of the value of blockchain by designing these governance protocols and dividing them into application layers and protocol layers, using the text to represent the layer of the network protocol of items in the UN SDGs. The existing application layers, physical layers, and protocol layers are different. This is because the application layer has an accurate stack structure to achieve blockchain decentralization. Moreover, due to the characteristics of blockchain, which is always verified with shared data, the change in the value of blockchain is attributed to

its critical role in the sharing of data. Prior to that, the definition of data is critical. First, existing network protocols define the headers of packets for the data transmission of applications. Transmitters are encapsulated, receivers are encapsulated to create headers for data transmission in protocols, and receivers are referred to as reverse capsules for interpreting and processing headers. Subsequently, hybrid governance can refer to a private–public-based approach to protocol. This meaning will be a breakthrough margin for one-sided protocols of existing single-oriented ones. Submitting blockchain data to a network of applications does not save it all. The protocol makes the agreement, validates the data through the consensus process, and requires approval before the data can be stored. It also tends to be the opposite of the level of applications at which sensitive data are not protected by privacy (see Figure 5).
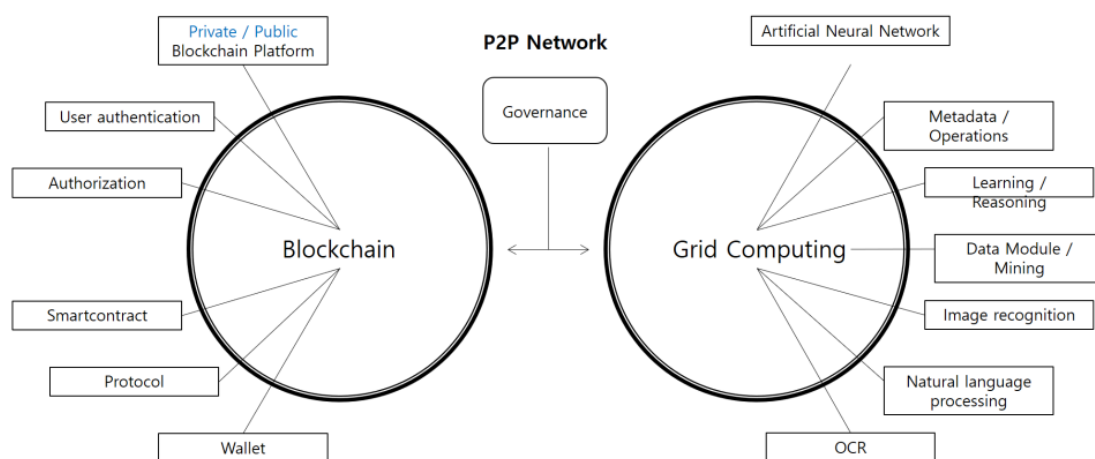

Figure 5. Protocol design for hybrid governance.

This meaning is designed to store the desired data whenever a particular event occurs. Modulation or artificial intelligences have a very difficult structure for modulation because of the control of protocols of the data. The hybrid blockchain protocol is designed to be used to verify carbon credits with hybrid structures that go beyond traditional private and public limits.

The task of developing and improving the most important carbon emission blockchain (MRV) must be the central task. Although the government submitted the information specification for the inference of greenhouse gas emissions after receiving third-party verification from the company concerned, the emission trading system will be submitted to the environment minister who is in charge of the emission trading system, and the emission certification committee will review the government certification status following third-party verification. The emission rights can be allocated free of charge, and the proportion of the emission rights allocated free of charge has increased the elasticity of operations by making the global carbon emission rights determined by the Presidential Decree considering the industry's international competitiveness, international trends, and impact on the national economy, such as prices. In other words, emission rights are allocated free of charge by the percentage specified by the allocation plan: 100% during the first planning period, 97% during the second period, and 90% after the third period. It should be noted that Korea's free quota ratio is slightly different from the EU-ETS (EU Emissions Trading System) calculation method. For the EU-ETS, excluding the proportion of emissions allocated on a paid basis is a free allocation ratio; for countries, the percentage of "standard greenhouse gas emissions" of each allocated company is "multiplied by the mandatory reduction rate specified by the company's past average greenhouse gas emissions" to get the free allocation ratio. Therefore, considering the emission rights reserved by the EU-ETS, even though the EU-ETS has a free allocation ratio of 90%, the companies subject to each quota may be allocated all of the standard greenhouse gas emissions free of charge; in Korea's emission trading system, however, only 90% of each allocated company's standard greenhouse gas emissions

are allocated free of charge. Thus, if the allocated company had a similar emission rate in the past, they should purchase 10%.

Ultimately, even if Korea's emission trading system has a free quota ratio of 100%, if 20% of the total emission rights were to be reserved, the EU-ETS ratio would have the same effect as 80% based on the standard. An important factor here is the monitoring service for MRVs using artificial intelligence blockchains. Monitoring means the collection, storage, and management of all data necessary to determine the baseline and to measure artificial emissions and leaks within the business boundaries. Monitoring plans should be established for existing CDM (Clean Development Mechanism) projects and reflected in the project plans. The key elements of the monitoring plan are the data and variables to be monitored, and other data retention deadlines, responsibilities, and authority for data collection and management, quality assurance and management procedures, uncertainty levels, measurement methods, and calibration cycles for measuring equipment should be included; these should include artificial intelligence and blockchain mechanisms. For the data and variables to be monitored, the business plan should include data (variables) names, units of measurement, descriptions of data, data sources, applicable numbers, methods, and procedures, monitoring cycles, quality assurance and management procedures, and the purpose of data use. If sampling is included in the monitoring method, the corresponding sampling plan listed in the project plan is prepared in accordance with the relevant guidance (UNFCCC 2015c), including the sampling design, data to be collected, and implementation plan. The organization of monitoring plans for all CDM projects shall comply with the CDM Business Standards (UNFCCC 2015d). In addition, each approved methodology or new baseline and monitoring methodology will differ in all other details, such as monitoring target, frequency, quality assurance and management procedures, and their levels. Therefore, specific criteria should be established for each item of the monitoring plan in the project plan based on an already approved methodology or a new methodology applied to the CDM project.

Finally, verification of whether such carbon emissions rights are being duly traded is performed based on the CDM verification and certification standards as the procedure for CDM operating bodies to assess the reduction of greenhouse gas emissions by business participants over a specified period of time. The CDM operating body verifies that the project activities comply with the CDM's detailed principles and requirements of the procedure when carrying out the verification. The CDM-certified bodies that perform verification and certification utilize the engine data of the blockchain and present a platform for it considering the grace period and revision of the form.

The above (see Figure 6) stores MRV data, GHG data, and unstructured/structured data in the Web Application Server (WAS). The natural network is mapped to reflect this. These analyzed engines are stored in the Deep Learning repertoire. These stored databases are stored in the real-time enterprise (RTE) server, and the data analyze and deliver databases that can analyze real-time data.

① Transfer MRV data to Web Application Server (WAS).
② GHG data to WAS.
③ Send structured and unstructured data to WAS.
④ Transfer Neural Network data.
⑤ Application of Blockchain Agreement Algorithm.
⑥ Save to Deep Learning data repository.
⑦ Exception Saving on a Processable Server.
⑧ Real-time Enterprise (RTE) is saved to server.
⑨ Real-time DB (DataBase), divided into storage DBs.
⑩ Store on final set database server.
⑪ Display on dashboard.
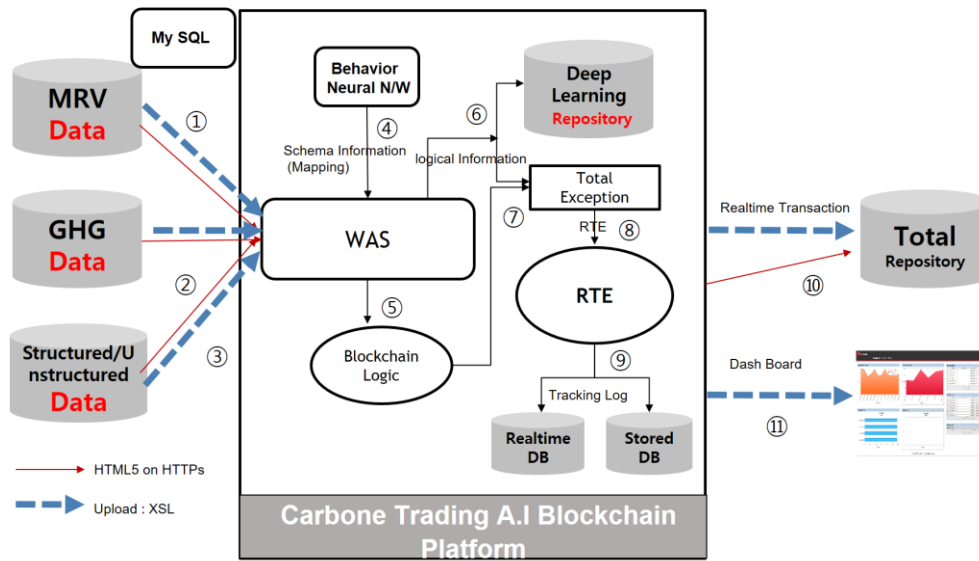
Figure 6. Carbon trading AI (Artificial Intelligence) blockchain platform.

3.5. Verification Method using Hybrid Governance Protocol

Looking at blockchain-based technology, there are protocols that use the blockchain concept, and the structure is based on protocol-based tokens. Blockchain itself is a distributed database or a data structure. Each node distributes and stores data using encryption technology. The protocol is one that can communicate between blockchain nodes (see Figure 7). Nodes using the same protocol can communicate with each other. An environment where various kinds of software can operate based on the protocol is produced. There are various tokens that operate in such protocol-based environments. Existing blockchains do not provide development environments, such as development environments or virtual machines, so they do not have tokens, but must be accessed in terms of initial value storage. Various kinds of tokens used on the basis of smart contracts can be seen as a program that performs each unique type of contract. Compared to communication, there are protocols for exchanging over the Internet and file/email with protocols such as HTTP, FTP, and SMTP based on TCP/IP technology, and various programs are produced using such protocols. Various programs such as websites, email, and file sharing are kinds of tokens, and there are attempts to create a decentralized world free of intermediaries through blockchain technology.

Figure 7. Interchain blockchain diagram.

3.5.1. Hybrid Governance Protocol Applicable to UN SDGs

A protocol in communication is one wherein a computer or a system communicates with another. Pre-promised operational regulations are required to perform data transfers quickly and accurately a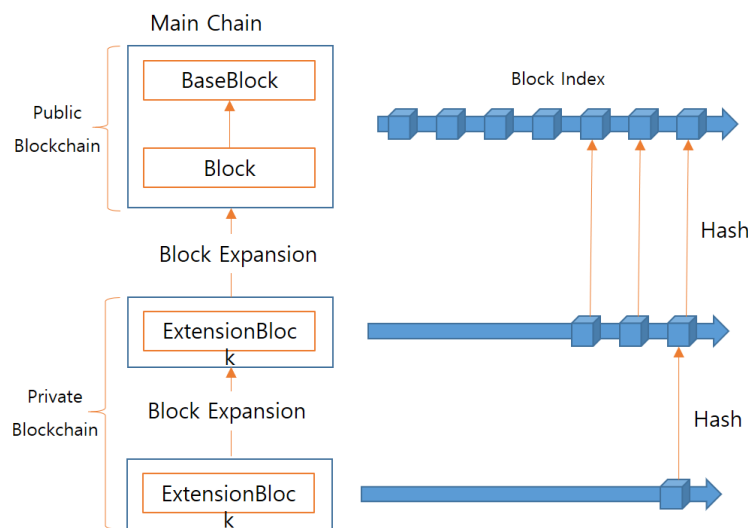nd to provide error detection and recovery functions. The Internet has communication over the network based on protocols such as TCP/IP, SMTP, HTTP, and HTTPS. A standard is always necessary, and the network always requires interoperability.

(1) TCP/IP (Transmission Control Protocol/Internet Protocol): A collection of communication protocols used by computers to access the Internet.
(2) HTTP (Hypertext Transfer Protocol): Communication protocol used to exchange documents.
(3) SMTP (Simple Mail Transfer Protocol): Simple e-mail communication protocol used to send and exchange e-mail between computers.

Next, we went through Web 1.0 and 2.0, and on top of these protocols were applications like Google and Facebook. Their business model was to build their own data and, based on that (centralized), demand/charge services directly from customers or collect advertising fees. At that time, the DB was closed, owned. Being able to obtain data and information only by using that service limited the possibility of creating new value from an open source from a different angle. Blockchain leads to a "change in protocol level" that has enabled these existing Web services. With an open-source, distributed DB, anyone can access data and share information freely. It is all about hardware, software, networks, and data. Blockchain protocols allow everyone to download software, become nodes, and replicate and use data. Joel Mongro [49] of Placeholder VC/Union Square Ventures describes blockchain as the embodiment of the Fat Protocol, unlike the traditional web-based Thin Protocol. The value created through the development of protocols and the return on the value created were low because information was locked in the application. Over the next few years, however, blockchain will rebuild protocols in decentralized form, which will revolve around the development and value creation of technologies.

(1) If the data existed in the application layer in the existing web base, blockchain shares the data with anyone on an open source basis.
(2) The underlying protocol project itself can be easily financed by developers through tokenization, and those who develop the dApp on top of that protocol also benefit as the protocol ecosystem grows.

While monetization over protocol was to create and sell S/W (Software) that utilizes the protocol, blockchain allows people who agree to the protocol to purchase each token and create better value for that protocol, resulting in an increase in value and price so that people can immediately obtain economic rewards. Thus, creating a new protocol and becoming dominant create the value of the token, giving rise to the underlying protocol project itself. They share computing power (Data Base), but they can decentralize and manage their resources. Now that the security tokenization is in earnest, we think it will be possible to develop more active protocol levels. In the early days, when one thinks of Netscape and Google, the Web was more like a thin protocol. In fact, data showed that most investments were made in infrastructure corresponding to protocols/core throughout 2017. Project financing in infrastructure amounts to 10 billion USD, with the sum of infra, payment, finance, exchange, and computing, which correspond to protocols and major vertical apps, practically making up the majority. Actually, the return is also high here. In a token economy, all assets are tokenized, and people take advantage of the goods/services written on top of the protocols they support, purchase token/coins in the process, and, in return, get rewarded as much as all participants contribute. However, we have a long way to go, and we do not think that human-developed technology itself will solve the social problems that we care about. On the other hand, if we remain still for many reasons, the world of blockchain and decentralization will not be as beautiful as expected [50].

Certificate-Based Hybrid Blockchain

The certificate-based hybrid blockchain's public key password is used to authenticate the certificate based on the certificate containing the information of the certificate. In Korea, however, the Korean government has prepared a system for issuing public certificates through the 1999 Autobiography Act to certify the certificates through five public certificates under the best certificate authority, Root CA. For foreign countries, personal in-device, Eve modem device authentication, and WiMAX industry certificates are provided through Verisign's device certification service. In addition, the certificate-based authentication technology is being used in VoIP (Voice over Internet Protocol) and network surveillance cameras, and the station is expanding. Certificate-based authentication technology provides high stability through strong authentication functions and supports anti-denial functions. Nonetheless, device certification processing software algorithm requires high computational throughput. Therefore, it is not suitable for use in IoT (Internet of Things) devices that have power and performance. As such, blockchain is used instead of certificates for authentication to present a functional and usable enough blockchain.

Authentication of Hybrid Blockchain based on Cryptographic Protocol

A protocol that authenticates objects based on the private and public blockchains' public key passwords and symmetric key passwords is used primarily in wireless Internet security protocols. It supports various tables, such as 802.1x/802.11i and WPA. The cryptographic protocol-based authentication method can include technologies such as ID/password-based authentication, MAC-address-based authentication, and certificate-based device certificate authentication depending on the cryptographic protocol used. A variety of authentication methods can be provided to select the combined authentication method according to the use environment, and the anti-denial function can be supported according to the code protocol adopted. Depending on the security-based encryption technology, however, if any vulnerability in encryption technology is found, it can lead to vulnerability in authentication technology. These blockchain technologies offer many blockchain architectures based on various encryption technologies.

Certification of Hybrid Blockchain based on MAC Address

MAC address is an authentication method using a unique identification address (MAC) address assigned to the underlying hybrid network interface, which is used primarily for network rooting in intranet environments. It has a difference that compares the MAC address registered in the server with the message sent from the device when the device requests one in the network, and it is easier and faster than the ID/password-based authentication method. With the advent of IoT, however, there is a need for new MAC address forms to be defined, and new tables are being defined. MAC addresses can be tightened, so without extra security equipment, they are vulnerable to attacks by spoofing and others. These hybrid-based blockchain types can be applied to a variety of industry groups for hybrid-based blockchain authentication based on the MAC address of a computer system. In addition, blockchain is proposed for authentication work for authentication and protocol.

Authentication of Hybrid Blockchain based on ID/Password

This is a technology used mainly in server/client authentication environments by storing each user ID and password of blockchain users in the server's DB and authenticating them based on stored knowledge. To prevent a list of passwords stored on a server from being exposed and consequently disabling authentication, a method of storing values through a hash function is often adopted. To ensure greater safety, hide SSIDs (Service Set IDentifier), use the WEP key between AP and device, adopt the PAP authentication method, and use the RFID method. The ID/password method in the IoT environment has problems, such as the server's load due to the characteristics of the IoT environment,

where many devices are used without human intervention, and it is important to exclude human intervention in the additional process of device modification.

The problem is that it is not suitable for authentication technology in an IoT environment because it does not provide an anti-witching function. Based on blockchain technology for these IDs/passwords, it provides the necessary skills for the most basic authentication.

3.5.2. Hybrid Governance Protocol for Design Pattern

Visitor patterns are often used with composition patterns. In the picture above, when dealing with the class that implements an element on the left, the composition pattern is used to implement the visitor pattern by implementing the individual objects and their parent objects in the form of a list. In general, NodeBlock allows a member variable and a method to be written together within an object; in a visitor pattern, however, the variable and method are created separately. For a similar pattern, Java does not support multiple inheritances from multiple different objects simultaneously. The term multiple inheritance here means that language internally supports double dispatch, and that multiple inheritance is not supported. The non-identifier pattern eventually results in the object's inheritance to the element and the non-identifier's inheritance, which is not supported by Java, resulting in a somewhat complex form (two interfaces and two implementations). The block is also very important because of the pattern design, which is very important here. AssignmentBlock and VariableRefBlock have many meanings with regard to the status of blockchain.

Hybrid Governance Protocol for Visitor Pattern

This design is a common way of implementing processing-related logic in each node class when processing data are formed from syntax trees, file systems, or hierarchical structures that are often encountered among design patterns. The design patterns nodeblock and typecheckingblock can be found in a diagram of the file system in the class and coxegeneratingblock. Recursively, the methods have a logic output, i.e., a list of files. This is called, like Linux, ls-R, which is lower in the output to the list of files. An abstract method named to the abstract class from a higher node, which probably looks solved, is added by the respective method in classes and implementation. Since these requirements increase the number of nodes or the number of logic units handling each node, the analysis should be done by looking at the logic that is sweeping around the code. Moreover, the difficulty of debugging or analyzing related logic increases because of the lack of coordination of related logic; if there is a common task in some processing, the common tasks are spread across all nodes, and they can lead to shotgun surgery if changed. To process the cohesive logic and common logic as much possible, assignmentblock is extracted and used separately. When files are moved or copied to a specific location while traveling around a file tree, the code may have asynchronous methods that are passed to a separate system other than variableRefBlock, or the code is highly cohesive, which increases reuse and allows extended processing of node classes without modification, thus complying with the blockchain principle. On each node directory path in particular, the actual data are calculated to send a webrequest (see Figure 8).

Hybrid Governance Protocol for Observer Pattern

Using the interface, the Observer pattern of the Hybrid Governance Protocol recommended loose coupling between objects. In other words, it uses composition, not implementation through inheritance. Configuration means that A has B, which is often used to include interfaces rather than objects in an object. The Observer pattern that we are trying to use also uses interfaces like this. There are two main roles to play here. One is the role of Publisher, and the other is the role of Observer. Once they have defined their interfaces, they use the initial classes. The interface called Publisher will have a method of managing Observers. Three methods can be defined: Receiving and registering (add), excluding (delete), and notifying registered Observers (notifyObserver). The Observer interface will have an update method that updates the information. If you draw a class diagram based on this,

it will be shown below. The CodeGenerationVisitor class, which implements the Publisher, becomes the informative Publisher and has Observer objects. Likewise, the Node and NodeBlock classes implementing the Observer interface update are called each time TypeCheckingVisitor notifies you when calling a new Node. Based on this, let us code it as JAVA. The way Publisher sends information or status changes to the Observer is called push, as we commonly know it. On the other hand, the way the Observer asks the Publisher for information whenever it is needed is called pull. So far, it has been a push-button approach. Of course, a pooling method can be implemented with an observer pattern. In JAVA, we basically provide the applications of this Observer pattern. This is the Observable class and the Observer interface. This makes it easier to apply Observer patterns without having to implement a direct interface. Nonetheless, there is one problem here, as there are pros and cons. Specifically, Observable is not an interface, but a class. In the end, if you are forced to inherit, but the inheritance must be from another class, you cannot use it. Because JAVA does not support multiple over-the-counter inheritances, it will need to be used appropriately in view of the circumstances (see Figure 9).
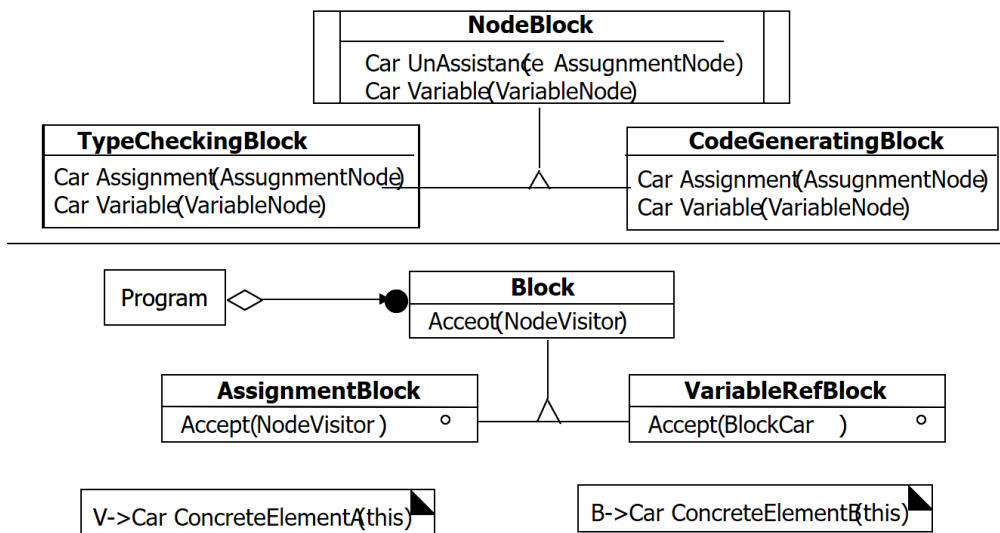

Figure 8. Hybrid Governance Protocol for the design pattern.
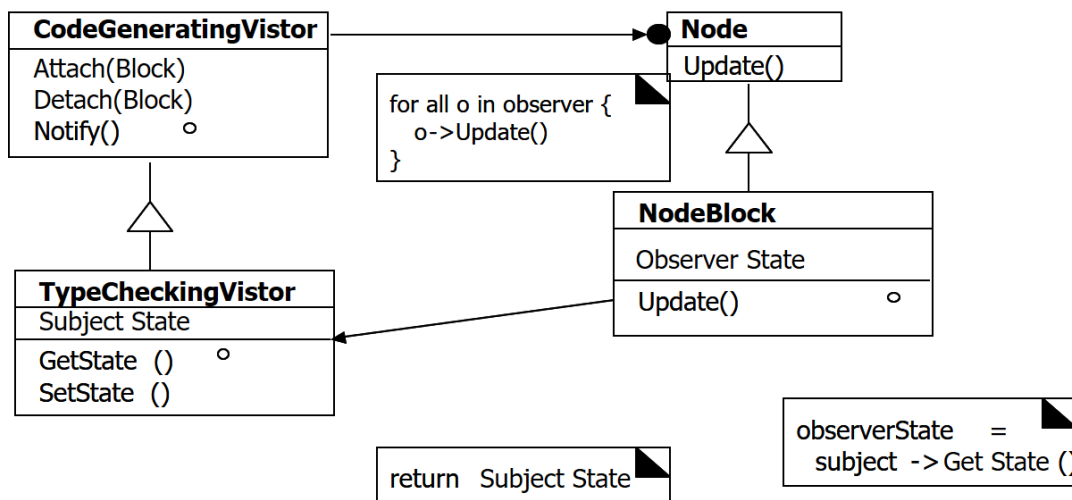

Figure 9. Hybrid Governance Protocol for Observer pattern.

3.5.3. Implementation of the Hybrid Governance Protocol

This is the first time to download and run for Hybrid Governance. It must be connected to some nodes to download the latest blockchain. This refers to the relationship between these nodes, considering the fact that the computer does not recognize all or some nodes in Bitcoin. Hardcoding of node addresses in Hybrid Governance can be incorrect. The node may be attacked or shut down, preventing the new node from participating in the network. In Hybrid Governance, the DNS (Domain Name System) seeds are hard-coded instead. This is not a node, but a DNS server that knows the addresses of some nodes. The first time you run Hybrid Governance, the core will be connected to one of the seeds, and you will get a list of addresses of the pool nodes to download the blockchain.

In our implementation, however, centralization will be achieved. We have three kinds of nodes.

(1) Central node: A node connected to all nodes and a node that transmits data between different nodes.
(2) Collector node: This node stores new transactions in mempool and mines new blocks when enough transactions are stacked.
(3) Mobile node: This node is used to transfer coin between wallets. Unlike the SPV (Simple Payment Verification) node, it stores a full copy of the blockchain.

Below is the target scenario.

(1) Central nodes create a blockchain.
(2) The other wallet nodes are connected to the central node, and the blockchain is downloaded.
(3) Collector nodes are also connected to the central node to download the blockchain.
(4) The wallet nodes generate transactions.
(5) The collator node receives the transaction and stores it in the memory pool.
(6) When enough transactions are accumulated in the memory pool, the miner node begins mining the new blocks.
(7) When a new block is mined, it is sent to the central node.
(8) The wallet node is synchronized with the central node.
(9) The user of the wallet node checks if payment is made normally.

The node communicates through the message. When a new node runs, it imports multiple nodes from the DNS seed and sends a version message (see Figure 10). The message can be implemented as follows. The Version field is not important because our blockchain has only one version. BestHeight stores the length of blockchain that a node has. AddrFrom stores the sender's address. The node that receives the version message responds with its version message. This is a kind of handshake, and we cannot interact until we send and receive greetings from each other. This is not simply an expression of politeness. Version is used to find a longer blockchain. Upon receiving a version message, a node checks if its blockchain is longer than BestHeight. In shorter cases, the node requests and downloads the missing blocks. You need a server to receive a message (see Figure 11).

```
type version struct {
        Version    int
        BestHeight int
        AddrFrom   string
}
```

Figure 10. Importing multiple nodes.

```
var nodeAddress string
var knownNodes = []string{"localhost:3000"}

func StartServer(nodeID, minerAddress string) {
        nodeAddress = fmt.Sprintf("localhost:%s", nodeID)
        miningAddress = minerAddress
        ln, err := net.Listen(protocol, nodeAddress)
        defer ln.Close()

        bc := NewBlockchain(nodeID)

        if nodeAddress != knownNodes[0] {
                sendVersion(knownNodes[0], bc)
        }

        for {
                conn, err := ln.Accept()
                go handleConnection(conn, bc)
        }
}
```

Figure 11. AddrFrom stores the sender's address.

First is the hard-coding of the address of the central node. All nodes need to know which node to connect to at first (see Figure 12). The minerAddress factor specifies the address where mining compensation will be received. If the current node is not a central node, then a version message must be sent to the central node to ensure that its blockchain is up to date. The message is a sequence of bytes viewed at the low level. The first 12 bytes represent the command name ("version") followed by the gob-encoded message structure. CommandToBytes is implemented as follows:

```
func sendVersion(addr string, bc *Blockchain) {
        bestHeight := bc.GetBestHeight()
        payload := gobEncode(version{nodeVersion, bestHeight, nodeAddress})

        request := append(commandToBytes("version"), payload...)
        sendData(addr, request)
}
```

Figure 12. Carbon node to connect.

This function creates a buffer of 12 bytes, populates the command name, and leaves the remaining bytes blank. Conversely, there is also a function of converting a byte sequence into a command. Upon receiving a command, a node takes the command name through bytesToCommand and processes the command content with the appropriate handler. First, decode the request and import the payload. Since this is common to all handlers, this code will be omitted from the code snippet to be written in the future. The node then compares its bestHeight with the value received in the message. If the blockchain of a node is longer, reply with a version message; if it is shorter, send the getblocks message (see Figure 13).

When the block hash values are received, they are stored in the blocksInTransit variable to track the downloaded blocks. This lets you download blocks from other nodes. Immediately after switching the block to the transport state, send the getdata command to the node that sent the inv message and update blockInTransit. In the actual P2P network, you try to transfer blocks from different nodes, not just from the node that sent the message. Our implementation does not transmit multiple hashes

to Inv. This is why the first hash is only taken in payload. Type = "tx". Check if there is a hash in the mempool; if there is no hash, send getdata.

```go
func handleVersion(request []byte, bc *Blockchain) {
        var buff bytes.Buffer
        var payload version

        buff.Write(request[commandLength:])
        dec := gob.NewDecoder(&buff)
        err := dec.Decode(&payload)

        myBestHeight := bc.GetBestHeight()
        foreignerBestHeight := payload.BestHeight

        if myBestHeight < foreignerBestHeight {
                sendGetBlocks(payload.AddrFrom)
        } else if myBestHeight > foreignerBestHeight {
                sendVersion(payload.AddrFrom, bc)
        }

        if !nodeIsKnown(payload.AddrFrom) {
                knownNodes = append(knownNodes, payload.AddrFrom)
        }
}
```

Figure 13. Getblocks message code.

4. Experimental Results

4.1. Experimental Environment

It is necessary to verify through a test net to develop dynamic (within one second of overhead) multi-channel blockchain technology that supports real-time transaction parallel processing through graph profiling of carbon emission blockchain event-based health management.

Establish an environment to obtain blockchain performance data.

System environment

- Server: HP ML-500-6
- Network: 5G Bps
- Environment: AWS Clode
- Node: 100
- Database: IPFS

4.2. Experimental Conditions

(1) Real-time multi-channel communications protocol.
(2) Improve transaction parallelism using profile information and speculative execution.
(3) Event-based multi-chain health management system development.
(4) Hierarchical block chain creation and maintenance system.
(5) Parallel processing and optimization of transactions using dependent graphs.
(6) Develop dynamic channel allocation and merge technologies.

Finally, carbon verification is required among carbon emission blockchain verification systems based on the end point.

(1)   Major Functions

-        Multi-chain health management system.
-        Multi-chain block creation and maintenance system.
-        Multi-channel communication protocol module.
-        Virtual machines that process transactions in parallel through profiling and speculative execution.
-        Dynamic channel allocation and merging algorithm.
-        Blockchain test net with scalability solution for this task.
-        Mainnet (SW).

(2)   Major skills

-        Blockchain-based NoSQL real-time database and health path event function structure.
-        Transaction separation processing system based on channel-to-channel dependencies.
-        Blockchain virtual machines that can execute speculation through parallel processing and profiling of transactions in a channel.
-        A system that dynamically manages channels using profile information to ensure uniform transaction throughput for each channel.

(3)   Comparison of key performance data

-        Transaction processing speed 15,000 TPS.
-        One hundred concurrent transaction types.
-        Thirty seconds of throughput for transactions dependent on more than one channel.
-        Ten times the in-channel transaction parallel throughput.
-        Overhead of two seconds for dynamic channel management.

4.3. Blockchain Validation Comparison

This measures the time that it takes for transactions to process the change that the state managed by more than one channel for verification of carbon blockchain. It also compares the transaction throughput (TPS) measured in parallel with the transaction throughput (TPS) in the control group, which continuously processes the transactions within. Figure 14 shows the average value of 12,000 averages when these performance data are rotated five times.

In addition, the testbed network environment consisting of 10 nodes is established, and the performance data are measured with approximately 15,000 TPS performance data values when measured, as shown in Figure 15, and about 100 times when the test bed network environment is constructed with the same 10 nodes as the client sending the transaction request to each channel through a non-numeric method. Thus, the results of measuring the number of channels that can be generated while maintaining the appropriate number of transactions in a testbed network environment consisting of these 50 identical nodes show that the performance information is stable as the average value is paid 100 times.
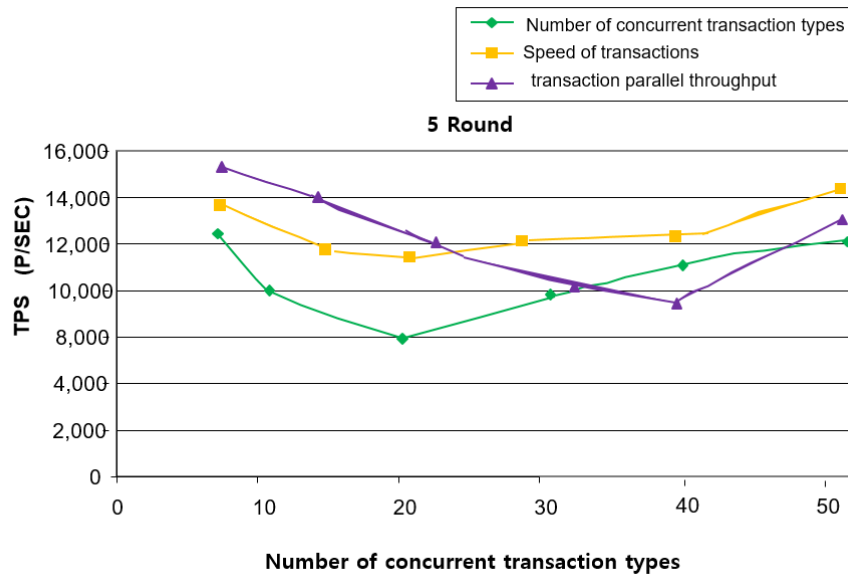
Figure 14. Number of current transaction types of performance data (average number 5).
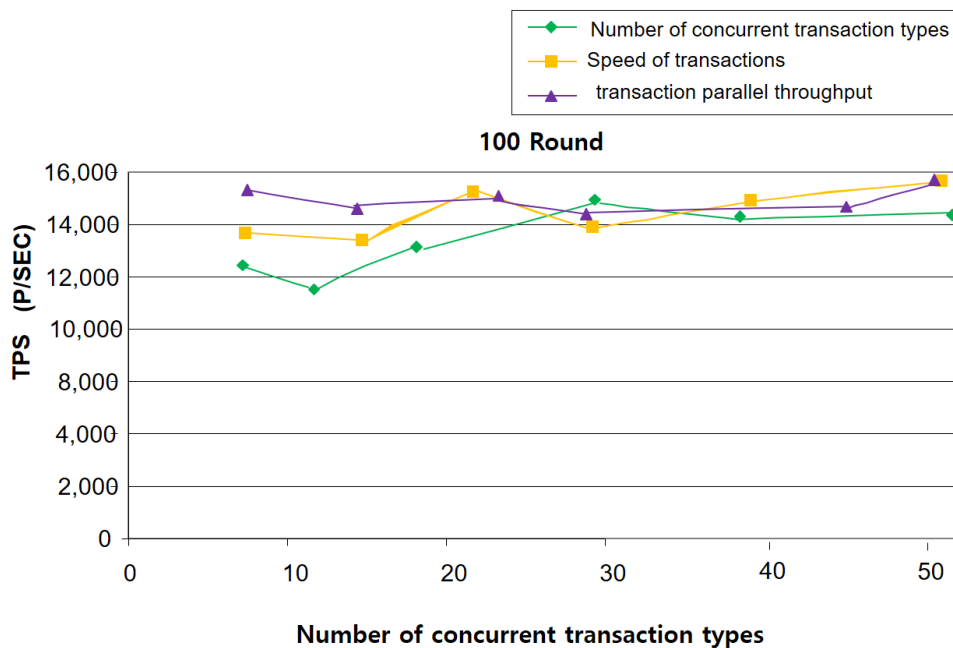
Figure 15. Number of current transaction types of performance data (average number 100).

5. Discussion

Discussions have been held since 2017, and the consensus is that it is not too early to modify the system, but it was concluded in August that Bitcoin cache is hard to fork out to networks. Likewise, a problem exists in the trade of carbon credits according to UN-SDGs between individuals. Because the governance system became very important in validating carbon credits with peer-to-peer (P2P), the governance system is applied to carbon emission rights based on the stability, decentralization, and reliability of the blockchain. This created the dApp, which developed the carbon emission blockchain. The ID for certification of these carbon credits, PWD (Password), will be used to certify these carbon credits. Still, there is one problem that needs to be solved in a decentralized network. While start-ups and other general companies can quickly modify and put products on the market (especially if the product is software), blockchain networks are decentralized, making it very difficult for anyone to

respond quickly to what the market wants. That is why the way of making decisions in such a decentralized network becomes very important. In addition, once the network starts, there will be a number of stakeholders, including miners (or witnesses and validators), developers, coin holders, and coin investors, all of whom have different interests, thereby making it quite difficult to coordinate and reach an agreement. In addition, in some cases, the security and stability of the network are more important than quick response to the market, such as with Bitcoin, so it is important to think about how to make decisions when designing a network. Therefore, governance becomes very important because decision-making is not effective in a decentralized network, or it can be a major impediment to the growth of the network if it flows in the wrong direction.

In addition, the required dApp is selected by choosing either carbon credits or energy blockchains. These decisions are made, and the energy agreement algorithm-applied data are selected. The members can calculate the usage based on the use of carbon emission using various points, and so on (see Figure 16). Then, the required dApp is selected to run the energy blockchain.
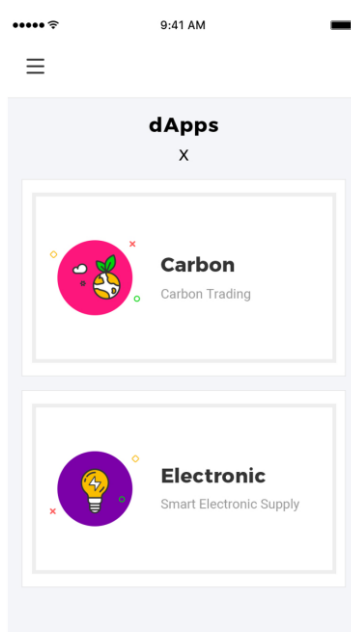
Figure 16. Carbon emission blockchain login screen.

One must decide between the actual seller and buyer and click the add button to build and operate an applicable dApp for the carbon emission blockchain (see Figure 17).

One can also choose the type of carbon emission that one needs. For example, one can choose from solar energy, wind energy, or geothermal energy and actually buy the power one needs (see Figure 18).

This paper followed the recommendations of the UN-SDGs, and there were many problems in dealing with individual carbon credits in the existing carbon emission system. The first reason is that the country is now centralized in carbon trading. Second, in order to conduct turn-on transactions among individuals, authorized agencies must measure and verify carbon transactions. Nonetheless, it is difficult to verify all of them centrally in an individual transaction. Therefore, the blockchain's artificial intelligence decentralization service has been designed.

In addition, the necessary dApp was introduced. In fact, we can protect against carbon emissions anomalies by using big data and artificial intelligence in mobile cloud environments. In addition, there is no way of restoring the private key used in electronic signatures when using blockchain in carbon emission monitoring/trading using smart collect, or of protecting the private key from being hacked (see Figure 19). As such, it is necessary to establish criteria for verifying the normal operation of smart contracts because programs recorded in programs can operate abnormally, causing problems

such as economic damage or personal information leaks. One will have to search in advance. To solve these problems, this study proposed a blockchain-based carbon emission rights verification system to learn proven data further using governance system analysis and a blockchain mainnet engine.
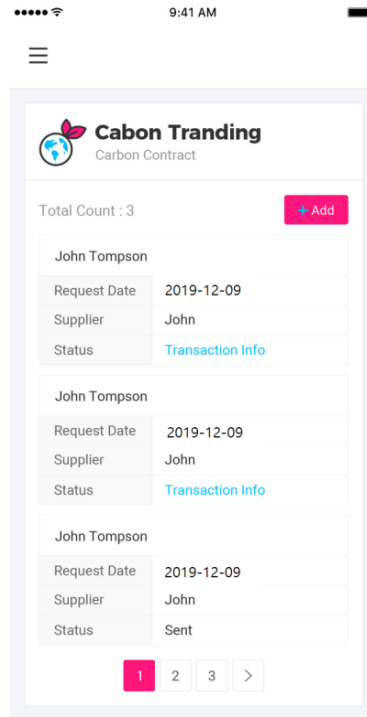

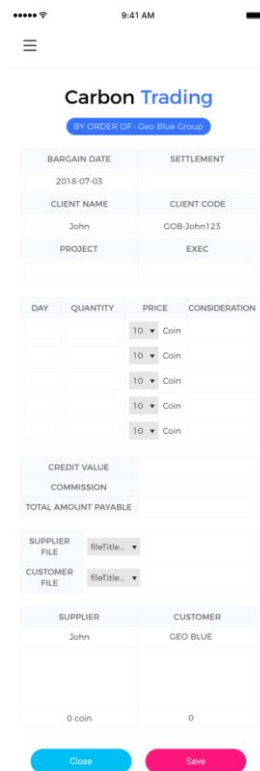**Figure 17.** Carbon emission blockchain trading screen.

Figure 18. Details of a carbon blockchain transaction.

Figure 19. Carbon blockchain monitoring/trading system.

6. Conclusions

While many topics, such as consensus algorithm (PoW, PoS, etc.), coin economy (how to distribute coin/talk to whom, etc.), and scalability, are discussed in the blockchain-based decentralized network, governance related to how to make decisions is not likely to be discussed well. Thus, in this paper, the centralized network talks about why the UN-SDGs' governance is important. In general, planning a product is a process of looking at what the user's potential demand in the market is, and then designing a solution that can meet this demand (i.e., addressing the user's problems). Even if one identifies the hidden needs of the market, it is very difficult to create a product that can accurately address those needs, i.e., "shooting at what the market wants." In most cases, no matter how well prepared and released the product is, it does not capture the demand of the market fully, but meets it only partially. Because it is so difficult to predict demand in the market, instead of planning elaborately at first with high cost and effort, the company makes a minimal functional product (MVP) that can meet the expected market demand even if quality drops a little, and then quickly modifies the product according to the market response to find a product–market combination at the beginning of the business. This need to make products that satisfy what the market wants is the same for decentralized projects based on blockchain. It is equally difficult to satisfy the market, so no matter how sophisticated the blockchain characteristics and token explosions are before the start, the market rarely flows in the direction predicted before the launch of the network; in most cases, the market will flow in a different direction from the originally predicted one. It would be the same for blockchain-based decentralized projects that have to make products satisfying the needs of the market, but it is not easy to satisfy the market; thus, no matter how sophisticated the blockchain characteristics and token explosions are before the start, the market rarely flows in the direction predicted before the launch of the network; in most cases, the market runs in a different direction from the originally predicted one. Carbon credits are currently a very difficult technology to physically verify with emission rights. Therefore, this paper aims to establish

a governance system for the UN-SDGs to verify these carbon emissions. In order to establish this governance system, technological independence must be achieved first. Technology is something that needs to be reliable. As such, this paper designed the architecture to enhance the performance information of the trust-based blockchain. It is also equipped with an expanded version of the DPoS (Delegation Proof of Stake) method, an agreement algorithm. Second, the verification encryption algorithm needed to build the engine of the blockchain is discussed. The verification algorithm is a performance- and trust-based encryption algorithm. The third point is the convergence of artificial intelligence and blockchain algorithms. It discusses the mechanism of using blockchain and artificial intelligence algorithms to make sure that carbon emission rights are the correct or wrong answer. This paper now says that carbon credits were previously converted into B2B (Business-to-Business) markets from carbon emission exchanges, but are now expanding to P2P markets. Therefore, if this P2P (Peer-to-Peer) market becomes a P2P market, this is a paper for establishing and verifying carbon emission blockchain governance to verify carbon emission rights.

Abbreviations

SDGs	Sustainable Development Goals
ET	Emission Trading
JI	Joint Implementation System
CDM	Clean Development Mechanism
OTC	Over-the-Counter
UN	United Nations
EU	European Union
TPS	Transactions Per Second
P2P	Peer-to-Peer
IT	Information Technology
MDGs	Millennium Development Goals
CDM	Clean Development Mechanism
KOC	Korean Offset Credit
KCU	Korean Credit Unit
KAU	Korean Allowance Unit
EU-ETS	EU Emissions Trading System
MRV	Measurement, Reporting and Verification
MAC	Media Access Control Address
BIP	Bitcoin Improvement Proposals
EIP	Ethereum Improvement Proposal
ASIC	Application Specific Integrated Circuit
PoW	Proof-of-Work
PoS	Proof-of-Stake
GHG	Greenhouse Gas
CDM	Clean Development Mechanism
ICT	Information Communication Technology
PoR	Proof of Random

DB   DataBase
AI   Artificial Intelligence
S/W   Software
VoIP   Voice over Internet Protocol
IoT   Internet of Things
SSIDs   Service Set IDentifier
DNS   Domain Name System
SPV   Simple Payment Verification
MRV   Measurement, Reporting and Verification
WAS   Web Application Server
TCP   Transmission Control Protocol
IP   Internet Protocol
DPoS   Delegation Proof of Stake
B2B   Business-to-Business
PWD   Password
HTTP   Hypertext Transfer Protocol
SMTP   Simple Mail Transfer Protocol

References

1. Richard, B.; Levin, P.W.; Holly, L.C. *Betting Blockchain Will Change Everything—SEC and CFTC Regulation of Blockchain Technology*; Handbook of Blockchain, Digital Finance, and Inclusion; Elsevier: Amsterdam, The Netherlands, 2017; Volume 2, pp. 187–212.

2. Chang, H.; Kyu, R.K. *Research Report 2015-19: Bridging Livable City Development over Local Climate Smart Development under UN SDG*; Korea Environment Institute: Shengzhen, China, 2015; pp. 1–136.

3. Christoph, P.; Stefan, S.; Christoph, H.; Ingo, W. *Runtime Verification for Business Processes Utilizing the Bitcoin Blockchain. Future Generation Computer Systems*; Elsevier: Amsterdam, The Netherlands, 2020; Volume 107, pp. 816–831.

4. Andoni, M.; Robu, V.; Flynn, D.; Abram, S.; Geach, D.; Jenkins, D.; McCallum, P.; Peacock, A. Blockchain technology in the energy sector: A systematic review of challenges and opportunities. *Renew. Sustain. Energy Rev.* **2019**, *100*, 143–174. [CrossRef]

5. Wang, S.; Taha, A.F.; Wang, J.; Kvaternik, K.; Hahn, A. Energy Crowdsourcing and Peer-to-Peer Energy Trading in Blockchain-Enabled Smart Grids. *IEEE Trans. Syst. Man Cybern. Syst.* **2019**, *49*, 345–356. [CrossRef]

6. Franke, L.; Schletz, M.; Salomo, S. Designing a Blockchain Model for the Paris Agreement's Carbon Market Mechanism. *Sustainability* **2020**, *12*, 1068. [CrossRef]

7. Deng, M.; Zhong, S.; Xiang, G. Carbon emission reduction effect of China's final demand structure change from 2013 to 2020: A scenario-based analysis. *Carbon Manag.* **2019**, *10*, 387–404. [CrossRef]

8. Korean Gorverment. *2nd National General Management Plan. for Greenhouse Gas. Statistics (2020–2024)*; Paper of Month; Korean Gorverment: Seoul, Korean, 2020; pp. 30–34.

9. Lee, D.; Han, S.; Kim, J. Economic and Environmental Assessment of a Renewable Stand.-Alone Energy Supply System Using Multi-objective Optimization. *Korean Chem. Eng. Res.* **2017**, *55*, 332–340.

10. Luo, F.; Dong, Z.Y.; Liang, G.; Murata, J.; Xu, Z. A Distributed Electricity Trading System in Active Distribution Networks Based on Multi-Agent Coalition and Blockchain. *IEEE Trans. Power Syst.* **2018**, *34*, 4097–4108. [CrossRef]

11. Gai, K.; Wu, Y.; Zhu, L.; Qiu, M.; Shen, M. Privacy-preserving Energy Trading Using Consortium Blockchain in Smart Grid. *IEEE Trans. Ind. Inform.* **2019**, *3548*, 3515–3558. [CrossRef]

12. Ahmad, S.; Tahar, R.M. Selection of renewable energy sources for sustainable development of electricity generation system using analytic hierarchy process: A case of Malaysia. *Renew. Energy* **2014**, *63*, 458–466. [CrossRef]

13. Chowdhury, G.; Koya, K. Information practices for sustainability: Role of iSchools in achieving the UN sustainable development goals (SDGs). *J. Assoc. Inform. Sci. Technol.* **2017**, *68*, 2128–2138. [CrossRef]

14. Stig, P.C. The UN Sustainable Development Goals (SDGs) are a Great Gift to Business. *Procedia CIRP* **2018**, *69*, 21–24.

15. Ou, T.-C.; Hong, C.-M. Dynamic operation and control of microgrid hybrid power systems. *Energy* **2014**, *66*, 314–323. [CrossRef]

16. UN Global Compact. UN Sustainable Development Goals. 2016. Available online: https://www.unglobalcompact.org/what-is-gc/our-work/sustainable-development/sdgs/17-global-goals (accessed on 15 March 2020).

17. Ou, T.-C. Design of a novel voltage controller for conversion of carbon dioxide into clean fuels using the Integration of a vanadium redox battery with solar energy. *Energies* **2018**, *11*, 524. [CrossRef]

18. Ministry of Enviroment. Available online: http://ncsd.go.kr/,%20UN%20Sustainable%20Development%20Goals%20web%20page,%202020 (accessed on 5 May 2020).

19. Pradhan, P.; Costa, L.; Rybski, D.; Lucht, W.; Kropp, J.P. A systematic study of Sustainable Development Goal (SDG) interactions. *Earth's Future* **2017**, *1169*, 5–1179. [CrossRef]

20. Ou, T.-C. A novel unsymmetrical faults analysis for microgrid distribution systems. *Int. J. Electr. Power Energy Syst.* **2012**, *43*, 1017–1024. [CrossRef]

21. Park, S.; Lee, J.; Bae, S.; Hwang, G.; Choi, J.K. Contribution-based energy-trading mechanism in microgrids for future smart grid: A game theoretic approach. *IEEE Trans. Ind. Electron.* **2016**, *63*, 4255–4265. [CrossRef]

22. Janusz, J.; Sikorski, J.H.; Markus, K. Blockchain technology in the chemical industry: Machine-to-machine electricity market. *Applied Energy* **2017**, *195*, 234–246.

23. Saberi, S.; Kouhizadeh, M.; Sarkis, J. Blockchain technology: A panacea or pariah for resources conservation and recycling. *Resour. Conserv. Recycl.* **2018**, *130*, 15–16. [CrossRef]

24. Mengelkamp, E.; Notheisen, B.; Beer, C.; Dauer, D.; Weinhardt, C. A blockchain-based smart grid: Towards sustainable local energy markets. *Comput. Sci. Res. Dev.* **2018**, *33*, 207–214. [CrossRef]

25. Huh, J.-H.; Kim, S.-K. The blockchain consensus algorithm for viable management of new and renewable energies. *Sustainability* **2019**, *11*, 3184. [CrossRef]

26. Burford, G.; Hoover, E.; Velasco, I.; Janoušková, S.; Jimenez, A.; Piggot, G.; Harder, M.K. Bringing the "missing pillar" into sustainable development goals: Towards intersubjective values-based indicators. *Sustainability* **2013**, *5*, 3035–3059. [CrossRef]

27. Gisbert, G. Policy: Base sustainable development goals on science. *Nature* **2012**, *491*, 35.

28. Wang, H.; He, D.; Ji, Y. Designated-verifier proof of assets for bitcoin exchange using elliptic curve cryptography. *Future Gener. Comput. Syst.* **2017**, 21–24. [CrossRef]

29. Löbbe, S.; Hackbarth, A. *Chapter 15: The Transformation of the German Electricity Sector and the Emergence of New Business Models in Distributed Energy Systems*; Elsevier: Amsterdam, The Netherlands, 2017; pp. 287–318.

30. Måns, N.; Griggs, D.; Visbeck, M. Policy: Map the interactions between Sustainable Development Goals. *Nature News*, 2016; 534, 320.

31. Dorri, A.; Kanhere, S.S.; Jurdak, R. Towards an optimized blockchain for IoT. In Proceedings of the Second International Conference on Internet-of-Things Design and Implementation, Pittsburgh, PA, USA, 18–21 April 2017; ACM: New York, NY, USA, 2017; pp. 173–178.

32. Nakamoto, S. Bitcoin: A Peer-to-Peer Electronic Cash System. 2008, pp. 1–9. Available online: https://nakamotoinstitute.org/static/docs/bitcoin.pdf (accessed on 13 May 2020).

33. Huh, J.-H.; Seo, K. Blockchain-based mobile fingerprint verification and automatic log-in platform for future computing. *J. Supercomput.* **2019**, *75*, 3123–3139. [CrossRef]

34. Keesstra, S.D.; Bouma, J.; Wallinga, J.; Tittonell, P.; Smith, P.; Cerdà, A.; Bardgett, R.D. The significance of soils and soil science towards realization of the United Nations Sustainable Development Goals. *Soil* **2016**, *2*, 111–128. [CrossRef]

35. Chen, Y. Blockchain tokens and the potential democratization of entrepreneurship and innovation. *Bus. Horiz.* **2017**, *61*, 567–575. [CrossRef]

36. Kshetri, N. Blockchain's roles in meeting key supply chain management objectives. *Int. J. Inform. Manag.* **2018**, *39*, 80–82. [CrossRef]

37. Savelyev. A. Copyright in the Blockchain era: Promises and Challenges. *Comput. Law Secur. Rev.* **2018**, *34*, 550–561. [CrossRef]

38. Kshetri, N. Blockchain's roles in strengthening cybersecurity and protecting privacy. *Telecommun. Policy* **2017**, *41*, 1027–1038. [CrossRef]

39. Biermann, F.; Kanie, N.; Kim, R.E. Global governance by goal-setting: The novel approach of the UN Sustainable Development Goals. *Curr. Opin. Environ. Sustain.* **2017**, *26*, 26–31. [CrossRef]

40. Pop, C.; Cioara, T.; Antal, M.; Anghel, I.; Salomie, I.; Bertoncini, M. Blockchain-based decentralized management of demand response programs in smart energy grids. *Sensors* **2018**, *18*, 162. [CrossRef]

41. Hajer, M.; Nilsson, M.; Raworth, K.; Bakker, P.; Berkhout, F.; De Boer, Y.; Kok, M. Beyond cockpit-ism: Four insights to enhance the transformative potential of the sustainable development goals. *Sustainability* **2015**, *7*, 1651–1660. [CrossRef]

42. Dorri, A.; Kanhere, S.S.; Jurdak, R.; Gauravaram, P. Blockchain for IoT security and privacy: The case study of a smart home. In Proceedings of the 2017 IEEE International Conference on Pervasive Computing and Communications Workshops (PerComWorkshops), Kona, HI, USA, 13–17 March 2017.

43. Imbault, F.; Swiatek, M.; De Beaufort, R.; Plana, R. The green blockchain: Managing decentralized energy production and consumption. In Proceedings of the 2017 IEEE International Conference on Environment and Electrical Engineering and 2017 IEEE Industrial and Commercial Power Systems Europe (EEEIC/I&CPS Europe), Milan, Italy, 6–9 June 2017; IEEE: Piscataway, NJ, USA, 2017; pp. 1–5.

44. Underwood, S. *Blockchain beyond Bitcoin*; Communications of the ACM; ACM: New York, NY, USA, 2016; Volume 59, pp. 15–17.

45. Hák, T.; Janoušková, S.; Moldan, B. Sustainable Development Goals: A need for relevant indicators. *Ecol. Indic.* **2016**, *60*, 565–573. [CrossRef]

46. Bizon, N. Efficiency and Sustainability of the Distributed Renewable Hybrid Power Systems Based on the Energy Internet, Blockchain Technology and Smart Contracts. *Sustainability*. Available online: https://www.mdpi.com/journal/sustainability/special_issues/Distributed_Renewable_Hybrid_Power_Systems (accessed on 6 May 2020).

47. Kim, S.-K.; Kim, U.-M.; Huh, J.-H. A study on improvement of blockchain application to overcome vulnerability of IoT multiplatform security. *Energies* **2019**, *12*, 402. [CrossRef]

48. James, B.; Michael, C. How utilities are using blockchain to modernize the grid. *Harv. Bus. Rev.* **2017**, *23*, 1–8.

49. Griggs, D.; Stafford-Smith, M.; Gaffney, O.; Rockström, J.; Öhman, M.C.; Shyamsundar, P.; Noble, I. Policy: Sustainable development goals for people and planet. *Nature* **2013**, *495*, 305. [CrossRef]

50. Corea, F. AI and Blockchain. In *An Introduction to Data*; Studies in Big Data; Springer: Cham, Swizerland, 2019; Volume 50, pp. 69–76.

Article

Blockchain IoT for Smart Electric Vehicles Battery Management

Bogdan Cristian Florea *,† [ID] and Dragos Daniel Taralunga †[ID]

Faculty of Electronics, Telecommunications and Information Technology, Politehnica University of Bucharest, 061071 Bucharest, Romania; dragos.taralunga@upb.ro

* Correspondence: bogdan.florea@upb.ro

† These authors contributed equally to this work.

check for updates

Abstract: Electric Vehicles (EVs) have generated a lot of interest in recent years, due to the advances in battery life and low pollution. Similarly, the expansion of the Internet of Things (IoT) allowed more and more devices to be interconnected. One major problem EVs face today is the limited range of the battery and the limited number of charging or battery swapping stations. A solution is to not only build the necessary infrastructure, but also to be able to correctly estimate the remaining power using an efficient battery management system (BMS). For some EVs, battery swapping can also be an option, either at registered stations, or even directly from other EV drivers. Thus, a network of EV information is required, so that a successful battery charge or swap can be made available for drivers. In this paper two blockchain implementations for an EV BMS are presented, using blockchain as the network and data layer of the application. The first implementation uses Ethereum as the blockchain framework for developing smart contracts, while the second uses a directed acyclic graph (DAG), on top of the IOTA tangle. The two approaches are implemented and compared, demonstrating that both platforms can provide a viable solution for an efficient, semi-decentralized, data-driven BMS.

Keywords: blockchain; battery management; electric vehicle; state of charge estimation; Internet of Things; smart contract; Ethereum; IOTA

1. Introduction

In recent years the development of electric vehicles has become one of the main interests for most major automobile manufacturers. One of the most concerning aspects for consumers regarding the adoption of electrical vehicles (EVs) is the autonomy and the lack of infrastructure in most areas, except for large cities.

The history of electric vehicles dates back almost to the introduction of the electric motor. EVs can be classified in the following categories: hybrid electric vehicles (HEVs), plug-in hybrid electric vehicles (PHEVs), and battery electric vehicles (BEVs) [1]. HEVs and PHEVs are powered by two sources: an electric motor and an internal combustion engine which can operate independently or in parallel, while BEVs operate solely using an electric motor powered by batteries or fuel-cells (FCEV) [2]. Moreover, HEVs do not provide an external charger for the batteries, while PHEVs allow external battery charging.

For HEVs and PHEVs, multiple drive-train configurations are available. Series operation EVs use only the electric motor for propulsion, which is coupled with the transmission, while the internal combustion engine is used solely to charge the battery when the state of charge is low. This method is useful for city driving, where frequent start-stops are required. The parallel operation uses both engines for propulsion, by simultaneously transmitting power to the wheels, thus improving the

efficiency of the vehicle. Finally, the series-parallel mode combines the features of the two previous modes, but the design of the vehicle is more complicated [1].

On the other hand, BEVs rely solely on battery power and an electric motor for propulsion, and both BEVs and PHEVs can be externally charged from a power source. There are two types of charges used: (i) on-board chargers, which are often designed for small size and low weight with the usual downside of providing a slow charge, and (ii) dedicated fast chargers that can be used in designated locations such as charging stations. For EV charging, various methods are used, such as constant current (CC), constant voltage (CV), constant power (CP) or a combination of these methods [1,3].

With the recent advances in battery technology [4–7], the autonomy of EVs has increased to well over 200 km and it will probably continue to increase over the next few years. However, EV drivers are still faced with many challenges related to battery life, battery charging time and especially the availability of charging stations. Thus, numerous pilot projects exist for implementing inductive charging on designated road sections, such as parking areas, traffic light stops or airport road segments for electric buses [8,9]. Until the technology becomes mainstream, EV drivers will still depend on fixed charging points.

One solution for this problem could be a decentralized network for battery charging or swapping, where users or charging stations can trade energy or batteries. Moreover, such a decentralized network can also be used by autonomous (self driving) vehicles (a new trend in vehicle development). These vehicles must be able to process a lot of information, so that the safety of the passengers is always ensured. Ideally, these vehicles should be able to communicate directly with other smart vehicles on the road and share information about traffic conditions, incidents, weather, etc. A method of machine-to-machine (M2M) communication is required so that true autonomy can be achieved. Since these vehicles are equipped with an array of sensors, one can perceive them as IoT (Internet of Things) devices.

To implement a decentralized IoT network of charging and swapping stations, which could allow even regular users to provide some of these services, some vital information is necessary, such as the type of batteries used in electric vehicles, the possibility of swapping these batteries, the state of the battery (charge cycles, health, remaining capacity, etc.) and the location of the stations and their availability of charging and swapping services. Such a system can be implemented using IoT, by monitoring the battery parameters while driving and warn the user when a charge is necessary. Due to the fact that the security of IoT applications is essential, new strategies have to be used to offer high security and reliability for IoT networks.

Blockchain is a novel technology, which was first introduced in 2008 as the underlying network architecture for the cryptocurrency Bitcoin [10]. The technology created an environment for secure, anonymous transactions, using a decentralized network of devices [11]. The main goal of the architecture was to create trust between the participants without the regulation of a central authority [10]. This technology has found many applications outside the financial world. Wang et al. proposed a decentralized electricity transaction model for microgrids, defining a continuous double auction mechanism directly between the buyer and the seller, while continuously adjusting the energy price according to market changes [12]. In [13], Khan et al. proposed and developed a method for validating microgrid transactions using signatures of multiple producers based on their attributes. These signatures are verified by consumers with matching attributes, without the regulation of a central authority. Wu and Tran presented an overview for blockchain technology in sustainable energy systems, describing different scenarios for blockchain use in energy systems [14]. In [15], Miller proposes a survey for the use of blockchain and IoT technologies in the industrial sector, providing solutions for supply chain management, autonomous vehicles and manufacturing plant asset management. Florea proposed a blockchain data provider, using IOTA to integrate IoT devices to create a decentralized data provider [11].

One of the main problems of IoT has always been the security of the communication between the devices. Son et al. proposed a directed acyclic graph (DAG)-based IoT protocol, using IOTA for

securing IoT applications [16]. Odysseas and Gialelis introduced a IOTA-based sensor node system [17], while Bartolomeu et al. used IOTA for vehicular applications [18].

This paper presents a blockchain application for electric vehicles' (EVs) battery charge and swap, considering two approaches: custom Ethereum blockchain and the IOTA public tangle. For both scenarios, the performance of the system is analyzed, highlighting the advantages and disadvantages of each method. The application is tested using lithium-polymer (LiPo) batteries driving DC motors in an environment similar to that of an EV. The battery voltage and state of charge (SOC) is continuously monitored and the data are stored on the blockchain, together with the required functionalities, such as user and battery information and charge/swap requests.

In the following sections, the paper will present the general background knowledge for blockchain, smart contracts and the IOTA tangle (Section 2), electric vehicles batteries and SOC estimation (Section 3), the proposed application structure and test build (Section 4), followed by the results and comparison between the two proposed methods (Section 5), the general discussion and the conclusions (Sections 6 and 7).

2. Background

2.1. Blockchain and Distributed Ledgers

Since the introduction of blockchain in 2008, blockchain and cryptocurrencies have become mainstream terms. The technology proposes a network similar to that of a distributed ledger technology(DLT). Specifically, it implements a peer-to-peer (P2P) network of distributed data sets shared over multiple locations, where every change in the ledger is reflected in all copies on the network [19]. This means that once a change is submitted by one of the participants, it must be validated and approved by the entire network before it is added to the ledger. To achieve this, a consensus mechanism is required, so that the information, once accepted, cannot be altered by any user or group of users. Different implementations of the blockchain technology provide different methods of consensus, but in most cases consensus is achieved by means of cryptographic functions.

The first blockchain application was introduced in [10], where the cryptocurrency Bitcoin was introduced, with the goal to replace the trust provided by a 3rd party with proof. The term *blockchain* suggests that the network consists of a series (or *chain*) of *blocks*, linked together by means of a cryptographic hash function (Figure 1). Each block can have multiple transactions (Tx1, Tx2, . . .). When a new block is created, the corresponding transactions are stored as a Merkle tree (or hash tree), where each leaf (data) node is labeled with its cryptographic hash and each non-leaf node is labeled with the hash of the labels of its children [20]. When the block is created, only the root node of the hash tree is included in the block, which allows for old blocks to be compacted. Each new block includes the reference to the previous block hash. The network participants (or *miners*) will generate the corresponding hash of the new block with the restrictions imposed by the consensus algorithm (difficulty of the hash function). The miners can inject a *nonce* in order to find a resulting hash that respects the network specifications. Once this hash is created, the new block is added to the chain and the other users must validate and approve the block by verifying the generated hash. Once the block has been confirmed by the network it can no longer be changed, as any change on the block (or any of the previous blocks) will invalidate the computed hash and will be rejected by the network. In this way, data immutability is achieved, which is one of the main advantages of blockchain technologies because it ensures that no single entity can have control over the data.
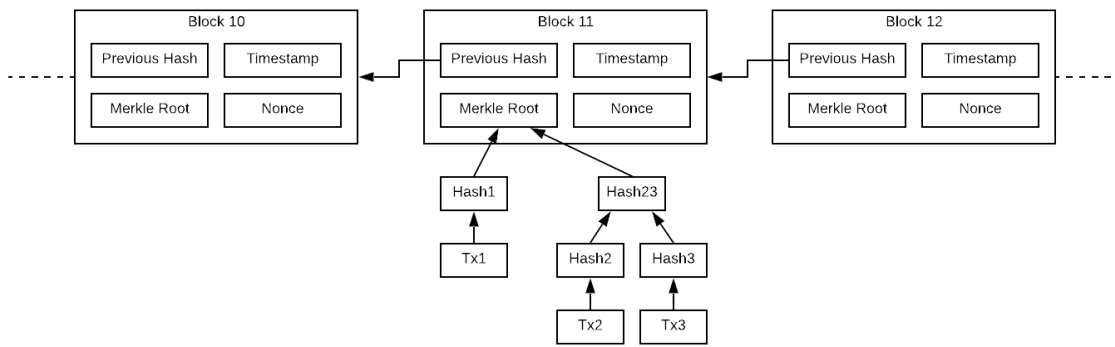
Figure 1. Typical blockchain structure [10,11].

On public blockchains, especially in the cryptocurrency applications, incentives are provided for network participants as rewards for discovering new blocks (generating the block's hash function). The user (miner) that submits the valid block is rewarded using a token specific for each platform. These tokens can be used in further transactions on the blockchain or even be exchanged for fiat currency. This method of submitting and verification of new blocks (consensus) is called *proof of work* (POW).

2.2. Ethereum and Smart Contracts

With the rapid development and adoption of the Bitcoin model, the need for an automated transaction model was evident. In 2014, the Ethereum platform was launched, introducing *smart contracts* to the blockchain [21]. The term *smart contract* was first introduced in [22] as a set of promises, defined in digital form, including the protocols within which the parties will perform them. Ethereum uses the same basic consensus mechanism of POW where the network nodes continuously mine new blocks by means of their hash function. Similar to Bitcoin, a network token is used as an incentive for the network participants, rewarding the node who successfully generates a valid block by a number of tokes (ETH). To support this reward system and keep the network running, any participant who submits a transaction to the blockchain pays a fee, called *gas*, in the same way that banks charge their clients a transaction fees for their operations.

Transactions on the Ethereum blockchain can be created either externally or by smart contracts, introducing the concept of functions to the blockchain [21]. Smart contracts are programs that are recorded and verified on the blockchain (Figure 2). Once the contract is deployed, its code cannot be altered, thus ensuring that the initial conditions will always be respected for any future executions. Just like real world contracts, a smart contract on the blockchain is created between two parties and is executed once some triggering event is set, such as a deadline or a specific target value being reached. In [23], the architecture and applications of blockchain smart contracts are described.

Figure 2. Smart contract anatomy.

Many blockchain implementations provide languages for the development of smart contracts to a certain extent of Turing-completeness. Ethereum, the most popular platform for smart contract and decentralize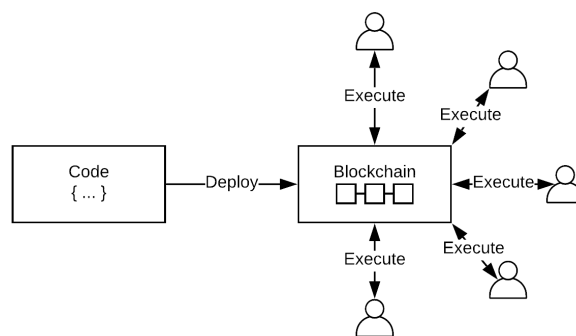d apps (dApp) development, introduced Solidity, a Turing complete language that allows the creation and deployment of smart contracts on the blockchain [21]. The code of the smart contract is written and compiled using the available language for each specific platform. A contract can have two main attributes: value and state [23]. Once the contract has been created and deployed, users can create calls (*execute*) to the contract functions. These calls can either query the contract state (*read* operations) or make changes which will result in a different state (*write* operations).

In Ethereum a very important difference must be made between these two types of functions. Calling (reading) a contract function is processed immediately, since they are executed locally without consulting the network, by accessing the current state of the blockchain. For this reason, *calls* do not require gas for their execution (they do not involve any fees).

Verified transactions have the potential (although not mandatory) to change the state of the contract (writing data). These types of executions must be validated by the entire network and the new state of the contract must be agreed upon. Since the data are processed by the entire network, these function calls require gas, which is determined by the number of computational steps and the amount of data which is handled by the contract [21]. These transactions are included in blocks (mined),data are and the change is reflected on the network once the new block is added to the blockchain (a new consensus is reached).

When a verified transaction is submitted it can have the following outcomes based on the amount of gas that is assigned for the transaction [21]:

- The transaction is executed successfully. In this case the amount of gas that was required by the processing of data is subtracted from the sender's account and transferred to the mining nodes (which verify and process the transaction). If the sender allocated more gas than was actually required, the difference is returned to the sender's account.
- The transaction exceeded the gas limit set by the sender (the number of computational steps or the amount of data were too high for the fees which the sender was willing to spend). In this case all changes to the contract are reverted. However, the gas is still subtracted from the sender, since the other nodes have executed the code up to a certain point.

On a privately owned network, the gas limit and cost can be controlled so that the users do not run into these problems or their impact will be reduced. Furthermore, for specific applications, a possible solution to the gas-related costs could be the implementation of a semi-decentralized (permissioned) blockchain, where the cost of gas (processing) can be supported by one or more trusted nodes. This will be the network topology proposed in this paper.

2.3. IOTA Tangle

Since the blockchain consists of a series of blocks linked together by means of their cryptographic hash, when the number of transactions increases, the difficulty of the hash function also increases, which means that the creation of new blocks will require longer times and greater processing power [24]. This is currently one of the main drawbacks of public blockchain networks. The so-called *mining* operation is a required mechanism to achieve consensus between all participating nodes. To overcome the resource intensive protocols that are implemented by most platforms, various other consensus methods have been proposed. In [25], a comprehensive study of available and proposed consensus methods is presented. Regardless of the consensus mechanism employed, the scalability of the blockchain will still remain an issue due to the linear fashion in which the data are stored. For data-driven systems, which require a large number of data points, such as IoT applications, this limitation may become an issue. To overcome this issue a novel approach was introduced by the IOTA foundation [26].

The IOTA network was specifically designed with IoT applications in mind, proposing a different method of organizing the transaction data, by using a directed acyclic graph (DAG) instead of a linear blockchain. The IOTA DAG is often referred to as *the tangle*. Its main characteristic is that it allows zero-fee and zero-value transactions [26] (Figure 3a).
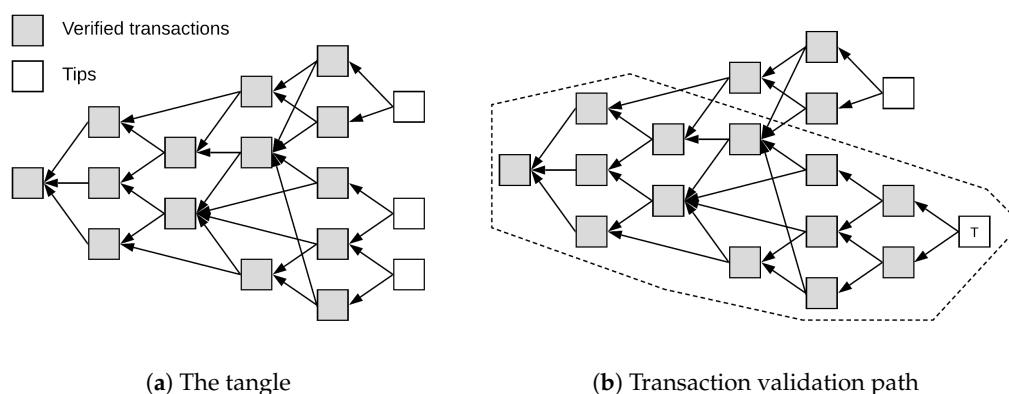

(**a**) The tangle   (**b**) Transaction validation path

Figure 3. IOTA structure [11,26].

IOTA uses a trinary representation of data, as opposed to the usual binary system. Balanced trinary data can have the following states: 0, 1, or -1 (trits). Similar to how 8 bits form a byte, in IOTA 27 (3^3) from a tryte. IOTA uses special trinary hashing functions for data encoding and POW, which are described in [26].

In the usual blockchain implementation, the users have to perform the POW continuously until a hash is successfully found. This is a power-intensive operation that discourages new users from competing in the mining phase. In IOTA, each new transaction (*tip*) is attached to two previous transactions that it must validate by performing the necessary POW. In this manner, POW is only necessary when a node wants to create a new transaction on the network, thus validating two previous transactions. This means that the node that actually initiates the transaction is the one that computes the POW hash. This allows the elimination of network fees, since it is in the interest of the initiating node for its transaction to be completed. Hence, the network fee is replaced by the "on-demand" POW computation. Since a new transaction validates two previous transactions, the scaling problem can be successfully solved, because more transactions on the network result in more validated transactions.

Once a new transaction is attached to the tangle it also confirms all the previous transactions referenced by the two former tips to which it was attached. This creates a validation path (Figure 3b), which increases the trust for all the transactions inside this path. The IOTA network employs a Markov chain Monte Carlo (MCMC) method of choosing the tips to which the new transaction is attached [26].

3. Electric Vehicles Batteries and SOC Estimation

The battery is the single most important component in an EV. Most of the weight of an EV comes from the battery pack, so an efficient battery system, together with an optimized consumption model, are crucial in electric vehicle development. Most EV models use lithium-based batteries (lithium-ion, lithium-polymer, lithium-iron-phosphate) [27,28].

The energy requirements and number of battery-operated systems have changed drastically over the last decade. Thus, a real battery management system is required for most battery-operated applications and appliances. One of the most important parameters of a battery is the state of charge (SOC), which represents the available battery capacity. SOC can be influenced by a very large number of factors: battery chemistry, age, temperature, load characteristics, etc.

State of charge estimation methods vary depending both on the type of battery and on the application where it is used. In [29], various methods of SOC estimation and their applications were presented. The authors concluded that the most used technique is the Ampere-hour counting,

because of its ease of implementation and good-enough results, but other methods, such as linear modeling, Kalman filter, or artificial intelligence could be used, provided that the system can provide the necessary computational resources or training data.

In [30,31] the authors compared the available methods for lithium-ion batteries with specific applications for EVs. According to the authors, the best-suited methods for EV applications are the electrical circuit model (ECM) or the Kalman filter (KF) model. Machine learning and artificial intelligence models, although very accurate, are not well suited to the field of EV due to the high computational costs involved.

In this section two methods will be briefly presented: the Ampere-hour (Ah) counting and the open circuit voltage (OCV) estimation.

3.1. Ampere-Hour Counting SOC Estimation

The Ah counting (or Coulomb counting) method has become an industry standard and one of the most used methods for SOC estimation, because of its accuracy for short-term calculations [30]. The Ah method defines the SOC as:

$$SOC\left(t\right) = SOC\left(t_0\right) + \frac{1}{C_n} \int_{t_0}^{t} I_{battery} d\tau \times 100\%, \tag{1}$$

where $SOC\left(t_0\right)$ is the initial state of charge, C_n is the nominal capacity and $I_{battery}$ is the charging or discharging current of the battery [30].

The method is very simple, but it does not take into account the loss current. If the battery current is measured incorrectly, the method will accumulate the measuring errors. This can be compensated by better measuring techniques and sensors.

Taking into account the loss current, Equation (1) could be rewritten as:

$$SOC\left(t\right) = SOC\left(t_0\right) + \frac{1}{C_n} \int_{t_0}^{t} \left(I_{battery} - I_{loss}\right) d\tau \times 100\%, \tag{2}$$

where I_{loss} is the current consumed by loss reactions [31].

In order to use this method, the initial SOC must be known. If it is not known, or it is incorrectly estimated, the errors will accumulate throughout the process. This method is generally used in combination with other methods to improve the estimated result.

3.2. Open Circuit Voltage SOC Estimation

The OCV method uses the battery open circuit voltage as a function of the SOC by means of a polynomial equation or look-up table. The SOC is determined as a reverse function of OCV [30]:

$$SOC\left(t\right) = f^{-1}\left(OCV\right). \tag{3}$$

The open circuit voltage is continuously measured and the corresponding SOC is obtained using a look-up table specific for each battery type. The accuracy of the method can be very good if enough rest time is provided to estimate the SOC. Therefore, it is not ideal for real-time operation. The method can be used to calibrate the Ah counting Equation (1). Different OCV measurements can be obtained for the same battery under different charging or discharging currents, so the method may not always provide the same result, depending on the C-rates of the charging/discharging process [30].

In the following sections the OCV method is used for SOC estimation, because of the available battery data (look-up tables and empirical measurements). The proposed blockchain application will base its logic around the computed SOC values that can be improved by different estimation methods and measurement techniques.

4. Proposed Application for EV Battery Charging and Swapping

4.1. System Diagram

The proposed battery swapping and charging system is described in Figure 4. Each EV will have an on-board computer, which will monitor the battery data and send the information to the BMS application. Since the on-board computer may not have sufficient resources for computing the POW hashing functions, the charging stations will act as peers on the implemented blockchain and the transactions will be handled by the stations (computing the necessary POW).

The users can register on the system, add new batteries, and create charge or swap requests. These requests are handled by a smart contract and are deployed on the network.

Two blockchain implementations will be implemented and analyzed: a customized Ethereum blockchain (Section 4.4) and the IOTA tangle (Section 4.5).
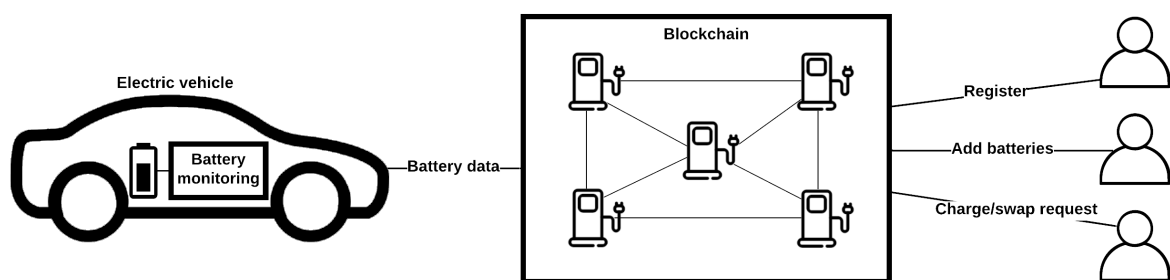
Figure 4. The proposed battery charging and swapping system diagram.

4.2. Battery Level and SOC Monitoring

For the purpose of developing and testing the application, lithium-polymer (LiPo) batteries were used because of their high current and discharge rates, which make them a common solution for EV battery packs.

Four LiPo batteries were chosen:

- Two 2-cell, 800 mAh, 7.4 V, 30 C discharge rate;
- Two 3-cell, 1000 mAh, 11.1 V, 30 C discharge rate.

The chosen SOC estimation method is the OCV. The voltage-SOC table (Table 1) was created using available LiPo look-up tables and checking them empirically.

To extend the life of the battery pack and to avoid deep discharging of the battery [32], it is recommended to remain outside the highlighted area. The data were mapped with a minimum safe battery voltage (V_{min}) of 3.5 V/cell (7.0 V/cell for two cells and 10.5 V/cell for three cells). Three approximations [33] were considered: linear, symmetric sigmoidal, and asymmetric sigmoidal.

Table 1. LiPo Voltage-SOC (state of charge) table.

SOC	Cell Voltage (V)	2 Cells Voltage (V)	3 Cells Voltage (V)
100%	4.20	8.40	12.60
95%	4.15	8.30	12.45
90%	4.11	8.22	12.33
85%	4.08	8.16	12.25
80%	4.02	8.05	12.07
75%	3.98	7.97	11.95
70%	3.95	7.91	11.86
65%	3.91	7.83	11.74
60%	3.87	7.75	11.62
55%	3.85	7.71	11.56
50%	3.84	7.67	11.51
45%	3.82	7.63	11.45
40%	3.80	7.59	11.39
35%	3.79	7.57	11.36
30%	3.77	7.53	11.30
25%	3.75	7.49	11.24
20%	3.73	7.45	11.18
15%	3.71	7.41	11.12
10%	3.69	7.37	11.06
5%	3.61	7.22	10.83
0%	3.27	6.55	9.82

The highlighted values represent the unsafe battery operating range.

The linear approximation is described by the following relation:

$$SOC = \frac{V - V_{min}}{V_{max} - V_{min}},$$

(4)

where V is the battery voltage, V_{max} is the maximum voltage (for 100% charge), and V_{min} is the minimum safe voltage, as described in the previous paragraph.

The symmetric sigmoidal approximation was fitted using a 4-parameter logistics function (4PL):

$$SOC = d + \frac{a - d}{1 + \left(\frac{V_{normalized}}{c}\right)^b},$$

(5)

where:

$$V_{normalized} = \frac{V - V_{min}}{V_{max} - V_{min}},$$

(6)

and the parameters a, b, c, and d have the following meaning: a and d control the position of the horizontal asymptotes (upper and lower, respectively), b controls the slope of the response, and c controls the position of the transition region [34].

The asymmetric sigmoidal approximation was fitted using a 5-parameter logistics function (5PL):

$$SOC = d + \frac{a - d}{\left[1 + \left(\frac{V_{normalized}}{c}\right)^b\right]^g},$$

(7)

where a, c, and d are defined in (5) and $V_{normalized}$ is defined in (6). In this case, the b parameter solely controls the approach to the top asymptote and together with g controls the approach to the bottom asymptote [34].

Using curve fitting tools, the parameters for the 4PL function were determined as: $a = 0$, $b = 2.9$, $c = 1/1.9$, and $d = 112$. With these values, Equation (5) becomes:

$$SOC = 112 - \frac{112}{1 + (1.9 \cdot V_{normalized})^{2.9}}. \tag{8}$$

In the case of the 5PL function the parameters are: $a = 0$, $b = 8$, $c = 1/3.5$, $d = 270$, and $g = 0.045$. With these values Equation (7) becomes:

$$SOC = 270 - \frac{270}{\left[1 + (3.5 \cdot V_{normalized})^8\right]^{0.045}}, \tag{9}$$

The voltage data in Table 1 are plotted together with the three approximations in Figure 5 for a 2-cell battery, with $V_{max} = 8400$ mV and $V_{min} = 7000$ mV.

(**a**) Linear   (**b**) Symmetric sigmoidal   (**c**) Asymmetric sigmoidal
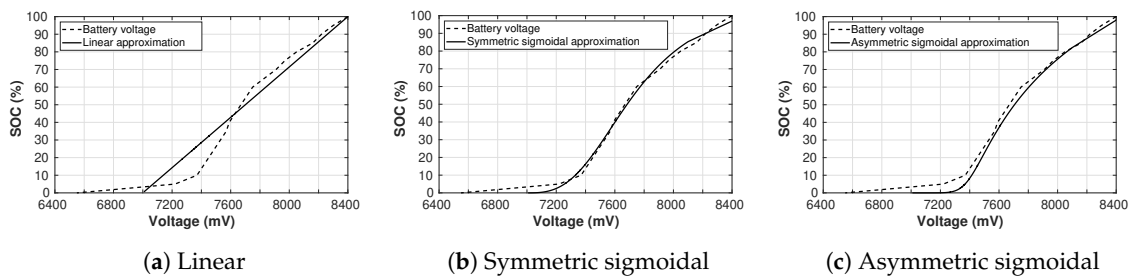
Figure 5. Battery state of charge approximations.

It can be noted that both the 4PL (Figure 5b) and 5PL (Figure 5c) approximations provide good results, while the linear approximation (Figure 5a) is not suitable for SOC estimation of LiPo batteries. In the next section the 4PL approximation is chosen, as it requires less computational effort with very good results.

4.3. Battery Monitoring System

The battery monitoring system should be available on any registered EV. For this application, the BMS measures the battery voltage and, using Equation (8), estimates the remaining charge. The data are processed by a micro-controller and sent via I2C (inter-integrated-circuit) communication to an on-board computer (in this case a Raspberry Pi), which generates the transaction and submits the data to the blockchain network.

A monitoring board (Figure 6) was designed and implemented. An ATMega164p micro-controller is used to measure the battery voltage and compute the SOC using the 4PL approximation (8).

The board monitors all four test batteries simultaneously, which can also power the microcontroller using the power switch. The battery voltages are read from the analog pins of the microcontroller (A0–A3). Since the battery voltages are higher than the 5V accepted by the microcontroller, the voltage is adjusted using voltage dividers.

For the 3-cell batteries the voltage dividers are formed using $R1$ and $R2$ ($R3$ and $R4$ for the second battery), providing a ratio of 3.12. The divider ratio for the 2-cell batteries is 1.68 ($R5$ and $R6$ for the 3rd battery and $R7$ and $R8$ for the 4th).
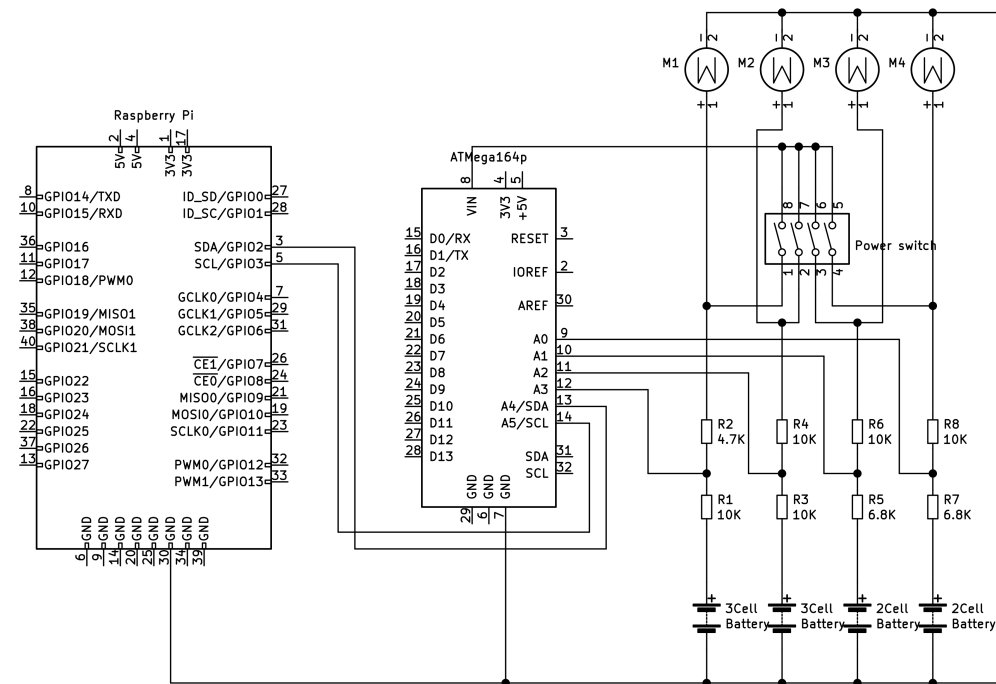
Figure 6. Battery monitoring board.

For the 3-cell batteries the read voltage ranges between 0 and 4.03 V and for the 2-cell batteries between 0 and 5 V.

The microcontroller transmits the data to the Raspberry Pi via I2C communication. The data are averaged over a series of 60 samples and the blockchain transaction is created. The anatomy of the transaction depends on the blockchain implementation and will be detailed in the following sections.

A battery test bed was designed and implemented (Figure 7), using a Raspberry Pi as an on-board computer for collecting the battery data and relaying the information to the blockchain.
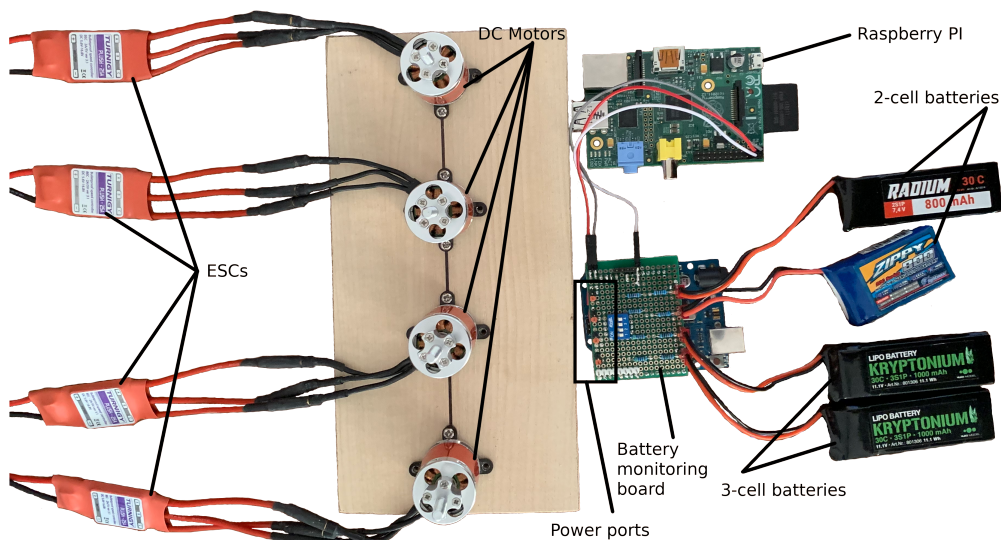
Figure 7. Battery test bed.

The transactions are created using the Python libraries `Web3.py` (Ethereum) and `PyOTA` (IOTA). These libraries implement the necessary functions for creating and submitting the transactions for their respective networks. The methods for each implementation will be described in their respective sections below.

For user interaction, a web application has been developed using `NodeJS` and the libraries specific for each platform (`Web3.js` for Ethereum and `iota.js` for IOTA). The web application allows the users and stations to register on the network, add new batteries and manage their requests.

The overall system architecture is presented in Figure 8.
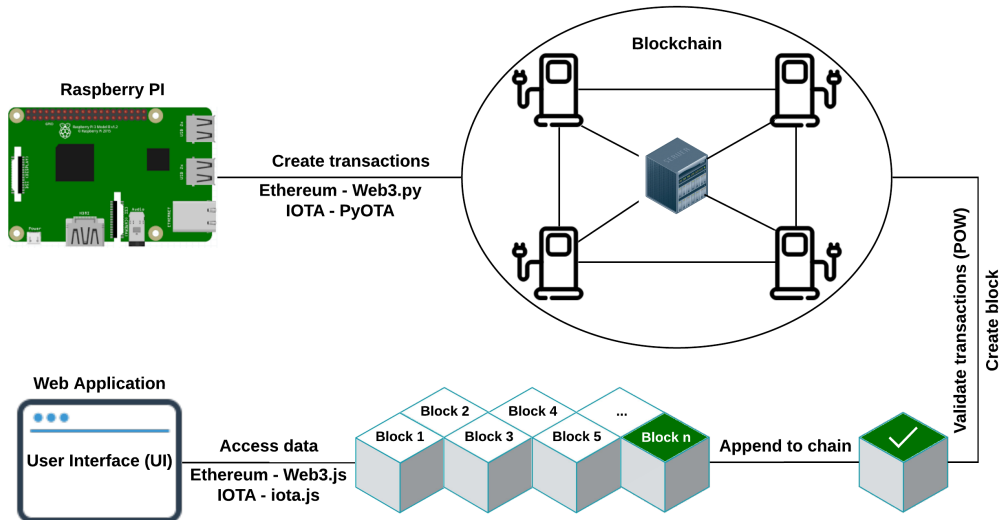
Figure 8. The blockchain interface for the proposed battery swapping and charging system. POW: proof of work.

4.4. Ethereum Blockchain

The first implementation of the charging/swapping application uses a smart contract deployed on a custom Ethereum blockchain.

In Ethereum, participating nodes have to perform POW to discover new blocks. To motivate users into participating in the block discovery process, a transaction fee (called *gas*) is paid by the user submitting the transaction. On the public chain the gas cost can be very high depending on the payload of the transaction. This makes the public Ethereum chain not well suited for data transactions, such as IoT applications.

On a customized chain, the gas cost and difficulty of the hash function can be controlled, in order to be used for specific applications, such as the battery management of electric vehicles.

On the main network any user with sufficiently capable processing resources can join. In a custom deployed network user access can be handled according to the application needs, thus allowing the implementation of permissioned blockchains.

In this paper, a permissioned network is created where the registration of new users or charging stations is handled by a master node. This creates a semi-decentralized network, but it can provide certain advantages, which will be highlighted in this section.

Users of the network are the EV owners. The EV computer (Raspberry Pi in this study) will sync to the network in light mode, where only the current state of the network and block headers are synced. For all processing operations a light node depends on the full node peers on the network (it does not take part in the *mining* process). The semi-decentralized structure ensures that there is at least one full node that is the master node of the application. Transactions and the necessary POW are handled by the charging/swapping station nodes, which will be synced as full nodes on the network.

When a user or station registers on the network via a web application, the master node creates a new address on the blockchain, which will be used to identify the user. The newly created address is stored and managed by the master node.

The registration process is handled by a smart contract deployed on the network. The proposed smart contract is described in Figure 9.
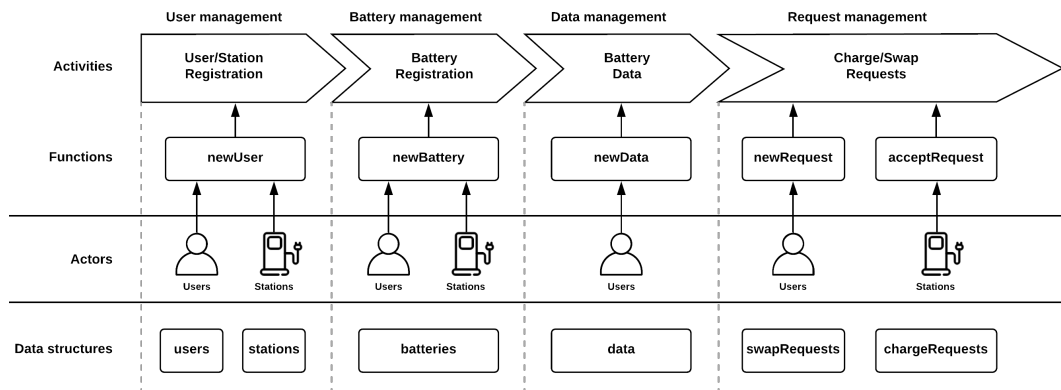
Figure 9. The smart contract structure.

The user management section provides the functions for registering new users or stations and for displaying their information.

The user and station information are stored inside the smart contract using the following structure:

```
struct User {
uint id;
uint balance;   // user balance
uint8 userType; // user or station
bool set;       // differentiate between unset and zero struct values
}
```

Upon registration, each user will have a unique id generated (similar to the primary keys in relational databases) and it can have an initial balance of virtual tokens that can be used to perform transaction on the network. The `userType` field specifies if the user is an EV owner or a charging station.

Each user or station is associated with an address by using a special `mapping` type, which maps the user address to the user data. All users can be accessed through the `user` variable.

```
mapping (address => User) public users;
```

The `newUser` function has the following prototype:

```
function newUser(address _address, uint8 _type) public
```

The function checks if a user with the specified address exists. If the address is not found, a new user object is created and its mapping is assigned. The `newUser` transaction is shown in Table 2 and the result is described in Table 3. The new user has an initial balance of 50 tokens.

In Table 2, the **From** address is different from the new user address (in the **Decoded input** field). The **From** address is the address of the master, as this is the node that actually creates the transaction. In this way, the gas cost required by the transaction is actually paid by the master instead of the user.

The gas used for this transaction would correspond to 0.00234 ETH on the main Ethereum network. For an ETH price of 258 USD (as of May 2019) the transaction cost would be around 0.60 USD. By running a separate network and allowing only mining nodes to submit transactions, the user is not required to have an actual Ethereum token (ETH) balance. Table 3 shows that for a **call** (read) operation, there is no cost involved, as the function only queries and returns the user data.

Table 2. New user transaction on the Ethereum blockchain.

Transaction hash	0x6cf7bdea3c4c8be4c023558e9a7089d840bb18115da1b11aa3ba55f77dd42b2c
From	**0x468fa9e5c2e87816688bcc96176bbe3e711ea4be**
To	BatteryContract.newUser(address, uint8) **0x6b2010a939adce6728d0e61d68c14d19c797a380**
Gas	117179
Input	0x7636a94c0000000000000000000000000062650b2f80d471d29372a4be9acf28365cd419c 100000000000000000000000000000000000000000000000000000000000000000

Decoded input	{
	    "address _address": "**0x62650b2f80d471d29372a4be9acf28365cd419c1**",
	    "uint8 _type": 0
	}

Logs	[
	    {
	        "from": "0x6b2010a939adce6728d0e61d68c14d19c797a380",
	        "topic": "0x05cdcffc20f5068d145a89a6ba9848186e191098da4d73e256368398e0a76ff7",
	        "event": "newUserEvent",
	        "args": {
	            "_address": "0x62650b2f80d471d29372a4be9acf28365cd419c1",
	            "_id": "0",
	            "length": 2
	        }
	    }
	]

Value	0 wei

Table 3. New user result on the Ethereum blockchain.

Transaction hash	call 0x468fa9e5c2e87816688bcc96176bbe3e711ea4be 0x6b2010a939adce6728d0e61d68c14d19c797a380 0xa87430ba0000000000000000000000000062650b2f80d471d29372a4be9acf28365cd419c1
From	0x468fa9e5c2e87816688bcc96176bbe3e711ea4be
To	BatteryContract.users(address) 0x6b2010a939adce6728d0e61d68c14d19c797a380
Input	0xa87430ba0000000000000000000000000062650b2f80d471d29372a4be9acf28365cd419c1

Decoded input	{
	    "address": "0x62650B2f80D471d29372a4Be9aCf28365cd419c1"
	}

Decoded output	{
	    "0": "uint256: id 0",
	    "1": "uint256: balance 50",
	    "2": "uint8: userType 0",
	    "3": "bool: set true"
	}

Once users are registered they can add new batteries for their EVs. The battery information is stored in a structure as follows:

```
struct Battery {
uint id;
bytes32 manufacturer;  // eg. Yuki
bytes32 model;         // eg. Radium
bytes32 batteryType;   // eg. LiPo
uint32 capacity;       // eg. 800 (mAh)
uint8 cells;           // eg. 2
uint manufactureDate;  // Unix timestamp
uint32 maxChargeCount; // eg. 200
```

```
bool set;               // differentiate between unset and zero struct values
}
```

The `newBattery` function has the following prototype:

```
function newBattery(address _address, bytes32 _manufacturer, bytes32 _model,
bytes32 _batteryType, uint32 _capacity, uint8 _cells,
uint256 _manufactureDate, uint32 _maxChargeCount) public
```

The function requires the battery owner's address (which was provided after registering) and the battery information. The resulting transaction is presented in Table A1. Since the amount of data written to the contract is much higher than the `newUser` transactions, the gas cost is almost double.

When a battery runs low, the user can manually submit a charge or swap request to the contract `newRequest` method (Table A2):

```
function newRequest(address _address, uint _batteryId, uint8 _requestType,
uint _timestamp) public
```

The `_requestType` parameter specifies if it is a charge or swap request. Note that the request does not specify a specific station. All stations can view the request and whichever one can provide the requested service can accept it (Table A3). The function `acceptRequest` has the following definition:

```
function acceptRequest(address _address, uint _userIndex, address _station,
uint _stationIndex, uint _approved) public
```

where the `_address` and `_userIndex` represent the user address and their battery identifier is used to locate the battery in the structure mapping; the `_station` and `_stationIndex` are used to specify the station's battery and the `_approved` parameter is the timestamp of the approval. The function changes the owners of the two batteries and the change will be reflected on the network once the transaction is confirmed. The result after the request is accepted is presented in Table A4.

The previous requests are created by the users/stations using the web interface. The battery information is submitted by the on-board computer and the data are stored in the smart contract using the following structure:

```
struct BatteryData {
uint id;
uint8 SOC;           // percentage
uint32 voltage;      // mV
uint32 chargeCount;  // eg. 7
uint timestamp;      // eg. 1562662637000
bool set;
}
```

The Raspberry Pi collects the data and averages them over 60 samples (30 samples/minute). The `newData` contract function is called from the Python script:

```
function newData(address _address, uint _id, uint _index, uint8 _soc,
uint32 _voltage, uint32 _chargeCount, uint _timestamp) public
```

where the `_address`, `_id`, and `_index` parameters are used to identify the user and the battery, `_voltage` and `_soc` are the actual measurements, and `_chargeCount` and `_timestamp` are the current charge count and the date and time of the measurement.

In this section, a full implementation of a battery swapping/charging system is described, using an Ethereum smart contract on a custom network. This approach allows further actions or improvements to be added to the smart contract, while the transaction costs are supported by the master node due to the semi-decentralized, permission-based approach.

Using the same contract on the main Ethereum network would be unfeasible, due to the high transaction costs (gas). The nature of the application is perfectly suited for a permission-based network, since the aim of the application is to transfer data rather than tokens on the blockchain.

4.5. IOTA Tangle

The Ethereum implementation uses the power and flexibility of smart contracts to implement the application logic on the blockchain ensuring that all nodes run the same code and data immutability.

The first difference between IOTA and other blockchain platforms is the way the data are stored (directed acyclic graph vs. linear chained blocks). This solves the scalability issue by linking a new transaction to two previous transactions by validating them, as described in Section 4.5.

Since the IOTA network does not have transaction fees, the implementation can run on the public network. One important disadvantage is that IOTA does not (*yet*) support smart contracts, and thus the application logic has to be handled by a master node, resulting in a semi-decentralized system. In this case, the master node has to perform extra operations to extract and filter the data from the tangle, whereas in the Ethereum version these operations were handled directly by the smart contract functions.

To implement the required functionality, the transaction structure is used (Table 4) by routing the different types of transactions to their specific actions.

Table 4. IOTA transaction anatomy [26].

Field	Description	Length (trytes)
address	Sender's or recipient's address, depending if the transaction withdraws or receives tokens	81
signatureMessageFragment	A signature if the transaction withdraws tokens or a tryte-encoded message otherwise. This can be split across multiple transactions	2187
value	The amount of tokens transferred	27
tag	User-defined tag	27
timestamp	Unix timestamp (seconds since Jan. 01 1970) of when the transaction was issued. In IOTA, the timestamp is not currently enforced and can be arbitrary	9
bundle	The hash of the bundle of the transaction	81
currentIndex	Index of the current transaction in the bundle	9
lastIndex	Index of the last transaction in the bundle	9
trunkTransaction	Hash of a parent transaction	81
branchTransaction	Hash of a parent transaction	81
attachmentTimestamp	Unix timestamp of when the POW was completed	9
nonce	The POW field of the transaction	27

To route the transaction to specific actions, the **tag** field is used, similar to a function call of a smart contract. Based on this the application will filter the data and assign it to the appropriate structures.

For example, the equivalent of the `newUser` operation from the Ethereum implementation would have the structure described in Table 5.

The tag field specifies the action of the transaction. Since the application is running on the public development network, any user can create a transaction with this tag. However, since all transactions are still handled by the master node as the sender, the application will only filter its own transactions from the tangle.

Since the IOTA implementation uses only raw transactions, their structure for the other operations are similar to the one presented in Table 5. Each operation has a corresponding tag field: `IOTABMSNEWUSER` for the new user transactions; `IOTABMSNEWBATTERY` for the new battery operation; `IOTABMSNEWDATA` for battery data information; and `IOTABMSNEWREQUEST` and `IOTABMSACCEPTREQUEST`

for the request operations. Because the IOTA implementation uses the public Devnet tangle, these tags can be used to examine the transaction details at https://devnet.thetangle.org.

For this implementation, the monitoring board collects the data over 60 samples, at the same rate of 30 samples/minute. The data are stored directly on the tangle, so the Raspberry Pi has to create a new transaction using the `ProposedTransaction` class from the PyOTA Python library:

```
tx = ProposedTransaction(
address=Address(IOTAAddress),
value=0,
tag=Tag(b'IOTABMSDATA'),
message=TryteString.from_string(IOTAJSONData)
)
```

where `IOTAAddress` is the address of the master node and `IOTAJSONData` is a JSON object containing the measurement information, with the same properties as the `newData` function from the Ethereum implementation. The `ProposedTransaction` object is a transaction that was created locally and has not yet been submitted to the network. To actually broadcast the transaction, the `send_transfer` function is used:

```
IOTAApi.send_transfer(
depth=3,
transfers=[tx],
min_weight_magnitude= 14,
inputs=BatteryAddress
)
```

where `BatteryAddress` is the address of the registered battery (acting as the sender of the message), `depth` is the maximum depth in the tangle for the tip selection mechanism, and `min_weight_magnitude` is an optional parameter used to specify the POW difficulty. Note that the `transfers` parameter contains a list of transactions (in this case only one), since there is no value transferred between the two addresses. When transferring IOTA tokens, at least two transactions are required: one that adds tokens to the recipient and one that subtracts the same amount from the sender.

Ideally, the POW should be performed locally. However, the Raspberry PI does not have the necessary resources to compute the POW, so the transaction is handled by the master node of the system, which computes the validation hashes for two selected tips. If the master node is not reachable, the transaction data are stored locally and resubmitted when the connection can be established.

The biggest challenge and limitation of this implementation is the battery swapping operation. Since the swap request is not sent to a particular station (similar to the Ethereum implementation), the station that accepts the request has to do so by creating a new transaction. This new transaction has to somehow reference the swap request submitted by the user. Two solutions can be outlined for this problem: either reference the swap request transaction hash in the `message` field of the transaction, together with the rest of the information, or override the IOTA's tip selection mechanism and attach the `acceptRequest` transaction directly to the related request transaction using the `trunkTransaction` or `branchTransaction` fields (Table 4). For this implementation, the first method was preferred.

The main difference between the IOTA implementation and the Ethereum one is that the code which handles the data storage and processing is not contained in a smart contract (distributed across all nodes), but runs solely on the master node. This makes the IOTA implementation more centralized than its Ethereum counterpart, due to the fact that the master node still represents a single point of failure for the application.

Table 5. New user transaction on the IOTA tangle.

Transaction hash	AMCSQBBEUNDBITQMW9ZYDXA9H9YBMO9QQZMAQARQGFFWUZX9HOUYHFI ENRBAUTQ9IZZ9ZSWBMULFZ9999
From	UHLEMW9QSZBRM9QVQGICTIMKWQNWDPQLYPHCMMHR9JDDYJXHGAOVLJR LEWACCLJTXFOJLJAAJLXVRUDIW
To	SMVIZBPLNBFOALXONUIREQZZWN9HTLVJQVEDUDVNGMLYP9SQDOLMMWC 9WXRKXFJZMLQZU9TMRSWJCDZKD
Bundle	STODQIOYCBKLUQWWHARYLQUEKLFDZNNSVASDQSHCHEXWZEG9ZKCH9LJ KV9YTHJZDTUJDGSESUHUQYYDA9
Index in bundle	0/0
Trunk transaction	Y9YHCOTRWEMFREDJ9HWRWSKONSUGADUCSXZDDMJLVD9IJYDWSNCG9PN PWTCEWWTOXHKKBWYVDUIOXM999
Branch transaction	Y9YHCOTRWEMFREDJ9HWRWSKONSUGADUCSXZDDMJLVD9IJYDWSNCG9PN PWTCEWWTOXHKKBWYVDUIOXM999
Tag	**IOTABMSNEWUSER**9999999999999
Message	ODGAPCSCSCFDTCGDGDGADBGABCWBECSBICLBZBVBXBLBPBYBKBVBGCY BXBDCSBACOB9CICICFCXBCBRBCCVBECTB9CECOBNBDCNBECXBQBWBVBH CZBCBBC9CNBYBVBWBWBFCMBCBFCGCACUBGCPBTBICWBVB9CICDCCBCC WBACBCFCTBMBNBICUBNBGAQAGAHDMDDDTCGADBGAUAGAQAGAQCP C9DPCBDRCTCGADBZAUAQAGAHDXCADTCGDHDPCADDDGADBGAVAZAZ ABBYAYAWAXAWACBVAYAWAGAQD

Decoded message	{
	    "address": "SMVIZBPLNB...MRSWJCDZKD",
	    "type": "0",
	    "balance": 50,
	    "timestamp": "1558442329142"
	}

In the case of smart contracts, the corresponding function is executed whenever a transaction is submitted. In the IOTA implementation the master node has to monitor the network state continuously using the transaction **tag** field and decide which function should be executed locally. Here, the tangle is used only as a decentralized data storage (instead of a traditional database management system). When the user wants to access the information from the web application, the master node queries the tangle for the raw data and any necessary processing is done before presenting the data to the user.

Off-chain processing is recommended when working with distributed applications, since computational power is expensive on any blockchain implementation, but it is much more difficult to work with unstructured data than with organized data structures achieved through smart contracts.

One important difference between the IOTA implementation and the Ethereum counterpart is the fact that Ethereum requires at least two full nodes (the master node and at least one charging station) to perform the POW and create new blocks on the network. In IOTA, the charging stations can be connected to the tangle, but this is not mandatory, since the actual POW is done by the device that creates the transaction (the master node in this implementation). This reduces the setup time and the necessary hardware requirements for the stations, but has the downside that if the master node is not available, the system may encounter some down-times.

5. Results

Figures 10 and 11 show the voltage and state of charge plots for a 2-cell and 3-cell battery, respectively. These results are obtained directly in the front-end application and can be viewed by the users. They can help improve the SOC estimation by accounting for battery age and other environmental factors, and possibly allow stations or users to properly service or replace batteries in

safe operating conditions. It can be noted that the SOC vs. Voltage plot (Figures 10c and 11c) is similar to the theoretical 4-PL approximation in Figure 5b, which is the expected result.
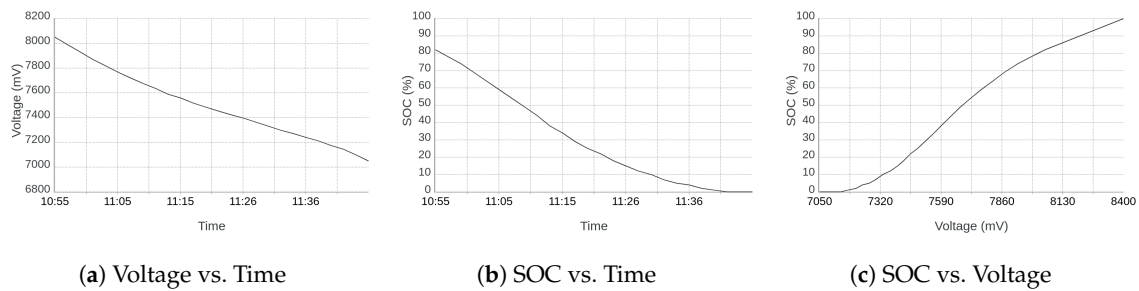

(**a**) Voltage vs. Time   (**b**) SOC vs. Time   (**c**) SOC vs. Voltage

Figure 10. Experimental results for 2-cell battery.

(**a**) Voltage vs. Time   (**b**) SOC vs. Time   (**c**) SOC vs. Voltage
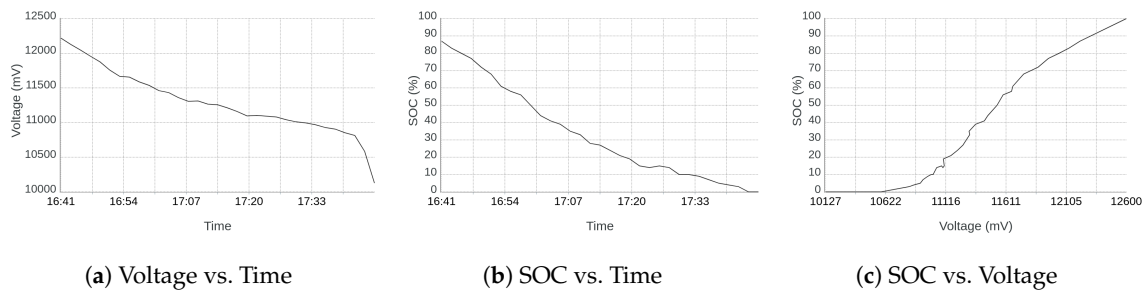
Figure 11. Experimental results for 3-cell battery.

To compare the two implementations, the transaction times were measured for a set of 500 transactions submitting new battery data (Figure 12). For the Ethereum blockchain (Figure 12a), running with two mining nodes (one master node and one charging station), the time from submitting a transaction until its first confirmation by the network ranged between 1.65 and 75.45 s, with an average of 12.97 s per transaction. These confirmation times can vary depending on the network congestion, the number of operations required in the contract function and the difficulty of the network, which, in the case of a permission-based chain, can be controlled by the network administrator.
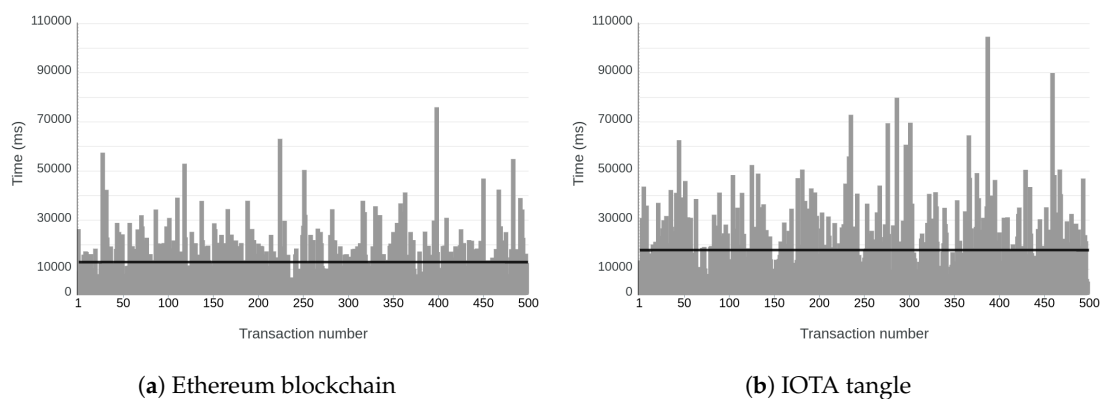

(**a**) Ethereum blockchain   (**b**) IOTA tangle

Figure 12. Transaction confirmation times.

For the IOTA tangle the results for the same transactions are presented in Figure 12b. It can be seen that the transaction times are slightly higher than the Ethereum implementation, with an average of 17.86 s and the minimum and maximum values of 3.78 and 104.14 seconds, respectively. These differences can be easily explained by the different approach of the two platforms. While in Ethereum, mining nodes perform the POW operations continuously, in IOTA these operations are performed only when a new transaction is submitted. In the proposed implementation the IOTA POW is not done locally due to the limited resources of the Raspberry Pi board. Instead, the required operations are performed by a public node outside the application infrastructure (in this case, the IOTA Devnet node).

Depending on the load of the node and the network congestion, the expected transaction recording time can vary. However, the benefit is an easier setup and fewer resources necessary for the master and station nodes of the BMS application.

6. Discussion

The Ethereum blockchain demonstrates that the technology is mature enough to be used in many fields of industry, offering the possibility of developing any kind of application logic on the blockchain in a decentralized manner. The main disadvantage of this approach is the rather complicated setup required to deploy the blockchain and smart contract. Since the application would not be suited to function on the main network, due to the high transaction fees, the creation of a separate network is absolutely necessary. Hence, one advantage is the possibility to manage the network settings and difficulty, so that the response time can be reduced, compared to a transaction on the public blockchain. Another advantage, which will be considered in future works, is to setup the blockchain using a different consensus mechanism, such as proof-of-authority (POA), where designated nodes can add new blocks to the chain without requiring a swarm of mining nodes.

IOTA was considered as an alternative because of its zero-fee transaction model and its scalability, which allows the application to run on the main tangle with minimal additional setup. The lack of smart contracts is the main disadvantage of this approach, because the application logic has to be maintained by one or more central nodes and it is more susceptible to failures, while possible changes of the application may affect its overall functionality on the network. These problems could be resolved when smart contracts become available in IOTA (which were already announced as of 2019), but the implementation may provide additional difficulties that cannot yet be estimated.

The main problem of the proposed IOTA implementation is the tag-based routing system, which can be replicated by users not registered on the battery management application. This can be solved either by having one or more trusted nodes (or *oracles*) that will generate the transactions on behalf of their users (as proposed in this paper), or by using masked authenticated messages (MAM) [35] as a means to create direct channels of communication between data publishers (EV owners) and subscribers (stations). This approach will be further studied in future works.

Battery charging requests on IOTA can be easily created because they do not involve changing the ownership of the battery, but, without the capabilities of on-chain processing, swap requests can be more difficult to handle, as they require the front-end application to search through the transaction history to find the latest state of the requested batteries. Due to this fact, IOTA is better related to producer–consumer applications, where sensors or embedded devices are the data producers and the users query and use the data off-tangle (data flow is unidirectional).

An issue for any application which relies on user information and value exchange (tokens, electricity, batteries, fiat currency, etc.) must deal with the privacy issues that may arise from these interactions. Several methods can be considered, depending on the type of blockchain that is being used and on the visibility of the blockchain network. Feng et al. [36] and Jia et al. [37] introduced such methods that deal with blockchain privacy.

The Ethereum-based implementation presented in this paper uses a private blockchain network where user access control (UAC) methods can be implemented to protect the user information. Furthermore, sensitive user information can be encrypted using a private–public key mechanism.

The proposed IOTA implementation uses the public tangle; thus, MAM can be used to establish a direct channel between the involved parties when an exchange is requested (battery swap or driver-to-driver charging).

These issues are an interesting extension for this study and the authors plan on extending the results of the current paper with an in-depth study on blockchain data privacy and protection.

7. Conclusions

In this paper, a complete battery management system for electric vehicles was presented using blockchain technology to create a semi-decentralized network of electric vehicles and charging stations that are able to share data (battery information and condition) based on continuous monitoring.

Blockchain is a relatively young technology that has seen major growth and adoption in the last 10 years with the development of cryptocurrencies. The underlying architecture makes it a strong candidate for data-driven applications, such as electric and autonomous vehicles.

To analyze the feasibility of the proposed application, two distinct implementations were considered and tested: the first method uses an Ethereum blockchain, powered by a smart contract, which allows the distributed processing and sharing of data, while at the same time ensuring data immutability and privacy. The second approach uses the IOTA network, which lacks the support for smart contract development, but provides zero-fee transactions and is built with data-driven applications in mind, thus allowing better application scaling.

The results show that both platforms can be used for developing blockchain IoT applications having acceptable transaction confirmation times for the purpose of the proposed battery monitoring system, which does not require real-time confirmations. Ethereum is still the main platform for developing decentralized applications, which can be deduced from the large number of projects and research papers available. This may change in the future especially for IoT and data-driven applications, as alternative approaches specially designed for this field mature and become available.

Abbreviations

The following abbreviations are used in this manuscript:

4PL	4-Parameter Logistics
5PL	5-Parameter Logistics
Ah	Ampere-Hour
BEV	Battery Electric Vehicle
BMS	Battery Management System
DAG	Directed Acyclic Graph
DLT	Distributed Ledger Technology
ECM	Electrical Circuit Model
ESC	Electronic Speed Control
EV	Electric Vehicle
FCEV	Fuel-Cell Electric Vehicle
I2C	Inter-Integrated Circuit
IoT	Internet of Things
HEV	Hybrid Electric Vehicle
KF	Kalman Filter
LiPo	Lithium-Polymer
M2M	Machine to Machine
MAM	Masked Authenticated Messages
OCV	Open Circuit Voltage
P2P	Peer to Peer
PHEV	Plug-in Hybrid Electric Vehicle
POA	Proof of Authority
POW	Proof of Work
SOC	State of Charge
UAC	User Access Control

Appendix A. Ethereum Transactions

Table A1. New battery transaction on the Ethereum blockchain.

Transaction hash	0xe3bdb085f2dc0c7423bc7a8a50c3c75f431faccf7fe9ced9c8889e755845455d
From	0x468fa9e5c2e87816688bcc96176bbe3e711ea4be
To	BatteryContract.newBattery(address,bytes32,bytes32,bytes32,uint32,uint8,uint256,uint32) 0x6b2010a939adce6728d0e61d68c14d19c797a380
Gas	**213278**
Input	0x2b069245 . . . 000000c8

Decoded input	{
	    "address _address": "0x62650b2f80d471d29372a4be9acf28365cd419c1",
	    "bytes32 _manufacturer": "0x59756b69",
	    "bytes32 _model": "0x4b727970746f6e69756d0000",
	    "bytes32 _batteryType": "0x4c69506f",
	    "uint32 _capacity": 1000,
	    "uint8 _cells": 3,
	    "uint256 _manufactureDate": "1526989237000",
	    "uint32 _maxChargeCount": 200
	}

Logs	[
	    {
	        "from": "0x6b2010a939adce6728d0e61d68c14d19c797a380",
	        "topic": "0xf01d0b1897e49a087d6d16276d60ab14a343d4e4b451af73bfc055cab1888c7c",
	        "event": "newBatteryEvent",
	        "args": { . . . }
	    }
	]

Table A2. New swap request transaction on the Ethereum blockchain.

Transaction hash	0xdb90386e3ab9877e7da06699cb975fcf97020211f3c351755302961146d1d5b5
From	0x468fa9e5c2e87816688bcc96176bbe3e711ea4be
To	BatteryContract.newRequest(address,uint256,uint8,uint256) 0x6b2010a939adce6728d0e61d68c14d19c797a380
Gas	141145
Input	0xc286525a . . . e5153348

Decoded input	{
	    "address _address": "0x62650B2f80D471d29372a4Be9aCf28365cd419c1",
	    "uint256 _batteryId": "0",
	    "uint8 _requestType": 0,
	    "uint256 _timestamp": "1558621533000"
	}

Logs	[
	    {
	        "from": "0x6b2010a939adce6728d0e61d68c14d19c797a380",
	        "topic": "0x28d61e4489683b71fb18e12434540b0f2e409d794b88c706069480866c22f893",
	        "event": "newRequestEvent",
	        "args": { . . . }
	    }
	]

Table A3. New accept swap request transaction on the Ethereum blockchain.

Transaction hash	0x3a78d06023f5d493cb1a55f21c0bbf0f803d98a6373dba5bd0c92e87401bf26b
From	0x468fa9e5c2e87816688bcc96176bbe3e711ea4be
To	BatteryContract.acceptRequest(address,uint256,address,uint256,uint256) 0x6b2010a939adce6728d0e61d68c14d19c797a380
Gas	469526
Input	0xeca01e5a0000000000000000000000000062650b2f80d471d29372a4be9acf28365cd419c10000 0000000000000000000000000000000000000000000000000000000000000000000000000000000 0000001365af95d86cf447dbe6b991be87d5c4a59a3e38000000000000000000000000000000000 0000000000000000000000000000000000000000000000000000000000000000000000000000000 000000016ae5153348

Decoded input	{
	    "address _address": "0x62650B2f80D471d29372a4Be9aCf28365cd419c1",
	    "uint256 _userIndex": "0",
	    "address _station": "0x1365af95D86cF447dbe6B991bE87d5c4A59A3E38",
	    "uint256 _stationIndex": "0",
	    "uint256 _approved": "1558621533000"
	}

Logs	[
	    {
	        "from": "0x6b2010a939adce6728d0e61d68c14d19c797a380",
	        "topic": "0xf1e21ec30699d34039ffbb472baadcc06326aa1a6fc32b220f936f2a58a8a495",
	        "event": "acceptedRequestEvent",
	        "args": { . . . }
	    }
	]

Table A4. Accepted request result on the Ethereum blockchain.

Transaction hash	call 0x468fa9e5c2e87816688bcc96176bbe3e711ea4be 0x6b2010a939adce6728d0e61d68c14d19c797a380 0x9ecebe2a0000000000000000000000000062650b2f80d471d29372a4be9acf28365cd419c10000 00000000000000000000000000000000000000000000000000000000000000000
From	0x468fa9e5c2e87816688bcc96176bbe3e711ea4be
To	BatteryContract.requests(address, uint256) 0x6b2010a939adce6728d0e61d68c14d19c797a380
Input	0x9ecebe2a0000000000000000000000000062650b2f80d471d29372a4be9acf28365cd419c10000 00000000000000000000000000000000000000000000000000000000000000000

Decoded input	{
	    "address": "0x62650B2f80D471d29372a4Be9aCf28365cd419c1"
	    "uint256": "0"
	}

Decoded output	{
	    "0": "uint256: id 0",
	    "1": "uint256: batteryId 0",
	    "2": "uint8: requestType 0",
	    "3": "uint256: timestamp 1558621533000",
	    "4": "address: station 0x1365af95D86cF447dbe6B991bE87d5c4A59A3E38"
	    "5": "uint256: approved 1558621533000"
	    "6": "bool: set true"
	}

References

1. Yong, J.Y.; Ramachandaramurthy, V.K.; Tan, K.M.; Mithulananthan, N. A review on the state-of-the-art technologies of electric vehicle, its impacts and prospects. *Renew. Sustain. Energy Rev.* **2015**, *49*, 365–385. [CrossRef]
2. Eberle, U.; von Helmolt, R. Sustainable transportation based on electric vehicle concepts: A brief overview. *Energy Environ. Sci.* **2010**, *3*, 689–699. [CrossRef]
3. Dharmakeerthi, C.H.; Mithulananthan, N.; Saha, T.K. Modeling and planning of EV fast charging station in power grid. In Proceedings of the 2012 IEEE Power and Energy Society General Meeting, San Diego, CA, USA, 22–26 July 2012; pp. 1–8.
4. Hannan, M.A.; Hoque, M.M.; Hussain, A.; Yusof, Y.; Ker, P.J. State-of-the-Art and Energy Management System of Lithium-Ion Batteries in Electric Vehicle Applications: Issues and Recommendations. *IEEE Access* **2018**, *6*, 19362–19378. [CrossRef]
5. del Valle, J.A.; Anseán, D.; Carlos Viera, J.; Antuña, J.L.; González, M.; García, V. Analysis of Advanced Lithium-Ion Batteries for Battery Energy Storage Systems. In Proceedings of the 2018 IEEE International Conference on Environment and Electrical Engineering and 2018 IEEE Industrial and Commercial Power Systems Europe (EEEIC/I CPS Europe), Palermo, Italy, 12–15 June 2018; pp. 1–6.
6. Liu, C.; Liu, L. Optimizing Battery Design for Fast Charge through a Genetic Algorithm Based Multi-Objective Optimization Framework. *ECS Trans.* **2017**, *77*, 257–271. [CrossRef]
7. O'Malley, R.; Liu, L.; Depcik, C. Comparative study of various cathodes for lithium ion batteries using an enhanced Peukert capacity model. *J. Power Sources* **2018**, *396*, 621–631. [CrossRef]
8. Helber, S.; Broihan, J.; Jang, Y.J.; Hecker, P.; Feuerle, T. Location Planning for Dynamic Wireless Charging Systems for Electric Airport Passenger Buses. *Energies* **2018**, *11*, 258. [CrossRef]
9. Liu, H.; Tan, L.; Huang, X.; Zhang, M.; Zhang, Z.; Li, J. Power Stabilization based on Switching Control of Segmented Transmitting Coils for Multi Loads in Static-Dynamic Hybrid Wireless Charging System at Traffic Lights. *Energies* **2019**, *12*, 607. [CrossRef]
10. Nakamoto, S. Bitcoin: A Peer-to-Peer Electronic Cash System. 2008. Available online: https://bitcoin.org/bitcoin.pdf (accessed on 3 March 2020).
11. Florea, B.C. Blockchain and Internet of Things data provider for smart applications. In Proceedings of the 2018 7th Mediterranean Conference on Embedded Computing (MECO), Budva, Montenegro, 10–14 June 2018.
12. Wang, J.; Wang, Q.; Zhou, N.; Chi, Y. A Novel Electricity Transaction Mode of Microgrids Based on Blockchain and Continuous Double Auction. *Energies* **2017**, *10*, 1971. [CrossRef]
13. Khan, S.; Khan, R. Multiple Authorities Attribute-Based Verification Mechanism for Blockchain Mircogrid Transactions. *Energies* **2018**, *11*, 1154. [CrossRef]
14. Wu, J.; Tran, N.K. Application of Blockchain Technology in Sustainable Energy Systems: An Overview. *Sustainability* **2018**, *10*, 3067. [CrossRef]
15. Miller, D. Blockchain and the Internet of Things in the Industrial Sector. *IT Prof.* **2018**, *20*, 15–18. [CrossRef]
16. Son, B.; Lee, J.; Jang, H. A Scalable IoT Protocol via an Efficient DAG-Based Distributed Ledger Consensus. *Sustainability* **2020**, *12*, 1529. [CrossRef]
17. Odysseas, L.; Gialelis, J. An IOTA Based Distributed Sensor Node System. In Proceedings of the 2018 IEEE Globecom Workshops (GC Wkshps), Abu Dhabi, UAE, 9–13 December 2018; pp. 1–6.
18. Bartolomeu, P.C.; Vieira, E.; Ferreira, J. IOTA Feasibility and Perspectives for Enabling Vehicular Applications. In Proceedings of the 2018 IEEE Globecom Workshops (GC Wkshps), Abu Dhabi, UAE, 9–13 December 2018; pp. 1–7.
19. Ibáñez, L.; Simperl, E.; Gandon, F.; Story, H. Redecentralizing the Web with Distributed Ledgers. *IEEE Intell. Syst.* **2017**, *32*, 92–95. [CrossRef]
20. Merkle, R.C. A Digital Signature Based on a Conventional Encryption Function. In *Advances in Cryptology (CRYPTO '87)*; Pomerance, C., Ed.; Springer: Berlin/Heidelberg, Germany, 1988; pp. 369–378.
21. Buterin, V. A Next Generation Smart Contract and Decentralized Application Platform. 2014. Available online: https://github.com/ethereum/wiki/wiki/White-Paper (accessed on 3 March 2020).

22. Szabo, N. Smart Contracts: Building Blocks for Digital Markets. 1996. Available online: http://www.fon.hum.uva.nl/rob/Courses/InformationInSpeech/CDROM/Literature/LOTwinterschool2006/szabo.best.vwh.net/smart_contracts_2.html (accessed on 3 March 2020).

23. Wang, S.; Ouyang, L.; Yuan, Y.; Ni, X.; Han, X.; Wang, F.Y. Blockchain-Enabled Smart Contracts: Architecture, Applications, and Future Trends. *IEEE Trans. Syste. Man Cybern. Syst.* **2019**, *49*, 2266–2277. [CrossRef]

24. O'Dwyer, K.J.; Malone, D. Bitcoin mining and its energy footprint. In Proceedings of the 25th IET Irish Signals Systems Conference 2014 and 2014 China-Ireland International Conference on Information and Communications Technologies (ISSC 2014/CIICT 2014), Limerick, Ireland, 26–27 June 2014; pp. 280–285.

25. Wang, W.; Hoang, D.T.; Hu, P.; Xiong, Z.; Niyato, D.; Wang, P.; Wen, Y.; Kim, D.I. A Survey on Consensus Mechanisms and Mining Strategy Management in Blockchain Networks. *IEEE Access* **2019**, *7*, 22328–22370. [CrossRef]

26. Popov, S. The Tangle. 2018. Available online: https://assets.ctfassets.net/r1dr6vzfxhev/2t4uxvsIqk0EUau6g2sw0g/45eae33637ca92f85dd9f4a3a218e1ec/iota1_4_3.pdf (accessed on 3 March 2020).

27. Miao, Y.; Hynan, P.; von Jouanne, A.; Yokochi, A. Current Li-Ion Battery Technologies in Electric Vehicles and Opportunities for Advancements. *Energies* **2019**, *12*, 1074. [CrossRef]

28. Iclodean, C.; Varga, B.; Burnete, N.; Cimerdean, D.; Jurchiş, B. Comparison of Different Battery Types for Electric Vehicles. *IOP Conf. Ser. Mater. Sci. Eng.* **2017**, *252*, 012058. [CrossRef]

29. Piller, S.; Perrin, M.; Jossen, A. Methods for state-of-charge determination and their applications. *J. Power Sources* **2001**, *96*, 113–120. [CrossRef]

30. Rivera-Barrera, J.P.; Muñoz-Galeano, N.; Sarmiento-Maldonado, H.O. SoC Estimation for Lithium-ion Batteries: Review and Future Challenges. *Electronics* **2017**, *6*, 102. [CrossRef]

31. Zhang, R.; Xia, B.; Li, B.; Cao, L.; Lai, Y.; Zheng, W.; Wang, H.; Wang, W. State of the Art of Lithium-Ion Battery SOC Estimation for Electrical Vehicles. *Energies* **2018**, *11*, 1820. [CrossRef]

32. Prochazka, P.; Cervinka, D.; Martis, J.; Cipin, R.; Vorel, P. Li-Ion Battery Deep Discharge Degradation. *ECS Trans.* **2016**, *74*, 31–36. [CrossRef]

33. Weng, C.; Sun, J.; Peng, H. A unified open-circuit-voltage model of lithium-ion batteries for state-of-charge estimation and state-of-health monitoring. *J. Power Sources* **2014**, *258*, 228–237. [CrossRef]

34. Gottschalk, P.G.; Dunn, J.R. The five-parameter logistic: A characterization and comparison with the four-parameter logistic. *Anal. Biochem.* **2005**, *343*, 54–65. [CrossRef] [PubMed]

35. Brogan, J.; Baskaran, I.; Ramachandran, N. Authenticating Health Activity Data Using Distributed Ledger Technologies. *Comput. Struct. Biotechnol. J.* **2018**, *16*, 257–266. [CrossRef]

36. Feng, Q.; He, D.; Zeadally, S.; Khan, M.K.; Kumar, N. A survey on privacy protection in blockchain system. *J. Netw. Comput. Appl.* **2019**, *126*, 45–58. [CrossRef]

37. Jia, B.; Zhou, T.; Li, W.; Liu, Z.; Zhang, J. A Blockchain-Based Location Privacy Protection Incentive Mechanism in Crowd Sensing Networks. *Sensors* **2018**, *18*, 3894. [CrossRef]

Article

Implementing Blockchain Technology in Irrigation Systems That Integrate Photovoltaic Energy Generation Systems

Florentina Magda Enescu [1,*], Nicu Bizon [1,2,3,*] , Adrian Onu [4], Maria Simona Răboacă [2] , Phatiphat Thounthong [5] , Alin Gheorghita Mazare [1] and Gheorghe Șerban [1]

[1] Faculty of Electronics, Communications and Computers, University of Pitesti, 110040 Piteşti, Romania; alin.mazare@upit.ro (A.G.M.); gheorghe.serban@upit.ro (G.Ș.)

[2] National Research and Development Institute for Cryogenic and Isotopic Technologies—ICSI Rm. Valcea, 240050 Ramnicu Valcea, Romania; simona.raboaca@icsi.ro

[3] Doctoral School, Polytehnic University of Bucharest, 060042 Bucharest, Romania

[4] R&D Department, ASSIST Software, 720043 Suceava, Romania; adrian.onu@assist.ro

[5] Renewable Energy Research Centre (RERC), King Mongkut's University of Technology North Bangkok, Bangkok 10800, Thailand; phatiphat.t@fte.kmutnb.ac.th

* Correspondence: florentina.enescu@upit.ro (F.M.E.); nicu.bizon@upit.ro (N.B.)

check for updates

Abstract: Traditionally, the energy industry has been slow in adopting new disruptive technologies and the transition to a new energy market will require a new digital transformation plan, involving all parties from the energy market. Although it now seems to be an impossible and hard-to-accept scenario, especially by the big players in the industry, the pilot projects so far demonstrate that blockchain can play a major role in the future energy market, even if the technology is still in the first stages of the adoption life cycle. This article attempts to describe a solution to provide alternative irrigation systems for small farmers. The solution involves creating associations of small farmers that will use green energy from photovoltaic panels for the irrigation of agricultural lands. The efficiency of the proposed system can be monitored not only through digital hardware connected to photovoltaic panels and water pumps, but also by using the new blockchain technology that stimulates innovation and growth in the energy and a high level of automation though smart contracts. To accelerate the transition to the green energy economy, a SolarCoin version similar to the Bitcoin cryptocurrency has also been proposed, which is a utility token that creates new possibilities for energy and water trading.

Keywords: irrigation system; photovoltaic water pumping systems (PWPS); floating photovoltaic panels; SCADA; blockchain; SolarCoin

1. Introduction

It is expected that in about 12 years, more than half of the electricity produced in the European Union will come from renewable energy sources, and the decarbonization of electricity is expected to be achieved by 2050 [1]. Under these conditions, the entire energy industry will have to go through a massive transformation, which will affect everyone in the value chain from the production, consumption, distributors, and networks [2–5].

The use of solar energy in various applications has grown over the past few years, and the irrigation sector is one of its most appropriate uses [6–8]. Many agricultural producers are attracted to this solution as it helps to maximize their profits by reducing the costs of electricity or fuel [9–11]. In addition, during the cold season after the irrigation interruption, electricity obtained from the

photovoltaic panels can still be used at high capacity to supplement the energy required to run the farm [4,12,13].

Photovoltaic systems are ideal in isolated areas that do not have access to the national energy system. Below, the most important advantages of applying the photovoltaic systems in agriculture have been listed [14–16]:

If the annual electricity consumption is known, then the photovoltaic system is easy to design because the network-connected systems have a small number of components and do not require too much space.

Research has confirmed that plants can also work with unfiltered water or chemical fertilizers dissolved in water.

Photovoltaic technology is getting cheaper. It does not rely on intense sunlight. The technology is simple enough to be easily implemented.

Irrigation is mandatory in obtaining profits from agriculture.

When pumping water, farmers need energy, but energy distributors sell it at too high a price for farmers' incomes and they are not interested in using irrigation channels.

Existing irrigation channels have deteriorated over time due to abandonment, which can be due to bad intentions.

This can be argued by the collection of images from a farm (see Figure 1) that resorted to these possibilities of realizing the irrigation of agricultural lands by using renewable energy, obtained with the help of PV (photovoltaic) panels [17].

Figure 1. Photovoltaic panels used for irrigation.

In the study carried out, the surplus of energy obtained in the months with a greater number of hours with brightness will not be stored in batteries but will be traded by cooperatives from which the farm is part to another cooperative or farm to the national system.

Regarding the maintenance of the panels (cleaning), high costs are not necessary, and in the case of a large number of panels, there are automatic systems for cleaning by miniroboting [18]. The possible lack of the national energy system in the area where the farm (cooperative) is located must also be considered [19].

Considering the adoption level of solar energy, it might be recommended for the small producers to make use of any additional income source, such as SolarCoin. Being based on blockchain technology [20–31], SolarCoin is global and decentralized, similar in many ways to cryptocurrency such as Bitcoin, but more efficient and environmentally friendly [32–34]. SolarCoin stands out because,

unlike other types of cryptocurrency, it ensures contribution to an economically and environmentally beneficial activity by vertically produced solar energy [35–37].

The study [38] has showed that despite the barriers to using blockchain technology, these technologies contribute to the Sustainability Development Goals by producing a series of changes and practices in various fields. In [39], the blockchain technology has been taken into consideration for an irrigation system.

We are proposing a software solution based on Ethereum blockchain and Distributed Ledger technology that aims to reduce the costs for farmers related to irrigation systems. A somewhat similar blockchain-based software platform was built and launched in Australia—Power Ledger (https://www.powerledger.io/) is a platform where businesses and consumers can trade energy peer-to-peer. The platform primarily caters to clean energy, such as wind and solar energy, that can be produced by individuals and businesses and then shared.

The main objectives and the novelty of this study are as follows:

(1) The proposal of a new solution to create individual microgrids for the small producer associations in a way that is most advantageous for both the producers and consumers, by assuring a reliable and transparent energy tracking solution achieved through decentralization of data and use of blockchain technologies;

(2) Presenting the possibilities of acquiring energy through blockchain utility tokens and SolarCoin technologies and comparing the obtained results in order to choose the solution that can bring the most benefits compared to the size of association;

(3) Proposing a way of placing the photovoltaic park so that agricultural lands cannot be affected, and the water stored in the channel is kept at a higher quality.

(4) Analyzing the current stage of the irrigation system used as a case study to integrate photovoltaic energy system and proposing solutions to solve the afore identified issues.

Also, this study presents the energy production of a photovoltaic system that may be coupled with the proposed Photovoltaic Water Pumping System (PWPS) when more energy for irrigation is necessary.

Thus, the structure of the paper is as follows: Different possibilities of energy transaction's first advanced methods and Blockchain SolarCoin variant are presented in Section 2. The model of the energy consumption flow within a farmers' association is presented in Section 3. The experimental study for an irrigation system based on renewable energy is presented in Section 4. The design of the photovoltaic energy system needed to supply the water pumps and the SCADA system for the association, and the analysis of the energy generated by the photovoltaic system during a year are also discussed based on the main results presented in an appendix. The proposed approach to reduce costs for the system under study is presented and discussed in Section 5. The last section concludes the paper.

2. Current State of Irrigation Systems

Regarding the water balance in Europe, 44% of captured water is used for energy production, 24% for agriculture, 21% for water supply to the population, and 11% for industry [1]. However, this distribution varies depending on location; in southern Europe, for example, agriculture accounts for 60% of the total water captured, with the percentage even reaching 80% in certain areas [1].

It is supposed that with the change of rainfall regimes, some parts of Europe will have more freshwater resources in the future and other parts will not be able to cover the overall need.

Crop irrigation is an area in which innovative practices and new policies can significantly facilitate the efficient use of water. In southern European countries such as Greece, Italy, Portugal, Cyprus, Spain, and southern France, arid or semi-arid conditions require the use of irrigation. In these areas, almost 80% of the water used in agriculture is currently used for irrigation [1–3]. A methodology that allows an optimal estimation of water quantity and energy used in an irrigation system in Spain has

been presented in [4]. Another example, which has been verified in the long run by such a system, was developed by Daud and Mahmoud in Jordan [5]. The water is extracted from a well and the available average solar radiation is 5.5 kWh/m^3/day. The tests proved the safety of the system with a general efficiency of more than 3%. This result was compared with similar studies that reported a high efficiency for photovoltaic solar water pumping systems [6–8].

In Romania, the situation is entirely different. The agricultural lands are large, there are many freshwater sources, and before 1989, Romania had an irrigation network spread over an area of 3.2 million hectares, which was almost entirely destroyed with the installations being stolen or left to waste. Most functional irrigation systems from 1989 have been dismantled and some have not even been built [3].

In May 2009, irrigation facilities for 563,000 hectares of agricultural land were in operation, of which 553,000 hectares (or 99%) were contracted by irrigation water user organizations [3].

In the irrigation field, Romania has a deficit of 2.6 million unrecorded hectares. In 2009 in Romania, 2.6 million hectares of land were unrecorded when it comes to irrigation statistics (today the area is even larger). According to these statistics, 300,000 hectares of land is irrigated, but in fact, there are only 100,000 hectares. Other sources indicate an irrigated area of 560,000 hectares [3].

For small farmers (usually with between 1 to 10 ha of land) located in areas with no electricity, it is appropriate and necessary to use funding opportunities for the purchase of mobile drip irrigation equipment (dripping or spraying) and for the insurance provision of electricity for the water pumps based on the photovoltaic panels [9–11].

Romania has one of the largest agricultural potentials in Europe, having a really high hydrological potential and a major advantage for organic farming (pollution of agricultural lands is still low compared to other EU countries).

Unfortunately, due to the destruction of the old irrigation system and the absence of a coherent governmental plan or other viable solution, a significant part of the agricultural area has been deserted.

To rehabilitate irrigation systems, high investments are needed, but besides that, there is the possibility for small farmers to not be able to afford purchasing water from rehabilitated irrigation systems, as the costs are high compared to the obtained incomes [17–19].

Although difficult to query for data in distributed databases, as stated in [39], they still provide fast processing. The biggest advantage of distributed ledger technology (DLT) is the ability to build trust in digital ecosystems [40].

Taking into consideration the security risks of a highly automated decentralized digital system for this kind of applications, the possible risks involved cannot be neglected. The Ethereum blockchain is one of the most used for deploying and running smart contracts, with lots of decentralized applications already in production [20–22]. As an open-source platform, it is already being code reviewed by the community, and thus it is one of the most secure platforms to run smart contracts on [23–25]. It is worth mentioning that all the software modules require core development principles, such as security in depth, unit testing, pre-and post-condition sanity checks, code consistency, and regular audits [26–28].

The performances of a photovoltaic system supervised by Supervisory Control and Data Acquisition (SCADA) system highlighted in [41,42] and the online surveillance on mobile applications as shown in [43] further accentuate the possibility of their application in this work oriented towards agriculture.

As has been shown, agriculture is facing problems due to water management and the cost of purchasing electricity. The work presented in [44] does not evaluate the performance of the blockchain technology applied in support of the community and the possibilities of communication with the blockchain network. The same is approached in [45] in managing the agro-food supply chain through the use of IoT of the consumption data.

How to use a water pumping system in irrigation system is fully described [46]. In this method, the water demands for irrigation are met and qualitatively analyzed, and energy products for

photovoltaic systems and the surplus of economic energy are redirected to the necessary coverage in the area.

So, an experimental study of renewable energy-based irrigation system is presented here in order to highlight the SCADA interfaces for a farmer and for the association, and the main features and advantages of the implemented blockchain-based application compared with the aforementioned proposals.

The location selected for the study is located in the Oltenia area of Romania, a geographical area where the solar radiation is high, and the quantity of natural water is reduced.

It is an area with low potential both economically and socially. The analyzed area is considered as agricultural area. The cultivation of the land is the main means of existence of most families. According to the [47] existing irrigation system, "it worked partially year after year, in an increasingly advanced state of degradation: pumps and equipment were damaged, they clogged channels, some pipes were stolen directly from the field".

With the help of the World Bank [47] the system was rehabilitated, but even after that it was only partially functioning due to the bureaucratic and impractical way of administration. The electricity subsidy needed to start the pumps, considered state aid, has been canceled since 2010, which has made it impossible for small farmers to bear the costs [47].

This area features a photovoltaic park with high energy efficiency. Nearby there is a system with a non-functional irrigation channel with a high degradation status, which is not currently in use (see Figure 2). Farmers in the area do not have the possibility to use water for crop irrigation during the droughts of the year (spring-summer), even if the channel is supplied with water.

Figure 2. Images from the area where the study has been carried out.

The problem of rehabilitation of the channel and pumping stations has been raised, but the small farmers cannot accept the connection to these systems as the costs of running water in the channel are very high compared to their income. Considering the possibility of using renewable energy through photovoltaic panels, whose costs are in a continuous decline, their concentration in micro grids, and the possibility to establish from the beginning their profitability by tracking the production of the photovoltaic park near the pumping station, three possible irrigation solutions will be explored in this study:

- Energy supply from the national energy system for land improvements and water supply to small producers;
- Use of the electricity produced by a nearby photovoltaic park, which delivers the energy to the national energy system and this can be used by farmers to supply the water pumps for the rehabilitation of the existing irrigation system;
- Establishing an association to deal with the management and production of electricity with renewable sources and the administration of the existing irrigation channels.

The first solution was already tried in another agricultural area in our country, by rehabilitating an irrigation system with European funds [47]. Considering the data presented in [48]—parliamentary report reveals the deterioration of the irrigation system—it is shown that in terms of the state of the pumping states, "they are mostly inoperative or require rehabilitation of a smaller or greater extent. On the whole of the analyzed areas, only five hours from the pumping stations are functional". It turned out to not be efficient, and the investment could not be amortized as expected. Water can be delivered to farmers, but at a high price. So, individual producers cannot afford it.

Innovations in electronics, information technology, as well as in energy storage solutions, allow the emergence of dispersed energy systems based on unconventional sources. The high costs and the random and intermittent nature of some of these energy sources make some a far-away alternative, or in other words, a possibility only in the future when there is no alternative, and the technologies of capitalization will be much more advanced, and of course, cheaper than they are currently. However, the prospect of capitalizing other forms of energy (unconventional energies) is very close, as they are also the energy hope of mankind. For these reasons, the latter solution is the most advantageous method to be accepted by small farmers and this can be demonstrated with this study.

3. Comparison of the Advanced Methods for Energy Transaction

SolarCoin represents an alternative digital coin that uses a Proof-of-Stake blockchain to stimulate solar electricity production [49–51].

The technology allows safe quantification of the amount of energy generated and used. SolarCoin owners—individuals or large solar panels—are proposing to build a currency transaction based on the assumption that electricity produced from solar energy is worth more in the world than its value in traditional energy markets [52–54].

SolarCoin represents tokens emitted in circulation when checking the production of solar energy. They can be traded just as normal cryptocurrency, being available at the moment on four different public crypto-currency exchanges. All the transactions are gathered, checked, and synthesized in specific blocks—which create the blockchain for the SolarCoin. It is a high-trust database underlying the project: A distributed, trustworthy, and verifiable ledger of the total energy produced by PV panels [55–57]. It remunerates the producers of solar power with blockchain-based tokens at a rate of 1 SolarCoin (SLR) for each 1 MWh of produced solar energy [58–60].

The technology behind the project is a POST (Proof of Stake Time) blockchain derived from the Vericoin implementation. Being an alternative to the proof-of-work blockchains, SolarCoin is more efficient than Bitcoin because it requires miners to solve computational puzzles [61–63].

SolarCoin is a zero-charge supplementary recompense, which does not depend on other stimuli that the producers of solar energy could receive (such as grants from the government, fixed green energy prices, tax reductions, green certificates, etc.). Anyone who produces solar energy in order to reduce CO_2 gas emissions can be rewarded with SolarCoin [64,65].

A. SolarCoin Economy:

The holder of a solar power plant is qualified to obtain SolarCoin as a zero-charge recompense for the generation of solar energy. For solar plants with a power of less than 20 kW, the right to coins lies with the consumer of the electricity produced rather than the financial holder [62,63].

B.   Working principle [66,67]:

Step 1: To qualify for a SolarCoin grant, owners must register their facilities through the SolarCoin Foundation. The registrations can be realized directly on the website of the foundation through a SolarCoin associate or through a tracking program.

The record includes evidence of plant ownership, network connection documentation (verifiable by an independent entity), solar power production parameters (e.g., meter readings), and KYC data (Know-Your-Customer).

Step 2: Upon completion of the registration, the foundation generates SolarCoin to the owner's SolarCoin digital wallet directly.

Step 3: SolarCoin is issued every six months to plant owners who are registered.

So, the SolarCoin will become a good/[an asset] with increasing liquidity, and it will be transparently released and tracked through blockchain, which can be stored in electronic wallets (e.g., mobile devices, computer) or offline (e.g., paper wallets).

Because environmental issues are getting more and more visible through the media (e.g., with the Amazon rainforest fires), green energy is getting more attention. This means more affordable photovoltaic panels, and that the SolarCoin demand and prices might go up in the following years, becoming additional revenue for solar power producers. Owners who generate solar energy could use/sell this energy and also obtain SolarCoin that can be reclaimed, exchanged, or used.

C.   Profit SolarCoin [68]:

Use of the SolarCoin may be an important stimulant for the investors in solar energy in order to increase the capacity of production. Investors will take the commitment to put money into solar energy by relying on:

1.   The price of the installation;
2.   The cost of the solar energy it generates;
3.   Expected earnings from any additional incentives they receive.

SolarCoin implements the remarkable features of blockchain technology in order to obtain a new situation:

•   A supplementary zero-charge reward for solar power producers;
•   The first digital coin to preserve natural funds;
•   The first stimulus program for solar energy that is non-governmental, global, and decentralized.

Partnerships can also be rewarded with SolarCoin—all contributing to building the ecosystem. SolarCoin ensures the distribution of digital coins to a beneficial and real economic and environmental activity: Vertically produced solar energy. SolarCoin is, thus, able to develop into a special, limitless stimulus for solar energy, independently of any other national or local stimuli [69]. Also, it is worth mentioning that all of the transactions are clear and can be visualized by any user of the blockchain explorer. Due to their distribution, blockchains can diminish the cost and duration of transactions. More significantly, the blockchain technology is prepared to transform the value exchange, eliminating the requirement of having intermediate energy distributors or banks [70–72].

This being the context of the problem, the scope of this study is related to the development of modern land improvement systems at low exploitation prices in order to be accessible to all farmers [73–75]. Table 1 summarizes the main features of purchasing and, in turn, distributing the energy surplus produced in a household/association using photovoltaic panels.

Manufacturers can opt for the method they consider to be the one that can bring them a high profit from an economic point of view. When choosing the optimal solution, the following table might be helpful, but obviously, there are many other details to be taken into consideration, such as the location, the number of possible members of the association, the current status of the nearby irrigation channel, etc. [76–78].

Table 1. Characteristics of purchasing energy technologies.

Technology Type	Stimulates Innovation	Global and Decentralized	Stimulus for Solar Energy	Open-source Community Project	Reward	Tokens
Photovoltaic plant connected to the national power system	NOT	NOT	NOT	NOT	NOT	NOT
Blockchain—utility tokens	YES	YES	NOT	NOT	Tokens	YES
Blockchain—SolarCoin	YES	YES	YES	YES	1 SolarCoin (SLR) per 1 MWh of solar energy produced	NOT

The aforementioned features (see Table 1) of the possible implementation solutions are explored in the next sections of this study and compared with the proposed solution.

4. The model of the Energy Consumption Flow within a Farmers' Association

The association of farmers in the studied area, in the first stage, will acquire collective energy from the energy suppliers. The greater the participation in this association, the easier it is to estimate the consumption time (due to the law of large numbers) and thus the easier it is to negotiate a discount with the energy provider. At the end of the period, a balance sheet of the consumer profiles of the integrated users will be made. Profit earned by associates can be invested in the next year.

In the next stage, knowing the energy consumption, it is possible to estimate the electric energy needed by the association, and in these conditions, it can be purchased in the case of Romania directly from OPCOM (the Romanian Electricity and Gas Market Operator). Under these conditions, with the classic system, the association can obtain a profit that is invested in the acquisition of renewable sources that lead to independent energy, but also to energy storage solutions.

The solar radiation flux reaching the earth's surface has an energy potential corresponding to the impressive amount of 172 billion GW [79]. This energy source could permanently ensure the need for ever-increasing consumption. However, from a practical point of view, with regards to the actual volume that can be used, this becomes a very complex problem.

Photovoltaic water pumping systems (PWPS) consist of a series of photovoltaic panels, a motor, and a pump (Figure 3). Depending on the design, the system may contain batteries for storing electricity and charging the regulator. The motor is chosen according to the required power and the nature of the current provided by the system. If the motor uses alternating current, it is necessary to install an inverter. PWPS without an energy storage system are cheaper and require less maintenance compared to battery systems. Adding a water storage tank to the PWPS is a more economical method of storing energy than using a battery and useful if irrigation if possible, using gravity afterward. If the tank is built deep, some energy from the PWPS is required to take the water out. Photovoltaic solar energy is considered to be an important resource for regions of Romania where direct solar radiation can reach up to 1000 W/m^2, even if some cost is involved, mostly due to batteries lifespan, panel maintenance (cleaning), and upfront costs [80].

Attention is paid to the daily variation of the volume of water pumped. A threshold value (at which the pump starts/stops) of the total solar irradiance on the surface of the photovoltaic module is set to 450 W/m^2, which means that when the total solar irradiance is less than 450 W/m^2, the pump does not work. It starts at 450W/m^2 and the water flow increases with the increase of solar irradiance.

At this stage, when 6000 Wh is needed for a pump, the energy produced by the photovoltaic park in the analyzed area can be used.
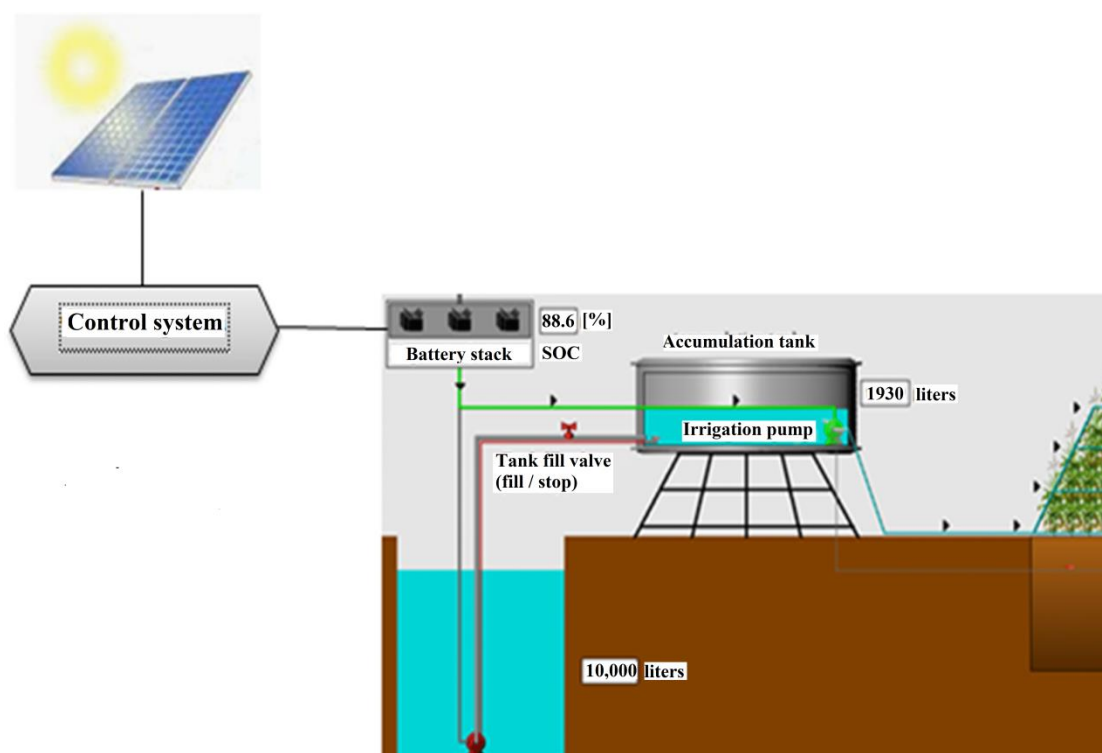
Figure 3. Photovoltaic system for pumping water.

Being a legal entity, the association can build its own photovoltaic park by acquiring photovoltaic panels. In this way, the association will be able to trade the energy produced both to the consumers inside the association and to the association's neighboring consumers. The profit obtained will come in the endowment of the photovoltaic park.

The profit is simply obtained by registering in the SOLARCOIN database, through which each farmer and the respective association can win SolarCoin. These can be purchased and subsequently reinvested, for energy acquisition and other resources. The SolarCoin Foundation will ask for registration data on the purchase of photovoltaic panels, as provided in the operating status [67,68].

The amount of additional energy generated will be sold through the novelty blockchain system. An important objective of the association is the realization of a software application that monitors the performance of each user.

The association is the owner of the equipment that will be given in the form of commodities to the persons in the association on the ground of which they are located. In this case, a solution for optimal land use would be to place the panels above the channel, as well as to hygienically protect the water in the canal.

The unused energy surplus will be traded on behalf of the association to members who, at that time, have an energy demand not covered by their own production or to the national energy system (Energy Distributor) (see Figure 4).
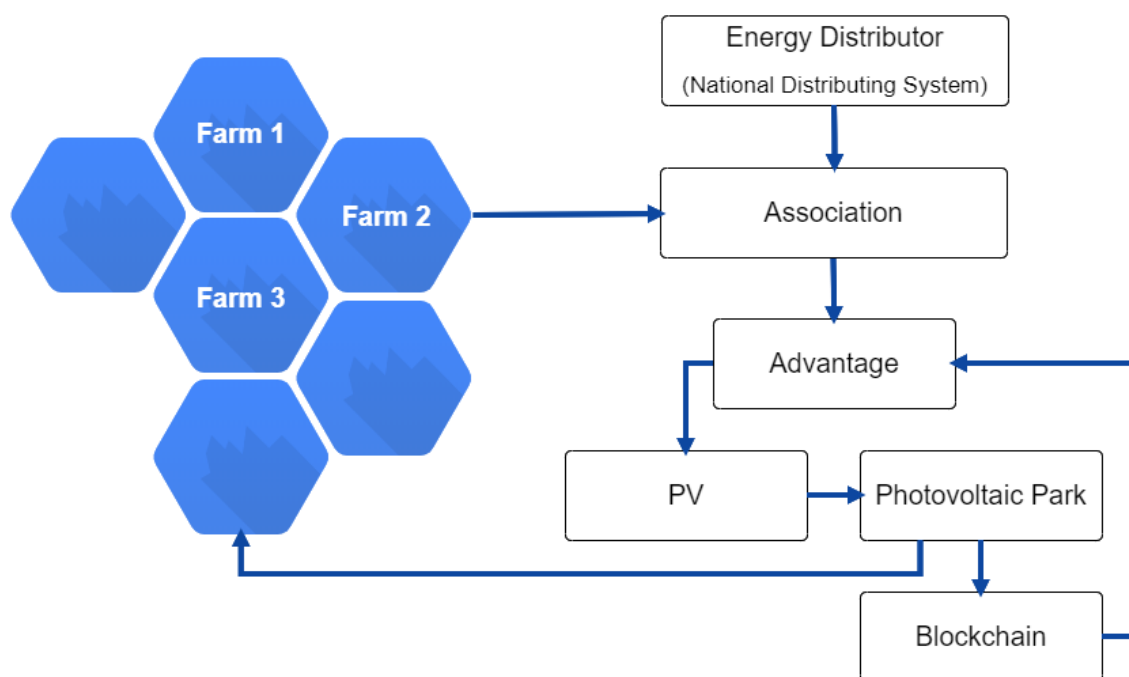
Figure 4. Proposed diagram for the software platform used in the association in order to make the activity profitable.

5. Experimental Study for an Irrigation System Based on Renewable Energy

The direct connection of the photovoltaic module to the water pumping system is the cheapest commercial solution. At a high-level description, the system consists of a photovoltaic module directly connected to the DC motor of a centrifugal pump. Due to its simplicity (not including batteries and the control system), such a system is simple and reliable. The pump was monitored for five months, during the spring and summer months when the crops were irrigated, in order to evaluate the volume of pumped water and its distribution over time and the influence of the solar radiation regime on the performance of the system. The first information is essential for photovoltaic system sizing to ensure optimal operation of the water pumping system. The second information may provide an overview on the case study in order to generalize the results obtained.

A. Choosing Panels:

For each member of the association, the energy requirement for pumping water will be calculated depending on the area owned. In order to determine the number of photovoltaic panels and the total power generated by the photovoltaic system, the steps and relationships mentioned in the Appendix A may be used.

B. SCADA system for association members—users:

The CitectSCADA®software from Schneider Electric has been used to implement the tracking system. A friendly interface (see Figures 5 and 6) allows tracking and control of the actual state of the irrigation system by both cultivators and the association.

At the beginning of the study, an isolated agricultural farm was analyzed, from an energy point of view and water supply, equipped with photovoltaic panels to generate the energy required to supply the water pump (depth), which was distributed in the irrigation system. With the help of this interface (see Figure 5), the state of the system can be monitored and controlled, namely: Average temperature, water level in the basin, battery charge level, and soil moisture.

Starting from this, it was continued to reduce costs and increase the reliability of the system. So, these unique farms will be constituted in cooperatives or associations (see Figure 6) that will be able to manage the situation of production, consumption of energy and water, costs, surplus of energy

realized, when appropriate, not by storage in batteries but by sale (smart contracts and utility token) to other farmers from outside cooperatives, either by feeding the national system.
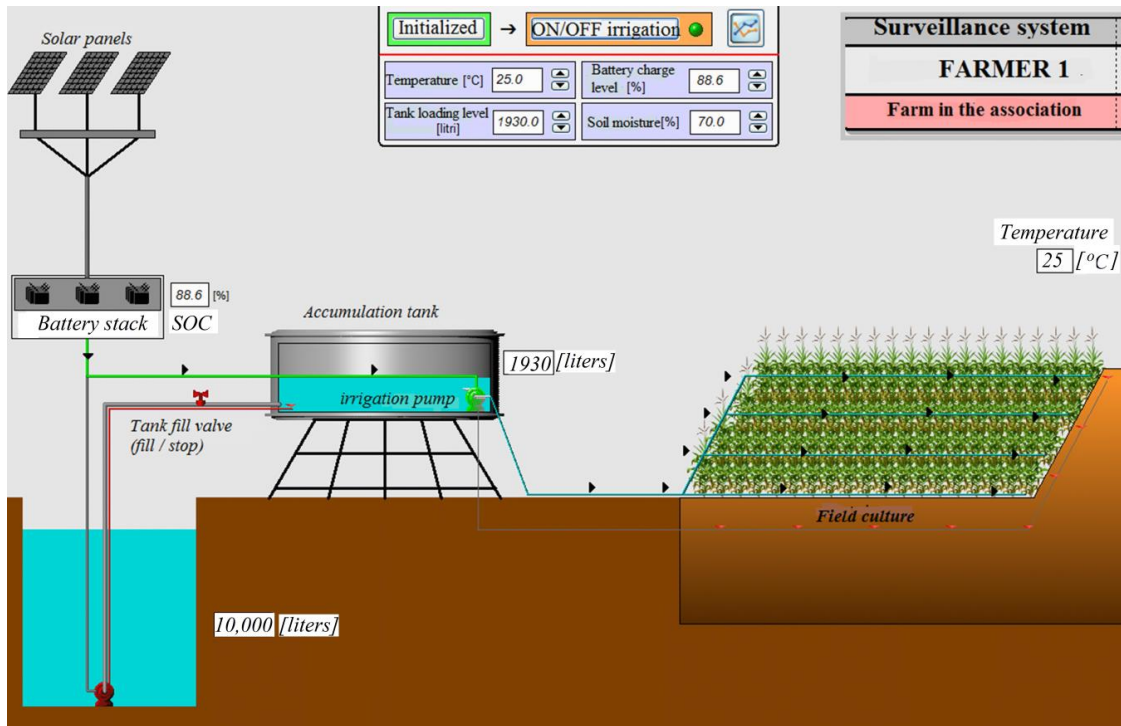

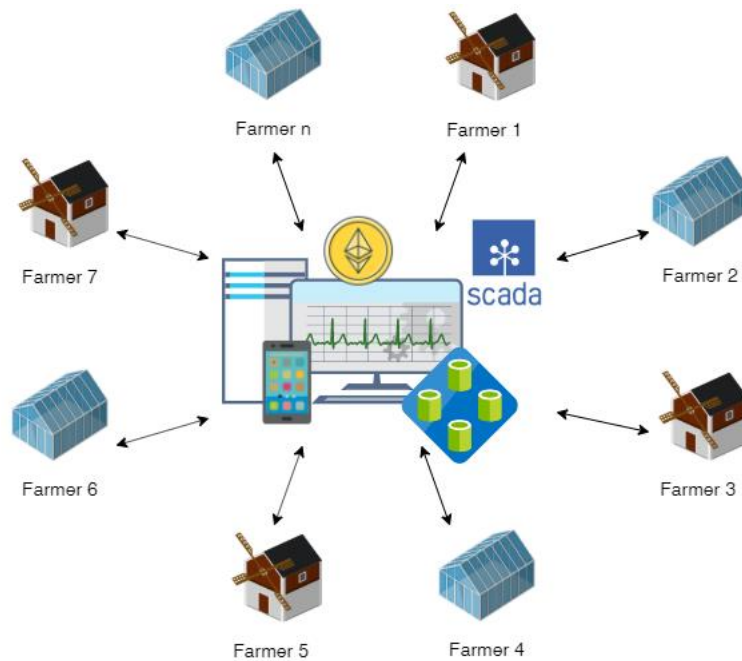**Figure 5.** Human-Machine Interface (HMI) Supervisory Control and Data Acquisition (SCADA)—Farmer 1.

Figure 6. SCADA system at the farmers' association level.

In Figure 6, we can see how the farmers will interact with our proposed system. Basically, the association of farmers will allow members to interact with the platform through the mobile application, which will interact via the backend with the utility token (Ethereum blockchain), distributed database, and the SCADA system for the monitoring and controlling the energy and water.

In order to have control over the amount of energy produced by the association, but also over the consumption of each member, each of the members will be equipped with a system for tracking and measuring the amount of consumed energy. So, the system will be provided with sensors and a warning system to alert users on the state of humidity and the necessity of watering the crops.

All energy consumption and surplus energy data will be stored in distributed ledger databases. These data will be accessible for both the associate and the association so that each of the two entities knows very well the stage they are in. In this way, each will be able to monitor the quality of the system and correct any losses. The system architecture is shown in Figure 7.
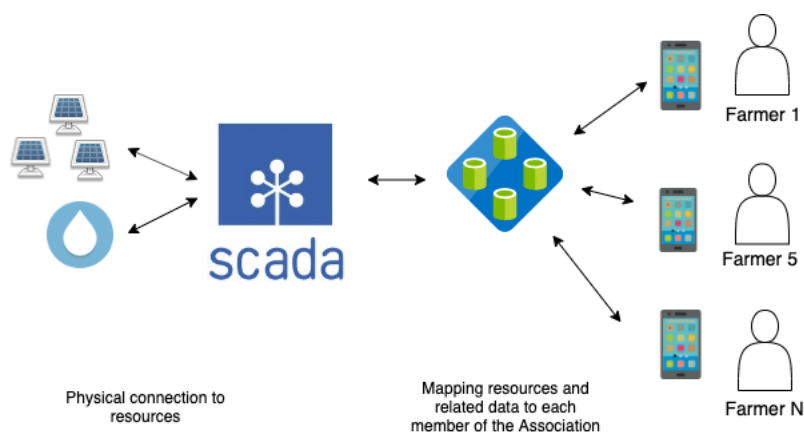
Figure 7. The architecture of the monitoring system—farmers' association.

C. Analysis of the photovoltaic power generation:

In the first phase, if the agricultural association cannot generate enough energy from its own resources, it can resort to the use of green energy resources in the immediate vicinity. At the end of this stage, it can be decided how the profit may be used for the acquisition of photovoltaic panels by the association, in order to create its own photovoltaic park (as it is shown in Figure 4).

A scheme of the proposed working model for the association to make the activity profitable is presented in Figure 8.

Step 1

In the first stage (first year), in order to be able to carry out its cooperative activity (the association), it acquires the necessary electricity from the national system, until the proposed objectives are achieved. By using the irrigation system, it is obvious that the production and quality of the farmers' products will increase, compared to the incomes obtained before using the irrigation system.

The material advantage obtained will be reinvested in the following year in the acquisition of photovoltaic panels.

Step 2

Near the irrigation channel, a photovoltaic park is located. Considering that this photovoltaic park is located in the studied area, it was possible to track, through the SCADA system existing in the park, the amount of energy produced daily and especially during the spring–summer periods, when the farmers need electricity to supply the pumps.

By realizing the cooperative (the farmers' association), the energy can be negotiated from that existing photovoltaic park or from the stock exchange. In this way, the association can save funds by reducing costs by purchasing electricity.

The money obtained will be invested in the purchase of photovoltaic panels that will be conceded by the farmers from the cooperative, or if the PV purchase will be considerable, it will be made own photovoltaic park. Also, income can be obtained in the form of SolarCoiN, by simply registering in the database, from the respective platform of the PV holders (demonstrating through documents).

Step 3

This is the time when the association has its own photovoltaic park, they can produce their own electricity, and therefore the benefits will be great in terms of production costs. With the help of the proposed platform, the surplus of energy, especially the electricity produced in the months in which it is not irrigated, will be delivered (sold) to the farmers outside cooperatives for their own needs or to another association, thus creating a chain of associations. During the periods of the year in which it is not irrigated, the energy will be delivered for cost for domestic purposes.
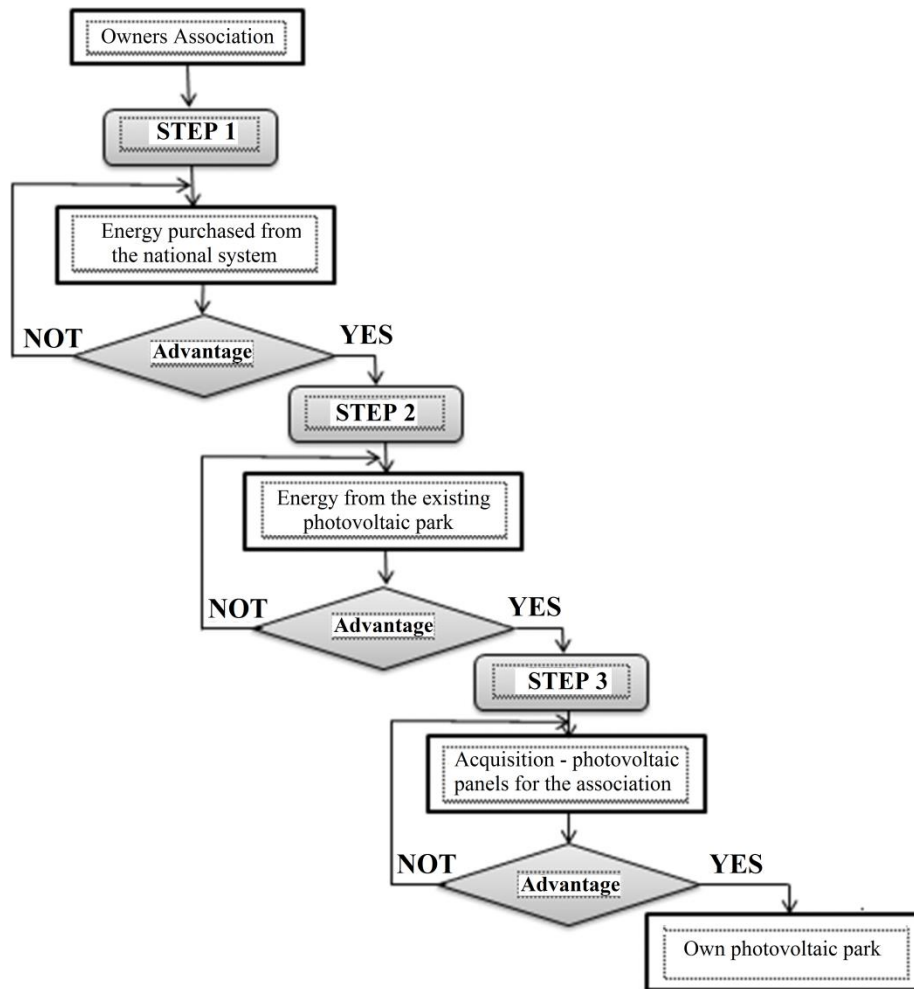
Figure 8. Diagram of the working model for the association.

The availability of energy from the 7.5 MW photovoltaic park (30,646 modules and 14 inverters covering 17 ha in the vicinity of the irrigation channel; see Figure 9) is estimated massed on the energy production budget and performance presented in the Appendix B.

The energy production budget for a calendar year is presented in Table A1 and Figures A1 and A2 of the Appendix B based on the values obtained from the SCADA system of the photovoltaic park.

Analyzing the values recorded during the peak months (May–September), when it is necessary to supply the electric power for the pumps from the irrigation system stations, it can be ascertained that they meet the requirements. Also, analyzing the values of the extra-season months, a profit may be obtained by either delivering the energy for the household needs of the members of the association or delivering it into the national energy system (see Figure 10).
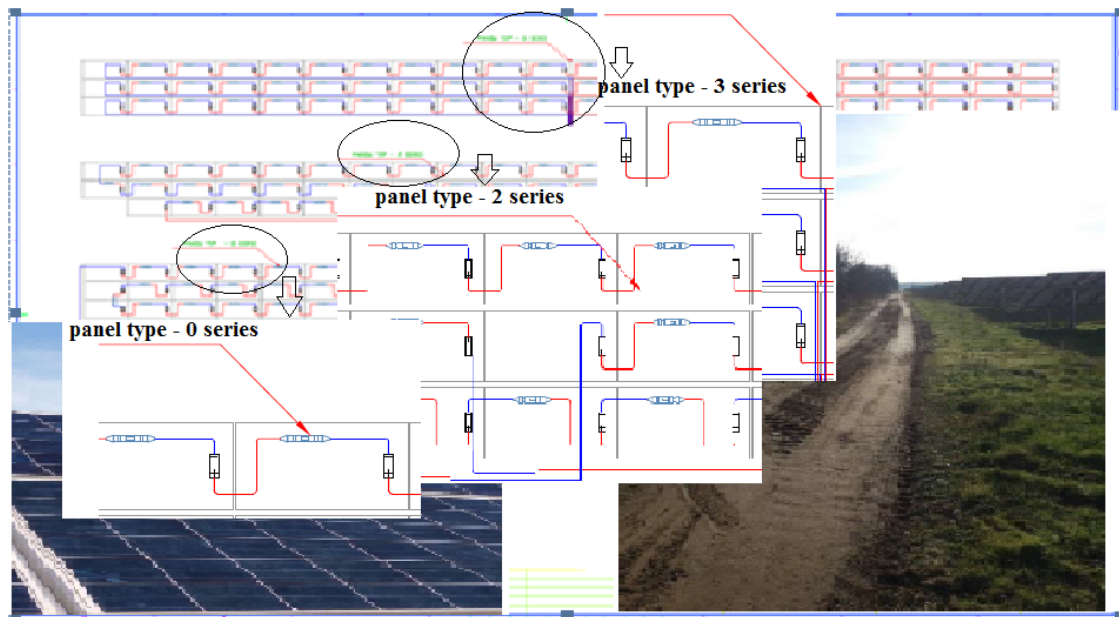
Figure 9. Map of the photovoltaic park.
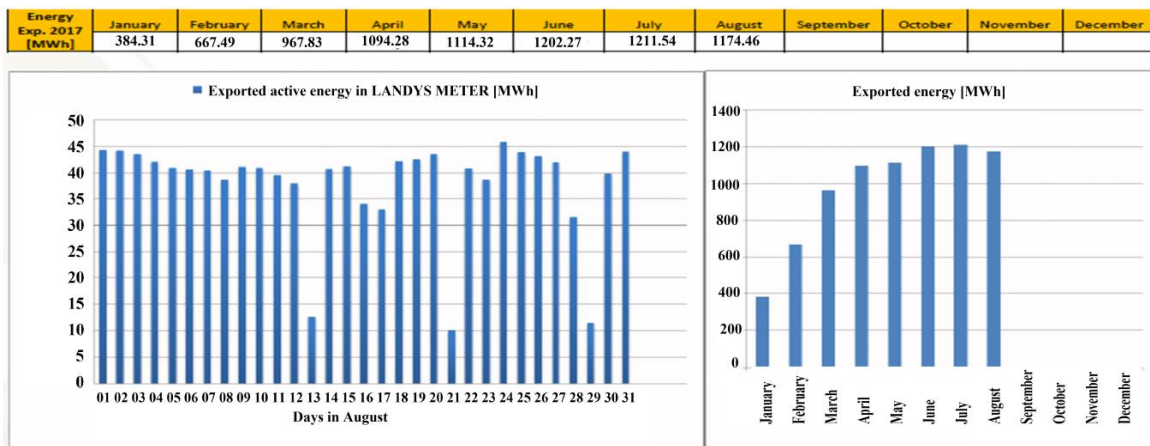
Figure 10. Graph with annual energy production delivered to national energy system.

The performance of the park of photovoltaic panels during time T (PR_T) can be estimated using the relationship (1):

$$PR_T = \frac{Energy\ produced\ during\ a\ certain\ period\ T\ [kWh]}{\frac{Average\ incident\ solar\ radiation\ during\ T}{1000\ W/m^2} \cdot Peak\ plant\ wattage \cdot T[h]} \tag{1}$$

For example, the results obtained are presented in Tables A2 and A3 for December, which looks to be the month with the least energy produced (see Figures A3 and A4). This assumption is validated by the energy availability of the photovoltaic park presented in Figure 11.
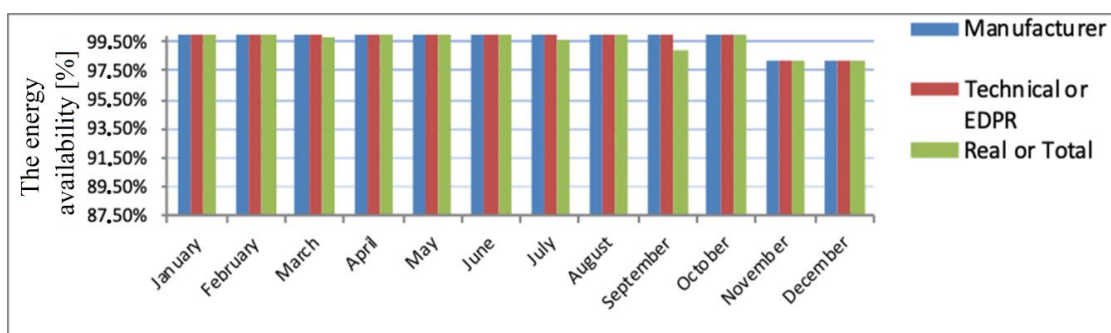
Figure 11. The energy availability of the photovoltaic park.

6. The Proposed Approach to Reduce Costs

Considering the solutions presented and discussed in the first part of the study and the need of the small producers to use the irrigation system (and they are aware of this necessity), this study proposes new methods of generating income for producers while keeping low prices for water purchased from the irrigation channels.

Three scenarios have been proposed depending on the area chosen for the study as well as the existing resources. In the proposed methodology, the reduction of costs will be first (see Figure 8). This can be mainly achieved by lowering the energy price using the renewable energy and the proposed method for energy transactions.

6.1. The System Description

6.1.1. Current System

The current solution (energy supply from the national electricity system) has proven to be unprofitable and thus unacceptable to small farmers due to high costs involved (see the argumentation made in Introduction). So, the energy cost must be reduced by use of renewable energy sources.

6.1.2. Use of a Photovoltaic Park

Another solution is to use energy from a photovoltaic park located close to the farms. If the photovoltaic park is equipped with a SCADA system for real-time monitoring and control of the power generation, then the farmers' association can be easily connected and monitored.

The analysis of the data (see the previous section) has shown that such a system is energy efficient but also cost-effective for the owner of this photovoltaic park. However, this solution is not so attractive for the farmers because the energy obtained is delivered at the price set by the distributors.

6.1.3. Acquisition of Individual Photovoltaic Panel Manufacturers

So, one of the profitable small businesses of the coming years will be that of small electricity production, due to a continuously growing of energy demand and high prices on the energy market. However, for small energy producers, it is almost impossible to distribute energy and obtain profits because, today, only big manufacturers have access to the energy market. Consequently, only associations of small producers could enter the market (see Figure 12). The local distributor would be obliged to take over the quantity produced by them at a fixed price. The price would be up to 50% lower than the actual market price.

So, this solution would be advantageous for the small farmer in order to benefit from a considerable profit, but it is difficult to be implemented in this stage. Thus, for a start, a simple and beneficial solution for the farmers' association will be proposed in next section.
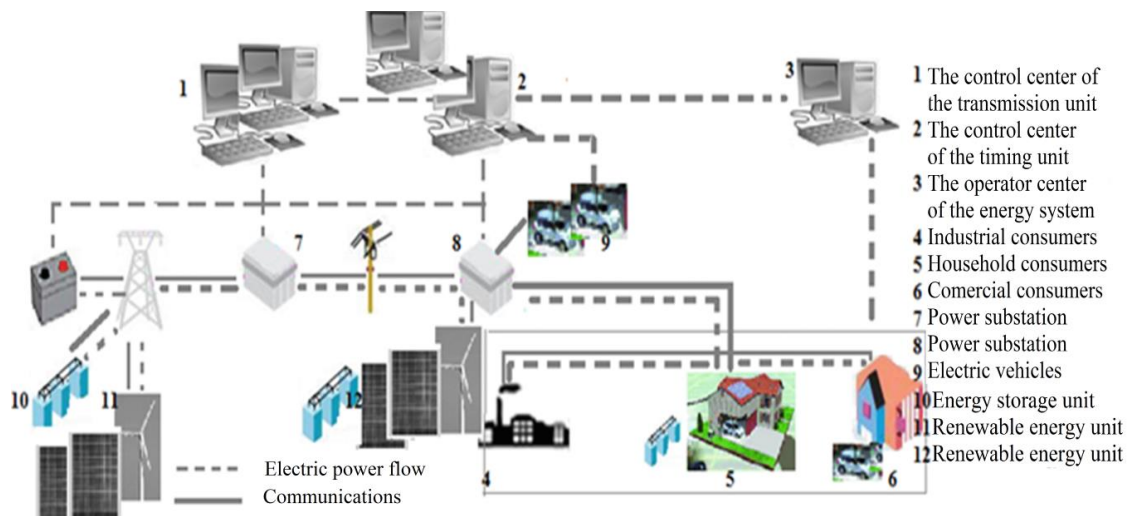
Figure 12. The national power system that integrates the green energy producers.

6.1.4. Manufacturers Associations

The small farmers will join an association that will concede the abandoned irrigation channel. The energy produced by photovoltaic panels will be directly used, without being pumped into the national power system and then used.

Equipping the irrigation channels with photovoltaic panels will be done in such a way that the association will make a profit. The association will continue to expand the photovoltaic park in an efficient way, taking into consideration the supply and demand, just like in the market economy. In order not to occupy the land necessary for the agriculture, the water channel can be also covered with floating photovoltaic panels that resist corrosion, and the anchors should last for 25 years or more (see Figure 13).

Figure 13. Photovoltaic panels mounted on the irrigation channel.

In comparison with the photovoltaic system mounted on the ground, the photovoltaic system mounted on the surface of the channel has the following advantages:

- The panels do not occupy land;

- They are not visible;
- The water in the channel cools the solar installation, thus avoiding the overheating that occurs in the case of photovoltaic panels that use silicon components (each module has a maximum power of 200 kW);
- It generates 11–30% more energy (due to water cooling) than an ordinary "ground" photovoltaic park where the panel can move (more efficient if the panel can move depending on the brightness);
- The floating system is mounted on a light support through which light passes so that the animals in the water can live;
- Reduce water evaporation;
- Inhibit algae inflorescences;
- The colder air reduces the aging of solar cells and obviously increases the performance in operation, granting a longer operating period;
- Requires a smaller cleaning process over time, with a smaller amount of water, than the case of the terrestrial photovoltaic panel [81–83].

The association will be interested in selling the energy surplus, especially in the months when the soil does not need extra water or can be motivated to increase the capacity in order to meet the demand of possible external consumers. Also, some of the energy will be used by association members.

There will be a so-called blockhouse of a restricted community, real-time counting of local energy generation and use, and the analysis of related data. The proposed solution is similar, but more efficient than that proposed in other peer–peer solar energy trading projects, as will be explained below.

6.2. Blockchain Application for the Association

The following software solution is proposed for the management of water and energy in an association, which adds a value through the transparency and decentralization of the data. Using blockchain technology, the solution aims to reduce overall costs of irrigation in associations of small farmers. The following components are proposed: A backend application, which processes all the events and transactions and smart contracts; a mobile application, which enables farmers to buy and sell energy and water; and a distributed ledger database, which offers a high degree of transparency and could build trust in the network of farmers in the association.

The detailed components of the platform.

I. The backend module—the backend module will play the main role in the proposed software solution. It will interact with the clients through the mobile application, with the blockchain, and with the databases; SQL and a distributed ledger database (e.g., BigchainDB) will be able to store the accounts (associations and association's members) with all the details such as photovoltaic panels owned, the energy produced, water used, application programming interfaces (APIs) for the mobile applications, SCADA systems, and with the Ethereum main-net blockchain. The Distributed Ledger Technology's (DLT) role is to add a high degree of transparency and to build trust in the network through the decentralization of data.

The administrators of the association can access the backend module trough a web interface in order to set up and configure details such as farmers' accounts, permissions, authentication, etc.

II. The ERC20 utility token—will be created on the Ethereum blockchain using the Solidity programming language. The token will have a fixed total supply and will be used as currency inside the associations to create an internal trading market. Members of the association will be rewarded with the token depending on the amount of energy produced with the owned photovoltaic panels. Buying water from the irrigation channel will also be made using the token.

Farmers will interact with the smart contracts through the mobile application.

III. The Mobile application will be used by the association members to control and monitor the energy produced and the water consumed. Also, it can be used to trade the utility token, allowing households outside of the association to buy water from the irrigation channel (see Figures 14 and 15).
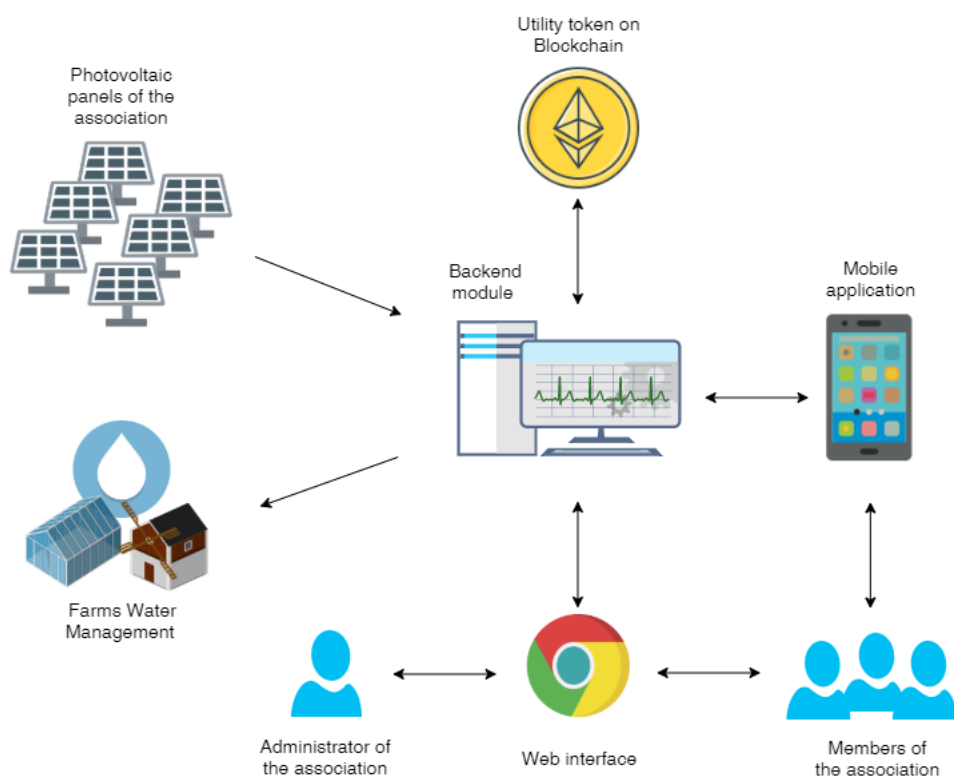
Figure 14. Visual representation of the digital platform proposed.

The architecture of the proposed platform is represented in Figure 14 (high-level) and in the technically detailed diagram from Figure 15. Members of the association (the farmers) will use the mobile application to interact with the utility token (buying and selling the token, energy, and water). The administrators of the association will be able to set up the new members into the system, along with their hardware: Photovoltaic panels and water meters. This will be achieved using the SCADA system and smart waters meters with Ethernet connectivity.

A.   Working principle:

The operating principle is simple to use by a wide range of users.

Step 1: A member of the association will access the platform from a mobile application and will sign into the account. The new members will have the option to create new accounts. A complete set of self-serving features will be implemented.

Step 2: The farmers will fill in the identification data and purchase documents of the photovoltaic panels and after the configuration of the smart water metering and SCADA system, the platform will map to the account the correct amount of energy produced and to all the tokens earned so far. The administrators of the association will enroll the new farmers into the system.

Step 3: Users will be able to spend their tokens via the platform by exchanging tokens for water from irrigation channel, for energy, or simply selling them to the highest bidder (other users of the platform, a member of the association, or to an external user).

Step 4: Users will have the possibility to hide any personal data, and the information stored in the distributed ledger database will contain only pseudorandomized data, following the General Data Protection Regulation (GDPR) accordingly.

After completing these steps, the entire system will be automated by the internal economy created with the help of the utility token. This proposed concept can be used for an association or can be configured for a cluster of associations. At a higher scale, the blockchain will produce even greater benefits as members will be able to avoid energy distributors' costs almost entirely.

B. Access to data:

The identity of the owner and the authenticity of photovoltaic acquisition documents are verified through a hash and after that can be accessed by the members of the association, the management of the association, or other interested households.

After enrolling each member in the database, it can access data with daily energy production, the amount of available energy available for sale, daily consumption of households in the association, and households who want to join the association. The same thing goes for the water used or that will be used, and the number of tokens owned by each member.

C. System Automation:

Using the SCADA system and smart water metering solution, the entire system will reach a high level of automation. The operations not automated will be the members enrolling in the system and physically connecting the devices to the irrigation channel.
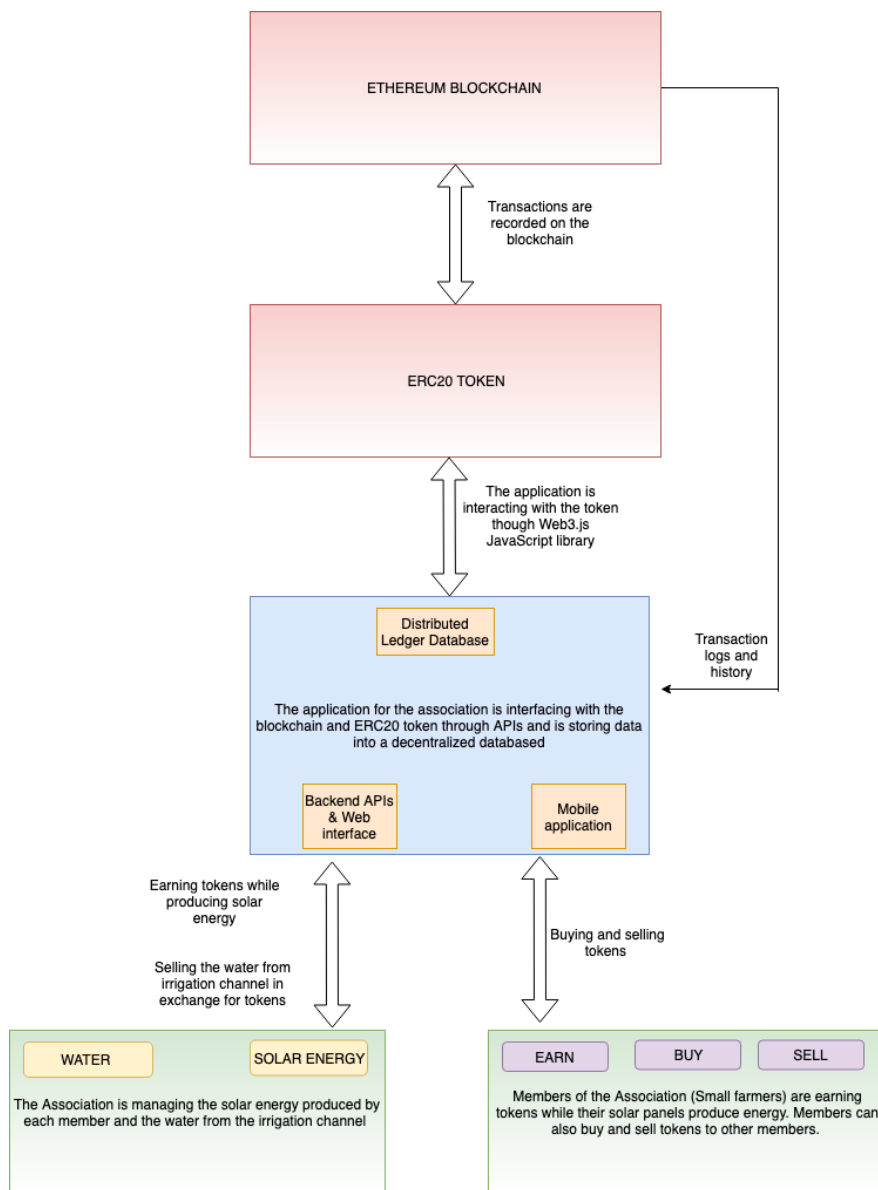
Figure 15. Blockchain-based smart contract system for irrigation systems.

D.   Implementing a prototype and some samples of the obtained results:

In the implemented prototype, an ERC20 token, a basic backend API, and a basic web interface has been developed with the following functionalities: Creating accounts, profiles, and sending and receiving tokens.

(a)   Smart Contracts:

The platform interface was built using Truffle framework and web3.js library for interfacing with the Ropsten Ethereum testnet.

The following snippets of code represent the token created using Solidity (Figure 16) and deployment to the testnet blockchain (Figure 17). As it can be observed below, our implementation makes use of the open-source contracts library called Open Zeppelin.

```solidity
pragma solidity ^0.5.2;

// --------------------------------------------------------------------
// 'Small Irrigation System Token' token contract
//
// Deployed to : 0xD8d3E3f498a9b32d40e124C20Cc5618c21C4Cd48
// Symbol      : SIST
// Name        : Small Irrigation System Token
// Total supply: 1_000_000_000_000
// Decimals    : 8
//
// --------------------------------------------------------------------

//Open source ERC20 implementations
import "openzeppelin-solidity/contracts/ownership/Ownable.sol";
import "openzeppelin-solidity/contracts/token/ERC20/ERC20Detailed.sol";
import "openzeppelin-solidity/contracts/token/ERC20/ERC20Burnable.sol";

contract SmallIrrigationSystemToken is Ownable, ERC20Burnable, ERC20Detailed {

    mapping (address => bool) public transferAgents;

    constructor(
        string memory name,
        string memory symbol,
        uint8 decimals,
        uint256 amount
    )
        ERC20()
        ERC20Detailed(name, symbol, decimals)
        Ownable()
        public
    {
        require(amount > 0, "amount has to be greater than 0");
        uint256 totalSupply = amount.mul(8 ** uint256(decimals));
        _mint(msg.sender, totalSupply);
    }
```

Figure 16. ERC20 implementation of the token's constructor.

The contract developed and deployed as an experiment is named "Small Irrigation System Token" (Figure 16). The constructor is an optional function declared with the constructor keyword, which is executed upon contract creation, and where you can run contract initialization code. The name of the token contract is the long name by which the token contract should be known. The symbol represents the short name by which the token contract should be known; in our case, it is "SIST". Decimals refer to how divisible a token can be, from 0 (not at all divisible) to 18 (maximum Ethereum decimals). The "Amount" defined in the contract refers to the number of tokens that will be minted (created on the first deploy). Contracts used from OpenZeppelin open-source smart contract library are the following: ERC20, ERC20Detailed, and ERC20Burnable; these three offer a secure way of implementing basic token functionalities such as sending and receiving tokens.

```
    modifier canTransfer(address _sender) {
        require(!isBanned[_sender]);
        _;
    }

    function transfer(address _to, uint _value) public canTransfer(msg.sender) returns (bool success) {
        return super.transfer(_to, _value);
    }

    function setBanState(address addr, bool state) public onlyOwner {
        require(addr != address(0x0));
        isBanned[addr] = state;
    }

    function setTransferAgent(address addr, bool state) public onlyOwner {
        require(addr != address(0x0));
        transferAgents[addr] = state;
    }


}
```

Figure 17. Token's transfer and ban functions.

As a security measure, the association's administrator could make use of the above smart contract functions. The administrator is named by the "setTransferAgent" function and he could deny specific users to use the token. These functions will be called every time a transfer is initiated and will check if the specific account is allowed to make transactions.

(b)   Deploy the contract to Ropsten:

The token deployment to the testnet blockchain will be made with the Truffe framework.

1.   Build the smart contract with the following console command: *truffle buil*
2.   Deploy the contract: *truffle deploy –network ropsten*

Once the contract is deployed, the platform can make use of the token enabling transfers between members and exchanges for energy or water. Initial functional and security testing can be achieved using Remix Ethereum IDE.

(c)   The interface for the mobile application:

The user interface proposed for the mobile application should be minimalistic and user-friendly, making it very intuitive and easy to use (see Figure 18).

So, the farmers will interact with the platform via the mobile application shown in Figure 17. One of the challenges to be faced will be the quality of user experience and training.

6.3. Discussion

After running the experiment, we could create the associations, farmer accounts, simulate energy and water data, and perform transactions via the Ethereum Blockchain. There is a clear set of advantages of the blockchain technology used in associations of small farmers.

- Secure payment and transaction systems based on the blockchain.
- The blockchain technology offers a high level of transparency, as each member of the association can see the number of tokens owned and all transfers.
- Implementing the DLT will enhance the trust in associations, as everyone could see relevant data such as the amount of energy produced and the amount of water consumed.

The next step of the experiment is to integrate the next version of the proposed platform into an association of small farmers. This will help to receive feedback on the user interaction and

functionalities of the small farmers. Also, the first tests within the association will provide a direction for scaling the platform and supporting transactions between multiple associations or villages and will confirm the effectiveness of developing an internal economy inside the associations. The internal economies will ensure the system is highly performant and is maintained properly even in the winter when the demand for water is not that high. Also, the internal economy needs to reduce the overall cost of irrigation water.
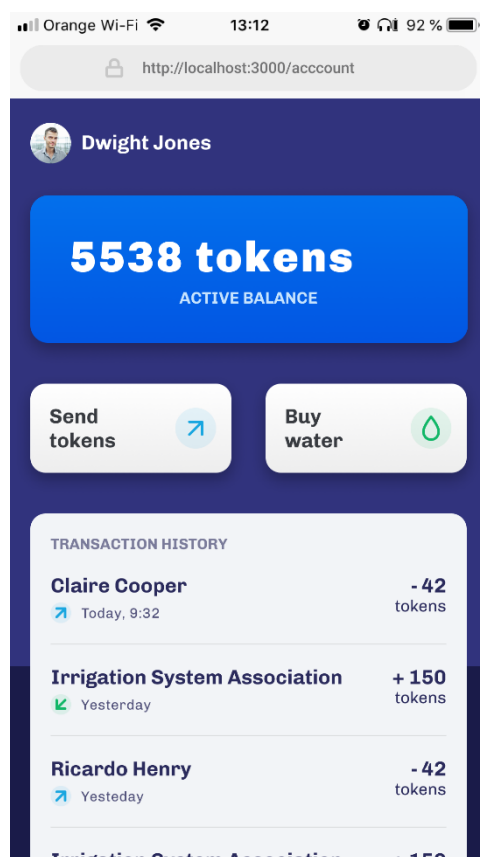
Figure 18. Sample screen of the interface proposed for the mobile application.

Implementing the blockchain-based system in just one association would be the first step in the digital transformation of the irrigation industry and even the solar energy industry. Once this step is confirmed and achieves a good level of adoption, the next step is to enable association-to-association transactions or village-to-village.

7. Conclusions

The advantages of the photovoltaic systems for isolated areas without access to the national energy system led to an attempt to propose the rehabilitation of irrigation systems.

The proposed solution is based on creating associations of small farmers that are using the irrigation system connected at photovoltaic panels. The efficiency of the proposed system is monitored not only through the location and type of photovoltaic panels, but also by using the new blockchain technology. Creating an internal economy inside the small farmers association can be a great benefit for the members. Firstly, the token value will be dictated by the demand, offering opportunities for the producers to maintain the infrastructure even in the winter when all the activities in the agriculture industry will be at a low level. Secondly, the non-members interested in acquiring energy or water from the association can make use of the internal economy to get the best price available at that time.

Innovative and sustainable solutions for agro-power-problems, interchange smoothness, and Human–Machine Interface (HMI) are important contributions of this paper, where the energy efficiency and chain-power-requirements are also considered. To validate the objectives of this study, an experimental renewable energy-based irrigation system with SCADA interfaces based on the proposed blockchain applications has been used.

So, the main findings of this study are as follows:

(1) The advantages of the proposed experimental renewable energy-based irrigation system using the energy of photovoltaic panels and a blockchain-based transaction system have been shown;

(2) The investment can be quickly recovered if a large number of farmers are involved in the same association through this blockchain-based application (see the energy production vs. budget presented during a year);

(3) The comparison of the blockchain utility tokens and SolarCoin technologies has been performed.

From the research, it is fact that the takeover of the agricultural irrigation activity by an association is one of the best solutions for enforcing agricultural production, but also for getting benefits from the community by reducing the costs of electricity in part or in some cases totally. An important profit is also obtained by selling the surplus energy you get.

Also, it should not be forgotten that a decommissioned and uncleaned channel can be rehabilitated to become functional.

Abbreviations

DLT	Distributed Ledger Technology
GDPR	General Data Protection Regulation
HMI	Human-Machine Interface
KYC	Know-Your-Customer
OPCOM	The Romanian Electricity and Gas Market Operator
PR_T	The performance of the photovoltaic park during T period
PV	Photovoltaic
PWPS	Photovoltaic Water Pumping Systems
POST	Proof of Stake Time
SQL	Structured Query Language
SLR	SolarCoin
SCADA	Supervisory Control and Data Acquisition

Appendix A

Design of the photovoltaic system:
The number of photovoltaic panels can be established using the following steps and relationships:

1. Calculate the energy needed to charge the batteries:

$$\eta_{BATTERY} = 0.7 \Rightarrow W_1 = \frac{W_{DAY}}{\eta_{BATTERY}} = \frac{3529.41}{0.7} = 5042.01 \ Wh \tag{A1}$$

2. Determine of the energy required to be supplied daily:

$$\eta_{BATTERY\_CHARGER} = 0.85 \Rightarrow W_2 = \frac{W_1}{\eta_{BATTERY\_CHARGER}} = \frac{5042.01}{0.85} = 5931.78\ Wh \tag{A2}$$

3. Evaluate the power of a module:

$$\left.\begin{array}{l}\eta_{panelFV} = 0.9 \\ P = 190\ W\end{array}\right\} \Rightarrow P_{REALmode} = P_{FV}\cdot\eta_{panelFV} = 190\cdot0.9 = 171\ W \tag{A3}$$

4. Estimate the average number of hours for standard illumination (hours/day) for the least favorable month (December):

$$N_{HOURSenviroment} = 6\ hours \tag{A4}$$

5. Estimate the energy obtained per day:

$$W_{dayFV} = P_{REALmode}\cdot N_{HOURSenviroment} = 171\cdot6 = 1026\ Wh \tag{A5}$$

where: P_{FV}—the power of a photovoltaic panel; $\eta_{panelFV}$—the yield of a photovoltaic panel. $N_{HOURSenviroment}$—the approximate illumination time.

6. Calculate the number of needed PV modules:

$$N_{MODULES} = \frac{W_4}{W_{dayFV}} = \frac{5931.78}{1026} = 5.78 panels \approx 6\ panels \tag{A6}$$

7. Calculate the number of modules in series for Un = 24V:

$$N_{seriesMODULES} = \frac{U_n}{V_{mp}} = \frac{24}{35.8} = 0.67 \approx 1\ piece \tag{A7}$$

8. Calculate the number of modules in parallel:

$$N_{parallelMODULES} = \frac{N_{MODULES}}{N_{seriesMODULES}} = \frac{6}{1} = 6\ pieces \tag{A8}$$

9. Calculate the number of modules needed to be purchased:

$$N_{MODULES} = N_{seriesMODULES}\cdot N_{parallelMODULES} = 1\cdot6 = 6\ pieces \tag{A9}$$

10. Estimate the total power generated by the photovoltaic system:

$$P_N = 190\ W(from\ datasheet) \Rightarrow P_{TOTAL} = N_{MODULES}\cdot P_N = 6\cdot190 = 1140\ W \tag{A10}$$

Appendix B

The energy production budget and performance of the 7.5 MW photovoltaic park:

Table A1. Production budget.

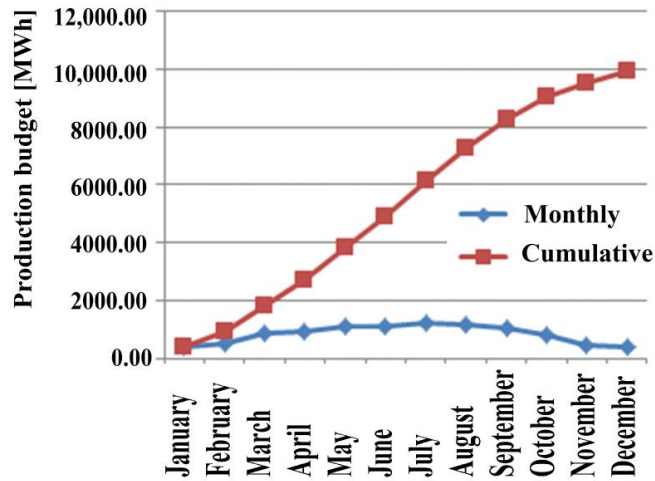|	Monthly (MWh)	Cumulative (MWh)
January	386.81	386.81
February	520.76	907.57
March	882.30	1789.88
April	943.31	2733.18
May	1102.99	3836.17
June	1086.91	4923.08
July	1204.52	6127.59
August	1141.43	7269.02
September	1017.09	8286.11
October	776.11	9062.22
November	463.85	9526.07
December	407.93	9934.00

Figure A1. Graph with solar photovoltaic production (MWh) each month of one year and cumulatively from the beginning of the calendar year.
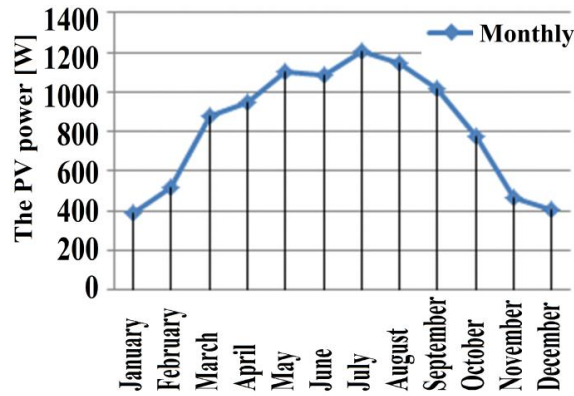

Figure A2. Monthly energy production (MWh) of the photovoltaic park.

Table A2. Energy production in December.

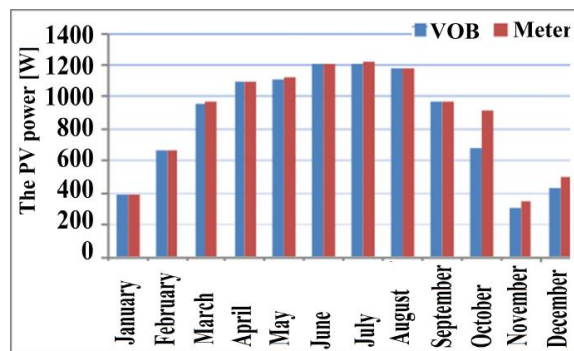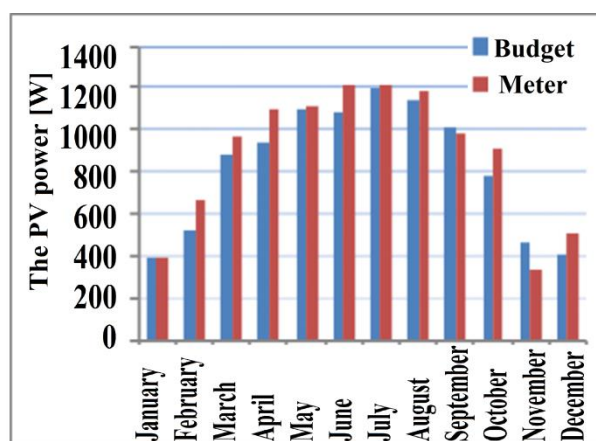|	Production (MWh)	
Source	**December**	**Cumulative**
SCADA [MWh]	437.93	10,209.23
Meter [MWh]	505.45	10,584.23
|Difference| [MWh]	67.97	375.00
Dev. SCADA vs. Meter [%]	13.45	3.54

Figure A3. Production representation (MWh)–SCADA vs. meter.

Table A3. Production—meter vs. budget.

	Production Status: Real vs. Budget	
Source	December	Cumulative
SCADA [MWh]	407.93	9934.00
|Difference Meter| [MWh]	97.52	650.23
Dev. Meter [%]	23.21	6.55

Figure A4. Production representation (MWh)—meter vs. budget.

References

1. Agri-Environmental Indicator—Irrigation. Available online: https://ec.europa.eu/eurostat/statisticsexplained/ (accessed on 1 September 2019).
2. Wu, J.; Tran, N.K. Application of Blockchain Technology in Sustainable Energy Systems: An Overview. *Sustainability* **2018**, *10*, 3067. [CrossRef]
3. Water for Agriculture. Available online: https://www.eea.europa.eu (accessed on 1 September 2019).
4. Galindo, J.; Torok, S.; Salguero, F.; de Campos, S.; Romera, J.; Puig, V. Optimal Management of Water and Energy in Irrigation Systems: Application to the Bardenas Canal. *IFAC Pap. Online* **2017**, *50*, 6613–6618. [CrossRef]
5. Daud, A.K.; Mahmoud, M.M. Solar powered induction motor-driven water pump operating on a desert well, simulation and field tests. *Renew. Energy* **2015**, *30*, 701–714. [CrossRef]
6. Bizon, N. Energy Harvesting from the Partially Shaded Photovoltaic Systems—Chapter 7. In *Optimization of the Fuel Cell Renewable Hybrid Power Systems*; Springer: New York, NY, USA, 2017; pp. 285–301.
7. Shinde, V.B.; Wandre, S.S. Solar photovoltaic water pumping system for irrigation: A review. *Afr. J. Agric. Res. (AJAR)* **2015**, *10*, 2267–2273.
8. Babkir, A. Comparative assessment of the feasibility for solar irrigation pumps in Sudan. *Renew. Sustain. Energy Rev.* **2018**, *81*, 413–420. [CrossRef]
9. Nallapaneni, M.K.; Jayanna, K.; Mallikarjun, P. Floatovoltaics: Towards improved energy efficiency, land and water management. *Int. J. Civ. Eng. Technol. (IJCIET)* **2018**, *9*, 1089–1096.
10. Wattana, V.; Tharwon, A.; Danupol, H. When blockchain meets Internet of Things: Characteristics, challenges, and business opportunities. *J. Ind. Inf. Integr.* **2019**. [CrossRef]
11. O'Dwyer, E.; Panb, I.; Acha, S.; Shah, N. Smart energy systems for sustainable smart cities: Current developments, trends and future directions. *Appl. Energy* **2019**, *237*, 581–597. [CrossRef]
12. Hua, H.; Qin, Y.; Hao, C.; Cao, J. Optimal energy management strategies for energy Internet via deep reinforcement learning approach. *Appl. Energy* **2019**, *239*, 598–609. [CrossRef]
13. Hirsch, A.; Parag, I.; Guerrero, J. Microgrids: A review of technologies, key drivers, and outstanding issues. *Renew. Sustain. Energy Rev.* **2018**, *90*, 402–411. [CrossRef]
14. Reka, S.; Dragicevic, T. Future effectual role of energy delivery: A comprehensive review of Internet of Things and smart grid. *Renew. Sustain. Energy Rev.* **2018**, *91*, 90–108. [CrossRef]

15. Zha, X.; Ni, W.; Wang, X.; Liu, R.P.; Guo, Y.J.; Niu, X.; Zheng, K. The impact of link duration on the integrity of distributed mobile networks. *IEEE Trans. Inf. Forensics Secur.* **2018**, *13*, 2240–2255. [CrossRef]

16. Li, Z.; Bahramiradb, S.; Paasob, A.; Yan, M.; Shahidehpour, M. Blockchain for decentralized transactive energy management system in networked microgrids. *Electr. J.* **2019**, *32*, 58–72. [CrossRef]

17. Karavas, C.S.; Arvanitis, K.; Papadakis, G. A Game Theory Approach to Multi-Agent Decentralized Energy Management of Autonomous Polygeneration Microgrids. *Energies* **2017**, *10*, 1756. [CrossRef]

18. Cioara, T.; Anghel, I.; Bertoncini, M.; Salomie, I.; Arnone, D.; Mammina, M.; Velivassaki, T.H.; Antal, M. Optimized Flexibility Management enacting Data Centres Participation in Smart Demand Response Programs. *Future Gener. Comput. Syst.* **2018**, *78*, 330–342. [CrossRef]

19. Islam, R.; Sarker, P.C.; Subarto Kumar Ghosh, S.K. Prospect and advancement of solar irrigation in Bangladesh: A review. *Renew. Sustain. Energy Rev.* **2017**, *77*, 406–422. [CrossRef]

20. Ding, W.; Wang, G.; Xu, A.; Chen, H. Research on Key Technologies and Information Security Issues of Energy Blockchain. *Zhongguo Dianji Gongcheng Xuebao/Proc. Chin. Soc. Electr. Eng. (CSEE)* **2018**, *38*, 1026–1034.

21. Dorri, A.; Kanhere, S.S.; Jurdak, R.; Gauravaram, P. Blockchain for IoT security and privacy: The case study of a smart home. In Proceedings of the 2017 IEEE International Conference on Pervasive Computing and Communications Workshops (PerCom Workshops), Kona, HI, USA, 13–17 March 2017; pp. 618–623. [CrossRef]

22. Kiayias, A.; Russell, A.; David, B.; Oliynykov, R. Ouroboros: A provably secure proof-of-stake blockchain protocol. In Proceedings of the CRYPTO 2017, 37th Annual International Cryptology Conference, Santa Barbara, CA, USA, 20–24 August 2017; Springer: New York, NY, USA, 2017; pp. 357–388.

23. Wang, X.; Yang, W.; Noor, S.; Chen, C.; Guoc, M.; van Dam, K.H. Blockchain-based smart contract for energy demand management. *Energy Procedia* **2019**, *158*, 2719–2724. [CrossRef]

24. Hertig, A. How Do Ethereum Smart Contracts Work? 2018. Available online: https://www.coindesk.com/information/ethereum-smart-contracts-work/ (accessed on 1 September 2019).

25. Li, Y.; Yang, W.; He, P.; Chen, C.; Wang, X. Design and management of a distributed hybrid energy system through smart contract and blockchain. *Appl. Energy* **2019**, *248*, 390–405. [CrossRef]

26. Hassan, M.U.; Rehmani, M.H.; Chen, J. Privacy preservation in blockchain based IoT systems: Integration issues, prospects, challenges, and future research directions. *Future Gener. Comput. Syst.* **2019**, *97*, 512–529. [CrossRef]

27. Makhdoom, I.; Abolhasan, M.; Abbas, H.; Ni, W. Blockchain's adoption in IoT: The challenges, and a way forward. *J. Netw. Comput. Appl.* **2019**, *125*, 251–279. [CrossRef]

28. Novo, O. Blockchain meets IoT: An architecture for scalable access management in IoT. *IEEE Internet Things J.* **2018**, *5*, 1184–1195. [CrossRef]

29. Liu, N.; Yu, X.; Wang, C.; Li, C.; Ma, L.; Lei, J. An Energy Sharing Model with Price-based Demand Response for Microgrids of Peer-to-Peer Prosumers. *IEEE Trans. Power Syst.* **2017**, *32*, 3569–3583. [CrossRef]

30. Unguru, M. Blockchain Technology: Opportunities for the Energy Sector. Available online: http://www.nos.iem.ro/handle/11748/1279 (accessed on 30 January 2020).

31. Wang, T.; Zheng, Z.; Rehmani, M.H.; Yao, S.; Huo, Z. Privacy preservation in big data from the communication perspective—A survey. *IEEE Commun. Surv. Tutor.* **2019**, *21*, 753–778. [CrossRef]

32. Viji Priya, G.; Krishna Priya, G.; Vivek, M.; Ashwini, R. A survey on security attacks and challenges in bitcoin. *Int. J. Comput. Eng. Technol. (IJCET)* **2018**, *9*, 65–74.

33. Conti, M.; Kumar, E.S.; Lal, C.; Ruj, S. A survey on security and privacy issues of bitcoin. *IEEE Commun. Surv. Tutor.* **2019**, *20*, 3416–3452. [CrossRef]

34. Nakamoto, S. Bitcoin: A Peer-to-Peer Electronic Cash System. 2008. Available online: https://bitcoin.org/bitcoin.pdf (accessed on 1 September 2019).

35. Ateniese, G.; Magri, B.; Venturi, D.; Andrade, E. Redactable blockchain—or-rewriting history in bitcoin and friends. In Proceedings of the IEEE European Symposium on Security and Privacy (EuroS&P), Paris, France, 26–28 April 2017; pp. 111–126.

36. Ross, K. ACWA Power Adopts Blockchain Currency SolarCoin. 2018. Available online: https://www.renewableenergyworld.com/2018/01/18/acwa-power-adopts-blockchain-currency-solarcoin/#gref (accessed on 1 September 2019).

37. Blockchain: Unchaining Utilities to the Future. Available online: https://www.arabianindustry.com/utilities/features/2018/oct/7/blockchain-unchaining-utilities-to-the-future-5987215/ (accessed on 1 September 2019).

38. Hughes, L.; Dwivedi, K.Y.; Misra, S.K.; Rana, P.N.; Raghavan, V.; Akella, V. Blockchain research, practice and policy: Applications, benefits, limitations, emerging research themes and research agenda. *Int. J. Inf. Manag.* **2019**, *49*, 114–129. [CrossRef]

39. Zhao, Y.; Peng, K.; Xu, B.; Liu, Y.; Xiong, W.; Han, Y. Applied engineering programs of energy blockchain in US. In Proceedings of the 10th International Conference on Applied Energy (ICAE2018), Hong Kong, China, 22–25 August 2018. *Sci. Direct Energy Procedia* **2019**, *158*, 2787–2793. [CrossRef]

40. Muzammal, M.; Qu, Q.; Nasrulin, B. Renovating blockchain with distributed databases: An open source system. *Future Gener. Comput. Syst.* **2019**, *90*, 105–117. [CrossRef]

41. Enescu, F.M.; Bizon, N. SCADA Applications for Electric Power System—Chapter 12. In *Reactive Power Control in AC Power Systems*; Springer: New York, NY, USA, 2017; pp. 561–609.

42. Enescu, F.M.; Bizon, N.; Moraru, C.M. Issues in Securing Critical Infrastructure Networks for Smart Grid Based on SCADA, Other Industrial Control and Communication Systems: Modeling, Analysis and Practice. In *Power Systems Resilience*; Springer: New York, NY, USA, 2018.

43. Enescu, F.M.; Marinescu, C.-N.; Ionescu, V.M.; Stirbu, C. System for monitoring and controlling renewable energy sources. In Proceedings of the 2017 9th International Conference on Electronics, Computers and Artificial Intelligence (ECAI), Targoviste, Romania, 29 June–1 July 2017. [CrossRef]

44. Bordel, B.; Martin, D.; Alcarria, R.; ROBLES, T. A Blockchain-based Water Control System for the Automatic Management of Irrigation Communities. In Proceedings of the 2019 IEEE International Conference on Consumer Electronics (ICCE), Las Vegas, NV, USA, 11–13 January 2019; p. 5.

45. Caro, M.P.; Ali, M.S.; Vecchio, M.; Giaffreda, R. Blockchain-based traceability in Agri-Food supply chain management: A practical implementation. In Proceedings of the 2018 Conferince IEEE: IoT Vertical and Topical Summit on Agriculture—Tuscany (IOT Tuscany), Tuscany, Italy, 8–9 May 2018; p. 4.

46. Chilundo, R.J.; Diana Nevesc, D.; Urânio, S.; Mahanjane, U.S. Photovoltaic water pumping systems for horticultural crops irrigation: Advancements and opportunities towards a green energy strategy for Mozambique. *Sustain. Energy Technol. Assess.* **2019**, *33*, 61–68. [CrossRef]

47. Casa pepenilor. Available online: https://www.dor.ro/casa-pepenilor/ (accessed on 2 December 2019).

48. De ce Aeceta Distruge Agricultura Romaniei. Un Raport Parlamentar Dezvaluie Delapidarea Sistemului de Irigatii. Available online: https://www.ancheteonline.ro/2012/08/de-ce-seceta-distruge-agricultura-romaniei-un-raport-parlamentar-dezvaluie-delapidarea-sistemului-de-irigatii/ (accessed on 2 December 2019).

49. Ahl, A.; Yarime, M.; Tanaka, K.; Tanaka, K.; Sagawa, D. Review of blockchain-based distributed energy: Implications for institutional development. *Renew. Sustain. Energy Rev.* **2019**, *107*, 200–211. [CrossRef]

50. Bousfield, D. Crypto-coin hierarchies: Social contestation in blockchain networks. *Artic. Glob. Netw. May* **2019**, *19*, 291–307. [CrossRef]

51. Andoni, M.; Robu, V.; David Flynn, D.; Abram, S.; Geach, D.; Jenkins, D.; McCallum, P.; Peacock, A. Blockchain technology in the energy sector: A systematic review of challenges and opportunities. *Renew. Sustain. Energy Rev.* **2019**, *100*, 143–174. [CrossRef]

52. Tan, S.; Wang, X.; Jiang, C. Privacy-Preserving Energy Scheduling for ESCOs Based on Energy Blockchain Network. *Energies* **2019**, *12*, 1530. [CrossRef]

53. Brilliantova, V. Blockchain and the future of energy. *Technol. Soc.* **2019**, *57*, 39–45. [CrossRef]

54. Zhong, L.; Wu, Q.; Xie, J.; Li, J.; Qin, B. A secure versatile light payment system based on blockchain. *Future Gener. Comput. Syst.* **2019**, *93*, 327–337. [CrossRef]

55. Kumar, N.M. Blockchain: Enabling wide range of services in distributed energy system. *BeniSuef Univ. J. Basic Appl. Sci.* **2018**, *7*, 701–704. [CrossRef]

56. Khaqqi, K.N.; Sikorski, J.J.; Hadinoto, K.; Kraft, M. Incorporating seller/buyer reputation-based system in blockchain-enabled emission trading application. *Appl. Energy* **2018**, *209*, 8–19. [CrossRef]

57. Rathore, S.; Pan, Y.; Park, J.H. BlockDeepNet: A Blockchain-Based Secure Deep Learning for IoT Network. *Sustainability* **2019**, *11*, 3974. [CrossRef]

58. SolarCoin: A Blockchain-Based Solar Energy Incentive. 2018. Available online: https://solarcoin.org/wp-content/uploads/SolarCoin_Policy_Paper_EN-1.pdf (accessed on 1 September 2019).

59. Produce One Megawatt Hour. Get One Free SolarCoin. Available online: https://solarcoin.org (accessed on 1 September 2019).

60. SolarCoin Monetary Policy Proposal to Accelerate the Renewable Energy Transition. Available online: https://medium.com/solarcoin/solarcoin-monetary-policy-proposal-to-accelerate-the-renewable-energy-transition-f46b5d6e7f19 (accessed on 1 September 2019).

61. Yang, L. The blockchain: State-of-the-art and research challenges. *J. Ind. Inf. Integr.* **2019**. [CrossRef]

62. Birleanu, F.G.; Anghelescu, P.; Bizon, N. Malicious and Deliberate Attacks and Power System Resiliency. In *Power Systems Resilience*; Springer: New York, NY, USA, 2018; pp. 223–246.

63. Huh, S.; Cho, S.; Kim, S. Managing IoT devices using Blockchain platform. In Proceedings of the 2017 19th International Conference on Advanced Communication Technology (ICACT), Pyeongchang, Korea, 19–22 February 2017; pp. 464–467.

64. Zappia, F.; Chen, L.; Pavone, P.; Pisani, R. A Model of Interaction between the Financial Sector and the Energy Sector: The Hypothesis of Energy Currency. *Chin. Bus. Rev.* **2018**, *17*, 532–534.

65. T'Serclaes, P. Blockchain Could Be the Missing Link in the Renewable Energy Revolution. World Economic Forum. 21 September 2017. Available online: https://www.weforum.org/agenda/2017/09/blockchainenergy-efficiency-finance/ (accessed on 1 September 2019).

66. Andrillon, F. SolarCoin: Incentivising Solar PV Energy Production through Blockchain Innovation. Available online: https://www.pv-tech.org/guest-blog/solarcoin-incentivising-solar-pv-energy-production-through-blockchain-innov (accessed on 1 September 2019).

67. Cryptocurrencies, Blockchain and Pollution. Available online: http://ecoprofit.ro/criptomonedele-blockchain-ul-si-poluarea/ (accessed on 1 September 2019).

68. Could SolarCoin Help ACWA Boost Its Profits From Solar? Available online: https://www.greentechmedia.com/articles/read/could-solarcoin-help-acwa-boost-its-profits-from-solar (accessed on 1 September 2019).

69. Mihalache, S.F.; Pricop, E.; Fattahi, J. Chap. In *Power Systems Resilience*; Springer: New York, NY, USA, 2018; pp. 269–287.

70. Casino, F.; Dasaklis, T.K.; Patsakis, C. A systematic literature review of blockchain-based applications:Current status. classification and open issues. *Telemat. Inform.* **2019**, *36*, 55–81. [CrossRef]

71. Dinh, T.T.A.; Liu, R.; Zhang, M.; Chen, G.; Ooi, B.C.; Wang, J. Untangling blockchain: A Data Processing View of Blockchain Systems. *IEEE Trans. Knowl. Data Eng.* **2018**, *30*, 1366–1385. [CrossRef]

72. Nasrulin, B.; Muzammal, M.; Qu, Q. ChainMOB: Mobility Analytics on Blockchain. In Proceedings of the 19th IEEE International Conference on Mobile Data Management (MDM), Aalborg, Denmark, 25–28 June 2018; pp. 292–293.

73. Wang, X.; Zha, X.; Ni, W.; Liu, R.P.; Guo, J.Y.; Niu, X.; Zheng, K. Survey on blockchain for Internet of Things. *Comput. Commun.* **2019**, *136*, 10–29. [CrossRef]

74. Reyna, A.; Martín, C.; Chen, J.; Soler, E.; Díaz, M. On blockchain and its integration with IoT. Challenges and opportunities. *Future Gener. Comput. Syst.* **2018**, *88*, 173–190. [CrossRef]

75. Rathorea, P.K.S.; Dasb, S.S.; Chauhana, D.S. Perspectives of solar photovoltaic water pumping for irrigation in India. *Energy Strategy Rev.* **2018**, *22*, 385–395. [CrossRef]

76. Ranjbarana, P.; Yousefia, H.; Gharehpetianb, G.B.; Astaraeia, F.R. A review on floating photovoltaic (FPV) power generation units. *Renew. Sustain. Energy Rev.* **2019**, *110*, 332–347. [CrossRef]

77. Cazzaniga, R.; Cicu, M.; Rosa-Clot, M.; Rosa-Clot, P.; Tina, G.M.; Ventura, C. Floating photovoltaic plants: Performance analysis and design solutions. *Renew. Sustain. Energy Rev.* **2018**, *81*, 1730–1741. [CrossRef]

78. Sahu, A.; Yadav, N.; Sudhakar, K. Floating photovoltaic power plant: A review. Floating photovoltaic plants: Performance analysis and design solutionso. *Renew. Sustain. Energy Rev.* **2016**, *66*, 815–824. [CrossRef]

79. Balaj, I.C. Possibilities of Using Solar Energy in Land Improvement Arrangements. Available online: https://dspace.upt.ro/jspui/bitstream/123456789/353/1/Teza%20doctorat%20Balaj%20Ciprian.pdf (accessed on 2 December 2019).

80. Maican, E. *Renewable Energy Systems*; Publishing House Printech: Bucureşti, Romania, 2015; ISBN 978-606-23-0359-4. isbn.pub.ro.

81. Campana, P.E.; Wasthage, L.; Nookuea, W.; Tan, Y.; Yan, J. Optimization and assessment of floating and floating-tracking PV systems integrated in on- and off-grid hybrid energy systems. *Solar Energy* **2019**, *177*, 782–795. [CrossRef]

82. Liu, L.; Sun, Q.; Li, H.; Yin, H.; Ren, X.; Wennersten, R. Evaluating the benefits of Integrating Floating Photovoltaic and Pumped Storage Power System. *Energy Convers. Manag.* **2019**, *194*, 173–185. [CrossRef]

83. Sahu, A.K.; Sudhakar, K. Effect of UV exposure on bimodal HDPE floats for floating solar application. *J. Mater. Res. Technol.* **2019**, *8*, 147–156. [CrossRef]

MDPI